Methods in Molecular Biology 2127

Springer Protocols

Camilo Perez
Timm Maier *Editors*

Expression, Purification, and Structural Biology of Membrane Proteins

Humana Press

METHODS IN MOLECULAR BIOLOGY

Series Editor
John M. Walker
School of Life and Medical Sciences
University of Hertfordshire
Hatfield, Hertfordshire, UK

For further volumes:
http://www.springer.com/series/7651

For over 35 years, biological scientists have come to rely on the research protocols and methodologies in the critically acclaimed *Methods in Molecular Biology* series. The series was the first to introduce the step-by-step protocols approach that has become the standard in all biomedical protocol publishing. Each protocol is provided in readily-reproducible step-by-step fashion, opening with an introductory overview, a list of the materials and reagents needed to complete the experiment, and followed by a detailed procedure that is supported with a helpful notes section offering tips and tricks of the trade as well as troubleshooting advice. These hallmark features were introduced by series editor Dr. John Walker and constitute the key ingredient in each and every volume of the *Methods in Molecular Biology* series. Tested and trusted, comprehensive and reliable, all protocols from the series are indexed in PubMed.

Expression, Purification, and Structural Biology of Membrane Proteins

Edited by

Camilo Perez and Timm Maier

Biozentrum, University of Basel, Basel, Basel Stadt, Switzerland

Humana Press

Editors
Camilo Perez
Biozentrum
University of Basel
Basel, Basel Stadt, Switzerland

Timm Maier
Biozentrum
University of Basel
Basel, Basel Stadt, Switzerland

ISSN 1064-3745 ISSN 1940-6029 (electronic)
Methods in Molecular Biology
ISBN 978-1-0716-0372-7 ISBN 978-1-0716-0373-4 (eBook)
https://doi.org/10.1007/978-1-0716-0373-4

This Humana imprint is published by the registered company Springer Science+Business Media, LLC, part of Springer Nature.
The registered company address is: 1 New York Plaza, New York, NY 10004, U.S.A.

Preface

Membrane proteins mediate fundamental biological processes such as signal transduction, transport processes across membranes, sensing of chemical signals, and coordination of cell–cell interactions. Numerous diseases in humans are linked to membrane proteins, making them important targets for drug development. Inhibitors targeting membrane proteins of pathogens are highly relevant for establishing novel antimicrobial treatments. Therefore, understanding the molecular mechanisms of membrane proteins is not only of fundamental biological interest but also provides opportunities for improving human health. However, membrane protein research entails several specific challenges, such as low expression yields, the requirement for solubilization, and the need for highly sensitive tools for structural and mechanistic characterization. In this book, the reader finds a comprehensive collection of protocols on membrane protein production for structural and mechanistic characterization. The purpose of this book is to collect up-to-date advanced protocols and advice from leading experts in the area of membrane protein biology that can be applied to structural and functional studies of any membrane protein system.

The first six chapters consist of methods for cloning and expression of membrane proteins and membrane protein complexes in prokaryotic and eukaryotic systems including Gram-negative and Gram-positive bacteria, *Saccharomyces cerevisiae*, and insect cells. For cases where overexpression of membrane proteins is not feasible, isolation from native material provides an alternate strategy. An example for such strategy is provided by Bodensohn et al. in Chapter 6, which provides protocols for the isolation of organelles and membranes from the plant *Arabidopsis thaliana*.

Optimization of purification protocols is frequently necessary to achieve high-quality membrane protein preparations. The importance of such steps should not be taken lightly since sample quality is a major determinant for the success of any advanced structural and biophysical characterization. Chapters 2–4, 7–10, and 19 detail approaches for purification of prokaryotic and eukaryotic membrane proteins. They include helpful troubleshooting advices to overcome common pitfalls in membrane protein production.

Over the last several years, nanobodies, small recombinant binders derived from camelid single-chain antibodies, have become widely used tools in membrane proteins research. They are applied to modify protein activity and to trap specific conformational states, useful in particular for subsequent structural analysis. Chapters 11–13 describe methods for membrane protein immobilization for the selection of nanobodies, for recombinant production of nanobodies and "macrobodies" (enlarged nanobodies, e.g., for electron microscopy applications), and for the identification of conformation-selective nanobodies.

Mechanistic studies often require reconstitution of membrane proteins into native-like lipid environments that allow both structural and biophysical investigations. Such methods include the incorporation of membrane proteins into liposomes, bicelles, and nanodiscs. Chapters 14, 15, 17, and 25 include protocols for the reconstitution of membrane proteins in such lipid environments and outline applications and advantages of particular membrane mimics.

Single-particle cryo-electron microscopy (cryo-EM) is a powerful tool for investigating the structure and mechanism of membrane proteins in multiple environments, including

detergent micelles and lipid nanodiscs. Chapters 16–18 describe protocols for electron microscopy grid preparation, data collection, and analysis.

Standard and advanced crystallization techniques, such as lipid cubic phase (LCP) crystallization, have enabled the determination of high-resolution structures of multiple membrane proteins. Chapters 19–21 describe recent advances in methods for X-ray crystallography of membrane proteins. *In meso* in situ serial X-ray crystallography (IMISX) minimizes crystal manipulation in LPC, and advanced microcrystal preparation techniques as well as high viscosity injectors enable the analysis of membrane proteins using serial X-ray crystallography on X-ray free electron lasers or synchrotron sources.

Biophysical methods, such as hydrogen/deuterium exchange measured by mass spectrometry (HDX-MS) and atomic force microscopy (AFM), are robust methods to study the structure and dynamics of membrane proteins. Chapter 22 describes a protocol for the study of detergent-solubilized membrane proteins by HDX-MS, while Chapter 23 provides methods for single-molecule AFM analysis.

Recent advances in nuclear magnetic resonance (NMR) spectroscopy are described in Chapters 24 and 25. In these chapters, the authors describe protocols for sample preparation and characterization of membrane proteins by solid-state NMR under magic angle spinning (MAS) and by solution-state NMR with protein in lipid nanodiscs.

We cordially thank all the authors who through this book shared their knowledge and experience with the broad scientific community. We are convinced that this book will guide and encourage young researchers and newcomers to the field to tackle bold studies on membrane proteins. We thank John Walker, the series editor, for his help and encouragement and the staff at Humana Press who helped to produce this volume.

Basel, Switzerland

Camilo Perez
Timm Maier

Contents

Preface . . . . . *v*
Contributors . . . . . *xi*

1 Cloning and Multi-Subunit Expression of Mitochondrial Membrane Protein Complexes in *Saccharomyces cerevisiae* 1
Porsha L. R. Shaw, Kathryn A. Diederichs, Ashley Pitt, Sarah E. Rollauer, and Susan K. Buchanan

2 Membrane Protein Production in *Escherichia coli* 13
Benjamin C. McIlwain and Ali A. Kermani

3 Membrane Protein Production in *Lactococcus lactis* for Structural Studies 29
Chloe Martens

4 Expression and Purification of Membrane Proteins in *Saccharomyces cerevisiae* 47
Martin S. King and Edmund R. S. Kunji

5 Membrane Protein Expression in Insect Cells Using the Baculovirus Expression Vector System 63
Jacques Boivineau, Matthias Haffke, and Veli-Pekka Jaakola

6 Membrane Extracts from Plant Tissues 81
Uwe Bodensohn, Christoph Ruland, Roman Ladig, and Enrico Schleiff

7 Membrane Protein Solubilization and Quality Control: An Example of a Primary Active Transporter 93
Charlott Stock and Inga Hänelt

8 GPCR Solubilization and Quality Control 105
Tamara Miljus, David A. Sykes, Clare R. Harwood, Ziva Vuckovic, and Dmitry B. Veprintsev

9 Affinity Purification of Membrane Proteins 129
Elisabeth Graeber and Volodymyr M. Korkhov

10 Purification of Membrane Proteins by Affinity Chromatography with On-Column Protease Cleavage 139
Stephan Hirschi and Dimitrios Fotiadis

11 Biotinylation of Membrane Proteins for Binder Selections 151
Benedikt T. Kuhn, Iwan Zimmermann, Pascal Egloff, Lea M. Hürlimann, Cedric A. J. Hutter, Christian Miscenic, Roger J. P. Dawson, Markus A. Seeger, and Eric R. Geertsma

12 Production and Application of Nanobodies for Membrane Protein Structural Biology 167
Janine Denise Brunner and Stephan Schenck

13 Identifying Conformation-Selective Heavy-Chain-Only Antibodies Against Membrane Proteins by a Thermal-Shift Scintillation Proximity Assay 185
Peter Stohler and Roger J. P. Dawson

14 Reconstitution of Membrane Proteins into Platforms Suitable for Biophysical and Structural Analyses 191
Philipp A. M. Schmidpeter, Nattakan Sukomon, and Crina M. Nimigean

15 Reconstitution of Proteoliposomes for Phospholipid Scrambling and Nonselective Channel Assays 207
Maria E. Falzone and Alessio Accardi

16 Membrane Protein Cryo-EM: Cryo-Grid Optimization and Data Collection with Protein in Detergent 227
Magnus Bloch, Mònica Santiveri, and Nicholas M. I. Taylor

17 Single-Particle Cryo-EM of Membrane Proteins in Lipid Nanodiscs 245
Valeria Kalienkova, Carolina Alvadia, Vanessa Clerico Mosina, and Cristina Paulino

18 Fast Small-Scale Membrane Protein Purification and Grid Preparation for Single-Particle Electron Microscopy 275
Natalie Bärland and Camilo Perez

19 Stabilization and Crystallization of a Membrane Protein Involved in Lipid Transport 283
Bing Zhang and Camilo Perez

20 In Meso In Situ Serial X-Ray Crystallography (IMISX): A Protocol for Membrane Protein Structure Determination at the Swiss Light Source 293
Chia-Ying Huang, Vincent Olieric, Martin Caffrey, and Meitian Wang

21 Membrane Protein Preparation for Serial Crystallography Using High-Viscosity Injectors: Rhodopsin as an Example 321
Tobias Weinert and Valérie Panneels

22 Hydrogen/Deuterium Exchange Mass Spectrometry for the Structural Analysis of Detergent-Solubilized Membrane Proteins 339
Darragh P. O'Brien, Véronique Hourdel, Alexandre Chenal, and Sébastien Brier

23 Mechanical Unfolding and Refolding of Single Membrane Proteins by Atomic Force Microscopy 359
Noah Ritzmann and Johannes Thoma

24 Sample Preparation and Technical Setup for NMR Spectroscopy with Integral Membrane Proteins 373
Hundeep Kaur, Anne Grahl, Jean-Baptiste Hartmann, and Sebastian Hiller

25 Exploring Lipid and Membrane Protein Dynamics Using Lipid-Bilayer Nanodiscs and Solution-State NMR Spectroscopy 397
Stefan Bibow

Index *421*

Contributors

Alessio Accardi • *Department of Biochemistry, Weill Cornell Medical College, New York, NY, USA; Department of Anesthesiology, Weill Cornell Medical College, New York, NY, USA; Department of Physiology and Biophysics, Weill Cornell Medical College, New York, NY, USA*

Carolina Alvadia • *Department of Biochemistry, University of Zurich, Zurich, Switzerland*

Natalie BÄrland • *Biozentrum, University of Basel, Basel, Switzerland*

Stefan Bibow • *Biozentrum, University of Basel, Basel, Switzerland*

Magnus Bloch • *Structural Biology of Molecular Machines Group, Protein Structure & Function Programme, Novo Nordisk Foundation Center for Protein Research, Faculty of Health and Medical Sciences, University of Copenhagen, Copenhagen, Denmark*

Uwe Bodensohn • *Institute of Molecular Biosciences, Goethe University, Frankfurt am Main, Germany*

Jacques Boivineau • *Chemical Biology & Therapeutics, Novartis Institutes for BioMedical Research, Novartis Pharma AG, Novartis Campus, Basel, Switzerland*

Sébastien Brier • *Biological NMR Technological Platform, Center for Technological Resources and Research, Department of Structural Biology and Chemistry, Institut Pasteur, CNRS UMR3528, Paris, France*

Janine Denise Brunner • *Laboratory of Biomolecular Research, Division of Biology and Chemistry, Paul Scherrer Institute, Villigen, PSI, Switzerland*

Susan K. Buchanan • *Laboratory of Molecular Biology, National Institute of Diabetes & Digestive & Kidney Diseases, National Institutes of Health, Bethesda, MD, USA*

Martin Caffrey • *Membrane Structural and Functional Biology (MS&FB) Group, School of Medicine and School of Biochemistry and Immunology, Trinity College Dublin, Dublin, Ireland*

Alexandre Chenal • *Biochemistry of Macromolecular Interaction Unit, Department of Structural Biology and Chemistry, Institut Pasteur, CNRS UMR3528, Paris, France*

Vanessa Clerico Mosina • *Department of Structural Biology at the Groningen Biomolecular Sciences and Biotechnology Institute, University of Groningen, Groningen, The Netherlands*

Roger J. P. Dawson • *Roche Pharma Research and Early Development, Therapeutic Modalities, Roche Innovation Center Basel, F. Hoffmann-La Roche Ltd, Basel, Switzerland*

Kathryn A. Diederichs • *Laboratory of Molecular Biology, National Institute of Diabetes & Digestive & Kidney Diseases, National Institutes of Health, Bethesda, MD, USA*

Pascal Egloff • *Institute of Medical Microbiology, University of Zurich, Zurich, Switzerland*

Maria E. Falzone • *Department of Biochemistry, Weill Cornell Medical College, New York, NY, USA*

Dimitrios Fotiadis • *Institute of Biochemistry and Molecular Medicine, University of Bern, Bern, Switzerland*

Eric R. Geertsma • *Institute for Biochemistry, Biocenter, Goethe University Frankfurt, Frankfurt, Germany*

Elisabeth Graeber • *Institute of Biochemistry, ETH Zurich and Paul Scherrer Institute, Villigen, Switzerland*
Anne Grahl • *Biozentrum, University of Basel, Basel, Switzerland*
Matthias Haffke • *Chemical Biology & Therapeutics, Novartis Institutes for BioMedical Research, Novartis Pharma AG, Novartis Campus, Basel, Switzerland; Global Discovery Chemistry, Novartis Institutes for BioMedical Research, Novartis Pharma AG, Novartis Campus, Basel, Switzerland*
Inga HÄnelt • *Institute of Biochemistry, Biocenter, Goethe University Frankfurt, Frankfurt, Germany*
Jean-Baptiste Hartmann • *Biozentrum, University of Basel, Basel, Switzerland*
Clare R. Harwood • *Centre of Membrane Proteins and Receptors (COMPARE), University of Birmingham and University of Nottingham, Midlands, UK; Division of Physiology, Pharmacology & Neuroscience, School of Life Sciences, University of Nottingham, Nottingham, UK*
Sebastian Hiller • *Biozentrum, University of Basel, Basel, Switzerland*
Stephan Hirschi • *Institute of Biochemistry and Molecular Medicine, University of Bern, Bern, Switzerland*
Véronique Hourdel • *Environment and Infectious Risks Unit, Department of Infection and Epidemiology, Institut Pasteur, Paris, France*
Chia-Ying Huang • *Swiss Light Source, Paul Scherrer Institut, Villigen, PSI, Switzerland*
Lea M. Hürlimann • *Institute of Medical Microbiology, University of Zurich, Zurich, Switzerland*
Cedric A. J. Hutter • *Institute of Medical Microbiology, University of Zurich, Zurich, Switzerland*
Veli-Pekka Jaakola • *Confo Therapeutics, Ghent, Belgium*
Valeria Kalienkova • *Department of Structural Biology at the Groningen Biomolecular Sciences and Biotechnology Institute, University of Groningen, Groningen, The Netherlands; Department of Biochemistry, University of Zurich, Zurich, Switzerland*
Hundeep Kaur • *Biozentrum, University of Basel, Basel, Switzerland*
Ali A. Kermani • *Department of Molecular, Cellular, and Developmental Biology, University of Michigan, Ann Arbor, MI, USA*
Martin S. King • *Medical Research Council Mitochondrial Biology Unit, University of Cambridge, Cambridge, UK*
Volodymyr M. Korkhov • *Institute of Biochemistry, ETH Zurich and Paul Scherrer Institute, Villigen, Switzerland*
Benedikt T. Kuhn • *Institute for Biochemistry, Biocenter, Goethe University Frankfurt, Frankfurt, Germany*
Edmund R. S. Kunji • *Medical Research Council Mitochondrial Biology Unit, University of Cambridge, Cambridge, UK*
Roman Ladig • *Institute of Molecular Biosciences, Goethe University, Frankfurt am Main, Germany*
Chloe Martens • *Laboratory for the Structure and Function of Biological Membranes, Center for Structural Biology and Bioinformatics, Université Libre de Bruxelles, Brussels, Belgium*
Benjamin C. McIlwain • *Department of Molecular, Cellular, and Developmental Biology, University of Michigan, Ann Arbor, MI, USA*

Tamara Miljus • *Laboratory of Biomolecular Research, Paul Scherrer Institute, Villigen, PSI, Switzerland; Department of Biology, ETH Zürich, Zürich, Switzerland; Centre of Membrane Proteins and Receptors (COMPARE), University of Birmingham and University of Nottingham, Midlands, UK; Institute of Metabolism and Systems Research, College of Medical and Dental Sciences, University of Birmingham, Birmingham, UK*

Christian Miscenic • *Roche Pharma Research and Early Development, Therapeutic Modalities, Roche Innovation Center Basel, F. Hoffmann-La Roche Ltd, Basel, Switzerland*

Crina M. Nimigean • *Department of Anesthesiology, Weill Cornell Medicine, New York, NY, USA; Department of Physiology and Biophysics, Weill Cornell Medicine, New York, NY, USA*

Darragh P. O'Brien • *Biochemistry of Macromolecular Interaction Unit, Department of Structural Biology and Chemistry, Institut Pasteur, CNRS UMR3528, Paris, France; Nuffield Department of Medicine, Target Discovery Institute, University of Oxford, Oxford, UK*

Vincent Olieric • *Swiss Light Source, Paul Scherrer Institute, Villigen, PSI, Switzerland*

Valérie Panneels • *Division of Biology and Chemistry, Laboratory of Biomolecular Research, Paul Scherrer Institute, Villigen, PSI, Switzerland*

Cristina Paulino • *Department of Structural Biology at the Groningen Biomolecular Sciences and Biotechnology Institute, University of Groningen, Groningen, The Netherlands*

Camilo Perez • *Biozentrum, University of Basel, Basel, Switzerland*

Ashley Pitt • *Laboratory of Molecular Biology, National Institute of Diabetes & Digestive & Kidney Diseases, National Institutes of Health, Bethesda, MD, USA*

Noah Ritzmann • *Department of Biosystems Science and Engineering, Eidgenössische Technische Hochschule (ETH) Zürich, Basel, Switzerland*

Sarah E. Rollauer • *Laboratory of Molecular Biology, National Institute of Diabetes & Digestive & Kidney Diseases, National Institutes of Health, Bethesda, MD, USA; Vertex Pharmaceuticals, Boston, MA, USA*

Christoph Ruland • *Institute of Molecular Biosciences, Goethe University, Frankfurt am Main, Germany*

Mònica Santiveri • *Structural Biology of Molecular Machines Group, Protein Structure & Function Programme, Novo Nordisk Foundation Center for Protein Research, Faculty of Health and Medical Sciences, University of Copenhagen, Copenhagen, Denmark*

Stephan Schenck • *Laboratory of Biomolecular Research, Division of Biology and Chemistry, Paul Scherrer Institute, Villigen, PSI, Switzerland*

Enrico Schleiff • *Institute of Molecular Biosciences, Goethe University, Frankfurt am Main, Germany; Buchmann Institute for Molecular Life Sciences, Goethe University, Frankfurt am Main, Germany; Frankfurt Institute of Advanced Studies, Frankfurt, Germany*

Philipp A. M. Schmidpeter • *Department of Anesthesiology, Weill Cornell Medicine, New York, NY, USA*

Markus A. Seeger • *Institute of Medical Microbiology, University of Zurich, Zurich, Switzerland*

Porsha L. R. Shaw • *Laboratory of Molecular Biology, National Institute of Diabetes & Digestive & Kidney Diseases, National Institutes of Health, Bethesda, MD, USA*

Charlott Stock • *Institute of Biochemistry, Biocenter, Goethe University Frankfurt, Frankfurt, Germany*

Peter Stohler • *Roche Pharma Research and Early Development, Therapeutic Modalities, Roche Innovation Center Basel, F. Hoffmann-La Roche Ltd, Basel, Switzerland*
Nattakan Sukomon • *Department of Anesthesiology, Weill Cornell Medicine, New York, NY, USA*
David A. Sykes • *Centre of Membrane Proteins and Receptors (COMPARE), University of Birmingham and University of Nottingham, Midlands, UK; Division of Physiology, Pharmacology & Neuroscience, School of Life Sciences, University of Nottingham, Nottingham, UK*
Nicholas M. I. Taylor • *Structural Biology of Molecular Machines Group, Protein Structure & Function Programme, Novo Nordisk Foundation Center for Protein Research, Faculty of Health and Medical Sciences, University of Copenhagen, Copenhagen, Denmark*
Johannes Thoma • *Wallenberg Centre for Molecular and Translational Medicine, Department of Chemistry and Molecular Biology, University of Gothenburg, Gothenburg, Sweden*
Dmitry B. Veprintsev • *Laboratory of Biomolecular Research, Paul Scherrer Institute, Villigen, PSI, Switzerland; Department of Biology, ETH Zürich, Zürich, Switzerland; Centre of Membrane Proteins and Receptors (COMPARE), University of Birmingham and University of Nottingham, Midlands, UK; Division of Physiology, Pharmacology & Neuroscience, School of Life Sciences, University of Nottingham, Nottingham, UK*
Ziva Vuckovic • *Laboratory of Biomolecular Research, Paul Scherrer Institute, Villigen, PSI, Switzerland; Department of Biology, ETH Zürich, Zürich, Switzerland; Drug Discovery Biology, Monash Institute of Pharmaceutical Sciences, Monash University, Parkville, VIC, Australia*
Meitian Wang • *Swiss Light Source, Paul Scherrer Institute, Villigen, PSI, Switzerland*
Tobias Weinert • *Division of Biology and Chemistry, Laboratory of Biomolecular Research, Paul Scherrer Institute, Villigen, PSI, Switzerland*
Bing Zhang • *Biozentrum, University of Basel, Basel, Switzerland*
Iwan Zimmermann • *Institute of Medical Microbiology, University of Zurich, Zurich, Switzerland*

Chapter 1

Cloning and Multi-Subunit Expression of Mitochondrial Membrane Protein Complexes in *Saccharomyces cerevisiae*

Porsha L. R. Shaw, Kathryn A. Diederichs, Ashley Pitt, Sarah E. Rollauer, and Susan K. Buchanan

Abstract

Saccharomyces cerevisiae is a useful eukaryotic expression system for mitochondrial membrane proteins due to its ease of growth and ability to provide a native membrane environment. The development of the pBEVY vector system has further increased the potential of *S. cerevisiae* as an expression system by creating a method for expressing multiple proteins simultaneously. This vector system is amenable to the expression and purification of multi-subunit protein complexes. Here we describe the cloning, yeast transformation, and co-expression of multi-subunit outer mitochondrial membrane complexes using the pBEVY vector system.

Key words pBEVY, *Saccharomyces cerevisiae*, Multi-subunit expression, Mitochondrial membrane protein, LiAc/SS transformation, Membrane protein complexes

1 Introduction

The large and intricate nature of multi-subunit mitochondrial membrane protein complexes make them exceedingly difficult to express and purify for structural and biochemical experiments. Turning to the *Saccharomyces cerevisiae* expression system can offer benefits to overcome the problems faced in obtaining suitable yields of these challenging proteins [1]. *S. cerevisiae* can increase the yield and stability of mitochondrial membrane proteins since the proteins are targeted to the yeast mitochondria and expressed in a native environment. After growth, the mitochondria can be isolated using differential centrifugation to provide a partially purified membrane sample to further purify the expressed protein [2–4].

The creation of the pBEVY vector system has made it possible to co-express multiple proteins in *S. cerevisiae* [5]. The vector system consists of three vectors, pBEVY-GT, pBEVY-GL, and pBEVY-GU, each with a bi-directional galactose promoter,

Camilo Perez and Timm Maier (eds.), *Expression, Purification, and Structural Biology of Membrane Proteins*, Methods in Molecular Biology, vol. 2127, https://doi.org/10.1007/978-1-0716-0373-4_1,

allowing for the expression of two unique proteins on each vector, for a total of six proteins simultaneously. Using the pBEVY vector system, we have developed protocols for expressing multi-subunit mitochondrial membrane complexes in *S. cerevisiae*. In this chapter we describe our protocols for cloning, yeast transformation [6–8], and small-scale mitochondrial purification [4, 9].

2 Materials

Prepare all solutions using ultrapure water (purified deionized water to a resistivity greater than 18.2 MΩ·cm at 25 °C). Prepare and store all reagents at room temperature (unless otherwise noted).

2.1 Cloning of Yeast Expression Vectors

1. 10× TBE buffer: 0.89 M Tris base, 0.89 M boric acid, 0.02 M EDTA.
2. Insert vectors containing Sam50, Sam37, or Sam35; here genes optimized for *S. cerevisiae* expression were ordered from Genewiz.
3. Template pBEVY vectors were provided from the Kunji lab (*see* Acknowledgments).
4. Kits for plasmid miniprep and for gel extraction as well as for cloning (e.g., In-fusion® HD Eco-dry mix).
5. UV-Vis spectrometer for measuring DNA concentration.
6. High-fidelity DNA polymerase (i.e., Q5 high-fidelity DNA polymerase (NEB)).
7. Quenching buffer: 10 mM Tris–HCl, pH 8.5, 10 mM EDTA, pH 8.0.
8. Primer sets (forward and reverse) designed from In-Fusion Cloning Primer Design Tool (Takara Bio, USA).
9. Water bath set at 42 °C.
10. Plate incubator set at 37 °C.
11. LB agar plates containing carbenicillin (100 μg/mL) (LB/carb).
12. LB media.
13. PCR Tubes.
14. Inoculation loops and cell spreaders.
15. 1.5 mL microcentrifuge tubes.
16. PCR tubes.
17. PCR thermocycler.
18. Laboratory incubator shaker set at 220 rpm at 37 °C.

2.2 Yeast Transformation

1. *S. cerevisiae* strain W303.1B.
2. 20% (w/v) D-(+)-glucose. Filter sterilize with 0.22 μm filter.
3. Plastic petri dishes (100 mm × 15 mm).
4. YP agar with 2% glucose: 10 g/L yeast extract, 20 g/L peptone, 20 g/L bacto agar, 2% glucose. For 200 mL batch add 2 g yeast extract, 4 g peptone, and 2 g bacto agar to 180 mL water in a 500 mL Erlenmeyer flask. Autoclave. After cooling at 20 mL of 20% glucose, swirling to gently mix, then pour plate (*see* **Note 1**).
5. YPD media: 10 g/L yeast extract, 10 g/L peptone, 2% glucose. For a 200 mL batch, add 2 g yeast extract, 4 g peptone to 180 mL water in a 500 mL bottle. Autoclave. Add 20 mL glucose once completely cool (*see* **Note 2**).
6. 10× TE buffer pH 8.0: 100 mM Tris–HCl, pH 8.0, 10 mM EDTA, pH 8.0. Autoclave.
7. 1 M LiAc. Autoclave.
8. 50% PEG 3350. Filter sterilized with 0.22 μM filter.
9. TE/LiAc solution: 1× TE buffer pH 8.0, 100 mM LiAc. Add 500 μL 10× TE buffer pH 8.0, 500 μL 1 M LiAc to 4 mL water in a 15 mL falcon tube. Make fresh for each transformation, keep on ice.
10. Salmon sperm carrier DNA: 2 mg/mL. Boil at 100 °C for 10 min before use. Place on ice to slightly cool before adding to cells and vectors.
11. PEG/TE/LiAc: 40% PEG 3350, 1× TE buffer pH 8.0, 100 mM LiAc. Add 500 μL 10× TE buffer pH 8.0, 500 μL 1 M LiAc to 4 mL of 50% PEG 3350 in a 15 mL falcon tube (*see* **Note 3**). Make fresh for each transformation, keep on ice.
12. Plastic petri dishes (100 mm × 15 mm).
13. Selection agar with 2% glucose: 6.9 g/L yeast nitrogen base without amino acids, complete supplement mixture dropout (*see* **Note 4**), 20 g/L bacto agar. For a 500 mL batch add 10 g bacto agar, 3.45 g yeast nitrogen base without amino acids, complete supplement mixture dropout (*see* **Note 4**) to 450 mL water in a 500 mL bottle. Autoclave.
    (a) Once agar has cooled, microwave and slightly cool before adding 20% D-(+)-glucose to 2% final concentration (if making all 500 mL for plates add 50 mL 20% glucose). Gently swirl to mix, then pour plate (*see* **Note 1**).
14. Incubator for cell growth.
15. Spectrophotometer at 600 nm to measure OD. Used with plastic cuvettes.
16. Water bath.

17. Centrifuge.
18. 50 mL sterile conical tubes.
19. 15 mL sterile conical tubes.
20. 1.5 mL sterile microcentrifuge tubes.
21. 250 mL sterile Erlenmeyer flask.
22. Sterile loop.

2.3 Growth

1. Selection agar with 2% glucose: 6.9 g/L yeast nitrogen base without amino acids, complete supplement mixture dropout (*see* **Note 4**), 20 g/L bacto agar, 2% glucose. For a 500 mL batch add 3.45 g yeast nitrogen base without amino acids, complete supplement mixture dropout, and 10 g bacto agar to 450 mL water in a 500 mL bottle. Autoclave.
   (a) Once agar cools microwave and slightly cool before adding 20% D-(+)-glucose to 2% final concentration (if making all 500 mL for plates add 50 mL 20% D-(+)- glucose). Gently swirl to mix, then pour plate (*see* **Note 1**).
2. 20% (w/v) D-(+)-glucose. Filter sterilize with 0.22 μm filter.
3. Selection media: 6.9 g/L Yeast Nitrogen Base without amino acids, complete supplement mixture dropout (*see* **Note 4**), 2% glucose. For a 500 mL batch, add 3.45 g yeast nitrogen base without amino acids, and complete supplement mixture dropout to 450 mL water in a 500 mL bottle. Autoclave. Once cool, add 50 mL 20% D-(+)-glucose (*see* **Note 2**).
4. YPG media: 10 g/L yeast extract, 20 g/L peptone, 30 mL glycerol, 0.1% glucose. For a 1 L batch add 10 g yeast extract, 20 g peptone, and 30 mL glycerol to 965 mL water in a 2 L Erlenmeyer flask. Autoclave. Once cool, and right before use add 5 mL 20% D-(+)-glucose.
5. 20% (w/v) D-galactose. Filter sterilize with 0.22 μm filter (*see* **Note 5**).
6. Cold, sterile ultrapure water.
7. Incubator for cell growth.
8. Spectrophotometer at 600 nm to measure OD. Used with plastic cuvettes.
9. Centrifuge.
10. 50 mL sterile conical tubes.
11. 250 mL sterile Erlenmeyer flask.
12. Sterile loop.

2.4 Small-Scale Mitochondrial Preparation

1. Breaking Buffer: 650 mM sorbitol, 100 mM Tris–HCl, pH 8.0, 5 mM EDTA, pH 8.0, 5 mM amino hexanoic acid, 5 mM benzamidine, 0.2% BSA. Add 200 mL water to a 500 mL beaker along with 50 mL of 1 M Tris–HCl, pH 8.0, and 5 mL of 500 mM EDTA pH 8.0. Weigh 59.20 g sorbitol, 0.33 g amino hexanoic acid, and 0.3 g benzamidine and mix. Make up to 500 mL with water and mix 1.00 g of BSA (*see* **Note 6**). Store at 4 °C.
2. Wash Buffer: 650 mM sorbitol, 100 mM Tris–HCl, pH 7.5, 5 mM amino hexanoic acid, 5 mM benzamidine. Add 100 mL water to a 250 mL beaker along with 25 mL of 1 M Tris–HCl pH 7.5. Weigh 29.60 g sorbitol, 0.16 g amino hexanoic acid, and 0.15 g benzamidine. Mix and bring up to 250 mL with water. Store at 4 °C.
3. 200 mM PMSF. Weigh out 0.87 g and mix in 50 mL 100% ethanol. Store at 4 °C.
4. Tris-buffered glycerol (TBG) storage buffer: 100 mM Tris–HCl, pH 8.0, 10% glycerol. Add 400 mL water to a 500 mL graduated cylinder along with 50 mL of 1 M Tris–HCl, pH 8.0, stock, and 50 mL glycerol. Mix and sterile filter, store at 4 °C.
5. Sterile filter, 0.22 μm.
6. 50 mL conical tubes.
7. Glass beads, 0.5–0.75 μm.
8. Vortex mixer.
9. Centrifuge.
10. 40 mL centrifuge tubes.
11. 1 mL glass homogenizer.
12. BCA assay.

2.5 Western Blot for Expression

1. Polyacrylamide gel electrophoresis (PAGE) system.
2. Precast SDS-PAGE gel (i.e., 4–12% Bis-Tris gels).
3. LDS sample buffer (4×): 424 mM Tris–HCl, 564 mM Tris Base, 8% LDS, 40% Glycerol, 2.04 mM EDTA, 0.88 mM SERVA Blue G250, 0.7 mM Phenol Red pH 8.5.
4. MES-SDS Running Buffer (20×): 1 M MES, 1 M Tris base, 2% (w/v) SDS, 20 mM EDTA, pH 7.3.
5. Pre-stained protein marker.
6. Western blot transfer system (i.e., dry blotting system).
7. Western blot box.
8. Phosphate buffered saline pH 7.4 (PBS, 10×): 1.5 M NaCl, 66 mM phosphate pH 7.4.

9. 1× PBS containing 0.1% Tween-20 (PBST): Dilute 100 mL of PBS 10× to 1 L with water and mix 1 mL of Tween-20.
10. Blocking buffer: 3% BSA in PBST, add 6 g of BSA to 200 mL of PBST, mix and store at 4 °C.
11. Antibody (i.e., anti-polyhistidine-peroxidase and anti-strep-tactin-HRP).
12. Chemical substrate (i.e., 3,3′-diaminobenzidine).

3 Methods

All methods are carried out at room temperature unless otherwise stated.

3.1 Cloning of Yeast Expression Vectors

1. Design primers using the In-Fusion Cloning Primer Design Tool (*see* **Note 7**).
2. Calculate melting temperatures using a designated calculation tool for carrying out PCR using high-fidelity DNA polymerase.
3. Add 1 ng of vector to 0.5 μL of 100 μM forward primer and 0.5 μL of 100 μM reverse primer with 1 μL of 10 mM dNTPs, 0.5 μL of high-fidelity polymerase, 10 μL of corresponding reaction buffer, and water to a final volume of 50 μL.
4. Run PCR product on a 1.0% agarose + ethidium bromide gel at 90 V for 45 min in TBE buffer.
5. Gel extract vector and insert using gel extraction kit.
6. Add 90 ng of vector to 3× molar ratio of insert and bring to a final volume of 15 μL with water. Molar ratio was calculated using designated calculator tool.
7. Take the vector-insert mixture and add to In-fusion® HD Eco-dry mix.
8. Place reactions at 42 °C for 30 min in PCR machine.
9. Quench reactions with 40 μL quenching buffer.
10. Add 5 μL of quenched reaction mix to 100 μL of Stellar competent cells (*see* **Note 8**).
11. Place cells and reaction mixture on ice for 30 min.
12. Heat-shock samples at 42 °C for 45 s.
13. Incubate samples on ice for 2 min.
14. Add 450 μL of SOC media to samples and incubate for 37 °C for 1 h.
15. Centrifuge samples at 9,000 × *g* for 10 min.
16. Resuspend samples in 110 μL of fresh SOC and plate 100 μL of cells on LB + antibiotic plates and incubate for 18–24 h for 37 °C.

17. Plate 5 μL of cells on LB + antibiotic plates and incubate for 18–24 h for 37 °C.
18. Select five different colonies and add to 5 mL LB + antibiotic and shake at 225 rpm at 37 °C for 18 h.
19. Miniprep samples and send for sequencing.

3.2 Yeast Transformation

Keep cultures sterile. Complete all steps near flame and use sterilized pipette tips, conical tubes, and flasks.

1. Prepare competent *S. cerevisiae* cells.
   (a) Streak yeast strain W303.1B from glycerol stock (*see* **Note 9**) onto YPD plate using a sterile loop. Incubate at 30 °C for 48–72 h (*see* **Note 10**).
   (b) Select a single colony and inoculate 8 mL YPD media in a sterile 50 mL conical tube. Incubate culture for 16–18 h at 30 °C and 220 rpm.
   (c) Place 25 mL YPD media in a 250 mL flask (*see* **Note 11**). Inoculate flask with 1.2 mL of the overnight culture. Incubate at 30 °C and 220 rpm until an OD_{600nm} of 1 is reached (*see* **Note 12**).
   (d) Transfer cells into sterile 50 mL conical tube. Centrifuge at 1500 × *g* for 10 min at 4 °C. Discard the supernatant.
   (e) Resuspend cells in 25 mL cold, sterile ultrapure water by pipetting.
   (f) Centrifuge at 1500 × *g* for 10 min at 4 °C. Discard the supernatant.
   (g) Resuspend cells in 500 μL TE/LiAc solution by pipetting. Keep cells on ice.
2. *S. cerevisiae* transformation (keep cells sterile and on ice).
   (a) In a sterile 1.5 mL microcentrifuge tube, add 20 μL salmon sperm carrier DNA, 3 μL each vector (*see* **Note 13**), 100 μL competent yeast cells. Repeat for each transformation, change vectors if so desired.
   (b) Negative control: 3 μL sterile water.
   (c) Incubate at room temperature for 10 min.
   (d) Add 500 μL PEG/TE/LiAc solution to transformation reaction, pipette to mix.
   (e) Incubate at 30 °C for 30 min (*see* **Note 14**).
   (f) Heat-shock cells in a 42 °C water bath for 20 min.
   (g) Centrifuge at 700 × *g* for 3 min at room temperature.
   (h) Pipet off the supernatant and discard. Resuspend cells in 200 μL sterile ultrapure water by pipetting.
   (i) Plate 50 μL cells (*see* **Note 15**) on selection agar plates and incubate at 30 °C for 72 h.

3.3 Small-Scale Growth

1. Select a single colony using a sterile loop and inoculate 10 mL selection media in a sterile 50 mL conical tube. Incubate culture for 12–16 h (overnight) at 30 °C and 220 rpm.
2. Measure OD_{600nm} of starter culture. Expected OD_{600nm} 3–5. Calculate volume necessary for a 100 mL YPG culture to have a starting OD_{600nm} of 0.15 (*see* **Note 16**).
3. Inoculate 100 mL YPG media in 250 mL Erlenmeyer flask with starter culture (target starting $OD_{600nm} = 0.15$). Incubate 16–18 h at 30 °C at 220 rpm.
4. Measure OD_{600nm} of overnight YPG culture. Expected OD_{600nm} of 3–5. Induce cells with 2 mL 20% galactose (final galactose concentration is 0.4%).
5. Incubate for 4 h at 30 °C at 220 rpm.
6. Measure OD_{600nm} after 4-h induction. Expected OD_{600nm} of 4–7.
7. Centrifuge at 1500 × *g* for 5 min at 4 °C to harvest cells (*see* **Note 17**).
8. Resuspend pellet with cold sterile ultrapure water to a final volume of 40 mL (*see* **Note 18**).
9. Centrifuge at 1500 × *g* for 5 min at 4 °C. Discard supernatant.
10. Store cells in −80 °C freezer (*see* **Note 19**).

3.4 Small-Scale Mitochondrial Preparation

1. Prechill centrifuges to 4 °C.
2. Resuspend yeast cell pellet in a 50 mL falcon tube by adding 20 mL of breaking buffer and rocking at 4 °C for 10 min.
3. Add 1 mL of 200 mM PMSF to resuspended cell pellet.
4. Bring the resuspended cell pellet up to 25 mL with glass beads, adding approximately 2.5 mL of glass beads to the falcon tube.
5. Vortex resuspended pellet with glass beads for 1 min and place on ice for 30 s repeating five times, for a total time of 7 min.
6. Incubate the cells on ice for 1 min after vortexing is completed.
7. Remove cell debris and pellet glass beads by centrifuging at 2700 × *g* for 10 min at 4 °C.
8. Transfer supernatant to 40 mL centrifuge tubes and bring volume up to the top of the tube, adding about 15 mL of breaking buffer.
9. Pellet mitochondrial membrane sample by centrifuging at 68,000 × *g* for 30 min at 4 °C.
10. Remove supernatant and resuspend the mitochondrial membrane pellet with 35 mL of wash buffer by pipetting up and down.
11. Centrifuge the sample again at 68,000 × *g* for 30 min at 4 °C.
12. Resuspend the pellet in 1 mL of TBG storage buffer using a homogenizer.

13. Add the mitochondrial sample to a 1 mL Eppendorf tube, remove 10 µL of sample for BCA assay.
14. Determine total mitochondrial protein concentration using a BCA assay (*see* **Note 20**).

3.5 Western Blot for Expression

1. Dilute 15 µg of mitochondrial protein sample to 12 µL with TBG storage buffer and add 3 µL of LDS sample buffer (4×).
2. Set up gel electrophoresis system with a 12-well precast SDS-PAGE and 1× MES buffer.
3. Load 5 µL of protein ladder and 12 µL of mitochondrial gel sample onto the gel and run at a constant 180 V for 35 min until the loading dye reaches the bottom of the gel.
4. Set up a semi-dry western transfer following manufacturer's instruction (*see* **Note 21**).
5. After transfer is complete, add the membrane to 25 mL of blocking buffer and rock for 30 min at room temperature.
6. Add antibody to the blocking buffer and rock for 45 min at room temperature, we used anti-polyhistidine-HRP (1:5000) and anti-strep-tactin-HRP (1:4000).
7. Wash the membrane with 15 mL of PBST rocking for 5 min, repeating twice. Wash the membrane one last time with 15 mL of PBS rocking for 5 min at room temperature.
8. Add chemical substrate to visualize membrane following manufacturer's instructions (Fig. 1) (*see* **Note 22**).

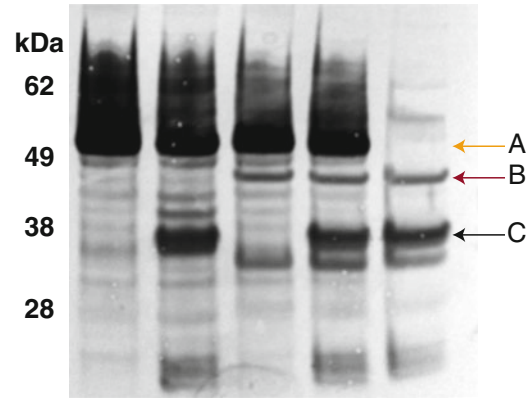

Fig. 1 Western blot showing expression levels of the SAM complex protein combinations from the mitochondrial protein sample. Lane 1 shows expression levels of Sam50 alone (marked by yellow arrow, **a**), Lane 2 shows expression levels of Sam50 and Sam35 (marked by red arrow, **b**), Lane 3 shows expression levels of Sam50 and Sam37 (marked by black arrow, **c**), Lane 4 shows expression levels of all three proteins, Sam50, Sam37, Sam35, and Lane 5 shows expression levels of Sam37 and Sam35

4 Notes

1. We use 25 mL YP agar with 2% glucose per plate.
2. We usually keep larger stocks of media without glucose and add glucose immediately before use to the amount of media we are going to use.
3. PEG 4000 can be used instead of PEG 3350.
4. Each complete supplement mixture dropout will have different amounts required per liter. Check manufacturer's instructions for the required amount.
5. Using warm ultrapure water will help dissolve galactose.
6. Dissolve BSA after the rest of the reagents have been dissolved to reduce foaming from the BSA.
7. We recommend checking the primer T_m provided by the In-fusion® design software using a different calculator, we use NEB T_m calculator, to ensure there is not a large difference between the T_m values for primer pairs. The length of the primers may need to be adjusted.
8. Transformation can be carried out with 2.5 μL of PCR product and 50 μL of Stellar ™ competent cells without any further modifications to the protocol.
9. Keep glycerol stock on dry ice.
10. Usually 48 h is sufficient for colony growth. We have completed successful transformations with plates up to 1 week old.
11. One 25 mL culture will give five transformation reactions. We recommend making two 25 mL cultures in case extra cells are needed.
12. Usually an OD_{600nm} of 1 is reached in 4.5 h.
13. For three vector transformation, use 2.5 μL of each vector.
14. Put in 30 °C incubator with no shaking.
15. Plate 100 μL cells for three vector transformations.
16. Glycerol stocks of samples can be made for later use from the selection media overnight culture. To make glycerol stock of transformant, mix 0.30 mL, 50% sterile glycerol, and 0.70 mL selection media overnight culture. Freeze in dry ice for 10 min, store in −80 °C freezer.
17. We usually do this by pouring half of the culture into a sterile 50 mL falcon tube, centrifuging, decant the supernatant, and repeating the process to spin down the whole culture.
18. For the first transformation, we recommend saving a small sample (50 μL) for a whole-cell Western blot to compare protein yield to isolated mitochondrial sample. For gel sample,

add 20 μL cells, 20 μL water, and 14 μL 4× loading dye. Boil 10 min at 99 °C before loading 10 μL of each sample.

19. Cells can be kept in −20 °C freezer if the mitochondrial preparation will be done the next day.
20. We run a standard curve with each assay and run a 1/10 dilution of the mitochondrial sample to ensure the protein concentration is within the linear range of the BCA assay.
21. We use the iBlot2 semi-dry system that allows transfer to PVDF membrane in 7 min reducing the time before results.
22. For some of our proteins, there is unequal expression when we co-express the proteins on the same vector (using both the Gal10 and Gal1 promoters). For this reason, we have expressed the three proteins of the Sam complex on three different vectors, all using the Gal1 promoter. We recommend you to check both variations when co-expressing new proteins.

Acknowledgments

The authors would like to thank Dr. Edmund Kunji (Cambridge, UK) for the yeast expression strain and the pBEVY vectors. This work was supported by the Intramural Research Program of the NIH, the National Institute of Diabetes & Digestive & Kidney Diseases.

References

1. Routledge SJ, Mikaliunaite L, Patel A, Clare M, Cartwright SP, Bawa Z, Wilks MD, Low F, Hardy D, Rothnie AJ, Bill RM (2016) The synthesis of recombinant membrane proteins in yeast for structural studies. Methods 95:26–37. https://doi.org/10.1016/j.ymeth.2015.09.027
2. Daum G, PC B, Schatz G (1982) Import of proteins into mitochondria. Cytochrome b2 and cytochrome c peroxidase are located in the intermemembrane space of yeast mitochondria. J Biol Chem 257(21):13028–13033
3. Glick BS, Pon LA (1995) Isolation of highly purified mitochondria from *Saccharomyces cerevisiae*. Methods Enzymol 260(1):213–223
4. Meisinger C, Sommer T, Pfanner N (2000) Purification of Saccharomcyes cerevisiae mitochondria devoid of microsomal and cytosolic contaminations. Anal Biochem 287 (2):339–342. https://doi.org/10.1006/abio.2000.4868
5. Miller CA, Martinat MA, Hyman LE (1998) Assessment of aryl hydrocarbon receptor complex interactions using pBEVY plasmids expression vectors with bi-directional promoters for use in *Saccharomyces cerevisiae*. Nucleic Acids Res 26(15):3577–3583. https://doi.org/10.1093/nar/26.15.3577
6. Gietz RD, Schiestl RH (2007a) Frozen competent yeast cells that can be transformed with high efficiency using the LiAc/SS carrier DNA/PEG method. Nat Protoc 2(1):1–4. https://doi.org/10.1038/nprot.2007.17
7. Gietz RD, Schiestl RH (2007b) High-efficiency yeast transformation using the LiAc/SS carrier DNA/PEG method. Nat Protoc 2(1):31–34. https://doi.org/10.1038/nprot.2007.13
8. Gietz RD, Schiestl RH (2007c) Quick and easy yeast transformation using the LiAc/SS carrier DNA/PEG method. Nat Protoc 2(1):35–37. https://doi.org/10.1038/nprot.2007.14
9. Deters D, Müller U, Homberger H (1976) Breakage of yeast cells Large scale isolation of yeast mitochondria with a continuous-flow disintegration. Anal Biochem 70(1):262–267

Chapter 2

Membrane Protein Production in *Escherichia coli*

Benjamin C. McIlwain and Ali A. Kermani

Abstract

Escherichia coli is the workhorse of the structural biology lab. In addition to routine cloning and molecular biology, *E. coli* can be used as a factory for the production of recombinant membrane proteins. Purification of homogeneous samples of membrane protein expressed in *E. coli* is a significant bottleneck for researchers, and the protocol we present here for the overexpression and purification of membrane proteins in *E. coli* will provide a solid basis to develop lab- and protein-specific protocols for your membrane protein of interest. We additionally provide extensive notes on the purification process, as well as the theory surrounding principles of purification.

Key words Membrane protein, *E. coli*, Crystallography, Ion channel, Transporter.

1 Introduction

Membrane protein production has historically been difficult—membranes make up only a small fraction of the total cell volume, and purification of stable membrane proteins requires solubility in a membrane mimetic, often detergents. The revolution in membrane protein structural biology has been propelled forward by the development of methods and techniques to use bacterial cells to produce membrane proteins. *E. coli* is especially useful due in-part to its simple, well-understood genetics, and high levels of recombinant protein expression [1]. The genomes of *E. coli* are easy to manipulate genetically, and users expend minimal culturing costs as *E. coli* utilize inexpensive carbon sources and have a short (~20 min) doubling time. Not without drawbacks, *E. coli* expression is not suitable for proteins that require posttranslational modifications and complex membrane components. Proteins can form in inclusion bodies. *E. coli* is not typically suitable for the expression of eukaryotic membrane proteins. However, robust yields of

Authors "Benjamin C. McIlwain and Ali A. Kermani" contributed equally to this work

Camilo Perez and Timm Maier (eds.), *Expression, Purification, and Structural Biology of Membrane Proteins*, Methods in Molecular Biology, vol. 2127, https://doi.org/10.1007/978-1-0716-0373-4_2,

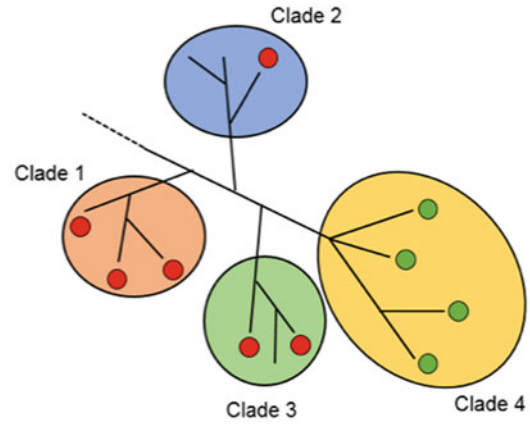

Fig. 1 Construction of a phylogenetic tree can help identify clades of related proteins. Our experience shows that closely-related proteins will often exhibit similar expression

prokaryotic membrane proteins, in the range of 1–10 mg/L culture, can be obtained from *E. coli* cultures. Here, we present a general protocol for the overexpression and purification of membrane proteins in *E. coli*, which has been used to purify and characterize numerous bacterial membrane proteins, including diverse targets from our laboratory [2–5].

1.1 Homolog Screening and Biochemical Tractability

Proper insertion of recombinant membrane proteins into the *E. coli* membrane is difficult to predict, and misinsertion often leads to misfolding and degradation. Online tools are available that simulate membrane integration and estimate the likelihood that a particular sequence will express in *E. coli* [6]. In addition, it is often useful to screen several (between 4 and 10) homologs to find a biochemically tractable protein with high yield. We have found that construction of a phylogenetic tree (Fig. 1) is a useful way to identify clades of related proteins. In our experience, if a clade contains one high-yielding homolog (green circles), other members of this clade are often worth investigating to identify additional biochemically tractable homologs.

2 Materials

2.1 Transformation

1. SOC media, 2% tryptone, 0.5% yeast extract, 10 mM NaCl, 2.5 mM KCl, 10 mM $MgCl_2$, 10 mM $MgSO_4$, and 20 mM glucose.
2. LB media, 1% tryptone, 0.5% yeast extract, 1% NaCl, pH 7.0–7.5. Sterilize by autoclaving 20 min at 15 psi, 121 °C.
3. Bead or water bath at 42 °C.
4. Disposable cell spreaders.

2.2 Protein Expression

1. TB media, dissolve 24 g of yeast extract, 20 g tryptone, and 4 mL of glycerol in 900 mL of deionized water. Sterilize by autoclaving for 20 min at 15 psi, 121 °C. Add 100 mL of filter-sterilized phosphate buffer (0.17 M KH_2PO_4, 0.72 M K_2HPO_4) to a final volume of 1 liter.
2. Isopropyl ß-D-1-thiogalactopyranoside (IPTG) stock, 1 M in deionized water. Filter sterilize prior to use.

2.3 Protein Purification

1. Lysis buffer, 20 mM Tris–HCl pH 6.5, 4 M urea, 2% sodium dodecyl sulfate (SDS).
2. Breaking buffer, 50 mM Tris–HCl pH 7.5, 100 mM NaCl.
3. Phenylmethylsulfonyl fluoride (PMSF) stock, 200 mM stock in isopropanol.
4. Protease inhibitor cocktail, prepare a 100× stock by dissolving 100 mg leupeptin and 25 mg pepstatin in 70% methanol. Stir for 30 min at 4 °C, then aliquot and store at −80 °C.
5. n-Decyl-ß-D-maltopyranoside (DM) detergent.
6. Wash buffer, 20 mM Tris–HCl pH 7.5, 100 mM NaCl, 5 mM DM.
7. FPLC buffer, 10 mM HEPES-HCl pH 7.5, 200 mM NaCl, 5 mM DM.
8. BioRad *Econo*-column chromatography columns.
9. Immobilized metal affinity chromatography (IMAC) resin of choice.
10. Amicon centrifugal filter units.
11. Size exclusion column (e.g., Superdex Increase 10/30).
12. Probe ultrasonicator.
13. Dialysis cassettes.

3 Methods

3.1 Heat-Shock Transformation (See Note 1)

1. Thaw one aliquot (~50–100 µL) of *E. coli* C41 (DE3) competent cells on ice for 5 min (*see* Table 1). Add 1–10 ng of plasmid DNA to cells (*see* **Note 2**). Mix the cells by gentle shaking or tapping. Do not vortex the competent cells. Incubate on ice for 20–30 min.
2. Heat shock the cells by incubating them at 42 °C for 30–60 s. Transfer the cells to ice for an additional 3–5 min (*see* **Note 3**).
3. Recover the transformed cells by culturing them in 500 µL of SOC media at 37 °C at 220 rpm for 1 h.
4. Plate the recovered cells on LB agar plates supplemented with appropriate antibiotic (*see* **Notes 4** and **5**). To ensure even distribution of cells on the plate, use a disposable cell spreader. Incubate the plates overnight at 37 °C.

3.2 Small-Scale Expression Screening of Recombinant Protein

Membrane proteins can be extremely sensitive to expression conditions. Therefore, when working with a new target, our first step is always to screen different growth and induction conditions using Western blot in order to identify the expression conditions that maximize protein expression.

1. Transform the plasmid DNA carrying the encoding gene into competent cells (*see* Table 1). For transformation refer to Subheading 3.1.
2. Incubate the transformed plates overnight at 37 °C.
3. Dislodge the transformed cells from each LB agar plate with 10 mL of LB media and using a disposable cell spreader.
4. Dilute the dislodged cells from each plate into a separate 50 mL falcon tube containing 10 mL of LB media supplemented with appropriate antibiotic to an OD_{600} of ~0.1 (prepare nine cultures for each transformant) (*see* Fig. 2).
5. Grow the cells at 37 °C, 220 rpm to the OD_{600} of 0.8–1.0.
6. Induce cultures with varying IPTG concentrations, and for various induction times (*see* Fig. 2).

Table 1
Commonly used *E. coli* strains for overexpression of membrane proteins

Competent cell line	Features
BL21(DE3) *see ref* [10]	This strain does not express the T7 RNA polymerase. These cells are deficient in *Lon* and *OmpT* proteases that minimize protein degradation. Most common competent cell lines are derived from BL21. DE3 indicates that the host is a strain of λDE3 and carries a chromosomal copy of the T7 RNA polymerase gene. Such strains are suitable for the production of proteins from target genes cloned in pET vectors by induction with IPTG.
C41(DE3) C43(DE3) *see ref* [12]	Contain an uncharacterized mutation that increases overexpression of membrane proteins—prevents cell death associated with the production of toxic proteins.
Rosetta	BL21 derivatives designed to enhance the expression of proteins that contain codons rarely used in *E. coli*. Achieved through use of the pRARE plasmid encoding rare tRNA codons.
BL21(DE3) pLysS *see refs* [10, 11]	pLysS plasmid that encodes T7 lysozyme, an inhibitor of T7 polymerase that lower background expression of target gene.
NiCo21(DE3)	Major endogenous *E. coli* proteins that bind to metal affinity resin are deleted or tagged. Minimizes *E. coli* protein contamination of IMAC purification.
Lemo21(DE3) *see refs* [13, 14]	Allow tunable expression of difficult clones, through varying levels of lysozyme. Lysozyme production is modulated by L-rhamnose (0–2 mM). Fine-tuning of T7 expression can alleviate inclusion body formation.

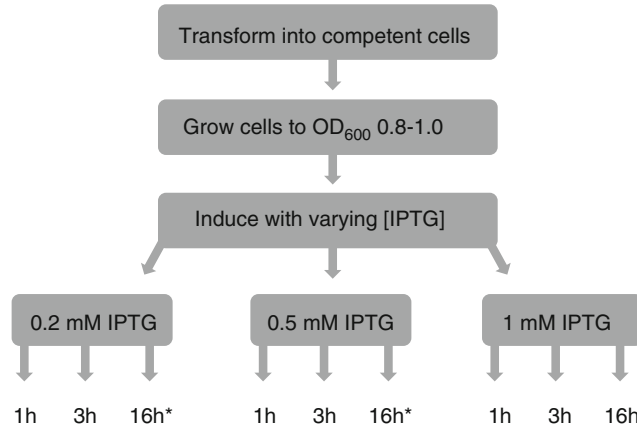

Fig. 2 Strategy of induction screening for membrane protein expression in *E. coli*. DNA construct is transformed into competent cell line of choice (*see* **Note 3**), and grown to a high OD_{600}. Mini-cultures are then induced with varying concentrations of IPTG, and induction stopped after 1, 3, or 16 h (overnight) by harvesting via centrifugation. Cell pellets are lysed and samples run on SDS-PAGE gel. Typically, membrane protein expression is too low to visualize from cell extract using a Coomassie stained gel. Therefore, we recommend transferring to a nitrocellulose membrane and Western blot used to quantify target protein expression. $*$ denotes temperature to be reduced for overnight induction, usually 16 °C

7. Transfer 1 mL of each culture to a separate microcentrifuge tube and pellet cells using a benchtop centrifuge at maximum speed for 3–5 min at 4 °C.
8. Lyse the cells by adding 200 μL of Lysis Buffer to each microcentrifuge tube. Make sure the cells are completely lysed by pipetting up and down and vortexing for a few minutes.
9. Centrifuge the lysate using a benchtop centrifuge at maximum speed for 3–5 min. Decant supernatant to a fresh 1.5 mL microcentrifuge tube and discard the pellet.
10. Mix the supernatant with 50 μL of loading buffer (4×). Spin down the samples for 10 min to remove aggregates and remaining unbroken cells.
11. Run a SDS-PAGE gel by loading 10 μL of each sample.
12. Run a Western blot using anti-His antibody as the primary antibody to check expression of recombinant protein grown under different conditions.

3.3 Overexpression of Recombinant Protein

After screening to identify the best conditions for overexpression, we scale up to 1-liter growths to test expression and purification conditions.

1. Dislodge the transformed cells from LB agar plate by adding 10 mL of freshly prepared TB media (*see* **Note 4**) and a disposable cell spreader. Use these cells to inoculate 1 liter of TB media supplemented with appropriate antibiotic (*see* **Note 5**).
2. Grow the cells at 37 °C, 220 rpm to the OD_{600} of 0.8–1.0. Measure the OD using a spectrophotometer (*see* **Note 6**).
3. Induce the cells using freshly prepared 1 mM IPTG (*see* **Note 7**) and grow for an additional 1–3 h at 37 °C, shaking at 220 rpm.
4. Harvest the cells by centrifugation for 16 min at 5000 × *g*, 16 °C. Discard supernatant and refrigerate the pellet for immediate purification or store at −80 °C for several weeks.

3.4 Cell Lysis and Detergent Extraction (See Notes 8–11)

1. Resuspend the bacterial cell pellet in 40 mL of breaking buffer supplemented with 1× protease inhibitor cocktail, 10 μg/mL DNase, 0.2 mg/mL lysozyme, 2 mM $MgCl_2$, and 1 mM PMSF. Incubate on ice for 30 min to allow genomic DNA digestion and cell wall lysis.
2. Lyse cells using a probe ultrasonicator (*see* **Note 8**) using six on/off cycles of 30 s each. To prevent excessive heating, it is essential to keep the beaker containing the sample on ice.
3. Add 2% w/v n-Decyl-ß-D-maltopyranoside (DM) (*see* **Note 11**) and 1 mM PMSF to the cell lysate. Incubate on a rotary mixer at room temperature for 2 h. Often, several detergents may need to be screened to determine the one that produces the best results for your protein. Complementary methods such as FSEC (*see* **Note 12**) can be used to screen detergents in which the target protein is stable.
4. Centrifuge the cell lysate at 24,000 × *g* for 45 min at 16 °C. Remove supernatant from the pellet by decanting. Discard the pellet.
5. Adjust the pH of cell lysate to approximately 7.5 using Tris–HCl pH 8.0, prior to loading to the affinity column.

3.4.1 Membrane Preparation (Alternative to Whole Cell Lysate Detergent Extraction)

1. Lyse cells as in Subsection 3.4.1, and pellet cell debris with high-speed centrifugation (7–11,000 × *g* for 45 min).
2. Pour supernatant into prechilled ultracentrifuge tubes and centrifuge at 100,000 × *g* for 45 min (tubes must be at least 70% full to prevent collapse under high vacuum of ultracentrifuge).
3. Following centrifugation, pour out remaining supernatant and collect waxy membrane pellet. Weigh membrane pellet.
4. Add 2% (w/w) DM to the waxy membrane pellet, along with a small volume of chilled breaking buffer (between 10 and 20 mL) and agitate using a small magnetic stirrer for 1 h at 4 °C.

5. Following solubilization, transfer solubilized material to a pre-chilled ultracentrifuge tube. Top up tube with breaking buffer, and centrifuge at 100,000 × *g* for 45 min.
6. Adjust the pH of supernatant to approximately 7.5 using Tris–HCl, pH 8.0, prior to loading to the affinity column.

3.5 Affinity Purification of Histidine-Tagged Membrane Protein (See Note 13)

1. Pack an *Econo*-column with 2 mL of cobalt resin slurry (50% ethanol) per liter of culture. Wash the column with 5 column volumes (CV) of deionized water to remove ethanol and equilibrate the column with 5 CV of wash buffer.
2. Load the protein onto the column using a peristaltic pump, with a flow rate of 1 mL/min.
3. Wash nonspecific proteins from the column using 5 CV of Wash buffer supplemented with 20 mM imidazole.
4. Elute the recombinant protein using an imidazole gradient from 20 mM to 400 mM or use stepwise increases in imidazole concentration.
5. Confirm the fractions containing the purified target protein by running a SDS-PAGE gel.

3.6 Affinity Tag Cleavage Using Proteases (See Note 14)

1. Combine the fractions containing the purified target protein and concentrate the combined sample using an Amicon centrifugal filter unit to less than 1 mL.
2. Dialyze the purified protein against wash buffer to remove imidazole.
3. Add 1 U of thrombin per mg of protein and incubate overnight at 4 °C. Remove 10 μg of protein before adding thrombin and keep it in a fresh microcentrifuge tube. Check the degree of His-tag removal by running the thrombin-treated sample against the undigested sample on a SDS-PAGE gel (*see* **Note 15**).

3.7 Size Exclusion Chromatography (See Notes 16 and 17)

1. Wash and equilibrate the size exclusion column with 2 CV of water and FPLC buffer, respectively.
2. Remove precipitation from protein sample prior to loading to size exclusion column by spinning the sample in a microcentrifuge tube filter at maximum speed for 1 min at room temperature.
3. Run the sample over the column with a flow rate of 0.5–1 mL/min. The protein elution peak should be symmetrical and monodisperse. If not, different detergents (or different homologs of the protein) should be screened in order to determine

purification conditions that yield a stable, well-folded sample. Collect the fractions containing the target protein and examine purity on a SDS-PAGE gel.

4. Protein is now ready for biochemical analysis, structural studies, or reconstitution into proteoliposomes.

4 Notes

1. An alternative method to heat-shock transformation is to perform electroporation [7]. Electroporation increases the permeability of cells to charged molecules (such as DNA) by applying brief, but intense electrical fields. Prechill microcentrifuge tubes and electroporation cuvette on ice. To prevent arcing during transformation, ensure the salt concentration in DNA sample is low. Add the SOC media to electroporated cells immediately after electroporating. Any delay can result in low transformation efficiency.
2. Expression vectors are used to introduce a specific gene into a target cell, for that cell to then be used for protein expression. Expression vectors contain the gene of interest (protein to be made) as well as regulatory elements such as repressors, promoters, and enhancers [8, 9]. The *pET* expression system is widely used, and under the control of T7 RNA polymerase. The *pBAD* expression allows tightly controlled, titratable expression of protein. pBAD is useful for the expression of toxic proteins. The *Duet* vector (pETDuet) is designed to co-express two target proteins in *E. coli*.
3. In the laboratory, artificially competent cells are exposed to conditions cells would never encounter in nature (high [divalent cation] or heat shock) and incubated with the DNA to be incorporated into the competent cell genome for expression. There are a variety of competent cell strains available for membrane protein production in *E. coli* [10–14].
4. Cultures of *E. coli* require specific formulations of growth media. *TB* (*terrific broth*): Highly enriched media for high-density growth of *E. coli*. Contains tryptone, yeast extract, glycerol, K_2HPO_4. *LB* (Luria-Bertani): Widely used media containing peptone, yeast extract, and NaCl.

   M9 minimal salts: Primarily used for growth requiring labeled proteins, supplemented with vitamins, carbon sources, and amino acids.
5. Plasmids carry *antibiotic resistance genes*, conferring antibacterial resistance. There are several classes of antibiotics, each with distinct mechanisms of action (Table 2). There are reviewed in reference [15]. A brief description follows: *Ampicillin* is an

Table 2
Commonly used antibiotics for working with *E. coli*

Antibiotic	Stock (mg/mL)	Working (μg/mL)
Ampicillin	100	100
Chloramphenicol[b]	25	25
Kanamycin	50	50
Tetracycline[a]	10	10
Gentamycin	10	10
Streptomycin	25	25
Carbenicillin	100	100

Listed antibiotics are soluble in H_2O, except where superscript a indicates solubility in 70% ETOH and superscript b indicates solubility in 100% ETOH. Antibiotics should be filter-sterilized and kept at −20 °C until use

irreversible inhibitor of transpeptidase, as enzyme crucial to bacterial cell wall synthesis. *Kanamycin* interferes with bacterial protein synthesis by binding to the 30S subunit of prokaryotic ribosomes and causing incorrect amino acids to be placed in the growing peptide chain. *Chloramphenicol* is a macrolide class of antibiotic that binds to the 50S ribosomal subunit, preventing peptide bond formation. *Gentamycin* also interferes with bacterial protein synthesis by binding to the 30S ribosome, leading to incorrect amino acid incorporation. The resulting translated protein often mis-folds and aggregates. *Tetracycline* inhibits protein production in bacteria by blocking aminoacyl-tRNA binding to the 30S ribosome, preventing incorporation of new amino acids to the peptide chain. *Streptomycin* binds to the 30S ribosome and prevents peptide synthesis entirely by blocking binding of formyl-methionyl-tRNA, which initiates peptide chain formation. *Carbenicillin* is more resistant to enzymatic breakdown than ampicillin.

6. There are defined phases of bacterial cell growth (lag, log, stationary, and death), and induction of cells during the log phase (where bacteria are dividing rapidly) is best for overproduction of membrane protein expression in *E. coli*. It is not uncommon for OD_{600} to decrease slightly after induction, although substantial decrease may indicate that protein expression is toxic.
7. Induction of gene expression in *E. coli* is essential for the large-scale production of membrane proteins. *IPTG* triggers transcription of the *lac operon*, binding to the lac repressor and permitting the transcription of genes under the control of the *lac operon*. IPTG is not hydrolyzed by β-galactosidase, so remains present during induction of bacteria. IPTG is effective

in the range of 100 μM–3 mM, although it is essential to test varying ITPG concentrations for membrane protein expression (*see* Fig. 2). *Arabinose* triggers transcription of proteins under the control of the *pBad* promoter. Expression of *pBad* with arabinose allows for highly regulated protein expression. *pBAD* is inhibited by low concentrations of glucose, however, and it is not appropriate for protein expression in minimal media containing glucose as a carbon source.

8. Cell disruption can be performed using a probe sonicator or a French press homogenizer. *Ultrasonication* uses high frequency sound waves to shear cells. This causes heating of the sample (so the sample must be kept on ice), and sound waves can often shatter glass beakers, so investment in metal beakers is advised. A *French press homogenizer* uses high pressure to pass cells through a narrow aperture, disrupting the cells. Often 2–3 passes through a French press homogenizer. Disrupted cell lysate will often contain contaminants such as soluble proteins, unbroken cells, and cell debris. These contaminants should be removed via centrifugation before continuing. Efficient cell lysis is essential for ensuring high yield of protein. Use a manual Teflon or glass homogenizer prior to cell lysis. Add the resuspended cell pellet (*from 3-4-1*) into the glass tube and gently stroke the pestle up and down several times until no visible clumps remain.
9. Addition of *protease inhibitors* to cell lysate during protein purification is critical to prevent degradation of the target protein throughout the purification steps. *Leupeptin* is a cysteine, threonine, and serine protease inhibitor. It inhibits trypsin, plasmin, and papain. *Pepstatin* is an inhibitor of aspartyl proteases, including pepsin and cathepsins D and E. *PMSF* is a serine protease inhibitor and inhibits chymotrypsin, thrombin, and trypsin. *AEBSF* is a serine protease inhibitor that inhibits chymotrypsin, kalikrein, plasmin, thrombin, and trypsin. AEBSF has similar specificity to PMSF, but it is more stable at low pH.
10. DNase is widely used during protein purification to degrade genomic DNA to prevent increasing sample viscosity. Alternatively, benzonase can degrade both DNA and RNA, with a working concentration of 5 U/mL. 1–2 mM Mg^{2+} is required for benzonase activity; therefore including more than 1 mM EDTA can inhibit benzonase activity.
11. Detergents play an indispensable role in the extraction and purification of membrane proteins from bacterial cell extracts [16–19] (Table 3). Detergent molecules are made up of a hydrophilic "head group" and a hydrophobic "tail." Hydrophilic head group allows detergent molecules to partition into

Table 3
Commonly used detergents in membrane protein purification

	CMC (mM)	CMC (% w/v)	Extract	Purify
Nonionic detergents				
DM	1.8	0.087	21 mM	2.4–5 mM
n-Dodecyl β-D-maltoside (DDM)	0.17	0.0087	20 mM	0.26–0.24 mM
Nonyl-glucoside (NM)	6.5	0.2	25–35 mM	
Octyl-glucoside (OG)	23–25	0.67–0.73	51 mM	27–40 mM
Triton X-100	0.22–0.24	0.001–0.016	0.1–0.5%	
Digitonin	<0.5	0.02		
Ionic detergents				
SDS	8	0.23		
Zwitterionic detergents				
CHAPS	8	0.5		
Fos-Choline 12	1.5	0.047		
LDAO	1–2	0.023	51 mM	1.4–4 mM
Bile acid salts				
Sodium cholate	14	0.73		

the lipid bilayer and solubilize membrane proteins, and can be categorized based on the head group charge: *Ionic detergents* (*SDS*, *CTAB*) are effective at extracting proteins from the membrane for analysis by gel or Western blot. These detergents are harsh and denaturing as they disrupt protein–protein interactions. *Bile acid salts* (*Na-cholate*, *deoxycholic acid*) are ionic detergents but are milder than SDS or CTAB. *Nonionic detergents* (*maltosides*, *glucosides*) are mild and non-denaturing. These detergents disrupt protein–lipid and lipid–lipid interactions. *Zwitterionic detergents* (*Fos-Choline*, *CHAPS*) have both positive and negative charges in their head group. They are electrically neutral but may interrupt protein–protein interactions. They are classed as intermediately mild. The *Critical Micelle Concentration (CMC)* is an important factor to consider when solubilizing membrane proteins as it is essential that membrane proteins be encased by detergent micelles. The CMC for a detergent describes the concentration at which detergent monomers self-assemble into protein-surrounding micelles. Caution is suggested for detergent screening to ensure the chosen detergent does not affect the function of the protein, as has fueled controversy about substrate binding in membrane proteins [20, 21].

12. *Fluorescence-detection size exclusion chromatography* (FSEC) [22–25] is a method where the target protein is fused to a green fluorescent protein (GFP) molecule, and unpurified protein sample is analyzed by FSEC. This method only requires small (nanogram) quantities of protein and allows evaluation of protein expression, monodispersity, and approximate molecular mass.
13. *Hexahistidine*-tagged (6× His-tag) proteins can be purified using immobilized metal affinity chromatography (IMAC) (Fig. 3). His-tagged proteins bind metal-ion ligated resin and are eluted using imidazole (*low imidazole wash*: 10–40 mM, *high imidazole protein elution wash*: 400 mM). Ni^{2+} resin is used most commonly, but for membrane proteins with typically low yields, Co^{2+} is more specific and yields a cleaner sample. Protein can be loaded onto resin using either a peristaltic pump over an assembled gravity column of resin or by batch binding. Binding of target protein to resin is most efficient when cell lysate pH is >6.5 (pKa of His is ~6). His-tags

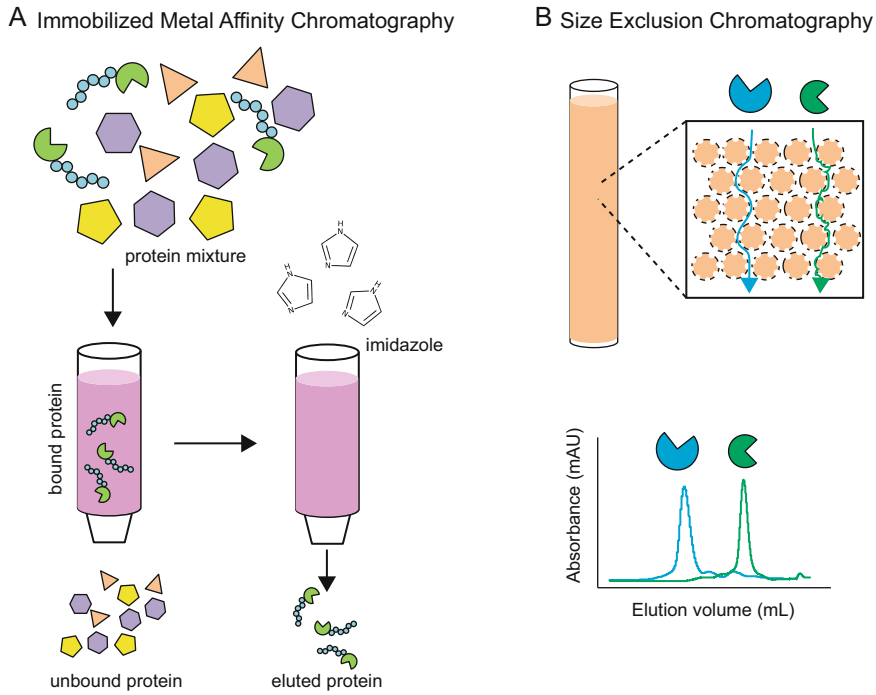

Fig. 3 Chromatographic principles used in the protocol. (**a**) Immobilized metal affinity chromatography (IMAC) resin is loaded with sample containing His-tagged target protein, as well as cellular debris remaining from cell lysis and detergent extraction. Nonspecific binding proteins are eluted with washing, and the target protein is eluted from the column via addition of imidazole (400 mM). Details for this technique are outlined in Subsection 3.5 (**b**) In size exclusion chromatography, purified samples are run over a column of porous beads and transit time through column is directly correlated with size of protein. This technique is outlined in Subsection 3.7

are generally placed at the C-terminal end of the protein to be purified. Proteins with an attached *maltose-binding protein* (MBP) affinity tag are purified using amylose-resin-based chromatography. The elution of MBP-fused proteins is achieved using a maltose-containing buffer. MBP can be attached to both the N- and C-terminal ends of the protein to be purified. The *1D4* epitope tag is derived from the C-terminus of bovine rhodopsin and is eluted from immobilized anti-1D4 resin using 1D4 peptide. Since the carboxy terminus is part of the epitope, the 1D4 tag can only be placed on the C-terminal end. The *FLAG-tag* is a hydrophilic epitope tag. FLAG binds to immobilized anti-FLAG monoclonal antibodies in a Ca^{2+}-dependent manner. Elution of FLAG-tagged protein is either with FLAG peptide, low pH glycine buffer, or with EDTA to chelate Ca^{2+} [25].

14. Affinity tags can be easily removed by introducing a specific protease site between the affinity tag and the target protein (Table 4). Affinity tag removal has been reviewed in [26] and a brief description of common affinity tag removal methods follows. The most commonly used endopeptidases are *enterokinase*, *factor Xa*, *thrombin*, *Lys-C*, and *tobacco etch virus* (TEV). *Enterokinase* is a protease that cleaves after the lysine residue at its recognition site. It can sometimes show nonspecific protease activity at other basic residues. DDDK is part of the FLAG-tag, so enterokinase is an ideal tool for removal of FLAG fusion tags. *Factor Xa* is the endopeptidase formed by activation of Factor X. Factor Xa cleaves after the arginine residue at its recognition site. It is notorious for nonspecific cleavage of peptides, so caution is suggested. Laboratory-grade *Thrombin* is a serine protease purified from bovine plasma. The human thrombin is an essential component of the coagulation cascade where it cleaves fibrinogen to fibrin. Thrombin offers a high degree of specificity. *TEV protease* is a sequence-specific cysteine protease. Drawbacks of TEV protease use include deactivation by self-cleavage. *Lys-C* is a serine endopeptidase that cleaves on the carboxyl side of lysine residues.

Table 4
Commonly used proteases to remove affinity tags

Protease	Recognition sequence	Working
Enterokinase	XDDDDK|XX	1 U per 25 μg
Factor Xa	XIEGR|X	1 U per 50 μg
Tobacco Etch Virus (TEV) protease	XENLYFQ|GX	10 U per 200 μg
Thrombin	XLVPR|GSX	1 U per 100 μg
Lys-C	XXK|XXX	1:20 enzyme-to-protein

15. It is essential to optimize the protease cleavage protocol for each individual protein. In order to find the optimum, set up a series of reactions by varying protease concentration (up to 10 U per mg of protein) and incubation time. Monitor the degree of digestion by running 5 μg of digested protein against undigested protein. A shift in the band size of digested protein indicates affinity tag removal.
16. *Size exclusion chromatography* (SEC) is a chromatographic method where molecules in solution are separated by their size (Fig. 3). The chromatography column is packed with fine, porous beads that are *dextran polymers* (Sephadex), *agarose* (Sepharose), or *polyacrylamide* (Sephacryl). As buffer containing protein is run over the column, smaller proteins will visit porous surface of beads with a delayed transit time through the column, whereas larger protein molecules will not, resulting in the separation of a solution of particles based on size. Important factors to consider are column length (longer = higher resolution), column width (more bead bed volume), and flow rate (0.5–1 mL/min). Sample volume between 0.5 and 2% of total column volume generates the best resolution. A protein concentration in the range of 5–10 mg/mL is sufficient for high-resolution separation.
17. An alternative to SEC is *ion-exchange chromatography*, which includes *anion-exchange* and *cation-exchange*. Column contains resin bearing either positive (binds acidic amino acids) or negative charge (binds basic amino acids) charge, therefore affinity for the column will depend strongly on protein sequence. The protein is eluted from the ion-exchange column with a gradient of salt (KCl or NaCl), or by altering pH of the buffer. Purification of membrane proteins will often utilize anion-exchange chromatography. It is important to avoid using anionic detergents with anion-exchange columns, and cationic detergents with cation-exchange columns.

Acknowledgment

We would like to thank Randy Stockbridge as well as other members of the Stockbridge lab for helpful suggestions, guidance, and feedback on this chapter.

References

1. Wallin E, Heijne GV (1998) Genome-wide analysis of integral membrane proteins from eubacterial, archaean, and eukaryotic organisms. Protein Sci 7(4):1029–1038
2. Stockbridge RB, Lim HH, Otten R, Williams C, Shane T, Weinberg Z, Miller C (2012) Fluoride resistance and transport by riboswitch-controlled CLC antiporters. Proc Natl Acad Sci 109(38):15289–15294
3. Stockbridge RB, Robertson JL, Kolmakova-Partensky L, Miller C (2013) A family of

fluoride-specific ion channels with dual-topology architecture. elife 2:e01084

4. Kermani AA, Macdonald CB, Gundepudi R, Stockbridge RB (2018) Guanidinium export is the primal function of SMR family transporters. Proc Natl Acad Sci 115(12):3060–3065
5. McIlwain BC, Newstead S, Stockbridge RB (2018) Cork-in-bottle occlusion of fluoride ion channels by crystallization chaperones. Structure 26(4):635–639
6. Marshall SS, Niesen MJ, Müller A, Tiemann K, Saladi SM, Galimidi RP, Zhang B, Clemons WM Jr, Miller TF III (2016) A link between integral membrane protein expression and simulated integration efficiency. Cell Rep 16 (8):2169
7. Dower WJ, Miller JF, Ragsdale CW (1988) High efficiency transformation of E. coli by high voltage electroporation. Nucleic Acids Res 16(13):6127–6145
8. Wagner S, Bader ML, Drew D, de Gier JW (2006) Rationalizing membrane protein overexpression. Trends Biotechnol 24(8):364–371
9. Hartley JL (2006) Cloning technologies for protein expression and purification. Curr Opin Biotechnol 17(4):359–366
10. Studier FW, Moffatt BA (1986) Use of bacteriophage T7 RNA polymerase to direct selective high-level expression of cloned genes. J Mol Biol 189(1):113–130
11. Zhang X, Studier FW (1997) Mechanism of inhibition of bacteriophage T7 RNA polymerase by T7 lysozyme. J Mol Biol 269(1):10–27
12. Miroux B, Walker JE (1996) Over-production of proteins in Escherichia coli: mutant hosts that allow synthesis of some membrane proteins and globular proteins at high levels. J Mol Biol 260(3):289–298
13. Wagner S, Klepsch MM, Schlegel S, Appel A, Draheim R, Tarry M, Högbom M, Van Wijk KJ, Slotboom DJ, Persson JO, De Gier JW (2008) Tuning Escherichia coli for membrane protein overexpression. Proc Natl Acad Sci 105 (38):14371–14376
14. Schlegel S, Löfblom J, Lee C, Hjelm A, Klepsch M, Strous M, Drew D, Slotboom DJ, de Gier JW (2012) Optimizing membrane protein overexpression in the Escherichia coli strain Lemo21 (DE3). J Mol Biol 423 (4):648–659
15. Kohanski MA, Dwyer DJ, Collins JJ (2010) How antibiotics kill bacteria: from targets to networks. Nat Rev Microbiol 8(6):423
16. Seddon AM, Curnow P, Booth PJ (2004) Membrane proteins, lipids and detergents: not just a soap opera. Biochim Biophy Acta 1666 (1–2):105–117
17. Garavito RM, Ferguson-Miller S (2001) Detergents as tools in membrane biochemistry. J Biol Chem 276(35):32403–32406
18. Anandan A, Vrielink A (2016) Detergents in membrane protein purification and crystallisation. In: The Next Generation in Membrane Protein Structure Determination. Springer, Cham, pp 13–28
19. Schimerlik MI (1998) Overview of membrane protein solubilization. Curr Protoc Neurosci 2 (1):5–9
20. Wang H, Elferich J, Gouaux E (2012) Structures of LeuT in bicelles define conformation and substrate binding in a membrane-like context. Nat Struct Mol Biol 19(2):212
21. Quick M, Shi L, Zehnpfennig B, Weinstein H, Javitch JA (2012) Experimental conditions can obscure the second high-affinity site in LeuT. Nat Struct Mol Biol 19(2):207
22. Kawate T, Gouaux E (2006) Fluorescence-detection size-exclusion chromatography for precrystallization screening of integral membrane proteins. Structure 14(4):673–681
23. Hattori M, Hibbs RE, Gouaux E (2012) A fluorescence-detection size-exclusion chromatography-based thermostability assay for membrane protein precrystallization screening. Structure 20(8):1293–1299
24. Bird LE, Rada H, Verma A, Gasper R, Birch J, Jennions M, Löwe J, Moraes I, Owens RJ (2015) Green fluorescent protein-based expression screening of membrane proteins in Escherichia coli. J Vis Exp 95:e52357
25. Kosobokova EN, Skrypnik KA, Kosorukov VS (2016) Overview of fusion tags for recombinant proteins. Biochem Mosc 81(3):187–200
26. Waugh DS (2011) An overview of enzymatic reagents for the removal of affinity tags. Protein Expr Purif 80(2):283–293

Chapter 3

Membrane Protein Production in *Lactococcus lactis* for Structural Studies

Chloe Martens

Abstract

The expression and downstream purification of membrane proteins is the prerequisite for biophysical and structural studies of this major source of therapeutic targets. The gram-positive bacterium *Lactococcus lactis* is an attractive option for heterologous membrane protein expression and purification thanks to advantageous characteristics such as mild proteolytic activity and small genome size. Vectors designed for gene transcription under the control of inducible promoters are readily available. Specifically, the tightly regulated nisin-inducible gene expression system (NICE) allows to fine-tune the overexpression of different gene products. The expressed protein engineered with a suitable tag can be readily detected and purified from crude membrane extracts. The purpose of this protocol chapter is to detail the procedures of cloning, expression, isolation of the membrane vesicles, and affinity purification of a membrane protein of interest in *L. lactis*.

Key words Membrane protein, *Lactococcus lactis*, NICE expression system, pNZ8148, Ni-NTA affinity chromatography

1 Introduction

The field of structural biology of membrane proteins is booming, thanks to the progress of biophysical techniques [1] and computational tools [2], allowing unprecedented insights into their molecular mechanisms. However, the production of stable and functional membrane proteins for structural studies is still a challenge. A range of options are available to the structural biologist for the expression of protein targets, ranging from simple prokaryotic systems to complex eukaryotic host cells [3]. Within this spectrum, the gram-positive bacterium *Lactococcus lactis* is well established as a viable alternative for quick and efficient production of membrane proteins [4–6], including yeast [7], human [7], and plant [8] membrane proteins. The success of *L. lactis* host for large-scale production of heterologous proteins stems from the development of the nisin-controlled expression (NICE) system, derived from the

Camilo Perez and Timm Maier (eds.), *Expression, Purification, and Structural Biology of Membrane Proteins*, Methods in Molecular Biology, vol. 2127, https://doi.org/10.1007/978-1-0716-0373-4_3,

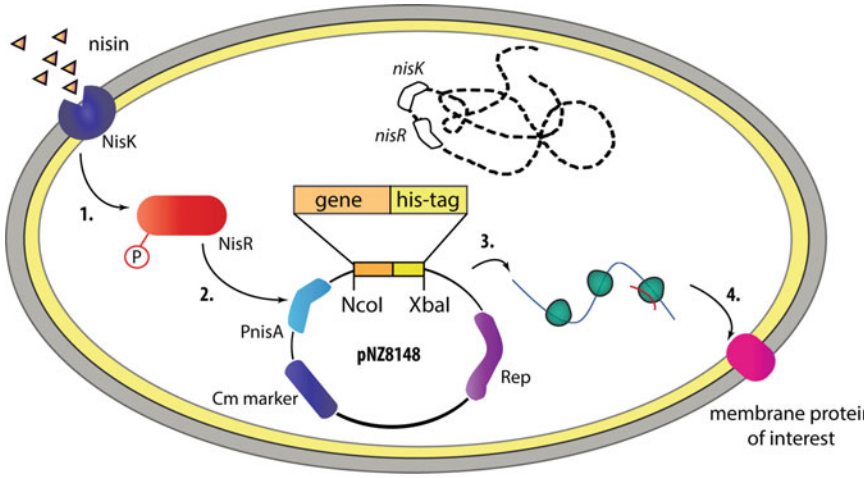

Fig. 1 Illustration of the Nisin-controlled gene expression (NICE) system for the expression of a his-tagged membrane proteins. (1) Upon binding of nisin, the histidine kinase receptor NisK autophosphorylates and transfers the phosphate group to the response regulator NisR. (2) Once activated, NisR induces the transcription of the gene of interest cloned into the vector pNZ8148, under the control of the promoter PnisA. (3) Translation of the membrane protein with its polyhistidine tag. (4) Expression of the membrane protein at the membrane of *L. lactis*

self-regulated production of the bacteriocin nisin A by specific *L. lactis* strains [9, 10]. The presence of subinhibitory amount of nisin in the extracellular media starts the regulatory cascade by binding to the receptor histidine kinase NisK. The receptor phosphorylates the NisR response regulator which induces the nisin operon at the promoter NisA and translation of the downstream gene cluster (Fig. 1). The introduction of *nisR* and *nisK* genes in the genome of the nisin-negative *L. lactis* strain MG1363 yielded the strain NZ9000 [10]. This strain is commercially available and can be transformed with plasmids containing the gene of any protein of interest under the control of the inducible promoter PnisA. Typically, the plasmid pNZ8148 is the standard vector for membrane protein expression in *L. lactis*. It contains the nisA promoter followed by a NcoI restriction site for translational fusion at the ATG site, a MCS followed by a terminator, a replicon derived from the plasmid pSH71 from *L. lactis*, and a chloramphenicol selection marker (Fig. 1) [9].

While *E. coli* is the gold standard prokaryotic host with many engineered strains available, *L. lactis* has some specific advantages that make it an interesting production system for downstream structural and functional studies. *L. lactis* is a food-grade bacterium that has been used in the dairy industry for decades, thus yielding a variety of well-characterized strains [11]. As a gram-positive bacterium, it possesses only one membrane making whole-cells studies [12] and functional characterization in membrane vesicles [13, 14] relatively straightforward. Because of its small genome size (2310

proteins) [15], the chances of redundancy during functional assays and of contamination during purification are reduced. In addition, *L. lactis* has a mild proteolytic activity, does not produce endotoxins, and does not form inclusion bodies. The introduction of external labels via the medium is facilitated by *L. lactis* auxotrophy for many amino acids [16, 17], a useful feature for the addition of selemethionine labels for crystal structure determination [18]. The few disadvantages are smaller cloning efficiency, and difficult mechanical lysis of the cells. Different strategies can be used to overcome these drawbacks and will be summarized in this chapter.

In this protocol, we detail the procedures for membrane protein production using *L. lactis*. Starting with the cloning and transformation of the gene of interest in a vector using the NICE expression system, we then describe growth and induction conditions, isolation of membrane vesicles and purification of the membrane protein by affinity chromatography with a polyhistidine tag. We also describe the procedure for small-scale expression test on whole *L. lactis* cells. The detergent-solubilized membrane protein can then be used for various biophysical studies, such as structural mass spectrometry, fluorescence [19] or paramagnetic spectroscopy [20], or crystallography [21].

2 Materials

All solutions are prepared using ultrapureultrapure water, from the molecular biology steps to protein purification. In theory, distilled water can be used for culture; however, we have found more consistent expression levels and purification yields using high-purity water. All the steps from cloning (Subheading 2.1) up to the collection of the cells after growth require sterile reagents, equipment, and conditions.

2.1 Cloning of Gene of Interest into L. lactis Compatible Vector

1. Codon optimized version of gene of interest (*see* **Note 1**).
2. Vector pNZ8148—available commercially (Mobitec).
3. *L. lactis* strains NZ9000—available commercially (Mobitec).
4. *L. lactis* strain NZ9700 for nisin production—available upon request.
5. Primers for gene amplification. Introduce NcoI restriction site on 5′ end and XbaI restriction site on 3′ end. Use manufacturer recommendation for primers design. We use Q5 high-fidelity PCR kit (NEB).
6. PCR kit containing high-fidelity and hot-start DNA polymerases, adapted buffer, and dNTPs. We use Q5 high-fidelity PCR kit (NEB).
7. Thermal cycler for PCR and PCR tubes.
8. Ligafast Rapid ligation kit (Promega).

9. NcoI and XbaI restriction enzymes with compatible buffer. We use FastDigest restriction enzymes.
10. DpnI enzyme.
11. 50% (w/v) Glucose autoclaved: weigh 500 g of glucose in a 1 L bottle and add water up to 1 L (*see* **Note 2**)
12. M17 broth (*see* **Note 3**).
13. Chloramphenicol stock: 5 mg/mL in absolute EtOH. Store at −20 °C.
14. GM17-Cm: Prepare M17 broth according to manufacturer's instructions and autoclave. Add glucose from stock to 0.5% (w/v) final concentration and chloramphenicol to 5 μg/mL.
15. Gel extraction kit (e.g., QIAquick gel extraction kit).
16. Plasmid Miniprep kit (e.g., QIAprep Spin miniprep kit).
17. Nanodrop™ spectrophotometer to measure DNA concentration and assess purity.

2.2 Transformation

1. Electroporation device—MicroPulser Electroporator.
2. Electroporation cuvettes, sterile. Cuvettes can be washed and reused. Clean the cuvettes by soaking in a solution of 70% EtOH. Dry the lids and the cuvettes under a UV lamp in a laminar flow hood. Close the cuvettes and keep until further use.
3. 0.5 M $CaCl_2$ stock in ultrapure water.
4. 0.5 M $MgCl_2$ stock in ultrapure water.
5. Steritop filter with a 500 mL process volume and a 0.22 μM membrane pore size.
6. M17 (Oxoid) concentrated twice (*see* **Note 3**). Mix 37.25 g in 500 mL ultrapure water and autoclave.
7. Wash solution 1, 0.5 M sucrose and 10% glycerol in 500 mL of ultrapure water. Filter-sterilize and keep at 4 °C.
8. Wash solution 2, 0.5 M sucrose, 10% glycerol, and 50 mM EDTA, pH 7.5, in 200 mL of ultrapure water. Filter-sterilize and keep at 4 °C.
9. GM17 medium, Prepare 100 mL of M17 (Oxoid) (*see* **Note 3**), autoclave and then add glucose to 0.5% (w/v) final concentration.
10. SGM17-G1 medium, Mix 3.725 g of M17 with 1 g of glycine in 50 mL of ultrapure water and autoclave in a 100 mL glass bottle. Mix with an equal volume of sucrose 1 M and glucose 1% (w/v) through a steritop to reach a final buffer composition of 1% (w/v) glycine, 0.5 M sucrose, and 0.5% (w/v) glucose.
11. SGM17-G2 medium, Mix 18.625 g of M17 with 10 g of glycine in 250 mL of ultrapure water and autoclave in a

500 mL glass bottle. Mix with an equal volume of sucrose 1 M and glucose 1% (w/v) through a steritop to reach a final buffer composition of 2% (w/v) glycine, 0.5 M sucrose, and 0.5% (w/v) glucose.

12. Recovery medium (1 mL per transformation reaction), M17 containing 0.5% (w/v) glucose, 0.5 M sucrose, 20 mM $MgCl_2$, and 2 mM $CaCl_2$. Mix 1 volume of M17 medium concentrated twice with 1 volume of a sterile solution containing 1 M sucrose, 1% (w/v) glucose, 40 mM $MgCl_2$, and 4 mM $CaCl_2$ (*see* **Note 4**).
13. SGM17-Cm plates. Plates are M17 with 1% agar, 0.5% (w/v) glucose, 0.5 M sucrose, and 5 μg/mL chloramphenicol. Mix 19 g of M17 broth (Oxoid) with 5 g agar in 250 mL ultrapure water and autoclave (*see* **Note 3**). Dissolve 171.1 g of sucrose in 250 mL of ultrapure water, add 5 mL glucose 50% (w/v). When the M17-agar solution cools down to ~65 °C, add the sucrose-glucose solution using a steritop filter. Add 50 μL from chloramphenicol stock solution and pour solution into sterile petri dishes (*see* **Note 4**).
14. Parafilm.
15. Glycerol 50% (v/v), autoclaved.
16. Eppendorf Thermal shaker.

2.3 Production of Nisin A

1. GM17 plates. Plates are M17 with 1% agar, 0.5% (w/v) glucose. Mix 19 g of M17 broth (Oxoid) (*see* **Note 3**), 2.5 g of glucose, and 5 g of agar in 500 mL ultrapure water and autoclave. When the GM17-agar solution cools down to ~65 °C, pour solution into sterile petri dishes.
2. GM17 media. Prepare 1 L by mixing 37.25 g M17 broth (Oxoid) (*see* **Note 3**), 5 g of glucose in 1 L of ultrapure water. Add a magnetic stirrer in the 1 L bottle and autoclave (*see* **Note 5**). Prepare another 250 mL bottle of the same media for small cultures.

2.4 Small-Scale Expression Tests

1. Nisin A (*see* **Note 6**).
2. HEPES cell wash buffer (*see* **Note 7**). 50 mM HEPES, pH 7.4. For 1 L, dissolve 11.915 g of HEPES in 900 mL ultrapure water. Adjust pH to 7.4 with 5 M NaOH and add ultrapure water to make 1 L. Filter through 0.22 μM membrane and store at 4 °C.
3. Trichloroacetic acid (TCA) 20% (v/v) in water.
4. Lysozyme, powder. Take it out of the −20 °C freezer 15 min before use (*see* **Note 8**).
5. Refrigerated Tabletop centrifuge for Eppendorf tubes.

2.5 Large-Scale Culture

1. 2 L glass bottle with GM17-Cm, autoclaved (*see* **Note 9**).
2. Chloramphenicol stock solution for large volumes: dissolve chloramphenicol in absolute EtOH to a final concentration of 50 mg/mL. Keep at −20 °C.
3. HEPES cell wash buffer (*see* **Note 7**). Prepare 2 L and keep at 4 °C.

2.6 Isolation of Inverted Membrane Vesicles

1. DNaseI from bovine pancreas. Make 1 mL aliquots of 10 mg/mL and store at −20 °C.
2. Potter tissue homogenizer.
3. High-Pressure Homogenizer Emulsiflex C3.
4. Ultracentrifugation tubes.
5. HEPES membrane buffer, 50 mM HEPES pH 7.4, 150 mM NaCl, 10% glycerol (v/v). For 1 L, dissolve 11.915 g of HEPES, 8.76 g of NaCl and 126 g of glycerol in 900 mL of ultrapure water. Adjust the pH to 7.4 with 5 M NaOH and add ultrapure water to make 1 L. Filter through 0.22 μM membrane and store at 4 °C.

2.7 Membrane Protein Purification for Biophysical Studies

1. Detergent β-dodecyl-maltoside (DDM)—Sol Grade. Powder. Take it out of the freezer 15 min before use.
2. DDM—Anal Grade. Prepare 1 mL aliquots of 10% (w/v) final concentration in ultrapure water.
3. Ni-NTA agarose (Qiagen). 1 mL of slurry per liter of culture.
4. Econo-Pac chromatography column (Biorad).
5. Imidazole stock 5 M, adjusted to pH 7.5 with HCl. Prepare 50 mL, filter through 0.22 μM membrane and protect from light.
6. HEPES desalting buffer. 50 mM HEPES pH 7.4, 100 mM NaCl, 10% glycerol (v/v). For 1 L, dissolve 11.915 g of HEPES, 8.76 g of NaCl and 126 g of glycerol in 900 mL ultrapure water. Adjust the pH to 7.4 with 5 M NaOH and add ultrapure water to make 1 L. Filter through 0.22 μM membrane and store at 4 °C.
7. HEPES wash buffer. Same as HEPES desalting buffer but with 20 mM imidazole. Add imidazole from stock in a 1:500 volume ratio.
8. HEPES elution buffer. Same as HEPES desalting buffer but with 250 mM imidazole. Add imidazole from stock in a 1:20 volume ratio.
9. PD-10 desalting column.
10. 100 mL Erlenmeyer flask.

3 Methods

3.1 Cloning of Gene of Interest into L. lactis Compatible Vector

Different strategies are available to insert a gene of interest into a plasmid. Here we report the classic ligation method, consisting in three steps. First, amplification of the gene of interest by PCR followed by restriction with the enzymes NcoI and XbaI. Then, ligation of the gene insert into vector pNZ8148 digested with the same restriction enzymes. Finally, transformation of *L. lactis* NZ9000 by electroporation and selection of successful transformants. This step can sometimes be a challenge for *L. lactis*, and alternative methods have been developed and are presented elsewhere [8, 22, 23]. In the example provided in this protocol, the protein gene is followed by a sequence coding for six histidines, for downstream affinity purification of the membrane protein.

3.1.1 Preparation of the Insert

1. Amplify your gene of interest by PCR, according to the manufacturer instructions (*see* **Note 10**). For example using the Q5 high-fidelity DNA polymerase: (1) Initial denaturation, 5 min at 98 °C; (2) Denaturation, 50 s at 98 °C; (3) Annealing, 50 s at 55 °C; (4) Elongation, 1 min + 1 min per kb of DNA template at 72 °C; repeat (2)–(4) 25 times; (5) Final Extension, 5 min at 72 °C. The ideal annealing temperature depends on the primers and has to be determined for each PCR reaction. We use the NEB calculator: https://tmcalculator.neb.com/#!/main
2. (optional: *see* **Note 11**). If the gene is on a plasmid extracted from a bacterial source: incubate PCR product with 2 μL of DpnI enzyme at 37 °C in thermal block for 2 h. Inactivate the enzyme by 20 min incubation at 80 °C.
3. Purify the DNA using the QIAquick PCR & Gel Cleanup Kit, according to the manufacturer instructions. Run an agarose gel to verify gene amplification.
4. Set up the digestion reaction. Mix 40 μL of the purified PCR product with 2 μL of NcoI, 2 μL of XbaI, and 5 μL of FastDigest buffer. Incubate the reaction for 15 min at 37 °C in thermal block. Inactivate the enzymes by 10 min incubation at 80 °C.
5. Purify the restricted DNA product using QIAquick PCR & Gel Cleanup Kit.

3.1.2 Preparation of the Vector

1. Inoculate 50 mL of sterile GM17-Cm with *L. lactis* NZ9000 cells transformed containing the plasmid pNZ8148 (*see* Subheading 3.2 for electrotransformation). Grow overnight at 30 °C without shaking. In the morning, pellet the cells by centrifugation, resuspend in 1 mL of resuspension buffer from the miniprep kit, supplemented with 10 mg of lysozyme. Incubate at 30 °C in a thermal shaker for 1 h. Extract the plasmidic DNA according to the kit's instructions.

2. Repeat **step 4** on the purified plasmid.
3. Run an agarose gel 1% to isolate the digested vector. Excise the top band (~3.5 kb) and purify the DNA using QIAquick PCR & Gel Cleanup Kit.

3.1.3 Ligation Reaction

1. Measure the DNA concentration of the restricted PCR product and the restricted vector on nanodrop (*see* **Note 12**). Use 100 ng of vector DNA and mix with insert DNA in a 6:1 insert:vector molar ratio, using the following equation:

$$\text{Amount of insert (ng)} = \frac{\text{size of insert (bp)}}{\text{size of vector (bp)}} \times 6 \times 100 \text{ (ng)}$$

   Add buffer and ligase according to manufacturer's instructions and incubate at 37 °C for 20 min in thermal block.
2. Clean up ligation product with QIAquick PCR & Gel Cleanup Kit. Elute in 50 μL of ultrapure water.
3. Concentrate the ligation product by solvent evaporation using a centrifugal evaporator to a final volume of 5 μL (*see* **Note 13**).

3.2 Transformation

3.2.1 Prepare Electrocompetent NZ9000 L. lactis Cells

1. In the morning, streak NZ9000 strain on GM17 plate. Incubate for ~30 h at 30 °C.
2. Inoculate 5 mL of sterile GM17 with a single colony from the plate. At the end of the day, inoculate 50 mL of SGM17_G1 with the day preculture. Grow overnight a 30 °C, without shaking.
3. In the morning, use 50 mL overnight culture to inoculate 500 mL SGM17_G2. Incubate at 30 °C with under slow agitation until OD reaches ~0.5 (~4 h).
4. Pellet cells by centrifugation at 4 °C (*see* **Note 14**) and resuspend in 400 mL of ice-cold wash solution 1. Centrifuge again and resuspend cells in 200 mL of ice-cold wash solution 2. Incubate the cells on ice for 15 min. Centrifuge the cells again and resuspend in 100 mL of wash solution 1. Centrifuge for the fourth and last time and resuspend the cells in 4 mL of ice-cold wash solution 1 (*see* **Note 15**).
5. Aliquots the competent cells in 50 μL Eppendorf tubes, snap-freeze in liquid nitrogen, and store at −80 °C.

3.2.2 Electro-transformation

1. Thaw an aliquot of competent cells on ice (*see* **Note 16**). Chill an electroporation cuvette by placing it at 4 °C or on ice.
2. Add the concentrated ligation product on the cells, pipet slowly once and transfer delicately to the chilled cuvette (*see* **Note 17**).
3. Set the following parameters on the electroporator: 2 kV, 25 μF capacitance, 200 Ω resistance.
4. Quickly dry the cuvette with a tissue, place the cuvette and electroporate (*see* **Note 17**). Immediately add 1 mL of ice-cold recovery medium, incubate 10 min on ice, then grow at 30 °C for 2 h.

5. Pellet the cells by high-speed centrifugation for 1 min on a tabletop centrifuge and remove 800 µL of supernatant. Resuspend the cells in the remaining liquid and plate all the cells on SGM17-Cm agar plates (*see* **Note 18**). Cover the plate with parafilm and incubate at 30 °C for 2 days.
6. Pick up three colonies per plate to inoculate 3 × 5 mL of GM17-Cm. Grow overnight at 30 °C. In the morning, prepare glycerol stocks by mixing 500 µL of culture with 500 µL of glycerol 50% (v/v). Snap-freeze and keep at −80 °C. Pellet the cells of the remaining culture and resuspend in 1 mL of the miniprep resuspension buffer, supplemented with 10 mg of lysozyme. Incubate at 30 °C in a thermal shaker for 1 h. Extract plasmidic DNA according to the kit's manufacturer instructions and verify correct gene cloning by sequencing. Keep the correct glycerol stocks accordingly and throw away the wrong ones, if any (*see* **Note 19**).

3.3 Production of Nisin A

1. In the morning, streak NZ9700 strain on GM17 plate. Incubate for ~30 h at 30 °C.
2. In the following afternoon, inoculate 20 mL of sterile GM17 with a single colony from the plate and grow overnight at 30 °C. Next morning, inoculate 1 L of GM17 and leave until next morning.
3. Pellet the cells by centrifugation. Aliquot the supernatant in 15 mL falcon tubes (~8 mL per falcon tube) (*see* **Note 20**). Store at −20 °C for up to 6 months.

3.4 Small-Scale Expression Tests

1. Inoculate 5 mL of GM17-Cm of with a verified glycerol stock. Grow overnight at 30 °C.
2. In the morning, inoculate 10 mL of fresh GM17-Cm with 500 µL of the overnight culture. Grow until OD at 660 nm reaches ~0.8. Add 10 µL of nisin (NZ9700 supernatant) and induce for 2 h.
3. Pellet 2 mL of culture in an Eppendorf tube. Resuspend in 1 mL HEPES cell wash buffer and add 10 mg of lysozyme. Vortex thoroughly and incubate at 30 °C for 1 h in thermal shaker.
4. Add 10 mM $MgSO_4$, 5 mM $CaCl_2$, and 10 µg/mL DNaseI. Incubate 10 min at 30 °C in thermal shaker.
5. Pellet the cells, resuspend in 500 µL of HEPES cell wash buffer, and perform lysis by basic shock by adding 50 µL of NaOH 1.85 M. Vortex and keep 10 min on ice.
6. Add 50 µL of TCA 20% (v/v) to precipitate proteins (*see* **Note 21**). Vortex and keep 10 min on ice.

7. Centrifuge at 4 °C in a tabletop centrifuge at full speed for 10 min and discard supernatant.
8. Resuspend cells in minimal volume of SDS-PAGE gel loading buffer and detect protein expression by SDS-PAGE followed by anti-his Western blot, following established procedures (*see* **Note 22**).

3.5 Growth

1. In the morning, inoculate 5 mL of GM17-Cm by scraping a verified glycerol stock. Grow at 30 °C for ~6 h, then inoculate 100 mL of GM17-Cm with the 5 mL day culture. Grow overnight at 30 °C (*see* **Note 23**).
2. Next morning, inoculate 1.9 L of GM17-Cm with the overnight culture. Monitor OD at 660 nm and induce when it reaches 0.8 (takes ~2 h) by adding 1.25 mL of NZ9700 supernatant per liter of culture (*see* **Note 24**).
3. Induce for 2 h and collect cells by centrifugation. Dispose of supernatant and weigh the cell pellet. Expect 5 g of cell paste per liter of culture.
4. Resuspend the cells in HEPES cell wash buffer and centrifuge again. Resuspend the washed pellet in a final volume of 10 mL of HEPES cell wash buffer per liter of culture. Freeze and keep at −80 °C. The cell pellet can be conserved for up to 6 months without noticeable changes in yield of purification (*see* **Note 25**).

3.6 Isolation of Inverted Membrane Vesicles

1. Thaw the cell pellet in a water bath and then keep on ice. Add lysozyme to 10 mg/mL final concentration, homogenize with a Potter tissue homogenizer, and incubate at 30 °C for 1 h in a water bath. Add 10 μg/mL DNaseI and 10 mM $MgSO_4$. Vortex and incubate for 10 min at 30 °C.
2. Break the cells by 4 passes at ~25,000 psi in a high-pressure homogenizer (Emulsiflex) (*see* **Notes 26** and **27**).
3. Separate cell debris from membranes by low-speed ultracentrifugation (~15,000 × *g*), 15 min, at 4 °C. Decant the supernatant in ultracentrifugation tubes and pellet the cell membranes by high-speed ultracentrifugation: 1 h, 125,000 × *g*, 4 °C (*see* **Note 28**).
4. Discard the supernatant and resuspend the membranes in 5 mL of HEPES membrane buffer per liter of culture, homogenize the membranes with Potter tissue homogenizer, and store at −80 °C. The membranes can be kept for up to 1 month.

3.7 Membrane Protein Purification for Biophysical Studies

1. Thaw the cell membranes on ice. In parallel or the day before, prepare the solubilization buffer. Mix the detergent DDM with HEPES membrane buffer to a final concentration of 2% (w/v). Agitate on a wheel until the detergent is dissolved and keep at 4 °C.

2. Mix the solubilization buffer and the membranes in a 1:1 volume, reaching a final detergent concentration of 1% (w/v). Decant in an Erlenmeyer with a magnetic stirrer and stir slowly for 2 h at 4 °C.
3. During solubilization, decant 1 mL of resin slurry per liter of culture in a 50 mL falcon tube. Wash the Ni-NTA resin with 15 column volumes (CV) of ultrapure water and equilibrate with 3 CV of HEPES wash buffer supplemented with 0.05% DDM. Keep the falcon with the equilibrated resin on ice (*see* **Note 29**).
4. Separate insoluble debris from solubilized proteins with 45 min high-speed ultracentrifugation (125,000 × *g*, 4 °C). Pour the supernatant in the falcon containing the equilibrated resin and add imidazole from stock to a final concentration of 10 mM to limit unspecific binding. Incubate on an orbital shaker or on a wheel at 4 °C for 2 h.
5. Pour the content of the falcon onto an Econo-pac column. Discard the flow-through, keeping 20 μL for SDS-PAGE analysis.
6. Wash the resin with 10 column volumes of HEPES wash buffer supplemented with 0.05% DDM (*see* **Note 29**). Keep 20 μL for SDS-PAGE analysis.
7. Elute his-tagged protein by stepwise addition of 3 CV of elution buffer supplemented with 0.05% DDM (w/v) (*see* **Note 29**). Measure the absorbance at 280 nm and pool the fractions containing protein (*see* **Notes 30** and **31**).
8. Remove the imidazole from the protein sample by exchanging the buffer on a PD10 desalting column equilibrated with HEPES desalting buffer supplemented with 0.02% DDM (w/v) (*see* **Note 29**). Aliquot and flash-freeze the protein in liquid nitrogen and keep at −80 °C until further use (*see* **Note 32**).

4 Notes

1. *L. lactis* has an AT-rich codon usage [15, 24]. For heterologous membrane production, it is important to codon-optimize the gene of interest, to avoid stalling during transcription. Codon optimization is a service available from most gene synthesis providers. Synthetic gene design is relatively cheap nowadays and can be used to add protease cleavage site and purification tags in one go.
2. 500 g of glucose will not readily dissolve in 1 L of water. Simply put the whole bottle in the autoclave, the remaining solid glucose will melt during the autoclaving procedure.

3. M17 broth is designed for the growth of lactic streptococci. The media is available from different brands such as Difco, Oxoid, and Biokar. There are important price differences between the three brands. For large-scale cultures, the cheapest brand Biokar is preferred. For more delicate experiments and small-scale use, we recommend using Difco or Oxoid medium. This applies to the growth of Lactis *NZ9700* strain for nisin A production, the preparation of electrocompetent cells, of SGM17-Cm plates, and of the recovery medium used after electroporation.
4. To prepare the recovery medium and the SGM17-Cm plates, we recommend sterilizing the sucrose by filter sterilization instead of autoclaving. We have observed caramelization of sucrose and subsequent decrease in transformation efficiency.
5. When growing *L. lactis* NZ9700 strain for nisin production, make sure to add a magnetic stirrer bar in the bottle used for the cells' growth before autoclaving, to allow stirring of the culture later on.
6. Nisin A is secreted by the *L. lactis* strain NZ9700, available upon request. The supernatant of an overnight culture of NZ9700 is used for induction (*see* Subheadings 2.3 and 3.3). Alternatively, Nisin A can be bought (Sigma) and used in a concentration ranging from 0.1 to 2 ng/mL. However, we have observed lower levels of expression using the commercially available nisin and recommend using the supernatant for induction.
7. We use HEPES for purification, but phosphate buffers are suitable as well. The ideal buffer depends on the protein under study and the assays that will be performed downstream.
8. Lysozyme digests the peptidoglycan cell wall of gram-positive bacteria. We use it to facilitate cell lysis for DNA extraction or protein purification.
9. *L. lactis* is anaerobic and oxygen tolerant [25]. The cells can be grown in 2 L bottles filled to the brim with GM17-Cm medium without shaking. Add the chloramphenicol after the bottles have cooled down.
10. When designing the primers for PCR amplification, make sure to introduce the appropriate restrictions sites NcoI and XbaI in the forward and reverse primers, respectively. NcoI will recognize the ATG start codon of the gene, and XbaI is introduced after the stop codon.
11. If the PCR is carried out on a plasmid extracted from a bacterial source, then the digestion of the parental methylated DNA by the enzyme DpnI is essential to avoid false positives at the transformation stage.

12. The purity of the restricted DNA is crucial for a successful ligation reaction. The absorbance ratios of DNA can provide an indication of contamination either by protein (at 280 nm) or by ethanol and isopropanol (at 230 nm). A value of 2 for the absorbance 260/230 ratio and a value of 1.8 for the 260/280 ratio of DNA are desirable.
13. Transformation efficiency in *L. lactis* cells is low compared to *E. coli*. Only few to no transformants will be obtained upon the transformation of a ligation product. Different strategies have been proposed to overcome this issue [22]. We found that concentrating the DNA by water evaporation in a rotavap followed by transformation of the entire ligation product clearly improved the number of successful transformants.
14. It is very important to keep the environment and the material sterile when preparing electrocompetent cells. All the tubes, flask, and buffers have to be autoclaved. The resuspension of the cells is done in an ice box under a laminar flow hood, sterilized with a UV lamp beforehand.
15. Glycine and EDTA weaken the cell membrane during growth. Sucrose is required as an osmotic stabilizer [26, 27].
16. When performing electrotransformation, add 50 ng of digested plasmidic DNA and 50 ng of intact plasmid DNA to the competent cells, as negative and positive controls, respectively. The digested DNA should not produce any transformants and the intact plasmid should produce 20–50 colonies.
17. During electroporation, it is important to avoid the formation of bubbles in the cuvette and to ensure that there is a contact between both sides of the cell, in order to avoid the formation of an arc during the pulse. Electroporation should be done under sterile conditions, e.g., under a hood or next to a flame.
18. We found that plating the entire cell culture on one petri dish gave better yields of transformation than the usual dilution procedure.
19. Once the gene of interest is inserted in the vector pNZ8148 and transformed into *L. lactis* NZ900 cells, any subsequent modification of the gene can easily be done using the protocol described in Subheadings 2.1 and 3.1 using appropriate primers. It is crucial however to methylate the parental DNA before the PCR reaction, to avoid false positives after transformation. We typically do this using the Dam methyltransferase enzyme (NEB).
20. The NICE expression system is tightly regulated, and the amount of nisin can be fine-tuned to control gene expression. The optimal amount of NZ9700 supernatant has to be optimized for each new target. This can easily be estimated by performing small-scale culture induced with a range of nisin

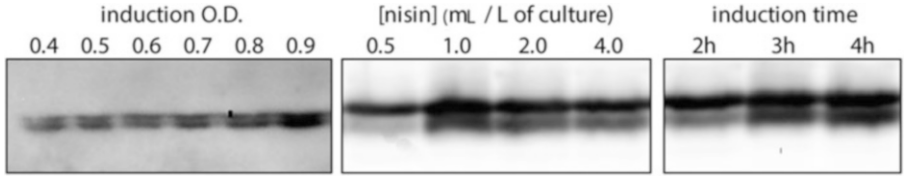

Fig. 2 Optimization of induction parameters using small-scale expression tests. Anti-his Western blot analysis detects the expression level of his-tagged LmrP in whole-cell extracts run on SDS-PAGE. Optimization of time of induction, amount of nisin for induction, and length of induction time are shown on the left, middle, and right panels, respectively. The double band is a gel migration artifact

dilutions and assessing the level of expression by Western blot (Fig. 2 and Subheading 3.4). We typically use 1.25 mL of supernatant in 1 L of culture for induction. 8 mL aliquots allow to induce 6 L of culture.

21. TCA is caustic, handle carefully.
22. Small-scale expression tests are used to see if the target protein is expressed before large-scale cultures. It can also be used to optimize the induction conditions. The amount of nisin to use, the optimal density for induction, and the time of induction can be monitored by Western blot (*see* Fig. 2).
23. We found that starting with a "pre-preculture" of 5–10 mL, which is then used to inoculate the larger overnight, 100 mL preculture gave more consistent growth curves on the day of culture.
24. Place the 2 L bottles with GM17-Cm in the incubator at 30 °C the day before the culture.
25. The stability upon storage depends on the protein itself. This number is a rough estimate based on our experience.
26. One-Shot (Constant system ltd) disruption systems are known to provide a more efficient lysis of *L. lactis* cells and provides higher yields of crude membranes than the combination of French Press and lysozyme incubation [28].
27. To avoid overheating of the sample, perform the lysis with a cell disruptor connected to a cooling system or in a cold room. If none of these options are available put the tubing in ice.
28. Cell debris are whitish and opaque while membranes are yellowish and translucid. Perform as many low-speed ultracentrifugation as needed to get rid of most of the white pellet. Two or three rounds of centrifugation are usually needed.
29. Detergent in solution is not stable. Typically, buffers containing detergent can be kept at 4 °C up to 1 week. We recommend adding the detergent from a frozen stock (either 10% (w/v) aliquot or powder) on the day of use.

30. Imidazole solutions tends to have contaminants that absorb at 280 nm. Make sure to blank with the elution buffer before measuring absorbance. We found that imidazole BioUltra (Sigma) does not absorb at 280 nm.
31. We use the Nanodrop™ reader to have a rough estimate of the protein centration. For an accurate measurement of protein concentration, we recommend the use of a more sensitive spectrophotometer or of a different assay (Pierce 660, BCA assay, Bradford assay). Neither the presence of detergent nor imidazole interferes with the aforementioned assays.
32. It is worth noting that the lipid composition of *L. lactis* membrane differs from that of *E. coli*, and this can have implications for biophysical and structural characterization [29, 30]. We have shown with native mass spectrometry that proteins expressed in *L. lactis* and purified using the detergent DDM retain significant amount of cardiolipin bound, but no other phospholipids are observed (Fig. 3). In contrast, proteins

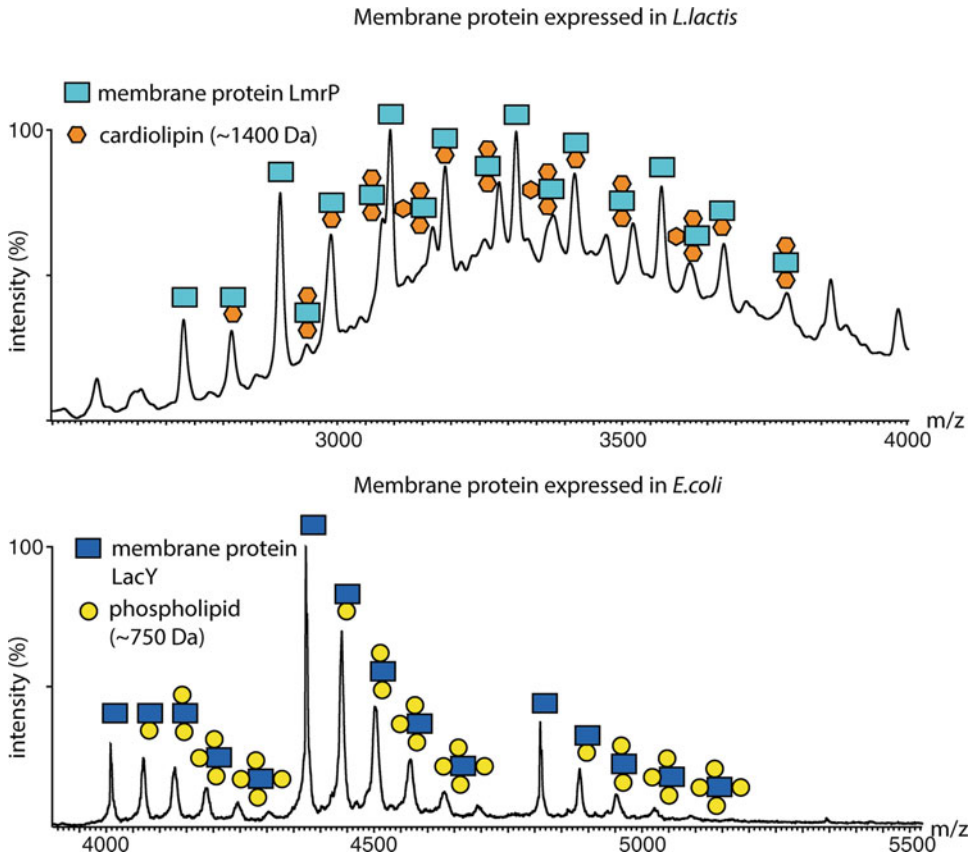

Fig. 3 Mass spectra of LmrP and LacY, expressed and purified from *L. lactis* and *E.coli*, respectively. Top panel shows LmrP retaining up to three cardiolipins (~1400 Da) bound. Lower panel shows LacY retaining up to five smaller size phospholipids (~750 Da) bound

purified from *E. coli* with the same procedure retain smaller adducts bound, likely a mixture of smaller phospholipids species such as phosphatidylethanolamine and phosphatidylglycerol.

Acknowledgments

We thank Matthieu Masureel for the small-scale expression tests. We acknowledge support from the Fonds de la Recherche Scientifique (FRS-FNRS) (Grant Number: 1.B.261.19F).

References

1. Cheng Y (2018) Membrane protein structural biology in the era of single particle cryo-EM. Curr Opin Struct Biol 52:58–63. https://doi.org/10.1016/j.sbi.2018.08.008
2. Chavent M, Duncan AL, Sansom MS (2016) Molecular dynamics simulations of membrane proteins and their interactions: from nanoscale to mesoscale. Curr Opin Struct Biol 40:8–16. https://doi.org/10.1016/j.sbi.2016.06.007
3. Pandey A, Shin K, Patterson RE, Liu XQ, Rainey JK (2016) Current strategies for protein production and purification enabling membrane protein structural biology. Biochem Cell Biol 94(6):507–527. https://doi.org/10.1139/bcb-2015-0143
4. Kunji ER, Slotboom DJ, Poolman B (2003) Lactococcus lactis as host for overproduction of functional membrane proteins. Biochim Biophys Acta 1610(1):97–108
5. King MS, Boes C, Kunji ER (2015) Membrane protein expression in Lactococcus lactis. Methods Enzymol 556:77–97. https://doi.org/10.1016/bs.mie.2014.12.009
6. Putman M, van Veen HW, Poolman B, Konings WN (1999) Restrictive use of detergents in the functional reconstitution of the secondary multidrug transporter LmrP. Biochemistry 38(3):1002–1008. https://doi.org/10.1021/bi981863w
7. Monne M, Chan KW, Slotboom DJ, Kunji ER (2005) Functional expression of eukaryotic membrane proteins in Lactococcus lactis. Protein Sci 14(12):3048–3056. https://doi.org/10.1110/ps.051689905
8. Frelet-Barrand A, Boutigny S, Moyet L, Deniaud A, Seigneurin-Berny D, Salvi D, Bernaudat F, Richaud P, Pebay-Peyroula E, Joyard J, Rolland N (2010) Lactococcus lactis, an alternative system for functional expression of peripheral and intrinsic Arabidopsis membrane proteins. PLoS One 5(1):e8746. https://doi.org/10.1371/journal.pone.0008746
9. Mierau I, Kleerebezem M (2005) 10 years of the nisin-controlled gene expression system (NICE) in Lactococcus lactis. Appl Microbiol Biotechnol 68(6):705–717. https://doi.org/10.1007/s00253-005-0107-6
10. de Ruyter PG, Kuipers OP, de Vos WM (1996) Controlled gene expression systems for Lactococcus lactis with the food-grade inducer nisin. Appl Environ Microbiol 62(10):3662–3667
11. Song AA, In LLA, Lim SHE, Rahim RA (2017) A review on Lactococcus lactis: from food to factory. Microb Cell Factories 16(1):55. https://doi.org/10.1186/s12934-017-0669-x
12. Wang W, van Veen HW (2012) Basic residues R260 and K357 affect the conformational dynamics of the major facilitator superfamily multidrug transporter LmrP. PLoS One 7(6):e38715. https://doi.org/10.1371/journal.pone.0038715
13. Mazurkiewicz P, Poelarends GJ, Driessen AJ, Konings WN (2004) Facilitated drug influx by an energy-uncoupled secondary multidrug transporter. J Biol Chem 279(1):103–108. https://doi.org/10.1074/jbc.M306579200
14. van den Berg van Saparoea HB, Lubelski J, van Merkerk R, Mazurkiewicz PS, Driessen AJ (2005) Proton motive force-dependent Hoechst 33342 transport by the ABC transporter LmrA of Lactococcus lactis. Biochemistry 44(51):16931–16938. https://doi.org/10.1021/bi051497y
15. Bolotin A, Wincker P, Mauger S, Jaillon O, Malarme K, Weissenbach J, Ehrlich SD, Sorokin A (2001) The complete genome sequence of the lactic acid bacterium Lactococcus lactis

ssp. lactis IL1403. Genome Res 11 (5):731–753. https://doi.org/10.1101/gr.169701

16. Delorme C, Godon JJ, Ehrlich SD, Renault P (1993) Gene inactivation in Lactococcus lactis: histidine biosynthesis. J Bacteriol 175 (14):4391–4399
17. Godon JJ, Delorme C, Bardowski J, Chopin MC, Ehrlich SD, Renault P (1993) Gene inactivation in Lactococcus lactis: branched-chain amino acid biosynthesis. J Bacteriol 175 (14):4383–4390
18. Berntsson RP, Alia Oktaviani N, Fusetti F, Thunnissen AM, Poolman B, Slotboom DJ (2009) Selenomethionine incorporation in proteins expressed in Lactococcus lactis. Protein Sci 18(5):1121–1127. https://doi.org/10.1002/pro.97
19. Hakizimana P, Masureel M, Gbaguidi B, Ruysschaert JM, Govaerts C (2008) Interactions between phosphatidylethanolamine headgroup and LmrP, a multidrug transporter: a conserved mechanism for proton gradient sensing? J Biol Chem 283(14):9369–9376. https://doi.org/10.1074/jbc.M708427200
20. Masureel M, Martens C, Stein RA, Mishra S, Ruysschaert JM, McHaourab HS, Govaerts C (2014) Protonation drives the conformational switch in the multidrug transporter LmrP. Nat Chem Biol 10(2):149–155. https://doi.org/10.1038/nchembio.1408
21. Malinauskaite L, Quick M, Reinhard L, Lyons JA, Yano H, Javitch JA, Nissen P (2014) A mechanism for intracellular release of Na+ by neurotransmitter/sodium symporters. Nat Struct Mol Biol 21(11):1006–1012. https://doi.org/10.1038/nsmb.2894
22. Geertsma ER, Poolman B (2007) High-throughput cloning and expression in recalcitrant bacteria. Nat Methods 4(9):705–707. https://doi.org/10.1038/nmeth1073
23. Geertsma ER, Poolman B (2010) Production of membrane proteins in Escherichia coli and Lactococcus lactis. Methods Mol Biol 601:17–38. https://doi.org/10.1007/978-1-60761-344-2_2
24. Grantham R, Gautier C, Gouy M, Jacobzone M, Mercier R (1981) Codon catalog usage is a genome strategy modulated for gene expressivity. Nucleic Acids Res 9(1): r43–r74
25. Pedersen MB, Iversen SL, Sorensen KI, Johansen E (2005) The long and winding road from the research laboratory to industrial applications of lactic acid bacteria. FEMS Microbiol Rev 29(3):611–624. https://doi.org/10.1016/j.femsre.2005.04.001
26. Holo H, Nes IF (1989) High-Frequency Transformation, by Electroporation, of Lactococcus lactis subsp. cremoris Grown with Glycine in Osmotically Stabilized Media. Appl Environ Microbiol 55(12):3119–3123
27. Wells JM, Wilson PW, Le Page RW (1993) Improved cloning vectors and transformation procedure for Lactococcus lactis. J Appl Bacteriol 74(6):629–636
28. Frelet-Barrand A, Boutigny S, Kunji ER, Rolland N (2010) Membrane protein expression in Lactococcus lactis. Methods Mol Biol 601:67–85. https://doi.org/10.1007/978-1-60761-344-2_5
29. Martens C, Stein RA, Masureel M, Roth A, Mishra S, Dawaliby R, Konijnenberg A, Sobott F, Govaerts C, McHaourab HS (2016) Lipids modulate the conformational dynamics of a secondary multidrug transporter. Nat Struct Mol Biol 23(8):744–751. https://doi.org/10.1038/nsmb.3262
30. Findlay HE, Booth PJ (2017) The folding, stability and function of lactose permease differ in their dependence on bilayer lipid composition. Sci Rep 7(1):13056. https://doi.org/10.1038/s41598-017-13290-7

Chapter 4

Expression and Purification of Membrane Proteins in *Saccharomyces cerevisiae*

Martin S. King and Edmund R. S. Kunji

Abstract

Saccharomyces cerevisiae is one of the most popular expression systems for eukaryotic membrane proteins. Here, we describe protocols for the expression and purification of mitochondrial membrane proteins developed in our laboratory during the last 15 years. To optimize their expression in a functional form, different promoter systems as well as codon-optimization and complementation strategies were established. Purification approaches were developed which remove the membrane protein from the affinity column by specific proteolytic cleavage rather than by elution. This strategy has several important advantages, most notably improving the purity of the sample, as contaminants stay bound to the column, thus eliminating the need for a secondary purification step, such as size exclusion chromatography. This strategy also avoids dilution of the sample, which would occur as a consequence of elution, precluding the need for concentration steps, and thus preventing detergent concentration.

Key words Membrane proteins, Mitochondria, Protein expression, *Saccharomyces cerevisiae*, Yeast, Nickel affinity chromatography, Purification by on-column proteolytic cleavage

1 Introduction

1.1 Expression of Mitochondrial Membrane Proteins in Saccharomyces cerevisiae

Membrane proteins account for approximately 30% of all open reading frames in sequenced genomes. They have many functions, including transport, maintenance of cellular homeostasis, transmission of signals, and control of cell–cell contacts. Given their central importance in physiology, their dysfunction has been implicated in an increasing range of diseases.

One of the most popular systems for the heterologous expression of membrane proteins is the baker's yeast *Saccharomyces cerevisiae* [1]. Yeast cells are able to post-translationally process eukaryotic membrane proteins in a way that prokaryotic expression systems cannot (such as *Escherichia coli* and *Lactococcus lactis* [2]). The genetics of *S. cerevisiae* is well understood; consequently, a wide range of techniques and strains have been developed for improved membrane protein production (as reviewed in [1]).

Camilo Perez and Timm Maier (eds.), *Expression, Purification, and Structural Biology of Membrane Proteins*, Methods in Molecular Biology, vol. 2127, https://doi.org/10.1007/978-1-0716-0373-4_4,

Furthermore, expression in yeast has cost benefits compared to insect [3] and mammalian [4] systems. The structural, biophysical, and functional characterizations of membrane proteins require a lot of material [5–11]. Since the expression levels of membrane proteins can be low, large-scale fermentation is required, for which reliable procedures are available [12, 13]. The protocols described below have been successful in expressing and purifying a wide range of mitochondrial inner membrane proteins, including members of the mitochondrial carrier family (SLC25), such as the mitochondrial ADP/ATP carrier [5–7], aspartate/glutamate carrier [14], phosphate carrier [15] and ATP-Mg/phosphate carriers [16, 17], as well as the mitochondrial pyruvate carrier [18], and also beta-barrels of the mitochondrial outer membrane, such as Sam50 and Mdm10 (unpublished data).

2 Materials

2.1 Strains and Plasmids

1. *Escherichia coli* XL1 blue (Stratagene).
2. *Saccharomyces cerevisiae* strain W303.1B (MATα leu2-3,112 trp1-1 can1-100 ura3-1 ade2-1 his3-11,15) (ATCC number: 201238) and derivative WB-12, which lacks *aac1* and *aac2*, for complementation studies [19]. Other yeast strains are available, most notably protease-deficient strains such as BJ2168 (MATα leu2 trp1 ura3-52 prc1-407 ptb1-1122 pep3-3) and FGY217 (MATα, ura3-52, lys2Δ201, pep4Δ) [1].
3. pYES2/CT expression vector (ThermoFisher Scientific), which uses the pGal promoter. Derivatives that use the promoters of the genes coding for the mitochondrial ADP/ATP carrier and phosphate carrier for constitutive expression of membrane proteins.

2.2 Growth Media

1. LB media, 1% tryptone, 0.5% yeast extract, 1% NaCl.
2. SOC recovery media, 2% tryptone, 0.5% yeast extract, 10 mM NaCl, 2.5 mM KCl, 10 mM $MgCl_2$, 10 mM $MgSO_4$, 20 mM glucose.
3. Synthetic-complete uracil-dropout (SC-Ura) medium (Formedium).
4. YPG medium, 1% yeast extract, 2% tryptone, 2% glycerol.
5. YPD medium, 1% yeast extract, 2% tryptone, 2% D-glucose.

2.3 Buffers

Prepare all solutions using ultrapure water and analytical-grade reagents. Follow all local waste disposal and health and safety regulations.

1. 30% glycerol (autoclaved)
2. TE/lithium acetate buffer, 10 mM tris, pH 8.0, 1 mM EDTA, 100 mM lithium acetate.

3. PEG 4000/TE/lithium acetate buffer, 40% PEG 4000, 10 mM tris, pH 8.0, 1 mM EDTA, 100 mM lithium acetate.
4. Breaking buffer, 0.65 M sorbitol, 100 mM tris–HCl, pH 8.0, 0.2% bovine serum albumin, 5 mM EDTA, 5 mM amino hexanoic acid, 5 mM benzamidine hydrochloride.
5. Wash buffer, 0.65 M sorbitol, 100 mM tris–HCl, pH 7.4, 5 mM amino hexanoic acid, 5 mM benzamidine hydrochloride.
6. Tris-buffered glycerol (TBG), 100 mM tris–HCl, pH 7.4, 10% glycerol.
7. Solubilization buffer, 20 mM imidazole, 150 mM NaCl, 20 mM HEPES-NaOH, pH 7.4, and an EDTA-free complete protease inhibitor tablet.
8. Buffer A, 20 mM HEPES-NaOH, pH 7.4, 150 mM NaCl, 20 mM imidazole, 0.1% detergent, and 0.1 mg mL^{-1} lipid.
9. Buffer B, 20 mM HEPES-NaOH, pH 7.4, 50 mM NaCl, 0.1% detergent and 0.1 mg mL^{-1} lipid.

2.4 Reagents

1. KOD hot-start DNA polymerase kit (Merck-Millipore).
2. SYBR Safe (ThermoFisher Scientific).
3. Salmon sperm DNA (Merck-Millipore).
4. Anti-6X his tag primary antibody produced in rabbit (Abcam).
5. Goat anti-rabbit secondary antibody (Abcam).
6. Tetraoleoyl cardiolipin (18:1) (Avanti Polar Lipids).
7. Nickel sepharose high performance (Amersham Biosciences).
8. Column PD-10, empty (GE healthcare).
9. Factor Xa protease (NEB).
10. Proteus "1-step batch" midi spin column (Generon).
11. BCA assay kit (ThermoFisher Scientific).

2.5 Equipment

1. PCR thermocycler.
2. NanoDrop.
3. GenePulser II (BioRad).
4. Agarose tanks and associated powerpack.
5. SDS-PAGE dual run and blot system.
6. Equipment for the development of X-Ray film.
7. Applikon 140 Pilot System with an eZ controller (fermentation).
8. ÄKTAprime (GE Healthcare) (protein purification).
9. 2.5 liter full-baffle TunAir shake flasks (Sigma).

10. For the disruption of yeast cells, we used mechanical breaking with glass beads of 0.5–0.75 mm diameter in a Dyno-Mill (Dyno-Mill, Multi-Lab).

3 Methods

A workflow for the protocol, from molecular biology to protein purification, is presented in Fig. 1.

1. First, obtain a codon-optimized gene encoding the membrane protein to be expressed, including an N-terminal *SacI* restriction site, an "AAAAA" Kozak sequence (optimal for expression in *S. cerevisiae* [20, 21]), an octa-his tag and a Factor Xa cleavage site, and C-terminal stop codons, followed by a *XhoI* restriction site (Fig. 2). We use GenScript (www.genscript.com) for gene synthesis.
2. Ensure that the synthesized gene does not contain additional *SacI* and *XhoI* restriction sites. In addition to the recognition site of Factor Xa (IEGR), we also include the three amino acids N-terminal to the recognition site (DAA) and the four amino acids C-terminal to the cleavage site (TSED) found in the naturally occurring substrate of bovine Factor Xa, prothrombin (Uniprot code, P00735) (Fig. 2). We have found this increases specific protease activity, probably due to the avoidance of steric hindrance between Factor Xa and the detergent micelle. Factor Xa is particularly useful as the enzyme is very efficient, even at 4–10 °C, but can exhibit non-specific proteolytic activity.
3. Design PCR primers to the N- and C-terminal regions of the codon-optimized gene, including six nucleotides 5′ to the *SacI* restriction site and six 3′ to the *XhoI* restriction site to allow for efficient digestion. We try to design primers to have a predicted melting temperature of 65–70 °C, which enables us to use an annealing temperature of 60–65 °C during PCR. We have found this reduces non-specific priming. We typically clone into the pYES2/CT vector and induce protein expression using galactose. However, other systems, including constitutively active promoters, are available, and their suitability needs to be determined empirically [1, 9].

3.1 Cloning the Target Gene into pYES2/CT and Transformation into Escherichia coli XL1 Blue

1. Set up the PCR reaction as follows: KOD 10× buffer (5 μL), 25 mM $MgSO_4$ (3 μL), 2 mM dNTP (5 μL), 10 μM forward primer (1.5 μL), 10 μM reverse primer (1.5 μL), ultrapure water (32 μL), KOD DNA polymerase (1 μL), and template DNA (10–50 ng) (1 μL). Use the following PCR parameters: initial denaturation, 2 min at 95 °C; denaturation, 20 s at 95 °C; annealing, 20 s at 60–65 °C; elongation, 40 s at

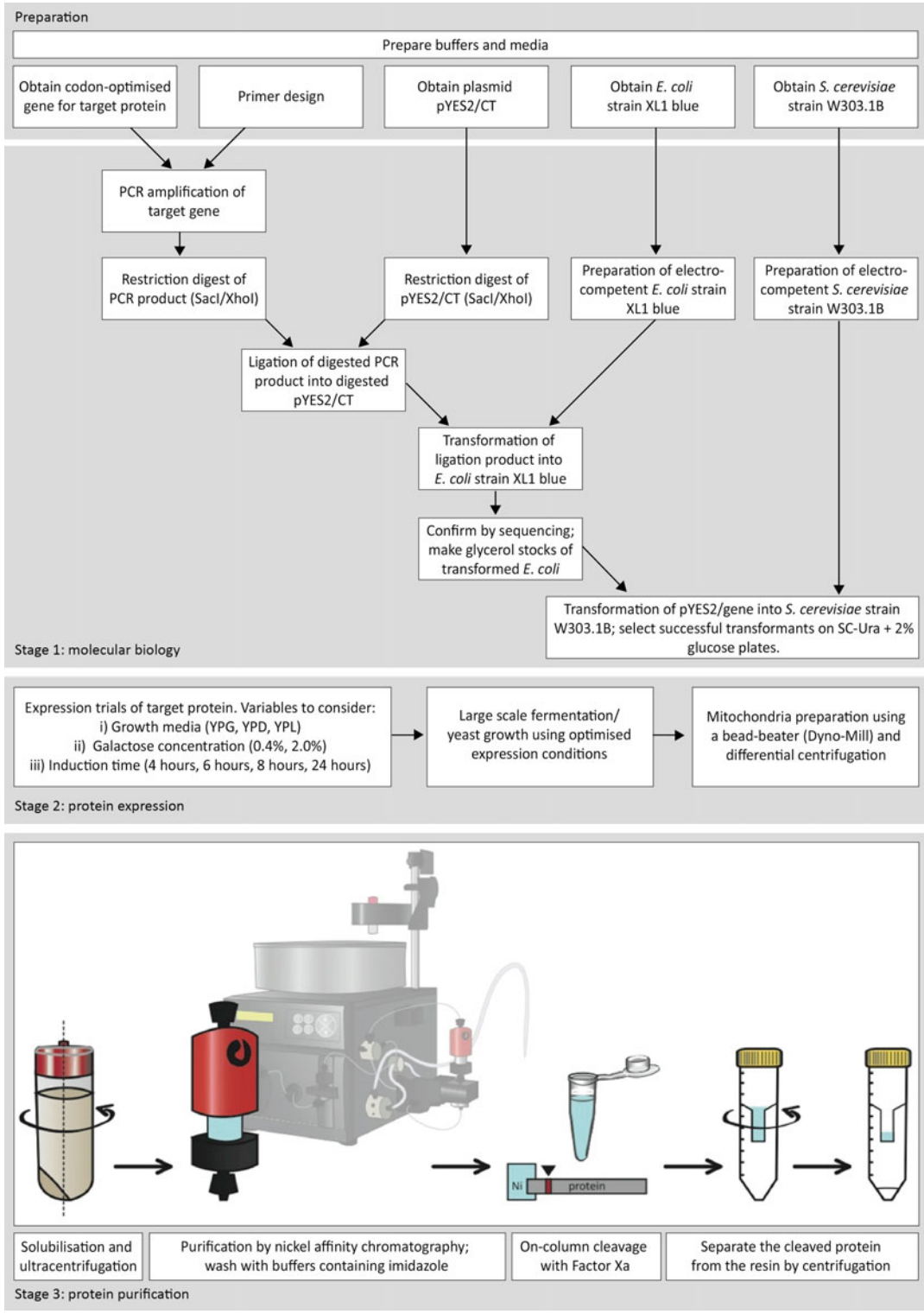

Fig. 1 Workflow

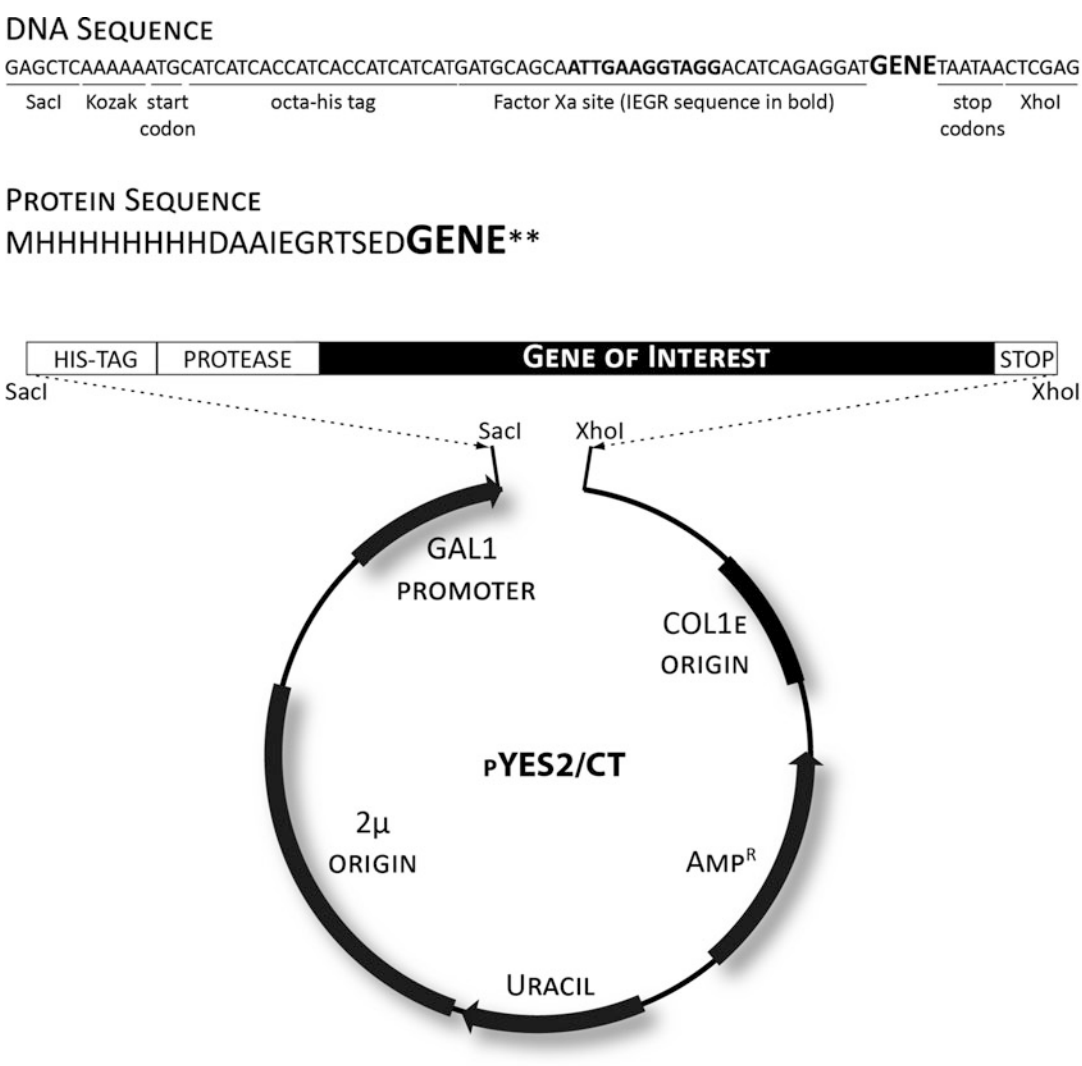

Fig. 2 Construct design. We synthesize our gene product of interest with an N-terminal extension that includes a *SacI* restriction site, an AAAAA Kozak sequence for optimal expression in *S. cerevisiae* [20, 21], an octa-his tag for nickel affinity purification, and a Factor Xa recognition site for on-column cleavage. C-terminal to the gene, we include two stop codons and a *XhoI* restriction site

70 °C; final elongation, 10 min at 70 °C. We use 30 cycles of denaturation, annealing, and elongation. Annealing temperature chosen according to the lowest T_m of the primers. Length of elongation is chosen according to the size of the expected PCR product; we typically use 40 s per 1000 bases.

2. Follow the QIAquick PCR purification protocol; elute plasmid with 50 µL pre-warmed EB buffer.
3. Run a 1% agarose gel using standard protocols to confirm PCR amplification has been successful.

4. Set up the restriction digestion reaction of both the PCR-amplified gene product and pYES2/CT vector: CutSmart buffer (5 μL), PCR product or vector (30 μL), SacI (10,000 units mL^{-1}) (2 μL), Xho (20,000 units mL^{-1}) (1 μL), ultrapure water (12 μL).
5. Incubate at 37 °C for an hour to ensure complete digestion; inactivate the restriction enzymes by incubation at 80 °C for 10 min.
6. Follow the QIAquick PCR purification protocol; elute digested gene product with 50 μL EB buffer and determine the DNA concentration.
7. Run the digested pYES2 vector on a 1% agarose gel following standard protocols; excise the top band, which represents the digested plasmid, with a sharp scalpel. Follow the QIAquick gel extraction protocol; elute plasmid with 50 μL EB buffer and determine the DNA concentration using the nanodrop.
8. Set up the ligation reaction at a 3:1 insert:vector molar ratio; use 100 ng of vector per ligation reaction, and calculate the amount of insert [amount of insert (ng) = 3 × (insert length/vector length) × amount of vector (ng)]. Use the following reaction mixture: T4 DNA ligase buffer (2 μL), vector (for a 4000 bp vector, use 100 ng DNA), insert (for a 1000 bp insert, use 75 ng DNA), T4 DNA ligase (1 μL), and ultrapure water (15 μL). These calculations are for a gene product of 1000 bp and a vector of 4000 bp.
9. Incubate at room temperature for 1 h; inactivate the enzyme by incubation at 65 °C for 10 min.
10. Transform ligated plasmid into *E. coli* XL1 blue (prepared according to the manufacturer's protocol) by electroporation. Pre-chill electrophoretic cuvettes on ice; thaw competent cells.
11. Transfer 80 μL of cells into the cuvette, add 3 μL ligation product, and mix gently by pipetting. Prepare 2 mL sterile Eppendorf tubes with 2 mL SOC media.
12. Use the following settings on a GenePulser II: voltage, 2.5 kV; capacitance, 25 uF; low-range resistance, 200 Ω; high-range resistance, infinite.
13. Place the prepared electrophoretic cuvettes into the electroporation chamber and pulse the cells; immediately add 1 mL SOC media to the cuvette and transfer back into 2 mL Eppendorf tubes.
14. Leave cells to recover at 37 °C for 1 h (without shaking).
15. Plate out 100 μL cells onto pre-warmed LB + 100 μg mL^{-1} ampicillin plates; incubate at 37 °C overnight.

16. Pick individual colonies; inoculate into LB media supplemented with 100 μg mL^{-1} ampicillin. Incubate overnight at 37 °C with shaking at 225 rpm.
17. Add 750 μL 30% autoclaved glycerol and 750 μL *E. coli* XL1 blue overnight culture in a sterile cryotube. Mix by inverting 12 times and store at −80 °C.
18. Centrifuge (3000 × *g*, 10 min, 4 °C); discard supernatant.
19. Follow the QIAprep miniprep protocol to isolate plasmid DNA. Store DNA at −20 °C for ligation into *S. cerevisiae* strain W303.1B.
20. Confirm by DNA sequencing that the gene has been successfully cloned.

3.2 Transformation in S. cerevisiae Strain W303.1B

1. Streak *S. cerevisiae* strain W303.1B from a glycerol stock onto a YPD plate; incubate at 30 °C for 3 days.
2. Set up a 5 mL culture of *S. cerevisiae* strain W303.1B in YPD; incubate at overnight at 30 °C with shaking at 225 rpm.
3. Inoculate 25 mL pre-warmed YPD media in 250 mL flasks with 1.2 mL overnight culture and incubate at 30 °C with shaking for 4 h.
4. Transfer cells into 50 mL falcon tubes; centrifuge (3000 × *g*, 10 min, 4 °C); discard the supernatant.
5. Resuspend cells in 25 mL ice-cold sterile ultrapure water by gentle pipetting; centrifuge (3000 × *g*, 10 min, 4 °C); discard the supernatant.
6. Prepare 5 mL TE/LiAc solution; keep on ice (*see* **Note 1**).
7. Resuspend cells gently in 500 μL ice-cold sterile TE/LiAc solution and keep on ice for transformation (one 25 mL culture will give five transformation reactions).
8. To a sterile 1.5 mL Eppendorf tube, add 20 μL of 2 mg/mL boiled salmon sperm carrier DNA (100 °C, 10 min), 1 μg plasmid DNA (typically 3 μL at 250–350 ng μL^{-1}) and 100 μL competent yeast cells (from **step 7**).
9. Incubate at room temperature for 10 min.
10. Prepare 5 mL PEG/TE/LiAc solution; keep on ice.
11. Add 500 μL of ice-cold sterile PEG/TE/LiAc solution to the transformation reaction and gently mix by pipetting.
12. Leave the mixture at 30 °C for 30 min.
13. Heat-shock the cells at 42 °C for 20 min.
14. Centrifuge (3000 × *g*, 3 min, room temperature); remove the supernatant and resuspend cells in 200 μL sterile water.
15. Plate out 100 μL of cells onto selection agar plates (SC-Ura + 2% glucose) and incubate at 30 °C for 48–72 h.

16. Pick individual colonies; inoculate into 2 mL SC-Ura + 2% glucose liquid media. Incubate overnight at 30 °C with shaking at 225 rpm.
17. Add 750 μL 30% autoclaved glycerol and 750 μL transformed *S. cerevisiae* overnight culture in a sterile cryotube. Mix by inverting 12 times and store at −80 °C.

3.3 Small-Scale Expression and Solubilization Trials

1. Streak the transformed *S. cerevisiae* from a glycerol stock onto a SC-Ura + 2% glucose plate; incubate at 30 °C for 3 days (*see* **Note 2**).
2. Set up a 10 mL culture in SC-Ura + 2% glucose; incubate overnight at 30 °C with shaking at 225 rpm.
3. Inoculate overnight culture into 100 mL YPG + 0.1% glucose to a starting OD_{600} of 0.2; incubate at overnight at 30 °C with shaking at 225 rpm.
4. After 16–20 h of growth, induce with galactose. Typically, we test two different concentrations (0.4 and 2.0% final galactose), each at four time-points (4, 6, 8, and 24 h) (*see* **Note 3**).
5. Transfer culture to a 50 mL falcon tube, and centrifuge (4000 × *g*, 10 min, 4 °C); discard the supernatant; add remaining culture to build up the pellet, and centrifuge (4000 × *g*, 10 min, 4 °C). Resuspend the pellet to a final volume of 30 mL MilliQ. Harvest cells as before.
6. Prepare breaking buffer (without bovine serum albumin) with added protease inhibitor tablet; use 1 tablet per 50 mL buffer. Add breaking buffer to each pellet to a total volume of 20 mL; add glass beads to a volume of 25 mL.
7. In the cold room, vortex cells with the glass beads for 2 min; rest on ice for 2 min and repeat three times (6 min total vortexing).
8. Remove cell debris and glass beads by centrifugation (4000 × *g*, 10 min, 4 °C).
9. Remove the supernatant; harvest mitochondria by centrifugation (45,000 × *g*, 30 min, 4 °C).
10. Remove the supernatant; resuspend the pellet in 2 mL TBG buffer using a homogenizer. Determine protein concentration using the BCA assay.
11. To a final volume of 500 μL, add 150 mM NaCl, 0.5 mg total protein and 2% dodecyl maltoside, 2% decyl maltose neopentyl glycol or 1% lauryl maltose neopentyl glycol (*see* **Note 4**).
12. Incubate for 1 h with rotation at 4 °C.
13. Withdraw 30 μL sample (total fraction) for SDS-PAGE analysis.

14. Transfer the remaining sample into MLA130 tubes; centrifuge (150,000 × *g*, 45 min, 4 °C).
15. Withdraw 30 μL supernatant (solubilizate) for SDS-PAGE analysis.
16. Ascertain expression and solubilization efficiency by Western blot using standard protocols. We load 10–20 μg total protein per lane, and test using an anti-His antibody (*see* **Note 5**).

3.4 Large-Scale Yeast Growth Using Fermentation

1. Set up 5 × 50 mL cultures in SC-Ura + 2% glucose; incubate overnight at 30 °C with shaking at 225 rpm (*see* **Note 6**).
2. Inoculate overnight cultures in 5 × 1 L SC-Ura + 2% glucose; incubate overnight at 30 °C with shaking at 225 rpm.
3. Inoculate 5 × 1 L secondary overnight cultures into 50 L of YPG + 0.1 glucose medium in the fermenter; incubate for 16–24 h at 30 °C with shaking at 225 rpm before induction with optimal galactose, determined from the expression trials.

3.5 Mitochondrial Preparation

1. Resuspend yeast cell pellets in 1 L of breaking buffer per 500 g of cells.
2. Lyse cells by passage through a Dyno-Mill at a flow rate of 3 L/h.
3. Centrifuge (3000 × *g*, 20 min, 4 °C); pool supernatant and discard pellet.
4. Harvest mitochondria by centrifugation (25,000 × *g*, 1 h, 4 °C); discard supernatant, and resuspend pellets in wash buffer.
5. Harvest mitochondria by centrifugation (25,000 × *g*, 1 h, 4 °C); discard supernatant, and resuspend pellets in TBG.
6. Harvest mitochondria by centrifugation (25,000 × *g*, 1 h, 4 °C); discard supernatant, and resuspend pellet to a final total protein concentration of 20 mg mL^{-1}.
7. Flash-freeze mitochondria in liquid nitrogen; store at −80 °C.

3.6 Lipid Preparation

1. Tetraoleoyl cardiolipin (18:1) is supplied as a powder in 100 mg aliquots (*see* **Note 7**).
2. Solubilize 100 mg lipid in 10 mL of 10% (w/v) detergent by vortexing for 2–3 h at room temperature to give 10 mg mL^{-1} lipid in a 10% detergent stock. Snap-freeze and store in liquid nitrogen until use (*see* **Note 8**).

3.7 Mitochondrial Membrane Protein Purification

1. Solubilize 1 g of yeast mitochondria in 1–2% detergent by mixing with solubilization buffer at 4 °C for 1 h (*see* **Note 9**).
2. Ultracentrifugation (140,000 × *g*, 45 min, 4 °C); take a sample of the solubilized fraction for SDS-PAGE/Western blot

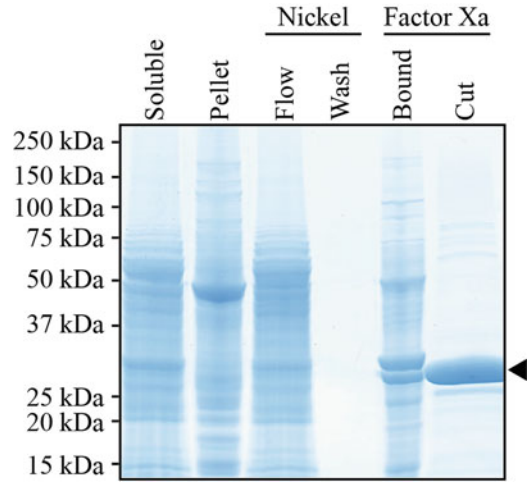

Fig. 3 SDS-PAGE analysis of the purification of a mitochondrial carrier protein. The protein (33 kDa; marked with an arrow) was heterologously expressed in *Saccharomyces cerevisiae* and purified using nickel affinity chromatography as described in Subheading 3.7. Mitochondria were solubilized in 2% dodecyl maltoside, and buffers contained 0.1 mg mL^{-1} tetraoleoyl cardiolipin. The band under the purified protein is a degradation product of the carrier, identified by mass spectrometry

analysis (Fig. 3, soluble), and resuspend the pellet to an equal volume for analysis by SDS-PAGE/Western blot (Fig. 3, pellet).

3. Load the soluble fraction onto a nickel-sepharose column at 1 mL min^{-1} on an ÄKTA prime (*see* **Note 10**); wash with 40 column volumes of buffer A, followed by 20 column volumes of buffer B, each at 3 mL min^{-1} (*see* **Note 11**). Alternatively, use batch binding: incubate the soluble fraction from **step 2** with nickel-sepharose for 1 h. Dispense into an empty PD-10 column, and collect flow-through for SDS-PAGE/Western blot analysis (Fig. 3, flow). Wash with 40 column volumes of buffer A, followed by 20 column volumes of buffer B by gravity flow; collect wash for SDS-PAGE/Western blot analysis (Fig. 3, wash).
4. Resuspend the column material with an equal volume of buffer B. Transfer to a vial containing 5 mM $CaCl_2$ and 10 μg Factor Xa and vortex thoroughly; incubate at 4 °C overnight with rotation (*see* **Note 12**).
5. Separate the cleaved protein from the resin by centrifugation (500 × *g*, 3 min, 4 °C) using a Proteus one-step purification column. Add an equal volume of buffer B as a chase, and centrifuge again. Take a sample of the flow-through for

SDS-PAGE/Western blot analysis (Fig. 3, cut). Resuspend the nickel resin to an equal volume for analysis by SDS-PAGE/Western blot (Fig. 3, bound and *see* **Note 13**).

6. Determine the protein concentration using the BCA assay or nanodrop; snap-freeze and store protein in liquid nitrogen (*see* **Note 14**).

4 Notes

1. To transform pYES2/CT into *S. cerevisiae* strain W303.1B, we use a protocol based on the lithium acetate/single-stranded carrier DNA/PEG method [22, 23]. This method is also applicable to other *S. cerevisiae* strains, including protease-deficient strains such as FGY217 and BJ2168 [1].
2. Before large-scale yeast growth and protein expression, it is important to optimize both the induction time and galactose concentration in small-scale expression trials. We have found large variations in expression levels between different conditions.
3. For proteins expressed under the control of a constitutive promoter, cells are harvested directly after approximately 18–20 h growth in YPG + 0.1% glucose.
4. It is important to ascertain whether protein can be solubilized from the mitochondrial membrane; insoluble protein is often indicative of protein-misfolding and aggregation. Typically, we test three detergents in solubilization assays: dodecyl maltoside, decyl maltose neopentyl glycol, and lauryl maltose neopentyl glycol [24]. We have found that the neopentyl glycol detergents are particularly stabilizing for small, alpha-helical membrane proteins, such as the mitochondrial carriers [5, 25]. The concentration of detergent needed for efficient solubilization is determined empirically.
5. If the protein is not expressed, many variables can be tested, as reviewed in [1].
6. After optimization of expression, we use fermentation to scale up yeast growth. We typically get about 700–900 g of yeast cells from a 50-L fermenter run after 20–24 h growth (including a 4-hour induction with 0.4% galactose final concentration) when grown in YPG + 0.1% glucose. From this, we routinely get approximately 1 g of an enriched mitochondrial fraction per 100 g of yeast cells, and approximately 1–3 mg purified protein per gram of enriched mitochondrial fraction.
7. We have found that lipid addition to the purification buffers is critical to ensure high yields of functional protein. Cardiolipin supplementation is especially important during the purification

of mitochondrial carriers. The structure of the ADP/ATP carrier has shown that cardiolipin is tightly bound [6, 7], and it is thought that cardiolipin is an important structural and functional element of all mitochondrial carriers [26], including uncoupling protein [27]. Other mitochondrial membrane proteins may have different lipid requirements [28]; these need to be determined empirically. Lipids supplied as a powder are extremely hygroscopic; we use an entire aliquot to prepare stocks. Lipids solubilized in chloroform are also available and are preferred when using small amounts.

8. Prepare lipids in the detergent to be used for protein purification.
9. Suitable detergents need to be empirically determined for each protein tested; we typically use either dodecyl maltoside or lauryl maltose neopentyl glycol for initial purification trials. Increasing the concentration of imidazole in the solubilization buffer reduces contaminant-binding but may also reduce binding of the target protein.
10. In order to increase purity and yield, it is important to "match" the amount of nickel resin used during binding with the amount of target protein. Too much nickel resin may increase contaminant-binding; too little may result in incomplete binding.
11. The concentration of imidazole used in both the solubilization and wash buffers can be further optimized.
12. Cleavage conditions need to be determined empirically. For example, addition of 10–20 mM imidazole to the cleavage reaction increases efficiency of cleavage, as Factor Xa can loosely associate with the resin. Depending on protein stability, the cleavage time and temperature may need to be optimized further. We have also used other proteases with great success, most notably TEV protease, which has the recognition site ENLYFQS. TEV protease is more specific than Factor Xa and is our protease of choice when Factor Xa non-specifically cleaves the gene product.
13. It is important to use SDS-PAGE/Western blotting to ascertain if the protein is being cleaved efficiently by the protease, and if protein is bound to the resin after cleavage and separation by centrifugation, which is indicative of protein unfolding.
14. After optimization, protein purified using this protocol is typically 90–95% pure (Fig. 3); additional steps, such as size exclusion chromatography, can increase purity further.

Acknowledgment

This research was supported by the Medical Research Council (grant MC_UU_00015/1). We thank Drs. Homa Majd and Chancievan Thangaratnarajah for help with preparing figures 1 and 2, respectively.

References

1. Routledge SJ, Mikaliunaite L, Patel A, Clare M, Cartwright SP, Bawa Z, Wilks MDB, Low F, Hardy D, Rothnie AJ, Bill RM (2016) The synthesis of recombinant membrane proteins in yeast for structural studies. Methods 95:26–37. https://doi.org/10.1016/j.ymeth.2015.09.027
2. King MS, Boes C, Kunji ER (2015) Membrane protein expression in *Lactococcus lactis*. Methods Enzymol 556:77–97. https://doi.org/10.1016/bs.mie.2014.12.009
3. Contreras-Gomez A, Sanchez-Miron A, Garcia-Camacho F, Molina-Grima E, Chisti Y (2014) Protein production using the baculovirus-insect cell expression system. Biotechnol Prog 30(1):1–18. https://doi.org/10.1002/btpr.1842
4. Goehring A, Lee C-H, Wang KH, Michel JC, Claxton DP, Baconguis I, Althoff T, Fischer S, Garcia KC, Gouaux E (2014) Screening and large-scale expression of membrane proteins in mammalian cells for structural studies. Nat Prot 9(11):2574–2585. https://doi.org/10.1038/nprot.2014.173
5. King MS, Kerr M, Crichton PG, Springett R, Kunji ER (2016) Formation of a cytoplasmic salt bridge network in the matrix state is a fundamental step in the transport mechanism of the mitochondrial ADP/ATP carrier. Biochim Biophys Acta 1857:14–22. https://doi.org/10.1016/j.bbabio.2015.09.013
6. Ruprecht JJ, Hellawell AM, Harding M, Crichton PG, Mccoy AJ, Kunji ERS (2014) Structures of yeast mitochondrial ADP/ATP carriers support a domain-based alternating-access transport mechanism. Proc Natl Acad Sci U S A 111(4):E426–E434. https://doi.org/10.1073/Pnas.1320692111
7. Ruprecht JJ, King MS, Zogg T, Aleksandrova AA, Pardon E, Crichton PG, Steyaert J, Kunji ERS (2019) The molecular mechanism of transport by the mitochondrial ADP/ATP carrier. Cell 176(3):435–447. https://doi.org/10.1016/j.cell.2018.11.025
8. Bamber L, Harding M, Butler PJG, Kunji ERS (2006) Yeast mitochondrial ADP/ATP carriers are monomeric in detergents. Proc Natl Acad Sci U S A 103(44):16224–16229. https://doi.org/10.1073/Pnas.0607640103
9. Bamber L, Harding M, Monné M, Slotboom DJ, Kunji ERS (2007) The yeast mitochondrial ADP/ATP carrier functions as a monomer in mitochondrial membranes. Proc Natl Acad Sci U S A 104(26):10830–10834
10. Bamber L, Slotboom DJ, Kunji ERS (2007) Yeast mitochondrial ADP/ATP carriers are monomeric in detergents as demonstrated by differential affinity purification. J Mol Biol 371(2):388–395
11. Crichton PG, Harding M, Ruprecht JJ, Lee Y, Kunji ERS (2013) Lipid, detergent, and Coomassie Blue G-250 affect the migration of small membrane proteins in blue native gels; mitochondrial carriers migrate as monomers not dimers. J Biol Chem 288(30):22163–22173. https://doi.org/10.1074/Jbc.M113.484329
12. Palmer SM, Kunji ERS (2012) Online monitoring of biomass accumulation in recombinant yeast cultures. Methods Mol Biol 866:165–179. https://doi.org/10.1007/978-1-61779-770-5_14
13. Palmer SM, Kunji ERS (2012) Online analysis and process control in recombinant protein production (review). Methods Mol Biol 866:129–155. https://doi.org/10.1007/978-1-61779-770-5_12
14. Thangaratnarajah C, Ruprecht JJ, Kunji ERS (2014) Calcium-induced conformational changes of the regulatory domain of human mitochondrial aspartate/glutamate carriers. Nat Commun 5. https://doi.org/10.1038/ncomms6491
15. Majd H, King MS, Palmer SM, Smith AC, Elbourne LD, Paulsen IT, Sharples D, Henderson PJ, Kunji ER (2018) Screening of candidate substrates and coupling ions of transporters by thermostability shift assays. elife 7. https://doi.org/10.7554/eLife.38821
16. Harborne SPD, King MS, Crichton PG, Kunji ERS (2017) Calcium regulation of the human mitochondrial ATP-Mg/Pi carrier SLC25A24 uses a locking pin mechanism. Sci Rep

7:45383. https://doi.org/10.1038/srep45383

17. Hofherr A, Seger C, Fitzpatrick F, Busch T, Michel E, Luan JT, Osterried L, Linden F, Kramer-Zucker A, Wakimoto B, Schutze C, Wiedemann N, Artati A, Adamski J, Walz G, Kunji ERS, Montell C, Watnick T, Kottgen M (2018) The mitochondrial transporter SLC25A25 links ciliary TRPP2 signaling and cellular metabolism. PLoS Biol 16(8). https://doi.org/10.1371/journal.pbio.2005651
18. Tavoulari S, Thangaratnarajah C, Mavridou V, Harbour ME, Martinou JC, Kunji ER (2019) The yeast mitochondrial pyruvate carrier is a hetero-dimer in its functional state. EMBO J 38(10). https://doi.org/10.15252/embj.2018100785
19. Hashimoto M, Shinohara Y, Majima E, Hatanaka T, Yamazaki N, Terada H (1999) Expression of the bovine heart mitochondrial ADP/ATP carrier in yeast mitochondria: significantly enhanced expression by replacement of the N-terminal region of the bovine carrier by the corresponding regions of the yeast carriers. Biochim Biophys Acta Bioenerg 1409 (3):113–124. https://doi.org/10.1016/S0005-2728(98)00155-8
20. Dvir S, Velten L, Sharon E, Zeevi D, Carey LB, Weinberger A, Segal E (2013) Deciphering the rules by which 5′-UTR sequences affect protein expression in yeast. Proc Natl Acad Sci U S A 110(30):E2792–E2801. https://doi.org/10.1073/pnas.1222534110
21. Hamilton R, Watanabe CK, de Boer HA (1987) Compilation and comparison of the sequence context around the AUG startcodons in Saccharomyces cerevisiae mRNAs. Nucleic Acids Res 15(8):3581–3593
22. Gietz RD, Schiestl RH (2007) High-efficiency yeast transformation using the LiAc/SS carrier DNA/PEG method. Nat Protoc 2(1):31–34. https://doi.org/10.1038/nprot.2007.13
23. Gietz RD, Woods RA (2002) Transformation of yeast by lithium acetate/single-stranded carrier DNA/polyethylene glycol method. Methods Enzymol 350:87–96
24. Chae PS, Rasmussen SG, Rana RR, Gotfryd K, Chandra R, Goren MA, Kruse AC, Nurva S, Loland CJ, Pierre Y, Drew D, Popot JL, Picot D, Fox BG, Guan L, Gether U, Byrne B, Kobilka B, Gellman SH (2010) Maltose-neopentyl glycol (MNG) amphiphiles for solubilization, stabilization and crystallization of membrane proteins. Nat Methods 7 (12):1003–1008. https://doi.org/10.1038/nmeth.1526
25. Crichton PG, Lee Y, Ruprecht JJ, Cerson E, Thangaratnarajah C, King MS, Kunji ER (2015) Trends in thermostability provide information on the nature of substrate, inhibitor, and lipid interactions with mitochondrial carriers. J Biol Chem 290(13):8206–8217. https://doi.org/10.1074/jbc.M114.616607
26. Klingenberg M (2009) Cardiolipin and mitochondrial carriers. Biochim Biophys Acta 1788 (10):2048–2058
27. Lee Y, Willers C, Kunji ER, Crichton PG (2015) Uncoupling protein 1 binds one nucleotide per monomer and is stabilized by tightly bound cardiolipin. Proc Natl Acad Sci U S A 112(22):6973–6978. https://doi.org/10.1073/pnas.1503833112
28. Horvath SE, Daum G (2013) Lipids of mitochondria. Prog Lipid Res 52(4):590–614. https://doi.org/10.1016/j.plipres.2013.07.002

Chapter 5

Membrane Protein Expression in Insect Cells Using the Baculovirus Expression Vector System

Jacques Boivineau, Matthias Haffke, and Veli-Pekka Jaakola

Abstract

Integral membrane proteins have a critical role in fundamental biological processes; they are major drug targets and therefore of high research interest. Recombinant protein production is the first step in the protein tool generation for biochemical and biophysical studies. Here, we provide simplified protocols that facilitate the generation of high-quality virus and initial expression analysis for integral membrane protein targets utilizing the baculovirus-mediated expression system in insect cells. The protocol steps include generation of viruses, virus quality control, and initial expression trials utilizing standard commercial baculovirus vector systems and are exemplified for G protein-coupled receptor targets. The viral quality, quantity, and recombinant protein expression are evaluated by microscopy, flow cytometry, fluorimetry, and SDS-PAGE, using either covalently fused fluorescent proteins or co-expressed fluorescence markers. Moreover, integral membrane protein expression levels, approximate molecular mass, and stability can be evaluated from small-scale expression and purification trials.

Key words Baculovirus, GPCRs, G protein-coupled receptors, Insect cells, Integral membrane protein, Sf9, *Spodoptera frugiperda*

1 Introduction

Integral membrane proteins (IMPs) such as G protein-coupled receptors (GPCRs; also known as heptahelical transmembrane (TM) proteins or 7TM), ion channels, transporters, and nuclear hormone receptors play key roles in physiology and are important therapeutic targets in the human body. It is estimated that GPCRs are targeted by more than 25% of currently prescribed drugs [1]. For instance, 6 drugs out of the top 10 and 60 of the top 200 most-selling drugs in the USA modulate GPCRs with estimated annual multibillion dollar sales [1]. GPCRs transmit signals from outside of cells through the biological lipid bilayer membrane to the G proteins, which amplify the signal and activate various downstream effectors. This leads to a biological response within

Camilo Perez and Timm Maier (eds.), *Expression, Purification, and Structural Biology of Membrane Proteins*, Methods in Molecular Biology, vol. 2127, https://doi.org/10.1007/978-1-0716-0373-4_5,

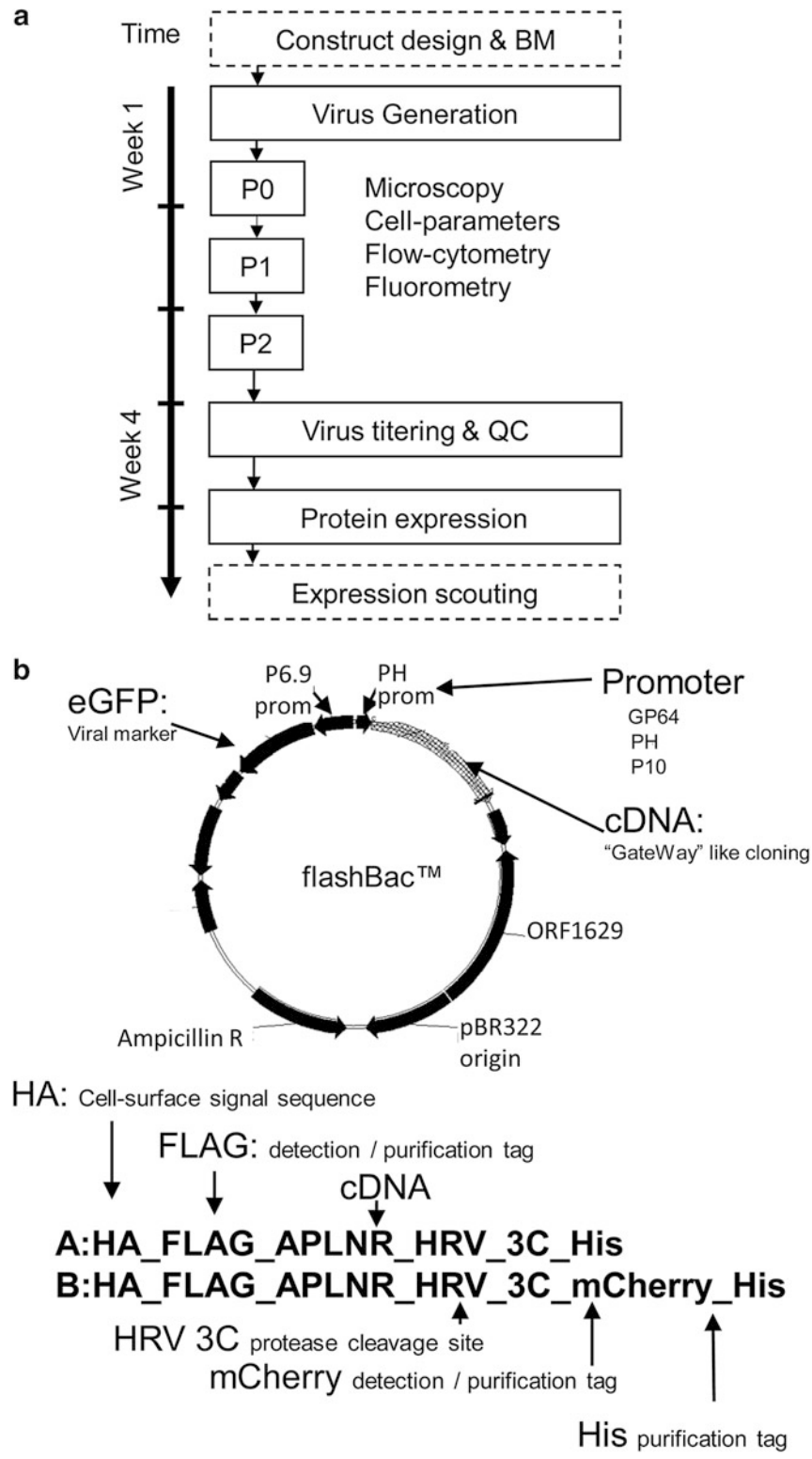

Fig. 1 Virus generation flowchart and molecular biology. (**a**) Pipeline for virus generation and initial protein expression test of IMP target with expected timelines. The dashed boxed are not included in the method

cells, signal transmission from cell to cell or even between different organs [2].

Nevertheless, until recently, rational structure-based drug discovery approaches for GPCRs have been very limited when compared to soluble proteins. This has been due to poor structural and biophysical understanding of ligand and protein–protein interactions for GPCRs at the molecular level. However, the field has changed dramatically in recent years due to a series of technical developments in GPCR protein chemistry and in structure elucidation tools: development of better insect- and mammalian-based expression systems, chaperone antibody generation, receptor mutagenesis for receptor conformational trapping and enhanced thermostability, fusion proteins, chemical stabilization for crystallogenesis, and improvement of cryo-EM resolution by direct detection cameras, to mention some examples [3, 4].

The first crucial step for structural biophysics, direct protein-based target engagement, and screening assays is the protein tool generation. Both mammalian- and insect cells-based expression systems have turned out to be very efficient for IMPs/GPCRs [4]. For instance, structures of 64 nominated by the GPCR community have been solved by X-ray crystallography and cryo-EM (https://gpcrdb.org/). More than 80% of these structures are obtained from recombinant proteins expressed in insect cell lines *Spodoptera frugiperda* 9 (Sf9) and *Trichoplusia ni* (Tni) (https://zhanglab.ccmb.med.umich.edu/GPCR-EXP/).

In this protocol, we describe how the baculovirus-mediated expression system can be used to produce highly infectious virus (Subheadings 3.1 and 3.2, Fig. 1) followed by a simple and fast expression analysis (Subheading 3.3, Figs. 2 and 3). The protocol is

Fig. 1 (continued) sections. (**b**) Upper panel: Backbone of flashBAC™ expression vector used for expression and purification of IMP/GPCR target. A target named as APLNR (Uniprot: P35414) is shown as example. Cloning is done by Type 2 restriction enzymes (golden gate cloning), i.e., any construct can be cloned starting directly from a PCR product. The eGFP under p6.9 promoter is used as transient viral marker. Early to late promoters (GP64, P10, and PH (polyhedrin)) can be used for screening optimal expression conditions. Lower panel: A: The expression cassette contains an N-terminal hemagglutinin tag (HA), which allows proper trafficking of the receptor to the plasma membrane, a FLAG tag used for detecting expression of GPCRs and sometimes in purification, the cDNA encoding the receptor (example as APLNR), a human rhinovirus 3C protease cleavage site sequence (HRV 3C) and 10 × His tag for purification. B: Shows a slightly modified expression cassette wherein the 3′ end of the GPCR is followed by mCherry fluorescent protein tag (mCherry) followed by 10 × His tag. The covalently fused mCherry is used for direct detection during expression and purification as well as characterization (i.e., thermostability, *see* Fig. 3). The anti-mCherry RFP-Trap® can be used as purification tag and eGFP as FRET pair for mCherry. The expression level and purification yields can be converted by comparing to known fluorescence standard protein concentrations (e.g., eGFP/mCherry proteins from BioVision). The fluorescence tags can be removed during the purification or preferably non-fluorescence tagged protein is used after initial screeningd

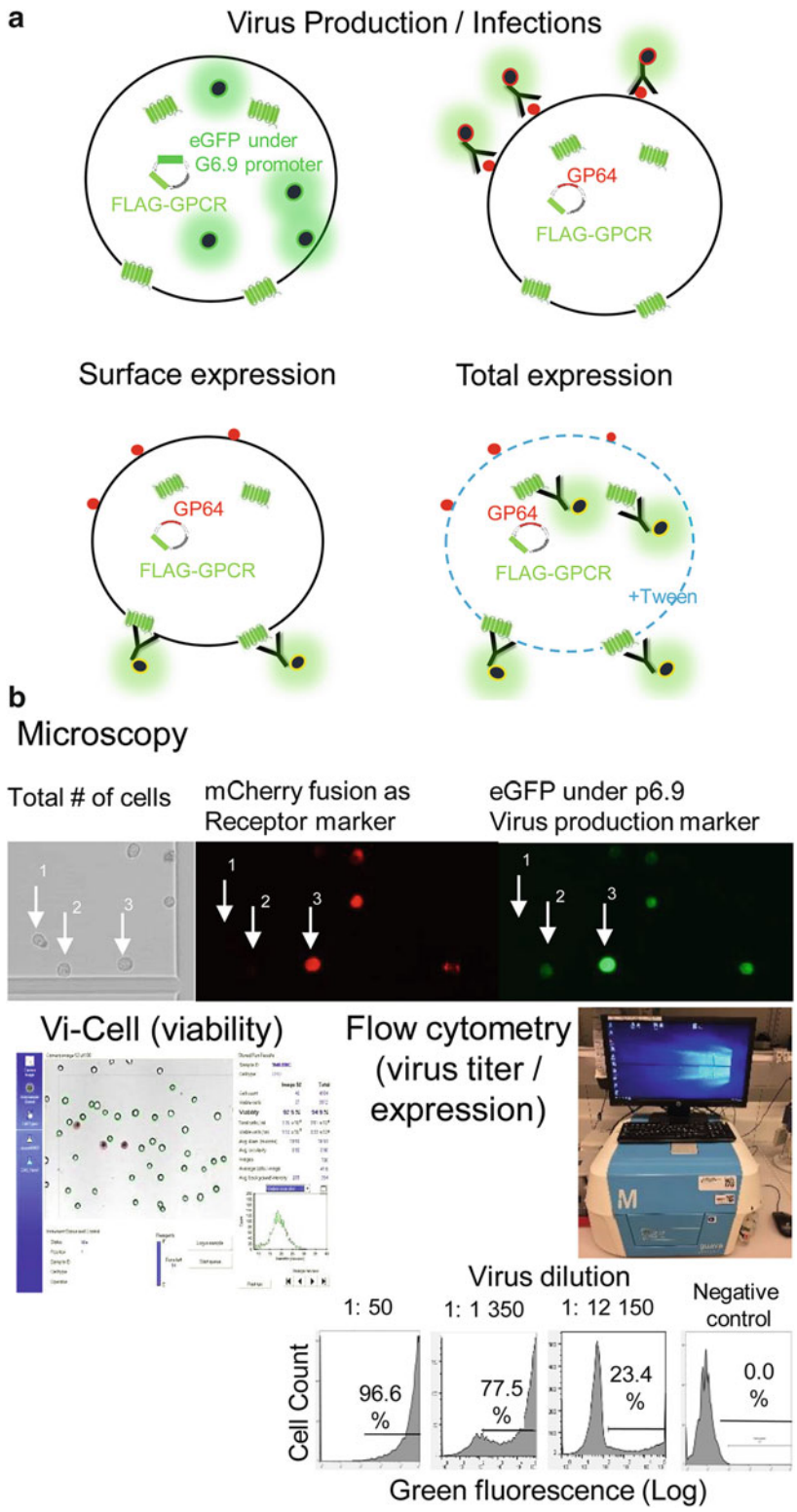

Fig. 2 Virus generation and cell expression analysis. (**a**) Fluorescence protein setup for virus and protein characterization. Upper panel: Left, eGFP fluorescent protein expressed under p6.9 virus can be used as viral

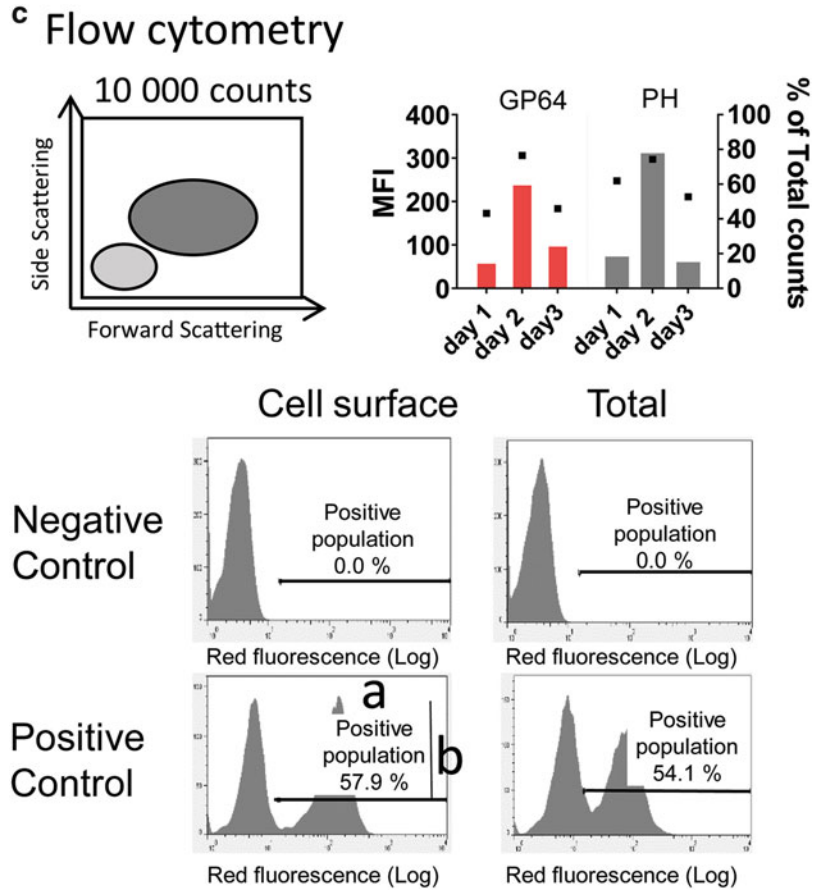

Fig. 2 (continued) expression marker and for indirect virus titering. Right, GP64 virus marker is expressed and localized in the plasma membrane after successful virus entry. The anti-GP64-Alexa488 antibody can be used as viral expression marker. Lower panel: Right, the direct recombinant protein expression can be followed with an anti-FLAG fluorescence conjugate and/or translationally fused fluorescence protein. Left, the degree of cell surface expression relative to intracellular expression is qualitatively estimated by using 1% Tween 20 for permeabilization. (**b**) Typical virus and protein expression analytics. Upper panel: Epi-fluorescence microscopy is used to characterize virus and protein expression based on fluorescence markers and cell morphology change upon viral expression. Left, brightfield-microscopy image ($\times$40), middle, red fluorescence image and right, green fluorescence image. Three individual Sf9 cells are highlighted with arrows showing a different pattern of fluorescence markers, cell swelling, and fluorescence intensities. Lower panel: Left, Vi-cell™ instrument is used for viability and cell counting by Trypan blue cell count (screen-capture of typical analysis is shown). The instrument also estimates the average cell diameter that can indicate viral infection. Right, Guava™ flow cytometry is used for viral titering and cell surface expression analysis. Typically different virus volumes are used to infect a fixed number of cells followed by analysis with antibodies and/or fluorescent markers to calculate virus titers and protein expression levels. (**c**) Typical examples of flow cytometry analysis. Upper panel: left, fixed number of particles is counted and gated based on particle size/dimension and fluorescence signals/intensities using fluorescence channels. Lower panel, using different gating, fluorescence intensities from markers (e.g., fused mCherry) and positive/negative controls, expression profiles such as expression levels and number of cells transfected can be extracted from the data (line a, population marked as positive expressing cells; line b, expression level is estimated from intensity of the marker). Upper: right, typical report of the expression data comparing two promoters and expression times with constant MOI/viral dilution

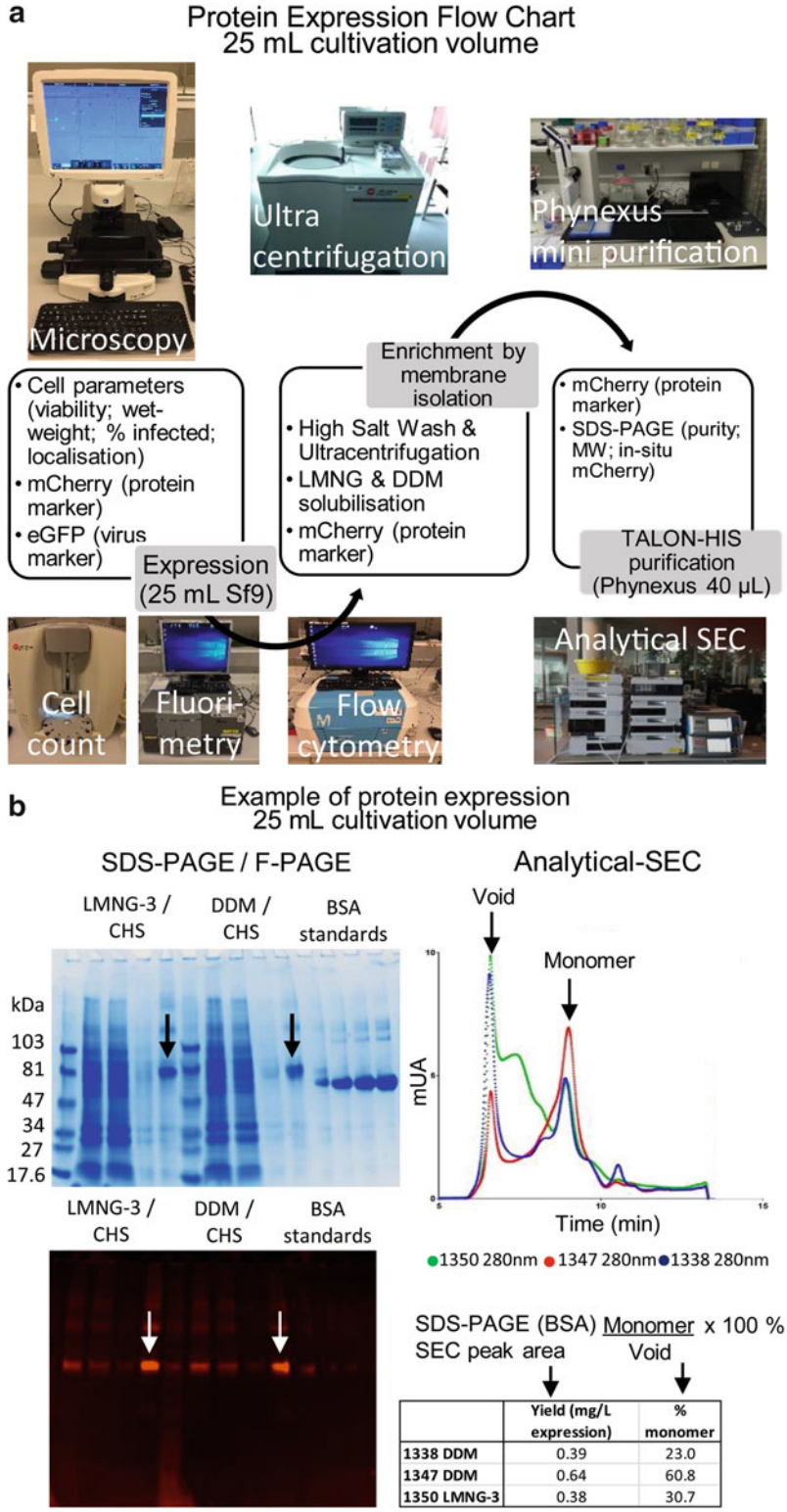

	Yield (mg/L expression)	% monomer
1338 DDM	0.39	23.0
1347 DDM	0.64	60.8
1350 LMNG-3	0.38	30.7

Fig. 3 Protein expression and analytics. (**a**) Schematic representation of the steps for protein expression and purification from insect cells and analysis. Main parameters and typical instruments used in each step are

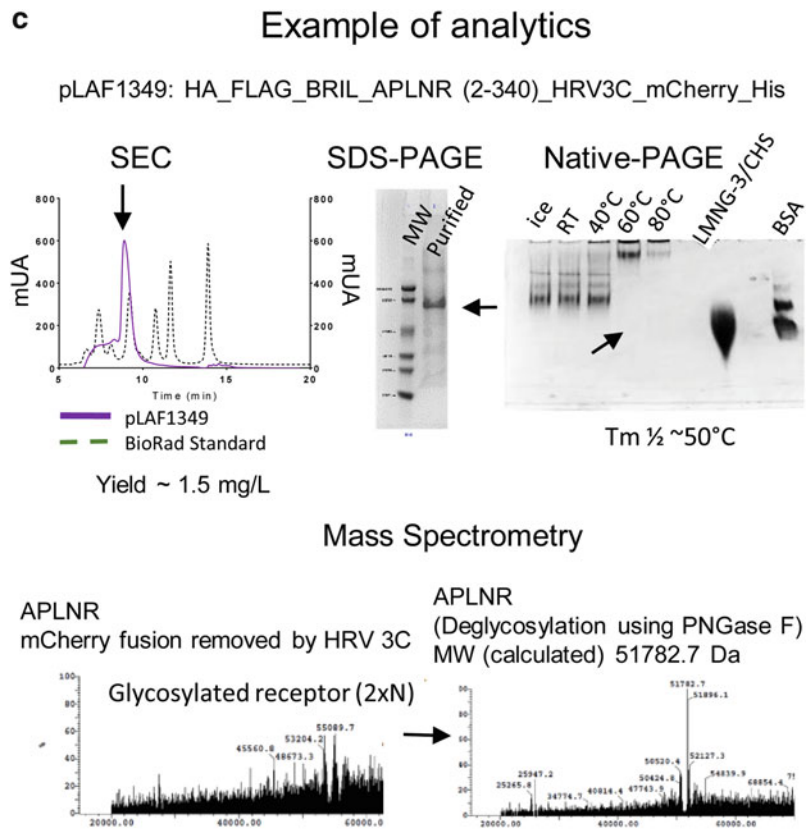

Fig. 3 (continued) shown. See text for details. (**b**) Anticipated results from the 25 mL protein expression screening using potent virus (10^9 virus/mL), 2×10^6 cells/mL, and a medium-expression protein. See text for details (APLNR target screening is used as example). Left, SDS-PAGE and fluorescence-SDS-PAGE is used to follow up the protein at different purification steps. Extractions with LMNG-3/CHS (lanes 2–5) and DDM/CHS (lanes 7–10) are shown. Lanes 2 and 7 show the input samples, lanes 3 and 8 the flow-through. Lanes 4 and 9 show the wash step. Samples from the elution step were loaded on lanes 5 and 10. Arrows indicate protein eluted from 40 μL TALON matrix. The yields from a medium-expression target allow full analysis using SDS-PAGE, mass spectrometry, SEC, and initial thermostability. Right, analytical-SEC profile of purified GPCR targets from 25 mL screening expression (different constructs vs. detergent). Yields, oligomerization, and monodispersity can be estimated from the peak profiles. (**c**) Typical example of scaled up protein expression and purification (1 L). Construct "pLAF1349" of APLNR protein was scaled up to 1 L expression scale, based on 25 mL screening results. The expression and purification were done in identical conditions as for small-scale. Typical analysis includes SEC, SDS-PAGE, estimation of aggregation and thermostability by different methods, and confirmation of protein identity by intact-MS. We typically enzymatically remove the mCherry tag (HRV 3C protease) and deglycosylate (PNGase F) the protein sample prior to MS analysis to obtain a more accurate protein mass (sample in the left is showing high degree of heterogeneity/different types of N-glycosylation)

adaptable to any standard protein laboratory and easily scalable to produce high-quality protein for structural biophysics (Fig. 3). The protocol can be modified to a high-throughput format or scaled up to 10 L volumes typically delivering more than 10 mgs of isolated protein (Fig. 3).

2 Materials

2.1 Materials for Virus Generation

1. Insect cell growth medium, such as Sf-900™ III SFM (Life Technologies), SF-4 Baculo Express ICM (BioConcept), Grace's insect medium with L-Glutamine.
2. 10% Fetal Calf Serum (FCS)-insect cell growth medium: take 900 mL of insect cell growth medium and add 100 mL of fetal calf serum, heat inactivated. Filter the medium through 0.22 μm under a laminar flow hood. Store at 4 °C.
3. Insect cells in log phase of growth in suspension.
4. Transfection agent compatible with insect cells, such as polyethylenimine (PEI) (Polysciences, Inc., Cat. Number 23966) dissolved in water at 1 mg/mL, Cellfectin® (Life Technologies), Fugene HD (Promega).
5. FlashBac Gold baculovirus expression system (Oxford Expression Technologies Ltd).
6. DNA vector with the gene of interest must be compatible with the flashBac baculovirus expression system (pIEx/Bac™-3/"flashBAC"-based expression vector).
7. Water bath.
8. Sterile water.
9. Sterile microcentrifuge tubes.
10. Incubator at 27 °C, with and without shaker for flasks.
11. Laboratory sealing film.
12. 12-well plate, non-cell binding.
13. Bioreactors, e.g., Erlenmeyer flasks with vented caps, 24-well plates, 50 mL tubes with vented caps.
14. Centrifuge with cooling system.
15. Microscope, with fluorescence imaging capabilities.
16. Light protective (dark/amber) 15 mL and 50 mL tubes.
17. Trypan blue and microscope counting chambers (hemocytometers) or cell counting instrument.
18. 0.22 μm filter tubes and bottles.

2.2 Material for Virus Quality Control, Titering, and Storage

1. Bioreactors: Erlenmeyer flasks with vented caps, 24-well deep-well plate.
2. Insect cell growth medium.
3. Insect cells on a log phase in suspension.
4. Virus stock solutions previously amplified.
5. Incubator at 27 °C, with shaker for flasks/50 mL tubes.
6. Anti-gp64 fluorescent-label-conjugated antibody (Expression Systems, Cat. Number 97201).
7. Antibody (Sigma-Aldrich, Cat. Number F1804-5MG) against the FLAG epitope label, conjugated with PerCP/Cy5.5 conjugation kit (AbCam, Cat. Number ab102911).
8. PBS 1× pH 7.4.
9. Assay plate, 96-well U-bottom.
10. Porous sheet, such as AirPore Tape Sheets (Qiagen).
11. Trypan blue and microscope counting chambers (hemocytometers) or cell counting instrument.
12. PBS-4% (w/v) BSA: Dissolve 2 g of bovine serum albumin (BSA) into 50 mL PBS 1× pH 7.4. Filter through 0.22 μm filter.
13. Benchtop flow cytometer.
14. Fluorimeter (optional).
15. Freezing medium: Mix 85% of cell culture medium, 5% glycerol, 10% fetal calf serum. Filter the medium through 0.22 μm filter under a laminar flow hood. Store at 4 °C.
16. Cryo-vials of 1.5 mL to 2 mL.

2.3 Material for Protein Expression

1. Bioreactors: Erlenmeyer flasks with vented caps, 24-well deep-well plate.
2. Insect cell growth medium.
3. Insect cells in log phase growth in suspension.
4. Virus stock solutions, previously amplified.
5. Incubator at 27 °C, with shaker for flasks/50 mL tubes.
6. Trypan blue and microscope counting chambers (hemocytometers) or cell counting instrument.
7. Centrifuge with cooling system.
8. Polytron PT1300D (Kinematica, Cat. Number PT1300D).
9. Hypotonic buffer: 10 mM HEPES-NaOH, pH 7.5, 10 mM $MgCl_2$, 20 mM KCl and EDTA-free protease inhibitor cocktail.

10. Solubilization solution: 10% (w/v) glycerol, 10% (w/v) lauryl maltose neopentyl glycol-3 (LMNG-3)/2% (w/v) cholesteryl hemisuccinate (CHS).
11. Wash buffer: 50 mM HEPES-NaOH, pH 7.5, 800 mM NaCl, 10% (w/v) glycerol, 20 mM imidazole, 0.01% (w/v) LMNG-3/0.002% (w/v) CHS.
12. Elution buffer: 50 mM HEPES-NaOH, pH 7.5, 800 mM NaCl, 10% (w/v) glycerol, 300 mM imidazole, 0.01% (w/v) LMNG-3/0.002% (w/v) CHS.
13. IMAC resin such as TALON Superflow Metal Affinity Resin (Clontech).
14. Imidazole.
15. Ultracentrifuge with polycarbonate tubes.
16. SDS-PAGE equipment and buffer (1× Tris-Glycine SDS buffer).
17. Analytical-SEC buffer: 50 mM MES-NaOH, pH 6.0, 500 mM NaCl, 0.01% (w/v) LMNG-3, filtered through 0.1 μm.
18. 1× PBS.
19. Balance.
20. Primary antibody against the protein of interest, conjugated to a fluorescent label. If the antibody does not have a fluorescent label, prepare the antibody using a conjugation kit, such as the PerCP/Cy5.5 Conjugation kit (AbCam, Cat. Number ab102911) and follow the manufacturer's instructions. Dilute the antibody at the correct concentration, according to the manufacturer's instructions or experimental data.
21. Assay plate, 96-well U-bottom.
22. PBS-4% (w/v) BSA: Dissolve 2 g of BSA into 50 mL PBS 1× pH 7.4. Filter through 0.22 μm filter.
23. Benchtop flow cytometer.
24. Fluorimeter.

3 Methods

3.1 Generation of BaculoVirus Expression System Using the FlashBAC System

In this section, we describe the generation of highly potent virus for GPCR targets. A general pIEx/Bac™-3/"flashBAC"-based expression vector has been described for various IMP/GPCR targets [4]. The constructs of interest are amplified by using PCR with *LguI* restriction sites at 5′ and 3′ ends of the gene, respectively. Shown in Fig. 1b is the expression cassette that contains an N-terminal hemagglutinin (HA) tag, which allows trafficking of the construct to the plasma membrane, a FLAG tag that is used for detection of proteins or which can be used for purification as

well, cDNA, followed by HRV 3C protease cleavage sequence, and a 10 histidine residues (10× His) tag. Typically, as shown in Fig. 1b, mCherry fluorescence protein (mCherry) fusions with the same tags are cloned in parallel to aid fast construct screening. The flashBAC vector has enhanced green fluorescence protein (eGFP) tag under a p6.9 promoter as viral expression marker. It is advisable to test different promoters (Polyhedrin PH, GP64 and P10) and several sets of constructs to obtain optimal expression profiles for the individual constructs/targets (time, yield, and quality). We typically produce P2 viruses before starting expression testing (Subheading 3.2).

3.1.1 Generation of P0 Virus Stock

1. Incubate the DNA carrying the gene of interest for 1 h in a water bath at 55 °C the day before the experiment to sterilize it. Prepare a minimum of 2 μL of plasmid DNA at a final concentration of 100 ng/μL in sterile water and then keep it at 4 °C.
2. Prepare the flashBac transfection mix in a sterile 1.5 mL microcentrifuge tube per construct: 360 μL insect cell growth medium; 1.8 μL of flashBac Gold baculovirus Expression System viral DNA; 1.8 μL of Transfection agent, 1.8 μL of DNA vector.
3. Prepare a negative control: 360 μL + (3 × 1.8) μL = 365.4 μL of insect cell growth medium. Gently tap the tube with fingers (2–3 times) and incubate at room temperature for 30 min. Tap the tube two to three times during the incubation time.
4. Meanwhile, prepare 0.75×10^6 insect cells per construct in a sterile centrifuge tube and spin down for 3 min at 100 × *g*, 21 °C. Discard the supernatant and resuspend the cells at 0.5×10^6 cells/mL in insect cell growth medium.
5. In a 12-well plate, pipette 1.5 mL (i.e., 0.75×10^6 cells) of cells per well. Incubate 10–30 min without shaking to let them settle down and immobilize as a monolayer (check under microscope).
6. Remove the medium by taking care not to disturb the cells and add the flashBac transfection mix (365 μL). Incubate 5 h at 27 °C without shaking.
7. After incubation, add 2000 μL of 10% FCS-insect cell growth medium to all wells. Close the plate with laboratory sealing film. Incubate for 5 days at 27 °C, in a wet environment (to prevent evaporation) without shaking.
8. After 5 days, check the cells under the microscope. For the constructs in which there is no fluorescence marker, this will only enable to see the shape of the cells (*see* **Note 1**). Collect the supernatant of each construct in a dark 15 mL centrifuge tube (P0) without disturbing the cells. Store at 4 °C.

9. Add 2000 μL of insect cell growth medium supplemented with 10% FCS to the cells. Close the plate with laboratory sealing film and incubate 3 days at 27 °C, in a humid environment (to prevent evaporation), without shaking.
10. After 3 days, check the cells under the microscope. For the constructs in which there is no fluorescence marker, this will only enable to see the shape of the cells (*see* **Note 1**). Collect the supernatant of each construct in a dark 15 mL centrifuge tube (P0 backup). Store at 4 °C.

3.1.2 Generation of P1 Virus Stock

1. The day before infection, calculate the volume of cell culture required for the amplification (3 mL minimum volume per amplification, include one negative control) and dilute the cells in the insect cell growth medium to a final density between 0.75×10^6 cells/mL and 1.00×10^6 cells/mL, depending on the dividing time of the cells.
2. On the day of infection, dilute the cells to 1.00×10^6 cells/mL in 10% FCS-insect cell growth medium. Distribute the cells into one bioreactor per construct, and prepare one extra bioreactor as a negative control.
3. Add 1/100th cell culture volume of the P0 or P0 backup virus stock to the cells in the bioreactor. Leave the negative control free from virus.
4. Incubate for 24 h under orbital shaking at 27 °C, speed depending on the bioreactor and the shaker type. Check the cell density, the viability, and if possible, the average cell diameter of the infected cells and the negative control. If the cell density in the samples is between 80% and 100% of the cell density in the negative control, dilute the sample 1:1 with 10% FCS-insect cell growth medium.
5. Incubate in the same conditions an additional 24 h. Check the cell density, the viability, and if possible, the average cell diameter of the infected cells and the negative control. If the cell viability of the sample decreases below 86%, the harvesting process can start, otherwise incubate in the same conditions for 24 h before harvesting.
6. For harvesting P1 virus, centrifuge the culture at $3200 \times g$ for 10 min at 4 °C. Filter the supernatant through a 0.22 μm filter in a light protection container (P1). Store at 4 °C.

3.1.3 Generation of P2 Virus Stock

1. The day before infection, calculate the volume of cell culture required for the amplification (3 mL minimum volume per amplification, include one control) and dilute the cells in the insect cell growth medium to a final density between 0.75×10^6 cells/mL and 1.00×10^6 cells/mL, depending on the generation time of the cells.

2. On the day of infection, dilute the cells to 1.00×10^6 cells/mL in 10% FCS-insect cell growth medium. Distribute the cells into one bioreactor per construct and prepare one extra bioreactor as a negative control.
3. Add 1/100th cell culture volume of the P1 virus stock to the cells in the bioreactor. Leave the negative control free from virus.
4. Incubate for 24 h under orbital shaking at 27 °C, speed depending on the bioreactor and the shaker type.
5. Check the cell density, the viability, and if possible, the average cell diameter of the infected cells and the negative control. If the cell density in the samples is between 80% and 100% of the cell density in the negative control, dilute the sample 1:1 with 10% FCS-insect cell growth medium.
6. Incubate in the same conditions for further 24 h. Check the cell density, the viability, and if possible, the average cell diameter of the infected cells and the negative control. If the cell viability of the sample decreases below 86%, the harvesting process can start, otherwise incubate in the same conditions for additional 24 h before harvesting.
7. For harvesting, centrifuge the culture at $3200 \times g$ for 10 min at 4 °C. Filter the supernatant through a 0.22 μm filter in a light protection container (P2). Store at 4 °C.

3.2 Virus Quality Control, Titering, and Storage

In this section protocol steps for virus quality control, titering and storage are described. Typically virus potencies greater than 10^8–10^9 viral particles/mL or working dilutions 1:1000–1:10,000 are expected from P2 virus. The virus is further amplified (P3/P4), and/or new virus is generated if desired potency is not achieved. Two protocols are described: titering virus by using a GP64 antibody or employing GFP marker fluorescence and cell viability. The expression test described in the Subheading 3.3 can be combined with the viral titering or done as a follow-up step.

The cell surface expression and total expression is followed by flow cytometry, fluorimetry, and microscopy (Fig. 2). For mCherry-tagged proteins and eGFP viral markers, direct fluorescence measurements can be used [5]. For other constructs and alternative viral marker, we use a fluorescent-label-conjugated antibody against the FLAG epitope to detect surface expression and the anti-GP64 to detect viral expression, respectively [6].

Described below is the standard protocol for the cell surface expression of FLAG epitope-tagged constructs. The same protocol can be adapted for the GP64 viral expression marker. Measurement parameters for both flow cytometry and fluorimetry need to be adjusted depending on instrument details including negative and positive controls. The fluorescence values can be converted to concentration from fluorescence protein standards (GFP, mCherry), which need to be assayed in parallel.

3.2.1 Titration with Flow Cytometry and GP64 Viral Expression Marker/eGFP Viral Expression Marker

1. The day before starting the experiment, split the cells to a density of 1.00×10^6 cells/mL in cell culture medium. Prepare 18 mL per virus stock solution +3 mL for the negative control. Incubate for 24 h under orbital shaking at 27 °C, speed depending on the shaker type.
2. Prepare a six-point, threefold serial dilution of viral stock into cell culture media into a 96-well plate (*see* **Note 2**):

   Add 135 µL of the virus solution to a well on column 1 and add 90 µL of cell culture media to the wells of the same row in columns 3, 5, 7, 9, and 11.

   Take 45 µL of virus from column 1 and add it to the well on column 3, pipette up and down, then take 45 µL from well on column 3 and add to well on column 5, continue this until you reach the well on column 11. The final volume in each well should be 90 µL.
3. Check the cell density and viability of the cell stock prepared the day before. Viability should be above 94%. Dilute the cells to 2.00×10^6 cells/mL into cell culture medium (18 mL per virus stock solution +3 mL for the negative control).
4. In a 24-deep well plate, distribute 3 mL of cells in each well (1 row per construct +1 well for the negative control) and infect with 60 µL of viral dilution: 1 row per dilution series, 1 dilution per well, i.e., 4 constructs can be tested in each plate. This can be done using a 12-channel pipette with one tip every two channels, this will fit the 24-well deep-well plate format.
5. Cover the plate with a porous sheet and incubate for 12–18 h under orbital shaking at 27 °C, speed depending on the shaker type.
6. After incubation, the total fluorescence signal can be measured with a fluorimeter.
7. Load 200 µL of cells in a 96-well assay plate (*see* **Note 3**) and measure the fluorescence signal using a Benchtop flow cytometer up to 20,000 counts.

   If the virus does not carry any fluorescence marker, use a labeled anti-gp64 antibody. Incubate 20 µL cells with 20 µL of the labeled antibody diluted in PBS—4% BSA for 30 min at 4 °C. Add 160 µL of PBS, then load the mix in a 96-well assay plate and measure the fluorescence signal using a Benchtop flow cytometer up to 20,000 counts.
8. Adjust settings for the negative control: fluorescence gain and thresholds to exclude debris (*see* **Note 3**).
9. Analyzing data with a FACS analysis software: Define a region as positive using the negative control (i.e., this region on the negative control should cover less than 0.5% of the total cell count). Report the percentage of the positive population versus

the virus dilution on an analysis software. Analyze using non-linear regression. The maximum value should be above 80%, meaning that more than 80% of the virus in the stock solution is potent. Note the dilution D for which 50% of the cells are infected. Calculate the titer of the virus stock solution using this equation:

$$\text{Infectious particles (IFP/mL)} = (0.5 \times \text{cell density } t_0 \times \text{volume})/(\text{inoculation volume} \times \text{D})$$

0.5 is the multiplicity of infection (MOI), meaning there is 0.5 infectious particle per cell

Cell density $t_0 = 2.0 \times 10^6$ cells/mL

Volume = 3 mL

Inoculation volume = 0.06 mL (60 µL virus stock solution was added to the cells)

3.2.2 Virus storage

1. Label a cryovial with the name of the construct and the virus titer. The titer will be two times less than the one calculated above due to dilution in **step 2**.
2. In a cryovial, add 500 µL of virus stock solution and 500 µL of freezing medium (1:2 dilution). Store at −80 °C.

3.3 Expression in Insect Cells

The initial expression screening and purification screening is done on a 25 mL scale. The initial purification protocol should be considered as a starting point for construct screening and should yield sufficient protein amounts for SDS-PAGE, SEC/F-SEC, and MS analysis (Fig. 3). Constructs should be further screened for expression, stability, and monodispersity using an expression culture of 5–250 mL from insect cells (Sf9, Sf21, and Hi5). An additional buffer and detergent screening process are advisable for the best expressing and monodisperse target. Routinely, 10–20 constructs are designed, expressed, purified, and analyzed for monodispersity in parallel. The protocol is scalable for large-scale expression in 1 L cultures (in 3 L Erlenmeyer flask; Fig. 3) or WAVE/Spinner flask for >10 L expression culture volume. It is advisable to check the protein activity and stability in the detergents prior to extensive scale-up. Additional analytical methods such as dynamic light scattering and static light scattering combined with SEC are also highly recommended.

3.3.1 Initial Small-Scale Expression

1. The day before the infection, check the cell parameters (viable cell density, viability) and dilute to 1.00×10^6 cells/mL with insect cell growth medium in a 50 mL bioreactor (*see* **Note 4**). Incubate for 24 h under orbital shaking at 27 °C, speed depending on the shaker type.

2. On the day of infection, check the cell parameters (viable cell density should be around 2.00×10^6 cells/mL) and add the volume of virus (from P2 or P3 stock) experimentally determined to reach the optimal dilution (*see* Subheadings 3.2). Incubate for 72 h under orbital shaking at 27 °C, speed depending on the shaker type (*see* **Note 5**).
3. Check the cell parameters (viable cell density, viability, and diameter). Cells were harvested by centrifugation ($800 \times g$) and stored at −80 °C until use (*see* **Note 6**).
4. Cell lysis is achieved by thawing the pellet in 5 mL hypotonic buffer. Additionally, cells are broken with a Polytron PT1300D, 3 × 30 s 16,000 rotations per minute (rpm). For lysate solubilization, 500 µL 10% glycerol (w/v), 10% (w/v) LMNG-3/2% (w/v) CHS (final concentration: 1% LMNG-3/0.2% CHS) are added and incubated by stirring for 2 h at 4 °C.
5. Transfer each solution into a polycarbonate tube and balance the tubes. Fill them with hypotonic buffer if necessary. Insolubilized material is removed by centrifugation at $150{,}000 \times g$ for 45 min at 4 °C. Imidazole is added to the supernatant to a final concentration of 20 mM and incubated with 40 µL TALON IMAC resin overnight (manual) or 2 h with a semi-automated IMAC robot tip. The resin is washed with 6 × 1 mL of 50 mM HEPES, pH 7.5, 800 mM NaCl, 10% glycerol (w/v), 20 mM imidazole, 0.01% LMNG-3/0.002% CHS (w/v). Bound receptor is eluted with 120 µL 50 mM HEPES, pH 7.5, 800 mM NaCl, 10% glycerol (w/v), 300 mM imidazole, 0.01% LMNG-3/0.002% (w/v) CHS. The eluted sample is analyzed in SDS-PAGE (20 µL), analytical-SEC (20 µL), and MS. The expression and purification yields and quality are analyzed by calculating obtained protein mass from SDS-PAGE (vs. BSA standard), analytical-SEC (peak height and area vs. BSA standard) or 280 nm absorbance measurements.

3.3.2 Expression

1. The day before the infection, check the cell parameters (viable cell density, viability) and dilute them to 1.00×10^6 cells/mL with insect cell growth medium in a bioreactor of appropriate size for the chosen expression volume (*see* **Note 4**). Incubate for 24 h under orbital shaking at 27 °C, speed depending on the bioreactor and the shaker type.
2. On the day of infection, check the cell parameters (viable cell density should be around 2.00×10^6 cells/mL) and add the volume of virus (from P2 or P3 stock) experimentally determined to reach the optimal dilution (*see* Subheadings 3.2).
3. Incubate for 72 h (or the optimal incubation time experimentally determined) at 27 °C, shaking speed depending on the

bioreactor and the shaker type. Take a 500 μL aliquot to analyze the expression by SDS-PAGE, Western blot, or other techniques.

4. Collect the culture into a container that can be centrifuged. Centrifuge at 3200 × *g* for 15–30 min at 4 °C. Discard the supernatant (*see* **Note 6**). If the container cannot be used for long-term storage, resuspend the pellet into insect cell growth medium or PBS and transfer into a suitable container. Centrifuge at 3200 × *g* for 10 min at 4 °C. Discard the supernatant.
5. Measure the wet weight and store the pellet at −20 °C.
6. Measure the cell parameters (viable cell density, viability, diameter, and microscope picture) using the aliquot taken in **step 3**. Perform a cell surface expression assay to check the protein expression level. This requires a fluorescent protein, a fluorescent tag on the expressed protein or a fluorescent antibody against the protein of interest.

3.3.3 Cell Surface Expression Assay

Cell surface expression of FLAG-tagged protein is evaluated by following Subheading 3.2.1 using anti-FLAG M2 antibody (Sigma-Aldrich).

4 Notes

1. Infected insect cells should appear larger and irregular in shape compared to uninfected control cells.
2. Microcentrifuge tubes can also be used for the serial dilutions. The advantage of using a 96-well U-bottom plate is that the infection performed afterwards is easier when using a multichannel pipette.
3. The details can change according to the flow cytometry instrument. Please refer to the manufacturer's instructions.
4. In general, the size of the expression culture should not exceed 20% of the maximal bioreactor volume.
5. You may want to test different cell types (Sf9, Sf21, Tni, High Five™), different infection volumes (or MOIs) on insect cells, different cell densities (typically between 1×10^6 and 4×10^6 cells/mL), different incubation times (typically between 24 and 96 h postinfection), medium (SF900III, SF-4 Baculo Express ICM), and promoters (PH, GP64, P10) to determine the parameters leading to the optimal expression profile. In that case, prepare a replicate for each condition you want to evaluate. Then, follow the steps either directly after harvesting or freeze the cell pellet as described and run all the samples in parallel.
6. For secreted protein, keep the supernatant as it contains your protein of interest.

Acknowledgment

The authors would like to thank Felix Freuler, Binesh Shrestha, Myriam Duckely, Sebastien Rieffel, Alexandre Lebrun, Aurelie Winterhalter, Simon Haenni, Sandra Holzinger, and the other members of the Protein Science team/Chemical Biology & Therapeutics at NIBR.

References

1. Santos R, Ursu O, Gaulton A, Bento AP, Donadi RS, Bologa CG, Karlsson A, Al-Lazikani B, Hersey A, Oprea TI, Overington JP (2017) A comprehensive map of molecular drug targets. Nat Rev Drug Discov 16(1):19–34. https://doi.org/10.1038/nrd.2016.230
2. Hauser AS, Chavali S, Masuho I, Jahn LJ, Martemyanov KA, Gloriam DE, Babu MM (2018) Pharmacogenomics of GPCR drug targets. Cell 172(1–2):41–54 e19. https://doi.org/10.1016/j.cell.2017.11.033
3. Erlandson SC, McMahon C, Kruse AC (2018) Structural Basis for G Protein-Coupled Receptor Signaling. Annu Rev Biophys. https://doi.org/10.1146/annurev-biophys-070317-032931
4. Munk C, Mutt E, Isberg V, Nikolajsen LF, Bibbe JM, Flock T, Hanson MA, Stevens RC, Deupi X, Gloriam DE (2019) An online resource for GPCR structure determination and analysis. Nat Methods 16(2):151–162. https://doi.org/10.1038/s41592-018-0302-x
5. Drew D, Newstead S, Sonoda Y, Kim H, von Heijne G, Iwata S (2008) GFP-based optimization scheme for the overexpression and purification of eukaryotic membrane proteins in Saccharomyces cerevisiae. Nat Protoc 3(5):784–798. https://doi.org/10.1038/nprot.2008.44
6. Hanson MA, Brooun A, Baker KA, Jaakola VP, Roth C, Chien EY, Alexandrov A, Velasquez J, Davis L, Griffith M, Moy K, Ganser-Pornillos BK, Hua Y, Kuhn P, Ellis S, Yeager M, Stevens RC (2007) Profiling of membrane protein variants in a baculovirus system by coupling cell-surface detection with small-scale parallel expression. Protein Expr Purif 56(1):85–92. https://doi.org/10.1016/j.pep.2007.06.003

Chapter 6

Membrane Extracts from Plant Tissues

Uwe Bodensohn, Christoph Ruland, Roman Ladig, and Enrico Schleiff

Abstract

The comparison of isolated plant cell membranous enclosures can be hampered if their extraction method differs, e.g., in regard to the utilized buffers, the tissue, or the developmental stage of the plant. Thus, for comparable results, different cellular compartments should be isolated synchronously in one procedure. Here, we devise a workflow to isolate different organelles from one tissue, which is applicable to different eudicots such as *Medicago* x *varia* and *Solanum lycopersicum*. We describe this method for the isolation of different organelles from one plant tissue for the example of *Arabidopsis thaliana*. All compartments are retrieved by utilizing differential centrifugation with organelle-specific parameters.

Key words Plant cell, Organelle and membrane isolation, Chloroplast, Mitochondria, Microsome, Envelope

1 Introduction

Biological membranes represent the boundary between different reaction spaces in the cell. The isolation of membranous compartments is fundamental for cell biological, biochemical and physiological studies of organelle function and protein distribution, e.g., [1–4]. For the detailed investigation of the structure, function, and composition of specific organelles, it is important to achieve very pure organelle fractions [2, 5–8].

The fractionation of cell lysate into specific organelles is most commonly achieved by density gradient or differential centrifugation [9, 10]. These procedures separate membranous enclosures according to their sedimentation characteristics. Most protocols are optimized for the purification of only a single compartment. These techniques usually prioritize high yield and homogeneity of a specific organelle over recovering multiple organelles from one tissue sample. However, the preparation of multiple cellular compartments from a single source by fractionation of a single cell type or tissue is required for the biochemical exploration of distributions and fluxes of metabolites, lipids, RNAs, and proteins [4, 11].

Camilo Perez and Timm Maier (eds.), *Expression, Purification, and Structural Biology of Membrane Proteins*, Methods in Molecular Biology, vol. 2127, https://doi.org/10.1007/978-1-0716-0373-4_6,

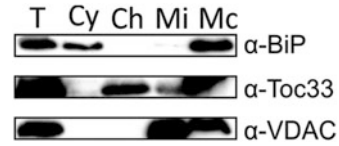

Fig. 1 Subfractionation of *Arabidopsis thaliana*. Arabidopsis seedlings were fractionated into a total (T), cytosolic (Cy), chloroplastidic (Ch), mitochondrial (Mi), and microsomal (Mc) entities. Fraction purity was verified with specific antibodies. α-BiP: endoplasmic reticulum (ER); α-Toc33: chloroplasts; and α-VDAC: mitochondria. This figure illustrates the typical trade-off between specific organelle enrichment and cross-contamination

Here we describe a method to isolate fractions enriched in organelles from a single homogenate of *Arabidopsis thaliana* leaf tissue. The fractions provide high-level enrichment (Fig. 1); however, they still contain contaminations of other organelles that needs to be controlled for. We also describe a method for large-scale chloroplast isolation with subsequent isolation of the chloroplast's outer and inner membrane in mixed envelope vesicles (MEV) to high purity.

2 Materials

2.1 Arabidopsis Tissue

1. Climate chamber specification: under a constant temperature and light regimes (16 h, 22 °C, light; 8 h, 18 °C, dark).
2. 9 × 9 × 8 cm pots.
3. Commercially available soil, e.g., "Hawita fruhstorfer Erde."
4. *Arabidopsis thaliana* Col-0.

2.2 Tissue and Cell Homogenization

1. Ultraturrax® T25.
2. SLA 1500 rotor for Sorvall™ RC 6 Plus centrifuge.

2.2.1 Isolation of Multiple Organelles

3. 1 L glass beaker.
4. Miracloth, pore diameter 80–120 μM.
5. Fine-hair or vegan paintbrush.
6. Grinding buffer (GB): 0.3 M sucrose, 25 mM tetrasodium pyrophosphate, 2 mM ethylenediaminetetraacetic acid (EDTA), 10 mM KH_2PO_4, 1% (w/v) polyvinylpyrrolidone-40 (PVP-40), 1% (w/v) bovine serum albumin (BSA), Adjust pH with hydrochloric acid (HCl) to pH 7.5. Add 20 mM (final concentration) sodium ascorbate and 20 mM (final concentration) cysteine just before use.

2.2.2 Large-Scale and Envelope Membrane Isolation

1. Blender (at least 2.5 L working volume, e.g., Waring™ Heavy Duty Blender).
2. F8-6x-1000y Rotor for Sorvall™.

3. Evolution™ RC centrifuge (Thermo Scientific).
4. Miracloth, pore diameter 80–120 μM.
5. Gauze (e.g., VWR No. 89178–490).
6. 2 × 5 L Erlenmeyer flask.
7. Fine-hair or vegan paintbrush.
8. 500 mM phenylmethylsulfonyl fluoride (PMSF) in methanol.
9. Grinding buffer (GB2): 50 mM Hepes-KOH, pH 7.6, 330 mM sorbitol, 1 mM EDTA, and 1 mM ethylene glycol-bis(ß-aminoethyl ether)-tetraacetic acid (EGTA), immediately before use add 1 mM PMSF and 1 mM β-mercaptoethanol.

2.3 Chloroplast Isolation

2.3.1 Chloroplast Isolation by the Procedure for Multiple Organelle Enrichment

1. HB-6 rotor for Sorvall™ RC 6 Plus centrifuge.
2. Sorbitol Resuspension Medium (SRM): 0.33 M sorbitol, 50 mM HEPES/KOH, pH 8.0.
3. Solutions for Percoll (GE Healthcare, No. 10607095) gradients (50 mL):

	Percoll	Sorbitol	Hepes 1 M	Water
42%	21 mL	3 g	2.5 mL	Fill to 50 mL
82%	41 mL	3 g	2.5 mL	Fill to 50 mL

2.3.2 Chloroplast Isolation by the Large-Scale Procedure

1. HB-6 Rotor for Sorvall™ RC 6 Plus centrifuge.
2. SLA-1500 Rotor for Sorvall™ RC 6 Plus centrifuge (Thermo Scientific).
3. Fine-hair or vegan paintbrush.
4. Wash buffer: equals grinding buffer GB2.
5. Percoll gradient buffer (final): 50 mM Hepes-KOH pH 7.6, 330 mM Sorbitol, 1 mM EDTA, 40%/80% Percoll, add 1 mM (final concentration) β-mercaptoethanol freshly before use.

	Percoll	Sorbitol	Hepes 1 M	EDTA	Water
40%	60 mL	9 g	7.5 mL	1.5 mL	Fill to 150 mL
80%	80 mL	6 g	5 mL	1 mL	Fill to 100 mL

2.4 Mitochondria Isolation

1. Gradient mixer (e.g., Sigma-Aldrich, No. 80–6196-09).
2. Surespin™ 630 rotor for Sorvall™ RC 6 Plus centrifuge (Thermo Scientific).
3. 2× Wash buffer (2× WB): 0.6 M sucrose, 20 mM Hepes-KOH, pH 7.4, 0.2% (w/v) BSA.

4. Mitochondria storage buffer (MSB): 0.4 M mannitol, 10 mM tricine-NaOH, pH 7.0, 1 mM EDTA, 0.2 mM phenylmethylsulfonyl fluoride (PMSF).
5. Light gradient solution (35 mL):

	Percoll	2× wash buffer	Water
2 Gradients	9.8 mL	17.5 mL	7.7 mL

6. Heavy gradient solution (35 mL):

	Percoll	2× wash buffer	PVP-40 20% (w/v)
2 Gradients	9.8 mL	17.5 mL	

2.5 Microsome Isolation

1. T-647.5 Rotor for pelleting (Thermo Scientific) for Sorvall™ RC 6 Plus centrifuge (Thermo Scientific).
2. TST-41.14 Rotor for gradients (Beckmann) for Sorvall™ RC 6 Plus centrifuge (Thermo Scientific).
3. Collection buffer (CB): 50 mM Tris–HCl, pH 8, 1 mM EDTA, 1% protease inhibitor cocktail (P.I.C., Sigma, No. P9599).
4. Sucrose gradient (10 mL):

	Sucrose	1 mM EDTA
20%	2 g	Fill to 10 mL
30%	3 g	Fill to 10 mL
40%	4 g	Fill to 10 mL

2.6 Envelope Isolation

1. F34-6-38 Rotor (Eppendorf) for Eppendorf centrifuge 5804 R.
2. TST-41.14 Rotor (Beckmann) for Sorvall™ RC 6 Plus centrifuge (Thermo Scientific).
3. Hyposomotic lysis buffer (hLB): 50 mM Hepes-KOH, pH 7.6, 1 mM EDTA, 1 mM EGTA, 1 mM PMSF, 1 mM β-mercaptoethanol.
4. Sucrose gradient buffer (50 mL): 50 mM Hepes-KOH, pH 7.6, 0.2/0.6/1.25 M Sucrose.

	Sucrose	Hepes 1 M	Water
0.2 M	3.4 g	2.5 mL	Fill to 50 mL
0.6 M	10.2 g	2.5 mL	Fill to 50 mL
1.25 M	21.4 g	2.5 mL	Fill to 50 mL

3 Methods

Carry out all steps of the isolation procedure at 4 °C utilizing chilled solutions and equipment. In order to prevent organelle damage through shear forces, cut pipette tips to enlarge the openings and brush organellar pellets into solution instead of resuspension with a pipette (*see* **Note 1**).

3.1 Plant Growth

1. Sow with 10–20 seeds per square cm.
2. Grow on soil for 14–21 days under a constant temperature and light regime (16 h, 22 °C, light; 8 h, 18 °C, dark).

3.2 Isolation of Multiple Organelles

1. Prepare the buffers listed in Subheadings 2.2.1, 2.3.1, 2.4, and 2.5. Store buffers at 4 °C.

3.2.1 Preparations Before Start of the Experiments

2. Prepare Percoll gradients with solutions described in Subheading 2.3.1. Overlay 6 mL 82% Percoll solution with 15 mL 42% Percoll solution (cut pipette tip).
3. Put the funnel in the neck of SLA 1500 bucket on ice, line it with four layers of Miracloth and presoak.

3.2.2 Preparation of the Continuous PVP Gradient

4. Set up the gradient mixer on top of a stirring block and add a stirrer.
5. Do a test run with water to check if the tubings are free, the flowrate is constant and the stirrer rotates properly.
6. Confirm that the connection between inner and outer chamber is closed.
7. Pour the light solution into the inner chamber (not connected to outlet tubing).
8. Pour the heavy solution into the outer chamber, place gradient chamber on stirring block.
9. Set peristaltic pump to medium flow rate, let heavy solution run into a surespin™ 630 compatible centrifugation tube until half dispersed.
10. Open connection between chambers and let solutions mix with stirrer until gradient mixer is empty.

3.2.3 Homogenization

11. Utilize the Ultraturrax® at the lowest power setting till the tissue is homogenized to a satisfactory degree (*see* **Note 2**). If you plan a Western blot analysis to investigate the localization of a defined protein, take a sample of the homogenate as cell lysate.

12. Pour homogenate into the funnel and filter it through the Miracloth. Bring the edges together and squeeze residual homogenate gently. If necessary, repeat **steps 2–4** till the plant material is fully used up.
13. Distribute the homogenate equally into SLA 1500 centrifugation tubes and centrifuge at 1500 × *g*, 4 °C for 5 min.
14. Transfer the *post-plastidic supernatant* into new tubes.
15. Resuspend the *nuclei/plastidic pellet* in SRM buffer with a small paintbrush. Pipette SRM onto paintbrush to release residual nuclei/plastids from it.

3.2.4 Chloroplast Isolation

16. Layer the resulting solution on top of a two-layer Percoll gradient prepared in **step 2** (Fig. 2).
17. Centrifuge Percoll gradients in a swingout rotor at 10,000 × *g*, 4 °C for 10 min with medium centrifuge break.
18. Collect nuclei and cell fragments, which are found in the pellet.
19. Collect thylakoids which can be recovered at the 42% interphase.
20. Collect intact plastids at the interphase between 82% and 42%.
21. Wash plastids twice with 5–10 mL SRM buffer with 2 min centrifugation at 1.100 × *g* 4 °C. Plastids can be stored short term at 4 °C in SRM in the dark or frozen away.

3.2.5 Mitochondria Isolation

22. Distribute post-plastidic fraction collected at **step 13** equally into SLA1500 centrifugation tubes and centrifuge at 17,400 × *g*, 4 °C for 20 min.
23. Transfer the *post-mitochondrial supernatant* into new tubes.
24. Resuspend the peroxisomal/mitochondrial pellet in 1× WB with a small paintbrush. Pipette 1× WB onto paintbrush to release residual peroxisomes/mitochondria from it.
25. Add 15 mL of 1× WB to each tube and preclear by centrifugation at 2450 × *g*, transfer supernatants to new tubes and pellet peroxisomes/mitochondria at 17,400 × *g*, 4 °C for 20 min.
26. Resuspend the peroxisomal/mitochondrial pellet in 1× WB with a small paintbrush. Pipette 1× WB onto paintbrush to release residual peroxisomes/mitochondria from it (keep volume minimal).
27. Overlay crude peroxisomal/mitochondrial enriched solution on one continuous PVP-40/Percoll gradient (if a lot of material is used, one should overlay 2 gradients, Fig. 3).

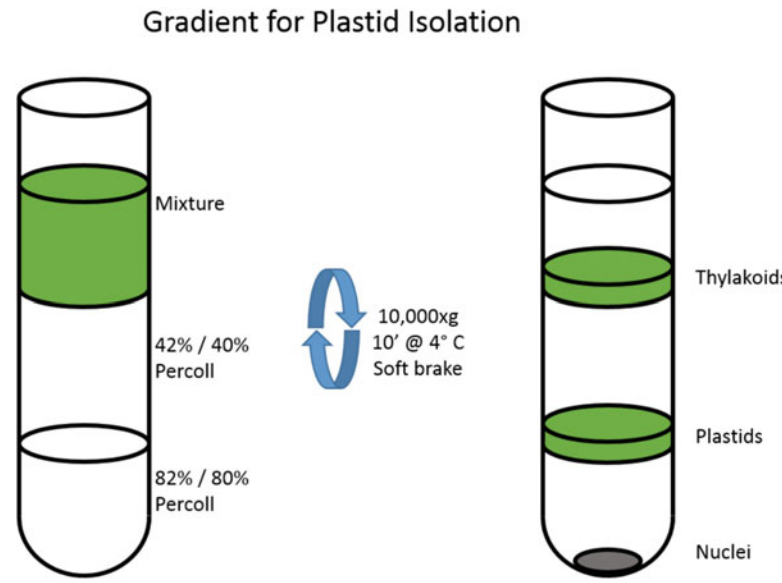

Fig. 2 Two-step Percoll gradient for the isolation of plastids of *Pisum sativum* (80%/40%) and *Arabidopsis thaliana* (82%/42%). Thylakoids are retrieved above the 40%/42% layer, and chloroplasts are recovered at the interface between the two Percoll layers

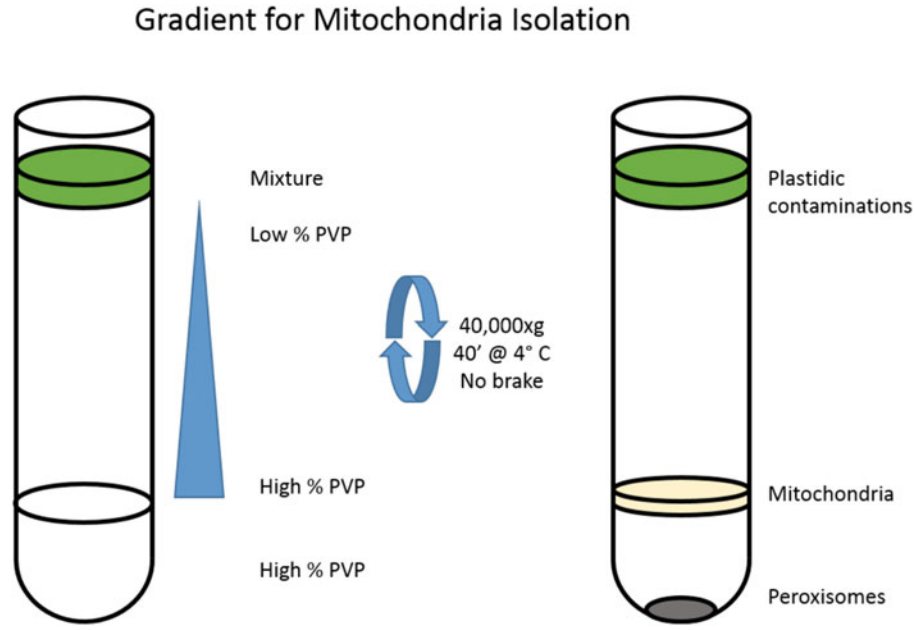

Fig. 3 Continuous PVP 40/Percoll gradient for the isolation of mitochondria from *Arabidopsis thaliana*. The mixture of enriched mitochondria, peroxisomes, and contaminants is layered on top of the gradient, and mitochondria are recovered in the bottom third of the gradient. The resulting pellet after centrifugation is enriched in peroxisomes (avoid recovery). Mitochondria will only be clearly visible if sufficient material is used for the gradient. Therefore, it is advised to layer all the material onto one gradient

28. Balance tubes and centrifuge at 40,000 × *g*, 4 °C, for 40 min with no brake (brake set to zero).
29. Mitochondria should appear as a light yellow/gray band reminiscent of an interphase in the lower third of the tube. The majority of peroxisomes form a dark pellet (*see* **Note 3**).
30. Remove and discard the solution to approximately 1 cm above the mitochondrial band.
31. Take up the mitochondrial fraction excluding the pellet and distribute solution equally in at least two tubes.
32. If *peroxisomal-enriched fraction* is required, resuspend the pellet in 1× WB.
33. Fill the buckets with the mitochondria containing solution (**step 30**) with 1× WB and centrifuge at 31,000 × *g*, 4 °C for 15 min with light break.
34. Carefully remove supernatant, fill tube with 1× WB and centrifuge at 18,000 × *g*, 4 °C for 15 min with middle break.
35. Aspirate solution and transfer soft mitochondrial pellet into 1.5 mL tube, centrifuge in microcentrifuge at 16,000 × *g* and resuspend pellet in mitochondria storage buffer.
36. Either use mitochondria directly or store them at −80 °C for further processing.

3.2.6 Microsomal Isolation

37. Distribute the post-mitochondrial fraction (**step 22**) equally, balance tubes with GB and centrifuge at 120,000 × *g*, 4 °C for 1 h.
38. Overlay 3 mL 40% sucrose solution with 3 mL 30% sucrose solution with another 4 mL 20% sucrose solution (cut pipette tip).
39. Resuspend microsomal pellet after centrifugation (**step 35**) in GB with pipette (small volume) and layer it on a three-step sucrose gradient (Fig. 4).
40. Balance tubes with GB and centrifuge at 100,000 × *g*, 4 °C for 18 h.
41. Microsomes are recovered at the interphase between 30% and 40% and mixed envelopes between 20% and 30%.
42. Microsomes are diluted 3:1 in CB and pelleted at 200,000 × *g*, 4 °C for 30 min and taken up in CB (Fig. 4).

This procedure yields a total cell fraction (**step 12**), a nuclear-enriched fraction (**step 18**), which can be further cleared if required, a thylakoid-enriched fraction as subfraction of chloroplasts (**step 19**), a chloroplast-enriched fraction (**step 21**), a peroxisomes-enriched fraction (**step 32**), a mitochondrial fraction (**step 36**), and a microsomes-enriched fraction (**step 42**). By

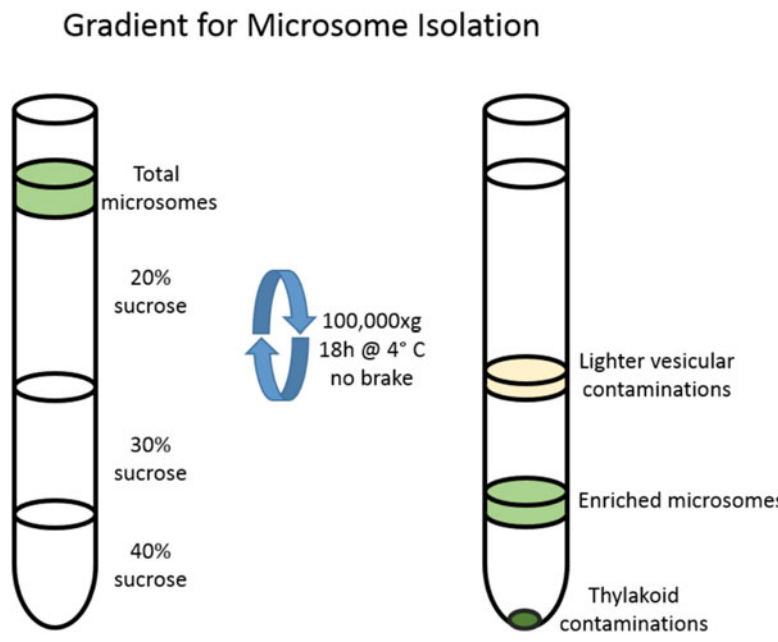

Fig. 4 Three-step sucrose gradient for microsome isolation from *Arabidopsis thaliana*. Fractions enriched in microsomes are recovered at the 40%/30% sucrose interphase after centrifugation

osmotic, salt, or carbonate treatment, the organelles can be further fractionated into soluble compartments or membranes.

3.3 Large-Scale Isolation of Chloroplasts and Chloroplast Membranes

For all the steps, it is important to keep samples cool at all times (*see* **Note 4**).

3.3.1 Preparations Before Start of the Experiments

1. Prepare 12 Percoll gradients by first pipetting 12 mL of the 40% solution into the centrifugation tubes, then adding 8 mL of the 80% solution by gently under-layering it.

3.3.2 Homogenization

2. Harvest roughly 2 kg of plant leaves (*see* **Note 5**).
3. Grind leaves in blender using grinding buffer (*see* **Note 6**).
4. Filter ground leaves through gauze and then through miracloth (*see* **Note 7**).
5. Centrifuge filtrate using F8-6x-1000y rotor at 1800 × *g*, 4 °C for 10 min.

3.3.3 Chloroplast Isolation

6. Discard supernatant and resuspend the pellet gently in 20 mL grinding buffer per bottle using the brush. Wash the brush in grinding buffer before using it to resuspend the pellets in order to equilibrate it.
7. Load the chloroplast suspension onto the Percoll gradients (12 mL per gradient, Fig. 2) and centrifuge for 15 min at 7500 g at 4 °C using the swing out rotor HB-6. Reduce deceleration for the centrifugation to about one-third of maximum.
8. Discard upper band containing thylakoids and buffer above the upper band, then take intact chloroplasts from the lower band into the bottles for the SLA-1500 rotor. Use cut pipette tips to minimize sheering forces.
9. Fill centrifugation bottles with grinding medium and centrifuge for 10 min at 1800 g at 4 °C using the SLA-1500 rotor.
10. Discard supernatant and resuspend gently using the brush. Distribute concentrated chloroplast suspension over 6 50 mL tubes, then fill them up with grinding buffer.
11. Centrifuge for 10 min at 1800 g at 4 °C with reduced deceleration in the Eppendorf F34–6-38 Rotor (it is also possible to use the HB-6 rotor with the respective centrifugation tubes and slightly less volume).

3.3.4 Mixed Envelope Isolation

12. Discard supernatant and add 30 mL hypo-osmotic lysis buffer (hLB, *see* Subheading 2.6, **step 3**) per tube. Resuspend pellet by gentle shaking and inverting. Keep samples cool at all times. Fill tubes to 50 mL and incubate on ice for 15 min.
13. After the osmotic shock, centrifuge for 15 min at 2250 g at 4 °C.
14. Transfer supernatant into T-647.5 ultracentrifugation tubes and discard the pellet containing thylakoids and other non-vesicular components. Fill the centrifugation tubes with lysis buffer, then centrifuge for 30 min at 100,000 × *g* at 4 °C.
15. Discard supernatant and resuspend the pellet in small volume of lysis buffer.
16. Crude mixed envelope can be stored at −80 °C after freezing in liquid nitrogen.

3.3.5 Purification of Mixed Envelope Membranes

17. The mixed envelop suspension is layered on top of a discontinuous sucrose gradient (Fig. 5).
18. For the step-gradient generation, use 3 mL 1.2 M sucrose as cushion, overlaid with 4 mL of 0.6 M and on top with 3 mL of 0.2 M sucrose solutions (*see* Subheading 2.6). The mixed envelope suspension is placed on top of the gradient and centrifuge for 1 h at 100,000 × *g* at 4 °C using the TST-41.14 rotor with no break (Fig. 5).

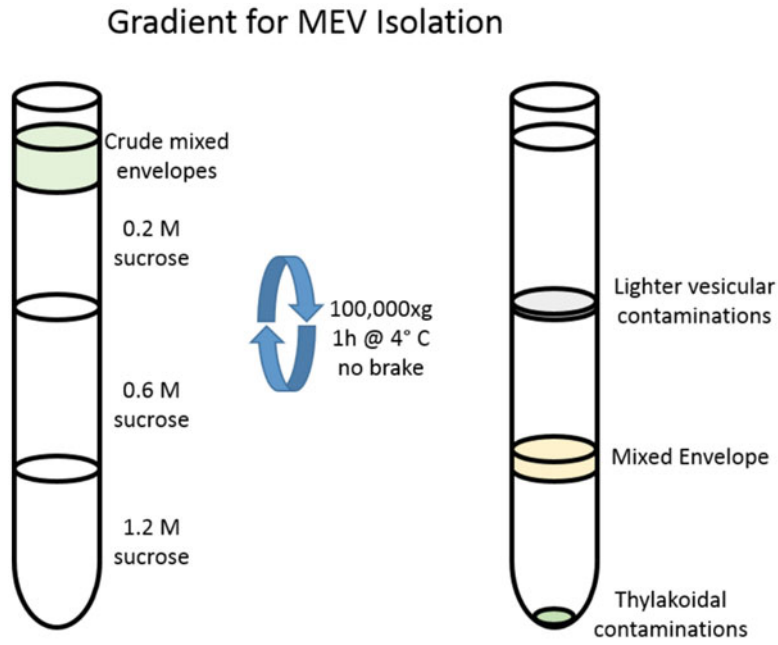

Fig. 5 Three-step sucrose gradient for MEV isolation from *Pisum sativum*. After centrifugation, MEV are retrieved at the 1.2 M/0.6 M interphase

19. Harvest mixed envelope from interphase between 0.6 M and 1.2 M sucrose solution.
20. Mixed envelope can be stored in sucrose or washed again. To wash them, transfer the sucrose-containing suspension into the T-647.5 tubes and add storage buffer of your choice to fill them up, then centrifuge for 1 h at 100000 g at 4 °C.
21. Discard the supernatant and resuspend the pellet in small amounts of the storage buffer of your choice, then freeze in liquid nitrogen and store at −80 °C.

4 Notes

1. When one is well accustomed with the protocol, the continuous PVP gradient and others can be poured during centrifugation time. Even discontinuous gradients can be overlaid during centrifugation times.
2. During homogenization, try to keep bubble and foam formation at a minimum. Rather use low settings and increase the lysis time to minimize foam formation.
3. The mitochondrial band is very weak and hard to perceive (looks more like an interphase than a clear band) during the initial runs. In order to circumvent this, it is advisable to load

the entire mitochondrial/peroxisomal pellet onto one gradient and balance the other with grinding buffer.

4. The cooling of all samples is ideally achieved by performing the purification in the cold room, but it is also acceptable to keep samples on ice at all times. All buffers should be prepared and cooled beforehand.
5. Ideally in the dark or green light to avoid starch formation, 16 h of darkness is sufficient.
6. Here it is recommended to first prepare half the material and then process the second half while the first is filtered. It is important to use low settings on blender to minimize sheering forces.
7. It is recommended to start with half the biomass and use only gravity flow to avoid foam formation. If flow is very low, it is acceptable to squeeze the gauze gently to increase flow. It is important to avoid foam as much as possible.

Acknowledgment

This work was supported by the Deutsche Forschungsgemeinschaft grant SCHL585/10-1.

References

1. Rödiger A, Baudisch B, Klösgen RB (2010) Simultaneous isolation of intact mitochondria and chloroplasts from a single pulping of plant tissue. Plant Physiol 167:620–624
2. Simm S, Papasotiriou DG, Ibrahim M, Leisegang MS, Müller B, Schorge T, Karas M, Mirus O, Sommer MS, Schleiff E (2013) Defining the core proteome of the chloroplast envelope membranes. Front Plant Sci 4:11
3. Jores T, Klinger A, Groß LE, Kawano S, Flinner N, Duchardt-Ferner E, Wöhnert J, Kalbacher H, Endo T, Schleiff E, Rapaport D (2016) Characterization of the targeting signal in mitochondrial β-barrel proteins. Nat Commun 7:12036
4. Hsueh YC, Flinner N, Gross LE, Haarmann R, Mirus O, Sommer MS, Schleiff E (2017) The chloroplast outer envelope protein P39 in Arabidopsis thaliana belongs to the Omp85 protein family. Proteins 85:1391–1401
5. Kleffmann T, Russenberger D, von Zychlinski A, Christopher W, Sjölander K, Gruissem W, Baginsky S (2004) The Arabidopsis thaliana chloroplast proteome reveals pathway abundance and novel protein functions. Curr Biol 14:354–362
6. Reumann S, Babujee L, Ma C, Wienkoop S, Siemsen T, Antonicelli GE, Rasche N, Lüder F, Weckwerth W, Jahn O (2007) Proteome analysis of Arabidopsis leaf peroxisomes reveals novel targeting peptides, metabolic pathways, and defense mechanisms. Plant Cell 19:3170–3193
7. Kruft V, Eubel H, Jänsch L, Werhahn W, Braun HP (2001) Proteomic approach to identify novel mitochondrial proteins in Arabidopsis. Plant Physiol 127:1694–1710
8. Millar AH, Sweetlove LJ, Giegé P, Leaver CJ (2001) Analysis of the Arabidopsis mitochondrial proteome. Plant Physiol 127:1711–1727
9. Rocha V, Ting IP (1970) Preparation of Cellular Plant Organelles from Spinach leaves. Arch Biochem Biophys 140:398–407
10. Schleiff E, Soll J, Küchler M, Kühlbarndt W, Harrer R (2003) Characterisation of the translocon of the outer envelope of chloroplasts. J Cell Biol 160:541–551
11. Hsueh YC, Ehmann C, Flinner N, Ladig R, Schleiff E (2017) The plastid outer membrane localized LPTD1 is important for glycerolipid remodelling under phosphate starvation. Plant Cell Environ 40:1643–1657

Chapter 7

Membrane Protein Solubilization and Quality Control: An Example of a Primary Active Transporter

Charlott Stock and Inga Hänelt

Abstract

When purifying a membrane protein, finding a detergent for solubilization is one of the first steps to master. Ideally, only little time is invested to identify the best-suited detergent, which on the one hand would solubilize large amounts of the target protein but on the other hand would sustain the protein's activity. Here we describe the solubilization screen and subsequent activity assay we have optimized for the bacterial P-type ATPase KdpFABC. In just 2 days, more than 70 detergents were tested for their solubilization potential. Afterwards, a smaller selection of the successful detergents was assayed for their ability to retain the activity of the membrane protein complex.

Key words Membrane protein, Solubilization, Detergent, ATPase assay

1 Introduction

The most prosperous environment for a membrane protein will always be its natural membrane. However, many structural, biochemical, and biophysical investigations require the initial purification of the membrane-bound protein. Despite new approaches like the protein extraction with styrene maleic acid co-polymers [1], detergents are still most widely used to solubilize membrane proteins and to shield their large hydrophobic surfaces in aqueous solutions. Until today one of the major bottlenecks is to find a detergent with a good solubilization efficiency that retains the activity of the protein of interest. The plethora of detergents available includes alkyl-maltosides and glucopyranosides like DDM and OG, amine oxides like LAPAO, ethylene glycols like $C_{12}E_8$, cholesterol-like detergents, e.g., CHAPS, lipid-like detergents, e.g., Fos-Choline-12, cyclohexyl maltosides (Cymals), and the new class of NG detergents [2–4].

The characteristic variable of a detergent is its critical micelle concentration (CMC). The CMC is the detergent concentration

Camilo Perez and Timm Maier (eds.), *Expression, Purification, and Structural Biology of Membrane Proteins*, Methods in Molecular Biology, vol. 2127, https://doi.org/10.1007/978-1-0716-0373-4_7,

allowing for the formation of detergent micelles and is dependent on the used solvent and temperature (*see* **Note 1**). Up to half of the mass in a protein–detergent complex can be assigned to detergents. These greatly influence the shape and biochemical properties of the complexes [5]. Particularly the length of the detergent's alkyl chains can be crucial. Long or short chains cause hydrophobic mismatch between the protein's hydrophobic surface and the detergent. This can lead to decreased solubilization efficiency and can bury functional sites rendering the protein inactive [6]. Further, detergents differ in charge being non-ionic, zwitterionic, or ionic which also has an impact on both the solubilization efficiency and the protein activity [7].

In most cases there is not one right detergent for each membrane protein. Some might work better for solubilization, others stabilize a highly functional form of your membrane protein of interest. Exchanging detergents after solubilization, addition of lipids to your buffers, or even the transfer into a new lipid environment can be necessary to stabilize your membrane protein for functional and structural analysis (*see* **Notes 2** and **3**).

In this chapter, we describe the small-scale solubilization screen and subsequent ATPase activity assay we applied to the bacterial P-type ATPase KdpFABC [8, 9]. KdpFABC is a heterotetramer composed of the P-type ATPase KdpB, the channel-like SKT (superfamily of K^+ transporters) member KdpA, and two smaller membrane-bound subunits KdpC and KdpF. Traditionally, the harsh industrial detergent mixture aminoxide WS-35, normally used to clean old oil barrels, was applied to solubilize KdpFABC [10–12]. Although resulting in active protein, aminoxide WS-35 appeared less favorable for structural investigations as no crystal structures had been solved in this undefined mixture. The performed assays showed us that also better-defined detergents could solubilize KdpFABC in its active state.

2 Materials

2.1 Membrane Preparation

1. Cell disruption buffer: 50 mM Tris–HCl, pH 7.5, 10 mM $MgCl_2$, 10% glycerol, 1 mM DTT, 2 mM EDTA, 0.5 mM PMSF, and DNAse.
2. Solubilization buffer: 50 mM Tris–HCl, pH 7.5, 10 mM $MgCl_2$, 10% glycerol, 0.5 mM PMSF, and DNAse.

2.2 Solubilization Screen

1. Isolated membranes at 10 mg/mL.
2. A variety of detergents supplied as 10% solutions (*see* **Note 4**).

2.3 Western Blot

1. SDS polyacrylamide gel (5% stacking and 12% resolving gel).
2. 3× loading dye: 20 mM Tris–HCl pH 6.8, 6% (w/v) SDS, 30% (v/v) glycerol, 0.06% (w/v) bromophenol blue, 7.5% (v/v) β-mercaptoethanol.
3. 10× electrophoresis buffer: 250 mM Tris, 1.9 M glycine, 1% SDS.
4. Nitrocellulose blotting membranes (GE Healthcare) and blotting paper (MN 440B, Macherey-Nagel).
5. Blocking buffer: 1× TBS, 5% (w/v) powdered milk, 0.1% (v/v) NaN_3, 0.1% (v/v) Tween 20.
6. TBS-T: 1× TBS, 0.1% (v/v) Tween 20.
7. Primary antibody: anti-His from mouse (dilution 3,000-fold in TBS-T, Sigma-Aldrich).
8. Secondary antibody: anti-mouse IgG-peroxidase produced in goat (dilution 20,000-fold in TBS-T, Sigma-Aldrich).
9. ECL-1: 0.1 M Tris–HCl, pH 8, 40 mM *p*-coumaric acid, 2.5 mM luminol.
10. ECL-2: 0.1 M Tris–HCl, pH 8, 0.03% H_2O_2.

2.4 IMAC (Ni-NTA) Purification of Protein

1. Protein in solubilization buffer solubilized with different detergents (1%) overnight (o/n) (o/n ~16 h).
2. Ni-charged resin (Ni Sepharose™ 6 Fast Flow, GE Healthcare).
3. Equilibration buffer: 50 mM Tris–HCl, pH 7.5, 150 mM NaCl, 20 mM $MgCl_2$, 10% (v/v) glycerol, 10 mM imidazole, and 5× CMC of detergent (*see* **Note 5**).
4. Wash buffer: 50 mM Tris–HCl, pH 7.5, 150 mM NaCl, 20 mM $MgCl_2$, 10% (v/v) glycerol, 30 mM imidazole, and 5× CMC of detergent.
5. Elution buffer: 50 mM Tris–HCl, pH 7.5, 150 mM NaCl, 20 mM $MgCl_2$, 10% (v/v) glycerol, 500 mM imidazole, 0.1 mM PMSF, and 5× CMC of detergent.

2.5 ATPase Activity Assay

1. 20 mM H_2SO_4 and 0.4 mM K_2HPO_4.
2. 5× ATPase buffer should be a buffer in which the protein of interest is stable in supplemented with 10- to 25-fold CMC of the probed detergent (*see* **Note 6**).
3. 1× ATPase buffer with two- to fivefold CMC of a detergent, prepared from 5× buffer.
4. 100 mM ATP, 100 mM KCl.
5. Malachite Green conc. solution: 50 mL ddH_2O, 10 mL H_2SO_4 (>96%), and 73.4 mg Malachite green.
6. 7.5% (w/v) $(NH_4)_6Mo_7O_{24}x4H_2O$ and 11% (v/v) Tween.

3 Methods

3.1 Membrane Preparation

1. Resuspend cells to OD_{600nm} 80–100 in cell disruption buffer (*see* **Note 7**).
2. Disrupt cells via sonification (*see* **Note 8**) or pressure homogenization (*see* **Note 9**) until the OD_{600nm} has reduced to at least one third of the starting value.
3. Separate undisrupted cells and cell debris via centrifugation at 26,000 × *g* for 15 min at 4 °C (e.g., Sorvall SS34 rotor 15,000 rpm).
4. Continue with the supernatant in an ultracentrifugation at 205,000 × *g* at 4 °C for 1 h to o/n (*see* **Note 10**) to obtain membranes (e.g., Ti45 Rotor at 42,000 rpm).
5. Resuspend the membrane pellet in solubilization buffer, determine the overall protein concentration in the membranes (with, e.g., Micro BCA™ Protein Assay Kit) and set it to 10 mg/mL.
6. Membranes can be stored at −80 °C until further use.

3.2 Solubilization Screen

1. Prepare a 100 µL sample of membranes at 10 mg/mL for each detergent to be tested.
2. Add 10 µL of detergent (10%) to each sample (*see* **Note 11**) and solubilize o/n.
3. Separate solubilized protein from non-solubilized protein via ultracentrifugation at 435,000 × *g*, 4 °C for 30 min (e.g., TLA100 rotor at 100,000 rpm).
4. Take 90 µL of each supernatant and store them for the analysis of the solubilization efficiency via Western blotting.

3.3 Western Blot

1. Mix 20 µL of supernatant from each solubilization reaction with 10 µL of 3× loading dye.
2. Run an SDS-PAGE (according to Laemmli) (*see* **Note 12**).
3. Transfer the protein from the SDS-PAGE to a nitrocellulose membrane (*see* **Note 13**).
4. Incubate the membrane in blocking buffer for 30 min. All following steps are carried out at 4 °C.
5. Wash the membrane three times for 10 min in TBS-T.
6. Incubate with the primary antibody for 1 h (*see* **Note 14**).
7. Wash the membrane three times for 10 min in TBS-T.
8. Incubate with the secondary antibody for 1 h.
9. Wash the membrane three times for 10 min in TBS-T.

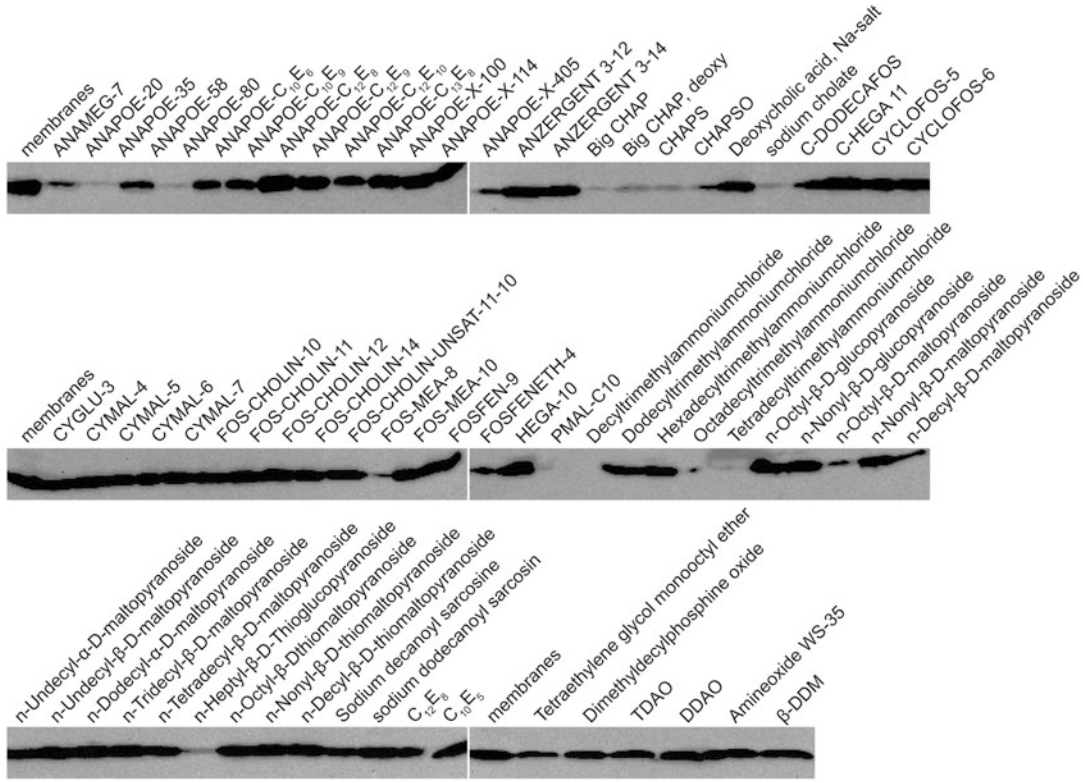

Fig. 1 Results of the solubilization screen with the bacterial P-type ATPase KdpFABC. The C-terminal His-tag on KdpC has been detected. In total 71 detergents were tested, of which 52 resulted in good, 7 in medium, and 12 in no solubilization of the protein complex (*see* **Note 15**)

10. Develop the WB by supplying the substrates of the horseradish peroxidase. Prepare solutions ECL-1 and ECL-2 separately and mix on the membrane 1 min prior to readout via chemiluminescence (*see* Fig. 1).

3.4 IMAC Purification of KdpFABC

1. Solubilize membranes prepared from 4 L of an *Escherichia coli* culture at a total protein concentration of 10 mg/mL with 1% of the tested detergent o/n.
2. Separate solubilized and unsolubilzed protein via ultracentrifugation (205,000 × *g* at 4 °C for 30 min, e.g., Ti45 Rotor at 42,000 rpm).
3. During ultracentrifugation, equilibrate the Ni-charged resin with 50 column volumes (cv) of ddH_2O and 50 cv of equilibration buffer.
4. Incubate the supernatant of the ultracentrifugation and the Ni-charged resin for 1 h at 4 °C under light agitation.
5. Load the complete sample volume on an empty gravity flow column (we use PP chromatography columns from Biorad).

6. Treat the bead material with 50 cv of wash buffer.
7. Elute the protein from the Ni-charged column in 4–5 steps (step 1: 0.5 cv, all further steps 1 cv) with elution buffer and determine the protein concentration via absorption at 280 nm. Exact protein concentrations are calculated by usage of the Lambert-Beer law with specific extinction coefficients related to the protein of interest (calculated with the ProtParam tool of the ExPASy server [13]).

3.5 ATPase Activity Assay

1. Prepare a phosphate standard curve (0, 0.4, 0.8, 2, 3.2, 4.8, and 6 nmol) diluting K_2HPO_4 in H_2SO_4 in 200 µL each.
2. The reaction volume used for each sample is 25 µL and is composed of ATP (in our case 2 mM), the substrate (in our case 1 mM KCl), and 5× ATPase buffer (*see* **Note 16**).
3. The volume in each reaction tube is set to 24 µL prior to the start of the reactions by the addition of 1 µL protein sample. Each reaction is incubated for exactly 5 min at 37 °C (*see* **Note 17**).
4. After 5 min the reaction is stopped by the addition of 175 µL of ice-cold 20 mM H_2SO_4 and the transfer of the sample on ice.
5. A malachite green working solution (2 mL malachite green concentrated solution, 500 µL 7.5% (w/v) $(NH_4)_6Mo_7O_{24} \times 4H_2O$ and 40 µL 11% (v/v) Tween) is prepared fresh and 50 µL are added to each sample and the prepared standard.
6. 175 µL of each sample and the standard curve are transferred into a 96-well plate and the absorption is determined at 621 nm within 10 min.
7. Triplicates of each sample are processed and are corrected by subtraction of the background absorption (measurement of ATPase assay without the addition of ATP, no transport should occur). ATPase activity is typically calculated as µmol formed P_i $*$ mg^{-1} of used ATPase $*$ min^{-1} of reaction time (*see* Fig. 2).

4 Notes

1. The detergent concentrations used for solubilization are far above the CMC, usually ≥1% (w/v), to ensure the proper solubilization of all membrane proteins. When after solubilization the detergent concentration is decreased during further purification steps, it is important to keep in mind that the number of detergent molecules per micelle increases when membrane proteins are incorporated into the micelles [6]. Be reminded that a CMC is not a fixed concentration but depends on several factors. When decreasing the detergent

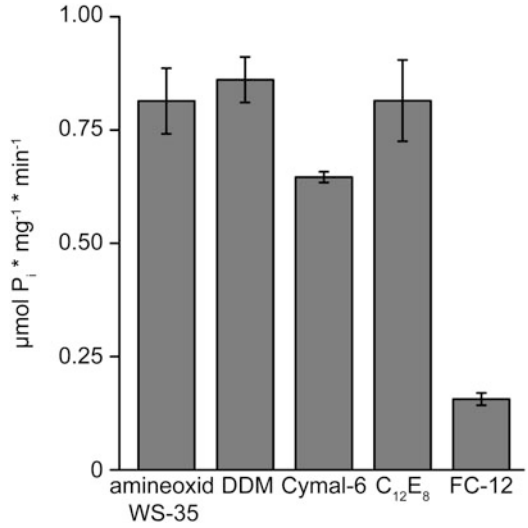

Fig. 2 Results of the ATPase assay with KdpFABC. In this case the detergent mixture aminoxide WS-35 (main component LAPAO) was thought to be the only detergent that could solubilize active KdpFABC complex for almost 20 years [26]. In recent years, it became apparent that also other detergents could be used for solubilization of active KdpFABC complexes [27]. In our hands, DDM, $C_{12}E_8$, and to some extent Cymal-6 preserved the activity of the protein. Only the harsh detergent Fos-Choline-12 (FC-12) failed to maintain the activity of KdpFABC

concentration (to 1–2× CMC) for downstream applications, make sure to repeatedly check the structural and functional integrity of your protein.

2. In structural biology, the importance of lipids for structural integrity (correct folding, oligomeric state) has caused a rise in the percentage of membrane protein structures solved not only in detergent [14]. Especially the application of lipidic mesophases, bicelles, or lipids added to the protein prior to crystallization (HiLiDe or addition of cholesterol-hemi-succinate) has given rise to several new membrane protein structures [15–19].
3. Specifically, for functional studies it can be necessary to examine your protein in different lipid surroundings. There are various scaffolds available into which detergent-solubilized membrane proteins and lipids can be reconstituted forming stable membrane patches. Membrane scaffold proteins (MSPs) are used to form nanodiscs, the protein saposin forms the salipro nanoparticles, and the co-polymer styrene maleic acid (SMA) can form SMALPs (SMA-lipid-particles) [20–22].
4. Use whichever detergents you have access to, you never know which one will work. Anatrace offers a variety of different detergent kits (partially their Solution Master detergent Kit,

cat. no. DSOL-MK, was used in this study). Definitely we would recommend to try $C_{12}E_8$ and Cymal-6 or similar detergents, a glucoside like OG, a maltoside like DDM, a NG-class detergent like LMNG, a medium size Fos-Choline like Fos-Choline-12, and a cholesterol-like detergent, e.g., CHAPS or CHAPSO.

5. Since the ATPase assay performed with the purified protein after IMAC is very sensitive for traces of phosphate and already minimal amounts of potassium trigger ATPase activity of KdpFABC ($K_M = 2$ μM), it is very important to use the purest chemicals available for buffer preparation [23].
6. We recommend starting with detergent concentrations between 2× and 5× CMC. At these concentrations your protein of interest should be solubilized if the detergent is operative. Later on, reduction of the detergent concentration to as low as 1.5× CMC is advisory, especially for structural applications.
7. We found that this range of OD_{600nm} yields optimal cell disruption efficiency.
8. We recommend cycles of 30 s sonification followed by 30 s breaks to avoid heating of the sample (e.g., Sonifier250 (Branson) at an intensity of 7 and a pulsed operation of 70%).
9. Cell disruption at 1 MPa is recommended and one cell passage is usually sufficient for *E. coli* cells (e.g., Stansted pressure cell homogenizer).
10. The duration of the ultracentrifugation depends on the amount of time needed for formation of a firm membrane pellet, the longer you centrifuge the more small membrane vesicles are spun down.
11. The final detergent concentration of ~1% is not enough in all cases. It is highly dependent on the critical micelle concentration (CMC), which is different for each detergent. In our hands 1% of detergent was enough to solubilize with detergents that have a CMC below 0.5%.
12. We advise you to load one sample of the purified membranes per gel to visualize the maximum amount of protein that can be solubilized from the membranes.
13. We typically use the ThermoFisher Pierce Power Blot Cassette with ThermoFisher 1-Step Transfer Buffer and the 7-min program for medium molecular weight proteins and one blotting paper at each side of the membrane.
14. The constructs we use carry a His_{10}-tag which we verify with an anti-His antibody from mouse and a secondary anti-mouse IgG-horseradish-peroxidase antibody produced in goat.

15. In an unanticipated case like ours, where more than 70% of detergents solubilized KdpFABC, a deliberate decision on which detergents to follow up is challenging. Always consider the downstream experiments you want to perform. For structural studies, it is advisory to examine published structures of related proteins or protein classes and to read up on the latest trends in your structural biology method of choice [14, 24]. If the protein is meant to be reconstituted into liposomes after purification, detergents with very low CMCs should be avoided since their subsequent removal is rather challenging [25]. Finally, the activity of your protein of interest should not be impaired by the applied detergent, especially during functional studies. Therefore, a rapid, versatile, and precise activity assay, like the ATPase assay presented in this chapter, is a very beneficial tool.
16. The buffer for the ATPase assay and the buffer the protein is supplied in should be as similar as possible. A buffer with a minimal amount of components is favorable since it decreases contamination sources. Therefore, depending on the timepoint of purification after which one wants to perform the ATPase assay, a buffer exchange is required. Here we typically use Zeba Spin Desalting Columns (Thermo Fisher, different sizes and MWCOs available). The used concentrations of ATP and substrate (here KCl) need to be selected carefully. In both cases they need to be well above the K_M value, but very high concentrations have been shown to reduce the ATPase activity. We recommend you to perform ATPase assays at different substrate and ATP concentrations to determine the optimal used concentrations.
17. The concentration of the used protein sample needs to be chosen such that the absorption values determined do not exceed the values determined for the standard curve. Further, to determine meaningful values, it is an absolute requirement for the reaction to run under steady-state conditions. This means, that enough substrate is supplied to guarantee steady concentrations of ATPase–substrate complex. We check this by monitoring the amount of produced product over time. Practically, we analyze samples taken after 1-minute intervals and plot the absolute amount of product produced (μmol P_i* mg^{-1} of used ATPase) against the time. This graph should be linear for the selected reaction time.

References

1. Dorr JM, Scheidelaar S, Koorengevel MC, Dominguez JJ, Schafer M, van Walree CA, Killian JA (2016) The styrene-maleic acid copolymer: a versatile tool in membrane research. Eur Biophys J 45(1):3–21. https://doi.org/10.1007/s00249-015-1093-y

2. Parker JL, Newstead S (2012) Current trends in alpha-helical membrane protein crystallization: an update. Protein Sci 21(9):1358–1365. https://doi.org/10.1002/pro.2122
3. Chae PS, Rasmussen SG, Rana RR, Gotfryd K, Chandra R, Goren MA, Kruse AC, Nurva S, Loland CJ, Pierre Y, Drew D, Popot JL, Picot D, Fox BG, Guan L, Gether U, Byrne B, Kobilka B, Gellman SH (2010) Maltose-neopentyl glycol (MNG) amphiphiles for solubilization, stabilization and crystallization of membrane proteins. Nat Methods 7 (12):1003–1008. https://doi.org/10.1038/nmeth.1526
4. Cho KH, Husri M, Amin A, Gotfryd K, Lee HJ, Go J, Kim JW, Loland CJ, Guan L, Byrne B, Chae PS (2015) Maltose neopentyl glycol-3 (MNG-3) analogues for membrane protein study. Analyst 140(9):3157–3163. https://doi.org/10.1039/c5an00240k
5. Ilgu H, Jeckelmann JM, Gachet MS, Boggavarapu R, Ucurum Z, Gertsch J, Fotiadis D (2014) Variation of the detergent-binding capacity and phospholipid content of membrane proteins when purified in different detergents. Biophys J 106(8):1660–1670. https://doi.org/10.1016/j.bpj.2014.02.024
6. Kunji ER, Harding M, Butler PJ, Akamine P (2008) Determination of the molecular mass and dimensions of membrane proteins by size exclusion chromatography. Methods 46 (2):62–72. https://doi.org/10.1016/j.ymeth.2008.10.020
7. Seddon AM, Curnow P, Booth PJ (2004) Membrane proteins, lipids and detergents: not just a soap opera. Biochim Biophys Acta 1666(1–2):105–117. https://doi.org/10.1016/j.bbamem.2004.04.011
8. Stock C, Hielkema L, Tascon I, Wunnicke D, Oostergetel GT, Azkargorta M, Paulino C, Hänelt I (2018) Cryo-EM structures of KdpFABC suggest a K^+ transport mechanism via two inter-subunit half-channels. Nat Commun 9(1):4971. https://doi.org/10.1038/s41467-018-07319-2
9. Huang CS, Pedersen BP, Stokes DL (2017) Crystal structure of the potassium-importing KdpFABC membrane complex. Nature 546 (7660):681–685. https://doi.org/10.1038/nature22970
10. Siebers A, Altendorf K (1988) The K^+-translocating Kdp-ATPase from Escherichia coli. Purification, enzymatic properties and production of complex- and subunit-specific antisera. Eur J Biochem 178(1):131–140
11. Gassel M, Siebers A, Epstein W, Altendorf K (1998) Assembly of the Kdp complex, the multi-subunit K^+-transport ATPase of Escherichia coli. Biochim Biophys Acta 1415 (1):77–84
12. Bramkamp M, Altendorf K (2005) Single Amino Acid Substitution in the Putative Transmembrane Helix V in KdpB of the KdpFABC Complex of *Escherichia coli* Uncouples ATPase Activity and Ion Transport. Biochemistry 44 (23):8260–8266
13. Wilkins MR, Gasteiger E, Bairoch A, Sanchez JC, Williams KL, Appel RD, Hochstrasser DF (1999) Protein identification and analysis tools in the ExPASy server. Methods Mol Biol 112:531–552
14. Parker JL, Newstead S (2016) Membrane Protein Crystallisation: Current Trends and Future Perspectives. Adv Exp Med Biol 922:61–72. https://doi.org/10.1007/978-3-319-35072-1_5
15. Loll PJ (2014) Membrane proteins, detergents and crystals: what is the state of the art? Acta Crystallogr F Struct Biol Commun 70 (Pt 12):1576–1583. https://doi.org/10.1107/S2053230X14025035
16. Caffrey M, Porter C (2010) Crystallizing membrane proteins for structure determination using lipidic mesophases. J Vis Exp 45. https://doi.org/10.3791/1712
17. Gourdon P, Andersen JL, Hein KL, Bublitz M, Pedersen BP, Liu X-Y, Yatime L, Nyblom M, Nielsen TT, Olesen C, Møller JV, Nissen P, Morth JP (2011) HiLiDe—systematic approach to membrane protein crystallization in lipid and detergent. Cryst Growth Des 11 (6):2098–2106. https://doi.org/10.1021/cg101360d
18. Kulig W, Tynkkynen J, Javanainen M, Manna M, Rog T, Vattulainen I, Jungwirth P (2014) How well does cholesteryl hemisuccinate mimic cholesterol in saturated phospholipid bilayers? J Mol Model 20(2):2121. https://doi.org/10.1007/s00894-014-2121-z
19. Faham S, Bowie JU (2002) Bicelle crystallization: a new method for crystallizing membrane proteins yields a monomeric bacteriorhodopsin structure. J Mol Biol 316(1):1–6. https://doi.org/10.1006/jmbi.2001.5295
20. Bayburt TH, Sligar SG (2010) Membrane protein assembly into Nanodiscs. FEBS Lett 584 (9):1721–1727. https://doi.org/10.1016/j.febslet.2009.10.024
21. Frauenfeld J, Loving R, Armache JP, Sonnen AF, Guettou F, Moberg P, Zhu L, Jegerschold C, Flayhan A, Briggs JA, Garoff H, Low C, Cheng Y, Nordlund P (2016) A saposin-lipoprotein nanoparticle system for membrane proteins. Nat Methods 13(4):345–351. https://doi.org/10.1038/nmeth.3801

22. Knowles TJ, Finka R, Smith C, Lin YP, Dafforn T, Overduin M (2009) Membrane proteins solubilized intact in lipid containing nanoparticles bounded by styrene maleic acid copolymer. J Am Chem Soc 131(22):7484–7485. https://doi.org/10.1021/ja810046q
23. Fendler K, Dröse S, Altendorf K, Bamberg E (1996) Electrogenic K^+ transport by the Kdp-ATPase of Escherichia coli. Biochemistry 35(24):8009–8017
24. Gewering T, Januliene D, Ries AB, Moeller A (2018) Know your detergents: A case study on detergent background in negative stain electron microscopy. J Struct Biol 203 (3):242–246. https://doi.org/10.1016/j.jsb.2018.05.008
25. Geertsma ER, Nik Mahmood NA, Schuurman-Wolters GK, Poolman B (2008) Membrane reconstitution of ABC transporters and assays of translocator function. Nat Protoc 3 (2):256–266. https://doi.org/10.1038/nprot.2007.519
26. Siebers A, Kollmann R, Dirkes G, Altendorf K (1992) Rapid, high yield purification and characterization of the K(+)-translocating Kdp-ATPase from Escherichia coli. J Biol Chem 267 (18):12717–12721
27. Damnjanovic B, Weber A, Potschies M, Greie JC, Apell HJ (2013) Mechanistic analysis of the pump cycle of the KdpFABC P-type ATPase. Biochemistry 52(33):5563–5576. https://doi.org/10.1021/bi400729e

Chapter 8

GPCR Solubilization and Quality Control

Tamara Miljus, David A. Sykes, Clare R. Harwood, Ziva Vuckovic, and Dmitry B. Veprintsev

Abstract

G protein-coupled receptors (GPCRs) are versatile membrane proteins involved in the regulation of many physiological processes and pathological conditions, making them interesting pharmacological targets. In order to study their structure and function, GPCRs are traditionally extracted from membranes using detergents. However, due to their hydrophobic nature, intrinsic instability in aqueous solutions, and their denaturing effects, the isolation of properly folded and functional GPCRs is not trivial. Therefore, it is of crucial importance to solubilize receptors under mild conditions and control the sample quality subsequently. Here we describe widely used methods for small-scale GPCR solubilization, followed by quality control based on fluorescence size-exclusion chromatography, SDS-PAGE, temperature-induced protein unfolding (CPM dye binding) and fluorescent ligand binding assay. These methods can easily be used to assess the thermostability and functionality of a GPCR sample exposed to different conditions, such as the use of various detergents, addition of lipids and ligands, making them valuable for obtaining an optimal sample quality for structural and functional studies.

Key words GPCR solubilization, FSEC, In-gel fluorescence, Thermal shift assay, Fluorescent ligand binding assay

1 Introduction

1.1 GPCR Production in Mammalian Cells

GPCRs have been produced in a number of expression systems ranging from cell-free expression, to bacterial *E. coli*, yeast, insect, and mammalian cell cultures. By far the most successful systems for the production of proteins for structural studies have been insect and mammalian cell cultures [1]. The reader is referred to a number of reviews and resources already available on the topic of production of recombinant GPCRs for structural studies [1–7].

1.2 GPCR Solubilization

In order to study the structure and function of membrane proteins in vitro, they first have to be extracted from the native membrane bilayer they were expressed in, most often insect or mammalian cell membranes. Detergents were traditionally employed for

Camilo Perez and Timm Maier (eds.), *Expression, Purification, and Structural Biology of Membrane Proteins*, Methods in Molecular Biology, vol. 2127, https://doi.org/10.1007/978-1-0716-0373-4_8,

the extraction of membrane proteins, and are still widely used [8]. Detergents are surfactants, amphiphilic compounds with well-segregated polar and apolar domains that reduce the interfacial surface tension in mixtures. They tend to aggregate into water-soluble micelles, this process is known as micellization. Micellization is driven by the favorable thermodynamic effect of the bulk water phase on the detergent molecules. Micelles are characterized by their critical micelle concentration (CMC, detergent concentration above which monomers self-assemble into micelles) and aggregation number (i.e. the number of detergent monomers present within a micelle). Their nature allows detergents to interact with hydrophobic membrane proteins and form a protective belt around them, keeping them water-soluble inside of formed micelles. However, a solubilized protein may or may not be in its native conformation, depending on its inherent protein stability, the detergent used, and the biochemical procedure it was exposed to [9]. Both the hydrophilic and hydrophobic groups of a detergent influence the stability of the membrane protein solubilized in it. While hydrophobic parts interact with the solubilized protein and prevents aggregation, the hydrophilic part is responsible for the proteins' extraction from membranes. Based on their properties, detergents can be classified as harsh ionic detergents, with the tendency for protein denaturation due to disruption of inter- and intramolecular protein–protein interactions (e.g., sodium dodecyl sulfate (SDS)). Mild non-ionic detergents, such as maltosides (e.g., n-dodecyl β-D-maltoside (DDM)) [10], glucosides, and polyoxyethylene glycols, which disrupt protein–lipid interactions rather than protein–protein interactions, whilst zwitterionic detergents have intermediate effects, such as 3-[(3-cholamidopropyl)dimethylammonio]-1-propanesulfonate (CHAPS).

Although detergents are of critical use for the extraction of GPCRs from membranes, they can interfere with certain biochemical applications and therefore their concentrations may have to be kept at the minimum to just above the CMC (2 or 3× the CMC is usually used), either by dilution of protein solution, dialysis, or gel filtration. For certain applications, it may be possible or desirable to replace detergents with other membrane mimics such as nanodiscs or liposomes [11], by the removal of detergent monomers by dialysis or adsorption to hydrophobic beads, various chromatography types or by enclosure into cyclodextrin cages.

The stability of GPCRs for biophysical studies is improved by reconstitution into liposomes [12], amphipols [13], or nanodiscs [14] right after solubilization, which mimic their natural environment within the membrane. Alternatively, GPCRs are extracted from membranes using a novel technique based on encapsulating proteins within styrene maleic acid lipid particles (SMALPs),

overcoming the problems associated with the usage of detergents [15]. A good overview of various available solubilization and reconstitution technologies is presented here [11].

1.3 Quality Control

Because the solubilization process is harsh on membrane proteins, it is important to check the quality and functionality of the membrane protein sample following its solubilization. In addition, quality control at this stage can be used to screen a number of conditions, such as the usage of various detergents, lipids, ligands, cofactors, and other additives, in order to prepare the best protein sample quality possible.

1.3.1 FSEC

In fluorescence-detection size-exclusion chromatography (FSEC), size-exclusion chromatography is coupled with a fluorescence detector. Since many recombinant proteins can be fluorescently tagged by green fluorescent protein (GFP), FSEC presents a reliable, fast, and simple method for the analysis of the protein homogeneity and degree of aggregation, and is used to guide the development of a purification protocol. It can readily be used to assess protein sample quality straight after solubilization (on crude cell lysates) to find optimal buffer compositions, detergents, supplementation lipids, stabilizing ligands, cofactors, or other additives that may help stabilize the receptor. The method can also be performed on purified receptor samples, as well as for characterization of complex formation and protein degradation over time [16, 17].

1.3.2 Thermal Shift Assays

Thermal shift assays are valuable tools for characterizing purified receptor proteins, allowing an assessment of their relative thermostability, when various solubilization methods are used, and an assessment of stabilizing interactions with cognate ligands [18]. Here we cover assays based on FSEC and gel electrophoresis, as well as a CPM assay. Although none of these protein thermostability measurement methods yields a "true" melting temperature for the protein since the denaturation of GPCRs is an irreversible process. However, in most cases they can readily be used to compare relative protein stability under different conditions, therefore facilitating the optimization of protein preparations for further studies. FSEC- and gel-based assays can be performed with crude cell lysates from a relatively small cultured sample, such as one 10 cm dish.

FSEC-Based Thermal Shift Assay

For receptors which are very unstable and cannot be purified, the thermostability of a fluorescently labeled protein can be measured by FSEC based on protein aggregation [19]. In this case, solubilized protein samples are incubated over a range of different temperatures, followed by centrifugation and filtration to remove large aggregates, and finally by FSEC analysis. As the

temperature increases, the protein aggregates and the peak corresponding to the solubilized protein shifts to a higher molecular weight. Protein peaks decrease in intensity due to the majority of high-molecular-weight aggregates being removed by centrifugation prior to loading on the column. However, this method is not high-throughput, as there are usually 10 samples per condition (corresponding to incubations over a range of temperatures) to be analyzed on FSEC separately.

Gel-Based Thermal Stability Assay

If HPLC instrumentation is not available, the stability of a fluorescently labeled membrane protein can also be readily assessed by gel electrophoresis. Similar to FSEC analysis, receptor stability is assessed by heating samples of receptor to different temperatures and monitoring the amount of fluorescent signal left in each sample following removal of aggregates by centrifugation. The fluorescence intensity of each sample indicates the quantity of stable protein in each sample. Since a crude extract is analyzed, there is no need for a purification step which allows the test to be performed on transiently transfected cells and early on in the crystallization pipeline.

CPM Assay

When a purified protein sample is available (*see* Subheading 3 for small-scale purification protocol), fluorescence-based thermal shift assays employ either an environmentally sensitive or chemical conjugation-sensitive fluorophores to monitor protein denaturation, enabling higher-throughput melting temperature (T_m) determination with reduced protein requirements compared to the aforementioned techniques. Solvatochromic dyes which show an increase in their fluorescent quantum yield when moving from polar to non-polar environments [20–22] work well with soluble proteins, but have limited utility with hydrophobic proteins and detergent-solubilized membrane proteins due to strong interference of the dye with hydrophobic components [23]. The thermal stability of integral membrane proteins such as GPCRs is better studied using more specific thiol-reactive dyes such as N-[4-(7-diethylamino-4-methyl-3-coumarinyl)phenyl]maleimide (CPM) or BODIPY-FL-cysteine [18, 24–26]. If a purified protein can be obtained, the CPM assay is a preferred method for measuring receptor stability as a single sample is heated and fluorescence is instantly measured, allowing multiple conditions to be analyzed simultaneously. In the following protocols, we outline the use and validation of the thiol-reactive CPM dye as a general tool to monitor thermal unfolding of a detergent-solubilized GPCR, as well as its utility as a tool to characterize low-molecular-weight ligands.

1.3.3 Ligand Binding Assay

In order to test the functionality of a purified receptor, a simple method is required which can rapidly discriminate between active and inactive material. The most widely used procedure is ligand binding, which relies on the binding of a receptor-specific ligand usually a radiochemical. Ligand binding assays are a cornerstone of pharmacology and have been used for decades in screening campaigns to discover inhibitors and activators of GPCR function. Such techniques are useful for determining the presence and the extent of active receptor in any given sample. Radioligand binding assays [27] can be formulated in many different ways using either a filtration technique to separate the bound from free ligands or alternatively in a homogenous format, the so-called mix and measure procedures which do not require a separation step and allow real-time measurement of protein stability. Similarly, fluorescent-ligand-based techniques can be used, such as those based on resonance energy transfer (RET), where the protein of interest is labeled with a donor fluorophore (e.g., fluorescence resonance energy transfer (FRET)) [28] or alternatively a luciferase enzyme is used as an energy donor (e.g., bioluminescence resonance energy transfer (BRET)) [29]. Although the acceptor ligand usually has to be modified by addition of the fluorescent moiety, potentially affecting its physicochemical and/or binding properties, these methods are widely used and continuously evolving due to their inherent sensitivity, reliability, and high speed, making them suitable to perform in 384- or 1536-well formats. Alternatively, ligand binding to the receptor can be assessed by detecting the change in fluorescence anisotropy of a relatively small fluorescent ligand upon binding to a large protein molecule [30].

2 Materials

Prepare all solutions using ultrapure water (an electrical resistivity of 18 MΩ cm at 25 °C) and analytical-grade reagents. Prepare and store all reagents at room temperature, unless otherwise specified. Filter-sterilize all the buffers through 0.22 μm filter using either a vacuum powered filtration unit (disposable or reusable, for larger volumes) or a syringe (for small volumes).

2.1 GPCR Solubilization

1. Detergent stock solutions: 10% DDM (n-dodecyl β-D-maltoside) containing 1 or 2% CHS (cholesteryl hemisuccinate) in 200 mM Tris buffer, pH 8.0. To make the stock solution, add 30 mL of water and 10 mL of 1 M Tris buffer, pH 8.0, to a 50-mL falcon tube. Add 5 g of DDM, close the tube and incubate under gentle rotation until the detergent is dissolved. Add 0.5 or 1 g of CHS to the detergent solution. Sonicate using a probe sonicator until the solution becomes translucent. Bring the volume to 50 mL with water, for a final Tris buffer

concentration of 200mM, close the tube and incubate under gentle rotation at room temperature until the solution becomes transparent. Aliquot and store at 4 °C, or −20 °C for long-term (over 24 h) storage. Following the same procedure, prepare 10% CHAPS and 2% CHS in 200 mM Tris buffer, pH 8.0.

2. Solubilization buffer (SB), 50 mM HEPES, 2 mM EDTA, 300 mM NaCl, 10% glycerol, 1× protease inhibitors (PI Complete, Roche), 1% DDM, 0.5% CHAPS, 0.3% CHS, pH 7.5. Add all the buffer components from stock solutions made in water, filter-sterilize, and then add the detergent(s) from stock solutions to avoid excessive foaming. Store at −20 °C long term or at 4 °C if to be used within several days. The exact composition of detergents used in the solublization process may depend on the receptor under study but 1% DDM with 0.2% CHS is a good starting point. However, if it does not produce functional receptor, alternative detergents or a mix of detergents may have to be experimentally tested.
3. Ultracentrifuge (e.g., Optima MAX, Beckman Coulter for small-scale solubilization) and ultracentrifuge tubes.

2.2 Small-Scale Purification Using a Combination of a Twin-Strep-Tag and Strep-Tactin-Coated Magnetic Beads

1. MagStrep "type 3" XTMagnetic (Strep-Tactin® XT coated) beads (IBA Lifesciences, Germany).
2. Magnetic separator (IBA Lifesciences, Germany).
3. Washing buffer (WB), 20 mM HEPES, 150 mM NaCl, 10% glycerol, pH 8.0.
4. Elution buffer (EB), 20 mM HEPES, 150 mM NaCl, 10% glycerol, 0.02% DDM, 10 mM biotin, pH 8.0. Buffer conditions should be adapted and optimised to suit the protein of interest.

2.3 In-gel Fluorescence

1. SDS-PAGE gels and appropriate buffer, e.g., TruPAGE Precast 12% gels (Sigma-Aldrich) and TruPAGE TEA Tricine SDS Running buffer (Sigma-Aldrich). Please note that NuPage Bis-Tris-based gels are not compatible with the detection of GFP-tagged proteins, although tris-glycine-based gels are.
2. Gel imager fitted with fluorescence detection, e.g., Amersham Imager 600 (GE Healthcare).
3. 5× SDS-PAGE sample buffer, 250 mM Tris–HCl, 50% glycerol, 10% SDS, 5% β-mercaptoethanol, 0.5% bromophenol blue dye, pH 6.8.
4. SDS-PAGE protein standards, e.g., Precision Plus Protein Standards (Biorad).

2.4 FSEC

1. High-pressure chromatography system (e.g., ÄKTA) fitted with a fluorescence excitation system and detector.
2. Size-exclusion column (e.g., GE Healthcare Superdex 200 Increase 5/150 or TOSOH TSKgel SuperSW3000).
3. FSEC running buffer (RB), 50 mM HEPES, 300 mM NaCl, 0.02% DDM and 0.004% CHS, pH 7.5.

2.5 CPM Assay

1. RotorGene Q qPCR instrument and 72-Well Rotor (Qiagen, Germany).
2. Strip tubes and caps, 0.1 mL (Qiagen).
3. CPM dye stock solution, 3 mg/mL in anhydrous DMSO. Dissolve solid CPM dye in an appropriate amount of anhydrous DMSO, aliquot in black tubes, close tightly and store at −20 °C. CPM dye can degrade when exposed to light.
4. Assay buffer, 20 mM HEPES, 150 mM NaCl, 10% glycerol, 0.02% DDM, 0.002% CHS, pH 7.45. Assay buffer composition can be modified, but avoid using Tris-based buffers due to its pH being highly temperature-dependent.

2.6 HTRF-Based Ligand Binding Assay

2.6.1 Receptor Labeling with Terbium Cryptate

1. 1× Tag-lite medium: Add 10 mL of LABMED (5× concentrated from Cisbio Bioassays, France) to a 50 mL Sterilin container. Add ultrapure water to a volume of 50 mL. Mix and store at 4 °C.
2. Labeling medium, 100 nM SNAP-Lumi4-Tb in 1× Tag-lite medium. Add 20 μL of 100 mM SNAP-Lumi4-Tb DMSO stock (Cisbio Bioassays, France) to 20 mL of Tag-lite medium. Mix and store at −20 °C.
3. Cell wash buffer, Dulbecco's phosphate buffered saline (D-PBS, Sigma-Aldrich).
4. Cell culture medium, Dulbecco's modified Eagle's medium (DMEM)—high glucose (D6429, Sigma-Aldrich), supplemented with 10% fetal calf serum (FCS, Sigma-Aldrich, F7524). Store at 4 °C.
5. Cell Dissociation Solution Nonenzymatic 1× (C5789, Sigma-Aldrich).

2.6.2 Membrane Preparation

1. Membrane preparation buffer, 10 mM HEPES, 10 mM EDTA, pH 7.4. Dissolve 2.38 g HEPES and 3.80 g of disodium EDTA in 1 L of water and adjust pH to 7.4 with 3 M HCl. Store at 4 °C for up to 1 week.
2. Membrane storage buffer, 10 mM HEPES, 0.1 mM EDTA, pH 7.4. Dissolve 2.38 g HEPES and 0.038 g of disodium EDTA in 1 L of water and adjust pH to 7.4 with 3 M NaOH. Store at 4 °C for up to 1 week.

3. Tissue homogenizer (e.g., Ultra-Turrax, Ika-Werk, Germany).
4. 25 mL centrifuge tubes (Universals) and bench top centrifuge (e.g., Heraeus Megafuge 8 centrifuge).
5. Ultracentrifuge (e.g., Optima MAX, Beckman Coulter) and ultracentrifuge tubes.
6. Protein concentration determination kit: e.g., Pierce Bicinchoninic Acid Protein Assay Kit (Thermo Scientific).

2.6.3 Ligand Binding

1. Fluorescently labeled ligand such as the propranolol derivative labeled with a red fluorescent probe (propranolol-red, Hello-Bio, UK) designed to bind the beta2 adrenergic receptor (β_2AR). Prepare a 10 μM stock solution by adding 1 μL of 1 mM propranolol red to 99 μL of assay buffer in a 0.5 mL Eppendorf.
2. Assay buffer, 20 mM HEPES, 150 mM NaCl, 10% Glycerol, 0.5% BSA, 1% DMSO, 0.1% DDM, pH 7.5. Alternative assay buffer components can be considered. For example, cholesteryl hemisuccinate (CHS) may be required to maintain the functionality of some receptors.
3. Plate reader, e.g., Pherastar FS (BMG Labtech).
4. White 384-well Optiplates (PerkinElmer, UK) or equivalent microplate.
5. 384-well compatible multichannel pipettors (8 or 12 channel) and reagent reservoirs (e.g., Matrix).
6. Optical plate sealers, e.g., MicroAMP™ Optical Adhesive Film (Thermo Scientific). Optical plate seals are only necessary if significant evaporation of the sample is expected.

3 Methods

All procedures are performed on ice or at 4 °C, unless otherwise specified.

3.1 GPCR Solubilization

1. Express GPCR stably or transiently in adherent HEK293 cells. Wash cells with PBS and harvest into phosphate buffered saline (PBS) containing 2 mM EDTA or using a plastic cell scraper. Pellet cells by centrifugation at 500 × *g* for 5 min, and use immediately or flash-freeze in liquid nitrogen and store at −80 °C (*see* **Note 1**).
2. Resuspend approximately 10 million cells (one 10-cm dish when grown in adherent culture) in 600 μL of solubilization buffer (SB) (*see* **Notes 2–4**).
3. Incubate under gentle rotation for 1 h.

4. Centrifuge the lysate at 150,000 × *g* for 30 min to remove non-solubilized material.
5. Transfer the supernatant containing the solubilized protein to a precooled 1.5 mL tube.

3.2 Small-Scale Purification of Twin-Strep-Tagged GPCR Using Strep-Tactin-Coated Magnetic Beads

Some of the techniques described here require purified protein samples achieved using the following purification procedure.

1. Use 20 μL of 5% Strep-Tactin-coated magnetic beads suspension per estimated nanomole of Twin-Strep-tagged target protein. Remove the supernatant from the required volume of MagStrep "type 3" XTMagnetic beads using a magnetic rack.
2. Wash the magnetic beads three times in wash buffer (WB) to remove any trace of the storage buffer using the magnetic rack.
3. Prepare Twin-Strep-tagged protein sample: harvest and solubilize HEK293 cells expressing the Twin-Strep-tagged target protein as described earlier in Sect. 3.1.
4. Resuspend the magnetic beads in the solubilized protein sample and incubate for 2–24 h under gentle rotation (80 rpm).
5. Retain the target-protein-bound magnetic beads using the magnet and wash three times with WB.
6. Resuspend the magnetic beads in elution buffer (EB) containing 10 mM biotin and incubate for 2–4 h under gentle rotation.
7. Place the sample back on the magnet to remove the magnetic beads from the supernatant containing the now purified protein.

3.3 In-gel Fluorescence

1. Solubilize the fluorescently labeled protein as described earlier in Sect. 3.1.
2. Mix the protein sample with 5× SDS-PAGE protein loading dye.
3. Load an appropriate amount of protein on a gel, depending on gel well size. Load protein markers (*see* **Note 5**).
4. Run the gel at 130 V for about 1.5 h.
5. Measure fluorescence on a gel imager (*see* **Note 6**).

3.4 FSEC

1. Equilibrate the column (e.g., GE Healthcare Superdex 200 Increase 5/150 or TOSOH TSKgel SuperSW3000) with at least 2 column volumes (CV) of RB (*see* **Notes 7–9**).
2. Prepare a protocol for automated chromatography, depending on the HPLC system used. For each sample to be analyzed, the protocol should contain the following steps:

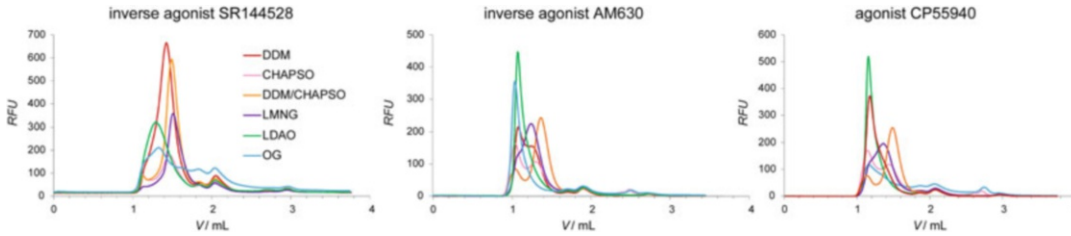

Fig. 1 Quality control of cannabinoid CB2 receptor construct (CB2-eGFP-TwinStrep-1D4) solubilized in various detergents in the presence of inverse agonists (SR144528 and AM630) or an agonist (CP55940), analyzed by FSEC on an ÄKTA Ettan LC system using a GE Healthcare Superdex 200 Increase 5/150 column. Although all three tested ligands have the same effect on CB2 stability in the "best" detergent (DDM/CHAPSO), the ability of ligands to stabilize the receptor in harsher conditions, such as using only DDM for solubilization, decreases in the following order: SR144528 > AM630 > CP55940

(a) RB should be run before sample injection to ensure a stable baseline, e.g., 1.2 mL for TOSOH TSKgel SuperSW3000 column.

(b) Auto-zero the fluorescence signal before sample injection to allow comparison between samples.

(c) Sample injection, e.g., 10 μL.

(d) Flow the RB for 1 CV, e.g., 5 mL for TOSOH TSKgel SuperSW3000 column.

3. Set an appropriate flow rate, e.g., 0.15 mL/min, for TOSOH TSKgel SuperSW3000 column.
4. Set column pressure limit and automatic run pause in case the maximal pressure is reached, to prevent column damage (e.g., 10 MPa for TOSOH TSKgel SuperSW3000) (*see* **Note 10**).
5. Set appropriate excitation and detection wavelengths to detect the protein of interest, e.g., for eGFP-fused protein excitation at 485 nm and detection at 530 nm.
6. Prepare protein samples in glass vials compatible with the instrument's automatic injection module, and load into the module in the manner dictated by the protocol. For example, if 10 μL protein is to be injected, use 30 μL protein sample in vials (*see* **Notes 11** and **12**).
7. Start the protocol (*see* **Note 13**).
8. At the end of the run, export the resulting chromatograms for further analysis (*see* Fig. 1).

3.5 FSEC-Based Thermal Shift Assay

1. Following the same method described above, solubilize approximately 10 million HEK293 cells in 600 μL SB, and clear the lysate by centrifugation (*see* **Note 14**).
2. Aliquot the supernatant (or eluate in the case where purified protein is used, adjusting the amount of material used and the sample volumes) into ten 1.5 mL tubes of 45 μL each.

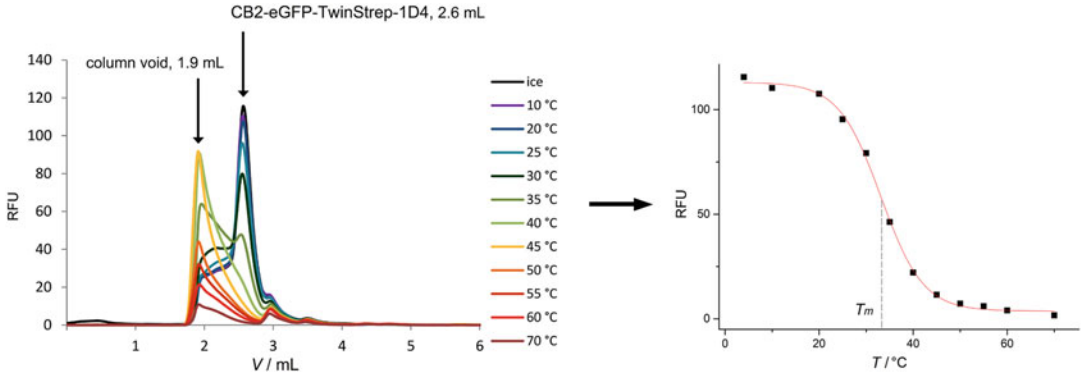

Fig. 2 Extraction of a melting temperature from fluorescence size-exclusion chromatograms. Chromatograms of cannabinoid CB2 receptor construct (CB2-eGFP-TwinStrep-1D4) were obtained on an ÄKTA Ettan LC system using a TOSOH TSKgel SuperSW3000 column as described. The peak retention volume of a chromatogram corresponding to the sample kept on ice was found (2.6 mL). The relative fluorescence at that volume was read for all other samples corresponding to incubation at various temperatures. The relative fluorescence was plotted versus the incubation temperature, the data were fitted into Boltzmann equation, and a melting temperature (T_m) was extracted

3. Incubate aliquots over a relevant temperature range for 30 min using a heating block. After incubation, store the sample on ice until loading onto the column (*see* **Note 15**).
4. Remove the largest protein aggregates by centrifugation at 20,000 × *g*, 4 °C, 30 min.
5. Analyze all the samples on FSEC as described earlier.
6. Repeat for different test conditions, e.g., solubilization with various detergents, addition of ligand, protein purification, addition of lipids during purification.
7. For each tested condition, find and note the peak retention volume of a chromatogram corresponding to the sample kept on ice.
8. Read relative fluorescence at that retention volume for all other samples corresponding to incubation at various temperatures.
9. Plot the resulting relative fluorescence versus the incubation temperature, fit the data into Boltzmann equation (e.g., using Origin, OriginLab or Prism 8, GraphPad), and extract the melting temperature (T_m) as a midpoint on the sigmoidal curve (*see* Figs. 2 and 3).

3.6 Gel-Based Thermal Stability Assay

1. Aliquot the supernatant (or eluate in cases where purified protein is used, adjusting the amount of material used and the total sample volume) into ten 1.5 mL tubes of 60 µL each (*see* **Note 16**).
2. Transfer all the samples simultaneously into a heat block at 25 °C. Heat for 5 min.

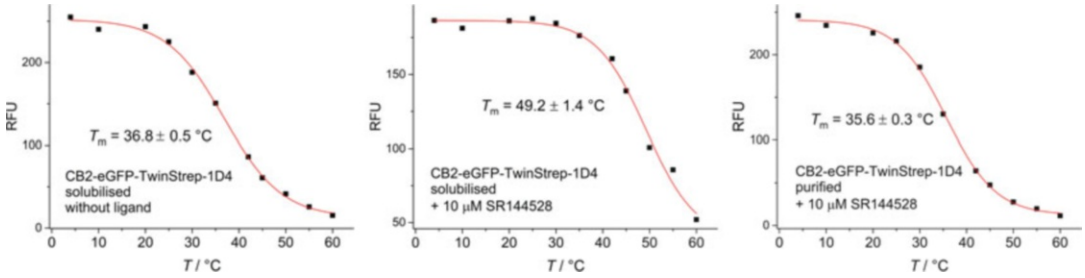

Fig. 3 Relative stability of a solubilized or purified CB2 receptor construct, with or without inverse agonist, as measured by FSEC. Thermostability of CB2-eGFP-TwinStrep-1D4 construct was analyzed on ÄKTA Ettan LC system using TOSOH TSKgel SuperSW3000 column, and melting temperatures of crude cell lysate or purified receptor, with or without addition of 10 μM inverse agonist SR144528, were determined as described. An increase in CB2 thermostability upon binding of an inverse agonist allows its purification (thermostability measurements of a purified apo-CB2 was impossible due to protein aggregation even at low temperatures)

3. After 5 min, take one sample out of the heat block and put on ice. Increase the heated temperature by 5 °C. Heat the remaining samples for another 5 min after the temperature is stabilized.
4. Repeat until all samples are removed from the heat block.
5. Centrifuge all the samples at 21,000 × *g* for 40 min at 4 °C to remove the largest protein aggregates.
6. Analyze the samples by SDS-PAGE as described earlier.
7. For each temperature point, determine the fluorescence intensity of folded protein sample using a software for quantitative image analysis, such as ImageJ (*see* **Note 17**).
8. Plot the resulting relative fluorescence versus the incubation temperature, fit the data into Boltzmann equation (e.g., using Origin, OriginLab or Prism 8, GraphPad), and extract the melting temperature (T_m) as a midpoint on the sigmoidal curve (*see* Fig. 4).

3.7 CPM Thermal Stability Assay Using Purified Receptor Proteins

1. Prepare a series of protein samples in μg quantities, e.g., 2, 4, 8, and 10 μg per 50 μL diluted in assay buffer from a stock of purified and concentrated receptor protein. This will correspond to approximately 0.5 to 2.5 μM of protein in the final sample (*see* **Note 18**).
2. Prepare a concentration series of CPM dye, e.g., 0.25, 0.5 and 1.0 μg per 7 μL by diluting stock CPM dye solution (3 mg/mL, 7.5 mM) in assay buffer (*see* **Note 18**).
3. Mix 25 μL of assay buffer, 50 μL of protein dilution and 7 μL of CPM dye dilution in the first row (A1–12) on a 96-well polypropylene plate so that each combination of protein and CPM dye concentration is prepared. The total reaction volume is

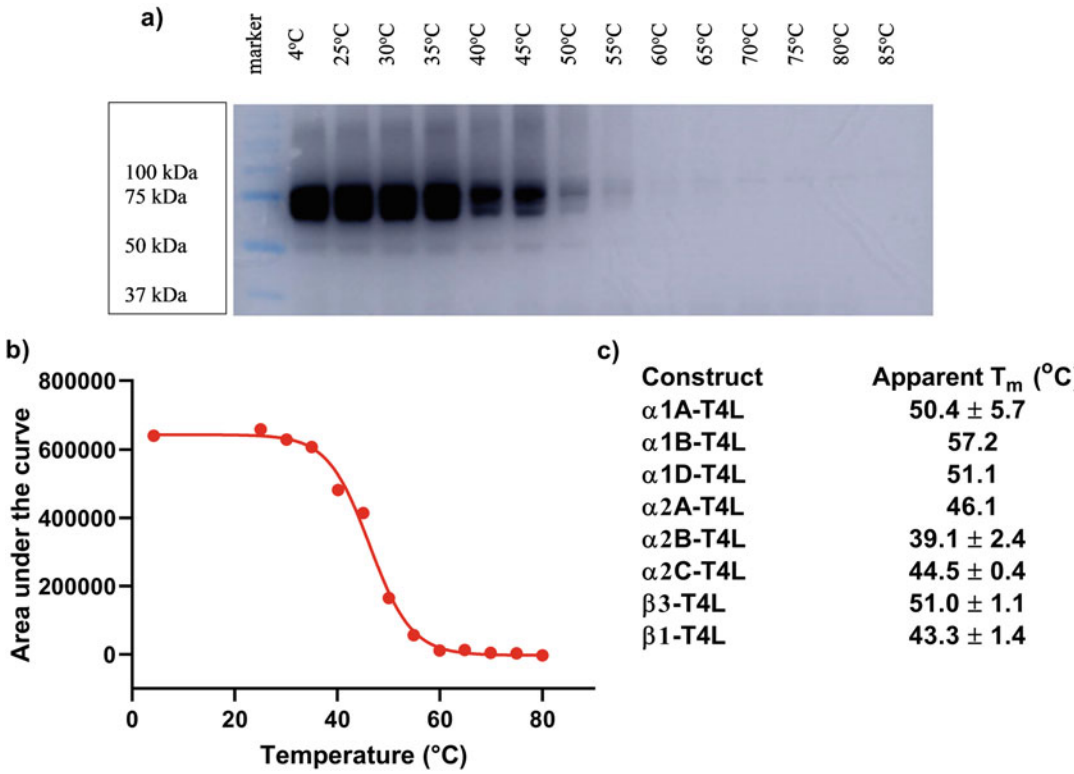

Fig. 4 Relative thermostability of alpha and beta adrenergic receptor constructs as measured by a gel-based thermostability assay. A receptor protein sample (alpha2C-T4L-AR with transferred mutations from turkey beta1 adrenergic receptor) was loaded on TruPAGE Precast 12% gels and run in TruPAGE TEA Tricine SDS Running buffer, 120 V, 1 h 40 min. GFP fluorescence was imaged using Amersham imager (**a**), followed by extraction of the relative intensities with an in-house program, plotted against the sample temperature (**b**). Using this method, melting temperatures were determined for various receptor constructs (**c**)

82 μL. Resulting CPM concentration is approximately 7.5, 15, and 30 μM. The samples should be kept on ice for a maximum of 5 min following the dye addition. If additional incubation is required, protect the samples from light as CPM dye can start degrading.

4. Add 25 μL of the receptor-dye reaction mixtures to PCR tubes in triplicates (*see* **Note 19**).
5. Measure fluorescence using a Rotorgene Q qPCR instrument. Ramp the temperature from 25 °C to 85 °C with a 4 °C increase per minute. Set the gain to the first sample in the run which is the reference consisting of protein and dye. Monitor CPM dye binding by excitation at 365 nm, and emission at 460 nm (*see* **Note 20**).
6. Analyze the data using the instrument software program "melt," which calculates the first derivative and reports the

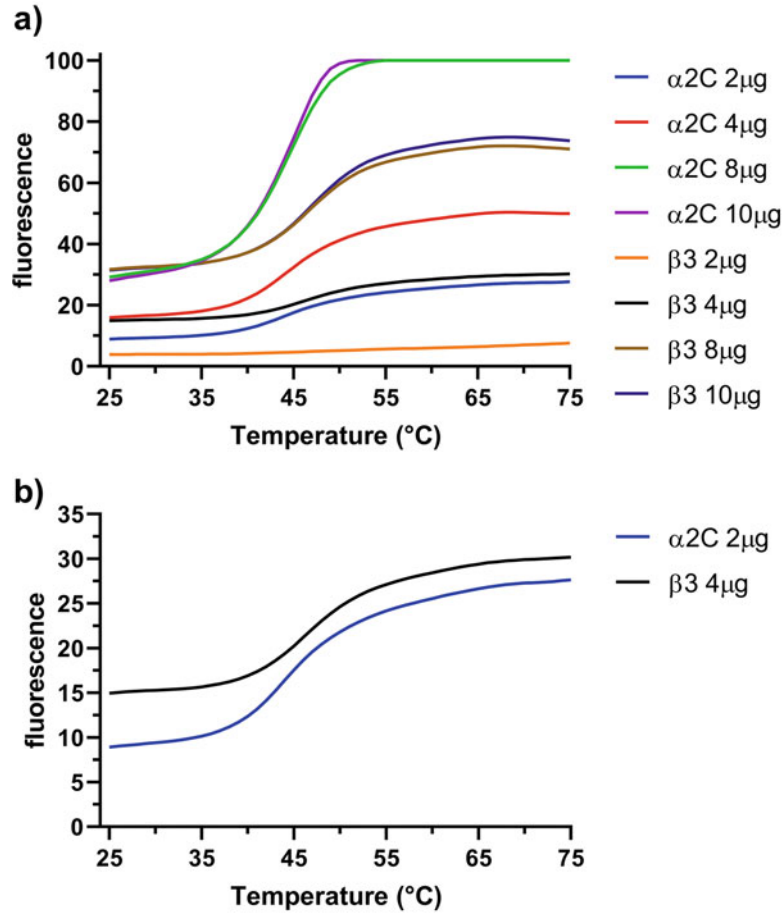

Fig. 5 The thermostability of adrenergic receptor constructs, as measured by the CPM assay. Generally, a higher protein (alpha2C-T4L-AR or beta3-T4L-AR) concentration results in higher fluorescent signal detected at a fixed CPM dye concentration of 15 μM per sample. If the concentration of the protein is too low, the fluorescence difference is too small to be observed, while with a high concentration of the protein, the fluorescence signal saturates and can lead to artificially decreased melting temperature (**a**). Selected protein concentrations of the alpha2C-T4L-AR and beta3-T4L-AR (**b**)

reflection point of each sample curve. Data is smoothed using "heavy" digital filter settings by using a sliding window of experimental data points. Invert the signal to give a maximum representing the T_m on the positive site. Calculate the melting temperatures as an average of each triplicate (triplicates on average do not differ for more than 0.5 °C; *see* Figs. 5 and 6).

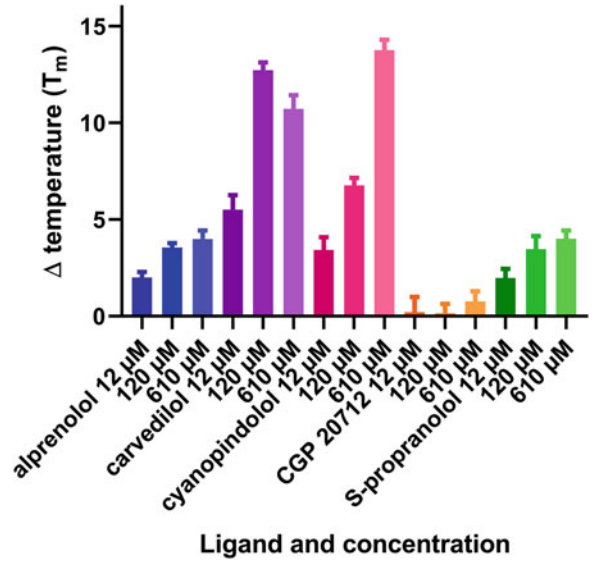

Fig. 6 Effect of ligand addition on beta3-T4-AR thermostability as measured by CPM assay. Melting temperatures were extracted using Rotorgene Q qPCR instrument software as described, shown as mean and standard deviation of three independent experiments. All compounds were tested at three different concentrations (12, 120, and 610 μM), at a fixed CPM dye concentration of 15 μM per sample

3.8 HTRF-Based Ligand Binding Assay

All steps are performed at room temperature unless otherwise stated.

3.8.1 Labeling of SNAP-Tagged GPCR with Terbium

1. Aspirate the cell culture medium from a T175 cm^2 flask containing confluent adherent HEK293 cells expressing a GPCR fused with a SNAP-tag.
2. Wash the cells twice with D-PBS and once with 10 mL of Tag-lite medium.
3. Add 10 mL of Tag-lite labeling medium containing 100 nM of SNAP-Lumi4-Tb and incubate at 37 °C under 5% CO_2 for 1 h.
4. Wash the cells twice with D-PBS to remove the excess of SNAP-Lumi4-Tb (*see* **Note 21**).
5. Detach the cells using 5 mL of enzyme-free Hank's-based Cell Dissociation Solution and collect in a 25 mL Universal centrifuge tube containing 5 mL of ice cold DMEM supplemented with 10% fetal calf serum (*see* **Note 22**).
6. Pellet by centrifugation at 500 × *g* for 5 min, and proceed immediately to the membrane preparation step or flash-freeze pellets in liquid nitrogen and store at −80 °C (*see* **Note 23**).

3.8.2 Membrane Preparation and Solubilization

All steps in the membrane preparation protocol are performed at 4 °C.

1. Add 20 mL of membrane preparation buffer to each pellet (from a T175 cm^2 flask), resuspend, and homogenize using an electrical homogenizer, e.g., Ultra-Turrax (position 6, four 5-s bursts).
2. Centrifuge the cell homogenate at 48,000 × *g* for 30 min.
3. Discard the supernatant, resuspend the pellet in 20 mL of membrane preparation buffer, re-homogenize and centrifuge as described above.
4. Discard the supernatant and resuspend the pellet in membrane storage buffer (0.9 mL per T175 cm^2 flask).
5. Determine the membrane protein concentration using the Pierce Bicinchoninic Acid Protein Assay Kit and bovine serum albumin (BSA) as a standard, and adjust the sample concentration to of 5–10 mg/mL by dilution adding membrane storage buffer. Membrane aliquots are stored at −80 °C until required (*see* **Note 24**).
6. Pellet membranes via centrifugation at 21,000 × *g* for 40 min at 4 °C to remove the membrane storage buffer. Add solubilisation buffer comprised of 20 mM HEPES, 10% glycerol, 150 mM NaCl, 0.5% BSA, and 1% DDM. Mix well and incubate under gentle rotation for 1 h.
7. Centrifuge the lysate at 150,000 × *g* for 30 min to remove any non-solubilized material, and transfer the supernatant containing the solubilized protein to a 0.5-mL tube on ice. Solubilized receptor preperations may be used immediately or flash frozen in liquid nitrogen and stored at −80 °C.
8. Adjust the receptor concentration to 0.4–4 nM for use in the ligand binding assay (*see* **Note 25**).

3.8.3 Ligand Binding

1. To prepare serial dilutions of the fluorescent ligand, add 50 μL of assay buffer to 5 × 0.5 mL tubes. Add 50 μL of the 10 μM stock propranolol-red ligand solution to the second tube, mix by pipetting up and down. Continue the serial dilution by adding 50 μL from tube 2 to tube 3, from 3 to 4, and so on. The stock and serial dilutions yield final ligand concentrations of 10–0.3125 μM. In the assay plate, these six concentrations will be diluted 100×, yielding final ligand concentrations 100 nM–3.125 nM (*see* **Note 26**).
2. Perform the binding assay in a final volume of 40 μL per well in a white 384-well OptiPlate measuring total and nonspecific binding (NSB). Add 29.2 μL of assay buffer to wells in rows A–D (1–6) of a 384-well plate. Add 0.4 μL of DMSO to wells in rows A–B (1–6), this serves as vehicle for when measuring

total ligand binding compared to nonspecific binding (NSB). Add 0.4 μL of unlabeled 100 μM ICI 118,551, made up in DMSO, to wells in rows C–D (1–6), to determine NSB.

3. Transfer 0.4 μL of each of the 100× fluorescent ligand serial dilutions and stock (**steps 1** and **2**) to its corresponding well on the assay plate. Cover the plate with an optical plate seal to prevent evaporation.
4. Measure the fluorescent intensity of the sample prior to the receptor addition, and construct a standard curve (ligand concentration versus fluorescent intensity) (*see* **Note 27**).
5. Add 10 μL of 0.4–4 nM receptor dilution in assay buffer to wells 1–6 in rows A–D, to yield a final receptor concentration of 0.1–1 nM (*see* **Notes 28** and **29**). Freshly prepared or frozen receptor samples can be used.
6. Immediately transfer the plate to the plate reader and monitor binding over time at room temperature. Alternatively, read the plate every 30 min, with incubation at room temperature in between. Once the optimal incubation time has been determined, it can be used to read the subsequent plates (*see* **Note 30**). Monitor terbium fluorescence by excitation at 337 nm and detection at, e.g., 620 nm using standard HTRF settings. Monitor the fluorescent ligand emission, e.g., at 665 nm for red and 520 nm for green ligands. Calculate the FRET ratio by dividing the acceptor (fluorescent ligand) signal by the donor signal (terbium cryptate).
7. Saturation experiments allow the calculation of receptor tracer affinity (or the dissociation constant, Kd) expressed as a concentration. Calculate specific tracer binding by subtracting nonspecific binding (NSB) from total binding. Plot total, specific, and nonspecific ligand binding signal versus the concentration of fluorescent ligand added. Data are then routinely globally fitted to determine specific binding using the total binding data taking into account NSB. Outlined below is the GraphPad Prism 8 equation syntax for global fitting of saturation data, where total binding is added to column A and nonspecific binding into column B, with the parameter NS shared between both data sets:

   Nonspecific = NS∗X

   Specific = Bmax∗X/(KD + X)

   <A> Y = Specific + Nonspecific

   <B> = Nonspecific

   Data from a typical saturation curve showing the binding of propranolol-red to solubilized β_2AR are shown in Fig. 7.

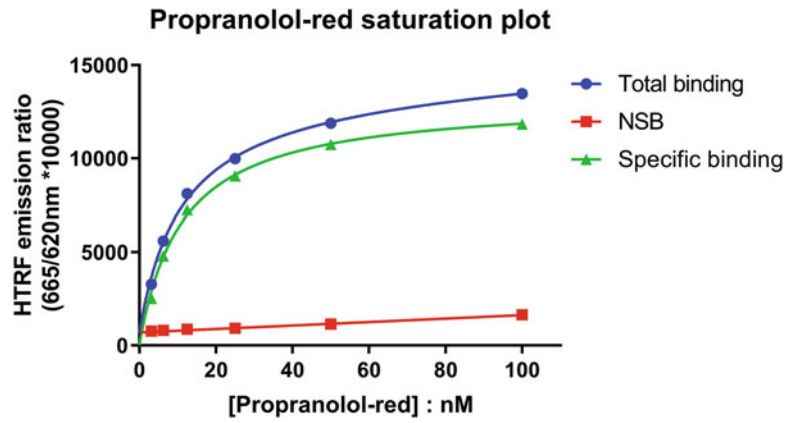

Fig. 7 Saturation binding of propranolol-red to the human β_2AR. The human β_2AR was expressed in HEK293 and labeled with terbium cryptate, followed by membrane preparation and receptor solubilization in 1% DDM. Receptor was incubated with increasing concentrations of propranolol-red (3.125–100 nM) at room temperature for 30 min, followed by HTRF measurements. Nonspecific binding (NSB) was determined in the presence of 1 μM non-fluorescent ligand ICI 118,551. Specific binding is calculated by subtracting NSB from total binding for each ligand concentration. Standard HTRF settings were used (4 laser flashes, integration delay 60 μsec, integration time 400 μsec). Data from a single experiment are shown. The affinity of propranolol-red binding to human β_2AR is estimated to be 10.9 nM

4 Notes

1. If a larger amount of cells is harvested, centrifugation time might need to be increased.
2. Instead of cells, prepared cell membranes can also be solubilized. In this case, prepare cell membranes following a standard protocol, and resuspend them in the appropriate volume of membrane storage buffer (typically 10 mM HEPES, 0.1 mM EDTA, pH 7.4). Remove the membrane storage buffer via centrifugation at 21,000 × *g* at 4 °C. Add a suitable solubilization buffer containing detergent, e.g., 1% DDM or 0.5% Lauryl Maltose Neopentyl Glycol (LMNG), and proceed with incubation for 1 h to solubilize the membranes.
3. Amount of solubilization buffer should be adjusted to the amount of material used and protein expressed.
4. Composition of SB can be optimized (e.g., detergent type and concentration, additives). Different detergents might need to be used at different concentrations (e.g., DDM is typically used at 1% and LMNG is typically used at 0.5%–1%). The detergent concentration could be optimized by determining the solubilization efficiency at different detergent concentrations.

5. Amount of protein loaded on gel might need adjustment, depending on protein expression levels, possible purification method, and its final concentration in the sample to be analyzed.
6. Alongside in-gel fluorescence, proteins subsequently can be nonspecifically stained (with protein stains such as Coomassie blue or InstantBlue Protein Stain, Expedeon), followed by detection on a gel imager or a scanner. While fluorescence detection visualizes only fluorescently tagged protein of interest (and its degradation products), protein stains visualize all proteins, indicating the efficiency level of the purification process.
7. Size-exclusion columns are often stored in 20% ethanol to prevent bacterial growth. In that case, wash the column with at least 2 CV of water before equilibration with RB to prevent precipitation of salt.
8. Filter and degas all buffers for size-exclusion chromatography to ensure optimal column performance and prevent damage.
9. Consider regular column cleaning according to the column manufacturer, and running calibration protein standards to assess column performance (e.g., Protein Standard Mix 15–600 kDa, Sigma).
10. Take care of the column maximum pressure allowance and set the appropriate flow rate, depending on the buffer used (more details in column user manual). Running pressure depends on RB composition, sample density, and flow rate. If pressure reaches maximal recommended value for the column, reduction of flow rate will result in reduced column pressure. If that is not possible, try to avoid viscous chemicals, for example, glycerol.
11. Make sure large protein aggregates are removed before loading to the column (either by filtration or by centrifugation) to avoid column clogging.
12. When protein homogeneity in samples treated with different detergents (either for solubilization or later for detergent screen) is screened, it is advisable to record FSEC chromatograms of empty micelles. As micelle size can vary between the detergents or detergent mixtures, the hypothetical retention volume of a protein sample will vary, too, and has to be considered when deciding on the best condition.
13. Ensure enough RB is provided for the protocol designed.
14. Ligand can be added to cells during the protein expression or after harvesting to increase protein stability and homogeneity.

15. Number of aliquots and temperatures can vary on the sample analyzed. We suggest using 10 different temperatures in the range 10–70 °C, keeping one sample on ice.
16. Number of samples to be incubated at different temperatures equals the number of data points for protein melting point determination. Number of samples and the incubation temperature range can be modified to suit the protein of interest.
17. In-gel fluorescence intensities can be analyzed by ImageJ. Briefly, rectangular areas on a gel corresponding to different protein samples are selected, followed by intensity measurements. For more detailed tutorials on intensity and gel analysis, readers are referred to the official ImageJ documentation, https://imagej.nih.gov/ij/.
18. The first step to generate a reliable measure of receptor thermostability using the CPM assay technique is to determine the optimal amount of the receptor protein and CPM dye. It is advisable to test different amounts and ratios of the receptor and the CPM dye, as other amounts than suggested in this protocol could be optimal for different proteins.
19. The CPM dyes spectral properties make it compatible with only a limited number of commercially available 96-well microtiter plate real-time PCR machines, reducing its use as a high-throughput screening (HTS) method in the 384- or 1536-well plate format [18].
20. The CPM dye, a coumarin derivative, has a short-wavelength excitation/emission maximum of 384/470 nm, making it prone to compound autofluorescence artifacts in fluorescence intensity assay formats [18].
21. If cells dissociate during the labeling or washing steps, resuspend them and pellet in the labeling medium or washing buffer (500 *g*, 5 min), remove excess liquid and wash by resuspending and pelleting. The number of wash steps can be reduced depending on the adherence properties of the cells. Coating flasks with poly-D-lysine prior to cell seeding can increase cell adherence.
22. If cells prove difficult to detach, use a scraper. The use of ice cold cell culture media during centrifugation step after labeling is thought to keep the cells viable and potentially minimizes internalization of the labelled receptor. The media also sequesters the unreacted terbium cryptate used in the labeling process because it contains serum albumin.
23. Solubilized receptor sample can be prepared directly from cell pellets, *see* Subheading 3.1.
24. If frozen membrane samples are used for solubilization, thaw the aliquots prior to use under the cold tap until ice melts. To

maintain the temperature of solution at 0 °C, the tube should be gently flicked while thawing. If freezing and thawing membranes render the receptor nonfunctional, consider adding 10% glycerol to the buffer and flash-freezing membranes in liquid nitrogen. Use small volume tubes (1.5–2.0 mL max) to maximize freezing speed and minimize damage by crystalline ice. The thawing procedure mentioned above (rapid but limited at 0 °C) minimizes damage by ice crystals formed during the thawing of the sample.

25. Receptor concentration is partly dependent on the affinity of the tracer used. For accurate quantification of pharmacological parameters (e.g., *Kd*), the concentration of the receptor used in the binding assay needs to be significantly lower than the affinity of the tracer.
26. A range of fluorescent ligand concentrations should be employed, 5–30-fold above and below the anticipated Kd of the fluorescent ligand.
27. To measure the relative levels of fluorescent ligand added to the assay plate, read the fluorescence intensity prior to the addition of receptor. This allows monitoring of inconsistent addition of the fluorescent ligand, as well as assessment of a potential effect of the unlabeled competitor compound on the fluorescent ligand intensity in solution (e.g., due to quenching), preventing misinterpretation of any HTRF signal reduction.
28. The concentration of the receptor used in the assay is partly dependent upon the affinity of the ligand. Less than 10% of the total fluorescent ligand added should specifically bind to the receptor. Significant tracer depletion can be overcome by increasing the concentration of fluorescent ligand or by reducing the concentration of protein (i.e., amount of membranes added) to a concentration below the *Kd* of the ligand. A value at least tenfold below the *Kd* is a good rule of thumb. If the sensitivity of measurements becomes a problem, use of the larger volume assay formats may help to compensate for the dilution of the sample.
29. Concentration of terbium-labeled receptor can be estimated from a standard curve constructed by diluting terbium labeling substrate (SNAP-Lumi4-Tb), assuming 100% labeling efficiency.
30. The optimal incubation to achieve equilibrium in ligand-receptor binding is dependent on the kinetic properties of the tracer. Ligands with slower off rates (many high affinity ligands belong to this class) will require a longer incubation time.

References

1. Munk C, Mutt E, Isberg V, Nikolajsen LF, Bibbe JM, Flock T, Hanson MA, Stevens RC, Deupi X, Gloriam DE (2019) An online resource for GPCR structure determination and analysis. Nat Methods 16(2):151–162. https://doi.org/10.1038/s41592-018-0302-x
2. Milic D, Veprintsev DB (2015) Large-scale production and protein engineering of G protein-coupled receptors for structural studies. Front Pharmacol 6:66. https://doi.org/10.3389/fphar.2015.00066
3. Xiang J, Chun E, Liu C, Jing L, Al-Sahouri Z, Zhu L, Liu W (2016) Successful strategies to determine high-resolution structures of GPCRs. Trends Pharmacol Sci 37 (12):1055–1069. https://doi.org/10.1016/j.tips.2016.09.009
4. Andréll J, Edwards PC, Zhang F, Daly M, Tate CG (2016) Generation of tetracycline-inducible mammalian cell lines by flow cytometry for improved overproduction of membrane proteins. In: Heterologous expression of membrane proteins. Methods Mol Biol:63–78. https://doi.org/10.1007/978-1-4939-3637-3_5
5. Magnani F, Serrano-Vega MJ, Shibata Y, Abdul-Hussein S, Lebon G, Miller-Gallacher J, Singhal A, Strege A, Thomas JA, Tate CG (2016) A mutagenesis and screening strategy to generate optimally thermostabilized membrane proteins for structural studies. Nat Protoc 11(8):1554–1571. https://doi.org/10.1038/nprot.2016.088
6. Franke B, Opitz C, Isogai S, Grahl A, Delgado L, Gossert AD, Grzesiek S (2018) Production of isotope-labeled proteins in insect cells for NMR. J Biomol NMR 71 (3):173–184. https://doi.org/10.1007/s10858-018-0172-7
7. Bird LE, Nettleship JE, Järvinen V, Rada H, Verma A, Owens RJ (2016) Expression screening of integral membrane proteins by fusion to fluorescent reporters. In: The next generation in membrane protein structure determination. Adv Exp Med Biol 922:1–11. https://doi.org/10.1007/978-3-319-35072-1_1
8. Prive GG (2007) Detergents for the stabilization and crystallization of membrane proteins. Methods 41(4):388–397. https://doi.org/10.1016/j.ymeth.2007.01.007
9. Seddon AM, Curnow P, Booth PJ (2004) Membrane proteins, lipids and detergents: not just a soap opera. Biochim Biophys Acta Biomembr 1666(1–2):105–117. https://doi.org/10.1016/j.bbamem.2004.04.011
10. Chae PS, Rasmussen SGF, Rana RR, Gotfryd K, Chandra R, Goren MA, Kruse AC, Nurva S, Loland CJ, Pierre Y, Drew D, Popot J-L, Picot D, Fox BG, Guan L, Gether U, Byrne B, Kobilka B, Gellman SH (2010) Maltose-neopentyl glycol (MNG) amphiphiles for solubilization, stabilization and crystallization of membrane proteins. Nat Meth 7 (12):1003–1008. http://www.nature.com/nmeth/journal/v7/n12/abs/nmeth.1526.html#supplementary-information
11. Skrzypek R, Iqbal S, Callaghan R (2018) Methods of reconstitution to investigate membrane protein function. Methods 147:126–141. https://doi.org/10.1016/j.ymeth.2018.02.012
12. Kimura T, Yeliseev AA, Vukoti K, Rhodes SD, Cheng K, Rice KC, Gawrisch K (2012) Recombinant cannabinoid Type 2 receptor in liposome model activates G protein in response to anionic lipid constituents. J Biol Chem 287 (6):4076–4087. https://doi.org/10.1074/jbc.M111.268425
13. Popot JL, Althoff T, Bagnard D, Banères JL, Bazzacco P, Billon-Denis E, Catoire LJ, Champeil P, Charvolin D, Cocco MJ, Crémel G, Dahmane T, de la Maza LM, Ebel C, Gabel F, Giusti F, Gohon Y, Goormaghtigh E, Guittet E, Kleinschmidt JH, Kühlbrandt W, Le Bon C, Martinez KL, Picard M, Pucci B, Sachs JN, Tribet C, van Heijenoort C, Wien F, Zito F, Zoonens M (2011) Amphipols From A to Z∗. Annu Rev Biophys 40(1):379–408. https://doi.org/10.1146/annurev-biophys-042910-155219
14. Ritchie TK, Grinkova YV, Bayburt TH, Denisov IG, Zolnerciks JK, Atkins WM, Sligar SG (2009) Chapter 11 - Reconstitution of membrane proteins in phospholipid bilayer nanodiscs. Methods Enzymol 464:211–231. https://doi.org/10.1016/S0076-6879(09)64011-8
15. Wheatley M, Charlton J, Jamshad M, Routledge SJ, Bailey S, La-Borde PJ, Azam MT, Logan RT, Bill RM, Dafforn TR, Poyner DR (2016) GPCR-styrene maleic acid lipid particles (GPCR-SMALPs): their nature and potential. Biochem Soc Trans 44(2):619–623. https://doi.org/10.1042/BST20150284
16. Hong P, Koza S, Bouvier ES (2012) Size-exclusion chromatography for the analysis of protein biotherapeutics and their aggregates. J Liq Chromatogr Relat Technol 35 (20):2923–2950. https://doi.org/10.1080/10826076.2012.743724

17. Kawate T, Gouaux E (2006) Fluorescence-detection size-exclusion chromatography for precrystallization screening of integral membrane proteins. Structure 14(4):673–681. https://doi.org/10.1016/j.str.2006.01.013
18. Bergsdorf C, Fiez-Vandal C, Sykes DA, Bernet P, Aussenac S, Charlton SJ, Schopfer U, Ottl J, Duckely M (2016) An alternative thiol-reactive dye to analyze ligand interactions with the chemokine receptor CXCR2 using a new thermal shift assay format. J Biomol Screen 21(3):243–251. https://doi.org/10.1177/1087057115619597
19. Hattori M, Hibbs RE, Gouaux E (2012) A fluorescence-detection size-exclusion chromatography-based thermostability assay for membrane protein precrystallization screening. Structure 20(8):1293–1299. https://doi.org/10.1016/j.str.2012.06.009
20. Pantoliano MW, Petrella EC, Kwasnoski JD, Lobanov VS, Myslik J, Graf E, Carver T, Asel E, Springer BA, Lane P, Salemme FR (2001) High-Density Miniaturized Thermal Shift Assays as a General Strategy for Drug Discovery. J Biomol Screen 6(6):429–440. https://doi.org/10.1177/108705710100600609
21. Ericsson UB, Hallberg BM, Detitta GT, Dekker N, Nordlund P (2006) Thermofluor-based high-throughput stability optimization of proteins for structural studies. Anal Biochem 357(2):289–298. https://doi.org/10.1016/j.ab.2006.07.027
22. Niesen FH, Berglund H, Vedadi M (2007) The use of differential scanning fluorimetry to detect ligand interactions that promote protein stability. Nat Protoc 2(9):2212–2221. https://doi.org/10.1038/nprot.2007.321
23. Yeh AP, McMillan A, Stowell MHB (2006) Rapid and simple protein-stability screens: application to membrane proteins. Acta Crystallogr Sect D Biol Crystallogr 62(4):451–457. https://doi.org/10.1107/s0907444906005233
24. Alexandrov AI, Mileni M, Chien EY, Hanson MA, Stevens RC (2008) Microscale fluorescent thermal stability assay for membrane proteins. Structure 16(3):351–359. https://doi.org/10.1016/j.str.2008.02.004
25. Hofmann L, Gulati S, Sears A, Stewart PL, Palczewski K (2016) An effective thiol-reactive probe for differential scanning fluorimetry with a standard real-time polymerase chain reaction device. Anal Biochem 499:63–65. https://doi.org/10.1016/j.ab.2016.01.016
26. Isom DG, Marguet PR, Oas TG, Hellinga HW (2011) A miniaturized technique for assessing protein thermodynamics and function using fast determination of quantitative cysteine reactivity. Proteins 79(4):1034–1047. https://doi.org/10.1002/prot.22932
27. Maguire JJ, Kuc RE, Davenport AP (2012) Radioligand binding assays and their analysis. In: Davenport A (ed) Receptor binding techniques, Methods in molecular biology (Methods and Protocols), vol 897. Humana, Totowa, pp 31–77. https://doi.org/10.1007/978-1-61779-909-9_3
28. Zwier JM, Roux T, Cottet M, Durroux T, Douzon S, Bdioui S, Gregor N, Bourrier E, Oueslati N, Nicolas L, Tinel N, Boisseau C, Yverneau P, Charrier-Savournin F, Fink M, Trinquet E (2010) A fluorescent ligand-binding alternative using Tag-lite(R) technology. J Biomol Screen 15(10):1248–1259. https://doi.org/10.1177/1087057110384611
29. Stoddart LA, Johnstone EKM, Wheal AJ, Goulding J, Robers MB, Machleidt T, Wood KV, Hill SJ, Pfleger KDG (2015) Application of BRET to monitor ligand binding to GPCRs. Nat Methods 12(7):661–663. https://doi.org/10.1038/nmeth.3398
30. Veiksina S, Kopanchuk S, Rinken A (2010) Fluorescence anisotropy assay for pharmacological characterization of ligand binding dynamics to melanocortin 4 receptors. Anal Biochem 402(1):32–39. https://doi.org/10.1016/j.ab.2010.03.022

Chapter 9

Affinity Purification of Membrane Proteins

Elisabeth Graeber and Volodymyr M. Korkhov

Abstract

Biochemical, biophysical, and structural studies of membrane proteins rely on the availability of highly pure and monodisperse membrane protein samples. One of the most powerful methods for isolation of the membrane protein of interest is affinity purification. This methodology typically relies on engineering an affinity tag into the protein of interest and an affinity resin that specifically recognizes the tag, allowing one to purify the target protein in a single step. In some cases, the affinity purification procedure is combined with additional steps to increase the purity and homogeneity of the final protein sample. Here, we describe several protocols for affinity purification of TSPO, a small membrane protein. The techniques we use include immobilized metal affinity chromatography (IMAC) and strep-II tag-based streptavidin affinity chromatography.

Key words IMAC, Ni-NTA, Strep-II tag, Streptactin, Detergent, TSPO

1 Introduction

1.1 Affinity Purification

Affinity tags and affinity resins are essential tools for purification of recombinant proteins that allow scientists to isolate highly pure preparations of a recombinant protein of interest. The choice of the affinity tag used to purify the protein of interest can determine the success of the protein purification experiment. Affinity tags such as the 6xHis or strep-II tag are routinely used for purification of soluble and membrane proteins. In the case of membrane protein purification, one can encounter a number of challenges [1]. The expression levels of the membrane proteins may be substantially lower in comparison to those of the soluble proteins. Overexpression of a membrane protein under certain conditions can lead to its misfolding and/or aggregation. Membrane proteins have to be extracted from the membranes prior to purification. Most commonly, this is done by detergent solubilization of the membrane, leading to formation of protein/micelle complexes stable in solution. Membrane protein solubilization procedures have to be optimized so that the extracted protein remains functional. Affinity

Camilo Perez and Timm Maier (eds.), *Expression, Purification, and Structural Biology of Membrane Proteins*, Methods in Molecular Biology, vol. 2127, https://doi.org/10.1007/978-1-0716-0373-4_9,

purification typically requires fusing the target protein to a tag, and this can potentially interfere with the correct membrane insertion and/or folding of the protein, affecting the yield and/or the quality of the final product of purification.

Here we describe protocols for efficient purification of membrane proteins based on His- or strep-tag affinity purification, applicable to proteins expressed in *E. coli*, mammalian, or insect cells.

1.2 Choice of Affinity Tag and Resin

The choice of the affinity tag has to be made when designing the construct, and it depends on the downstream applications that the protein will be used in after purification. It is possible to make the tag removable by introducing a protease cleavage site between the tag and the protein of interest.

One of the most commonly used affinity tags is the polyhistidine tag (His-tag), consisting of 6 (6xHis-tag) to 10 His residues (10xHis-tag). As membrane proteins are partly buried in the detergent micelle during purification, there is the risk of the affinity tag being inaccessible for binding to the affinity resin. A linker between the tag and the target protein or a longer version of the His-tag may facilitate tag accessibility. Furthermore, the tag position (N- or C-terminal) can be varied for better purification results. For purification using a His-tag, Ni-NTA resin or Co^{2+} affinity resin is used. In our hands, Co^{2+} resin provides a cleaner sample, which potentially makes it advantageous for purifying proteins that are expressed at lower levels.

Another tag commonly used for purification is the strep-II tag that consists of a Trp-Ser-His-Pro-Gln-Phe-Glu-Lys sequence [2]. This tag binds with high affinity to the streptactin resin and its relatively small size may be beneficial in applications where lack of interference from the tag is desired, such as in protein crystallization trials [3].

1.3 Considerations for the Choice of Detergent

A large number of detergents are now commercially available from a variety of sources. Invariably the detergent of choice has to be compatible with membrane protein stability upon purification. One of the most commonly used detergents for membrane protein solubilization is dodecyl maltoside (DDM), which has been used for purification and stabilization of a wide variety of membrane proteins in the past. Depending on the downstream usage of the protein, other detergents or detergent mixtures can be used during the purification procedure. The detergent can be exchanged during the wash step of the affinity chromatography or at a later stage (e.g., during gel filtration).

The choice of detergent used in membrane protein purification is dictated by the downstream experiments. For example, for membrane protein crystallization using vapor diffusion techniques, one would often use detergents with a small micelle size, such as LDAO

and octyl glucoside, as the small size of the micelle may potentially promote crystal contact formation. For cryo-EM analysis of membrane proteins, the optimal detergent has to be identified empirically by cryo-EM imaging of the grids containing the membrane protein purified in the presence of different detergents (e.g., DDM, LMNG, and digitonin). At the initial stages of analysis, the membrane protein sample purified in an optimal detergent should be uniformly distributed in the holes of the cryo-EM grids, allowing one to perform cryo-EM analysis of the membrane protein sample. Subsequent processing of the cryo-EM data following the established procedures is necessary to determine whether the chosen detergent is consistent with high-resolution structure determination.

Membrane proteins are typically solubilized using detergent at relatively high concentrations (0.5–2%). In the steps following solubilization, the concentration of detergent is typically decreased, but maintained at a level two- to threefold higher than the critical micelle concentration (CMC) of the given detergent. For example, we typically use DDM at a concentration of 0.02% (CMC of DDM is ~0.009%). In some cases, membrane proteins can be stabilized by addition of cholesteryl hemisuccinate (CHS) to the buffer [4] (*see* **Note 1**). Further details on the choice of detergents for protein purification are described elsewhere [5, 6].

2 Materials

Prepare all solution with ultrapure water. Filter all buffers using a 0.2 μm cut-off filter. Use detergents of analytical quality unless specified otherwise.

2.1 General Reagents and Materials

1. Tris–HCl, pH 7.5, 1 M stock solution.
2. NaCl, 5 M stock solution.
3. EDTA, 0.5 M stock solution.
4. 50% (v/v) glycerol.
5. 0.5 M phenylmethylsulfonyl fluoride (PMSF).
6. Detergents (*see* Subheading 1.3 regarding choice of detergent).
7. Empty chromatography columns for gravity flow (Bio-Rad).
8. Standard SDS-PAGE reagents.
9. Dulbecco's Modified Eagle's Medium (DMEM; mammalian cell culture).
10. Fetal calf serum (FCS; mammalian cell culture).
11. Lysogeny broth (LB; bacterial cell culture).

2.2 General Laboratory Equipment

1. Rod sonicator.
2. HPLC system with fluorescent detector.
3. Size exclusion chromatography (SEC) column.
4. Rotating wheel.
5. Magnetic stirrer.
6. Microliter spectrophotometer.
7. Imager with fluorescence detector.
8. Dounce homogenizer.

2.3 Small-Scale Solubilization of His-Tagged Proteins Fused to a Fluorescence Tag

1. Resuspension Buffer, 50 mM Tris, pH 7.5, 200 mM NaCl.
2. Equilibration Buffer, 50 mM Tris–Cl, pH 7.5, 200 mM NaCl, 0.02% DDM.

2.4 Large-Scale Purification of His-Tagged Proteins

All buffer solutions should be prepared on the day of the experiment and kept on ice:

1. Resuspension Buffer 1, 50 mM Tris–Cl, pH 7.5, 200 mM NaCl, 10% glycerol.
2. Resuspension Buffer 2, 50 mM Tris–Cl, pH 7.5, 200 mM NaCl, 20 mM imidazole.
3. Wash Buffer 1, 50 mM Tris–Cl, pH 7.5, 200 mM NaCl, 25 mM imidazole, 0.02% DDM, 10% glycerol.
4. Wash Buffer 2, 50 mM Tris–Cl, pH 7.5, 200 mM NaCl, 50 mM imidazole, 0.02% DDM, 10% glycerol.
5. Elution Buffer, 50 mM Tris–Cl, pH 7.5, 200 mM NaCl, 250 mM imidazole, 0.02% DDM, 10% glycerol.
6. Metal-chelate affinity resin, e.g., Ni-NTA Superflow (Qiagen; nitriloacetic acid-based tetradentate chelating agarose resin charged with Ni^{2+}), HisPur Cobalt Superflow (Thermo Scientific; tetradentate chelating agarose resin charged with Co^{2+}) (*see* **Note 2**).
7. Imidazole-HCl, pH 8.0, 1 M stock solution.

2.5 Removal of Affinity Tag by Reverse IMAC

1. Desalting column (HiPrep 26/10).

2.6 Purification of Strep-Tagged Membrane Protein

All buffer solutions should be prepared on the day of the experiment and kept on ice:

1. Resuspension Buffer, 50 mM Tris–HCl, pH 7.5, 200 mM NaCl, 0.5 mM EDTA.

2. Wash Buffer, 50 mM Tris–HCl, pH 7.5, 200 mM NaCl, 0.5 mM EDTA, 0.02% DDM.
3. Elution Buffer, 50 mM Tris–HCl, pH 7.5, 200 mM NaCl, 0.5 mM EDTA, 0.02% DDM, 50 mM biotin (*see* **Note 3**).
4. Strep-Tactin Superflow or Strep-TactinXT Superflow (IBA).
5. Desthiobiotin (when using Strep-Tactin Superflow) or biotin (when using Strep-TactinXT Superflow).

3 Methods

3.1 Small-Scale Solubilization of His-Tagged Proteins Fused to a Fluorescent Protein Tag

Presence of a fluorescent protein, such as GFP, tremendously facilitates the analysis of the protein of interest in small scale, helping to evaluate expression levels and stability of the protein.

The following procedure requires availability of cells expressing the protein of interest tagged with a fluorescent protein and a His-tag (the same protocol can be used for bacterial or mammalian cells, with minor adjustments, *see* **Note 4**). This protocol does not require an affinity purification step, as the protein quality is assessed by monitoring fluorescence of the GFP fusion with the target protein.

1. Grow the cells expressing the protein of interest in an appropriate cell culture medium. For example, for HEK293 cells use DMEM, supplemented with 10% FCS; for *E. coli*, use LB medium (or similar). Collect the cells by centrifugation and freeze the pellets until the day of experiment.
2. Resuspend the pellets in Resuspension Buffer. To avoid proteolysis, add 0.5 mM PMSF (*see* **Note 5**).
3. Sonicate the cells using a rod sonicator equipped with a microtip, following a protocol compatible with the instrument and tip type.
4. Add DDM to a final concentration of 1% (or other detergent of choice) (*see* **Note 6**).
5. Incubate for 1 h at 4 °C with constant rotation to solubilize the membrane protein.
6. Remove the insoluble material by ultracentrifugation (68,000 × *g*, 30 min, rotor TLA 100.3).
7. Analyze the supernatant by fluorescence size-exclusion chromatography (FSEC) using an appropriate column suitable for separation of proteins in the size range of the target membrane protein (using a flow of 0.3 mL/min, excitation 488 nm, emission 510 nm). A typical Equilibration Buffer for FSEC may have the following composition: 50 mM Tris–Cl, pH 7.5, 200 mM NaCl, 0.02% DDM.

3.2 Large-Scale Purification of His-Tagged Proteins

All steps are carried out with the samples and solutions kept on ice or at 4 °C.

1. Grow cells (e.g., HEK293 cells expressing the protein of interest) in an appropriate medium, harvest by centrifugation.
2. Resuspend the cell pellet in resuspension Resuspension Buffer 1, add DNAse (5 μg/mL), EDTA-free protease inhibitor cocktail, and 0.5 mM PMSF. Break the cells using a Dounce homogenizer, spin down by ultracentrifugation at 142,000 × *g* for 1 h at 4 °C. The membrane pellet can be frozen and stored at −80 °C until purification.
3. Resuspend the membrane pellet in Resuspension Buffer 2, 1:5 (w:v).
4. Add 5 μg/mL DNAse and EDTA-free protease inhibitor cocktail.
5. Add 1% detergent to the membranes.
6. Solubilization for 1 h at 4 °C using a 50 mL conical tube on a rotating wheel or a magnetic stirrer in a beaker for volumes larger than 45 mL.
7. Centrifugation 43,000 × *g*, 30 min, 4 °C.
8. Incubate supernatant with resin, 1 h, 4 °C.
9. Add supernatant and resin to a gravity column.
10. Let supernatant flow-though, collect, and pass through the resin again.
11. Wash with 10 column volumes (CV) Wash Buffer 1, followed by 20 CV Wash Buffer 2.
12. Elute with eight CV in fractions, measure concentration with microliter spectrophotometer and pool the protein-containing fractions.

3.3 Removal of Affinity Tag by Reverse IMAC

1. Exchange the buffer to the Wash Buffer using a desalting column.
2. Add protease, depending on the type of the cleavage site present in the protein expression construct (*see* **Note 7**). Ideally, the protease should carry the same tag as the expression construct, such that in the same step the protease can also be removed.
3. After appropriate time of incubation (*see* **Note 8**), add the mixture to Ni-NTA or Co^{2+} resin and incubate for 1 h.
4. Apply the mixture to a gravity column and collect the flow-through, which contains the cleaved protein. The cleaved protein tag and any uncleaved fusion protein remain bound to the affinity resin.
5. As a final step, the protein can be purified even further with a large-scale SEC.

3.4 Purification of Strep-Tagged Membrane Proteins

All steps are carried out on ice or at 4 °C.

1. Resuspend membrane pellet in Resuspension Buffer, 1:5 (w:v).
2. Add 5 μg/mL DNAse and protease inhibitor cocktail.
3. Add 1% detergent to the resuspended membranes.
4. Solubilize the membrane protein for 1 h at 4 °C using a 50 mL conical tube on a rotating wheel or a magnetic stirrer in a beaker for volumes larger than 45 mL.
5. Remove the insoluble material by centrifugation at 43,000 × *g*, for 30 min at 4 °C.
6. Add supernatant to the resin (*see* **Note 9**).
7. Pour the mixture into a gravity column.
8. Let supernatant flow through fast.
9. Wash with 10 CV Wash 1 and 20 CV Wash 2.
10. Elute with eight CV in fractions, measure concentration with a microliter spectrophotometer and pool the protein-containing fractions.
11. As a final step, the protein can be purified even further with a large-scale SEC.

3.5 Evaluation of Membrane Protein Purification

To evaluate the purification, examine the SEC or FSEC peak and load the samples from each purification step on an SDS-PAGE gel (Fig. 1). If you observe large quantities of your target protein in the flow-through, consider using a different resin or prolong the binding time. If the SDS-PAGE and SEC profile of the protein show signs of protein aggregation, multiple oligomeric states, proteolytic degradation, or contamination with unwanted proteins, consider changing your protocol. Common parameters for optimization of a purification procedure include (but are not limited to) the following: pH of the solutions during purification, concentration of salt used in the solution, type of detergent used for solubilization, presence of stabilizing agents (e.g., glycerol and CHS), and the type of affinity tag. Each case has to be evaluated carefully and the expected properties of the target membrane protein have to be taken into account.

4 Notes

1. We use CHS at a concentration of 0.004%.
2. Cobalt resin can provide a cleaner sample, but may also be more expensive.
3. Biotin does not readily dissolve in the buffer. We add it as the last ingredient during buffer preparation and dissolve it by vortexing and heating the buffer. As a final step the buffer is filtered using a 0.2 μm cutoff.

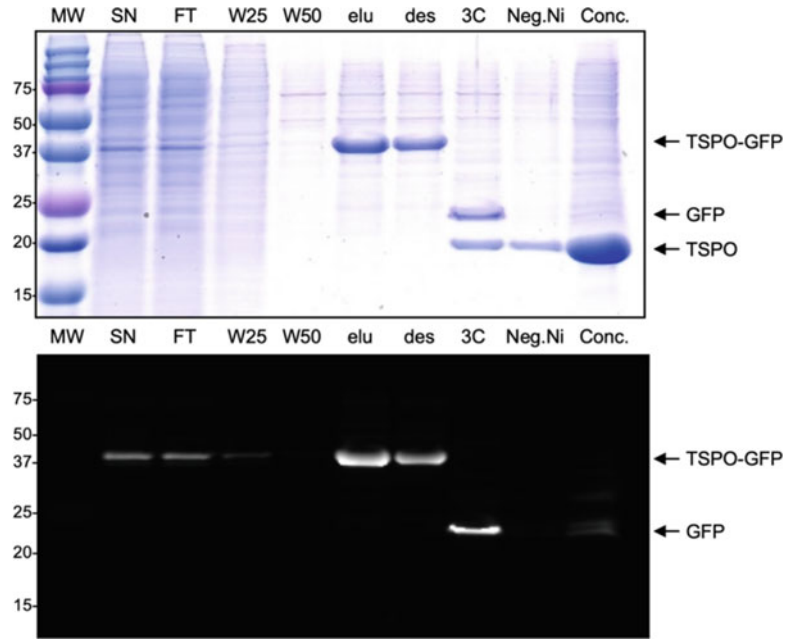

Fig. 1 SDS-PAGE analysis of fractions collected during purification of mammalian TSPO, an 18 kDa membrane protein. The construct used was TSPO-3C–GFP–10xHis (cleavable by 3C protease). The lanes are labeled as follows: MW—molecular weight marker; SN—supernatant collected after solubilization and centrifugation of the membranes prepared from HEK293 cells expressing TSPO; FT—flow-through after Ni-NTA affinity chromatography; W25—sample of flow-through during resin wash with Wash Buffer 1; W50—sample of flow-through during resin wash with Wash Buffer 2; elu—sample of protein eluted from the resin; des—desalted protein; 3C—sample of the eluted protein treated by 3C protease; Neg.Ni—sample of the flow-through after the reverse Ni-NTA procedure; Conc.—sample of a concentrated protein. The top image shows a Coomassie blue-stained gel (4–20% Mini-PROTEAN TGX gel). The bottom image shows the same gel prior to staining with the dye; the in-gel GFP fluorescence is monitored using Amersham Imager 600

4. Bacterial cells have a rigid cell wall that requires sonication to be broken. For mammalian cells, the cell membranes are broken by adding detergent in small-scale experiments and by using a dounce homogenizer in large-scale purification.
5. For mammalian cells, add EDTA-free protease inhibitor cocktail.
6. One of the most commonly used detergents is DDM, but small-scale tests can be used to identify the most appropriate detergent for solubilization and purification of a target membrane protein.
7. We commonly use 3C protease and perform cleavage at 4 °C for several hours or overnight.

8. The best incubation time can be determined by comparing results of several small-scale purification of the same construct done in parallel with 0,1, and 2 h incubation time.
9. We have observed that, depending on the construct, incubation with the resin for 1–2 h can be beneficial. This has to be tested for each protein.

References

1. Seddon AM, Curnow P, Booth PJ (2004) Membrane proteins, lipids and detergents: not just a soap opera. Biochim Biophys Acta Biomembr 1666(1):105–117. https://doi.org/10.1016/j.bbamem.2004.04.011
2. Schmidt TGM, Skerra A (2007) The Strep-tag system for one-step purification and high-affinity detection or capturing of proteins. Nat Protoc 2:1528. https://doi.org/10.1038/nprot.2007.209
3. Kimple ME, Brill AL, Pasker RL (2013) Overview of Affinity Tags for Protein Purification. Current protocols in protein science / editorial board, John E Coligan [et al] 73:Unit-9.9. doi: https://doi.org/10.1002/0471140864.ps0909s73
4. Hanson MA, Cherezov V, Griffith MT, Roth CB, Jaakola V-P, Chien EYT, Velasquez J, Kuhn P, Stevens RC (2008) A Specific Cholesterol Binding Site Is Established by the 2.8 Å Structure of the Human β2-Adrenergic Receptor. Structure 16(6):897–905. https://doi.org/10.1016/j.str.2008.05.001
5. Garavito RM, Ferguson-Miller S (2001) Detergents as Tools in Membrane Biochemistry. J Biol Chem 276(35):32403–32406. https://doi.org/10.1074/jbc.R100031200
6. Privé GG (2007) Detergents for the stabilization and crystallization of membrane proteins. Methods 41(4):388–397. https://doi.org/10.1016/j.ymeth.2007.01.007

Chapter 10

Purification of Membrane Proteins by Affinity Chromatography with On-Column Protease Cleavage

Stephan Hirschi and Dimitrios Fotiadis

Abstract

A protocol is described for the isolation of recombinant polyhistidine-tagged membrane proteins from overexpressing *Escherichia coli* cells. The gene encoding a target membrane protein is cloned into an expression plasmid and then introduced into *E. coli* cells for overexpression. Membranes from bacterial cells are isolated and the tagged target membrane protein is solubilized in detergent and subsequently bound to an affinity matrix. Tagged proteins are commonly eluted by an excess of a solute that competes for the binding to the matrix. Alternatively, amino acid sequence-specific proteases can be used to cleave off the affinity purification tag directly on the purification column (i.e., on-column cleavage). This selectively releases the target protein and allows subsequent elution. Importantly, this step represents an additional purification step and can significantly increase the purity of the isolated protein.

Key words Affinity chromatography, Membrane protein, On-column cleavage, Protease cleavage, Protein affinity tag

1 Introduction

Transmembrane proteins are essential components of cells that regulate the transport of solutes and the transduction of signals across the cell membrane. A plethora of different types of membrane proteins exist to perform these tasks, including receptors, transporters, channels, pumps, and many more [1, 2]. Due to their importance for cell communication and homeostasis, they are of high interest for the development of drugs. G-protein-coupled receptors (GPCRs) and ion channels together already make up more than 50% of all known drug targets [3]. Drug design and screening require functional characterization of the proteins of interest and benefit greatly from available structural information. To functionally and structurally characterize them, it is indispensable to extract target membrane proteins from their membrane environment and purify them [4]. The first obstacle in their

Camilo Perez and Timm Maier (eds.), *Expression, Purification, and Structural Biology of Membrane Proteins*, Methods in Molecular Biology, vol. 2127, https://doi.org/10.1007/978-1-0716-0373-4_10,

isolation is the acquisition of sufficient amounts of membrane protein for subsequent studies [1]. With a few exceptions, such as the visual rhodopsins, P-type calcium ATPases and aquaporins in eukaryotes or several outer membrane proteins in prokaryotes, the natural expression level of most membrane proteins is very low [5, 6]. For non-abundant membrane proteins, homologous or heterologous overexpression using bacteria, yeast, insect, or mammalian cells is required [5, 7]. Commonly used expression vectors encode specific N- or C-terminal tags that are added to the protein of interest to facilitate purification by affinity chromatography. Among the most popular tags for the purification of recombinant proteins are polyhistidine (His-tag), glutathione S-transferase (GST-tag), streptavidin-binding peptide (Strep-tag), and maltose-binding protein (MBP) [8]. In the presented purification protocol, we will be focusing on His-tagged membrane proteins and their purification using immobilized metal ion affinity chromatography (IMAC). This method exploits the strong interaction between histidine residues and immobilized transition metal ions such as Ni^{2+}, Co^{2+}, and Cu^{2+}. The most commonly used matrix for affinity purification of His-tagged proteins is nickel nitrilotriacetic acid (Ni-NTA) [9]. Purifications of highly expressed target proteins usually yield relatively pure protein in just one chromatographic step. This is mostly the case for proteins overexpressed in *E. coli*. However, when purifying His-tagged proteins from insect or mammalian cells, significantly more contamination is observed due to higher percentage of histidine residues in endogenous proteins [8]. The tagged target proteins are commonly eluted by an excess of a solute that competes for the binding to the affinity matrix (e.g., histidine or imidazole for IMAC). Elution can also be achieved by proteolytic cleavage of the affinity tag, thereby selectively releasing the target protein from the column [10]. This requires the introduction of a specific protease cleavage site between the target protein and the affinity tag. Viral proteases, such as the tobacco etch virus (TEV) and the human rhinovirus 3C (HRV 3C) proteases, have a very high amino acid sequence specificity and thus avoid digestion of the purified protein [10]. Removal of the purification tag can be performed directly on the affinity matrix and serves as an additional purification step. Due to the high specificity of the proteases, the protein purity can be significantly increased, especially when there is a high amount of unspecifically bound proteins resulting from a low expression level of the target protein [11, 12]. Furthermore, the removal of affinity tags is often a prerequisite for applications following purification (e.g., crystallization). Tagged versions of proteases are commercially available, which stay attached to the affinity matrix after cleavage of the target protein without contaminating it.

Here, we present a protocol for the purification of a His-tagged membrane protein expressed in *E. coli* using IMAC combined with

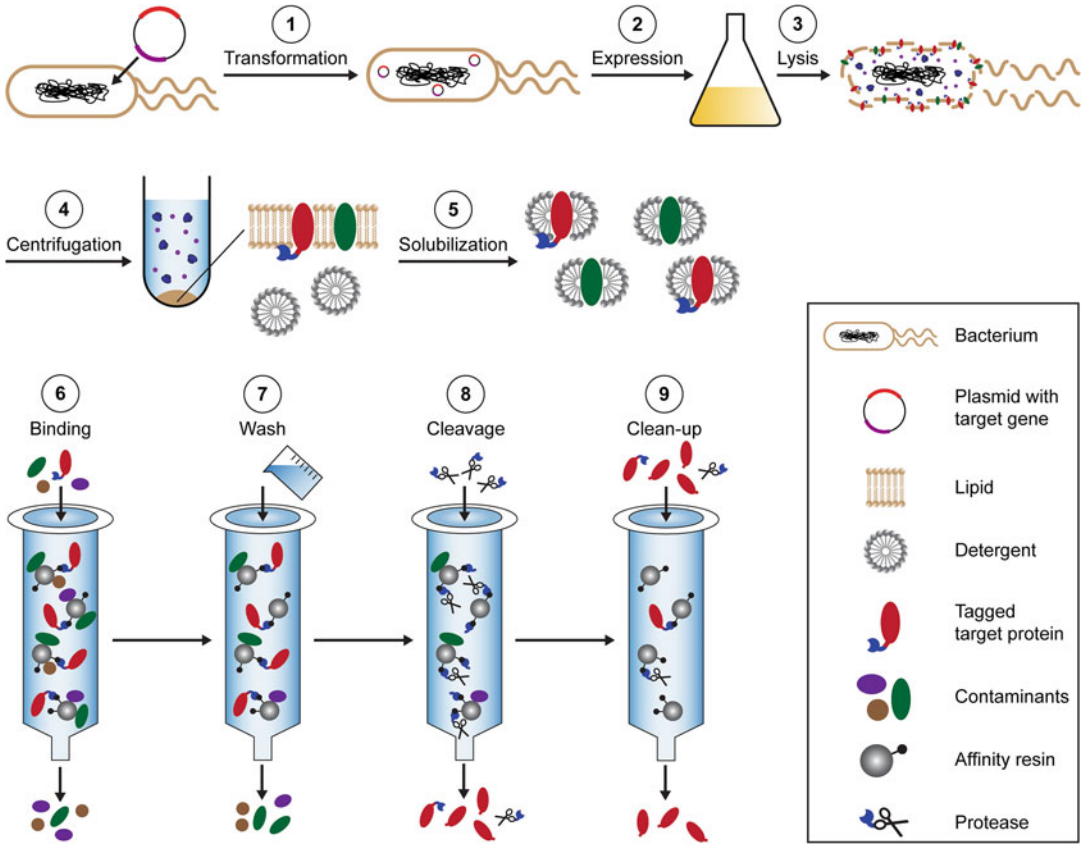

Fig. 1 Schematic illustration of the affinity chromatographic purification of a target membrane protein expressed in a bacterial host. (*1*) Transformation of competent bacteria with a plasmid containing the gene coding for the target membrane protein. (*2*) Cultivation of transformed bacteria and overexpression of target membrane protein. (*3*) Lysis of bacterial cells. (*4*) Isolation of bacterial membranes by ultracentrifugation. (*5*) Extraction of membrane proteins from lipid bilayers by detergent solubilization. (*6*) Binding of solubilized proteins to affinity matrix. (*7*) Removal of most unspecifically bound proteins. (*8*) Cleavage of affinity purification tag by specific protease and selective elution of target membrane protein. (*9*) Removal of uncleaved target protein and protease contaminants

proteolytic on-column tag removal. Several frequently encountered aspects about the isolation of recombinant membrane proteins are illustrated using the light-driven proton pump proteorhodopsin (PR) as an example [13]. The protocol describes the following steps (Fig. 1): Transformation of *E. coli* expression strain with plasmid containing gene of target protein, overexpression of target protein in *E. coli*, lysis of bacterial cells, isolation of *E. coli* membranes, solubilization of *E. coli* membranes, IMAC purification of target protein, and on-column protease cleavage. The protocol encompasses in-depth practical knowledge, specific recommendations for the selection of suitable materials and anticipated results (Fig. 2).

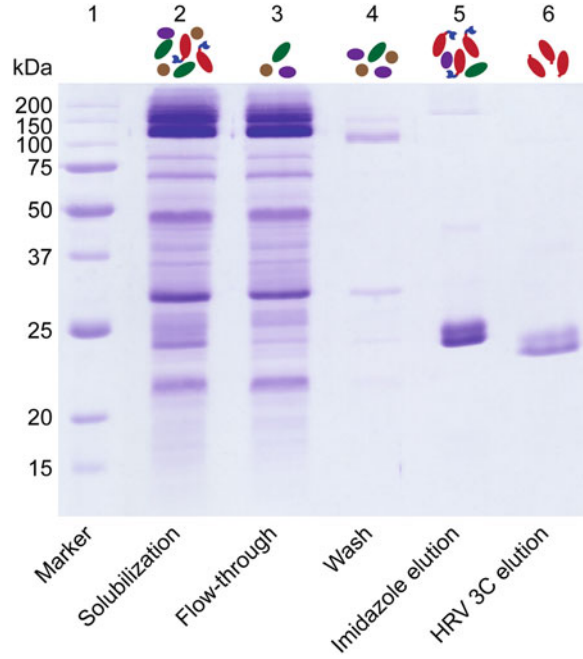

Fig. 2 Analysis of individual IMAC purification steps by SDS-PAGE. The first lane contains a mixture of known marker proteins with the indicated molecular weights. Lane 2 (solubilization): 2 μL of the solubilized *E. coli* membranes after ultracentrifugation; lane 3 (flow-through): 4 μL of non-bound protein fraction (note the reduction of the bands corresponding to PR compared to lane 2); lane 4 (wash): 4 μL of fraction eluted by wash step; lane 5 (imidazole elution): 2 μg of PR eluted with high imidazole concentration; lane 6 (HRV 3C elution): 2 μg of PR eluted by proteolytic on-column cleavage with HRV 3C (note the increased purity compared to the imidazole elution resulting from the additional purification step). Some membrane proteins, including PR, can exhibit double bands on SDS-PAGE (lanes 5 and 6), corresponding to incomplete removal of the N-terminal signal sequences during biosynthesis (*see* **Note 12**)

2 Materials

2.1 Overexpression in E. coli

Media and solutions for bacterial cell cultures can be prepared using standard deionized water, the rest should be prepared with ultrapure osmosis water (e.g., Milli-Q water).

1. Gene of interest (optionally codon optimized) in suitable expression vector for *E. coli* (for this protocol including T7 RNA polymerase promoter, *lac* operator, *lacI* repressor gene and tags for affinity purifications and/or detection), e.g., pET21 or derivatives. Here, we used the previously described pZUDF21 plasmid encoding a C-terminal HRV 3C cleavage site followed by a decahistidine-tag [14].

2. *E. coli* strain optimized for protein overexpression, e.g., BL21 (DE3) pLysS (New England BioLabs) or derivatives (*see* **Note 1**).
3. LB premix (e.g., LB broth, Miller formulation).
4. Ampicillin and chloramphenicol or appropriate antibiotics depending on the vector used (*see* **Note 2**).
5. Thermoshaker.
6. Erlenmeyer flasks.
7. Autoclave.
8. Shaker for liquid cultures.
9. Spectrophotometer and cuvettes.
10. Isopropyl-β-D-thiogalactopyranoside.
11. All-*trans* retinal (Sigma-Aldrich). Retinal is required as a cofactor only for the overexpression of rhodopsin-like proteins such as PR.
12. Large volume centrifuge and corresponding centrifugation tubes.
13. Membrane wash buffer, 50 mM Tris–HCl, pH 8 (adjusted at 4 °C), 450 mM NaCl.

2.2 Isolation of E. coli Membranes

All buffers used for the isolation of *E. coli* membranes should be prepared with ultrapure osmosis water (e.g., Milli-Q water).

1. *E. coli* cells overexpressing target protein (*see* Subheading 3.1).
2. Water bath.
3. Lysozyme.
4. Deoxyribonuclease I.
5. Microfluidizer (e.g., M-110P Microfluidizer, Microfluidics).
6. Large volume centrifuge and corresponding centrifugation tubes.
7. Ultracentrifuge and corresponding centrifugation tubes.
8. Glass homogenizer (at least 50 mL capacity) with Teflon pestle.
9. Membrane wash buffer, 50 mM Tris–HCl, pH 8 (adjusted at 4 °C), 450 mM NaCl.
10. Purification buffer, 20 mM Tris–HCl, pH 8 (adjusted at 4 °C), 300 mM NaCl, 10% (v/v) glycerol (*see* **Note 3**).

2.3 Immobilized Metal Ion Affinity Chromatography with On-Column Protease Cleavage

1. Isolated *E. coli* membranes containing target membrane protein (*see* Subheading 3.2).
2. n-Octyl-β-D-glucopyranoside (OG) or another suitable detergent such as malto- or glucopyranosides (*see* **Note 4**).
3. Purification buffer, 20 mM Tris–HCl, pH 8 (adjusted at 4 °C), 300 mM NaCl, 10% (v/v) glycerol (*see* **Note 3**).

4. Rotation shaker.
5. Ultracentrifuge and corresponding centrifugation tubes.
6. Wash buffer I, 20 mM Tris–HCl, pH 8 (adjusted at 4 °C), 300 mM NaCl, 60 mM imidazole, 10% (v/v) glycerol (*see* **Note 5**).
7. Ni-NTA resin.
8. Microcentrifuge.
9. Empty gravity flow columns (e.g., Wizard midi column, Promega).
10. Wash buffer II, 20 mM Tris–HCl, pH 8 (adjusted at 4 °C), 300 mM NaCl, 60 mM imidazole, 10% (v/v) glycerol, 1% (w/v) OG (*see* **Note 5**).
11. Elution buffer, 20 mM Tris–HCl, pH 8 (adjusted at 4 °C), 150 mM NaCl, 400 mM imidazole, 10% (v/v) glycerol, 1% (w/v) OG.
12. Cleavage buffer, 20 mM Tris–HCl, pH 8 (adjusted at 4 °C), 150 mM NaCl, 10% (v/v) glycerol, 1% (w/v) OG (*see* **Note 6**).
13. Razor blade.
14. Laboratory sealing film.
15. Recombinant His-tagged HRV 3C protease (e.g., Turbo3C protease (2 mg/mL), BioVision) (*see* **Note 6**).

2.4 Biochemical Analysis of Purified Membrane Protein

1. Purified target membrane protein (*see* Subheading 3.3).
2. Spectrophotometer.
3. Reagents and equipment for casting SDS/polyacrylamide gels.
4. Protein electrophoresis system.
5. Reagents for Coomassie Brilliant Blue R-250 staining of SDS/polyacrylamide gels.

3 Methods

3.1 Heterologous Overexpression in E. coli

1. Prepare LB medium using premixed LB for a small pre-culture (e.g., 100 mL) and a large main culture (e.g., 2 L). The scale can be adapted as required. Autoclave the media in advance to let them cool down before usage.
2. Transform the desired *E. coli* strain (*see* **Note 1**) with the expression vector containing the gene of the target membrane protein using common transformation protocols (e.g., heat shock of chemically competent cells). For this protocol, *E. coli* BL21(DE3) pLysS will be used as an example.

3. Supplement the small pre-culture with 100 mg/mL ampicillin and 35 mg/mL chloramphenicol (*see* **Note 2**) and inoculate it with the transformed *E. coli* cells. Incubate the cells in a shaker overnight at 37 °C and 180 rpm.
4. Supplement the main culture with 100 mg/mL ampicillin and 35 mg/mL chloramphenicol and inoculate it 1:100 with the overnight culture. Incubate the cells in a shaker at 37 °C and 180 rpm.
5. Continuously measure the optical density (OD) of the cell suspension at a wavelength of 600 nm using a spectrophotometer. When it reaches an OD_{600} of about 1.0, add IPTG to a final concentration of 0.1 mM and all-*trans* retinal to 5 μM to induce expression (*see* **Note 7**). Incubate the cells for 3 h at 37 °C and 180 rpm.
6. Harvest the cells by transferring them to large volume centrifugation tubes and centrifugation at 10,000 × *g* and 4 °C for 5 min.
7. To wash the cells once, resuspend them in membrane wash buffer and repeat the previous centrifugation step.
8. Resuspend the cells in membrane wash buffer and store them at −20 °C until further use.

3.2 Isolation of E. coli Membranes

1. Thaw the frozen cells in a water bath, then add a spatula tip of lysozyme and DNase, and stir for about 15 min to break the bacterial cell wall and digest genomic DNA. This should reduce the viscosity of the cell suspension and facilitate the next steps.
2. Lyse the cells by passing them through a Microfluidizer five times at 1500 bar, following the instructions of the manufacturer (*see* **Note 8**).
3. Centrifuge the lysate at 10,000 × *g* and 4 °C for 5 min to remove unlysed cells and cell debris.
4. Transfer the supernatant into ultracentrifugation tubes and pellet the cell membranes by ultracentrifugation at 150,000 × *g* and 4 °C for 1 h.
5. Homogenize the membrane pellet in 50 mL membrane wash buffer using a glass and Teflon homogenizer. Then wash the membranes at least once (better twice) by repeating the previous centrifugation and resuspension steps.
6. Finally, resuspend the membrane pellet in purification buffer as 2 mL aliquots corresponding to 1 L of bacterial cell culture.
7. Flash-freeze membrane aliquots in liquid nitrogen and store them at −80 °C until further use.

3.3 Immobilized Metal Ion Affinity Chromatography with On-Column Protease Cleavage

For assessment and potential troubleshooting (e.g., low protein yield or purity) of the purification process, it is strongly advised to take samples at each purification step. These are subsequently analyzed by SDS-PAGE (*see* Fig. 2) and can aid in the optimization of purification conditions.

1. Thaw a membrane aliquot and solubilize it in a total of 7 mL purification buffer containing 3% (w/v) OG (*see* **Note 4**) overnight at 4 °C with gentle rotation.
2. Ultracentrifuge the solubilized membranes at 100,000 × *g* and 4 °C for 1 h to remove non-solubilized components and aggregates.
3. In the meantime, equilibrate 0.5 mL of Ni-NTA (settled bed volume) by washing it twice with 2 mL wash buffer I in a 15 mL conical tube by centrifugation at 1000 × *g* for 1 min. Then resuspend the resin in a total of 7 mL wash buffer I.
4. Mix the supernatant of the solubilized membranes with the Ni-NTA suspension in a 50 mL conical tube and incubate for 2 h at 4 °C with gentle rotation.
5. Load the suspension onto a gravity flow column to separate the affinity resin with the bound target protein from unbound contaminants.
6. Wash the column with at least 20 mL (40 column volumes) of wash buffer II.
7. At this point the protein can be eluted by the addition of elution buffer if it should retain the His-tag (e.g., if subsequent applications require a His-tag). Otherwise, continue with the next step.
8. Wash the column with at least 2 mL (4 column volumes) of cleavage buffer to remove remaining imidazole.
9. Remove the liquid from the column by placing the gravity flow column in an empty 50 mL conical tube and centrifugation at 1000 × *g* and 4 °C for 1 min.
10. Cut off the column tip containing the resin using a razor blade.
11. Seal the bottom of the tip with sealing film, add 450 μL of cleavage buffer and 50 μL HRV 3C protease (*see* **Note 9**). Seal the top of the tip and incubate it overnight at 4 °C with gentle rotation.
12. Remove the bottom seal and elute the protein by centrifugation at 4000 × *g* and 4 °C for 2 min into a 2 mL tube. The yield (*see* **Note 10**) can be increased by adding an additional 250 μL of cleavage buffer to the tip and repeating the centrifugation to recover cleaved protein that may still be trapped in the resin.
13. Equilibrate 50 μL Ni-NTA (settled bed volume) by washing it twice with 1 mL cleavage buffer in an 1.5 mL tube by

centrifugation at 1000 × *g* for 1 min and incubate it with the eluted protein for 30 min at 4 °C with gentle rotation (*see* **Note 11**).

14. Wash a fresh gravity flow column with 5 mL cleavage buffer and transfer the suspension to elute the protein from the resin by centrifugation at 4000 × *g* and 4 °C for 2 min.

3.4 Biochemical Analysis of Purified Protein

1. Measure the protein concentration using a spectrophotometer or another common assay for the determination of protein concentration (e.g., Bradford or bicinchoninic acid (BCA) assay).
2. Assess the purity of the purified protein by SDS-PAGE (*see* **Note 12**) and Coomassie staining according to common protocols (*see* Fig. 2).

4 Notes

1. Specialized strains for protein overexpression such as BL21 (DE3) [15] are based on the T7 RNA polymerase system, inducible by IPTG, and are deficient in the Lon and OmpT proteases. Derivative strains, i.e., C41(DE3) and C43(DE3), were specifically developed for the overexpression of membrane proteins and frequently result in high expression levels [16]. The pLysS plasmid encodes T7 lysozyme, which suppresses basal expression from the T7 promoter, thus increasing the production of recombinant proteins that are toxic to the cells. The most suitable *E. coli* strain for overexpression of your target membrane protein should be determined using small test expression cultures and by assessing the expression level, e.g., by Western blot analysis or activity assays.
2. Ampicillin is required for the selection of pET21 transformed cells and chloramphenicol for maintaining the pLysS plasmid.
3. This is a standard purification buffer recommended as starting point. Optimal pH for binding of the His-tag to the Ni-NTA matrix is around 8, but a range from at least pH 7 to pH 9 can be used. Addition of stabilizing or reducing agents and essential cofactors can be explored. Information about the compatibility of the matrix with specific reagents can be obtained from the manual provided by the manufacturer.
4. A suitable detergent for the solubilization and purification of your target membrane protein should be determined beforehand [14]. Optimally, the detergent is able to efficiently extract the membrane protein from the membrane but is mild enough to stabilize it and preserve its function [17, 18]. Non-ionic detergents with low critical micelle concentration (CMC) are

usually mild and a good starting point. Commonly used detergents include the non-ionic alkyl-maltopyranosides or -glucopyranosides, such as n-dodecyl-β-D-maltopyranoside (recommended for first experiments) and OG. The detergent concentration for solubilization should be in great excess of the CMC, whereas for the following purification steps it is reduced to a several-fold of the CMC (e.g., two- to threefold) [14]. For most membrane proteins 2 h of solubilization at 4 °C is sufficient, but a few exceptions such as PR and some outer membrane proteins require longer solubilization (e.g., overnight).

5. The recommended imidazole concentration for preliminary experiments is around 20 mM and 40 mM for binding and washing, respectively. Additionally, a minimum of 300 mM NaCl should be used for the binding and washing steps to reduce unspecific binding. These conditions can be adapted accordingly if low protein purity (increase stringency of wash) or yield (decrease stringency of wash) is observed.
6. Optimal cleavage conditions for the cysteine proteases TEV and HRV 3C are 20 mM Tris–HCl, pH 8, 150 mM NaCl. The storage buffer should include a low concentration of reducing agent such as 5 mM β-mercaptoethanol. Specifications may vary between different versions of the proteases, consult the manual provided by the manufacturer.
7. Optimal expression conditions including OD_{600} at start of induction, IPTG concentration for induction and duration of expression need to be determined in small test expression cultures prior to the large overexpression (*see* **Note 1**). Typical values range from 0.5 to 1.0 for OD_{600} and 0.1 to 1.0 mM IPTG. Common temperature and duration for overexpression range from 3 to 4 h at 37 °C to overnight at 18 °C. Retinal is required as a cofactor only for the overexpression of rhodopsin-like proteins such as PR.
8. Alternative methods for mechanical cell lysis with similar efficiencies include French pressure cell press or probe sonication.
9. It is important that the tip contains enough liquid to mix the resin for efficient cleavage. Different ratios of protease to target protein can be tested to optimize cleavage efficiency.
10. The protease cleavage efficiency for some membrane proteins can be significantly reduced due to poor accessibility of the cleavage site (e.g., due to very short N- or C-termini). One possibility to increase the accessibility is the introduction of a flexible linker before the protease cleavage site, i.e., a short peptide consisting of glycine and serine repeats [19]. Another possible issue for efficient protease cleavage is the oligomeric state of the target protein. Increased oligomericity has been

shown to negatively affect the proteolytic removal of affinity tags [20].

11. This additional incubation with Ni-NTA removes potentially uncleaved target proteins as well as protease remnants.
12. Membrane proteins typically run at a slightly lower molecular weight on SDS/polyacrylamide gels than expected based on the molecular weight calculated from the amino acid sequence [21]. Occasionally, purified membrane proteins can exhibit double bands on SDS-PAGE (*see* Fig. 2) corresponding to incomplete processing of the signal sequence during their biosynthesis in *E. coli* [22]. This can be confirmed by N-terminal sequencing of the bands in question (e.g., by Edman degradation). Such protein heterogeneities can be prevented by using N-terminally truncated protein constructs (i.e., lacking the signal sequence), which result in more homogeneous samples but may reduce the expression levels [23].

Acknowledgments

Financial support from the University of Bern, the Swiss National Science Foundation (grant 31003_184980), and the National Centre of Competence in Research (NCCR) Molecular Systems Engineering to Dimitrios Fotiadis is gratefully acknowledged.

References

1. Lacapère J-J, Pebay-Peyroula E, Neumann J-M, Etchebest C (2007) Determining membrane protein structures: still a challenge! Trends Biochem Sci 32:259–270
2. von Heijne G (2007) The membrane protein universe: what's out there and why bother? J Intern Med 261:543–557
3. Santos R, Ursu O, Gaulton A et al (2017) A comprehensive map of molecular drug targets. Nat Rev Drug Discov 16:19–34
4. Lin S-H, Guidotti G (2009) Purification of membrane proteins. In: Methods Enzymol, 1st edn. Elsevier, Amsterdam, pp 619–629
5. Grisshammer R (2006) Understanding recombinant expression of membrane proteins. Curr Opin Biotechnol 17:337–340
6. Molloy MP, Herbert BR, Slade MB, Rabilloud T, Nouwens AS, Williams KL, Gooley AA (2000) Proteomic analysis of the *Escherichia coli* outer membrane. Eur J Biochem 267:2871–2881
7. Assenberg R, Wan PT, Geisse S, Mayr LM (2013) Advances in recombinant protein expression for use in pharmaceutical research. Curr Opin Struct Biol 23:393–402
8. Kimple ME, Brill AL, Pasker RL (2013) Overview of affinity tags for protein purification. Curr Protoc Protein Sci 73:Unit 9.9
9. Waugh DS (2005) Making the most of affinity tags. Trends Biotechnol 23:316–320
10. Waugh DS (2011) An overview of enzymatic reagents for the removal of affinity tags. Protein Expr Purif 80:283–293
11. Boggavarapu R, Hirschi S, Harder D, Meury M, Ucurum Z, Bergeron MJ, Fotiadis D (2016) Purification of human and mammalian membrane proteins expressed in *Xenopus laevis* frog oocytes for structural studies. Methods Mol Biol 1432:223–242
12. Bergeron MJ, Boggavarapu R, Meury M, Ucurum Z, Caron L, Isenring P, Hediger MA, Fotiadis D (2011) Frog oocytes to unveil the structure and supramolecular organization of human transport proteins. PLoS One 6: e21901

13. Béja O, Spudich EN, Spudich JL, Leclerc M, DeLong EF (2001) Proteorhodopsin phototrophy in the ocean. Nature 411:786–789
14. Ilgü H, Jeckelmann JM, Gachet MS, Boggavarapu R, Ucurum Z, Gertsch J, Fotiadis D (2014) Variation of the detergent-binding capacity and phospholipid content of membrane proteins when purified in different detergents. Biophys J 106:1660–1670
15. Rosano GL, Ceccarelli EA (2014) Recombinant protein expression in *Escherichia coli*: advances and challenges. Front Microbiol 5:1–17
16. Miroux B, Walker JE (1996) Over-production of proteins in *Escherichia coli*: mutant hosts that allow synthesis of some membrane proteins and globular proteins at high levels. J Mol Biol 260:289–298
17. Privé GG (2007) Detergents for the stabilization and crystallization of membrane proteins. Methods 41:388–397
18. Sonoda Y, Newstead S, Hu N-J et al (2011) Benchmarking membrane protein detergent stability for improving throughput of high-resolution X-ray structures. Structure 19:17–25
19. Chen X, Zaro JL, Shen W-C (2013) Fusion protein linkers: Property, design and functionality. Adv Drug Deliv Rev 65:1357–1369
20. Kenig M, Peternel Š, Gaberc-Porekar V, Menart V (2006) Influence of the protein oligomericity on final yield after affinity tag removal in purification of recombinant proteins. J Chromatogr A 1101:293–306
21. Rath A, Glibowicka M, Nadeau VG, Chen G, Deber CM (2009) Detergent binding explains anomalous SDS-PAGE migration of membrane proteins. Proc Natl Acad Sci U S A 106:1760–1765
22. Harder D, Hirschi S, Ucurum Z, Goers R, Meier W, Müller DJ, Fotiadis D (2016) Engineering a chemical switch into the light-driven proton pump proteorhodopsin by cysteine mutagenesis and thiol modification. Angew Chemie Int Ed 55:8846–8849
23. Hirschi S, Fischer N, Kalbermatter D, Laskowski PR, Ucurum Z, Müller DJ, Fotiadis D (2019) Design and assembly of a chemically switchable and fluorescently traceable light-driven proton pump system for bionanotechnological applications. Sci Rep 9:1046

Chapter 11

Biotinylation of Membrane Proteins for Binder Selections

Benedikt T. Kuhn, Iwan Zimmermann, Pascal Egloff, Lea M. Hürlimann, Cedric A. J. Hutter, Christian Miscenic, Roger J. P. Dawson, Markus A. Seeger, and Eric R. Geertsma

Abstract

The selective immobilization of proteins represents an essential step in the selection of binding proteins such as antibodies. The immobilization strategy determines how the target protein is presented to the binders and thereby directly affects the experimental outcome. This poses specific challenges for membrane proteins due to their inherent lack of stability and limited exposed hydrophilic surfaces. Here we detail methodologies for the selective immobilization of membrane proteins based on the strong biotin-avidin interaction and with a specific focus on its application for the selection of nanobodies and sybodies. We discuss the challenges in generating and benefits of obtaining an equimolar biotin to target-protein ratio.

Key words Biotin, Neutravidin, Streptavidin, FX cloning, Avi-tag, Panning, Phage display, Ribosome display, Nanobodies, Sybodies

1 Introduction

Antibody fragments and in particular nanobodies have become indispensable tools for studying structural and functional aspects of membrane proteins [1]. The generation of these binders involves the stringent phenotypic selection of individual members from libraries holding many variants. Central to this procedure is the selective immobilization of the target protein to enrich those members of the library that specifically interact with it. We recently developed an in vitro selection platform based on three large synthetic nanobody (sybody) libraries that allows the generation of binders under entirely defined and mild conditions compatible with membrane proteins [2]. A major hallmark of our platform is its optimization toward the routine selection of binders against membrane proteins, which entails successive alterations in display technology, immobilization surface, and the application of solution panning. The latter allows the free target protein to interact with

Camilo Perez and Timm Maier (eds.), *Expression, Purification, and Structural Biology of Membrane Proteins*, Methods in Molecular Biology, vol. 2127, https://doi.org/10.1007/978-1-0716-0373-4_11,

the displayed binders in solution, preceding a rapid (within minutes) immobilization on beads and subsequent pull-down of the target protein-binder complexes. Hereby delicate membrane proteins are protected from denaturation resulting from prolonged exposure to surfaces at high protein densities. Hence, the selective immobilization of the target protein is a key step in selection procedures.

Though seemingly trivial, the choice of the immobilization strategy is of great relevance as this may dramatically skew the selection and directly affect the quality and quantity of unique binders identified. Given the aim of obtaining multiple strong binders against different, three-dimensional epitopes, an ideal protein immobilization strategy should: (1) preserve the native three-dimensional structure; (2) allow a non-oriented, ideally random orientation of the target protein with high accessibility of potential epitopes; (3) capture the target protein selectively, rapidly (within a few minutes), and stably (over prolonged periods of several hours) in a variety of buffer conditions and a broad temperature range; and (4) allow near-complete capture of the target protein to avoid loss of binder diversity during solution panning. In addition, the strategy should not interfere with biogenesis and function of the target protein and should be facile to implement. Among the multitude of protein immobilization strategies [3], the biotin/avidin-based interaction fits these criteria best and is therefore widely used [4].

The interaction between the vitamin biotin and avidin or its variants streptavidin and neutravidin is one of the strongest non-covalent interactions known (K_d of ~10^{-14} M) and has a half-life of several days [5, 6]. The interaction remains stable over a broad range of temperatures [7], pH values, and denaturants [8, 9]. Avidin, streptavidin, and neutravidin are homotetrameric proteins with four biotin-binding sites. Streptavidin, derived from bacterial origin, and neutravidin, a deglycosylated form of avidin, are generally preferred over avidin, as the absence of glycosylation and their lower pI values reduce nonspecific binding [5, 8]. Importantly, naturally biotinylated proteins are rare: in *E. coli* or mammalian cells the number of proteins holding a covalently attached biotin amount to one and four, respectively [10, 11].

Biotinylation of a target membrane protein can be achieved chemically or enzymatically. Chemical biotinylation is most conveniently done by targeting the primary amine of a surface-exposed lysine residue using biotin derivatized with an N-hydroxysuccinimide (NHS) group. This reaction can be performed under comparably mild, biocompatible conditions. Due to the general abundance of lysines on protein surfaces, amine chemistry allows the introduction of biotin at different positions in the protein. Consequently, the target protein can be immobilized in several orientations allowing exposure of different potential epitopes, provided that only one biotin group is introduced.

A higher degree of labeling is disadvantageous as this may restrict flexibility and surface presentation and may even directly interfere with binding of the antibody by masking the epitope. As an alternative to the comparably abundant lysines, cysteines may be targeted using, e.g., biotin derivatized with a maleimide group. The main advantage of chemical biotinylation is the random target orientation during immobilization. This comes at the price of two disadvantages: chemical biotinylation typically results in a distribution of target proteins carrying none, one, or multiple biotin moieties; and biotinylation of lysines may modify, and thereby mask, potential epitopes.

The *E. coli* biotin protein ligase BirA requires biotin and ATP to biotinylate its only target, the biotin carboxyl carrier protein (BCCP) subunit of acetyl-CoA carboxylase, at a specific lysine in an evolutionary conserved amino acid sequence. Engineering of this sequence led to the identification of the Avi-tag, a 15 amino acid stretch, GLNDIFEAQ-K-IEWHE, that is biotinylated with high efficiency [12, 13]. Avi-tags fused to the N- or C-terminus [14] or even integrated in exposed loops [15] are efficiently biotinylated by BirA. Enzymatic biotinylation of membrane proteins can be done in vivo using native or co-expressed BirA or in vitro using the purified BirA protein. The main advantage of enzymatic biotinylation is its high efficiency and specificity, resulting in nearly complete and exclusive biotinylation of the lysin residue in the Avi-tag. Hence, the highly desirable biotin to target protein ratio of 1:1 can easily be achieved. However, enzymatic biotinylation has two major disadvantages: all target proteins are immobilized in the same orientation, which may render some epitopes inaccessible; this problem is exacerbated for homo-oligomeric target proteins, where several biotin moieties are introduced via the Avi-tag; and the attachment of the Avi-tag sequence to the open reading frame of the target protein requires molecular cloning and potentially construct optimization.

The biochemical quality of the membrane protein target is arguably the most critical parameter when performing binder selections. Hence, it is paramount that the biotinylation procedure does not compromise the structure and function of the target protein. Therefore, biotinylated target proteins need to be experimentally tested for activity and structural integrity using size exclusion chromatography, both for enzymatic and chemical biotinylation.

This chapter first details a facile cloning strategy for fusing sequences for N- or C-terminal Avi-tags to the target open reading frame. Subsequently, we describe approaches for enzymatic and chemical biotinylation of (Avi-tagged) membrane proteins and conclude with methodology to assess the degree of biotinylation. Together, this chapter provides all relevant information required to selectively immobilize membrane proteins using the biotin/avidin interaction.

2 Materials

2.1 FX Cloning

1. FX cloning vectors. *E. coli* expression vectors for the arabinose-controlled P_{BAD} promoter [16] and holding sequences coding for an Avi-tag in combination with an HRV 3C protease cleavable GFP-His-tag or His-tag (Fig. 1) are available on Addgene (#47069, #47071-47075). The optional intermediate vector pINIT_cat for subcloning is available on Addgene as well (#46858). All FX cloning vectors should be propagated in a CcdB-resistant *E. coli* strain such as DB3.1 [17].
2. Dedicated forward and reverse primers targeting the gene of interest and compatible with FX cloning. For ordering, choose the smallest synthesis scale and mere desalting as purification.

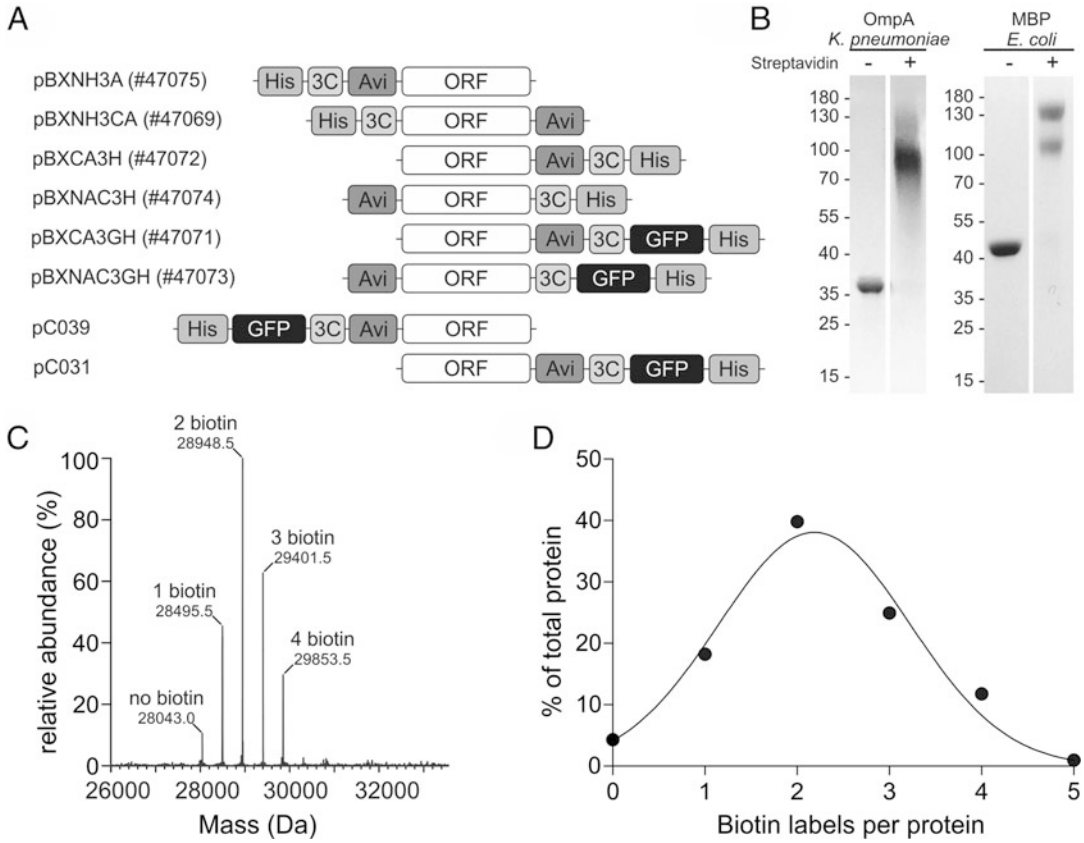

Fig. 1 Protein biotinylation toolkit. (**a**) FX cloning expression vectors for the introduction of Avi-tags. (**b**) Assessing the degree of biotinylation by a streptavidin-induced mobility shift in SDS-PAGE. Avi-tagged OmpA of *Klebsiella pneumoniae* and MBP of *E. coli* were enzymatically biotinylated in vitro using purified BirA. (**c**) GFP (126 μM) was chemically biotinylated with a fivefold molar excess of EZ-Link Sulfo-NHS-LC-Biotin (630 μM) in PBS for 30 min at 25 °C. The resulting biotinylation pattern was determined by mass spectrometry (ESI-MS). (**d**) Quantification of the biotinylation pattern. Less than 5% of GFP was devoid of biotin. The data were fitted with a Gaussian curve

Table 1
FX-cloning sequencing primers

Primer name	Primer sequence (5′–3′)
pINIT_cat forward	ATCTGTTGTTTGTCGGTGAACGC
pINIT_cat reverse	TGGCAGTTTATGGCGGGCGT
pBX forward	AGATTAGCGGATCCT
pBAD reverse	GCTGAAAATCTTCTCTCATCCG
interGFP reverse	CATTAACATCACCATCTAATTCAACAAGAA

3. Template DNA for the open reading frame of interest (e.g., genomic DNA or plasmid).
4. Phusion DNA polymerase, corresponding buffer, and dNTPs.
5. TAE buffer, TAE agarose gel, and agarose gel DNA extraction kit.
6. SapI restriction enzyme and corresponding buffer.
7. T4 DNA ligase.
8. 10 mM ATP: 10 mM Na_2-ATP, 10 mM $MgSO_4$. Dissolve in 50 mM KPi, pH 7.0 and adjust to pH 6.5–7.0 with NaOH. Store in small aliquots at −20 °C.
9. CcdB-sensitive *E. coli* strain (e.g., MC1061 [18]).
10. LB medium and LB-agar plate supplemented with the appropriate antibiotic. For ampicillin (Amp) and chloramphenicol (Cam), use 100 μg/mL and 34 μg/mL, respectively.
11. Miniprep kit (QIAGEN).
12. Sequencing primers for pINIT_cat or the arabinose-controlled P_{BAD} expression vectors (Table 1).

2.2 BirA-Based In Vitro Biotinylation

1. BirA at 8 mg/mL (228 μM) in 50 mM Tris–HCl pH 7.5, 200 mM KCl, 50% glycerol, 0.1 mM DTT. His-tagged BirA can be produced using pET21a-BirA (Addgene) as described [19] but it is also commercially available (e.g., from Sigma-Aldrich). Store for prolonged periods at −80 °C. Substocks stored at −20 °C will remain liquid and ready to use.
2. HRV 3C protease at 6 mg/mL (276 μM) in 50 mM Tris–HCl pH 7.5, 150 mM NaCl, 1 mM TCEP, and 50% glycerol. His-tagged 3C protease can be produced as described [20] but is also commercially available (e.g., from Sigma-Aldrich). Store 100 μL aliquots at −80 °C.
3. 200 mM ATP (dissolve in 50 mM KPi, pH 7.0 and adjust to pH 6.5–7.0 with NaOH).

4. 1 mM biotin in 50 mM Bicine buffer pH 8.3. Store in small aliquots at −20 °C.
5. 1 M MgOAc.
6. Ni-NTA resin or prepacked Ni-NTA column.

2.3 BirA-Based In Vivo Biotinylation

1. Expression vectors. Mammalian vectors for protein expression based on a pCDNA3.1(+) backbone (Thermo Fisher) controlled by a CMV promoter and holding a Kozak sequence preceding sequence coding for an N- (pC039) or C-terminal (pC031) Avi-tag in combination with an HRV 3C protease cleavable GFP-His-tag, respectively (Fig. 1).
2. BirA co-expression vectors. Co-expression of *E. coli* BirA in mammalian cell culture and under control of a CMV promoter is assured by the presence of an additional plasmid coding for BirA with a C-terminal Myc-tag for intracellular biotinylation, or BirA with an N-terminal IgH signal sequence and C-terminal KDEL ER-retention signal for biotinylation of extracellularly located Avi-tags.
3. Opti-MEM reduced serum medium (Thermo Fisher).
4. ExpiFectamine 293 transfection kit (Thermo Fisher; part of the expression kit).
5. Expi293 expression medium (Thermo Fisher) and Freestyle medium (Thermo Fisher).
6. Fernbach cell culture shaking flask (e.g., 3 L) plus CO_2-gassed shaker platform.
7. Optional: 2.1 mM biotin in Expi293 medium.
8. Steritop filter (250 mL, Millipore).

2.4 Chemical Biotinylation

1. PBS buffer pH 7.4, 137 mM NaCl, 2.7 mM KCl, 10 mM Na_2HPO_4, 1.8 mM KH_2PO_4.
2. EZ-Link Sulfo-NHS-LC-Biotin (Thermo Fisher).
3. Dimethyl sulfoxide (DMSO).

2.5 Assessing Degree of Biotinylation

1. Streptavidin at 1 mg/mL in MilliQ. Store in aliquots at −20 °C.
2. 5× SDS-PAGE sample buffer.
3. SDS-PAGE gel and setup.

3 Methods

3.1 FX Cloning

1. Design FX-cloning compatible primers targeting your gene of interest. This is most conveniently done online at the https://www.fxcloning.org website using a FASTA-formatted

sequence including a start and stop codon. Order the primer set optimized toward removal of stable hairpin structures (*see* **Note 1**).

2. Amplify the gene of interest by PCR. Prepare a 50 μL PCR reaction and add the DNA polymerase immediately prior to starting the reaction. Use a touch-down [21] program, e.g., (1) 30 s at 98 °C; (2) 10 s at 98 °C; (3) 15 s at 61 °C (annealing temperature decreased by 0.5 °C per cycle); (4) 15–30 s/kb at 72 °C; repeat (2)–(4) 14 times; (5) 10 s at 98 °C; (6) 15 s at 53 °C; (7) 15–30 s/kb at 72 °C; repeat (5)–(7) 14 times; (8) 120 s at 72 °C; (9) unlimited at 10 °C.
3. Analyze the product on a preparative TAE agarose gel. Purify the relevant band using a DNA gel extraction kit and quantify the DNA spectrophotometrically.
4. Mix 50 ng of pINIT_cat with the extracted insert in a molar ratio of vector:insert of 1:5 (*see* **Note 2**).
5. Add 1 μL 10× SapI buffer and adjust the volume to 9 μL with ultrapure water. Add 1 μL SapI (2 U) and incubate for 1 h at 37 °C in a PCR machine.
6. Heat inactivate the SapI for 20 min at 65 °C. Let the sample cool down and add 1.25 μL 10 mM ATP and 1.25 μL T4 DNA ligase (1.25 U). Incubate for 1 h at room temperature.
7. Heat inactivate the T4 DNA ligase for 20 min at 65 °C and transform 5 μL of the ligation mix to 100 μL chemically competent *E. coli* MC1061 cells (or an alternative CcdB-sensitive strain).
8. Plate 10% and 90% aliquots on LB-agar-Cam plates and incubate overnight at 37 °C.
9. Use a single colony to inoculate 5 mL LB-Cam and cultivate overnight. Isolate the plasmid using a miniprep kit, determine the concentration spectrophotometrically, and verify the insert by DNA sequencing using the pINIT_cat sequencing primers.
10. Mix 50 ng of the FX cloning Avi-tag expression vector (*see* **Note 3**) with pINIT_cat carrying the insert to a molar ratio of vector:pINIT_cat-derivative of 1:5. Add 1 μL 10× SapI buffer and adjust the volume to 9 μL with ultrapure water. Add 1 μL SapI (2 U) and incubate for 1 h at 37 °C in a PCR machine.
11. Heat inactivate the SapI for 20 min at 65 °C. Let the sample cool down and add 1.25 μL 10 mM ATP and 1.25 μL T4 DNA ligase (1.25 U). Incubate for 1 h at room temperature.
12. Heat inactivate the T4 DNA ligase for 20 min at 65 °C and transform 5 μL of the ligation mix to 100 μL chemically competent *E. coli* MC1061 cells.

13. Plate 10% and 90% aliquots on LB-agar-Amp plates. Incubate the plates overnight at 37 °C.
14. Use a single colony to inoculate 5 mL LB-Amp and cultivate overnight at 37 °C.
15. Archive the culture as a glycerol stock at −80 °C (*see* **Note 4**). This stock can serve for inoculation of expression cultures based on the araBAD promoter (*see* **Notes 5** and **6**).

3.2 BirA-Based In Vitro Biotinylation

1. Recombinantly express the target protein using previously established procedures [22] (*see* **Note 7**). Purify the Avi-tagged target protein (*see* **Note 8**) and determine the protein concentration spectrophotometrically.
2. Add 3C protease to a molar ratio of 1:10 to cleave off the decaHis-tag while dialyzing the sample for 1 h at 4 °C to remove excess imidazole (*see* **Note 9**).
3. Adjust the target protein concentration to 10–50 μM (either by dilution or using a concentrator unit). Add biotin to a molar ratio of target protein:biotin of 1:1.5, 5 mM ATP, 10 mM MgOAc and BirA to a molar ratio of target protein:BirA of 20:1 (*see* **Note 10**). Incubate the sample overnight at 4 °C (*see* **Note 11**).
4. Remove His-tagged BirA, HRV 3C protease, and potential remaining contaminants from the sample by reverse IMAC and collect the flow-through holding the biotinylated target protein.
5. Perform size exclusion chromatography (SEC) to remove soluble aggregates and excess of biotin from the sample (*see* **Note 12**). Determine the degree of biotinylation as outlined in Subheading 3.5.
6. Proceed with the selection of binders such as nanobodies and sybodies (*see* **Note 13**) or store the target protein (*see* **Notes 14** and **15**).

3.3 BirA-Based In Vivo Biotinylation

1. Generate mammalian expression vectors for the gene of interest in pC031 or pC039 to obtain a fusion protein with an N- or C-terminal Avi-tag (*see* **Notes 16** and **17**).
2. Split an Expi293 subculture (*see* **Note 18**), typically grown to 3-5 × 10^6 cells/mL, into a 3 L Fernbach shaking flask and adjust to a final volume of 0.6 L Expi293 medium with a density of 0.7 × 10^6 cells/mL.
3. Incubate the culture for 72 h at 37 °C, under humidified atmosphere and 5% CO_2 in a shaking incubator.
4. On the day of the transient transfection, adjust the culture to 830 mL with a density of 3.4 × 10^6 cells/mL by adding Expi293 medium and/or removing cells.

5. Add 20 mL biotin solution (final concentration of 50 μM) (*see* **Note 19**).
6. Pipet 50 mL Opti-MEM into a 100 mL sterile Schott bottle. Add 2.7 mL ExpiFectamine transfection reagent, shake gently, and incubate for 5 min at room temperature.
7. Pipet 50 mL Opti-MEM into a second 100 mL Schott bottle and add the two plasmid batches in a final amount of 1 mg to 0.1 mg, target protein expression plasmid:BirA expression plasmid, respectively. Shake gently and incubate for 5 min at room temperature.
8. Mix the contents of both bottles, filter sterilize, and incubate for 20–30 min at room temperature to form the transfection complex.
9. Add 100 mL of the formed transfection complex to the Fernbach shaking flask with 850 mL of cell culture for a final volume of 950 mL. Incubate further at 37 °C and 5% CO_2 with mild shaking.
10. Add sterile 5 mL Enhancer 1 and 50 mL Enhancer 2 from the ExpiFectamine 293 transfection kit at 16–20 h post-transfection and continue incubation.
11. Incubate for a total time of approximately 48-72 h post-transfection depending on the most optimal condition for protein expression. Harvest the cells by centrifugation at 3000 × *g* for 15 min, flash freeze the pellet in liquid nitrogen, and store at −80 °C.
12. Purify the biotinylated Avi-tagged target protein (*see* **Note 8**) and determine the protein concentration spectrophotometrically. Determine the degree of biotinylation as outlined in Subheading 3.5. Proceed with the selection of binders such as nanobodies and sybodies (*see* **Note 13**) or store the target protein (*see* **Notes 14** and **15**).

3.4 Chemical Biotinylation

1. Recombinantly express the target protein using previously established procedures [22]. Purify the target protein and employ preparative SEC using PBS, supplemented with the required detergent, as buffer (*see* **Note 20**). Determine the protein concentration spectrophotometrically.
2. Concentrate the target protein to 50-200 μM.
3. Dissolve EZ-Link Sulfo-NHS-LC-Biotin in highly pure DMSO to a concentration of 10 mM (*see* **Note 21**).
4. Add EZ-Link Sulfo-NHS-LC-Biotin to the target protein in fivefold molar excess and incubate at 25 °C for 30 min under gentle agitation (*see* **Note 22**).

5. Perform SEC to remove excess of biotin from the sample (*see* **Note 12**).
6. Determine the biotinylation pattern of the biotinylated target protein by mass-spectrometry (Fig. 1, *see* **Note 23**). In case mass spectrometry analysis is not available or cannot be carried out due to the target's high molecular weight, determine the degree of biotinylation as outlined in Subheading 3.5.
7. Proceed with the selection of binders such as nanobodies and sybodies (*see* **Note 13**) or store the target protein (*see* **Notes 14** and **15**).

3.5 Assessing Degree of Biotinylation

1. Mix two aliquots of 10 μg biotinylated target protein with 5× SDS-PAGE sample buffer.
2. Add streptavidin to one of the aliquots in a 1:1 molar ratio of target protein:streptavidin (*see* **Note 24**).
3. Analyze the control (no addition) and test (streptavidin addition) samples in adjacent lanes on SDS-PAGE.
4. Stain the gel with Coomassie Brilliant Blue R-250 and quantify the band intensities with the ImageJ software and calculate the degree of biotinylation (*see* **Notes 25** and **26**).

4 Notes

1. As the N- and C-termini of most proteins are comparably long and flexible, we generally do not insert a linker sequence between the target protein and the Avi-tag. Nevertheless, should this be desired, a sequence for a linker is best introduced at this step.
2. Alternatively, should subcloning of a sequence-verified open reading frame not be required, proceed with **Step 10** and use the purified PCR product to replace the pINIT_cat holding the insert.
3. Should an expression and purification strategy for the protein already be established, this combination of tags and fusions proteins should guide the choice for the expression vector. We recommend the production of protein variants with N- and C-terminal Avi-tags as this may allow the presentation of different surfaces of the target protein.
4. For other expression systems that require fresh transformations for expression cultures, e.g., those based on the T7 promoter, the stock serves as a plasmid source. No additional verification by DNA sequencing is required following the subcloning of a sequence-verified open reading frame from pINIT_cat to an FX cloning expression vector.

5. The FX-cloning expression vectors for fused Avi-tag allow recombinant expression in *E. coli* under the control of the P_{BAD} promotor with decaHis-tag. Instead of subcloning a sequence-verified ORF from pINITIAL to an FX cloning Avi-tag expression vector, PCR products can also be cloned immediately into an FX cloning Avi-tag expression vector. This requires sequence verification of each expression vector. If multiple expression vectors are constructed, subcloning from pINITIAL prevents excessive sequencing. If one aims for only a single Avi-tagged construct, we recommend starting with pBXNH3CA (Addgene #47069), which adds a cleavable N-terminal decaHis-tag and a C-terminal Avi-tag to the protein. In our hands, this vector resulted in good expression levels for a number of ABC transporters as well as maltose-binding protein (MBP) and GFP.
6. Should expression in alternative pro- or eukaryotic systems be preferred, the P_{BAD}-based expression vectors may serve as facile intermediates for fusing the Avi-tag sequences.
7. If the Avi-tagged target protein is expressed in *E. coli* and if the Avi-tag sequence is located in the cytoplasm, the Avi-tag will be biotinylated in vivo by virtue of the natively expressed BirA. The degree of biotinylation varies from case to case (subject to availability of biotin, level of target protein overexpression and accessibility of Avi-tag), but is often incomplete. The degree of in vivo biotinylation may be increased by co-expression of BirA and supplementation of the medium with biotin [14]. However, due to the relevance of complete biotinylation of the Avi-tag, our protocol ignores in vivo biotinylation of the target within *E. coli* and assures full biotinylation by performing an additional in vitro step. If required, the degree of native biotinylation can be assessed as outlined in Subheading 3.5.
8. The BirA-based biotinylation protocol describes the procedure for His-tagged target protein but can in principle be adapted to protocols involving other affinity-tags. The use of strep-tags [23] or fusions with streptavidin-binding-protein (SBP) [24] should be avoided as biotinylation of Avi-tags by endogenous BirA, which may reach a very high degree depending on the experimental conditions and target protein, will prevent elution from the respective columns.
9. Although BirA is inhibited by NaCl (over 100 mM) and glycerol (over 1%) [14], we generally use buffers containing 150 mM NaCl and 10% glycerol if the target membrane protein requires this for maintaining a well-folded state. We compensate for the reduced BirA activity by biotinylating for prolonged periods (overnight).

10. Addition of extra amount of detergent might be necessary to keep the detergent concentration well above the CMC.
11. The BirA-based biotinylation reaction can also be performed for 1 h at room temperature if the target protein is stable under these conditions. For most membrane proteins we recommend keeping the sample at 4 °C.
12. Removal of free biotin is often crucial for downstream processes. In case no size exclusion chromatography is performed, use dialysis or a desalting column to remove the excess biotin from the sample.
13. The outcome of the binder selection depends to a very large extent on the quality of the target protein used. Productive binder selections are expected if: (1) the SEC profile of the biotinylated target protein is monodisperse and very similar to that obtained for non-biotinylated target protein; (2) the fraction of non-biotinylated target protein is less than 10%; and (3) in case of chemical biotinylation: over-biotinylation is excluded, ideally as assessed by mass spectrometry.
14. If possible, the biotinylated target protein is supplemented with 10% glycerol, aliquoted, snap-frozen in liquid nitrogen, and stored at −80 °C. To assess if freezing is tolerated by the target protein, compare a frozen/thawed and untreated sample by SEC. If no discernible aggregation or protein loss is observed, freezing can be considered as tolerated.
15. We routinely freeze biotinylated membrane proteins for storage purposes. Having thus far analyzed more than a dozen membrane proteins in this manner, we never experienced aggregation problems due to freezing. Frozen biotinylated proteins remain stable at −80 °C for several years.
16. The preferred location of the Avi tag on the target protein depends on the quality and quantity of the fusion protein that can be obtained. Both parameters are most easily assessed by using fluorescence-detection size-exclusion chromatography (FSEC) analysis [25].
17. Biotinylation of Avi-tags during cultivation can be achieved in several additional expression systems [14, 26, 27]. These procedures also require the co-expression of BirA and growth medium supplemented with biotin.
18. Numerous expression screenings provided the tendency that Expi293 is more successful for expressing membrane proteins. As an alternative we recommend Freestyle 293-F cells. Implementation of the latter will require small adaptations of the described workflow for which we refer to the instructions from the supplier.

19. Supplementing the medium with biotin is optional. Over the course of many years and targets we observed virtually complete biotinylation even in the absence of supplemented biotin.
20. It is very important that compounds containing primary amines are absent from the purified protein sample for chemical biotinylation. A frequent source of primary amines stems from Tris-buffers. IMAC-purified protein is not pure enough regarding biogenic amines to be used for NHS coupling.
21. The NHS moiety of EZ-Link Sulfo-NHS-LC-Biotin reacts with water and is thereby inactivated. We therefore highly recommend preparing the Sulfo-NHS-LC-Biotin solution freshly. Keep solid EZ-Link Sulfo-NHS-LC-Biotin under argon at −80 °C for prolonged storage.
22. In case the target protein is unstable at 25 °C, the biotinylation reaction can be carried out at 4 °C. In this case, increase the biotin-target protein ratio to 10:1 and incubate for 60 min instead of 30 min.
23. A typical pattern contains different species containing either none, one, or several biotin moieties per target protein (Fig. 1). Ideally, the non-biotinylated species should not exceed 10% of the total species (in the example of GFP labeling shown in Fig. 1, non-biotinylated target accounts for around 5%). In case of over- or under-biotinylation, the biotin-target protein ratio needs to be adjusted accordingly, while keeping the target protein concentration and incubation time constant.
24. The biotinylation of target protein can be quantified by mobility shift in SDS-PAGE upon addition of streptavidin to the sample. Streptavidin remains folded and bound to the biotinylated target protein under conventional SDS-PAGE conditions [28]. Membrane protein samples are usually not boiled before SDS-PAGE. However, when boiling the sample is required add streptavidin afterward.
25. Due to the tetrameric architecture of streptavidin with four biotin-binding sites, multiple protein bands may be observed, e.g., (1) free streptavidin (53 kDa), (2) streptavidin associated with a single target protein, and (3) streptavidin associated with multiple (up to four) target proteins. In our hands, it is more straightforward to use the intensity loss of the target protein band upon streptavidin addition relative to the control sample for quantification. For more precise quantification we recommend mass spectrometry to analyze the degree of biotinylation. For qualitative analysis of target protein biotinylation, western blotting using a streptavidin-HRP conjugate can be employed.

26. Incomplete biotinylation might be advantageous regarding oligomeric proteins. Similar to the presence of multiple biotin labels on monomeric proteins, the occurrence of multiple biotin groups per oligomeric protein complex may restrict its flexibility upon immobilization and thereby decrease the variation and amount of protein surface accessible to the binders. We recommend a pull-down of biotinylated target protein with immobilized streptavidin and compare the pull-down efficiency with the mobility shift in SDS-PAGE to quantify the biotinylation per oligomeric unit.

Acknowledgments

We thank Martin Siegrist, Jean-Marie Vonach, and Marcello Foggetta for technical help during expression and fermentation as well as Roche Diagnostics in Munich, Penzberg for reagent generation. We acknowledge financial support from the German Research Foundation via the Cluster of Excellence Frankfurt (Macromolecular Complexes, to E.R.G.), and the SFB807 (Transport and Communication across Biological Membranes, to E.R.G.). Work in the Seeger group was supported by a SNSF Professorship of the Swiss National Science Foundation (PP00P3_144823, to M.A.S.), a SNSF NRP 72 grant (407240_177368, to M.A.S.), a SNSF BRIDGE proof-of-concept grant (20B1-1_175192, to P.E.), and a BioEntrepreneur-Fellowship of the University of Zurich (BIOEF-17-002, to I.Z.). R.J.P.D, E.R.G., and M.A.S. acknowledge a grant of the Commission for Technology and Innovation CTI (16003.1 PFLS-LS).

References

1. Steyaert J, Kobilka BK (2011) Nanobody stabilization of G protein-coupled receptor conformational states. Curr Opin Struct Biol 21:567–572
2. Zimmermann I, Egloff P, Hutter CA et al (2018) Synthetic single domain antibodies for the conformational trapping of membrane proteins. elife 7
3. Rusmini F, Zhong Z, Feijen J (2007) Protein immobilization strategies for protein biochips. Biomacromolecules 8:1775–1789
4. Fairhead M, Howarth M (2015) Site-specific biotinylation of purified proteins using BirA. Methods Mol Biol 1266:171–184
5. Green NM (1990) Avidin and streptavidin. Methods Enzymol 184:51–67
6. Piran U, Riordan WJ (1990) Dissociation rate constant of the biotin-streptavidin complex. J Immunol Methods 133:141–143
7. Marttila AT, Laitinen OH, Airenne KJ et al (2000) Recombinant NeutraLite avidin: a non-glycosylated, acidic mutant of chicken avidin that exhibits high affinity for biotin and low non-specific binding properties. FEBS Lett 467:31–36
8. Green NM (1975) Avidin. Adv Protein Chem 29:85–133
9. Sano T, Cantor CR (1990) Cooperative biotin binding by streptavidin. Electrophoretic behavior and subunit association of streptavidin in the presence of 6 M urea. J Biol Chem 265:3369–3373
10. Fall RR (1979) Analysis of microbial biotin proteins. Methods Enzymol 62:390–398
11. Robinson BH, Oei J, Saunders M et al (1983) [3H]biotin-labeled proteins in cultured human skin fibroblasts from patients with pyruvate carboxylase deficiency. J Biol Chem 258:6660–6664

12. Beckett D, Kovaleva E, Schatz PJ (1999) A minimal peptide substrate in biotin holoenzyme synthetase-catalyzed biotinylation. Protein Sci 8:921–929
13. Schatz PJ (1993) Use of peptide libraries to map the substrate specificity of a peptide-modifying enzyme: a 13 residue consensus peptide specifies biotinylation in Escherichia coli. Biotechnology (N Y) 11:1138–1143
14. Cull MG, Schatz PJ (2000) Biotinylation of proteins in vivo and in vitro using small peptide tags. Methods Enzymol 326:430–440
15. Brown MT, Steel BC, Silvestrin C et al (2012) Flagellar hook flexibility is essential for bundle formation in swimming Escherichia coli cells. J Bacteriol 194:3495–3501
16. Guzman LM, Belin D, Carson MJ et al (1995) Tight regulation, modulation, and high-level expression by vectors containing the arabinose P_{BAD} promoter. J Bacteriol 177:4121–4130
17. Hartley JL, Temple GF, Brasch MA (2000) DNA cloning using in vitro site-specific recombination. Genome Res 10:1788–1795
18. Casadaban MJ, Cohen SN (1980) Analysis of gene control signals by DNA fusion and cloning in Escherichia coli. J Mol Biol 138:179–207
19. Howarth M, Takao K, Hayashi Y et al (2005) Targeting quantum dots to surface proteins in living cells with biotin ligase. Proc Natl Acad Sci U S A 102:7583–7588
20. Ullah R, Shah MA, Tufail S et al (2016) Activity of the Human Rhinovirus 3C Protease Studied in Various Buffers, Additives and Detergents Solutions for Recombinant Protein Production. PLoS One 11:e0153436
21. Don RH, Cox PT, Wainwright BJ et al (1991) 'Touchdown' PCR to circumvent spurious priming during gene amplification. Nucleic Acids Res 19:4008
22. Marino J, Holzhuter K, Kuhn B et al (2017) Efficient Screening and Optimization of Membrane Protein Production in Escherichia coli. Methods Enzymol 594:139–164
23. Schmidt TG, Skerra A (1994) One-step affinity purification of bacterially produced proteins by means of the "Strep tag" and immobilized recombinant core streptavidin. J Chromatogr A 676:337–345
24. Keefe AD, Wilson DS, Seelig B et al (2001) One-step purification of recombinant proteins using a nanomolar-affinity streptavidin-binding peptide, the SBP-Tag. Protein Expr Purif 23:440–446
25. Kawate T, Gouaux E (2006) Fluorescence-detection size-exclusion chromatography for precrystallization screening of integral membrane proteins. Structure 14:673–681
26. Erdmann D, Zimmermann C, Fontana P et al (2010) Simultaneous protein expression and modification: an efficient approach for production of unphosphorylated and biotinylated receptor tyrosine kinases by triple infection in the baculovirus expression system. J Biomol Tech 21:9–17
27. Thie H, Binius S, Schirrmann T et al (2009) Multimerization domains for antibody phage display and antibody production. New Biotechnol 26:314–321
28. Viens A, Mechold U, Lehrmann H et al (2004) Use of protein biotinylation in vivo for chromatin immunoprecipitation. Anal Biochem 325:68–76

Chapter 12

Production and Application of Nanobodies for Membrane Protein Structural Biology

Janine Denise Brunner and Stephan Schenck

Abstract

Nanobodies, small recombinant binders derived from camelid single chain antibodies, have become widely used tools in a diversity of disciplines related to membrane proteins. They are applied as chaperones in crystallization and blockers or modifiers of protein activity among numerous other applications. Their simple architecture as a single polypeptide chain, in contrast to classical antibodies, enables straightforward cloning, library generation, and recombinant expression. The small diameter and the pointed wedge-like shape of the antigen-binding site underlies binding to hollows and crevices of membrane proteins and renders nanobodies often conformation specific making them a preferred type of chaperone. Here we describe a simple protocol for the recombinant production of nanobodies in *E. coli* and their purification. We expand the current repertoire of usage further by describing a procedure for enlarging nanobodies on their C-terminal end to generate "macrobodies," without interfering with their original characteristics. These enlarged nanobodies extend the application as a chaperone in crystallography and can serve to increase the mass for small targets in single particle electron cryo-microscopy, a field where nanobodies had so far only limited effect because of their small size.

Key words Nanobody, Macrobody, Nanobody expression, Complex formation, Nanobody enlargement, Nanobody generation, MBP fusion protein

1 Introduction

The VHH domain of camelid single-chain antibodies (unique among tetrapods) forms what has been termed nanobody [1]. After immunization of camelids (e.g., camels, dromedars, llamas, and alpacas), VHH domains can be cloned from a blood sample and screened in vitro [2]. Recently a number of synthetic libraries coupled to phage or yeast display has been constructed that make nanobodies even more accessible to researchers, circumventing animal immunization [3–5]. After selection nanobodies are usually produced in *E. coli,* a cheap and convenient host for the production of recombinant proteins.

Camilo Perez and Timm Maier (eds.), *Expression, Purification, and Structural Biology of Membrane Proteins*, Methods in Molecular Biology, vol. 2127, https://doi.org/10.1007/978-1-0716-0373-4_12,

Nanobodies have a number of highly advantageous properties that have made these binders a preferred choice for membrane protein research. They are highly soluble and monodisperse small proteins with a size of 12–15 kDa. The small diameter of their antigen-binding site is underlying their propensity to bind to cryptic epitopes within hollows and crevices of proteins. These areas often coincide with catalytic centers, substrate-binding sites, or functionally important hinge regions of proteins, and nanobodies that bind such epitopes are frequently found. Binding to such inaccessible epitopes is less pronounced for classical dual-chain mouse or rabbit antibodies, likely because of their larger antigen-binding area. The long antigen-binding loop CDR3 is the prominent element of nanobodies that predisposes for binding to crevices [6, 5].

Due to their excellent biochemical properties and ease of handling, nanobodies have become a widespread tool for a number of applications (Fig. 1). For instance, nanobodies can be functionally expressed in the cytosol of cells (intrabodies) [7], which is problematic with dual-chain antibodies. Tagged with fluorescent proteins (chromobodies) they can be used as a reporter [8–10]. Nanobodies can also be utilized as a tool for purification of proteins (e.g., directed against GFP [11, 12]) to facilitate the purification of lowly expressed proteins from extracts. In pharmacology, nanobodies are of great interest due to their frequently observed interference with protein function, which makes nanobodies promising agents in clinical approaches either as a drug or in diagnostics [13–15]. One of the most prominent applications of nanobodies is their use as chaperones in structural biology, especially for membrane proteins. They have been successfully applied as crystallization chaperones, by contributing to crystal contacts and/or by stabilizing the conformation of the target membrane protein. Increasing numbers of reported structures from complexes of nanobodies and target membrane proteins reflect this. Among them are membrane proteins from bacterial or eukaryotic origin, diverse as secondary active transporters [16–19], numerous GPCRs [5, 6, 20, 21], ion channels [22–24], and other membrane proteins [25–27].

One of the most advantageous properties for a number of applications of nanobodies is their small size. Also with respect to their propensity of binding to cervices, the small diameter of nanobodies is in favor for targeting such epitopes. However, the small size may also be limiting for the provision of crystal contacts in some cases and is insufficient to be clearly discernible in electron micrographs. Because of this inherent parameter, nanobodies may also fail to improve crystallization by providing crystal contacts and are currently of limited use for particle enlargement and classification in single particle cryo-EM. We have recently shown that nanobodies can also be produced as a fusion protein with a C-terminally

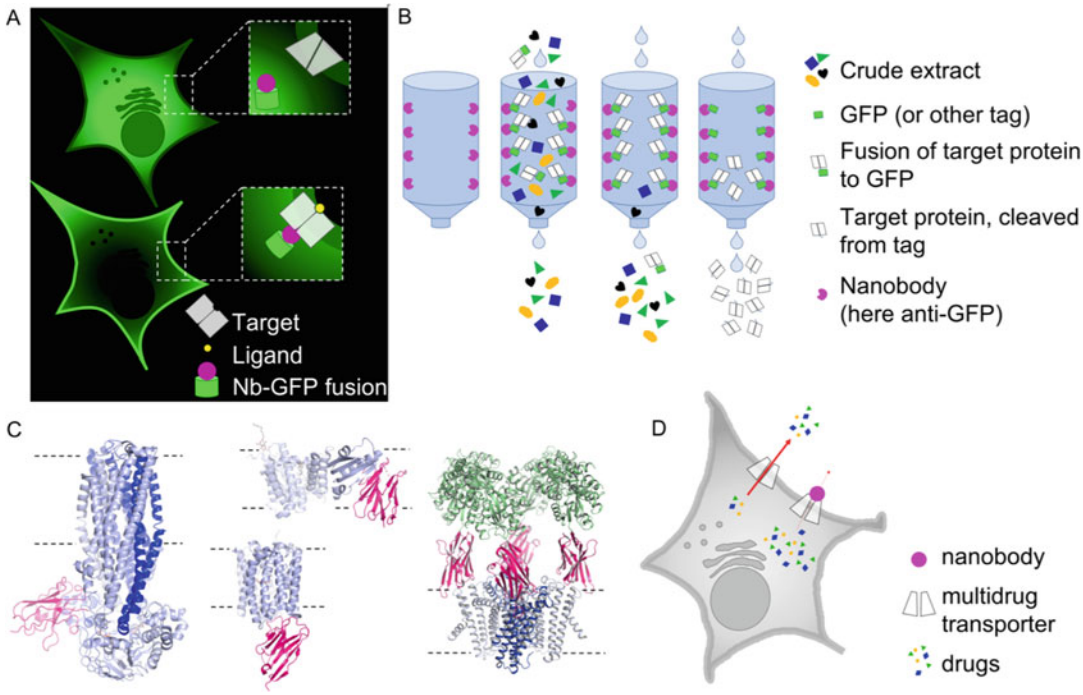

Fig. 1 Applications of nanobodies. (**a**) Chromobodies as reporters. GFP is fused to the nanobody at the C-terminus (top). The target protein is only recognized by the nanobody in a certain conformation (ligand-bound) leading to recruitment of the reporter to the membrane upon addition of ligand (bottom). (**b**) Purification of a target protein fused to GFP/YFP from cell lysate by using an anti-GFP/YFP nanobody covalently linked to Sepharose resin. (**c**) Membrane proteins (blue) crystallized in complex with nanobodies (pink). PglK from *Campylobacter jejuni* with inhibitory nanobody, PDB code 5NBD; LacY from *Escherichia coli* with a nanobody that stabilizes the open conformation, PDB code 6C9W; SLC26 transporter from *Deinococcus geothermalis* with nanobody, PDB code 5DA0; TMEM175 potassium channel from *Marivirga tractuosa* with macrobody [22] (Nb-MBP, pink-green), from left to right. (**d**) Inhibition of drug efflux in a tumor cell by a blocking nanobody as an example where nanobodies could serve as drugs or support a certain therapy

linked maltose-binding protein (MBP) to enlarge nanobodies and increase the space for crystallization [22]. The gain of mass by such a fusion protein can also help for obtaining phase information to solve a crystal structure by molecular replacement [22]. MBP is a proven fusion protein for crystallization [28] and therefore linkage to a nanobody may increase the chance for crystallization further, especially if unmodified nanobodies failed. These enlarged nanobodies that we termed "macrobodies" would also be of use in cryo-EM for efficient particle classification due to an increased size and addition of a new and clearly discernible structural feature in micrographs of macrobody-membrane protein complexes. An alternative and independently developed technique is "megabodies" that also serve to enlarge nanobodies for structural biology purposes [29, 30].

Numerous protocols for the generation and production of nanobodies have been published in recent years. Most of them rely on the periplasmic expression of nanobodies, to ensure correct disulfide bond formation. However, nanobodies were also successfully expressed in the intracellular environment of bacteria and eukaryotic cells [7–10, 31]. Here, we provide a reliable and rapid protocol for the expression and purification of nanobodies as fusions to MBP at their N-terminus in the periplasm of *E. coli* for structural biology approaches that generally require high amounts of protein. Our protocol is not including the generation and screening of libraries for which we recommend established protocols [2, 4]. The periplasmic expression provides the nonreducing environment to guarantee correctly folded binders and the N-terminal MBP fusion further facilitates high yield expression, also of "problematic" nanobodies. Originally, this technique was described by Salema and Fernández [32] and further developed by E.R. Geertsma (Institute of Biochemistry, University of Frankfurt, Germany) by integrating the FX-compatible vector pBXNPHM3 for high-throughput cloning [33] and expression of nanobodies as cleavable MBP fusion proteins [3, 8, 16, 17, 22]. In addition to a step-by-step protocol of this procedure we provide a single-step procedure for generating nanobodies with an additional non-cleavable C-terminally fused MBP moiety to convert them to "macrobodies" (*see* Fig. 2). We show examples of macrobodies directed against a non-canonical K^+ channel of the TMEM175 family [22]. Apart from their potential in crystallization and cryo-EM, this large format of nanobodies is also useful during screening procedures, e.g., using analytical size exclusion chromatography leading to a larger shift of the complex as exemplified with this channel protein.

2 Materials

2.1 Cloning and Transformation

1. PCR products (with flanking *SapI* sites) (*see* **Notes 1–3**).
2. Vector pBXNPHM3 (Addgene plasmid #110099) (*see* **Note 4**).
3. CutSmart Buffer or NEBuffer 4 (New England BioLabs).
4. *SapI* restriction enzyme (2 U/μL).
5. Adenosine triphosphate (ATP)-mix, 10 mM Na_2ATP, 10 mM $MgSO_4$, 50 mM KPi, pH 7, adjusted to pH 6.5–7 with NaOH.
6. T4 DNA ligase (1 U/μL).
7. Sterile water.
8. Transformation competent MC1061 (*see* **Note 5**).
9. Waterbath or thermoblock.

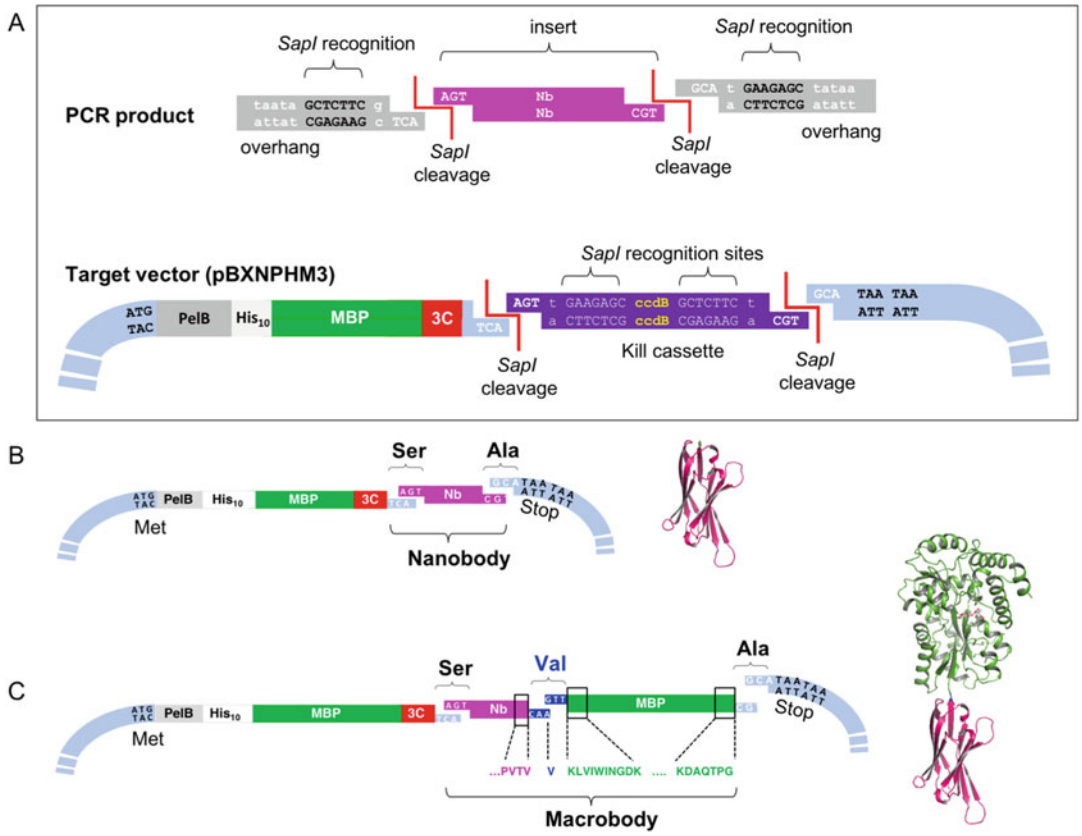

Fig. 2 FX-Cloning and expression constructs. (**a**) PCR product with overhangs and *SapI* cleavage sites indicated (top) and target vector with relevant features displayed (bottom). (**b**) FX-cloning compatible nanobody PCR product cloned into the pBXNPHM3 vector using the restriction enzyme *SapI*. Expression from this vector, His-tag purification and HRV 3C protease cleavage results in untagged nanobodies with minimal additional amino acids (Gly-Pro-Ser at the N-terminus and Ala at the C-terminus, *see* **Note 3**). (**c**) FX-cloning compatible target vector, nanobody PCR product and MBP PCR products after digestion with *SapI* enzyme. Expression from this vector, His-tag purification and HRV 3C protease cleavage will produce macrobodies with the same additional amino acids as in (**b**). PelB: Pectate lyase leader sequence, His_{10}: deca His-tag, MBP: maltose-binding protein, 3C: HRV 3C protease cleavage site, Nb: nanobody, ccdB: forms part of the kill cassette. Only the expression cassette of the vector and relevant features for the cloning strategy are shown. For a full map of the plasmid refer to the deposited map at addgene.org (*see* **Note 4**)

10. Luria Bertani broth (LB)-agar plates containing 100 mg/L ampicillin.
11. Glass beads/ Drigalski spatula.
12. Glycerol, sterile.

2.2 Expression

1. 100 mL Erlenmeyer flask.
2. 2 L Erlenmeyer flasks.
3. MC1061 *E. coli* transformed with the respective plasmid.
4. Ampicillin at 100 mg/mL aqueous solution, sterile filtered.

5. Autoclave.
6. Terrific broth, 23.6 g/L yeast extract, 11.8 g/L tryptone, 9.4 g/L K_2HPO_4, 2.2 g/L KH_2PO_4, 4 mL/L glycerol, deionized water, autoclaved.
7. Shaker.
8. L- (+)-Arabinose 20% aqueous solution, sterile filtered.
9. Centrifugation buckets, centrifuge, and rotor.
10. 50 mL centrifuge tubes.

2.3 Purification

1. Imidazole 3 M, pH 7.6.
2. Lysis buffer, 50 mM Tris pH 8.0, 0.5 mM ethylenediaminetetraacetic acid (EDTA), 150 mM NaCl, 10% glycerol, 25 mM imidazole (*see* **Note 6**).
3. Protease inhibitor cocktail or tablets.
4. $MgCl_2$ 1 M.
5. *DNase I* 10 mg/mL.
6. Cell disruptor (*see* **Note 7**).
7. Ultracentrifuge, rotor, and tubes.
8. Device for rotating tubes (tube rotator).
9. Ni-NTA affinity resin to bind in batch.
10. 50 mL centrifuge tubes.
11. Empty Chromatography column for gravity flow use.
12. Wash buffer, 10 mM Hepes-NaOH, pH 7.6, 150 mM NaCl, 10% glycerol, 40 mM imidazole.
13. Elution buffer, 10 mM Hepes-NaOH, pH 7.6, 150 mM NaCl, 10% glycerol, 300 mM imidazole.
14. Dialysis buffer, 10 mM Hepes-NaOH, pH 7.6, 150 mM NaCl, 10% glycerol.
15. HRV 3C protease (*see* **Note 8**).
16. Dialysis membranes, cutoff of 8 kDa or smaller.
17. Centrifugal filters for protein concentration (cutoff: nanobody 3 kDa, macrobody 30 kDa).

2.4 Size Exclusion Chromatography of Nanobodies and Macrobodies

1. Purified nanobody or macrobody.
2. Fluorescent size exclusion chromatography system and high-performance size exclusion column of suitable separation range and dimensions (e.g., 5 mm inner diameter, 150 mm length).
3. Gel filtration buffer NB, 10 mM Hepes-NaOH, pH 7.5, 150 mM NaCl.

2.4.1 Analytical Size Exclusion Chromatography of Nanobodies or Macrobodies

2.4.2 Preparative Size Exclusion Chromatography of Nanobodies or Macrobodies

1. Purified nanobody or macrobody.
2. Preparative size exclusion chromatography system and column of suitable separation range and dimensions (e.g., 10 mm inner diameter, 300 mm length).
3. A fraction collector to collect peak fractions for SDS-PAGE analysis.
4. Gel filtration buffer NB, 10 mM Hepes-NaOH pH 7.5, 150 mM NaCl.

2.5 Screening Complex Formation of Nanobodies with Membrane Protein Target

2.5.1 Analytical Size Exclusion to Verify or Identify Binders

1. Only for macrobodies: D-(+)-Maltose 500 mM, aqueous solution.
2. Target protein at desired concentration.
3. Detergent.
4. Purified nanobody or macrobody.
5. Fluorescent size exclusion chromatography system and column of suitable separation range and dimensions (e.g., 5 mm inner diameter, 150 mm length).
6. Gel filtration buffer CPLX, 10 mM Hepes-NaOH pH 7.6, 150 mM NaCl, detergent at 3× critical micelle concentration (cmc), *see* **Note 9**.
7. Fraction collector to collect eluted complex.

2.5.2 Preparative Size Exclusion to Isolate Complexes

1. Only for macrobodies: D-(+)-Maltose 500 mM, aqueous solution.
2. Target protein at desired concentration.
3. Detergent.
4. Purified nanobody or macrobody.
5. Size exclusion chromatography system and column for preparative scale (e.g., 10 mm inner diameter, 300 mm length).
6. Gel filtration buffer CPLX, 10 mM Hepes-NaOH, pH 7.6, 150 mM NaCl, detergent at 3× cmc.
7. Fraction collector to collect eluted complex.
8. Centrifugal filters for protein concentration (cutoff suitable to the size of the complex).

3 Methods

3.1 Cloning and Transformation of Standard Nanobody Format

1. Amplify the nanobody genes from template vectors by PCR with a proofreading polymerase using primers for FX-cloning (*see* **Note 1** and Fig. 2). Purify the amplicons from the gel using standard procedures.

2. Ligation reaction: Mix 100 ng of pBXNPHM3 vector with × ng of PCR-amplified insert (equimolar ratio), 1 μL CutSmart Buffer or NEB Buffer 4, 1 μL *SapI*, 1.25 μL ATP, 1.25 μL T4 DNA ligase and add water to reach a volume of 13 μL. Incubate at 30 °C for 1.5 h.
3. Thaw 100–200 μL chemically competent MC1061 bacteria on ice. Add 7 μL of the ligation reaction and mix carefully. Transform and recover in 0.8 mL LB. Shake at room temperature (RT) for 30 min.
4. Plate on LB-agar plates containing 100 μg/mL Ampicillin and incubate overnight at 37 °C.
5. Pick colonies for overnight culture using LB containing 100 mg/L at 37 °C in a shaker for subsequent plasmid isolation and sequence verification (*see* **Note 10**).
6. Prepare a glycerol stock of the overnight culture and freeze it using liquid nitrogen.

3.1.1 Cloning and Transformation of Macrobodies

1. Amplify the nanobody gene and the maltose-binding protein (MBP) gene (from the vector pBXNPHM3) by PCR with a proofreading polymerase (e.g., Phusion polymerase) using modified primers for FX-cloning of two subfragments (*see* **Note 2** and Fig. 2). Purify the amplicons from the gel using standard procedures.
2. Ligation reaction: Mix 100 ng of pBXNPHM3 vector with × ng of PCR-amplified inserts. Here, for two fragments to be inserted, equimolar amounts of the nanobody-gene and the MBP gene and the vector will be mixed. The overhangs guarantee correct insertion. Then add 1 μL CutSmart Buffer or NEB Buffer 4, 1 μL *SapI*, 1.25 μL ATP, 1.25 μL T4 DNA ligase and add water to reach a volume of 13 μL. Incubate at 30 °C for 1.5 h.
3. Proceed as in Subheading 3.1 with **step 3**.

3.2 Expression

The specifications in the following protocol refer to 1 L expression culture. The protocol applies for the production of nanobodies as well as macrobodies.

1. Inoculate a small Erlenmeyer flask containing 15 mL of terrific broth (TB) and 100 mg/L ampicillin with the respective glycerol stock, shake overnight at 37 °C.
2. Next day: Inoculate 1 L TB medium (e.g., in two 2 L Erlenmeyer flask) containing 100 mg/L ampicillin with 12–15 mL of the overnight culture. Shake at 37 °C with good aeration until OD_{600} of 0.7 is reached (approximately after 2–3 h).
3. Induce protein expression with a final concentration of 0.02% L- (+)-Arabinose (*see* **Note 11**).

4. Shake at a temperature of 37 °C for another 3–3.5 h. Ensure good aeration.
5. Measure OD_{600}. Harvest cells by centrifugation. Resuspend cells in lysis buffer using a minimal volume and transfer to a 50 mL centrifugal tube. Freeze the resuspended cells using liquid nitrogen and store at −80 or −20 °C until usage.

3.3 Purification

The following section describes the purification of nanobodies involving in-batch affinity purification, cleavage and removal of the His_{10}-tagged proteins followed by separation of the cleaved nanobodies from remaining contaminants by size exclusion. The same protocol applies for the purification of macrobodies. SDS-PAGE analysis of relevant steps during purification is shown in Fig. 3.

1. Thaw the frozen cell suspension and dilute to an OD_{600} of 150 with lysis buffer. Add protease inhibitors (*see* **Note 12**). All steps are performed on ice.
2. Add $MgCl_2$ and *DNase I* to a final concentration of 5 mM and 10 μg/mL, respectively (*see* **Note 13**).
3. Use a mixer or homogenizer to provide a clump-free suspension and lyse cells with a suitable cell disruptor (*see* **Note 14**).
4. Separate cell debris by centrifugation at 100,000 × *g* for 30 min. Continue with the supernatant.
5. In the meantime, transfer Ni-NTA affinity resin (0.5 mL bed volume per 1 L nanobody expression culture) into a 50 mL centrifugation tube. Wash resin with 10 column volumes (CV) of ultrapure water, centrifuge resin at 1500 g for 2 min, discard supernatant, wash with 10 CV of lysis buffer, centrifuge resin at 1500 g for 2 min.
6. Add the supernatant from Subheading 3.3, **step 4**, to the Ni-NTA affinity resin and incubate on a rotary device for at least 1 h at 4 °C.
7. Transfer the resin with the supernatant to an empty gravity-flow chromatography column of suitable size. Let the supernatant flow through. Wash resin with 20 CV of Wash buffer.
8. Elute protein in a minimal volume using Elution buffer. Measure protein concentration and take a sample for SDS-Page analysis.
9. Add HRV 3C protease to the eluted protein in a molar ratio of 1:20 and transfer the mixture to a dialysis membrane for overnight dialysis in Dialysis buffer. Add imidazole to a final concentration of 25 mM to the Dialysis buffer. *See* **Note 15**.
10. Next day: To remove the N-terminal MBP moiety bearing the deca-His-tag the dialyzed solution is subjected to reverse

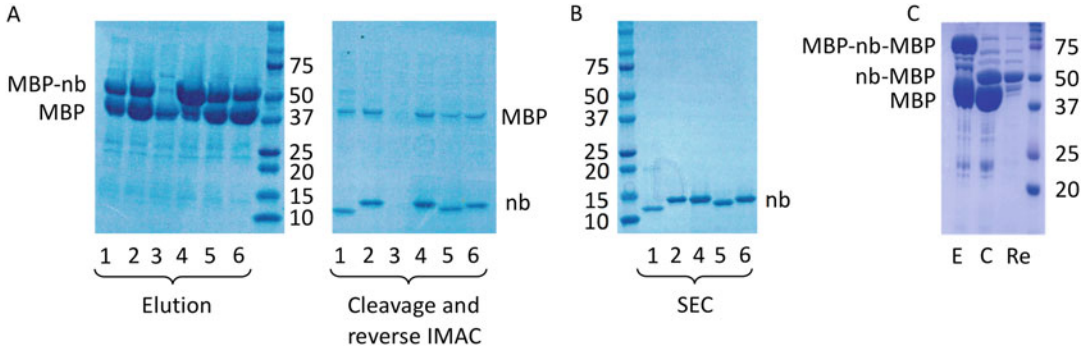

Fig. 3 Purity of nanobodies and macrobodies as analyzed by SDS-PAGE. (**a**) Eluate from NiNTA affinity resin for nanobodies 1–6 (lane 1–6, left) and flow-through containing cleaved nanobodies after re-IMAC (lane 1–6, right). His-MBP and His-tagged 3C protease are largely retained on the resin after the re-IMAC step. (**b**) Nanobodies were further purified by size exclusion chromatography (SEC) using a Superdex 75 10/300 column to separate nanobodies from MBP contaminants. (**c**) Macrobody purification. E: Eluate, C: Cleaved proteins after digest with HRV 3C protease, Re: Flow-through after reverse IMAC. Most of the cleaved tags (the N-terminal His-MBP and the His-tagged 3C protease) are retained on the resin. The N-terminally MBP-tagged macrobody (MBP-nb-MBP), the macrobody (nb-MBP), and cleaved His-MBP have molecular weights of ~ 93 kDa, ~53 kDa, and ~45 kDa, respectively. After elution from IMAC, a substantial amount of the purified protein can be MBP lacking nanobodies or macrobodies as seen in (**a**, lane 2, 5 or 6) or (**c**, lane E). This is also depending on the nanobody (see lane 4 in (**a**) where free MBP is not prominent), *see* **Note 5**. Positions of molecular weight markers are indicated on the right in kDa of molecular weight

Immobilized Metal Affinity Chromatography (IMAC), meaning that the flow through contains the protein of interest. This will also remove the His-tagged 3C protease (*see* **Note 8**). For reverse IMAC, prepare a fresh batch of Ni-NTA affinity resin (0.5 mL bed volume per 1 L nanobody expression culture) in the same way as in Subheading 3.3, **step 5**, except that beads are washed twice with 10 CV of Wash buffer after rinsing with water.

11. Take a sample for subsequent analysis by SDS-PAGE from the dialyzed and cleaved protein. Then mix the protein with the equilibrated resin and incubate for 20–30 min on a rotary device (*see* **Note 16**).
12. Transfer the resin with the supernatant to an empty gravity-flow chromatography column of appropriate size. Collect the flow through and add an additional 1–1.5 CV of Wash buffer to the resin to elute all unbound protein. Measure concentration and take a sample for SDS-Page analysis.
13. If necessary, concentrate nanobodies using centrifugal filters to a suitable concentration.
14. Run analytical size exclusion chromatography to analyze monodispersity of the nanobody or preparative gel filtration to recover the fractions containing the monodisperse protein of interest (*see* also Subheading 3.4).

15. Nanobodies can be stored at −80 °C after flash-freezing in liquid N_2. For freezing, the buffer should be supplemented with a final concentration of 20% glycerol to reduce freezing damage.

3.4 Size Exclusion Chromatography of Nanobodies and Macrobodies

Before using nanobodies the proteins have to be analyzed by size exclusion chromatography for monodispersity. Initial screens can be done in analytical scale with very small amounts of protein. If aggregates are observed, a preparative scale size exclusion chromatography (SEC) is mandatory for good performance in subsequent experiments.

3.4.1 Analytical Size Exclusion Chromatography of Nanobodies or Macrobodies

1. Inject 2–20 μg of nanobody or macrobody (in a max. volume of 50 μL) to a suitable gel filtration column (for a 5 mm inner diameter, 150 mm length column) equilibrated with Gel filtration buffer NB. Use tryptophan fluorescence (excitation 280 nm, emission 315 nm) and UV absorption at 280 nm for detection (*see* **Note 17**).
2. Analyze chromatograms for monodispersity. Some nanobodies may also form aggregates indicated by void volume peaks.

3.4.2 Preparative Size Exclusion Chromatography of Nanobodies or Macrobodies

1. Prepare nanobody at a suitable concentration in a volume of 500 μL (for a 10 mm inner diameter, 300 mm length column).
2. Inject to SEC and collect elution fractions (*see* Fig. 4a for representative size exclusion profiles of three different nanobodies).
3. Take samples of the peak fractions for analysis by SDS-PAGE.
4. Concentrate peak fractions to the required concentration and proceed to the next steps (e.g., complex formation with target membrane protein). Alternatively, the protein can be frozen using liquid nitrogen by supplementing with a final concentration of 20% glycerol.

3.5 Screening Complex Formation of Nanobodies with Membrane Protein Target

In order to obtain a stoichiometric complex of nanobodies with the target protein a size exclusion chromatography step is required to isolate this complex. First, analytical scale analysis will be performed to identify binders and then a preparative scale SEC is required to isolate a homogeneous complex for structural studies.

3.5.1 Analytical Size Exclusion to Verify or Identify Binders

1. Mix 2–20 μg of nanobody or macrobody (depending on detection limits and collection of fractions, *see* **Note 17**) in a 1.5-fold excess (mol/mol) with target protein (*see* **Note 18**). Incubate for 15–30 min on ice.
2. Inject ~3–30 μg of total protein (in a max. volume of 50 μL) to a suitable gel filtration column (for a 5 mm inner diameter, 150 mm length column) equilibrated with gel filtration buffer

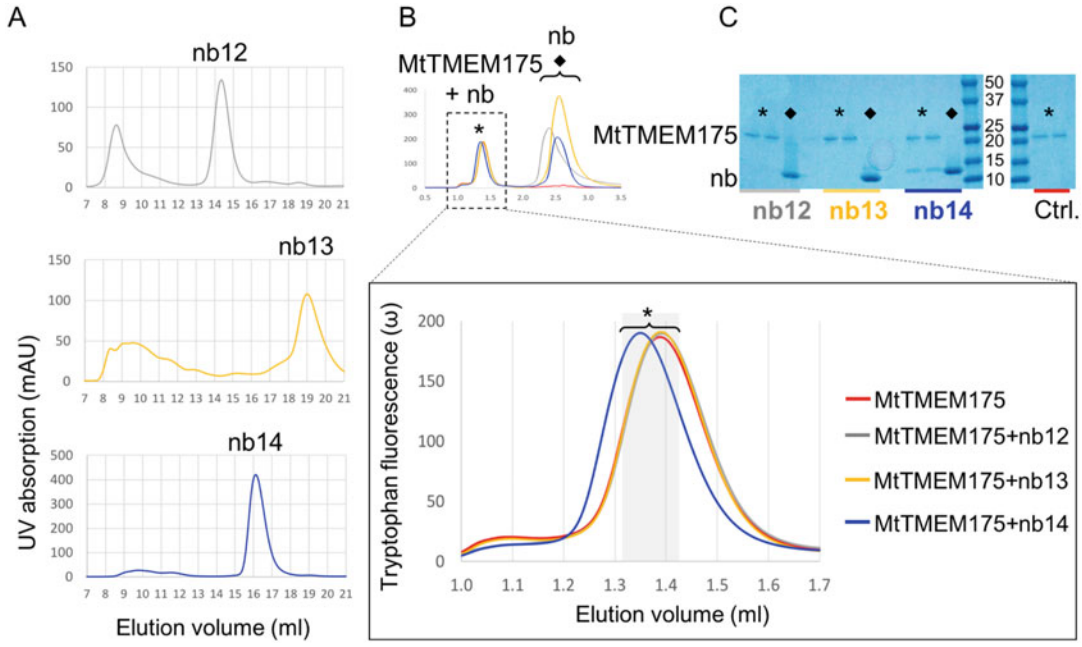

Fig. 4 Complex formation of MtTMEM175 with different nanobodies. (**a**) Size exclusion chromatography of nanobodies nb12-nb14 after affinity purification using a Superdex 75 10/300 column. (**b**) Analytical size exclusion chromatography in small scale on an HPLC system for evaluation of nanobody binders toward MtTMEM175. Purified MtTMEM175 was incubated with candidate nanobodies nb12, nb13 or nb14 and separated using a Superdex 200 5/150 column. Chromatograms were compared to un-complexed MtTMEM175 (red). MtTMEM175 has a molecular weight of 28 kDa and forms tetramers. Peaks were normalized to each other. (**c**) SDS-PAGE analysis of peak fractions. Asterisks and diamonds mark samples from the respective peak fractions in (**b**). The molecular weight marker is shown. Note that nb12 and nb13 do not form a complex with MtTMEM175 that is stable enough for size exclusion chromatography. Nb14 is co-eluting at higher molecular weight in complex with MtTMEM175 in a 1:1 stoichiometry, resulting in a shift relative to un-complexed MtTMEM175 (**b**) and is clearly detectable in SDS-PAGE (**c**)

CPLX. Use tryptophan fluorescence (excitation 280 nm, emission 335 nm) and absorption at 280 nm to detect protein. Compare chromatograms of un-complexed target protein with samples that contain nanobodies in complex with target protein (*see* **Note 19**). Figure 4 illustrates the screening of nanobodies and subsequent identification of a nanobody (nb14) binding to the MtTMEM175 tetramer in a 1:1 stoichiometry as detected by analytical size exclusion chromatography and SDS-PAGE.

3.5.2 Preparative Size Exclusion to Isolate Complexes

1. In a volume of 500 µL (for a 10 mm inner diameter, 300 mm length column) mix nanobody or macrobody in a 1.5 molar excess with target protein. Incubate for 30 min on ice (*see* **Note 18**).

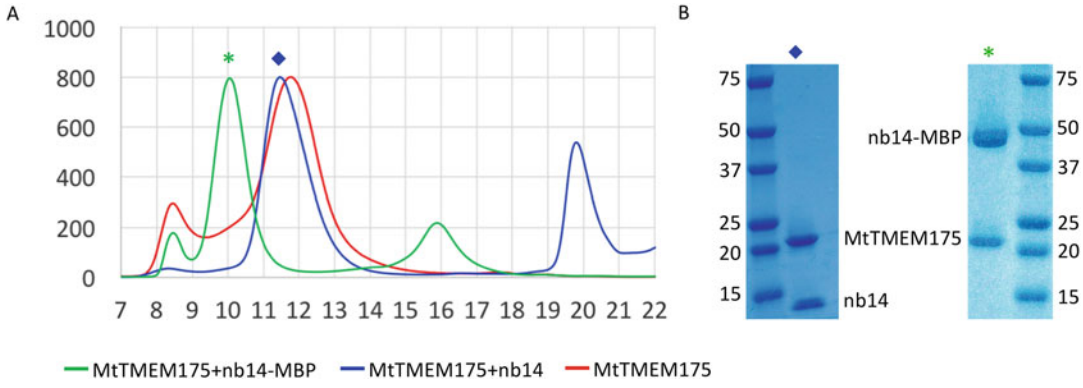

Fig. 5 Complex formation of the nanobody and macrobody with target protein. (**a**) Size exclusion chromatography of MtTMEM175 in complex with nb14 (blue) or nb14-MBP (macrobody, green) compared to uncomplexed MtTMEM175 (red). Peaks of MtTMEM175 and complexes are normalized. Note the much bigger shift in elution volume for the macrobody-MtTMEM175 complex compared to the nanobody-MtTMEM175 complex. MtTMEM175 has a molecular weight of 28 kDa and assembles to tetramers. Nanobody 14 and nb14-MBP bind MtTMEM175 with a 1:1 stoichiometry. (**b**) SDS-PAGE analysis following separation of MtTMEM175 in complex with nb14 and nb14-MBP (macrobody). An asterisk and a diamond symbol indicate samples from the respective peak fractions in (**a**). The positions of molecular weight markers are indicated in kDa of molecular weight

2. Inject to SEC equilibrated with gel filtration buffer CPLX and collect elution fractions of the complex (*see* **Note 19**).
3. Take samples of the peak fractions for analysis by SDS-PAGE. Figure 5 shows a representative analysis by size exclusion chromatography and corresponding SDS-PAGE of uncomplexed MtTMEM175 and MtTMEM175 in complex with nanobodies (nb14) or macrobodies (nb14-MBP).
4. Concentrate peak fractions to the required concentration and proceed to crystallization or electron microscopy.

4 Notes

1. The nanobody gene is modified by PCR such that it is compatible with FX-cloning [33] and FX vectors (see also Fig. 2). Primers for the standard nanobody format are generated as indicated here:
   Forward primers nanobody layout:
   5′-tatata**GCTCTTC**x*AGT***nanobodygene***-*3′
   Reverse primers nanobody layout:
   5′-tatata**GCTCTTC**x*TGC***nanobodygene**-3′.

   where "tatata" is a random overhang to facilitate *SapI* digest and "nanobodygene" corresponds to the 5′ and 3′ ends of the specific nanobody sequence. The *SapI* recognition

sequence is bold and underlined. X can be any nucleotide. The sticky ends (italic and underlined capitals) are coding for Ser (AGT) and Ala (TGC, reverse complement) from 5′ to 3′.

2. To clone macrobodies in one step into the vector pBXNPHM3 amplify the inserts (nanobodies from template vectors and MBP from the empty pBXNPHM3 vector) using a modified reverse primer for the nanobody gene and two additional primers for the MBP gene:
   Modified nanobody reverse primer:

   5′-tatata**GCTCTTC**a*AAC***nanobodygene**-3′

   Nanobodies end with the amino acid sequence VTV. The primer will add an additional valine (AAC, reverse complement) for linkage to MBP.

   MBP primers for fusion with nanobodies (will truncate MBP at the N-terminus by 5 amino acids, thus MBP will start with KLVIWIN and end with KDAQTPG, the sticky ends (italic and underlined capitals) are coding for Val (GTT) and Ala (TGC, reverse complement) from 5′ to 3′):

   Forward primer MBP:

   5′-tatata**GCTCTTC**x*GTT*aaactggtaatctggattaacgg-3′

   Reverse primer MBP:

   5′-tatata**GCTCTTC**x*TGC*acccggagtctgcgcgtctttc-3′.

3. FX-cloning generates an additional serine at the N-terminus of the protein of interest and an additional alanine at the C-terminus (*see* **Note 1**).

4. Most FX cloning compatible vectors and respective maps are available from Addgene (https://www.addgene.org). The Addgene entry for the plasmid pBXNPHM3 is #110099. All FX-cloning vectors, also pBXNPHM3 require a ccdB-insensitive strain for propagation, such as DB3.1 (gyrA462 endA1 Δ(sr1-recA) mcrB mrr hsdS20 glnV44 (=supE44) ara14 galK2 lacY1 proA2 rpsL20 xyl5 leuB6 mtl1). There are other commercially available strains that are ccdB insensitive.

5. Any strain that is sensitive to the gene product of ccdB can be used for cloning, e.g., MC1061 (F- Δ(araA-leu)7697 [araD139]B/r Δ(codB-lacI)3 galK16 galE15(GalS) λ- e14- mcrA0 relA1 rpsL150 spoT1 mcrB1 hsdR2). In principle, transformation competent MC1061 can be produced by several established protocols. For the generation of chemically competent MC1061 we have made very good experience by following the protocol from Inoue and colleagues [34]. A high competence is achieved when cells are grown below 16 °C.

   As an alternative to MC1061, *E. coli* HM140, a strain deficient in several periplasmic proteases [32], or similar can

be used for nanobody expression to prevent proteolytic activity in the bacterial host.

6. An imidazole concentration of 20–25 mM present in the buffer during binding of the His-tagged protein to Ni-NTA affinity resin decreases the binding of unspecific (contaminating) protein to the resin.
7. Any cell disruptor is suitable. If only small volumes have to be processed (e.g., 10–30 mL), sonication is a good method to crack cells (here, addition of lysozyme will aid in breaking cells); however, in case of large volumes (>200 mL) a microfluidizer® or a similar device is recommended. Alternatively, nanobodies can also be selectively isolated from periplasmic extracts [2]. In our hands, breaking whole cells is faster and the deca-His tag ensures high purity, also with whole cell extracts.
8. HRV 3C protease can be generated recombinantly (https://www.helmholtz-muenchen.de/pepf/protocols/purification/index.html). The expression of this construct (HRV 3C protease cloned into a pET-24d (+) vector) will produce His_6-tagged HRV 3C protease. If a different (e.g., GST-tagged 3C Protease) version of this protease is used, the procedure for the removal has to be modified accordingly.
9. Any buffer that is compatible with the biochemistry of the target protein can be taken.
10. For sequencing inserts cloned into the pBXNPHM3 vector use the pBAD reverse primer (see also https://www.addgene.org) with the sequence 5′-GATTTAATCTGTATCAGG-3′ in case of the standard format for nanobodies. For macrobodies, a primer that anneals at the coding sequence of the HRV 3C protease recognition site can be used as forward sequencing primer (5′-GTAGCCTGGAAGTTCTGTTCC-3′). The reverse cloning primers for nanobodies will be used for sequencing the 5′-end of the nanobody insert.
11. To induce protein production using pBX vectors, a concentration of 0.02% arabinose is often a good starting point; however, it might be advisable to determine the optimal arabinose concentration to enable maximal protein yields. See, for example, Geertsma and colleagues [35] for a procedure to evaluate expression using the tunable arabinose promoter.
12. Protease inhibitors might be added at this stage to prevent protein degradation.
13. Mg^{2+} is needed for the activity of *DNase I* and is further added to saturate EDTA with divalent metal ions in the lysis buffer to prevent chelation of Ni^{2+} from the Ni-NTA resin.

14. A clump-free suspension is needed to prevent clogging of the cell disruptor. Can alternatively be achieved by pipetting up and down using a serological pipette and an electrical pipette aid.
15. Take the volume in the dialysis membrane, which contains a concentration of 300 mM imidazole, into account when calculating the amount of imidazole to add. Imidazole is required to prevent binding of untagged proteins (here the nanobody) to the resin. At this concentration His-tagged proteins bind still very well to the resin.
16. For the reverse IMAC it is not recommended to incubate the resin with the protein for longer than 30 min to prevent unspecific binding of the untagged nanobodies to the resin.
17. Nanobodies are very small proteins that might lack a tryptophan which will be problematic for measuring protein concentration and during chromatography applications; however, this is a very rare event. If analytical FPLC is equipped with a fraction collector, complex formation can alternatively be confirmed by SDS-PAGE analysis of the fractions. This requires sufficient amounts of protein to be injected, i.e., much more than for a purely analytical chromatography.
18. In case of working with membrane proteins it is important to mix the respective components in the sequence below, to prevent damage to the membrane protein because of dilution of the detergent:
    (a) Nanobody or macrobody.
    (b) Detergent (to reach 3× cmc final concentration).
    (c) Salt and buffer to maintain the conditions required by the target protein.
    (d) Membrane protein.
    (e) When working with macrobodies for structural biology purposes, we added 3 mM maltose to the macrobody before incubation with the target protein. Maltose was also present in the Gel filtration buffer CPLX (2 mM). This will keep MBP in the maltose-bound conformation.
19. Binding results in shift to higher molecular weight (MW), but is very dependent on the binding stoichiometries and change in stokes radius. Note that the shift of the target protein peak can be minute after nanobody binding, dependent on the MW of the target protein and type of size exclusion column, making analysis by SDS-PAGE necessary.

References

1. Muyldermans S (2013) Nanobodies: Natural Single-Domain Antibodies. Annu Rev Biochem 82(1):775–797. https://doi.org/10.1146/annurev-biochem-063011-092449
2. Pardon E, Laeremans T, Triest S, Rasmussen SGF, Wohlkönig A, Ruf A, Muyldermans S, Hol WGJ, Kobilka BK, Steyaert J (2014) A general protocol for the generation of Nanobodies for structural biology. Nat Protoc 9 (3):674–693. https://doi.org/10.1038/nprot.2014.039
3. Zimmermann I, Egloff P, Hutter CAJ, Arnold FM, Stohler P, Bocquet N, Hug MN, Huber S, Siegrist M, Hetemann L, Gera J, Gmür S, Spies P, Gygax D, Geertsma ER, Dawson RJP, Seeger MA (2018) Synthetic single domain antibodies for the conformational trapping of membrane proteins. eLife 7:e34317. https://doi.org/10.7554/eLife.34317
4. McMahon C, Baier AS, Pascolutti R, Wegrecki M, Zheng S, Ong JX, Erlandson SC, Hilger D, Rasmussen SGF, Ring AM, Manglik A, Kruse AC (2018) Yeast surface display platform for rapid discovery of conformationally selective nanobodies. Nat Struct Mol Biol 25(3):289–296. https://doi.org/10.1038/s41594-018-0028-6
5. Wingler LM, McMahon C, Staus DP, Lefkowitz RJ, Kruse AC (2019) Distinctive activation mechanism for angiotensin receptor revealed by a synthetic nanobody. Cell 176 (3):479–490.e412. https://doi.org/10.1016/j.cell.2018.12.006
6. Rasmussen SGF, Choi H-J, Fung JJ, Pardon E, Casarosa P, Chae PS, Devree BT, Rosenbaum DM, Thian FS, Kobilka TS, Schnapp A, Konetzki I, Sunahara RK, Gellman SH, Pautsch A, Steyaert J, Weis WI, Kobilka BK (2011) Structure of a nanobody-stabilized active state of the β(2) adrenoceptor. Nature 469(7329):175–180. https://doi.org/10.1038/nature09648
7. Kirchhofer A, Helma J, Schmidthals K, Frauer C, Cui S, Karcher A, Pellis M, Muyldermans S, Casas-Delucchi CS, Cardoso MC, Leonhardt H, Hopfner K-P, Rothbauer U (2009) Modulation of protein properties in living cells using nanobodies. Nat Struct Mol Biol 17:133. https://doi.org/10.1038/nsmb.1727. https://www.nature.com/articles/nsmb.1727#supplementary-information
8. Schenck S, Kunz L, Sahlender D, Pardon E, Geertsma ER, Savtchouk I, Suzuki T, Neldner Y, Štefanić S, Steyaert J, Volterra A, Dutzler R (2017) Generation and characterization of anti-VGLUT nanobodies acting as inhibitors of transport. Biochemistry 56 (30):3962–3971. https://doi.org/10.1021/acs.biochem.7b00436
9. Irannejad R, Tomshine JC, Tomshine JR, Chevalier M, Mahoney JP, Steyaert J, Rasmussen SGF, Sunahara RK, El-Samad H, Huang B, von Zastrow M (2013) Conformational biosensors reveal GPCR signalling from endosomes. Nature 495(7442):534–538. https://doi.org/10.1038/nature12000
10. Traenkle B, Rothbauer U (2017) Under the Microscope: Single-Domain Antibodies for Live-Cell Imaging and Super-Resolution Microscopy. Front Immunol 8:1030–1030. https://doi.org/10.3389/fimmu.2017.01030
11. Kubala MH, Kovtun O, Alexandrov K, Collins BM (2010) Structural and thermodynamic analysis of the GFP:GFP-nanobody complex. Protein Sci 19(12):2389–2401. https://doi.org/10.1002/pro.519
12. Schellenberg MJ, Petrovich RM, Malone CC, Williams RS (2018) Selectable high-yield recombinant protein production in human cells using a GFP/YFP nanobody affinity support. Protein Sci 27(6):1083–1092. https://doi.org/10.1002/pro.3409
13. Stortelers C, Pinto-Espinoza C, Van Hoorick D, Koch-Nolte F (2018) Modulating ion channel function with antibodies and nanobodies. Curr Opin Immunol 52:18–26. https://doi.org/10.1016/j.coi.2018.02.003
14. Arezumand R, Alibakhshi A, Ranjbari J, Ramazani A, Muyldermans S (2017) Nanobodies As Novel Agents for Targeting Angiogenesis in Solid Cancers. Front Immunol 8:1746–1746. https://doi.org/10.3389/fimmu.2017.01746
15. Saerens D, Ghassabeh GH, Muyldermans S (2008) Single-domain antibodies as building blocks for novel therapeutics. Curr Opin Pharmacol 8(5):600–608. https://doi.org/10.1016/j.coph.2008.07.006
16. Ehrnstorfer IA, Geertsma ER, Pardon E, Steyaert J, Dutzler R (2014) Crystal structure of a SLC11 (NRAMP) transporter reveals the basis for transition-metal ion transport. Nat Struct Mol Biol 21:990–996. https://doi.org/10.1038/nsmb.2904
17. Geertsma ER, Chang Y-N, Shaik FR, Neldner Y, Pardon E, Steyaert J, Dutzler R (2015) Structure of a prokaryotic fumarate transporter reveals the architecture of the SLC26 family. Nat Struct Mol Biol 22:803–808. https://doi.org/10.1038/nsmb.3091
18. Kumar H, Finer-Moore JS, Jiang X, Smirnova I, Kasho V, Pardon E, Steyaert J,

Kaback HR, Stroud RM (2018) Crystal Structure of a ligand-bound LacY-Nanobody Complex. Proc Natl Acad Sci U S A 115 (35):8769–8774. https://doi.org/10.1073/pnas.1801774115

19. Ural-Blimke Y, Flayhan A, Strauss J, Rantos V, Bartels K, Nielsen R, Pardon E, Steyaert J, Kosinski J, Quistgaard EM, Löw C (2019) Structure of Prototypic Peptide Transporter DtpA from E. coli in Complex with Valganciclovir Provides Insights into Drug Binding of Human PepT1. J Am Chem Soc 141 (6):2404–2412. https://doi.org/10.1021/jacs.8b11343
20. Che T, Majumdar S, Zaidi SA, Ondachi P, McCorvy JD, Wang S, Mosier PD, Uprety R, Vardy E, Krumm BE, Han GW, Lee M-Y, Pardon E, Steyaert J, Huang X-P, Strachan RT, Tribo AR, Pasternak GW, Carroll FI, Stevens RC, Cherezov V, Katritch V, Wacker D, Roth BL (2018) Structure of the nanobody-stabilized active state of the kappa opioid receptor. Cell 172(1–2):55–67.e15. https://doi.org/10.1016/j.cell.2017.12.011
21. Koehl A, Hu H, Feng D, Sun B, Zhang Y, Robertson MJ, Chu M, Kobilka TS, Laeremans T, Steyaert J, Tarrasch J, Dutta S, Fonseca R, Weis WI, Mathiesen JM, Skiniotis G, Kobilka BK (2019) Structural insights into the activation of metabotropic glutamate receptors. Nature 566 (7742):79–84. https://doi.org/10.1038/s41586-019-0881-4
22. Brunner JD, Jakob RP, Schulze T, Neldner Y, Moroni A, Thiel G, Maier T, Schenck S (2018) Structural basis for ion selectivity in TMEM175 K^+ channels. https://doi.org/10.1101/480863
23. Fan C, Fan M, Orlando BJ, Fastman NM, Zhang J, Xu Y, Chambers MG, Xu X, Perry K, Liao M, Feng L (2018) X-ray and cryo-EM structures of the mitochondrial calcium uniporter. Nature 559(7715):575–579. https://doi.org/10.1038/s41586-018-0330-9
24. Hassaine G, Deluz C, Grasso L, Wyss R, Tol MB, Hovius R, Graff A, Stahlberg H, Tomizaki T, Desmyter A, Moreau C, Li X-D, Poitevin F, Vogel H, Nury H (2014) X-ray structure of the mouse serotonin 5-HT_3 receptor. Nature 512:276. https://doi.org/10.1038/nature13552. https://www.nature.com/articles/nature13552#supplementary-information
25. Ruprecht JJ, King MS, Zögg T, Aleksandrova AA, Pardon E, Crichton PG, Steyaert J, Kunji ERS (2019) The molecular mechanism of transport by the mitochondrial ADP/ATP carrier. Cell 176(3):435–447.e415. https://doi.org/10.1016/j.cell.2018.11.025
26. Bräuer P, Parker JL, Gerondopoulos A, Zimmermann I, Seeger MA, Barr FA, Newstead S (2019) Structural basis for pH-dependent retrieval of ER proteins from the Golgi by the KDEL receptor. Science 363 (6431):1103–1107. https://doi.org/10.1126/science.aaw2859
27. Perez C, Köhler M, Janser D, Pardon E, Steyaert J, Zenobi R, Locher KP (2017) Structural basis of inhibition of lipid-linked oligosaccharide flippase PglK by a conformational nanobody. Sci Rep 7:46641–46641. https://doi.org/10.1038/srep46641
28. Waugh DS (2016) Crystal structures of MBP fusion proteins. Protein Sci 25(3):559–571. https://doi.org/10.1002/pro.2863
29. Laverty D, Desai R, Uchański T, Masiulis S, Stec WJ, Malinauskas T, Zivanov J, Pardon E, Steyaert J, Miller KW, Aricescu AR (2019) Cryo-EM structure of the human α1β3γ2 $GABA_A$ receptor in a lipid bilayer. Nature 565 (7740):516–520. https://doi.org/10.1038/s41586-018-0833-4
30. Masiulis S, Desai R, Uchański T, Serna Martin I, Laverty D, Karia D, Malinauskas T, Zivanov J, Pardon E, Kotecha A, Steyaert J, Miller KW, Aricescu AR (2019) $GABA_A$ receptor signalling mechanisms revealed by structural pharmacology. Nature 565 (7740):454–459. https://doi.org/10.1038/s41586-018-0832-5
31. Pleiner T, Bates M, Trakhanov S, Lee C-T, Schliep JE, Chug H, Böhning M, Stark H, Urlaub H, Görlich D (2015) Nanobodies: site-specific labeling for super-resolution imaging, rapid epitope-mapping and native protein complex isolation. elife 4:e11349–e11349. https://doi.org/10.7554/eLife.11349
32. Salema V, Fernández LÁ (2013) High yield purification of nanobodies from the periplasm of E. coli as fusions with the maltose binding protein. Protein Expr Purif 91(1):42–48. https://doi.org/10.1016/j.pep.2013.07.001
33. Geertsma ER, Dutzler R (2011) A versatile and efficient high-throughput cloning tool for structural biology. Biochemistry 50 (15):3272–3278. https://doi.org/10.1021/bi200178z
34. Inoue H, Nojima H, Okayama H (1990) High efficiency transformation of Escherichia coli with plasmids. Gene 96(1):23–28. https://doi.org/10.1016/0378-1119(90)90336-P
35. Geertsma ER, Groeneveld M, Slotboom D-J, Poolman B (2008) Quality control of overexpressed membrane proteins. Proc Natl Acad Sci U S A 105(15):5722–5727. https://doi.org/10.1073/pnas.0802190105

Chapter 13

Identifying Conformation-Selective Heavy-Chain-Only Antibodies Against Membrane Proteins by a Thermal-Shift Scintillation Proximity Assay

Peter Stohler and Roger J. P. Dawson

Abstract

Over the last decades, the use of heavy-chain-only antibodies has received growing attention in academia and industry as research and diagnostic tools as well as therapeutics. Their generation has improved with the help of innovative new methods such as the sybody technology; however, identifying conformation-selective compounds against membrane proteins remains a major challenge. In this chapter, we apply a thermal shift scintillation proximity assay (SPA-TS) to identify sybodies from an in vitro display campaign with the ability to selectively stabilize the inhibitor-bound conformation of the human solute carrier (SLC) family transporter SC6A9 (GlyT1). Using detergent-purified GlyT1 protein and a tritium-labeled glycine uptake inhibitor small molecule, we find sybody candidates that increase the apparent melting temperature in SPA-TS by several degrees. The thermal shift stabilizes the GlyT1-inhibitor complex and qualifies the sybodies for structural studies and inhibitor-selective small molecule screening assays. The SPA-TS assay in its current form is adaptable to any antibody discovery campaign for membrane proteins and permits the generation of highly valuable tools in most stages of drug discovery and development.

Key words Heavy-chain-only, VHH, Sybody, Nanobody, Glycine transporter 1, SLC6A9, Human GlyT1, Crystallography, VHH profiling, Cryo-electron microscopy, Nanobody-enabled reverse pharmacology

1 Introduction

The scintillation proximity assay (SPA) format has been widely used in drug discovery and development to screen and profile small molecule compounds [1, 2]. Recently, SPA has been adapted to improve the quality and stability of detergent-solubilized membrane proteins [2]. The assay principle has been described with SPA beads generating a signal only in close proximity to a radiolabeled ligand. The proximity is created using a detergent-solubilized and His-tagged membrane protein such as GlyT1 upon binding to an SPA copper bead. Specific binding of the tritium-labeled glycine

Camilo Perez and Timm Maier (eds.), *Expression, Purification, and Structural Biology of Membrane Proteins*, Methods in Molecular Biology, vol. 2127, https://doi.org/10.1007/978-1-0716-0373-4_13,

uptake inhibitor analog then triggers bead scintillation. Free, excess ligand has a limited contribution and generates a negligible background signal. Applications for the SPA-TS permit the determination of optimal buffer conditions for membrane protein solubilization and purification. The assay can assess the optimal detergent type in a detergent screen, other buffer conditions including salt, pH, or additives, as well as the stabilization of membrane proteins by engineering (truncation, insertion, or mutagenesis). Furthermore, the assay permits the identification of optimal "binding moieties" including stabilizing small molecule ligands or conformation-specific lipids to keep the membrane protein in the preferred functional state for follow-up biophysical characterization or screening studies. Here, we detail the use of the scintillation proximity assay in thermal-shift mode (SPA-TS) for the selection of heavy-chain-only antibodies (sybodies) for the conformational trapping of the glycine 1 SLC transporter in the inhibited and disease-relevant state [3].

2 Materials

2.1 SPA Assay

1. 20 mg/mL YSi-copper SPA beads in water (PerkinElmer).
2. Citric acid monohydrate 1 M pH 6.4 (NaOH).
3. 4% Lauryl Maltose Neopentyl Glycol (LMNG) in H_2O.
4. 96-Well plate: Optiplate96 (PerkinElmer).
5. TopSeal (PerkinElmer).
6. His-tagged purified target protein (GlyT1, SLC6A9) diluted in citrate buffer.
7. 3H-labeled substrate Org24598 14 μM in ETOH (homemade).
8. Cold compound Org24598 10 mM in DMSO (homemade).
9. ≥99.5% Dimethyl sulfoxide.
10. Plate shaker: Bio-Shake iQ.
11. TopCount NXT Microplate Scintillation counter (PerkinElmer).
12. Buffer-1, 20 mM citrate pH 6.4, 150 mM NaCl, and 0.04% (w/v) LMNG.

2.2 Temperature Screen

1. 96-Well plate: twin tec PCR plate (Eppendorf).
2. Techne Prime Elite thermocycler.
3. Buffer-2, 20 mM Citrate pH 6.4, 150 mM NaCl, 0.04% LMNG.

3 Methods

3.1 SPA Assay

For the successful application of an SPA assay, an assay development phase is required that investigates the interaction between beads, protein, and tritiated ligand. In a first step, the optimal beads type and concentration as well as assay buffer is chosen. In a second step, the optimal protein concentration is determined by titration of protein sample. In a third step, we determine the molecular affinity (K_D) of the tritiated ligand to identify the optimal compound concentration for the assay.

1. For the detergent-purified and His-tag fusion of GlyT1 protein, apply tritiated and cold Org24598 compound and YSi-copper His-tag SPA beads, in buffer-1. In this case, the assay should exhibit high specific (SB) and low nonspecific (NSB) ligand binding signals (*see* **Note 1**).
2. Mix the SPA YSi-copper beads and the His-tag fusion of GlyT1 protein with and without 10 μM cold ORG24598 for NSB in 96-well plates at a volume of 150 μL per well.
3. Add 50 μL 3H ORG24598 at a final concentration of ligand of 6 nM in a total volume of 200 μL per well. Seal the plate by foil and shake at 1000 rpm for 20 min at 4 °C. Beads settled after a period of at least 30 min (*see* **Note 2**) before reading of the plate in a TopCount scintillation counter. The determination of total binding (TB) and nonspecific binding (NSB) of the tritiated ligand is determined by the radioactive counts per minute (CPM). Specific binding (SB) is calculated by subtraction of NSB from TB.
4. For protein titration, apply GlyT1 protein at low nM concentration (*see* **Note 3**). For example, use 0.3 mg beads and 0.05–0.15 μg (2.5–7.5 nM) protein per well in a 96-well plate. Concentrations would have to be adapted for 384-well plates. An optimal and linear signal should be observed for this protein concentration (Fig. 1).
5. The determination of the affinity (K_D) of the tritiated ligand is essential to identify the optimal assay concentration of the ligand in SPA. Dilute 3H-ORG24598 compound from 100 nM to 0 nM and bind to GlyT1 protein molecular K_D 12 nM. Therefore, the optimal ligand concentration is 6 nM (*see* **Note 4**).
6. To determine the corresponding NSB signal, use 10 μM cold ORG24598 (Fig. 2a, b). A TB:NSB signal ratio of around 10 was observed (*see* **Note 5**).

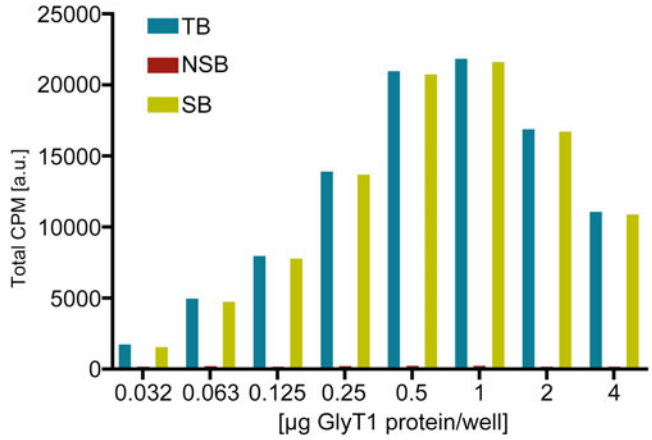

Fig. 1 SPA protein titration. 0–4 µg/well of a His-tag fusion of GlyT1 protein mixed at 6 nM 3H ORG24598 with 0.3 mg/well YSi-Copper SPA beads in a citrate buffer. SPA signal depletion occurred at higher protein concentration. *TB* Total binding, *NSB* Nonspecific binding, *SB* Specific binding

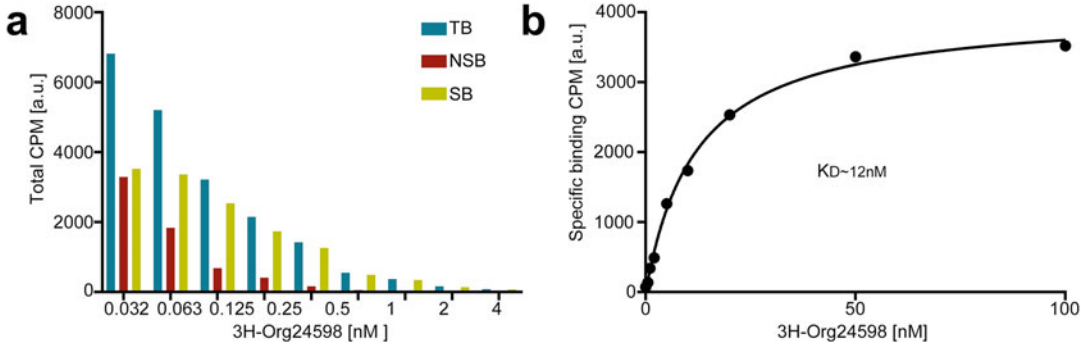

Fig. 2 Affinity determination for 3H-ORG24598 using GlyT1 protein. (**a**) 0–100 nM 3H ORG24598 TB, NSB, and SB in triplicate. An increase of the NSB at higher radioligand concentration is observed. (**b**) Specific binding signal (SB) for K_D determination

3.2 SPA-TS for Sybodies Trapping GlyT1 in the Inhibitor-Bound Conformation

1. For protein temperature screening with and without sybody, dilute GlyT1-HIS10 (1.0 mg/mL LMNG) in buffer-2 at 1:1000 ratio.
2. Add sybody #1–7 [3] to a final concentration of 1 µM.
3. Incubate for 1 h at 4 °C in a round shaker.
4. Distribute 150 µL sample/well in a 96-well twin tec PCR plate.
5. Run 10 min in Prime Elite with a temperature gradient from 23 to 50.9 °C.
6. Cool plate on ice.
7. To run the SPA assay. Add 15 µL SPA YSi beads (0.3 mg/mL) to each well of a 96-well Optiplate. Add 135 µL/well protein after temperature screen. Add 50 µL 3H-ORG24598 (24 nM, final 6 nM).

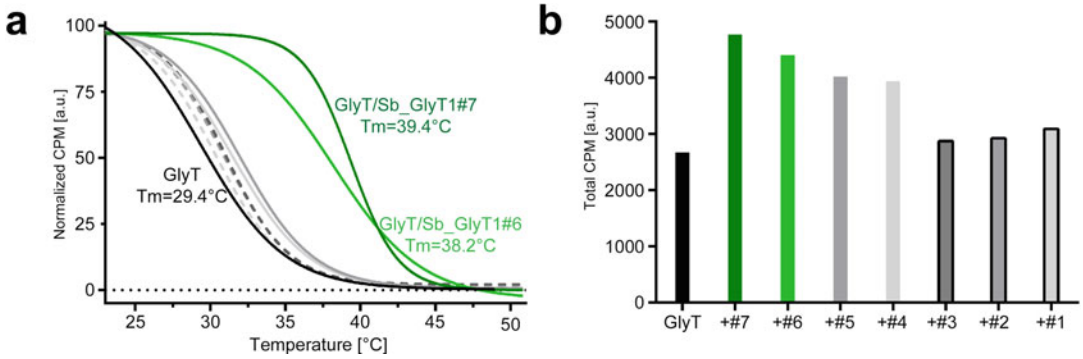

Fig. 3 Conformational trapping of GlyT1 protein by sybody. (**a**) SPA-TS analysis of sb_Glyt1#1–7 on GlyT1 using 3H-Org24598 binder. Shifts of the melting temperature (TM) are highest for sbGlyt1#6 and sbGlyt1#7 with values of 8.8 °C and 10 °C. (**b**) Absolute SPA signal with bound sybodies sb_Glyt1#1–7 [3] measured at 23 °C correlate well with SPA-TS values

8. Seal plate and shake for 20 min at 4 °C, 1000 rpm.
9. The results of the conformational trapping of GlyT1 protein by sybody are described in Fig. 3a, b.

4 Notes

1. Test copper SPA beads with radioligand in running buffer with and without His-tagged protein and imidazole. Unfavorable physicochemical properties of a ligand such as low solubility, hydrophobicity, and other factors can cause uncontrollable unspecific binding to the beads and consequently can disable any further SPA development. Good ligand properties enable an assay similar to the scheme published by Harder and Fotiadis [2] for beads, tritiated ligand, and membrane protein.
2. YSi beads are settling down quickly. For stable SPA signals let them settle for at least 30 min before reading the plate.
3. The amount and concentration of beads and protein is crucial for the SPA experiment. Elevated concentrations of protein can result in bead saturation and signal depletion due to the tritiated ligand to bind free, unbound protein.
4. Tritiated compound concentrations slightly below the K_D are beneficial for the assay outcome, reduces the NSB signal, and saves expensive reagent.
5. In SPA signal ratio of Total Binding (TB) versus Nonspecific Binding (NSB) is important for assay quality. We consider a ratio of 3 to be sufficient.

Acknowledgments

We thank Alain Gast for technical advice and assistance.

References

1. Bosworth N, Towers P (1989) Scintillation proximity assay. Nature 341:167–168
2. Harder D, Fotiadis D (2012) Measuring substrate binding and affinity of purified membrane transport proteins using the scintillation proximity assay. Nat Protoc 7:1569–1578
3. Zimmermann I, Egloff P et al (2018) Synthetic single domain antibodies for the conformational trapping of membrane proteins. elife 7:e34317

Chapter 14

Reconstitution of Membrane Proteins into Platforms Suitable for Biophysical and Structural Analyses

Philipp A. M. Schmidpeter, Nattakan Sukomon, and Crina M. Nimigean

Abstract

Integral membrane proteins have historically been challenging targets for biophysical research due to their low solubility in aqueous solution. Their importance for chemical and electrical signaling between cells, however, makes them fascinating targets for investigators interested in the regulation of cellular and physiological processes. Since membrane proteins shunt the barrier imposed by the cell membrane, they also serve as entry points for drugs, adding pharmaceutical research and development to the interests. In recent years, detailed understanding of membrane protein function has significantly increased due to high-resolution structural information obtained from single-particle cryo-EM, X-ray crystallography, and NMR. In order to further advance our mechanistic understanding on membrane proteins as well as foster drug development, it is crucial to generate more biophysical and functional data on these proteins under defined conditions. To that end, different techniques have been developed to stabilize integral membrane proteins in native-like environments that allow both structural and biophysical investigations—amphipols, lipid bicelles, and lipid nanodiscs. In this chapter, we provide detailed protocols for the reconstitution of membrane proteins according to these three techniques. We also outline some of the possible applications of each technique and discuss their advantages and possible caveats.

Key words Membrane proteins, Reconstitution, Amphipol, Bicelles, Nanodisc, Membrane scaffold, Membrane protein biophysics, Lipids

1 Introduction

Membrane proteins constitute about 30% of the proteome [1], are the connection between the inside and the outside of cells, and are entry points for pathogens and pharmaceuticals. It is thus of extreme importance to understand in molecular detail how specific proteins in the cell membrane work. In recent years, the number of high-resolution structures of membrane proteins has significantly increased mostly due to the developments in single-particle cryo-EM [2, 3], novel techniques in X-ray crystallography (lipidic cubic phase) [4], and continuously improving NMR techniques [5, 6]. Drawing conclusions from structural data and

Camilo Perez and Timm Maier (eds.), *Expression, Purification, and Structural Biology of Membrane Proteins*, Methods in Molecular Biology, vol. 2127, https://doi.org/10.1007/978-1-0716-0373-4_14,

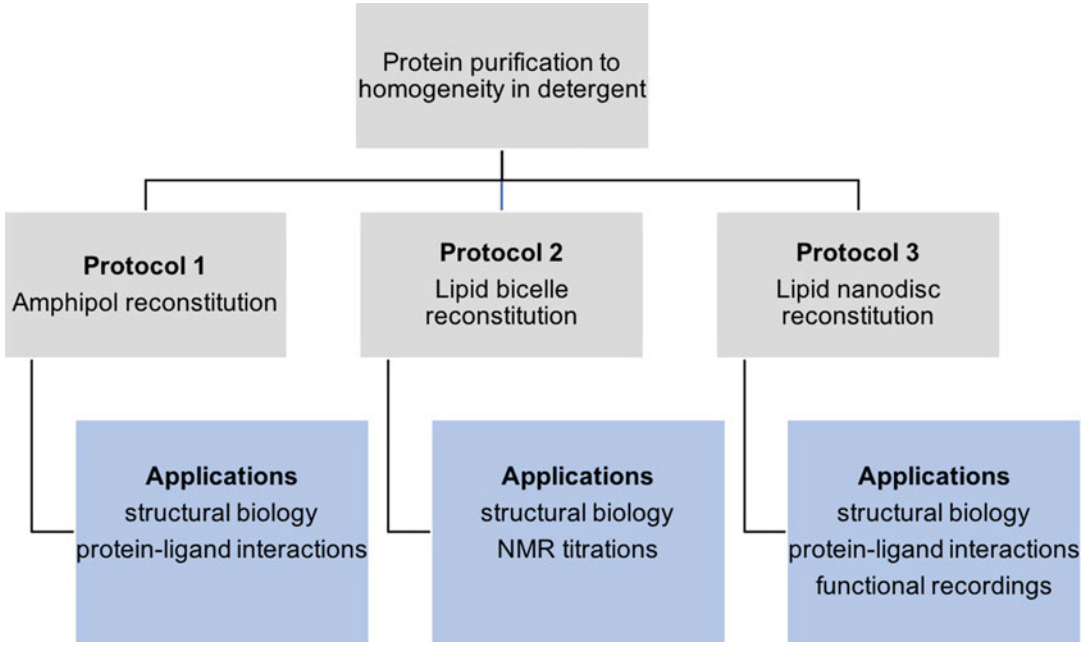

Fig. 1 Reconstitution of purified membrane proteins into native-like environments. Outline of the possibilities to transfer purified, integral membrane proteins solubilized in detergent into other platforms. For each platform, exemplary applications are listed

understanding molecular mechanisms that govern the function and regulation of these proteins is only possible if functional and biophysical data of the same proteins under comparable conditions are available. Previously, these data have been obtained for purified proteins in detergent. However, with more complex systems under investigation, the environment of the protein becomes increasingly important, and several techniques have been developed to provide a more native-like environment for integral membrane proteins, helping their stability, structural integrity, as well as their function and regulation under purified and defined conditions (Fig. 1) [7]. Although many detergents were deemed acceptable for many biophysical studies, they nevertheless display a non-native environment for membrane proteins. Their amphipathic character (Fig. 2a, b) leads to the formation of large micelles around protein molecules in order to preserve their structure even after extraction from cellular membranes. However, the presence of detergents can alter protein function and biophysical characteristics [8–12], the surface characteristics of aqueous buffers, and, in some cases, can even influence the function of extra-membranous protein domains [13].

To that end, multiple reconstitution platforms for membrane proteins have been developed. Here, we describe three of them—amphipols, lipid bicelles, and lipid nanodiscs—together with their

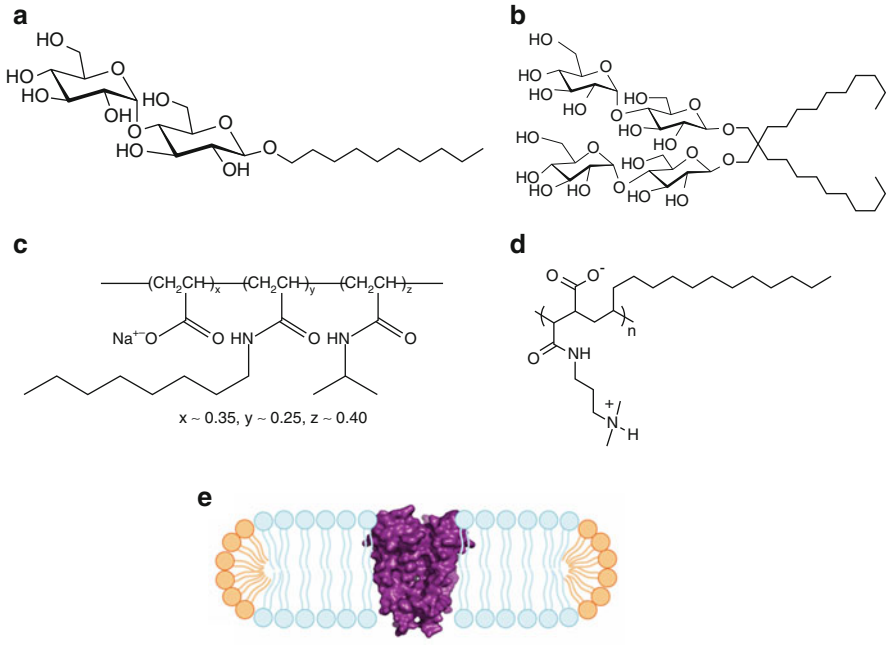

Fig. 2 Characteristics of detergents, amphipols, and bicelles. Chemical characteristics of hydrophilic headgroups and hydrophobic tails are present in detergent as shown for (**a**) *n*-Decyl-α-D-Maltopyranoside—DM, (**b**) Lauryl Maltose Neopentyl Glycol—LMNG, and amphipols as shown for (**c**) amphipol A8-35, and (**d**) PMAL-C12. Chemical structures were adapted from www.anatrace.com. (**e**) Cartoon of a lipid bicelle with a protein (KcsA ion channel, PDB: 1BL8 [75]) incorporated. Long-chain lipids in blue, short-chain lipids in orange, KcsA in magenta surface representation

advantages and caveats, indicating that the best solution for specific experimental needs has to be determined on a case-by-case basis (Fig. 1) [14].

1.1 Amphipols

Amphipols are amphipathic polymers that, in their chemical characteristics, resemble detergents, which combine a hydrophilic head group with a hydrophobic tail (Fig. 2a–d) [15–17]. However, amphipols can stabilize membrane proteins more efficiently by interacting more strongly with the protein compared to detergents that form a loo se micelle where single detergent molecules are in constant and rapid exchange with other detergent molecules in solution [18]. This is mostly due to the polymeric base structure of amphipols [19], which enables multiple hydrophobic chains of the same molecule to interact with the same protein (Fig. 2c, d). Furthermore, due to the very slow dissociation of the protein-amphipol complex [20], free amphipols can and should be removed from solution after reconstitution. The downsides of the approach are: (1) the protein reconstituted into amphipol is no longer accessible for ulterior functional studies, such as lipid bilayer recordings, as it is virtually impossible to remove these polymers from the

reconstituted protein, and (2) amphipol-reconstituted proteins may adopt different structural and functional characteristics compared to the protein in native membranes [21]. Nevertheless, amphipols have been proven to be excellent environments for protein-ligand interactions [22–25] as well as structural studies by crystallography [26] and cryo-EM [27–30].

1.2 Lipid Bicelles

Lipid bicelles closely resemble mixed detergent-lipid-micelles and are more native-like than amphipols as they provide a lipid environment for membrane proteins (Fig. 2e) [31]. The principle of lipid bicelles relies on the fact that lipid molecules in aqueous solution spontaneously assemble in bilayers (mostly in the form of liposomes) to separate their hydrophobic tails from water. By optimizing the molar ratio of long-chain lipids to short-chain lipids (a parameter usually designated as q), it is possible to induce the assembly of small patches of lipid bilayers with the protein incorporated. The long-chain lipids form the bilayer which is stabilized by a belt of short-chain lipids, which allow more curvature and protect the hydrophobic core of the bicelle (Fig. 2e) [32]. Lipid bicelles can be used for 3D-crystallography [33–36] and are an outstanding tool for analyzing membrane proteins by NMR [37–42].

1.3 Nanodiscs

A more complex, but at the same time a more native-like environment for membrane proteins, are lipid nanodiscs [43–47]. The detergent-free lipid bilayer is surrounded by a membrane-scaffolding protein (MSP) and the protein of interest is inserted inside the disc (Fig. 3). The MSP is a truncated form of apolipoprotein A-I. A multitude of MSPs is used to form nanodiscs [43, 44, 48], and they all share common characteristics—two monomers of MSP assemble to form a ring structure (Fig. 3c) [49–52]. The two subunits are held together by up to 28 intersubunit salt bridges, and the final ring structure creates an amphipathic environment (Fig. 3d–f) [53]. The outer surface of the nanodisc is fully accessible to aqueous solution, and thus is highly charged to ensure solubility. The inner surface of the ring, however, has to accommodate the lipid bilayer and accordingly carries charges along the top and bottom rims to mediate interaction with the solvent and the charged headgroups of the lipids, while in the core predominantly hydrophobic residues are exposed to provide an amenable environment for the acyl chains of the lipids [53, 54]. The high content of charged residues and the necessity of salt-bridges to stabilize the double-layered ring structure make MSP and in turn nanodiscs strongly pH-dependent assemblies. The diameter of the nanodisc can be varied either by varying the protein:MSP:lipid ratio or by selecting MSP of different chain lengths in order to accommodate the protein of interest (Fig. 3e–h) [43, 49, 55–59]. Nanodiscs can be assembled with various lipid

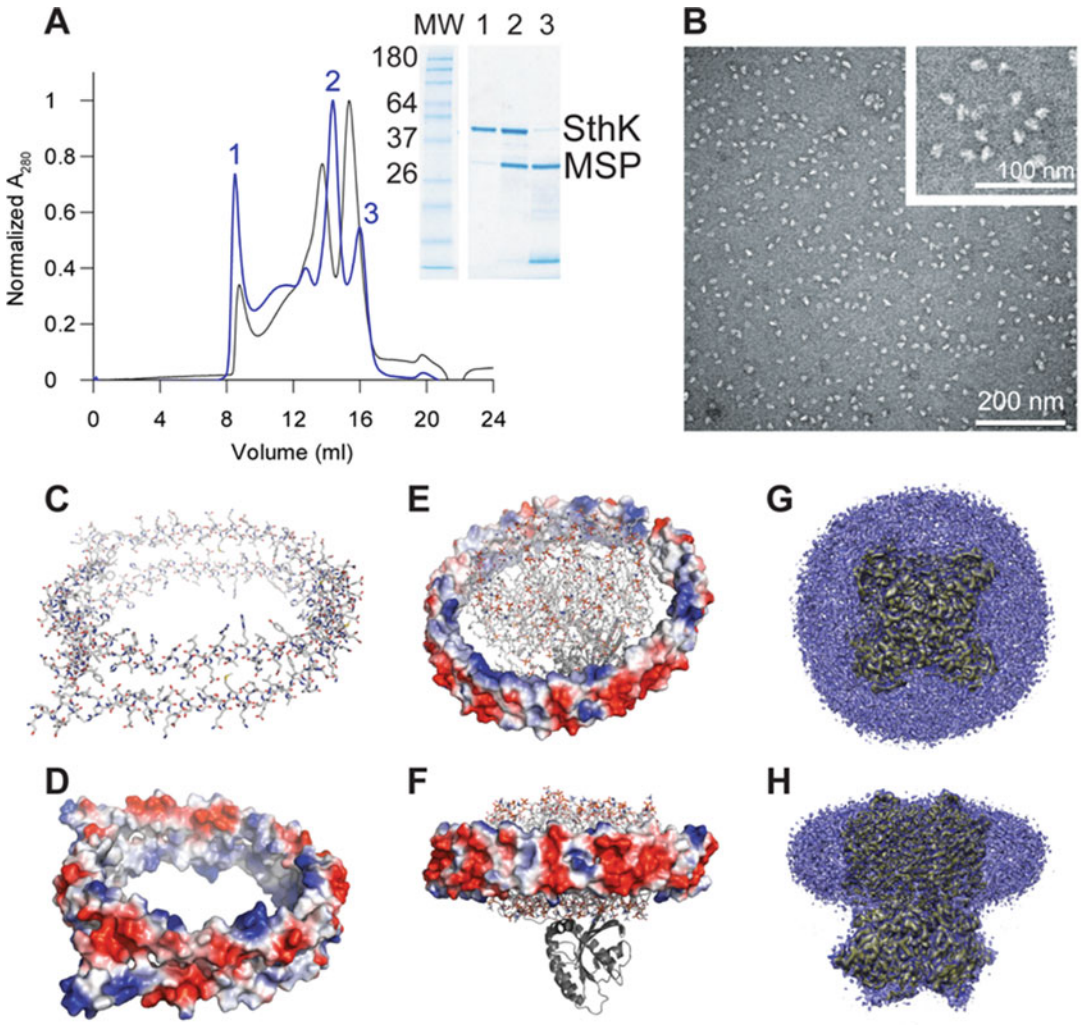

Fig. 3 Structural features of nanodiscs. (**a**) Gel filtration profiles (Superose 6 16/600) used to assess the reconstitution quality of the cyclic nucleotide-gated K^+ channel SthK into nanodiscs formed with different MSPs. Molar ratios of SthK:MSP2N2:POPG 1:1:125 (black) and SthK:MSP1E3:POPG 1:1:75 (blue) are shown. The bigger MSP (MSP2N2) shows an increased peak for empty nanodiscs. For the smaller MSP1E3, the SDS-PAGE clearly resolves the assembly of nanodiscs with aggregated SthK in the void peak (1), a peak for SthK inserted in MSP1E3 in nanodiscs (2) and empty nanodiscs (3). (**b**) Uranyl-acetate negative stain EM image of SthK in MSP1E3 (peak 2 in panel (**a**)) recorded on a JEM-1400 with 100 kV and a magnification of 150,000. (**c**) Apolipoprotein A-I (PDB: 2N5E [52]) is shown in stick representation (colored by atom) and (**d**) colored by the surface electrostatics. (**e**) Top view and (**f**) side view of the GTPase K-RAS4B tethered to an apolipoprotein A-I nanodisc (PDB: 2MSD [76]) with the nanodisc colored by surface electrostatics, lipids shown in stick representation and the GTPase as cartoon. (**g**) Top view and (**h**) side view of the density from single particle cryo-EM of a ligand-gated ion channel (yellow, EMDB: 7484) incorporated into MSP1E3 nanodiscs (blue) [57]. Panels (**c**)–(**f**) were prepared using Pymol (www.pymol.org), panels (**g**, **h**) were prepared using UCSF Chimera [77]

types. Therefore, they are able to meet the lipid requirements of the protein incorporated as well as the intended applications. However, it is important to optimize the protein:MSP:lipid ratio in order to maximize the amount of nanodiscs with protein incorporated or obtain the desired nanodisc sizes (Fig. 3a, b). Recently, it was shown that, once assembled, nanodiscs can tolerate significant distortion of the enclosed membrane [58, 60].

In the following sections, we will provide detailed protocols for the reconstitution of integral membrane proteins into the three systems described above.

2 Materials

All three protocols presented here start from pure, homogenous protein in detergent micelles.

2.1 Amphipols Reconstitution

1. Amphipol stock solution, 100 mg/ml in ddH_2O. Rotate the solution at 4 °C overnight to fully hydrate the amphipol. Prepare 100 μl aliquots and store at −20 °C until needed.
2. Detergent removal column (Pierce, Thermo Scientific).
3. Superdex200 10/300 gel filtration column (GE Lifesciences).

2.2 Bicelles Reconstitution

1. Lipid powder (Avanti Polar Lipids).
2. *n*-Octyl-β-D-Glucopyranoside (β-OG). 10% stock solution.
3. Bio-Beads (SM-2, BioRad).
4. Water bath sonicator.

2.3 Nanodiscs Reconstitution

1. Lipid stock solution (*see* below).
2. Membrane-scaffolding protein (MSP).
3. Bio-Beads (SM-2, BioRad).
4. Spin-X column.
5. Superose6 10/300 gel filtration column (GE Lifesciences).

3 Methods

3.1 Amphipols Reconstitution

The reconstitution of membrane proteins into amphipols is the easiest of the three methods presented here and can be incorporated into any regular protein purification protocol.

1. Prepare amphipol stock solution ahead of time.
2. Purify the protein of interest to homogeneity. Determine the protein concentration by absorbance and concentrate to

10 mg/ml or higher if the protein is stable at high concentrations (*see* **Note 1**).

3. Mix protein in detergent with amphipol and incubate under gentle agitation at 4 °C for 2 h (*see* **Note 2**). Commonly used protein:amphipol ratios are between 1:1 and 1:3 (w/w).
4. Prepare detergent removal columns by washing with 3 column volumes (CV) of ddH_2O followed by 3 CV of protein purification buffer without detergent.
5. Apply the protein-amphipol mix to the pre-equilibrated detergent removal column and collect fractions of 500 μl.
6. Check fractions for their protein content by absorbance. Pool protein-containing fractions and concentrate to 10 mg/ml.
7. Further purify the protein in amphipol by gel filtration in the protein purification buffer without detergent. The reconstituted protein should elute from the gel filtration as a single, symmetric peak at a volume similar to that of the protein in detergent.

3.2 Lipid Bicelles Reconstitution via Liposomes

Lipid bicelles provide a more native-like environment for membrane proteins than amphipols. The reconstitution protocol for lipid bicelles is more complex and needs some optimization for each protein. The protein should be purified to homogeneity with gel filtration as last purification step since the bicelles are not further purified after reconstitution.

1. Hydrate long-chain lipids of choice (usually at least tetradecyl tails) to 20 mg/ml in reconstitution buffer, 20 mM potassium phosphate, 20 mM NaCl, pH 7, for at least 2 h at room temperature.
2. Sonicate the hydrated lipids in a water bath sonicator for 1–2 min.
3. Add β-OG from a 10% stock to reach a final concentration of 0.5% β-OG and incubate the lipid-detergent mix for 30 min at room temperature under constant agitation. Although β-OG is most widely used for bicelle reconstitutions, other detergents can be used provided that they are compatible with the structural integrity of the protein of interest.
4. Add your protein of interest to the lipid-detergent mix in a molar ratio of 1:100 protein:lipid, mix, and incubate above the phase transition temperature of the lipids for 1 h to prevent the lipids from entering the gel phase and provide enough time for mixed micelles to form.
5. Remove detergent by adding freshly prepared Bio-Beads (30 mg Bio-Beads per mg detergent, *see* **Note 3**) and incubate for 2 h under gentle agitation.

6. Transfer the solution to a new reaction tube, add again fresh Bio-Beads, and incubate overnight under gentle agitation.
7. Change Bio-Beads one more time and incubate for 2 h before transferring the liposome solution to a new reaction tube. Make sure to avoid transferring any Bio-Beads.
8. Spin down the liposomes at 100,000 × *g* for 1 h, 4 °C.
9. Prepare the final buffer of your experiment by adding short-chain lipids to the desired concentration (usually hexyl tail-lipids, *see* **Note 4**) and hydrate for 2 h at room temperature. Resuspend the pellet into this final buffer with short-chain lipids to reach the desired protein concentration. Most often, lipid bicelles are used for NMR applications with a protein concentration of 0.5–1 mM.
10. Perform five freeze/thaw cycles to homogenize the bicelles. Freezing is best executed in liquid N_2. To thaw the bicelles, incubate the reaction tube at room temperature.

3.3 Lipid-Nanodiscs Reconstitution

The most complex protocol to reconstitute membrane proteins for functional and biophysical assays is the incorporation of proteins into lipid-nanodiscs. These particles, however, represent an environment that is very close to the conditions in a cellular membrane and can be tailored to specific experimental setups.

For an optimal reconstitution, different protein:MSP:lipid ratios need to be screened to obtain nanodiscs with a single protein incorporated. Suboptimal reconstitution conditions can lead to aggregation, empty nanodiscs, or nanodiscs containing several proteins per disc (Fig. 3a, b) [61, 62]. In general, the protein:MSP molar ratio should be 1:2 for purified membrane protein [50]; however, molar ratios between 1 and 25 have been applied in practice [57, 63–67]. The optimal protein:MSP:lipid ratio can be determined by systematically testing different conditions in small-scale reconstitutions and monitoring the sample quality by size-exclusion chromatography followed by SDS-PAGE and negative stain EM (Fig. 3a, b).

3.3.1 Lipid Preparation

1. Transfer the appropriate amount of lipids from stock solutions (typically 10 or 25 mg/ml in chloroform) to a glass tube.
2. Dry lipids to a thin film under a constant nitrogen gas stream. Remove residual organic solvent by rinsing in one volume of pentane, and dry again under the gas stream. Alternatively, the dried lipids can be placed in a vacuum desiccator overnight for complete removal of the solvent.
3. Add buffer to the dried lipid film to obtain a 20 mM lipid stock. Gradually add the detergent suitable for the membrane protein while sonicating in a water bath sonicator until the lipid solution is clear. The typical final concentration of detergent is at

least twice the critical micelle concentration (CMC). The lipids can also be dissolved by several freeze/thaw cycles.

4. After solubilization lipid stock solutions can be stored at −80 °C for future use.

3.3.2 Bio-Beads Preparation

1. Wash the Bio-Beads with two volumes of methanol, followed by extensively washing with ddH_2O to remove the organic solvent.
2. Wash the Bio-Beads with three volumes of purification buffer without detergent.
3. Bio-Beads can be used freshly or stored at 4 °C in ddH_2O and 0.01% NaN_3 for up to 3 months [49].

3.3.3 Nanodiscs Assembly

1. MSP protein can be prepared in lab according to published protocols [68] (*see* **Note 5**).
2. Add lipid, MSP, and the membrane protein in a tube at the optimized ratio. The sample volume is dependent on the application and the desired yield of nanodiscs (*see* **Note 6**).
3. Incubate the reconstitution mixture by gently inverting for 1–2 h at a temperature above the phase-transition temperature of the lipid. In case of using a mix of lipids, the experimental temperature should be optimized according to the phase transition temperature of the main lipid components [69].
4. Start detergent removal to initiate the reconstitution by adding Bio-Beads (20 mg per 100 µl sample), and gently invert for ~2 h.
5. Transfer the reconstitution mixture to a new tube. Add fresh, pre-equilibrated Bio-Beads to the reconstitution mixture (20 mg per 100 µl). Gently invert overnight.
6. Transfer the reconstitution mixture to a new tube. Dilute the sample with sample buffer to the volume appropriate for gel filtration (typically 500 µl final volume).
7. Filter the sample through a 0.22 µm Spin-X centrifugation tube filter.
8. Apply the sample to a Superose 6 16/600 gel filtration column pre-equilibrated in sample buffer. Collect the peak fraction corresponding to the assembled nanodiscs and check for protein and MSP content by SDS-PAGE (Fig. 3a).
9. The different fractions can be finally checked by negative-stain EM for evidence of nanodisc formation, presence of protein in nanodiscs, and absence of liposomes (Fig. 3b).

4 Notes

1. Protein should be purified to homogeneity (usually after gel filtration chromatography) to avoid reconstitution of bad particles. However, if the protein of interest displays low stability in detergent, amphipol exchange can also be performed right after affinity purification as long as the protein appears clean on SDS-PAGE at this stage.
2. Due to the free carboxylic groups, amphipols are highly water soluble at neutral pH values. The solubility is decreased at acidic pH as well as at high salt concentrations, which might lead to aggregation of amphipols.
3. To freshly prepare Bio-Beads, wash the Bio-Beads with at least 2 volumes of methanol for 10 min to remove air, followed by at least 4 volumes of ddH_2O. Decant the water and wash with 2 volumes of reconstitution buffer.
4. The concentration of short-chain lipids is given by the q value that needs to be determined for each protein and adjusted to the experimental needs. The q value is defined as the molar ratio of long-chain:short-chain lipids, and it determines the size and order parameter of the bicelles. For solid state NMR, q values of 3–6 are used, whereas q values of 0.15–0.5 will yield fast-tumbling bicelles suitable for solution NMR. For more details *see* [39, 70].
5. The size of MSP determines to some extent the diameter of nanodiscs and thus the number of enclosed lipid molecules [49, 55]. The selection of MSP is mainly dependent on the size of the membrane protein. Ideally, the nanodiscs should be large enough to accommodate the protein and at least two layers of phospholipids to mimic the physiological environment [50, 69]. If the assembled nanodiscs are too large, it may result in floating of the protein within the discs, which may obscure structural data processing and interpretation [71]. Additionally, there is an increased chance of reconstituting more than one protein per nanodisc [62].

   A variety of MSP constructs with various numbers of amphipathic helices are available to generate nanodiscs with diameters between 9.8 and 17 nm [43, 49, 67]. In addition, truncated versions of MSP have been designed, allowing the preparation of nanodiscs with diameters ranging from 6 to 8 nm [69].

   Circular MSP (cMSP) has been developed to improve the homogeneity of nanodiscs, which are especially crucial for structural studies. cMSP is a variant of MSP with its N- and C-termini covalently linked by sortase A [72, 73]. The nanodisc sizes produced by this technique range from 8.5 up to

80 nm in diameter. Alternatively, cMSP generated from DnaE split intein can be used for smaller nanodiscs (7–26 nm in diameter) [74].

6. Based on our experience, well-defined, published reconstitution ratios can serve as a starting point for optimization, especially those from membrane proteins of a similar size with the protein of interest, as well as similar MSP and lipid types.

Acknowledgments

This work was funded by the National Institutes of Health (GM088352 and GM124451 to C.N.) and the American Heart Association (18POST33960309 to P.S.). We thank J. Rheinberger for providing the gel filtration profiles and the negative stain EM image in Fig. 3a, b.

References

1. Fagerberg L, Jonasson K, von Heijne G, Uhlén M, Berglund L (2010) Prediction of the human membrane proteome. Proteomics 10(6):1141–1149. https://doi.org/10.1002/pmic.200900258
2. Kühlbrandt W (2014) Cryo-EM enters a new era. Elife 3:e03678. https://doi.org/10.7554/eLife.03678
3. Cheng Y (2015) Single-particle cryo-EM at crystallographic resolution. Cell 161(3):450–457. https://doi.org/10.1016/j.cell.2015.03.049
4. Cherezov V (2011) Lipidic cubic phase technologies for membrane protein structural studies. Curr Opin Struct Biol 21(4):559–566. https://doi.org/10.1016/j.sbi.2011.06.007
5. Liang B, Tamm LK (2016) NMR as a tool to investigate the structure, dynamics and function of membrane proteins. Nat Struct Mol Biol 23(6):468–474. https://doi.org/10.1038/nsmb.3226
6. Warschawski DE, Arnold AA, Beaugrand M, Gravel A, Chartrand É, Marcotte I (2011) Choosing membrane mimetics for NMR structural studies of transmembrane proteins. Biochim Biophys Acta 1808(8):1957–1974. https://doi.org/10.1016/j.bbamem.2011.03.016
7. Hunte C, Richers S (2008) Lipids and membrane protein structures. Curr Opin Struct Biol 18(4):406–411. https://doi.org/10.1016/j.sbi.2008.03.008
8. McCoy JG, Rusinova R, Kim DM, Kowal J, Banerjee S, Jaramillo Cartagena A, Thompson AN, Kolmakova-Partensky L, Stahlberg H, Andersen OS, Nimigean CM (2014) A KcsA/MloK1 chimeric ion channel has lipid-dependent ligand-binding energetics. J Biol Chem 289(14):9535–9546. https://doi.org/10.1074/jbc.M113.543389
9. Quick M, Winther AM, Shi L, Nissen P, Weinstein H, Javitch JA (2009) Binding of an octylglucoside detergent molecule in the second substrate (S2) site of LeuT establishes an inhibitor-bound conformation. Proc Natl Acad Sci U S A 106(14):5563–5568. https://doi.org/10.1073/pnas.0811322106
10. Quick M, Shi L, Zehnpfennig B, Weinstein H, Javitch JA (2012) Experimental conditions can obscure the second high-affinity site in LeuT. Nat Struct Mol Biol 19(2):207–211. https://doi.org/10.1038/nsmb.2197
11. Dowhan W (1997) Molecular basis for membrane phospholipid diversity: why are there so many lipids? Annu Rev Biochem 66:199–232. https://doi.org/10.1146/annurev.biochem.66.1.199
12. Yu CA, Yu L (1980) Structural role of phospholipids in ubiquinol-cytochrome c reductase. Biochemistry 19(25):5715–5720
13. Seddon AM, Curnow P, Booth PJ (2004) Membrane proteins, lipids and detergents: not just a soap opera. Biochim Biophys Acta 1666(1–2):105–117. https://doi.org/10.1016/j.bbamem.2004.04.011
14. Raschle T, Hiller S, Etzkorn M, Wagner G (2010) Nonmicellar systems for solution NMR spectroscopy of membrane proteins.

Curr Opin Struct Biol 20(4):471–479. https://doi.org/10.1016/j.sbi.2010.05.006

15. Popot JL, Althoff T, Bagnard D, Banères JL, Bazzacco P, Billon-Denis E, Catoire LJ, Champeil P, Charvolin D, Cocco MJ, Crémel G, Dahmane T, de la Maza LM, Ebel C, Gabel F, Giusti F, Gohon Y, Goormaghtigh E, Guittet E, Kleinschmidt JH, Kühlbrandt W, Le Bon C, Martinez KL, Picard M, Pucci B, Sachs JN, Tribet C, van Heijenoort C, Wien F, Zito F, Zoonens M (2011) Amphipols from A to Z. Annu Rev Biophys 40:379–408. https://doi.org/10.1146/annurev-biophys-042910-155219
16. Tribet C, Audebert R, Popot JL (1996) Amphipols: polymers that keep membrane proteins soluble in aqueous solutions. Proc Natl Acad Sci U S A 93(26):15047–15050
17. Tehei M, Perlmutter JD, Giusti F, Sachs JN, Zaccai G, Popot JL (2014) Thermal fluctuations in amphipol A8-35 particles: a neutron scattering and molecular dynamics study. J Membr Biol 247(9–10):897–908. https://doi.org/10.1007/s00232-014-9725-1
18. Le Bon C, Marconnet A, Masscheleyn S, Popot JL, Zoonens M (2018) Folding and stabilizing membrane proteins in amphipol A8-35. Methods 147:95–105. https://doi.org/10.1016/j.ymeth.2018.04.012
19. Gohon Y, Giusti F, Prata C, Charvolin D, Timmins P, Ebel C, Tribet C, Popot JL (2006) Well-defined nanoparticles formed by hydrophobic assembly of a short and polydisperse random terpolymer, amphipol A8-35. Langmuir 22(3):1281–1290. https://doi.org/10.1021/la052243g
20. Perlmutter JD, Drasler WJ, Xie W, Gao J, Popot JL, Sachs JN (2011) All-atom and coarse-grained molecular dynamics simulations of a membrane protein stabilizing polymer. Langmuir 27(17):10523–10537. https://doi.org/10.1021/la202103v
21. Barrera NP, Zhou M, Robinson CV (2013) The role of lipids in defining membrane protein interactions: insights from mass spectrometry. Trends Cell Biol 23(1):1–8. https://doi.org/10.1016/j.tcb.2012.08.007
22. Schmidpeter PAM, Gao X, Uphadyay V, Rheinberger J, Nimigean CM (2018) Ligand binding and activation properties of the purified bacterial cyclic nucleotide-gated channel SthK. J Gen Physiol 150(6):821–834. https://doi.org/10.1085/jgp.201812023
23. Martinez KL, Gohon Y, Corringer PJ, Tribet C, Mérola F, Changeux JP, Popot JL (2002) Allosteric transitions of Torpedo acetylcholine receptor in lipids, detergent and amphipols: molecular interactions vs. physical constraints. FEBS Lett 528(1–3):251–256
24. Catoire LJ, Damian M, Giusti F, Martin A, van Heijenoort C, Popot JL, Guittet E, Banères JL (2010) Structure of a GPCR ligand in its receptor-bound state: leukotriene B4 adopts a highly constrained conformation when associated to human BLT2. J Am Chem Soc 132(26):9049–9057. https://doi.org/10.1021/ja101868c
25. Charvolin D, Perez JB, Rouvière F, Giusti F, Bazzacco P, Abdine A, Rappaport F, Martinez KL, Popot JL (2009) The use of amphipols as universal molecular adapters to immobilize membrane proteins onto solid supports. Proc Natl Acad Sci U S A 106(2):405–410. https://doi.org/10.1073/pnas.0807132106
26. Polovinkin V, Gushchin I, Sintsov M, Round E, Balandin T, Chervakov P, Shevchenko V, Utrobin P, Popov A, Borshchevskiy V, Mishin A, Kuklin A, Willbold D, Chupin V, Popot JL, Gordeliy V (2014) High-resolution structure of a membrane protein transferred from amphipol to a lipidic mesophase. J Membr Biol 247(9–10):997–1004. https://doi.org/10.1007/s00232-014-9700-x
27. van Pee K, Neuhaus A, D'Imprima E, Mills DJ, Kühlbrandt W, Yildiz Ö (2017) CryoEM structures of membrane pore and prepore complex reveal cytolytic mechanism of Pneumolysin. Elife 6. https://doi.org/10.7554/eLife.23644
28. Liao M, Cao E, Julius D, Cheng Y (2013) Structure of the TRPV1 ion channel determined by electron cryo-microscopy. Nature 504(7478):107–112. https://doi.org/10.1038/nature12822
29. Hirschi M, Herzik MA, Wie J, Suo Y, Borschel WF, Ren D, Lander GC, Lee SY (2017) Cryo-electron microscopy structure of the lysosomal calcium-permeable channel TRPML3. Nature 550(7676):411–414. https://doi.org/10.1038/nature24055
30. Li M, Zhou X, Wang S, Michailidis I, Gong Y, Su D, Li H, Li X, Yang J (2017) Structure of a eukaryotic cyclic-nucleotide-gated channel. Nature 542(7639):60–65. https://doi.org/10.1038/nature20819
31. Sanders CR, Landis GC (1995) Reconstitution of membrane proteins into lipid-rich bilayered mixed micelles for NMR studies. Biochemistry 34(12):4030–4040
32. Sanders CR, Schwonek JP (1992) Characterization of magnetically orientable bilayers in mixtures of dihexanoylphosphatidylcholine and dimyristoylphosphatidylcholine by solid-state NMR. Biochemistry 31(37):8898–8905

33. Ujwal R, Bowie JU (2011) Crystallizing membrane proteins using lipidic bicelles. Methods 55(4):337–341. https://doi.org/10.1016/j.ymeth.2011.09.020
34. Rasmussen SG, Choi HJ, Rosenbaum DM, Kobilka TS, Thian FS, Edwards PC, Burghammer M, Ratnala VR, Sanishvili R, Fischetti RF, Schertler GF, Weis WI, Kobilka BK (2007) Crystal structure of the human beta2 adrenergic G-protein-coupled receptor. Nature 450(7168):383–387. https://doi.org/10.1038/nature06325
35. Ujwal R, Cascio D, Colletier JP, Faham S, Zhang J, Toro L, Ping P, Abramson J (2008) The crystal structure of mouse VDAC1 at 2.3 A resolution reveals mechanistic insights into metabolite gating. Proc Natl Acad Sci U S A 105(46):17742–17747. https://doi.org/10.1073/pnas.0809634105
36. Faham S, Bowie JU (2002) Bicelle crystallization: a new method for crystallizing membrane proteins yields a monomeric bacteriorhodopsin structure. J Mol Biol 316(1):1–6. https://doi.org/10.1006/jmbi.2001.5295
37. Kim DM, Dikiy I, Upadhyay V, Posson DJ, Eliezer D, Nimigean CM (2016) Conformational heterogeneity in closed and open states of the KcsA potassium channel in lipid bicelles. J Gen Physiol 148(2):119–132. https://doi.org/10.1085/jgp.201611602
38. Dürr UH, Gildenberg M, Ramamoorthy A (2012) The magic of bicelles lights up membrane protein structure. Chem Rev 112 (11):6054–6074. https://doi.org/10.1021/cr300061w
39. De Angelis AA, Opella SJ (2007) Bicelle samples for solid-state NMR of membrane proteins. Nat Protoc 2(10):2332–2338. https://doi.org/10.1038/nprot.2007.329
40. Opella SJ, Marassi FM (2004) Structure determination of membrane proteins by NMR spectroscopy. Chem Rev 104(8):3587–3606. https://doi.org/10.1021/cr0304121
41. Morrison EA, Henzler-Wildman KA (2012) Reconstitution of integral membrane proteins into isotropic bicelles with improved sample stability and expanded lipid composition profile. Biochim Biophys Acta 1818(3):814–820. https://doi.org/10.1016/j.bbamem.2011.12.020
42. Bibow S, Hiller S (2018) A guide to quantifying membrane protein dynamics in lipids and other native-like environments by solution-state NMR spectroscopy. FEBS J 286:1610. https://doi.org/10.1111/febs.14639
43. Denisov IG, Grinkova YV, Lazarides AA, Sligar SG (2004) Directed self-assembly of monodisperse phospholipid bilayer nanodiscs with controlled size. J Am Chem Soc 126 (11):3477–3487. https://doi.org/10.1021/ja0393574
44. Banerjee S, Huber T, Sakmar TP (2008) Rapid incorporation of functional rhodopsin into nanoscale apolipoprotein bound bilayer (NABB) particles. J Mol Biol 377 (4):1067–1081. https://doi.org/10.1016/j.jmb.2008.01.066
45. Jonas A, Kézdy KE, Wald JH (1989) Defined apolipoprotein A-I conformations in reconstituted high density lipoprotein discs. J Biol Chem 264(9):4818–4824
46. Davidson WS, Thompson TB (2007) The structure of apolipoprotein A-I in high density lipoproteins. J Biol Chem 282 (31):22249–22253. https://doi.org/10.1074/jbc.R700014200
47. Leitz AJ, Bayburt TH, Barnakov AN, Springer BA, Sligar SG (2006) Functional reconstitution of Beta2-adrenergic receptors utilizing self-assembling Nanodisc technology. Biotechniques 40(5):601–602, 604, 606, passim. https://doi.org/10.2144/000112169
48. Grinkova YV, Denisov IG, Sligar SG (2010) Engineering extended membrane scaffold proteins for self-assembly of soluble nanoscale lipid bilayers. Protein Eng Des Sel 23(11):843–848. https://doi.org/10.1093/protein/gzq060
49. Ritchie TK, Grinkova YV, Bayburt TH, Denisov IG, Zolnerciks JK, Atkins WM, Sligar SG (2009) Chapter 11: Reconstitution of membrane proteins in phospholipid bilayer nanodiscs. Methods Enzymol 464:211–231. https://doi.org/10.1016/S0076-6879(09)64011-8
50. Efremov RG, Gatsogiannis C, Raunser S (2017) Lipid nanodiscs as a tool for high-resolution structure determination of membrane proteins by single-particle cryo-EM. Methods Enzymol 594:1–30. https://doi.org/10.1016/bs.mie.2017.05.007
51. McLean MA, Gregory MC, Sligar SG (2018) Nanodiscs: a controlled bilayer surface for the study of membrane proteins. Annu Rev Biophys 47:107. https://doi.org/10.1146/annurev-biophys-070816-033620
52. Bibow S, Polyhach Y, Eichmann C, Chi CN, Kowal J, Albiez S, McLeod RA, Stahlberg H, Jeschke G, Güntert P, Riek R (2017) Solution structure of discoidal high-density lipoprotein particles with a shortened apolipoprotein A-I. Nat Struct Mol Biol 24(2):187–193. https://doi.org/10.1038/nsmb.3345
53. Morgan CR, Hebling CM, Rand KD, Stafford DW, Jorgenson JW, Engen JR (2011)

Conformational transitions in the membrane scaffold protein of phospholipid bilayer nanodiscs. Mol Cell Proteomics 10(9): M111.010876. https://doi.org/10.1074/mcp.M111.010876

54. Schuler MA, Denisov IG, Sligar SG (2013) Nanodiscs as a new tool to examine lipid-protein interactions. Methods Mol Biol 974:415–433. https://doi.org/10.1007/978-1-62703-275-9_18
55. Bayburt TH, Sligar SG (2010) Membrane protein assembly into Nanodiscs. FEBS Lett 584 (9):1721–1727. https://doi.org/10.1016/j.febslet.2009.10.024
56. Koehl A, Hu H, Feng D, Sun B, Zhang Y, Robertson MJ, Chu M, Kobilka TS, Laermans T, Steyaert J, Tarrasch J, Dutta S, Fonseca R, Weis WI, Mathiesen JM, Skiniotis G, Kobilka BK (2019) Structural insights into the activation of metabotropic glutamate receptors. Nature 566 (7742):79–84. https://doi.org/10.1038/s41586-019-0881-4
57. Rheinberger J, Gao X, Schmidpeter PA, Nimigean CM (2018) Ligand discrimination and gating in cyclic nucleotide-gated ion channels from apo and partial agonist-bound cryo-EM structures. Elife 7. https://doi.org/10.7554/eLife.39775
58. Kalienkova V, Clerico Mosina V, Bryner L, Oostergetel GT, Dutzler R, Paulino C (2019) Stepwise activation mechanism of the scramblase nhTMEM16 revealed by cryo-EM. Elife 8. https://doi.org/10.7554/eLife.44364
59. Quentin D, Ahmad S, Shanthamoorthy P, Mougous JD, Whitney JC, Raunser S (2018) Mechanism of loading and translocation of type VI secretion system effector Tse6. Nat Microbiol 3(10):1142–1152. https://doi.org/10.1038/s41564-018-0238-z
60. Falzone ME, Rheinberger J, Lee BC, Peyear T, Sasset L, Raczkowski AM, Eng ET, Di Lorenzo A, Andersen OS, Nimigean CM, Accardi A (2019) Structural basis of Ca^{2+}-dependent activation and lipid transport by a TMEM16 scramblase. Elife 8. https://doi.org/10.7554/eLife.43229
61. Bayburt TH, Sligar SG (2003) Self-assembly of single integral membrane proteins into soluble nanoscale phospholipid bilayers. Protein Sci 12 (11):2476–2481. https://doi.org/10.1110/ps.03267503
62. Boldog T, Grimme S, Li M, Sligar SG, Hazelbauer GL (2006) Nanodiscs separate chemoreceptor oligomeric states and reveal their signaling properties. Proc Natl Acad Sci U S A 103(31):11509–11514. https://doi.org/10.1073/pnas.0604988103
63. Li Y, Soubias O, Li J, Sun S, Randazzo PA, Byrd RA (2019) Functional expression and characterization of human myristoylated-Arf1 in nanodisc membrane mimetics. Biochemistry 58:1423. https://doi.org/10.1021/acs.biochem.8b01323
64. Tsukamoto H, Szundi I, Lewis JW, Farrens DL, Kliger DS (2011) Rhodopsin in nanodiscs has native membrane-like photointermediates. Biochemistry 50(22):5086–5091. https://doi.org/10.1021/bi200391a
65. Ranaghan MJ, Schwall CT, Alder NN, Birge RR (2011) Green proteorhodopsin reconstituted into nanoscale phospholipid bilayers (nanodiscs) as photoactive monomers. J Am Chem Soc 133(45):18318–18327. https://doi.org/10.1021/ja2070957
66. Mörs K, Roos C, Scholz F, Wachtveitl J, Dötsch V, Bernhard F, Glaubitz C (2013) Modified lipid and protein dynamics in nanodiscs. Biochim Biophys Acta 1828 (4):1222–1229. https://doi.org/10.1016/j.bbamem.2012.12.011
67. Inagaki S, Ghirlando R, Grisshammer R (2013) Biophysical characterization of membrane proteins in nanodiscs. Methods 59(3):287–300. https://doi.org/10.1016/j.ymeth.2012.11.006
68. Bayburt TH, Grinkova YV, Sligar SG (2002) Self-assembly of discoidal phospholipid bilayer nanoparticles with membrane scaffold proteins. Nano Lett 2(8):853–856. https://doi.org/10.1021/nl025623k
69. Hagn F, Nasr ML, Wagner G (2018) Assembly of phospholipid nanodiscs of controlled size for structural studies of membrane proteins by NMR. Nat Protoc 13(1):79–98. https://doi.org/10.1038/nprot.2017.094
70. Mäler L, Gräslund A (2009) Artificial membrane models for the study of macromolecular delivery. Methods Mol Biol 480:129–139. https://doi.org/10.1007/978-1-59745-429-2_9
71. Hagn F, Etzkorn M, Raschle T, Wagner G (2013) Optimized phospholipid bilayer nanodiscs facilitate high-resolution structure determination of membrane proteins. J Am Chem Soc 135(5):1919–1925. https://doi.org/10.1021/ja310901f
72. Nasr ML, Baptista D, Strauss M, Sun ZJ, Grigoriu S, Huser S, Plückthun A, Hagn F, Walz T, Hogle JM, Wagner G (2017) Covalently circularized nanodiscs for studying membrane proteins and viral entry. Nat Methods 14 (1):49–52. https://doi.org/10.1038/nmeth.4079

73. Yusuf Y, Massiot J, Chang YT, Wu PH, Yeh V, Kuo PC, Shiue J, Yu TY (2018) Optimization of the production of covalently circularized nanodiscs and their characterization in physiological conditions. Langmuir 34 (11):3525–3532. https://doi.org/10.1021/acs.langmuir.8b00025
74. Miehling J, Goricanec D, Hagn F (2018) A split-intein-based method for the efficient production of circularized nanodiscs for structural studies of membrane proteins. Chembiochem 19(18):1927–1933. https://doi.org/10.1002/cbic.201800345
75. Doyle DA, Morais Cabral J, Pfuetzner RA, Kuo A, Gulbis JM, Cohen SL, Chait BT, MacKinnon R (1998) The structure of the potassium channel: molecular basis of K+ conduction and selectivity. Science 280 (5360):69–77
76. Mazhab-Jafari MT, Marshall CB, Smith MJ, Gasmi-Seabrook GM, Stathopulos PB, Inagaki F, Kay LE, Neel BG, Ikura M (2015) Oncogenic and RASopathy-associated K-RAS mutations relieve membrane-dependent occlusion of the effector-binding site. Proc Natl Acad Sci U S A 112(21):6625–6630. https://doi.org/10.1073/pnas.1419895112
77. Pettersen EF, Goddard TD, Huang CC, Couch GS, Greenblatt DM, Meng EC, Ferrin TE (2004) UCSF Chimera—a visualization system for exploratory research and analysis. J Comput Chem 25(13):1605–1612. https://doi.org/10.1002/jcc.20084

Chapter 15

Reconstitution of Proteoliposomes for Phospholipid Scrambling and Nonselective Channel Assays

Maria E. Falzone and Alessio Accardi

Abstract

Phospholipid scramblases catalyze the rapid trans-bilayer movement of lipids down their concentration gradients. This process is essential for numerous cellular signaling functions including cell fusion, blood coagulation, and apoptosis. The importance of scramblases is highlighted by the number of human diseases caused by mutations in these proteins. Because of their indispensable function, it is essential to understand and characterize the molecular function of phospholipid scramblases. Powerful tools to measure lipid transport in cells are available. However, these approaches provide limited mechanistic insights into the molecular bases of scrambling. Here we describe in detail an in vitro phospholipid scramblase assay and the accompanying analysis which allows for determination of the macroscopic rate constants associated with phospholipid scrambling. Notably, members of the TMEM16 family of scramblases also function as nonselective ion channels. To better understand the physiological relevance of this channel function as well as its relationship to the scrambling activity of the TMEM16s we also describe in detail an in vitro flux assay to measure nonselective channel activity. Together, these two assays can be used to investigate the dual activities of the TMEM16 scramblases/nonselective channels.

Key words Phospholipids, Scrambling, Scramblases, Lipid transport, TMEM16, Nonselective channel

1 Introduction

The eukaryotic cell membrane is asymmetric at rest with phosphatidylserine (PS) and phosphatidylethanolamine (PE) lipids sequestered to the inner leaflet of the bilayer while phosphatidylcholine (PC) and sphingolipids are exposed on the external leaflet. This asymmetry is generated and maintained by energy-dependent lipid flippases and floppases that transport lipids against their concentration gradients and is disrupted by phospholipid scramblases that transport lipids down their concentration gradients [1, 2]. Scramblase activation results in the exposure of PS on the extracellular surface, which is an essential signaling step in many processes including apoptosis, blood coagulation, and cell fusion

Camilo Perez and Timm Maier (eds.), *Expression, Purification, and Structural Biology of Membrane Proteins*, Methods in Molecular Biology, vol. 2127, https://doi.org/10.1007/978-1-0716-0373-4_15,

[3, 4]. The indispensable role of scramblases in these signaling processes underscores their importance and mutations in many scramblases cause human diseases including disorders of blood coagulation, muscle repair, and bone formation [3, 4]. Thus far, members of two protein families have been identified as phospholipid scramblases, the TMEM16 Ca^{2+}-activated scramblases [5–11] and the caspase-activated XK-related (Xkr) proteins [12, 13]. Additionally, several G-protein-coupled receptors (GPCR's), including rhodopsin, bacteriorhodopsin, and the β-adrenergic receptor, exhibit phospholipid scrambling activity in vitro [14–16]. Finally, several peptides mediate lipid scrambling in vitro [17, 18], and most recently a DNA nanostructure was shown to mediate rapid transbilayer lipid movement in synthetic vesicles and in cells [19], underscoring the diverse chemical natures and three-dimensional architectures of molecules that mediate lipid scrambling.

In cells, phospholipid scrambling can be measured using fluorescently labeled proteins, such as Annexin V and LactC2, that specifically recognize and bind to PS lipids [5, 20]. As the membranes of apoptotic cells lose integrity, these probes can access and bind PS on both membrane leaflets. Therefore, it is critical to use nuclear-staining probes such as propidium iodide or DAPI to separate apoptotic cells from healthy ones that externalize PS due to the activation of a scramblase. These assays are essential to determine if a protein is associated with scrambling in cells, and indeed enabled the identification of both TMEM16 and Xkr proteins as scramblases [5, 21]. However, these cell-based approaches provide only limited information about the activation mechanisms of the scramblases, on their transport kinetics and lipid specificity. Further, results from these assays leave a degree of ambiguity as to whether the identified proteins directly mediate lipid scrambling, or if they are indirect activators of other endogenous scramblases [22]. In vitro measurements of lipid scrambling using purified and reconstituted proteins circumvent these pitfalls and provide complementary information to that obtained from cell-based assays. The main advantages of in vitro assays are a near-complete control over the experimental system via the choice of membrane lipid composition, of the intra- and extra-liposomal solutions, and that —in some cases— they enable measurement of the kinetics of lipid transport [9, 23–25]. This allows a thorough characterization of the biophysical properties of the scramblases, which is essential to understand their function and their role in cellular signaling functions. The main limitations of the in vitro measurements are the requirement for purified protein, the lack of knowledge of the orientation of the reconstituted molecules in the liposomal membrane, and the use of non-native lipids due to the need for fluorescence to track their movement between leaflets. Recent advances in protein purification techniques have enabled the purification of several mammalian scramblases [9, 10], thus reducing the first hurdle, and some

reconstitution approaches result in a preferential mode of protein incorporation in the membrane, diminishing the caveats associated with the second limitation [26]. Finally, it is important to carry out extensive controls to ensure that the position and nature of the chemically modified lipids does not affect the observations [7].

Several in vitro assays to measure scrambling have been developed, most of which use fluorescent nitrobenzoxadiazole (NBD)-labeled lipids [7, 14, 27]. These assays quantify the fluorescent lipids in the outer leaflet of the liposomes by adding a membrane-impermeant reagent that chemically reduces the fluorophore (i.e., dithionite) or a lipid-extracting agent that quenches the fluorescence (i.e., BSA). Alternative assays using radiolabeled lipids have been developed to monitor transbilayer movement of natural lipids [28–31]. However, these approaches are generally limited in time resolution, require synthesis of radiolabeled lipids and, in some cases, the use of phospholipases to cleave the externalized radiolabels from the membrane. The most frequently used assay, which will be described here, utilizes the irreversible reduction of NBD by membrane-impermeant sodium dithionite. This assay has been used to characterize several TMEM16 scramblases as well as the secondary scramblase function of GPCRs [5–8, 12, 14–16, 21, 23].

In the absence of a scramblase protein, fluorescently labeled lipids distribute nearly evenly between liposomal membrane leaflets (Fig. 1a, top panel). Upon addition of an extra-liposomal reducing agent a ~50% decrease of fluorescence is expected [7, 14]. In the presence of an active scramblase, there is rapid and bidirectional movement of lipids between leaflets (Fig. 1a, lower panel). Thus, under the assumption that fluorescently labeled lipids are transported as well as unlabeled lipids, a ~100% loss in fluorescence is expected as all fluorophore-conjugated lipids are reduced (Fig. 1a, lower panel). The time constant associated with the chemical reduction of free NBD in solution by dithionite is fast, <1 s [7, 23]. However, the proximity of the fluorophore to the lipid membrane slows the reaction to ~10–30 s, depending on the lipid used and on whether the NBD label is conjugated to the head or the tail of the lipid. This enables the extraction of kinetic information on scrambling processes that occur on time scales comparable to or slower than the time constant of the chemical reduction [7, 23]. It is important to note that the fluorescence decay after dithionite in proteoliposomes containing a scramblase does not generally reach 0, but rather plateaus at a finite value. This reflects the fact that a fraction of the vesicles is refractory to protein reconstitution and/or are multilamellar, and therefore not accessible to the dithionite [7, 14, 23, 24, 32].

The TMEM16 scramblases also function as nonselective ion channels [7, 32] [20] [11], and some TMEM16 homologs function as bona fide Ca^{2+}-activated, Cl^- selective channels [33–35]. The physiological role of the nonselective ion channel activity

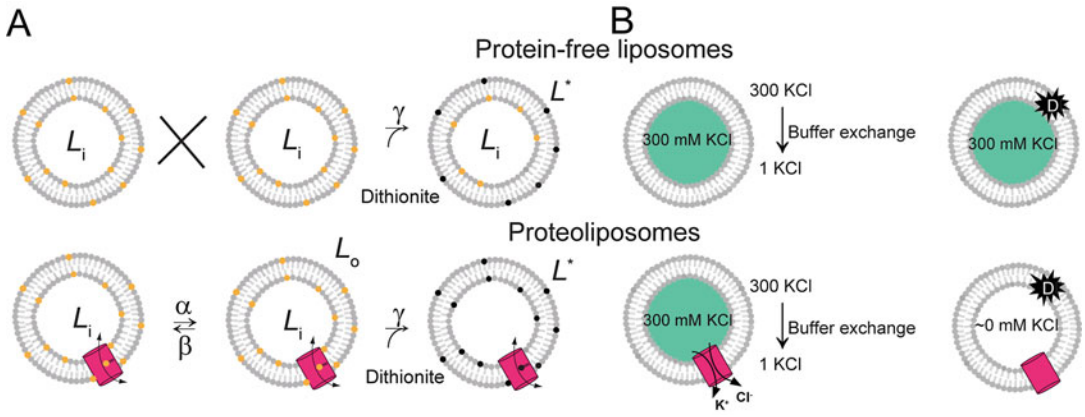

Fig. 1 Schematic of phospholipid scrambling and ion flux assays. (**a**) Schematic of the in vitro scramblase assay. Liposomes are reconstituted with NBD-labeled phospholipids (orange) that distribute equally in the two leaflets. Addition of extraliposomal sodium dithionite reduces the NBD fluorophore (black), causing 50% fluorescence loss in protein-free vesicles (top panel). When a scramblase is present (bottom panel), all NBD-phospholipids become exposed to dithionite, resulting in complete loss of fluorescence [7]. (**b**) Schematic of in vitro flux assay. Liposomes with high internal KCl concentration (300 mM) are buffer exchanged into low (1 mM) external KCl. In the absence of a scramblase (top panels), the KCl gradient is maintained after buffer exchange. The addition of dithionite (∗D) disrupts the liposomes and releases the remaining KCl which can be measured with a AgCl electrode. In the presence of an active nonselective channel (bottom panels), the KCl gradient is lost following buffer exchange due to ion flux. The addition of dithionite (*D) disrupts the liposomes and the remaining KCl is released which is measured with a AgCl electrode

of the TMEM16 scramblases is unknown. Initially, it was hypothesized that nonspecific ion transport was a by-product of scrambling, as ions and lipids might traverse the membrane through a proteolipidic pore [36, 37]. However, the identification of mutations that interconvert TMEM16 proteins between scramblases and Cl^- channels [20, 37], as well as scramblase mutants that affect only lipid scrambling but not ion transport, and vice versa [24], suggested this might not be the case. Indeed, recent structural work on the TMEM16A Cl^- channel and on the nhTMEM16 scramblase shows that these proteins form a protein-delimited pore [38–41]. In cells, the ion channel activity of the TMEM16 scramblases can be readily assayed using the patch clamp technique [10, 20, 37, 42]. However, in liposomes the nonselective nature of the TMEM16 scramblase/channels has only been measured using an end-point ion flux assay [7, 23, 24, 32]. In this assay, proteoliposomes are buffer exchanged from high external KCl to low KCl and the trapped internal Cl^- is measured using a Cl^- electrode following disruption of the liposomes with detergent. Only liposomes containing at least one active non-selective channel will lose their chloride content during the buffer exchange step. Thus, the ratio of the Cl^- trapped in TMEM16 proteoliposomes to that trapped in protein-free vesicles reflects the fraction of vesicles containing at

least one active channel. The assay is robust and sensitive enough to determine whether the reconstituted protein has nonselective channel activity. However, as an endpoint measurement, it provides no kinetic information. Thus, it can underestimate the effects of various manipulations (i.e. mutations and/or changes in ligand concentration) on the ion transport activity of the scramblase [7, 24]. Together, the scrambling and flux assays have been used to extensively characterize the TMEM16 scramblases contributing significantly to our understanding of both functions of these proteins [7, 23–25, 32]. Here, we provide a step-by-step description of scrambling and flux assays, including the details of liposome preparation, and of how to analyze the resulting data.

2 Materials

Prepare all solutions using deionized ultrapure water.

2.1 Liposome Reconstitution

1. 10 M KOH (50 mL).
2. 1 M HEPES pH 7.4 (1 L).
3. 2 M KCl (1 L).
4. Reconstitution buffer, 50 mM HEPES pH 7.4, 300 mM KCl, 50 mL: Add 2.5 mL of 1 M HEPES pH 7.4 stock and 7.5 mL of 2 M KCl to graduated cylinder. Bring volume up to 50 mL. Mix and store at room temperature.
5. 20 mg/mL phospholipid stocks in chloroform: adjust concentration of purchased stock to 20 mg/mL using chloroform or dissolved powdered lipids in chloroform.
6. 1 mg/mL NBD-labeled lipid stock in chloroform: adjust concentration of purchased stock to 1 mg/mL using chloroform or dissolved powdered lipids in chloroform.
7. Bio-Beads™ SM-2 Resin.
8. (3-((3-cholamidopropyl) dimethylammonio)-1-propanesulfonate) (CHAPS) powder.
9. Water-bath sonicator.
10. 4× Laemmli Sample Buffer (Bio-Rad).

2.2 Scrambling Assay

1. 1 M $Ca(NO_3)_2$ (50 mL).
2. 0.5 mL ethylene glycol-bis(β-aminoethyl ether)-*N*,*N*,*N*′,*N*′-tetraacetic acid (EGTA) pH 7.4 (50 mL): Add 25 mL H_2O to a beaker with a magnetic stirbar. Add 9.5 g of EGTA and mix on magnetic stirplate. Using a pH meter, slowly add in 10 M KOH to facilitate the dissolving until the final pH is 7.4. When the solid is dissolved and the pH is at 7.4. Bring volume up to 50 mL with H_2O. Filter and store at room temperature.

3. Assay Buffer +Ca^{2+}, 50 mM HEPES pH 7.4, 300 mM KCl, 0.5 mM $Ca(NO_3)_2$, 50 mL: Add 2.5 mL of 1 M HEPES pH 7.4 stock, 7.5 mL of 2 M KCl, and 25 μL of 1 M $Ca(NO_3)_2$ stock to graduated cylinder. Bring volume up to 50 mL with H_2O. Mix and store at room temperature.
4. Assay Buffer +EGTA, 50 mM HEPES pH 7.4, 300 mM KCl, 2 mM EGTA, 50 mL: Add 2.5 mL of 1 M HEPES pH 7.4 stock, 7.5 mL of 2 M KCl, and 200 μL EGTA from 0.5 M stock to graduated cylinder. Bring volume up to 50 mL with H_2O. Mix and store at room temperature.
5. 1 M Tris–HCl pH 10 (50 mL)
6. Sodium dithionite aliquots: Weigh a 10 mg aliquot of sodium dithionite into a 1.5 mL Eppendorf tube for every experiment that will be completed. Store on ice. This should be done the day of the experiment.
7. Liposome Extruder and 400 nm membrane.
8. Fluorescence spectrophotometer and a computer with an appropriate acquisition software.
9. Magnetic stirplate for fluorescence spectrophotometer.
10. Fluorescence cuvettes.
11. Magnetic stirbar that fits inside fluorescence cuvette.

2.3 Ion Flux Assay

1. Extracellular Solution +Ca^{2+}, 1 mM KCl, 50 mM HEPES pH 7.4, 300 mM Na-glutamate, 0.5 mM $Ca(NO_3)_2$, 100 mL: Add 60 mL H_2O to a beaker with a magnetic stirbar. Add 5 mL of 1 M HEPES pH 7.5 stock, 50 μL of 2 M KCl stock, and 50 μL of 1 M $Ca(NO_3)_2$ stock. Add 5.6 g of Na-glutamate monohydrate and mix on magnetic stirplate. When solid is dissolved adjust pH to 7.4 using KOH. Use graduated cylinder to bring volume to 100 mL with H_2O. Store at room temperature.
2. Extracellular Solution +EGTA, 1 mM KCl, 50 mM HEPES pH 7.4, 300 mM Na-glutamate, 2 mM EGTA, 100 mL: Add 60 mL H_2O to a beaker with a magnetic stirbar. Add 5 mL of 1 M HEPES pH 7.5 stock, 50 μL of 2 M KCl stock, and 400 μL of 0.5 M EGTA stock. Add 5.6 g of Na-glutamate monohydrate and mix on magnetic stirplate. When solid is dissolved adjust pH to 7.4 using KOH. Use graduated cylinder to bring volume to 100 mL with H_2O. Store at room temperature.
3. G50 beads swelled with extracellular solutions: Weigh 0.6 mg of G50 for every 10 mL of resin desired and place in a 50 mL falcon tube. Add extracellular solution up to desired volume. Rotate overnight (at least 4 h) at room temperature.
4. 100 mM KCl stock (50 mL).

5. 10 mM KCl stock (50 mL).
6. Agar bridges (100 mM KCl and 2% Agarose) stored in 100 mL KCl.
7. 1.5 M Octyl-beta-Glucoside (5 mL): Add 2.2 g of octyl-beta-glucoside to a 15 mL falcon tube with 2 mL of H_2O. Incubate at 37 °C for 10 min. When solid is dissolved, ensure the volume is 5 mL. The solution will be very viscous.
8. Thermo IEC Centra CL2 centrifuge.
9. Saturated solution of $FeCl_3$ or bleach.
10. Two chamber recording setup with flat-bottomed cylinders, ~3–4 mL volume secured on a magnetic stirplate.
11. A magnetic stirbar that fits inside the sample chambers.
12. AgCl electrode.
13. pH meter with an analog or digital electrical output.
14. A digitizer.
15. A computer with an appropriate acquisition software.

3 Methods

3.1 Preparation of Bio-Beads for Both Assays

1. Use 150 mg/mL Bio-Beads™ SM-2 Resin for each condition for each incubation. For lipid compositions with melting temperatures near room temperature complete four incubations. For lipid compositions with melting temperatures around or below 4 °C complete five incubations.
2. Weigh the desired amount of biobeads and add to a new 50 mL falcon tube.
3. Add 30 mL of methanol and rotate at room temperature for 20 min.
4. Let the biobeads settle and pour off the methanol, add 50 mL of H_2O, and rotate at room temperature for 20 min.
5. Let the biobeads settle and pour off the water, add another 50 mL of H_2O, and rotate at room temperature for 20 min.
6. Let the biobeads settle and pour off the H_2O, add 30 mL of reconstitution buffer, and rotate at room temperature for 20 min.
7. Let the biobeads settle, pour off the buffer and use a pipette to remove additional liquid.
8. Weigh the necessary amount of biobeads for each incubation into 2 mL Eppendorf tubes.

3.2 Lipid Preparation

For the scrambling assay, prepare a starting volume of 200 μL of 20 mg/mL lipids per condition (i.e., protein-free, with protein +/− ligand). For the flux assay, prepare a starting volume of 500 μL of 20 mg/mL lipids per condition. For both assays, always include a protein-free condition for each reconstitution.

1. Mix the desired chloroform-dissolved lipids together in glass tubes and dry under a stream of compressed nitrogen. For the scrambling assay, add 1% w/w of the desired NBD-labeled lipid (*see* **Note 1**).
2. Add an equal volume of pentane to the dried lipid film, gently resuspend the lipids and dry again under a stream of compressed nitrogen while rotating the tube to form a uniform lipid film on the bottom of the tube.
3. When all pentane has evaporated, add solid CHAPS to the dried lipid film to a concentration of 35 mM according to the final desired volume.
4. Add the desired reconstitution buffer volume (no more than 500 μL) taking care to wash down all the CHAPS on the sides of the tube (*see* **Note 2**).
5. Incubate for 20 min at room temperature to dissolve CHAPS.
6. Sonicate using bath sonicator until lipids are completely solubilized producing a clear and transparent solution (*see* **Note 3**).
7. When solution is clear, bring the volume up to final desired volume for 20 mg/mL lipids using reconstitution buffer.
8. Separate the lipids for each condition (i.e., protein-free and protein-containing).
9. Add the protein at desired ratio (for TMEM16's we use 5 μg protein/mg lipid).
10. Incubate at room temperature for 20 min.
11. Add lipids to 2 mL Eppendorf tubes with pre-weighed biobeads. Place individual tubes into a 50 mL falcon tube and incubate on a rotator for 2 h at 4 °C.
12. After 2 h, briefly spin down the individual tubes and transfer the lipids into the next tube of pre-weighed biobeads. Remove 15 μL of liposomes for SDS-PAGE analysis. Repeat 2-h incubation at 4 °C.
13. Change biobeads again after 2 h and rotate overnight (12–14 h) at 4 °C (*see* **Note 4**).
14. After the overnight incubation, change the biobeads one or two more times depending on the lipid composition (see bio-bead preparation section).

15. After the final incubation, remove the liposomes from the biobeads and transfer into glass tubes. Solution should be slightly cloudy. Remove 15 μL of liposomes for SDS-PAGE analysis.
16. Freeze at −80 °C if not using immediately.

3.3 Analysis of Reconstitution Efficiency Using SDS-PAGE

1. Remove 15 μL of liposomes from reconstitution as described above. Store at −80 °C without SDS loading dye until running the gel.
2. Thaw samples before use.
3. Add 5 μL of 4× SDS loading dye.
4. Run the SDS-PAGE gel as any other gel (*see* **Note 5**).

3.4 Freeze and Thaw Cycles to Introduce Ligand to the Inside of the Liposomes

1. Thaw liposomes if they are frozen.
2. Measure the volume of each condition. Loss of 10–30% of the starting volume is normal.
3. Add the desired amount of ligand according to the measured volume (i.e., Ca^{2+} or EGTA).
4. Sonicate liposomes for 2–3 s.
5. Flash freeze in liquid nitrogen.
6. Leave at room temperature to thaw.
7. Repeat 4–6.
8. Flash freeze (without sonicating) in liquid nitrogen for a third time.
9. Store at −80 °C until use and then thaw on ice.

3.5 Phospholipid Scrambling Assay

1. Set up the fluorometer to collect a 1200 s time-course with excitation at 470 nm and emission at 530 nm.
2. Thaw liposomes on ice if they are frozen.
3. Extrude the liposomes 21 times using 400 nm membrane (*see* **Note 6** and **7**).
4. Store the extruded liposomes at room temperature.
5. Add 1.98 mL of assay buffer to the cuvette with a stirbar.
6. Add 20 μL of extruded liposomes to the cuvette.
7. Start recording the fluorescence signal.
8. Add 60 μL of the 1 M Tris pH 10 stock to one aliquot of solid sodium dithionite and dissolve by vortexing.
9. At $t = 100$ s of the fluorescence recording, add 40 μL of the dithionite solution into the cuvette while still recording (*see* **Note 8**).
10. Record the fluorescence decay until the signal plateaus or for ~20 min.
11. After each experiment wash the cuvette and stirbar with water.

3.6 Quantification of Scrambling Activity

The scrambling assay described above can be utilized to extract detailed mechanistic information on the activity of the reconstituted protein. This information is contained in the steady-state level at which the fluorescence decay plateaus after dithionite addition and in the kinetics of the decay itself. Two analysis approaches have been used to extract mechanistic information: monitoring changes in the fluorescence at a fixed time point or analysis of the full-time course of fluorescence decay.

3.6.1 Approach 1: Fixed Time Fluorescence

When scrambling is fast compared to the rate of chemical reduction of the fluorophores, the kinetics of scrambling cannot be separated from those of the chemical reduction [7, 14, 23]. Therefore, the plateau value of the fluorescence decay is the only functional readout of the scrambling activity of the reconstituted proteins [7, 14, 15] as it directly reflects the fraction of liposomes containing at least one active scramblase. Indeed, when determined at various protein reconstitution densities, it can be used to determine the stoichiometry of the active scramblase complex [7, 15, 43]. However, the dynamic range of the signal associated with these changes is small; in ideal conditions, the maximal reduction is 50% of the total fluorescence, but in practice the range is ~30–40% due to the presence of liposomes lacking protein (Fig. 2a). This, together with the intrinsic variability of the plateau level, reduces the available range of the signal, potentially obfuscating the effects of changes in ligand concentrations or mutations that do not cause complete loss-of-function. To obviate—in part—these limitations, it is useful to consider the drop in fluorescence at a fixed time point when all lipids on the external leaflet have been reduced, which is $t = 3\tau$, where τ is the time constant of the decay in protein-free liposomes. This also allows to partially capture the effects of manipulations that reduce the rate of scrambling but not the final plateau [7, 10, 32, 44].

1. Normalize the trace to the fluorescence value at $t = 90$–95 s (right before the addition of dithionite).
2. Fit the normalized fluorescence decay of the protein-free liposomes to a single exponential function and determine the time constant.
3. Determine the normalized fluorescence value at $t = 3*\tau$ from the protein-containing traces and from the protein-free liposomes.
4. The relative change in fluorescence, ΔF, can be determined as the ratio of the change in a given condition, $\Delta F^* = F_{PF}(t = 3\tau) - F^*(t = 3\tau)$, to that measured in conditions of maximal activity, $\Delta F_{Max} = F_{PF}(t = 3\tau)$- $F_{Max}(t = 3\tau)$, where $F_{PF}(t = 3\tau)$ is the fluorescence value at $t = 3\tau$ measured in protein-free liposomes, and $F^*(t = 3\tau)$ and $F_{Max}(t = 3\tau)$,

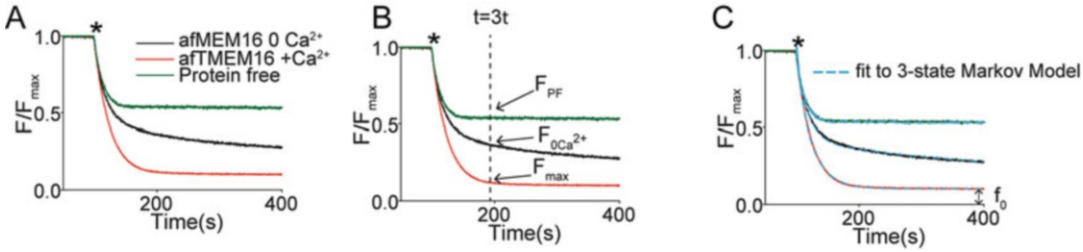

Fig. 2 Methods to analyze scrambling assay traces. (**a**) Normalized fluorescence decay from protein-free liposomes (green) and scramblase proteoliposomes (red, $+Ca^{2+}$ and black, 0 Ca^{2+}). * indicates the addition of dithionite to the extracellular solution. (**b**) Fixed point method of analyzing scrambling assay traces. The dashed line indicates $t = 3\tau$ and arrows point to the fluorescence values (F_{PF}, F_{0Ca2+} and F_{max}) used for the analysis (Eq. 1). For the traces in this example, $F_{PF} = 0.53F_{0Ca^{2+}} = 0.4$ and $F_{max} = 0.14$ so $\Delta F = 33\%$, indicating that removal of Ca^{2+} causes a 66% decrease in scrambling activity. (**c**) Normalized fluorescence decays fit (blue) to Eqs. 2 and 3 for scramblase proteoliposomes and protein-free vesicles, respectively. The fit of the fluorescence decay of protein-free liposomes determines L_i^{PF} and γ while that of the proteoliposomes determines f_0, α, and β. Arrows below the red trace denote f_0. Note the gain in dynamical range with the rate constant analysis. For the traces in this example, $f_0(+Ca^{2+}) = 0.2$, $\alpha(+Ca^{2+}) \sim \beta(+Ca^{2+}) \sim 0.1\ s^{-1}$, while $\alpha(0\ Ca^{2+}) \sim \beta(0\ Ca^{2+}) \sim 0.001\ s^{-1}$ and $f_0(0\ Ca^{2+})$ was constrained to be equal to the value in $+Ca^{2+}$, after verifying that the reconstitution efficiency is the same in the two conditions. Note that by fitting the complete trace to Eq. 2 the decrease in activity is ~100-fold, which reflects the dramatic slowdown of the scrambling process visible in the raw data

respectively, are the fluorescence values measured at $t = 3\tau$ for the experimental condition

$$\Delta F = \frac{100 \cdot \Delta F(t = 3\tau)}{\Delta F_{\mathrm{Max}}(t = 3\tau)} = \frac{100 \cdot (F_{\mathrm{PF}}(t = 3\tau) - F(t = 3\tau))}{F_{\mathrm{PF}}(t = 3\tau) - F_{\mathrm{Max}}(t = 3\tau)} \quad (1)$$

3.6.2 Approach 2: Analysis of the Kinetics of Fluorescence Decay

In conditions where the kinetics of scrambling are distinguishable from those of the NBD chemical reduction, the time course of fluorescence decay can be analyzed to determine the macroscopic rates of scrambling. Below we detail the analysis procedure as well as the main assumptions and limitations of the approach [23].

The time course of fluorescence decay after dithionite addition to a population of liposomes containing a scramblase is described by a three-state Markov model (Fig. 1a)

$$L_i \underset{\beta}{\overset{\alpha}{\rightleftarrows}} L_o \xrightarrow{\gamma} L^*$$

where L_i are fluorescent lipids in the inner leaflet, L_o are fluorescent lipids in the outer leaflet, L^* are the fluorescent lipids that were irreversibly reduced by sodium dithionite, α and β are the forward and reverse macroscopic rate constants of scrambling, and γ is the rate constant of dithionite reduction of NBD. It is important to note that α and β are macroscopic rate constants, reflecting the rate of lipid scrambling of a liposome. Therefore, α and β are the

product of the unitary rates of lipid transport (i.e., the conductance), of the number of active scramblases, and of the probability of the scramblase to be in a conductive conformation. This value depends on the number of active scramblase proteins reconstituted and on the number of liposomes. Since a fraction, $f_{0,}$ of liposomes is refractory to protein incorporation, the time course of fluorescence decay is described by the sum of three exponentials

$$F_{\text{tot}}(t) = f_0\left(L_i^{PF}(0) + \left(1 - L_i^{PF}(0)\right)e^{-\gamma t}\right) + \frac{(1-f_0)}{D(\alpha+\beta)} \times \left\{\alpha(\lambda_2+\gamma)(\lambda_1+\alpha+\beta)e^{\lambda_1 t} + \lambda_1\beta(\lambda_2+\alpha+\beta+\gamma)e^{\lambda_2 t}\right\} \quad (2)$$

where:

$$\lambda_1 = -\frac{(\alpha+\beta+\gamma) - \sqrt{(\alpha+\beta+\gamma)^2 - 4\alpha\gamma}}{2}$$

$$\lambda_2 = -\frac{(\alpha+\beta+\gamma) + \sqrt{(\alpha+\beta+\gamma)^2 - 4\alpha\gamma}}{2}$$

and

$$D = (\lambda_1+\alpha)(\lambda_2+\beta+\gamma) - \alpha\beta$$

where L_i^{PF} is the fraction of fluorescent lipids on the extracellular leaflet in protein-free liposomes. Importantly, L_i^{PF} and γ are experimentally determined by fitting the fluorescence decay of protein-free liposomes to:

$$F_{\text{PF}}(t) = L_i^{PF}(0) + \left(1 - L_i^{PF}(0)\right)e^{-\gamma t} \quad (3)$$

1. Measure scrambling in protein-free liposomes and in proteoliposomes prepared in the desired conditions.
2. Normalize the trace to the fluorescence value at $t = 90$–95 s (right before the addition of dithionite).
3. Fit the protein-free fluorescence decay to Eq. 3 to determine L_i^{PF} and γ.
4. Determine α, β, and f_0 by fitting the fluorescence decay of proteoliposomes to Eq. 1, with L_i^{PF} *and* γ constrained to the values determined above.

The value of f_0 corresponds to the fraction of protein-free liposomes or inaccessible to dithionite. This parameter is affected by the variability of the reconstitution efficiency of the protein into liposomes, and changes in f_0 affect the estimates of α, β. Thus, to compare the effects of different manipulations on the protein (i.e., +/− ligand or WT vs. mutant) on α, β it is necessary to ensure that

the efficiency of reconstitutions across the different conditions is comparable, as evaluated by the gels (see above). If this is the case, then the best procedure is to first determine f_0 for the WT protein in conditions of maximal activity, f_0(WT), and fix the f_0 values of the other conditions to f_0(WT). For example, for the Ca^{2+}-activated TMEM16 scramblases, the positive standard is the $+Ca^{2+}$ condition. To determine the rates in the absence of Ca^{2+} or of a mutant, the f_0 is constrained to the value of the WT protein in $+Ca^{2+}$ from the same reconstitution.

3.7 Flux Assay

3.7.1 Preparation of the Set-up

1. Strip the previous AgCl coating of the silver electrode with a razor blade.
2. Incubate the electrode in the saturated ferric chloride solution for 1 min.
3. Rinse with H_2O.
4. Place the electrode into the holder above the sample chamber and position the reference and sample electrodes into the appropriate chambers.
5. Add 100 mM KCl to the reference chamber, with enough to cover the end of the reference electrode.
6. Add 1.8 mL of extracellular solution to the sample chamber with a stirbar.
7. Connect the two chambers with the agar bridge by placing one end in each chamber. Ensure that the tip of the electrode and the ends of the agar bridges are inside the solution.
8. Start recording the voltage from the electrode.
9. To calibrate, add 18 μL of 10 mM KCl to the sample chamber and note the change in voltage.
10. Complete two more additions and 18 μL of 10 mM KCl noting the voltage each time.
11. Then complete three additions of 18 μL of 100 mM KCl noting the voltage each time.
12. Save the calibrations to the experimental record.

3.7.2 Preparation of the G-50 columns

13. Prepare one G50 column for each sample by adding 3 mL of swelled G-50 resin to a 5 mL column with filter.
14. Remove excess buffer by centrifuging for 5 s at 5000 rpm using a Thermo IEC Centra CL2 centrifuge 2–3 times.

3.7.3 Preparation of liposomes

15. Thaw liposomes on ice if they are frozen.
16. Extrude the liposomes 21 times using 400 nm membrane (*see* **Note 6** and 7).
17. Store the extruded liposomes at room temperature.

3.7.4 Flux measurement

18. Add 100 μL of liposomes to a prepared G50 column and spin for 1 min at 2000 rpm using a Thermo IEC Centra CL2 centrifuge.
19. While the sample is spinning, start the recording and add 18 μL of 10 mM KCl to the sample chamber for calibration. Note the voltage change.
20. Add 200 μL of the flow-through from the G50 column into the sample chamber.
21. Note the remaining volume in the tube to determine how dilute the final sample was.
22. After ~30s, add 40 μL of 1.5 M octyl-beta-glucoside to disrupt the liposomes and release the trapped Cl^-. Note the voltage change.

3.8 Flux Assay Analysis

1. Export the trace file from an ASCII or text format and import it to the analysis program of choice.
2. Measure the voltage at the following points (Fig. 3):

   At the beginning of the recording (V_0);
   After addition of the calibrating pulse (V_{cal});
   After addition of the liposomes (V_{lipo});
   After addition of detergent (V_{tot});

3. Use the Nernst equation to determine the experimental value of $\alpha = \frac{RT}{zF}$ (*see* **Note 9**) as

$$\alpha = \frac{\Delta V_{cal}}{\ln\left(1 + \frac{Vol_{Cal}}{1800} \cdot \frac{[Cl]_{cal}}{[Cl]_{in}}\right)} \tag{4}$$

   where Vol_{Cal} is the volume of the calibration pulse in μL, 1800 is the chamber volume at the beginning of the experiment expressed in μL, $[Cl]_{cal,in}$ are the Cl^- concentrations of the calibration pulse and of the external buffer in mM and $\Delta V_{cal} = V_{cal} - V_0$ expressed in mV.

4. Calculate the Cl^- concentrations from the measured voltages as follows:

$$[Cl]_{lipo} = \left([Cl]_{in} + \frac{9}{1000}[Cl]_{cal}\right) e^{(V_{lipo} - V_{Cal})/\alpha} \tag{5}$$

$$[Cl]_{tot} = \Delta Cl_{lipo}\, e^{(V_{tot} - V_{lipo})/\alpha} \tag{6}$$

   so that the Cl^- content of the liposomes is

$$\Delta Cl = [Cl]_{tot} - [Cl]_{prot} \tag{7}$$

The factor 9/1000 comes from the dilution of the 18 μL calibration pulse into the 2000 μL final volume.

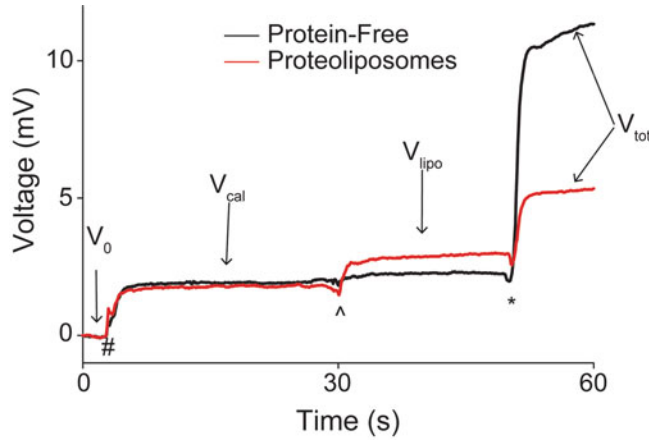

Fig. 3 Flux assay analysis. Raw trace for flux assay of protein-free liposomes (black) and proteoliposomes (red). Points needed for analysis are marked with arrows: V_0 is the beginning of the trace and measures the buffer before calibration; V_{cal} is measured after the addition of 18 μL of 10 mM KCl to calibrate the system (indicated by #); V_{lipo} is measured after the addition of liposomes (indicated by ^) and V_{tot} is the signal after the addition of detergent (indicated by *). This is the measure of the trapped Cl^- from inside the liposomes. For the traces in this example, ΔCl(Protein-free) =0.49 mM, and ΔCl(Proteoliposomes) = 0.16 mM, so that $A = 0.67$, indicating that ~67% of the liposomes contain at least one active nonselective channel

5. Calculate the channel activity of the sample, A, as the percentage of liposomes containing at least one active nonselective channel using the following equation:

$$A = \left(1 - \frac{\Delta Cl_{prot}}{\Delta Cl_{PF}}\right) 100 \tag{8}$$

where $\Delta Cl_{prot,PF}$ are, respectively, the chloride content of the proteoliposomes and of the protein-free vesicles.

4 Notes

1. It is helpful for sonication and lipid resuspension to separate lipids into tubes with no more than 2 mL of lipids. For example, if you need 4 mL of lipids, it is easier to prepare 2 tubes with 2 mL each rather than one tube with 4 mL.
2. Sonication is more effective with smaller volumes. It is best to resuspend the lipids and CHAPS in no more than 500 μL of buffer and bring the lipids to the final volume after they are resuspended. Of course, if your desired volume is less than 500 μL, then add the entire desired volume.

3. If lipids do not become clear with sonication alone, cycles of sonication and freezing and thawing can be helpful.
4. For lipid compositions with melting temperatures around room temperature (particularly POPE:POPG mixtures), it is very important to be strict with the incubation times. Leaving the liposomes longer (i.e., 15 h) results in a loss of protein from the liposomes.
5. To monitor the reconstitution efficiency and incorporation of the protein of interest, we use SDS-PAGE analysis of samples taken throughout the reconstitution (after the first incubation with biobeads and from the final sample before extrusion, see steps 12 and 15 above). This confirms that the protein was not lost during the reconstitution and is important for situations where a mutation or a ligand might result in reduced activity. Knowing the reconstitution efficiency is also important for the rate analysis as discussed later. In general, it is advisable to compare the intensity of the bands using densitometry [15]. This is of critical importance for samples with low protein-to-lipid ratios, as changes in the reconstitution efficiency can lead to large changes in the number of proteins inserted in each vesicle and in the total fraction of protein-free liposomes. At high protein-to-lipid ratios each liposome contains multiple copies of the reconstituted protein; a qualitative estimate of reconstitution efficiency can suffice, as small changes in the number of proteins per liposomes will not significantly affect the estimates of the kinetic parameters [39]. Adding SDS-loading dye to liposomes will make the solution viscous; ensure that care is taken when handling the sample and loading the gel.
6. For liposomes with melting temperatures around room temperature, they are likely to be in a gel phase after thawing on ice. Before extruding warm them by vortexing briefly or using your hands. This ensures that the gel material is not left inside the tube.
7. The number of times extruded must be odd so that you collect the extruded liposomes in the opposite syringe from which you loaded the sample.
8. It is important to have a fluorometer where solutions can be added without opening the lid to ensure recording of the initial kinetic information of the fluorescence decay after dithionite addition.
9. The empirical determination of α serves three purposes: it ensures that the system is responding properly, it offers a measure of the consistency of the instrument's response between experiments, and it is a check that no mistakes were made in the solution making.

Acknowledgement

The authors thank members of the Accardi lab for helpful discussions. This work was supported by NIH Grant R01GM106717 (to A.A.). M.E.F. is the recipient of a Weill Cornell Medicine Margaret & Herman Sokol Fellowship.

References

1. Pomorski T, Menon AK (2006) Lipid flippases and their biological functions. Cell Mol Life Sci 63(24):2908–2921
2. Bevers EM, Williamson PL (2016) Getting to the outer leaflet: physiology of Phosphatidylserine exposure at the plasma membrane. Physiol Rev 96(2):605–645. https://doi.org/10.1152/physrev.00020.2015
3. Kodigepalli KM, Bowers K, Sharp A, Nanjundan M (2015) Roles and regulation of phospholipid scramblases. FEBS Lett 589(1):3–14. https://doi.org/10.1016/j.febslet.2014.11.036
4. Nagata S, Suzuki J, Segawa K, Fujii T (2016) Exposure of phosphatidylserine on the cell surface. Cell Death Differ 23(6):952–961. https://doi.org/10.1038/cdd.2016.7
5. Suzuki J, Umeda M, Sims PJ, Nagata S (2010) Calcium-dependent phospholipid scrambling by TMEM16F. Nature 468:834–838
6. Suzuki J, Fujii T, Imao T, Ishihara K, Kuba H, Nagata S (2013) Calcium-dependent phospholipid scramblase activity of TMEM16 protein family members. J Biol Chem 288 (19):13305–13316. https://doi.org/10.1074/jbc.M113.457937
7. Malvezzi M, Chalat M, Janjusevic R, Picollo A, Terashima H, Menon AK, Accardi A (2013) Ca^{2+}-dependent phospholipid scrambling by a reconstituted TMEM16 ion channel. Nat Commun 4. https://doi.org/10.1038/ncomms3367
8. Brunner JD, Lim NK, Schenck S, Duerst A, Dutzler R (2014) X-ray structure of a calcium-activated TMEM16 lipid scramblase. Nature 516(7530):207–212
9. Bushell SR, Pike ACW, Falzone ME, Rorsman NJG, Ta CM, Corey RA, Newport TD, Shintre CA, Tessitore A, Chu A, Wang Q, Shrestha L, Mukhopadhyay S, Love JD, Burgess-Brown NA, Sitsapesan R, Stansfeld PJ, Huiskonen JT, Tommaro P, Accardi A, Carpenter EP (2019) The structural basis of lipid scrambling and inactivation in the endoplasmic reticulum scramblase TMEM16K. Nat Commun 10:3956. https://doi.org/10.1038/s41467-019-11753-1
10. Alvadia C, Lim NK, Clerico Mosina V, Oostergetel GT, Dutzler R, Paulino C (2019) Cryo-EM structures and functional characterization of the murine lipid scramblase TMEM16F. Elife 8:e44365. https://doi.org/10.7554/eLife.44365
11. Di Zanni E, Gradogna A, Scholz-Starke J, Boccaccio A (2017) Gain of function of TMEM16E/ANO5 scrambling activity caused by a mutation associated with gnathodiaphyseal dysplasia. Cell Mol Life Sci 75:1–14. https://doi.org/10.1007/s00018-017-2704-9
12. Suzuki J, Denning DP, Imanishi E, Horvitz HR, Nagata S (2013) Xk-related protein 8 and CED-8 promote phosphatidylserine exposure in apoptotic cells. Science 341 (6144):403–406
13. Suzuki J, Imanishi E, Nagata S (2016) Xkr8 phospholipid scrambling complex in apoptotic phosphatidylserine exposure. Proc Natl Acad Sci U S A 113(34):9509–9514
14. Menon I, Huber T, Sanyal S, Banerjee S, Barré P, Canis S, Warren JD, Hwa J, Sakmar TP, Menon AK (2011) Opsin is a phospholipid flippase. Curr Biol 21(2):149–153. https://doi.org/10.1016/j.cub.2010.12.031
15. Goren MA, Morizumi T, Menon I, Joseph JS, Dittman JS, Cherezov V, Stevens RC, Ernst OP, Menon AK (2014) Constitutive phospholipid scramblase activity of a G protein-coupled receptor. Nat Commun 5:5115. https://doi.org/10.1038/ncomms6115
16. Verchère A, Ou W-L, Ploier B, Morizumi T, Goren MA, Bütikofer P, Ernst OP, Khelashvili G, Menon AK (2017) Light-independent phospholipid scramblase activity of bacteriorhodopsin from Halobacterium salinarum. Sci Rep 7(1):9522–9522. https://doi.org/10.1038/s41598-017-09835-5
17. Kol MA, Van Laak ANC, Rijkers DTS, Antoinette Killian J, De Kroon AIPM, De Kruijff B (2003) Phospholipid flop induced by transmembrane peptides in model membranes is

modulated by lipid composition. Biochemistry 42(1):231–237. https://doi.org/10.1021/bi0268403

18. Mihajlovic M, Lazaridis T (2010) Antimicrobial peptides in Toroidal and cylindrical pores. Biochim Biophys Acta 1798(8):1485–1493. https://doi.org/10.1016/j.bbamem.2010.04.004
19. Ohmann A, Li C-Y, Maffeo C, Al Nahas K, Baumann KN, Göpfrich K, Yoo J, Keyser UF, Aksimentiev A (2018) A synthetic enzyme built from DNA flips 10(7) lipids per second in biological membranes. Nat Commun 9(1):2426–2426. https://doi.org/10.1038/s41467-018-04821-5
20. Yu K, Whitlock JM, Lee K, Ea O, Yuan Cui Y, Hartzell HC (2015) Identification of a lipid scrambling domain in ANO6/TMEM16F. Elife 4:1–23. https://doi.org/10.7554/eLife.06901
21. Suzuki J, Imanishi E, Nagata S (2014) Exposure of phosphatidylserine by Xk-related protein family members during apoptosis. J Biol Chem 289(44):30257–30267
22. Yang H, Kim A, David T, Palmer D, Jin T, Tien J, Huang F, Cheng T, Coughlin SR, Jan YN, Jan LY (2012) TMEM16F forms a Ca(2+)-activated Cation Channel required for lipid scrambling in platelets during blood coagulation. Cell 151(1):111–122
23. Malvezzi M, Andra KK, Pandey K, Lee B-C, Brown A, Iqbal R, Menon AK, Accardi A (2018) Out of the groove transport of lipids by TMEM16 and GPCR scramblases PNAS. doi:https://doi.org/10.1073/pnas.1806721115
24. Lee B-C, Khelashvili G, Falzone M, Menon AK, Weinstein H, Accardi A (2018) Gating mechanism of the extracellular entry to the lipid pathway in a TMEM16 scramblase. Nat Commun 9(1):3251. https://doi.org/10.1038/s41467-018-05724-1
25. Falzone ME, Rheinberger J, Lee B-C, Peyear T, Sasset L, Raczkowski AM, Eng ET, Di Lorenzo A, Andersen OS, Nimigean CM, Accardi A (2019) Structural basis of Ca^{2+}-dependent activation and lipid transport by a TMEM16 scramblase. Elife 8:e43229. doi: https://doi.org/10.7554/eLife.43229
26. Andra KK, Dorsey S, Royer C, Menon AK (2018) Structural mapping of fluorescently-tagged, functional nhTMEM16 scramblase in a lipid bilayer. J Biol Chem 293:12248. https://doi.org/10.1074/jbc.RA118.003648
27. Marx U, Lassmann G, Holzhutter HG, Wustner D, Muller P, Hohlig A, Kubelt J, Herrmann A (2000) Rapid flip-flop of phospholipids in endoplasmic reticulum membranes studied by a stopped-flow approach. Biophys J 78(5):2628–2640. https://doi.org/10.1016/S0006-3495(00)76807-X
28. Sanyal S, Frank CG, Menon AK (2008) Distinct flippases translocate glycerophospholipids and oligosaccharide diphosphate dolichols across the endoplasmic reticulum. Biochemistry 47:7937–7946
29. Sanyal S, Menon AK (2009) Specific transbilayer translocation of dolichol-linked oligosaccharides by an endoplasmic reticulum flippase. Proc Natl Acad Sci U S A 106(3):767–772
30. Sanyal S, Menon AK (2010) Stereoselective transbilayer translocation of mannosyl phosphoryl dolichol by an endoplasmic reticulum flippase. Proc Natl Acad Sci U S A 107:11289–11294
31. Wang L, Iwasaki Y, Andra KK, Pandey K, Menon AK, Bütikofer P (2018) Scrambling of natural and fluorescently tagged phosphatidylinositol by reconstituted G protein-coupled receptor and TMEM16 scramblases. J Biol Chem 293(47):18318–18327. https://doi.org/10.1074/jbc.RA118.004213
32. Lee B-C, Menon AK, Accardi A (2016) The nhTMEM16 Scramblase is also a nonselective Ion Channel. Biophys J 111(9):1919–1924. https://doi.org/10.1016/j.bpj.2016.09.032
33. Caputo A, Caci E, Ferrera L, Pedemonte N, Barsanti C, Sondo E, Pfeffer U, Ravazzolo R, Zegarra-Moran O, Galietta LJV (2008) TMEM16A, a membrane protein associated with calcium-dependent chloride channel activity. Science 322(5901):590–594. https://doi.org/10.1126/science.1163518
34. Yang YD, Cho H, Koo JY, Tak MH, Cho Y, Shim W-S, Park SP, Lee J, Lee B, Kim B-M, Raouf R, Shin YK, Oh U (2008) TMEM16A confers receptor-activated calcium-dependent chloride conductance. Nature 455(7217):1210–1215. https://doi.org/10.1038/nature07313
35. Schroeder BC, Cheng T, Jan YN, Jan LY (2008) Expression cloning of TMEM16A as a calcium-activated chloride channel subunit. Cell 134(6):11
36. Whitlock JM, Hartzell HC (2016) A pore idea: the ion conduction pathway of TMEM16/ANO proteins is composed partly of lipid. Pflugers Arch 468(3):455–473. https://doi.org/10.1007/s00424-015-1777-2
37. Jiang T, Yu K, Hartzell HC, Tajkhorshid E (2017) Lipids and ions traverse the membrane by the same physical pathway in the. Elife 16:1–26. https://doi.org/10.7554/eLife.28671

38. Paulino C, Neldner Y, Lam AKM, Kalienkova V, Brunner JD, Schenck S, Dutzler R (2017) Structural basis for anion conduction in the calcium-activated chloride channel TMEM16A. Elife 6:1–23. https://doi.org/10.7554/eLife.26232
39. Paulino C, Kalienkova V, Lam AKM, Neldner Y, Dutzler R (2017) Activation mechanism of the calcium-activated chloride channel TMEM16A revealed by cryo-EM. Nature 552 (7685):421–425. https://doi.org/10.1038/nature24652
40. Dang S, Feng S, Tien J, Peters CJ, Bulkley D, Lolicato M, Zhao J, Zuberbühler K, Ye W, Qi L, Chen T, Craik CS, Nung Jan Y, Minor DL Jr, Cheng Y, Yeh Jan L (2017) Cryo-EM structures of the TMEM16A calcium-activated chloride channel. Nature 552:426. https://doi.org/10.1038/nature25024
41. Khelashvili G, Falzone ME, Cheng X, Lee B-C, Accardi A, Weinstein H (2019) Dynamic modulation of the lipid translocation groove generates a conductive ion channel in Ca2+-bound nhTMEM16. Nat Commun 10(1):4972. https://doi.org/10.1038/s41467-019-12865-4
42. Scudieri P, Caci E, Venturini A, Sondo E, Pianigiani G, Marchetti C, Ravazzolo R, Pagani F, Galietta LJV (2015) Ion channel and lipid scramblase activity associated with expression of TMEM16F/ANO6 isoforms. J Physiol 59317(593):3829–384817. https://doi.org/10.1113/JP270691
43. Ploier B, Caro LN, Morizumi T, Pandey K, Pearring JN, Goren MA, Finnemann SC, Graumann J, Arshavsky VY, Dittman JS, Ernst OP, Menon AK (2016) Dimerization deficiency of enigmatic retinitis pigmentosa-linked rhodopsin mutants. Nat Commun 7:12832. https://doi.org/10.1038/ncomms12832
44. Kalienkova V, Clerico Mosina V, Bryner L, Oostergetel GT, Dutzler R, Paulino C (2019) Stepwise activation mechanism of the scramblase nhTMEM16 revealed by cryo-EM. Elife 8:e44364. https://doi.org/10.7554/eLife.44364

Chapter 16

Membrane Protein Cryo-EM: Cryo-Grid Optimization and Data Collection with Protein in Detergent

Magnus Bloch, Mònica Santiveri, and Nicholas M. I. Taylor

Abstract

Cryo-electron microscopy (cryo-EM) is a powerful tool for investigating the structure of macromolecules under near-native conditions. Especially in the context of membrane proteins, this technique has allowed researchers to obtain structural information at a previously unattainable level of detail. Specimen preparation remains the bottleneck of most cryo-EM research projects, with membrane proteins representing particularly challenging targets of investigation due to their universal requirement for detergents or other solubilizing agents. Here we describe preparation of negative staining and cryo-EM grids and downstream data collection of membrane proteins in detergent, by far the most common solubilization agent. This protocol outlines a quick and straightforward procedure for screening and determining the structure of a membrane protein of interest under biologically relevant conditions.

Key words Structural biology, Cryo-electron microscopy, Membrane protein, Detergent, Grid preparation, Negative staining, Vitrification, Data collection

1 Introduction

The development of cryo-EM as a technique for determining the structure of macromolecules began already in the 1970s, but only recently has the technique gained popularity with structural biologists. This is mainly due to technological advancements such as the development of direct electron detectors and sophisticated data analysis software, which has allowed for the determination of protein structures at near-atomic resolution (<4 Å) [1]. Cryo-EM represents an attractive alternative to X-ray crystallography, as it allows for structural investigation of proteins under near-native conditions without the need for crystallization. This becomes especially attractive in the context of membrane proteins, which are categorically difficult to crystallize.

Magnus Bloch and Mònica Santiveri contributed equally to this work.

Camilo Perez and Timm Maier (eds.), *Expression, Purification, and Structural Biology of Membrane Proteins*, Methods in Molecular Biology, vol. 2127, https://doi.org/10.1007/978-1-0716-0373-4_16,

Protein samples for analysis are ideally monodisperse and minimally heterogeneous, as determined by either PAGE or gel filtration. Additionally, negative staining grids are typically prepared prior to cryo-EM grids for a more detailed screening of sample quality. In negative staining, sample of a suitable concentration is applied to continuous carbon film grids, and after removal of excess sample, the grids are stained with a solution of a heavy metal salt such as uranyl acetate. The stain envelopes the sample molecules, which are visualized as negative densities in a suitable microscope, allowing for assessment of the dispersity and quality of the applied sample. This technique is particularly relevant when investigating membrane proteins, as preparation of samples of membrane proteins is generally an empirical discipline benefitting from rapid and reliable sample screening.

Structural investigation of any protein using cryo-EM involves preparation of a sufficiently pure, stable, and concentrated protein sample, which is then applied to a grid consisting of a mesh of metal, usually copper, supporting a thin, holey film typically made of carbon. The film can also be made of materials such as gold, or can be overlaid with another film made of graphene oxide, and may even be functionalized by modifying the film surface with a substance showing affinity for a target specimen, to allow for on-grid enrichment of the specimen [2]. Prior to sample application, the hydrophobic carbon film is rendered hydrophilic by glow discharging [3]. This process promotes a more even distribution of the sample on the grid, and favors embedding of sample molecules in solvent suspended within the film holes.

Immediately after sample application, excess sample is blotted away using filter paper and the grid plunged into liquid ethane. This plunging ensures rapid cooling of the sample, preventing the formation of crystalline ice. Instead, this rapid cooling facilitates vitrification of the aqueous sample, i.e., formation of a stable, amorphous, noncrystalline solid state, in which the protein molecules are safely and properly embedded [4].

Once grids have been prepared, the next step is screening them using a suitable microscope to determine conditions resulting in grids that will enable structure determination. Apart from sample quality, many factors affect the quality of the resulting grid, including grid type, blotting conditions, and method of sample application. Generally, thinner ice is achieved with smaller hole size [4] and more strict blotting parameters, and insufficient embedding of protein molecules in the film holes due to e.g. excessive adsorption to the carbon may be counteracted by multiple sequential sample applications.

Specimen preparation remains a major bottleneck in all cryo-EM research projects and structural investigation of membrane proteins is particularly a challenge as these must be extracted from their native lipid bilayer and kept stably in aqueous solution. The

most common approach to achieving this is the use of amphiphilic surfactant molecules known as detergents, which in aqueous solutions can form a collar around the hydrophobic transmembrane segment of membrane proteins shielding it from the surrounding hydrophilic environment. Depending on the solubilization conditions, detergent extraction may still preserve interactions of the membrane protein with its native lipids.

Detergents vary strongly in their physicochemical properties, which are often only defined for specific, controlled conditions, meaning that membrane protein solubilization using detergents is often very much an empirical discipline; a detergent that works well with one protein may work poorly with another, or may denature the target protein at higher concentrations, and a detergent suitable for extraction may not be suited for downstream purification and grid preparation. However, it is possible to outline some general principles and heuristics regarding the effects of detergents on membrane protein samples.

For instance, in principle a detergent must always be used at a concentration above its critical micelle concentration (CMC), as the detergent molecules otherwise do not form the micellar structures needed to accommodate the membrane protein. However, even at concentrations slightly above the CMC, excessive detergent molecules not associated with membrane protein may be present in the sample, which adversely affects the quality of the acquired micrographs. Generally, detergents with high CMCs such as *n*-octyl-ß-D-glucopyranoside (OG) give a background of detergent monomers, while use of detergents with low CMCs such as lauryl maltose neopentyl glycol (LMNG) usually results in a background of detergent micelles [5]. However, a detergent with a low k_{off} such as LMNG can remain stably bound to the protein even at sub-CMC concentrations, allowing the researcher to avoid a high background of empty micelles [6].

The most successful detergents used in high-resolution cryo-EM of membrane proteins appear to be mild detergents, such as *n*-dodecyl-β-D-maltopyranoside (DDM), octaethylene glycol monododecyl ether (C12E8), 7-cyclohexyl-1-heptyl-β-D-maltoside (CYMAL-7), and LMNG, which may be supplemented with various components such as cholesteryl hemisuccinate (CHS) that mimic the effects of native cholesterol molecules [7], or specific lipids such as 1-palmitoyl-2-oleoyl-sn-glycero-3-phosphocholine (POPC) [8] that may counteract potentially detrimental delipidation of the target membrane protein [9]. Digitonin is also widely and successfully used in high-resolution cryo-EM, but great care should be taken when handling this detergent, as it is toxic and poses a serious health risk if not handled properly. All of the detergents mentioned above are nonionic and considered to be mild and non-denaturing [10], but it may prove necessary in certain cases to resort to the use of ionic and zwitterionic detergents

such as CHAPSO [11] in order to obtain more efficient membrane extraction. Ionic and zwitterionic detergents are however considered to be denaturing and deactivating [10] and should thus be used with caution and preferably in combination with functional assays to assess the state of the solubilized membrane protein.

Apart from their direct effects on membrane proteins, detergents have the general effect of lowering the surface tension of the sample solvent, which makes it more difficult to obtain ice of suitable thickness during grid preparation [12]. In addition, detergents tend to form monolayers at the air-water interfaces of the grid, which along with the presence of free monomeric and micellar detergent molecules in the sample greatly increases the background scattering [13] (Fig. 1).

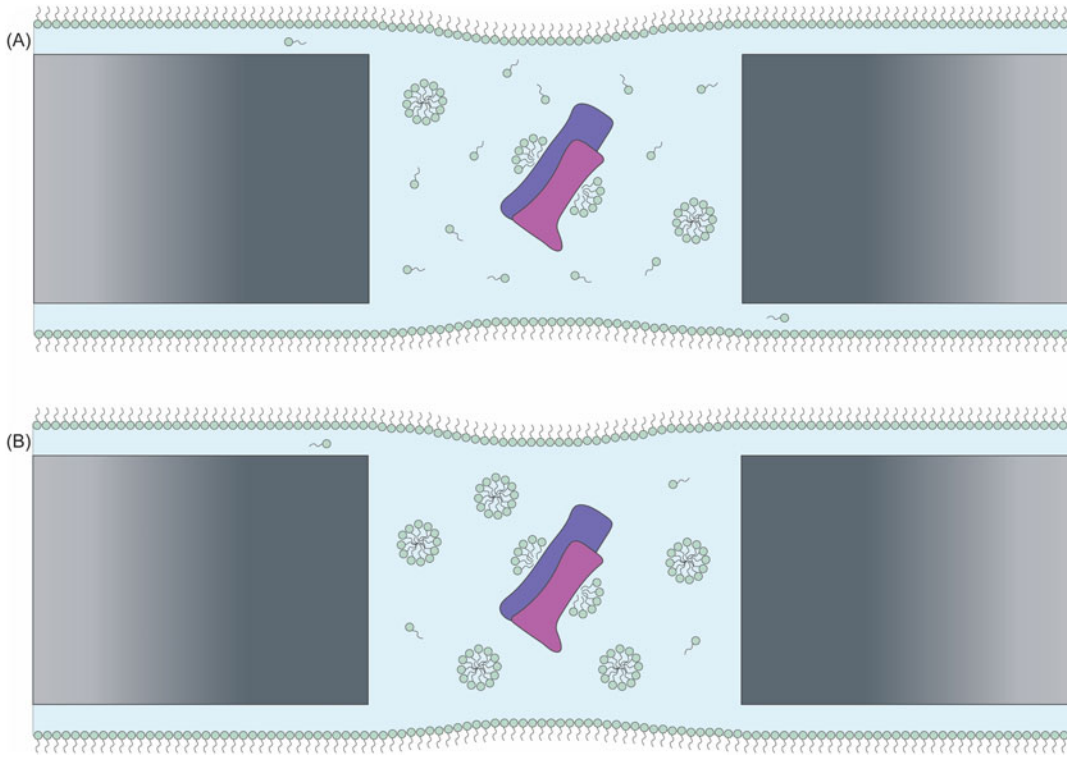

Fig. 1 *Schematic drawing of cryo-EM grids prepared using samples of a membrane protein complex in detergent*. Side view of cryo-EM grid films (dark gray rectangles) containing vitrified samples of a membrane protein complex (purple/pink mass) in detergent (light green). When a detergent with a high CMC is used (**a**) individual, free detergent molecules are more likely to exist as monomers, compared to when a detergent with a low CMC is used (**b**), where individual, free detergent molecules are more likely to be incorporated in micelles. Consequently, samples containing a detergent with a high CMC will usually result in grids with a background consisting mainly of detergent monomers, while samples containing a detergent with a low CMC will yield grids featuring many empty, background micelles. Note that in both cases (**a**, **b**), monolayers of detergent molecules form at the air-water interfaces of the grids, further adding to the background scattering (figure adapted from [13])

However, these solvent-modifying properties of detergents may also be turned into an advantage: For instance, fluorinated versions of detergents such as fos-choline-8 (FC-8) have been used to improve the distribution of solubilized membrane proteins in vitreous ice [14], and in fact detergents are routinely used for grid preparation of soluble proteins to avoid detrimental adsorption of protein molecules to the air-water interfaces, which can lead to protein denaturation and orientation bias [15]. While other strategies for extracting and reconstituting membrane proteins for structural studies exist, based on, e.g., amphipols, styrene-maleic acid copolymers (SMAs), and nanodiscs, detergents remain the most accessible and consequently most utilized tool for membrane protein solubilization and reconstitution.

This protocol provides a detailed description of important steps in the process of investigating membrane proteins in detergents by cryo-EM, including glow discharging, negative staining, and cryo-EM grid preparation. The process of data collection is briefly outlined to give the reader an idea of what lies beyond the bottleneck of specimen preparation.

2 Materials

It is assumed that a pure, stable, and sufficiently concentrated sample of membrane protein in a suitable detergent has been freshly prepared. Ideally, the sample has just eluted at a sufficiently high concentration as a monodisperse peak after gel filtration chromatography. For preparation of cryo-EM grids a good starting concentration is approximately 1 mg/ml, while a concentration of 0.01–0.03 mg/ml is sufficient for preparation of negative staining grids. It is recommended to clear the sample of any aggregation by high-speed centrifugation immediately prior to use and to keep the sample on ice at all times. Please refer to the figures of Subheading 3 for pictures of the required materials.

2.1 Glow Discharging of the Grid

1. Dual chamber CTA 010 glow discharger (Balzers Union).
2. Glass petri dish ($Ø < 10$ cm).
3. Whatman® filter paper, Grade 1.
4. Stainless steel Straight Style 0 Dumoxel- Tweezers (Dumont).
5. Suitable grids for either negative staining (e.g., Ted Pella Carbon Film, 200 mesh Cu) or cryo-EM (e.g., Quantifoil Holey Carbon Film, 200 mesh Cu).
6. Optical microscope (for distinguishing the film side) (optional).

2.2 Negative Staining Grid Preparation

1. Suitable, glow-discharged grids.
2. Membrane protein sample on ice.
3. Micropipette with tips.
4. Parafilm®.
5. Whatman® filter paper, Grade 1.
6. Stainless steel Negative-Action Style N5AC Dumoxel® Tweezers (Dumont).
7. Wash buffer or double-distilled water (ddH_2O) (for grid wash).
8. Staining solution (e.g., 2% uranyl acetate).
9. Grid storage box.
10. Loading station (optional).

2.3 Cryo-EM Grid Preparation

1. Suitable, glow-discharged grids.
2. Membrane protein sample on ice.
3. Micropipette with tips.
4. Vitrobot Mark IV cryo-plunger (FEI) with foot pedal.
5. ddH_2O (for humidifier).
6. Standard Vitrobot Filter Paper, Ø55/20 mm, Grade 595.
7. Vitrobot Plunge Tweezers assembly.
8. Metal tweezers.
9. Swissci Cryo-EM Grid-Box.
10. Styrofoam container.
11. Styrofoam cup assembly.
12. Suitable liquid nitrogen container (NB: liquid nitrogen can cause cryogenic burns and should only be used in well-ventilated areas).
13. Ethane gas flask with small hose fitted with pipette tip (NB: liquid ethane can cause cryogenic burns, whereas gaseous ethane is highly flammable and can form an explosive mixture with air).
14. Latex gloves and protective goggles.

2.4 Data Collection

For data collection, access to suitable transmission electron microscopes and support from trained personnel is required. Please refer to Subheading 3 for details.

3 Methods

3.1 Glow Discharging of the Grid

This section outlines a glow discharge procedure based on the use of a Balzers Union dual-chamber CTA 010 glow discharger, but

Fig. 2 *CTA 010 glow discharger and required materials.* Relevant elements are numbered: (1) Chamber metal lid, (2) glass vacuum chamber, (3) vacuum knob, (4) chamber knob, (5) pressure gauge, (6) timer, (7) current gauge, (8) voltage dial, (9) start button, (10) vent button, (11) petri dish with filter paper and grid, (12) metal tweezers, (13) grid box

other glow discharge devices may be used as well. Always refer to the manufacturer's protocol.

1. Using tweezers, gently transfer the grids to be glow discharged from their storage compartment to a piece of filter paper placed in a glass petri dish. Make sure not to damage the grids by only gripping the very edge of the grids with the tweezers. Make sure that the grids are placed with the film side facing up (*see* **Note 1**).
2. Once the grids are in place, gently place the petri dish inside one of the glass vacuum chambers (Fig. 2).
3. The chamber is closed by pushing and holding down the metal lid with one hand, while using the other to seal the chamber by turning the vacuum knob from "Closed" to "Open."
4. Depending on the chosen chamber, turn the chamber knob from "Off" to either "Left" or "Right." The vacuum pump now begins to evacuate the corresponding chamber. The chamber pressure can be monitored on the pressure gauge.
5. Set the timer to 30 s and the voltage to 185 V by turning the relevant dials.
6. Once the pressure gauge indicates a chamber pressure of ~0.1 mbar, press the start button to initiate the glow discharge.

A violet light should come on, and the current gauge indicates a current flow across the chamber.

7. Once the violet light turns off, switch the chamber knob to "Off," turn the vacuum knob to "Closed," and vent the vacuum chamber by gently tapping the vent button. Continue the venting until the pressure gauge indicates that the chamber pressure is once again atmospheric.
8. Gently lift off the metal lid and remove the petri dish with the glow-discharged grids from the vacuum chamber.

3.2 Negative Staining Grid Preparation

This section outlines a procedure for preparation of grids for negative staining EM.

Please note that only in the final step (**step 12**) should the grid be allowed to dry out completely.

1. Fix a 10 × 10 cm piece of parafilm in place on a clean surface.
2. Deposit three 50 μl droplets of wash buffer (*see* **Note 2**) or ddH_2O on the parafilm (Fig. 3).
3. Fold a piece of filter paper down the middle and fix it in place with one side being horizontal and the other being vertical (the latter is used for blotting).

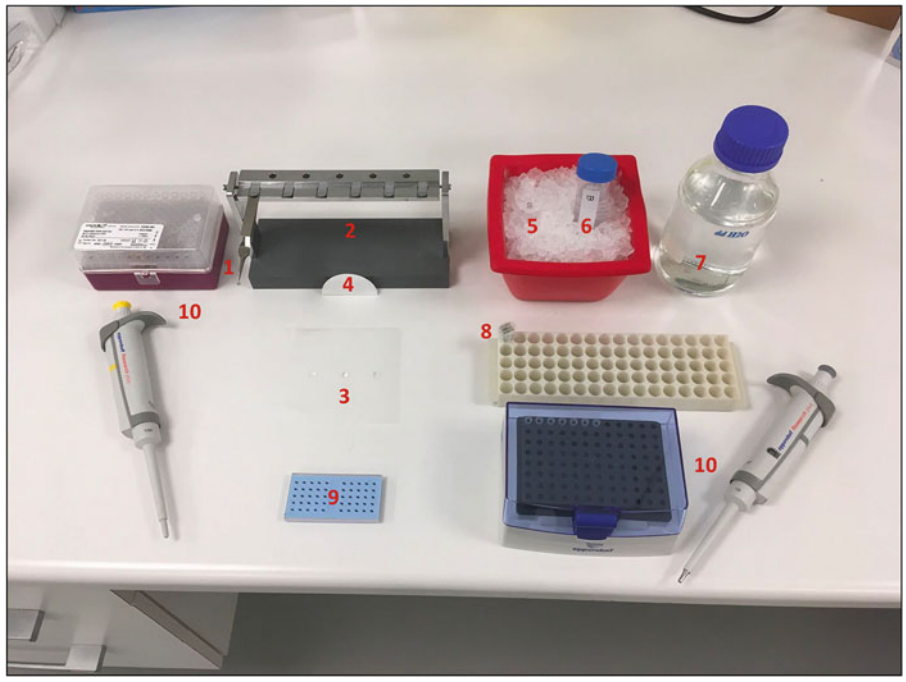

Fig. 3 Setup for preparation of negative staining grids. Relevant elements are numbered: (1) Metal tweezers with grid, (2) loading station, (3) parafilm with 50 μl droplets for grid wash, (4) filter paper, (5) membrane protein sample on ice, (6) wash buffer, (7) ddH_2O, (8) staining solution (2% uranyl acetate), (9) grid box (for storage), (10) micropipette and tips

4. Gripping only the very edge, a glow-discharged grid is picked up using the negative-action tweezers and the tweezers fixed in place on the loading station with the grid film side facing upwards (*see* **Note 3**).
5. Apply 3.5 μl sample on the film side of the grid (*see* **Note 4**). Wait for 60 s.
6. Pick up the tweezers and blot away excess sample by gently touching the side of the grid to the fixed filter paper until the grid is almost dry.
7. Immediately rotate the tweezers so that the grid film faces downwards and gently dip the film side of the grid into one of the droplets deposited on the parafilm while gently stirring. After a few seconds of stirring, move the grid out of the droplet, rotate the grid so that the film side faces upwards, and blot away excess wash liquid by gently touching the side of the grid to the fixed filter paper. This procedure is repeated for the remaining two droplets, and after washing the grid in the last droplet, the wash liquid is left on the film side of the grid.
8. Load 3.5 μl staining solution in a micropipette and hold it in one hand.
9. With the other hand, hold the tweezers so that the grid film faces upwards and blot away excess wash liquid by gently touching the side of the grid to the fixed filter paper until the grid is almost dry (*see* **Note 5**).
10. Immediately apply the staining solution (utilizing the "liquid bridge" principle) (*see* **Note 4**). Wait for 60 s.
11. Pick up the tweezers and blot away excess staining solution by gently touching the side of the grid to the fixed filter paper until the grid is almost dry (*see* **Note 6**).
12. Allow residual staining solution to evaporate and store the dry grid in a clean and dry grid box until use (*see* **Note 7**).

3.3 Cryo-EM Grid Preparation

This section outlines a cryo-EM grid preparation procedure based on the use of a specific cryo-plunger (FEI Vitrobot Mark IV), but other cryo-plungers (e.g., Gatan Cryoplunge 3 System or Leica Automatic Plunge Freezer EM GP2) may be used as well (*see* **Note 8**).

In order to reduce grid contamination, only high-quality liquid nitrogen and ethane should be used and all tweezers should be regularly cleaned and dried on a heating block between uses (*see* **Note 9**). One can further reduce grid contamination and improve reproducibility by preparing the grids in a temperature- and humidity-controlled room.

The level of liquid nitrogen should be carefully monitored and continuously adjusted to limit grid contamination and risk of grid

devitrification. Please note that after ethane plunging (sample vitrification) at no point must the grid be kept out of liquid nitrogen for extended periods of time as this will almost surely result in devitrification of the applied sample.

Latex gloves and protective goggles should be worn at all times.

1. On the display, the desired temperature and humidity of the blotting chamber are selected (*see* **Note 10**). Make sure that the humidifier canister is filled with ddH_2O (Fig. 4).

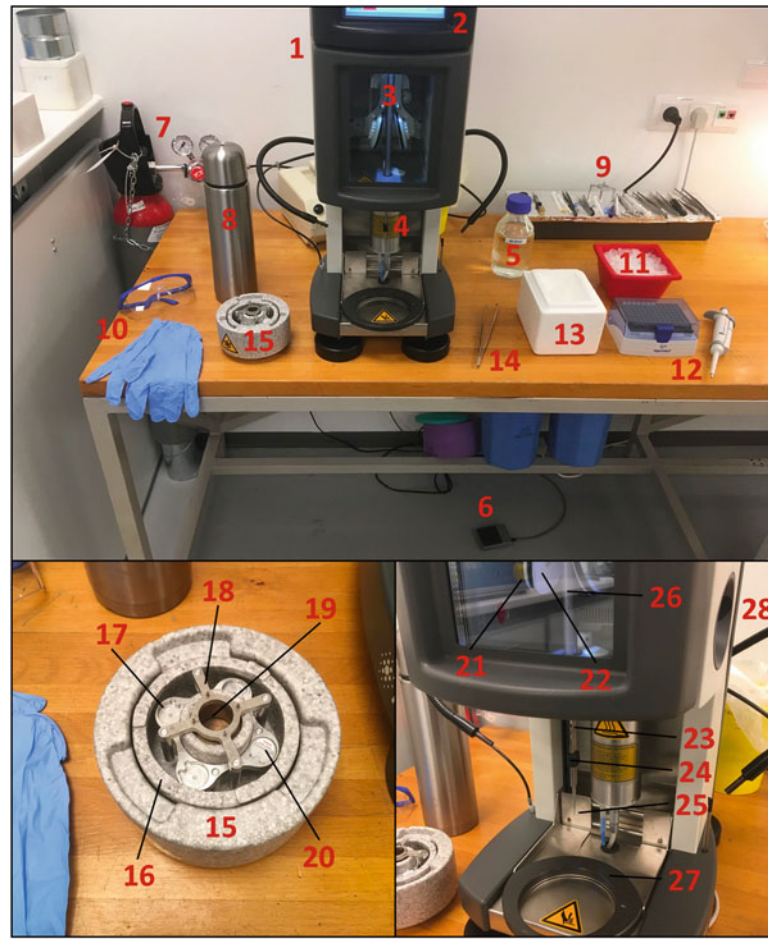

Fig. 4 Setup for preparation of cryo-EM grids. Relevant elements are numbered: (1) Vitrobot cryo-plunger, (2) display for putting in parameters, (3) blotting chamber, (4) humidifier canister, (5) ddH_2O for humidifier, (6) foot pedal, (7) ethane flask with hose, (8) liquid nitrogen container, (9) heating block, (10) gloves and protective goggles, (11) membrane protein sample on ice, (12) micropipette with tips, (13) styrofoam container, (14) transfer tweezers, (15) styrofoam cup, (16) styrofoam cylinder, (17) grid box holder, (18) aluminum spider, (19) ethane bucket, (20) grid box, (21) blotting arms, (22) filter paper, (23) plunge tweezers assembly, (24) black plastic belt, (25) grid, (26) plunge arm, (27) lift, (28) aperture

2. On the display, select the desired process parameters (*see* **Note 11**).
3. On the display, select the desired blotting parameters (*see* **Note 12**).
4. Fill a styrofoam container with liquid nitrogen and (using tweezers) gently submerge the ethane bucket, grid box holder, grid box, and aluminum spider.
5. Once all the parts are properly cooled (when nitrogen stops bubbling rapidly off the surface), fill the outer reservoir of the styrofoam cup with liquid nitrogen and (using metal tweezers) place the grid box holder and grid box inside it.
6. Using metal tweezers, carefully empty the ethane bucket of any liquid nitrogen and transfer it to the inner reservoir of the styrofoam cup, and then carefully place the aluminum spider on top of the bucket with its legs submerged in the liquid nitrogen of the outer reservoir (*see* **Note 13**).
7. Place the styrofoam cylinder floating on the liquid nitrogen of the outer reservoir (*see* **Note 14**) and keep it in place (*see* **Note 15**).
8. Using a small hose fitted with a pipette tip conduct gaseous ethane into the cooled ethane bucket (*see* **Note 16**).
9. Once the meniscus of the liquid ethane reaches the brim of the bucket, turn off the ethane flow and remove the hose.
10. Once the ethane starts to solidify (a milky crust appears on the insides of the bucket), the aluminum spider is removed (*see* **Note 17**). The solid crust should then melt away, leaving the ethane reservoir ready for use (*see* **Note 18**).
11. While wearing gloves, filter paper is attached to the pivoting blotting arms, and 1–2 test runs of the blotting process are performed to ensure that the process is executed properly (*see* **Note 19**).
12. Gripping only the very edge, a glow-discharged grid (*see* **Note 20**) is picked up using the plunge tweezers assembly, and the arms of the assembly are locked in place by sliding the black plastic belt down until it locks in place in the first indentation.
13. Attach the locked plunge tweezers assembly on the plunge arm and note which direction the grid film side is facing (*see* **Note 21**).
14. Using the foot pedal, instruct the Vitrobot to move the grid into the blotting chamber.

15. Place the styrofoam cup assembly on the lift, and (using the foot pedal) instruct the Vitrobot to lift the assembly (*see* **Note 22**).
16. Using the foot pedal, instruct the Vitrobot to move the grid into position for sample application.
17. Open the small aperture on the side of the blotting chamber and apply 3.5 μl sample to the grid film side (utilizing the "liquid bridge" principle) (*see* **Note 4**).
18. Using the foot pedal, instruct the Vitrobot to proceed with blotting (*see* **Note 23**). The Vitrobot automatically proceeds with plunging the grid into the liquid ethane and moving the styrofoam cup assembly down into position for detachment of the plunge tweezers (*see* **Note 24**). Readjust the liquid nitrogen level.
19. Using pre-cooled metal tweezers, gently open the cooled grid box and position it properly inside the grid box holder.
20. Gently detach the plunge tweezers assembly from the plunge arm while making sure that the grid is at all times fully submerged in liquid ethane and not sustaining damage from any contact with the wall of the ethane bucket.
21. Quickly transfer the grid from the ethane bucket to the liquid nitrogen of the outer reservoir of the foam cup (*see* **Note 25**).
22. While making sure that the grid is fully submerged in liquid nitrogen, keep the plunge tweezers closed with one hand and use the other to unlock the plunge tweezers by gently sliding up the black belt.
23. While making sure that the grid is fully submerged in liquid nitrogen, gently transfer the grid to a desired grid box compartment.
24. Using metal tweezers, gently close the grid box and keep it submerged in liquid nitrogen until use. For long-term storage, grid boxes should be kept in larger containers stored in sealed dewars of liquid nitrogen.

3.4 Data Collection

Access to a high-end cryo-transmission electron microscope (e.g., Thermo Fisher Scientific Titan Krios or JEOL 3200FSC) equipped with a high-end detector (e.g., Thermo Fisher Scientific Falcon 3EC or Gatan K2) is a prerequisite for acquiring a dataset of sufficient quality to allow for high-resolution (<4 Å) structure determination of any macromolecule. In addition to the manufacturer-provided microscope user interface, additional software packages for i.a. camera control (e.g., Thermo Fisher FluCam Viewer), image and spectrum acquisition (e.g., Thermo Fisher TEM Imaging and Analysis), and automated data collection (e.g., Thermo Fisher EPU, Leginon, SerialEM) are usually required.

While current software provides the user with some guidance for setting up the microscope, the support of a trained microscopist is still recommended to ensure proper microscope alignment. The following section briefly outlines the steps involved in setting up an automated data collection, which has been described in more detail elsewhere [16].

1. Prior to loading the prepared cryo-EM grids into the high-end microscope, these are typically assessed using a screening microscope (e.g., Thermo Fisher Scientific Tecnai or Glacios) for a relatively rapid assessment of grid quality (*see* **Note 26**).
2. Suitable grids are transferred to the high-end microscope and checked with live view camera to ensure agreement with screening results. A single grid is chosen for data collection.
3. The grid is brought to roughly eucentric height and the electron beam set up for each magnification level of the acquisition process. Decisions regarding data acquisition magnification, detector mode (i.e., linear or counting), and applied dose are made and suitable parameters chosen.
4. A more precise positioning at eucentric height is performed (typically by an automated process), and the different magnification levels are aligned with one another.
5. An atlas of the grid is generated and grid squares of suitable ice thickness are selected.
6. An acquisition template is generated. A suitable range of defocus values must be decided on (*see* **Note 27**).
7. Microscope alignments are performed to ensure parallel illumination and proper centering of the beam.
8. The current detector gain reference is validated or updated.
9. Automated data collection is initiated.

Especially the choice of data acquisition magnification, applied dose, and defocus value range strongly influences data quality, and implementation of an on-the-fly data preprocessing protocol involving at least motion correction and CTF estimation is highly recommended with regard to efficient optimization of data collection, as implemented for instance in the Focus software [17].

When working with small particles such as membrane proteins in detergents, the use of a phase plate may be necessary to increase contrast to allow for subsequent particle alignment. Many software packages exist for the analysis of cryo-EM data, such as RELION [18], cryoSPARC [19], and cisTEM [20], to name a few.

4 Notes

1. The orientation of the grids inside the storage compartment is usually stated on an attached label, but in cases of doubt it is usually possible to distinguish the film side using an optical microscope.
2. A good starting point is the buffer used for a potential preparative gel filtration, but other buffers may be tested as well.
3. If a loading station is not available, the negative-action tweezers can simply be placed on a suitable edge and fixed in place with a small weight.
4. Take great care not to touch the grid film directly with the pipette tip as this may critically damage it. Utilize the "liquid bridge" principle to safely apply your sample:

   (1) Gently initiate emptying of the pipette until a small droplet protrudes from the pipette tip. (2) Gently touch the grid film with this droplet, and as soon as contact is established (a "liquid bridge" is formed), gently extrude the remaining sample and allow it to flow onto the grid via this liquid bridge. Avoid emptying the pipette completely as this may introduce air bubbles into the applied droplet.
5. After the final blotting, only a very thin layer of wash liquid should remain on the grid film.
6. After the final blotting, only a very thin layer of stain should remain on the grid film.
7. In our experience, properly prepared negative staining grids can generally be stored at room temperature for long periods of time (weeks–months) without loss of quality.
8. Always refer to the manufacturer's protocol.
9. Alternatively, one can use a hair dryer or a drying oven.
10. Standard settings for working with aqueous biological samples are 4 °C (to maintain sample stability and viscosity) and 100% humidity (to limit evaporation of the applied sample).
11. In our experience, controlling all process steps using a foot pedal is much preferred to any automated options.
12. In our experience, the use of the following parameters is a good starting point in the absence of any preferences or previous experiences:

    Blot time: 3.0 s (specifies the time in which the blotting arms are pressed onto the grid).

    Blot force: 0 (zero corresponds to the middle value on a scale from −30 to +30, with input of a negative value resulting in weaker blotting, and input of a positive value resulting in more forceful blotting; note that the exact blotting procedure

depends on how and when the zero blot force was set, the exact angles of the blotting arms, etc.; therefore, optimal values for blot force need to be found for each individual system, as well as for different grids and samples).

Wait time: 0 s (specifies the time the operating system instructs the Vitrobot to wait between sample application and grid blotting).

Drain time: 0 s (specifies the time the operating system instructs the Vitrobot to wait between grid blotting and plunging).

Blot total: 1 (increasing this value allows for multiple sequential blots of the same grid).

13. The high thermal conductivity of aluminum ensures rapid and efficient transfer of heat from the ethane bucket to the outer reservoir.
14. Note that the two edges of the styrofoam cylinder are not identical, and that the smooth edge should be in contact with the liquid nitrogen of the outer reservoir, while the non-smooth edge should be facing upwards.
15. The styrofoam cylinder improves thermal insulation of the ethane bucket from the surrounding air but in cases of poor visibility may be temporarily removed.
16. To avoid introduction of ethane into the outer reservoir, do not initiate the flow of gaseous ethane until the hose outlet touches the floor of the ethane bucket. Keep the hose outlet connected to the floor of the ethane bucket and slowly initiate the flow of gaseous ethane until a milky mist occurs and a bubbling sound can be heard, indicating that the ethane is condensing inside the bucket. The mist should not be allowed to expand beyond the ethane bucket. Adjust the ethane flow accordingly.
17. This is done to limit the transfer of heat from the ethane bucket to the outer reservoir.
18. At atmospheric pressure, the melting point of ethane is at −183 °C, while the boiling point of liquid nitrogen is −196 °C, meaning that when the ethane of the bucket has partly solidified at least once, it is safe to assume that the temperature of the ethane reservoir remains stable at ~−180 °C, assuming that the outer reservoir is continuously replenished with liquid nitrogen and the styrofoam cylinder kept in place to ensure thermal insulation from the surroundings.
19. The test runs are optional, but in our experience, the blotting arms often become displaced when attaching the blotting

paper, and completing a few blotting cycles ensures that the arms are indeed properly positioned prior to the first grid blotting.

20. In the absence of any preferences or previous experiences, a good starting point is to use 200–400 mesh copper grids with carbon film of defined hole size and spacing, e.g., R 2/1 (indicates a hole diameter of 2 μm and a distance between holes of 1 μm).
21. This is important because the sample must be applied directly to the grid film.
22. Prior to initiating the lift, the liquid nitrogen level can be checked by pushing the styrofoam cylinder down: the liquid nitrogen should rise all the way to the brim of the styrofoam cup when the styrofoam cylinder is pushed all the way down, but should not spill over.
23. If wait time = 0 is employed, the Vitrobot will blot the grid immediately.
24. If drain time = 0 is employed, the Vitrobot will plunge the grid immediately after blotting.
25. Advanced user option: While still aiming to limit the time that the grid is exposed to air, a piece of filter paper may be used to gently remove excess ethane from the grid before submerging it in liquid nitrogen.
26. A good-quality cryo-EM grid is intact and not bent and features many grid squares containing ice of suitable and uniform thickness. Visibly damaged and bent grids should not be loaded into the microscope, and grids featuring prominent contamination should be discarded.
27. The defocus phase contrast method is the de facto standard method of cryo-TEM for generating sufficient micrograph contrast [21]. Usually, defocus values ranging from 1 to 3 μm at 100,000× magnification on a 300 keV microscope give good results.

Acknowledgment

The Novo Nordisk Foundation Center for Protein Research is supported financially by the Novo Nordisk Foundation (NNF14CC0001). This work was also supported by an NNF Hallas-Møller Emerging Investigator grant (NNF17OC0031006) and a DFF grant (8123-00002B) to NMIT. NMIT also acknowledges support of the Magda Sofie og Aase Lütz's Mindelegat (109366), Brødrene Hartmanns Fond (A33239), Agnes og Poul Friis Fond (81008-003), Civilingeniør Frode V. Nyegaard og Hustrus Fond,

and A.P. Møller Fonden (18-L-0326). NMIT is a member of the Integrative Structural Biology Cluster (ISBUC) at the University of Copenhagen.

References

1. Li X, Mooney P, Zheng S, Booth CR, Braunfeld MB, Gubbens S, Agard DA, Cheng Y (2013) Electron counting and beam-induced motion correction enable near-atomic-resolution single-particle cryo-EM. Nat Methods 10 (6):584–590. https://doi.org/10.1038/nmeth.2472
2. Drulyte I, Johnson RM, Hesketh EL, Hurdiss DL, Scarff CA, Porav SA, Ranson NA, Muench SP, Thompson RF (2018) Approaches to altering particle distributions in cryo-electron microscopy sample preparation. Acta Crystallogr D Struct Biol 74(Pt 6):560–571. https://doi.org/10.1107/s2059798318006496
3. Aebi U, Pollard TD (1987) A glow discharge unit to render electron microscope grids and other surfaces hydrophilic. J Electron Microsc Tech 7(1):29–33
4. Fahy GM, Wowk B (2015) Principles of cryopreservation by vitrification. In: Wolkers WF, Oldenhof H (eds) Cryopreservation and freeze-drying protocols. Springer New York, New York, NY, pp 21–82. https://doi.org/10.1007/978-1-4939-2193-5_2
5. Gewering T, Januliene D, Ries AB, Moeller A (2018) Know your detergents: a case study on detergent background in negative stain electron microscopy. J Struct Biol 203 (3):242–246. https://doi.org/10.1016/j.jsb.2018.05.008
6. Hauer F, Gerle C, Fischer N, Oshima A, Shinzawa-Itoh K, Shimada S, Yokoyama K, Fujiyoshi Y, Stark H (2015) GraDeR: membrane protein complex preparation for single-particle cryo-EM. Structure 23 (9):1769–1775. https://doi.org/10.1016/j.str.2015.06.029
7. Kulig W, Tynkkynen J, Javanainen M, Manna M, Rog T, Vattulainen I, Jungwirth P (2014) How well does cholesteryl hemisuccinate mimic cholesterol in saturated phospholipid bilayers? J Mol Model 20(2):2121. https://doi.org/10.1007/s00894-014-2121-z
8. Twomey EC, Yelshanskaya MV, Grassucci RA, Frank J, Sobolevsky AI (2016) Elucidation of AMPA receptor-stargazin complexes by cryo-electron microscopy. Science 353 (6294):83–86. https://doi.org/10.1126/science.aaf8411
9. Palsdottir H, Hunte C (2004) Lipids in membrane protein structures. Biochim Biophys Acta 1666(1–2):2–18. https://doi.org/10.1016/j.bbamem.2004.06.012
10. Seddon AM, Curnow P, Booth PJ (2004) Membrane proteins, lipids and detergents: not just a soap opera. Biochim Biophys Acta 1666 (1–2):105–117. https://doi.org/10.1016/j.bbamem.2004.04.011
11. Fan G, Baker ML, Wang Z, Baker MR, Sinyagovskiy PA, Chiu W, Ludtke SJ, Serysheva II (2015) Gating machinery of InsP3R channels revealed by electron cryomicroscopy. Nature 527(7578):336–341. https://doi.org/10.1038/nature15249
12. Cheng Y, Grigorieff N, Penczek PA, Walz T (2015) A primer to single-particle cryo-electron microscopy. Cell 161(3):438–449. https://doi.org/10.1016/j.cell.2015.03.050
13. Schmidt-Krey I, Rubinstein JL (2011) Electron cryomicroscopy of membrane proteins: specimen preparation for two-dimensional crystals and single particles. Micron 42 (2):107–116. https://doi.org/10.1016/j.micron.2010.07.004
14. Johnson ZL, Chen J (2017) Structural basis of substrate recognition by the multidrug resistance protein MRP1. Cell 168 (6):1075–1085.e1079. https://doi.org/10.1016/j.cell.2017.01.041
15. Chen J, Noble AJ, Kang JY, Darst S (2018) Eliminating effects of particle adsorption to the air/water interface in single-particle cryo-electron microscopy: bacterial RNA polymerase and CHAPSO.457267. https://doi.org/10.1101/457267. bioRxiv
16. Thompson RF, Iadanza MG, Hesketh EL, Rawson S, Ranson NA (2019) Collection, pre-processing and on-the-fly analysis of data for high-resolution, single-particle cryo-electron microscopy. Nat Protoc 14 (1):100–118. https://doi.org/10.1038/s41596-018-0084-8
17. Biyani N, Righetto RD, McLeod R, Caujolle-Bert D, Castano-Diez D, Goldie KN, Stahlberg H (2017) Focus: The interface between data collection and data processing in cryo-EM. J Struct Biol 198(2):124–133. https://doi.org/10.1016/j.jsb.2017.03.007

18. Scheres SH (2012) RELION: implementation of a Bayesian approach to cryo-EM structure determination. J Struct Biol 180(3):519–530. https://doi.org/10.1016/j.jsb.2012.09.006
19. Punjani A, Rubinstein JL, Fleet DJ, Brubaker MA (2017) cryoSPARC: algorithms for rapid unsupervised cryo-EM structure determination. Nat Methods 14(3):290–296. https://doi.org/10.1038/nmeth.4169
20. Grant T, Rohou A, Grigorieff N (2018) cisTEM, user-friendly software for single-particle image processing. Elife 7. https://doi.org/10.7554/eLife.35383
21. Danev R, Baumeister W (2016) Cryo-EM single particle analysis with the Volta phase plate. Elife 5. https://doi.org/10.7554/eLife.13046

Chapter 17

Single-Particle Cryo-EM of Membrane Proteins in Lipid Nanodiscs

Valeria Kalienkova, Carolina Alvadia, Vanessa Clerico Mosina, and Cristina Paulino

Abstract

Single-particle cryo-electron microscopy has become an indispensable technique in structural biology. In particular when studying membrane proteins, it allows the use of membrane-mimicking tools, which can be crucial for a comprehensive understanding of the structure-function relationship of the protein in its native environment. In this chapter we focus on the application of nanodiscs and use our recent studies on the TMEM16 family as an example.

Key words Cryo-EM, Single-particle, Nanodiscs, Membrane proteins, Structural biology

1 Introduction

Before 2014, single-particle cryo-electron microscopy (cryo-EM) was restricted to large protein complexes and resulted in low-resolution maps, whereas solely X-ray crystallography and NMR spectroscopy were able to deliver the resolution necessary to describe a structure and understand the biological function of proteins at an atomic level. However, advances in direct electron detection cameras, high-end microscopes, and image processing have revolutionized the field entirely. This "resolution revolution" [1] translates into structures at near-atomic resolution ($\geq$1.65 Å [2]), even for small (52 kDa [3]) and asymmetric proteins, making cryo-EM an indispensable technique for structure determination. Single-particle cryo-EM complements X-ray crystallography, while offering several advantages, as follows: (1) it requires only small amounts of protein, which can be immediately flash-frozen on EM grids to avoid further denaturation or degradation after

Valeria Kalienkova and Carolina Alvadia contributed equally to this work.

Camilo Perez and Timm Maier (eds.), *Expression, Purification, and Structural Biology of Membrane Proteins*, Methods in Molecular Biology, vol. 2127, https://doi.org/10.1007/978-1-0716-0373-4_17,

purification; (2) it is not limited by the formation of protein crystals, which are often restricted to energetically favored conformations; (3) it is hardly limited by buffer composition and allows the induction of conformational changes prior to freezing; (4) it is not hampered by compositional or conformational heterogeneity of the sample, providing a glimpse into structural dynamics; and (5) it enables the determination of both low- and high-resolution structures. Notably, while the resolution obtained with cryo-EM is on average lower than with X-ray crystallography, the common resolution obtained for membrane proteins is similar (about 2.8–3.8 Å, Table 1). These advantages have proven to be crucial to tackle several challenges faced when working with membrane proteins, allowing unprecedented research and making cryo-EM often the technique of choice to study the structure of membrane proteins.

Another emerging advantage of studying membrane proteins by cryo-EM is its compatibility with lipid membrane-mimicking tools, which can be resolved together with the target protein. The ability to study the structure of a membrane protein in its native environment is crucial, as the surrounding lipids can dramatically affect its conformation and functional properties [8, 18, 19, 26, 28, 33]. The optimal scenario would be to study membrane proteins in their native lipid environment within their cellular context, prior to any external interference by the researcher, i.e., membrane extraction and purification. While recent advances in cryo-electron tomography (cryo-ET) and sub-tomogram averaging allow, to some extent, to perform such studies [34–39], the technique faces significant challenges, i.e., (1) the preparation of samples; (2) the thickness and strong background signal of the sample; (3) the limitation in target protein size and the associated difficulty in identifying it within the membrane or the remaining proteome; (4) the low signal-to-noise ratio per image and accumulated radiation damage during whole tilt-series data acquisition; (5) the missing wedge, and (6) the achieving of high-resolution reconstructions. An alternative approach is to image proteins that were reintroduced into membrane vesicles after purification (proteoliposomes). This method provides a close representation of a native environment and offers full control of the buffer conditions on both sides of the membrane. Notably, it allows one to establish an electrochemical gradient across the membrane, which is crucial for the function of several classes of membrane proteins. However, the use of proteoliposomes also imposes multiple obstacles: (1) they are often heterogeneous in size and differ in protein reconstitution level; (2) they have a high membrane curvature, which might affect protein structure and function; (3) the position of the target protein within the proteoliposome is ambiguous, making it difficult to identify; and (4) the overall sample thickness, the fact that at least two layers of membrane are imaged and the strong scattering of phospholipid headgroups impose

Table 1
A representative use of nanodiscs for high-resolution structural characterization of membrane proteins by cryo-EM

Protein	MSP	Ligand	Lipid composition	Additives while freezing	Grid type	Angular distribution	Number of particles (initial/final)	Resolution (Å)	Source
ATPase V_0 proton channel	E3D1	–	Vacuolar membrane extract	–	UltrAuFoil 1.2/1.3	Isotropic	285,000/ 180,528	3.5	[4]
Kv	E3D1	–	POPC:POPG:POPE	–	UltrAuFoil R1.2/1.3	Isotropic	281,021/ 47,482	3.3	[5]
TRPM4	2N2	EDTA	Soybean polar lipid extract	–	Quantifoil Cu R1.2/1.3	Isotropic	528,648/ 47,247	3.2	[6]
		Ca^{2+}				Isotropic	829,078/ 45,346	3.1	
OSCA1.2	2N2	–	Soybean polar lipid extract	–	UltrAuFoil 1.2/1.3	Isotropic	788,948/ 76,797	3.1	[7]
MsbA	1D1	1D1	*E. coli* polar extract	–	Quantifoil 1.2/1.3	Isotropic	745,352/ 67,220	4.2	[8]
ATP synthase	E3D1	–	*E. coli* polar/DMPC	–	Quantifoil R1.2/1.3	Isotropic	541,565/ 160,937	3.6	[9]
		Oligomycin	POPC:cardiolipin			Isotropic	346,399/ 104,280	3.8	
ABCG2	1D1		Brain polar lipids: CHS 4:1	–	Quantifoil Cu Mesh 300	Isotropic	232,608/ 97,612	3.8	[10]
	1D1	Inhibitor bound	Brain polar lipids: CHS 4:1	–	Quantifoil Cu Mesh 300	Isotropic	2,098,186/ 402,348	3.56	[11]
Tc toxin	1D1	–	POPC	Fluorinated octyl-maltoside	C-flat 2/1, Protochips Thin layer of carbon	Anisotropic	30,061/ 13,042	3.46	[12]

(continued)

Table 1
(continued)

Protein	MSP	Ligand	Lipid composition	Additives while freezing	Grid type	Angular distribution	Number of particles (initial/final)	Resolution (Å)	Source
TRPML1	2N2	–	Soybean polar lipid extract	–	Quantifoil Cu R1.2/1.3	Isotropic	1167K/242K	5.8	[13]
	MSP1	–	POPC:POPG:POPE	–	Quantifoil Cu R1.2/1.3	Anisotropic	1,433,949/ 20,000 Closed I—9K Closed II—11K	3.6 overall 3.64—closed I 3.75—closed II	[14]
NOMPC	2N2	–	Soy PC	–	C-flat R1.2/1.3	Anisotropic	337,716/ 175,314	3.55	[15]
TRPV1	2N2	Apo	Soybean polar lipid extract	–	Quantifoil Cu R1.2/1.3	Isotropic	159,193/ 30,689	3.3	[16]
		Agonist				Anisotropic	218,787/ 73,929	2.95	
		Antagonist				Anisotropic	198,831/ 807,725	3.4	
MCU	1D1	–	POPC:cardiolipin	Fluorinated Fos-choline-8	Quantifoil Cu R1.2/1.3	Isotropic	577,209/ 51,737 577,209/ 44,990	4.8 5	[17]
mTMEM16A	2N2	2N2	Soy PC	–	Quantifoil Cu R1.2/1.3	Anisotropic	927,414/ 251,851	3.8	[18]
nhTMEM16	2N2	EGTA	POPC:POPG	–	Quantifoil Au R1.2/1.3	Isotropic	1,379,187/ 133,961	3.8	[19]
		Ca^{2+}					2,440,110/ 71,175	3.6	
		Ca^{2+}					2,440,110/ 33,310	3.7	
		Ca^{2+}					2,440,110/ 41,631	3.6	

afTMEM16	E3D1	EGTA	POPE:POPG	Fluorinated Fos-choline-8	UltrAuFoil R1.2/1.3	Isotropic	752,911/38,550	3.9	[20]
		Ca^{2+}					1,034,678/37,146	4.0	
		Ca^{2+}	POPE:POPG: ceramide				521,688/24,602	3.6	
mTMEM16F	2N2	EGTA	POPC:POPG	–	Quantifoil Au R1.2/1.3	Anisotropic	1,593,115/280,891	3.3	[21]
		Ca^{2+}				Anisotropic	1,019,012/186,487	3.5	
LRRC8A	E3D1	DCPIB	POPC	–	Quantifoil Au R1.2/1.3	Isotropic	752,842/25,153 (constricted)	3.4	[22]
							752,842/35,435 (expanded)	3.6	
	2N2	–				Isotropic	?/25,807	4.4	
TRPC6	2N2	BTDM	Soybean lipids	Fluorinated octyl-maltoside	GiG R1/1	Isotropic	326,026/53,528	3.8	[23]
TRPC3		OAG				Isotropic	625,074/22,220	4.4	
TRPV5	2N2	$PI(4,5)P_2$	Soy polar lipid extract	Fluorinated Fos-choline-8	Quantifoil 1.2/1.3	Isotropic	493,047/25,538	4	[24]
						Isotropic	493,047/~30,000	4.4	
PKD2	2N2	–	Soybean polar lipid extract	–	Quantifoil Cu 1.2/1.3	Isotropic	368,032/93,805	3	[25]
RyR1	E3D1	Ryanodine	Native, additionally soybean PC	Fluorinated octyl-maltoside	Quantifoil Cu R2/1	Isotropic	170,000/62,000	7.3	[26]
		ATP/Ca^{2+}				Isotropic	155,000/42,000	8.2	

(continued)

Table 1
(continued)

Protein	MSP	Ligand	Lipid composition	Additives while freezing	Grid type	Angular distribution	Number of particles (initial/final)	Resolution (Å)	Source
OST (oligosaccharyltransferase)	E3D1	–	*E. coli* polar lipids: Egg PC	–	Quantifoil Cu	Isotropic	486,361/110,091	3.3	[27]
hTRPV6	2N2	–	Soybean polar lipid extract	–	Au-coated CF-1.2/1.3-2 Au 200 mesh carbon	Isotropic	509,569/46,124	3.6	[28]
rTRPV6∗	CNW11					Isotropic	248,836/20,808	3.9	
VgrG1-Tse6-EF-Tu	1D1-ΔH5	–	POPC	–	Quantifoil 2/1 Additional 2 nm C	Isotropic	114,879/72,190	3.25	[29]
SthK	E3D1 (1E3)	–	POPG	Fluorinated Fos-choline-8	UltrAuFoil R1.2/1.3	Isotropic	179,504/51,115	3.42	[30]
		cAMP				Isotropic	572,844/81,501	3.35	
		cGMP				Isotropic	199,965/91,800	3.46	
$GABA_A$	2N2	–	POPC:brain extract	–	UltrAuFoil R1.2/1.3	Isotropic	370,757/55,449	3.22	[31]
Otop1	2N2	–	Soybean polar lipid extract	–	UltrAuFoil R1.2/1.3	Isotropic	1,517,125/67,425	2.98	[32]
Otop3		–		–		Isotropic	1,386,058/43,677	3.32	

This is not an exhaustive list

limitations on image processing and resolution. However, this method is being actively developed and recently yielded first promising results [40–42].

Currently, the best established and most commonly used strategy to mimic a membrane environment is the use of scaffold proteins or compounds that support the formation of soluble lipid bilayer patches. Multiple systems have been developed for this purpose, including Salipros [43, 44], peptidiscs [45], SMALPs [46], and nanodiscs [47]. The lipid-binding protein saposin A (SapA) and the short amphipathic bi-helical peptide NSPr can form compact lipoprotein particles, termed saposin-derived lipid nanoparticles (Salipro) and peptidiscs, respectively [43, 45, 48]. A benefit of Salipros and peptidiscs is that their scaffolds can accommodate membrane proteins of different sizes. It was recently shown that Salipros are suitable for high-resolution cryo-EM [44, 49] and potentially can be used to directly extract proteins from native membranes. However, the respective scaffold proteins of Salipros and peptidiscs appear to tightly wrap around the target protein, limiting the number of co-assembled lipids, which might not be sufficient to fully mimic a membrane environment [45, 48]. SMALPs are lipid patches formed by the insertion of styrene maleic acid copolymers (SMAs) into a lipid bilayer. Hereby, the protein of interest is directly extracted from the membrane, avoiding any exposure to detergent that can have a negative impact on its function and structure. More importantly, SMALPs preserve the native lipid composition, which can be crucial for a detailed understanding of the structure-function relationship [50]. Despite the advantages, there are only few examples of structural studies available using this approach [51–53], which might be related to some of its limitations, such as a poor extraction efficiency, especially for some types of membranes, and the fact that many SMAs are sensitive to divalent ions [54–56]. This chapter focuses on single-particle cryo-EM of membrane proteins in lipid nanodiscs, which is the most commonly used membrane-mimicking system.

A nanodisc is a self-assembled nanometer-sized discoidal phospholipid bilayer encircled by membrane scaffold proteins (MSPs), which keep the bilayer patch stable in solution [47, 57, 58]. Membrane scaffold proteins (MSPs) are amphipathic helical proteins derived from the human apolipoprotein A1 and were developed by Sligar and colleagues [47, 57]. Two antiparallel MSPs encircle a phospholipid bilayer disk, with each MSP associating with the hydrophobic alkyl chains of one of the leaflets (Fig. 1) [47, 59]. Unlike Salipros and peptidiscs, nanodiscs allow the incorporation of a large amount of bulk lipids around the target protein [60]. Nanodisc assembly is a well-established and well-described procedure [60–62] (Fig. 1), with multiple examples of its successful implementation in single-particle cryo-EM. A representative overview of studies using nanodiscs for high-resolution structural

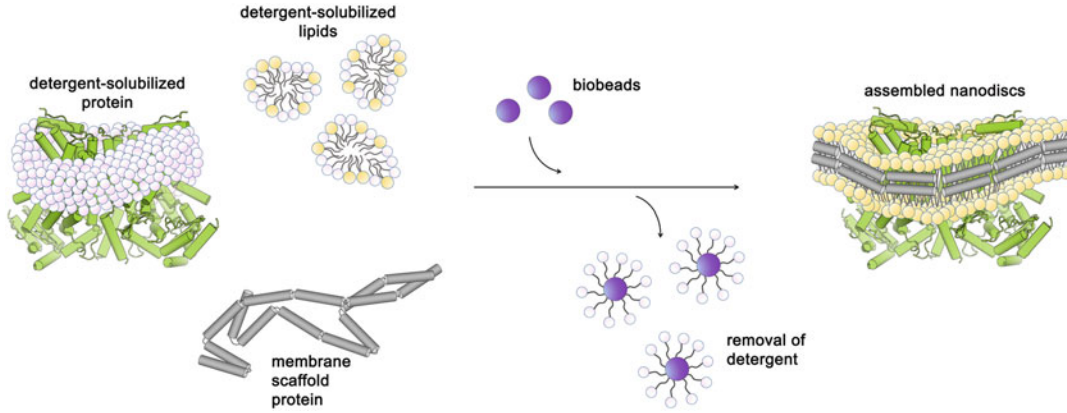

Fig. 1 Protein-nanodisc assembly. Schematic representation of the reconstitution of solubilized target protein into lipid nanodiscs. The target membrane protein is shown in green; the scaffold protein in gray; detergent and lipid molecules in pink and yellow spheres, respectively, with hydrophobic tails in gray and biobeads in purple

characterization of membrane proteins is shown in Table 1. The relative ease of nanodisc assembly and subsequent cryo-EM single-particle analysis make them an excellent model membrane system to study the effect of defined lipids on the structure and function of membrane proteins. In this chapter we discuss the general considerations when using nanodiscs for structural analysis by cryo-EM and will use our experience with proteins from the TMEM16 family as an example.

The TMEM16 family, which is exclusively found in eukaryotes, shows a remarkable dual functionality. It encompasses members functioning as Ca^{2+}-activated Cl^- channels, or Ca^{2+}-activated lipid scramblases—which catalyze the bidirectional diffusion of lipids between both membrane leaflets—or both [63]. The structures of the fungal lipid scramblase nhTMEM16 from *Nectria haematococca* [64] and that of the chloride channel mTMEM16A from mouse [18, 65, 66] revealed the architectural differences that underlie the functional diversity of the family. Whereas in the scramblase structure we observe a membrane-spanning and membrane-accessible cavity through which polar lipid headgroups can slide, the furrow is closed in the Cl^- channel structure to form a pore that allows the diffusion of ions through the membrane. Our recent studies on the murine TMEM16F and the fungal nhTMEM16 lipid scramblases [19, 21] in detergent and in nanodiscs, both in the presence and absence of Ca^{2+}, have further shed light on their regulation by Ca^{2+} and their mechanism of action. Strikingly, only when reconstituted into nanodiscs, but not in detergent, we were able to obtain a closed conformation of nhTMEM16 and sample the conformational plasticity of the transporter present under activating conditions, allowing us to propose a

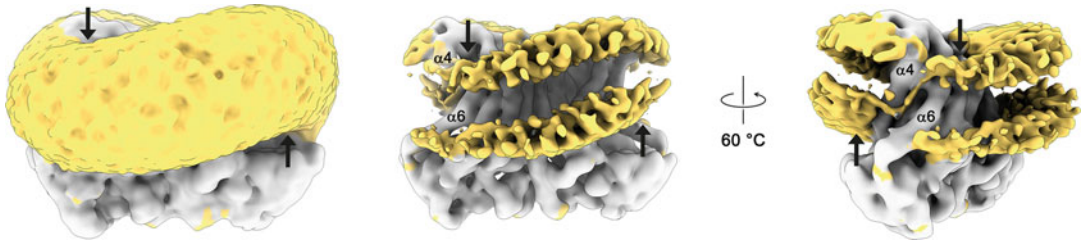

Fig. 2 Interaction of nhTMEM16 with the lipid environment. Shown is the low-pass-filtered map of the Ca^{2+}-bound nhTMEM16 open state in nanodiscs from the front (left and middle panels) and with a view on the subunit cavity (right). The location of the lipid headgroup regions of both leaflets is revealed at the higher contour (middle and right panels). The density corresponding to nhTMEM16 is colored in gray and the density of the nanodisc, composed of lipids surrounded by the 2N2 belt protein, and that of the additional density observed in the subunit cavity lined by transmembrane helices 4 and 6 are shown in yellow. The membrane distortion is indicated by black arrows

new mode of action. Another remarkable feature observed in all cryo-EM datasets obtained for nhTMEM16 is the deformation of the membrane at both entrances of the subunit cavity (Fig. 2). These studies, among others, highlight the power of investigating the structure of membrane proteins in nanodiscs by single-particle cryo-EM.

2 Materials

2.1 Lipid Preparation

1. Lipids of choice (solubilized in chloroform).
2. Glass pipettes.
3. Round-bottom glass flask.
4. Nitrogen stream.
5. Diethyl ether.
6. Desiccator.
7. Detergent of choice.
8. Argon stream.

2.2 Nanodisc Assembly

1. Purified membrane scaffold protein.
2. Purified target protein.
3. Detergent-solubilized lipids (from the previous section).
4. SM-II biobeads.
5. Filtration column.
6. Affinity chromatography column.
7. Detergent-free protein buffer.
8. Protein concentrator.
9. Size-exclusion chromatography setup.

2.3 Cryo-EM Sample Preparation

1. Cryo-EM grids.
2. Glow discharger.
3. Plunge-freezing device, e.g., Vitrobot IV (Thermo Fisher Scientific).
4. Ethane/propane mixture.
5. Liquid N_2.

2.4 Data Collection and Image Processing

1. High-end transmission electron cryo-microscope.
2. Ice thickness measurement software (in-house script [Rheinberger et al., manuscript in preparation]).
3. Data collection software.
4. Image processing software and image processing power.

3 Methods

For complementary protocols on protein reconstitution into nanodiscs please also *see* Chapter 14 in this issue.

3.1 Lipid Preparation

The formation of nanodiscs is not limited by the choice of lipids (Table 1), enabling the structural studies of proteins in their (nearly) native environment and in a defined lipid composition (*see* **Note 1**). Lipids are prepared as follows:

1. Weigh chloroform-solubilized lipids ($\rho = 1.49$ g/cm^3) and mix them in a round-bottom glass flask. For reconstitution of mTMEM16F and nhTMEM16 we used the lipids POPC and POPG at a molar ratio of 3:1 and 7:3, respectively [19, 21].
2. Evaporate the chloroform with a N_2 stream and redissolve the lipids in diethyl ether. Remove the organic solvents under N_2 stream, while gently rotating the flask, until a thin lipid film is formed. Remove traces of solvents by incubating the lipids in a desiccator overnight.
3. Rehydrate the lipids and solubilize them with at least twofold molar excess of detergent. The most important aspects when selecting the detergent are the stability of the target protein in its presence and the efficiency of its removal. For the reconstitution of TMEM16 proteins into nanodiscs, we solubilized 10 mM lipids in 30 mM DDM-β [19, 21].
4. Stir and, if necessary, perform multiple freeze-thaw cycles to ensure complete solubilization of the lipids. The obtained solution should be transparent and fairly viscous.
5. Transfer the solution into a tube and replace the oxygen with argon to prevent lipid oxidation. Store the lipids at −20 °C until further use.

3.2 Nanodisc Assembly

For the TMEM16 proteins, a POPC:POPG lipid mixture was used, which has a phase transition temperature of −2 °C, and assembly into MSP2N2 nanodisc (*see* **Notes 2–6**) was carried out at 4 °C as follows:

1. Incubate purified protein with the POPC:POPG lipid mixture on ice for 40 min.
2. Add MSP2N2 to the lipid-target protein mixture and further incubate for 40 min on ice (*see* **Note 7**). For mTMEM16F a molar ratio of 2:10:2200 of mTMEM16F:MSP2N2:lipids was found to be ideal for reconstitution, while for nhTMEM16 the optimal ratio was 2:10:1450 (*see* **Note 8**).
3. Transfer the mixture to a vessel of appropriate size. The vessel should allow complete mixing of the sample without having an excess of unfilled space, in order to minimize oxidation.
4. Slow removal of detergent is required to initiate nanodisc assembly. Add 50 mg of wet SM-II biobeads per mg of DDM added with the solubilized lipids. Note that detergent removal can also be accomplished by dialysis or detergent binding columns.
5. Incubate the sample overnight at 4 °C with gentle agitation. The incubation time required to completely remove detergent might vary.
6. After the self-assembly of nanodiscs, the sample should be clear. Remove the SM-II biobeads from the nanodisc sample, e.g., by column filtration.
7. In case the assembly reaction was carried out with an excess of lipids and MSP, it is necessary to remove the resulting empty nanodiscs after assembly (*see* **Note 9**). Add the assembled nanodisc solution to an affinity chromatography column and incubate for 0.5–2 h.
8. Wash the resin with 10–60 column volumes (CV) of wash buffer (e.g., 20 mM HEPES pH 7.5, 150 mM NaCl, 2 mM EGTA) (*see* **Note 10**) to remove empty nanodiscs and subsequently elute the nanodisc complex.
9. Optional: Cleave the affinity tag fused to the target protein.
10. Concentrate the sample using a concentrator with an appropriate-size cutoff (we routinely use a 100 kDa cutoff for TMEM16 proteins) and load the sample onto a Superose 6 10/300 GL size-exclusion column.
11. Pool the selected monodisperse peak fractions (Fig. 3, *see* **Note 11**).
12. Concentrate the target protein-nanodisc sample as desired (for TMEM16 protein-nanodisc complexes we had a protein concentration of 1.5 mg/mL, while in detergent samples we used

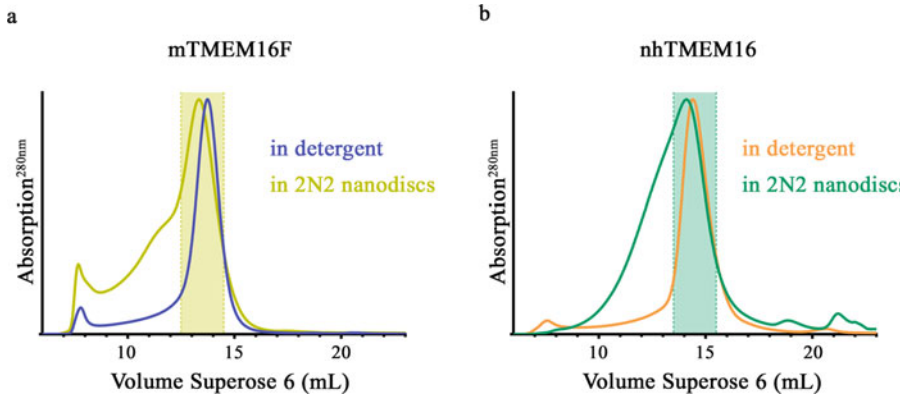

Fig. 3 Heterogeneity of nanodisc samples. Shown are size-exclusion chromatography profiles of mTMEM16F (left) and nhTMEM16 (right) when solubilized in detergent (blue and orange) and after reconstitution into the large 2N2 nanodiscs (yellow and green), respectively. The protein-nanodisc fractions used for subsequent sample preparation for cryo-EM are indicated by a yellow and green bar. The broader elution peak observed for the nanodisc samples might derive from empty nanodiscs, different sizes of protein-nanodisc complexes, or double incorporation of protein

a protein concentration of 3.3 mg/mL) and apply to the cryo-EM grids as fast as possible (*see* **Note 12**).

With regard to the biological function of TMEM16 proteins as lipid scramblases, we were interested in the interaction of TMEM16 with the surrounding bilayer. To ensure that the scramblase is embedded into a sufficiently large membrane area, we reconstituted and collected small datasets of nhTMEM16 at three different lipid-to-protein ratios (LPR) [19]. Strikingly, in all cases the shape of the nanodisc was not round (as observed for most membrane proteins), but oval, where nhTMEM16 is located close to the center with its long dimension parallel to the shortest diameter of the nanodisc (Fig. 4). This is likely a direct effect of scramblase incorporation and reflects a preferential localization of lipids far away from the catalytic lipid-translocating subunit cavity. Since increasing the amount of lipids per MSP only caused elongation of the nanodisc in one direction without changing its diameter near the subunit cavity, data collection was performed on the sample with the lowest LPR tested, which also had the most homogeneous assembly of approximately 165 × 140 Å in size [19].

3.3 Cryo-EM Sample Preparation

When preparing the assembly for the first time, we recommend to monitor the quality of the sample by using negative staining EM. This will allow to assess and compare the sample homogeneity and the overall suitability of the sample for single-particle cryo-electron microscopy. We also strongly advise to freeze the protein-nanodisc complexes for cryo-EM data collection as quickly as possible after purification.

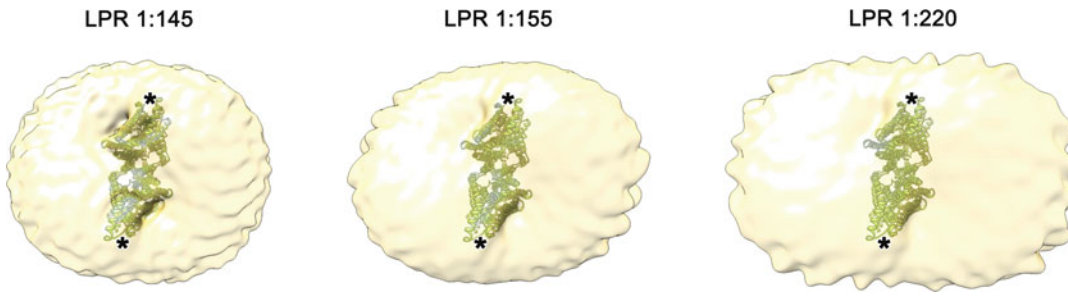

Fig. 4 Effect of LPR on the morphology of protein-nanodisc assemblies. Shown are low-pass-filtered cryo-EM maps obtained for nhTMEM16 when reconstituted into nanodiscs at indicated protein-to-lipid ratios (LPR) (mol/mol). The protein-nanodisc complexes in yellow are viewed from the extracellular side, nhTMEM16 model fitted into the density is displayed as green ribbon, and the location of the subunit cavities is indicated by an asterisk

The absence or presence of detergent in the buffer has an impact on the surface tension and how the sample drop behaves on the EM grid. Thus, optimal freezing conditions, e.g., glow-discharging time, protein concentration, additives, and blotting time, will differ for samples in nanodiscs compared to detergent micelles and need to be determined empirically. The ultimate goal is to obtain a cryo-EM sample with the highest number of homogeneous particles that are well separated and randomly oriented in a thin layer of ice. However, cryo-EM samples are rarely perfect. One of the biggest obstacles faced are preferred particle orientation (*see* **Note 13**) and protein denaturation at the air-water interface. Particle diffusion and adsorption to the air-water interface appear to be a determining factor of preferred particle orientation (*see* **Note 14**). However, other factors such as adhesion to additional support films, buffer composition and ionic strength, the protein itself, other additives, or ice thickness (e.g., when the ice is too thin to accommodate a certain orientation of the particles) also play a role. Despite it being a common perception, there is no clear evidence that the problem of favored orientation is enhanced by the use of nanodiscs, as it was possible to achieve isotropic map reconstructions at high resolution for various membrane proteins reconstituted into lipid nanodiscs (Table 1).

A number of tools and methods have emerged to optimize cryo-EM sample preparation and particle distribution. These include surfactants (*see* **Note 15**), multiple types of grids and grid modifications (*see* **Note 16**), multiple types of support films (*see* **Note 17**), sample additives (*see* **Note 18**), and freezing devices (*see* **Note 19**).

Grid preparation is as follows:

1. If applicable, perform modification of the grid (e.g., additional support film).

2. Glow-discharge the grids for 30′ at 15 mA. The grids should be used within the next 30 min.
3. Set the humidity and temperature at which the sample should be frozen. We routinely use 100% humidity and 15 °C on a Vitrobot Mark IV.
4. Apply the sample onto the grids (if applicable with additives, e.g., surfactants or ligands). For TMEM16 studies we used Quantifoil Au 1.2/1.3300 mesh holey carbon film grids.
5. Blot the grids for a selected amount of time (*see* **Note 20**). For TMEM16 a number of grids with different blotting times ranging from 2 to 7 s were prepared.
6. Plunge-freeze into the ethane/propane mixture and store grids in liquid N_2.

Although sample preparation was carried out in a similar manner (same type of grids, same freezing conditions, images acquired in regions of optimal ice thickness, etc.), notable differences could be observed between the TMEM16 datasets (Fig. 5). For mTMEM16F, the nanodisc samples displayed preferred particle orientation, which was not present in the equivalent detergent-solubilized sample. The anisotropy was less severe for the nanodisc dataset in the presence of Ca^{2+} than for the nanodisc dataset in the absence of Ca^{2+}, where the strong anisotropy distorted reconstruction and hampered a detailed interpretation of the cryo-EM map. The presence of Ca^{2+} being the only difference between those two nanodisc samples indicates a putative effect of the ionic strength on particle distribution. The fact that we did not encounter problems with particle orientation in the equivalent nanodisc datasets of nhTMEM16 suggests that nanodiscs themselves are not a determinant for anisotropy (Fig. 5). In fact, none of the datasets acquired for nhTMEM16, either in detergent or nanodiscs, suffered from preferred particle orientation, which suggests that the protein itself can play a role in particle distribution. Moreover, mTMEM16A, which is a close homolog of mTMEM16F, displayed improved particle distribution in nanodiscs compared to detergent in the same study [18].

3.4 Data Collection and Image Processing

Different software solutions can be used for automated cryo-EM data collection (e.g., SerialEM [67], EPU (Thermo Fisher Scientific), Leginon [68]). In the case of TMEM16, cryo-EM data were collected in an automated fashion using the EPU software.

1. Acquire an atlas of the grid.
2. Align the microscope.
3. Select holes for data collection. The best regions on the grid were screened and selected with an in-house written script (manuscript in preparation) that calculates the ice thickness (*see* **Note 21**).

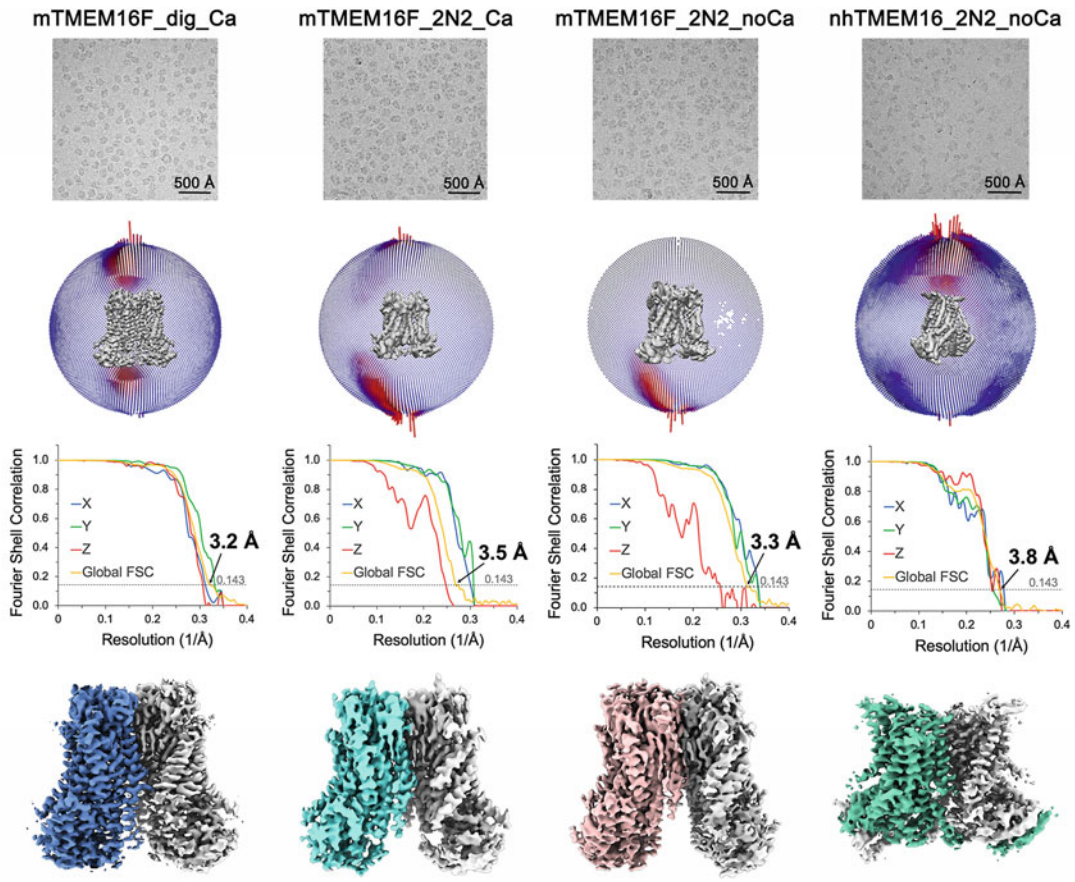

Fig. 5 Comparison of TMEM16 cryo-EM datasets. Shown are (from top to bottom) a representative cryo-EM image; the angular distribution of particles in the final map; the directional resolution values in *X*, *Y*, and *Z* compared to the global FSC resolution; and the final cryo-EM map of the indicated lipid scramblase with one protomer colored. Datasets shown are (from left to right) the Ca^{2+}-bound mTMEM16F in digitonin, the Ca^{2+}-bound mTMEM16F in nanodiscs, the Ca^{2+}-free mTMEM16F in nanodiscs, and the Ca^{2+}-free nhTMEM16 in nanodiscs. While the mTMEM16F datasets in nanodiscs, but not in detergent, suffered from favored particle orientation (Ca^{2+}-free stronger than Ca^{2+}-bound), this effect was not observed for the equivalent sample in nhTMEM16

4. Set up data collection. Define acquisition, autofocus, drift measurement areas, defocus range, and drift threshold. For the TMEM16 work, data was acquired on our in-house 200 kV Talos Arctica (Thermo Fisher Scientific) at a pixel size of 1.012 Å, an exposure time of 9 s with a sub-frame exposure time of 150 ms (60 frames), and a total electron exposure on the specimen of about 52 electrons per $Å^2$ with a defocus range from −0.5 to −2 μm and a drift threshold of 1 Å/s.
5. Start acquisition. Data quality was monitored on the fly using the software Focus [69]. At this stage it is possible to adjust the thickness range in order to optimize data collection.

6. Images showing contamination, an ice thickness or a defocus value out of the selected range, or a poor resolution in CTF estimation can be discarded.

Solutions to overcome problems of preferred particle orientation during data collection include the following: collect images in thicker ice (*see* **Note 22**), collect more images (*see* **Note 23**), or collect tilt images (*see* **Note 24**).

The resulting images are further analyzed with one of the available software packages for cryo-EM image processing (e.g., RELION [2, 70], cisTEM [71], cryoSPARC [72], EMAN2 [73], SPHIRE [74]). While the use of nanodiscs can impose additional challenges during image processing, standard image analysis procedures, as used for detergent-solubilized proteins, also apply to nanodisc samples. In particular, particle alignment of a target protein that is fully embedded in the nanodisc, with no protruding large soluble domains, can be very challenging (*see* **Notes 25** and **26**). Possible solutions include the application of C1 symmetry (*see* **Note 27**), use of binders (*see* **Note 28**), focused refinement (*see* **Note 29**), and signal subtraction (*see* **Note 30**).

4 Notes

1. Synthetic lipids, such as POPC and POPC:POPG mixtures, are widely used for nanodisc assembly as they provide a complete control over the lipid mixture and its characteristics. However, if the protein of interest requires a more complex lipid composition or the presence of unknown lipidic cofactors for its activity, the use of natural lipid extracts is also possible. Various polar lipid extracts from natural sources, such as *E. coli* membranes, soybean, and bovine heart, are commercially available or can be extracted in the laboratory [75].
2. The length of the MSP is the major determinant of the nanodisc diameter, which can range from 6 to 80 nm (Table 2) [76, 77, 79]. Thus, the choice of MSP is an important parameter and the size and oligomeric state of the target protein should be considered when choosing a scaffold protein. If the selected MSP forms nanodiscs that are considerably larger than the protein of interest, multiple incorporations of the target protein will be possible and/or the target protein may "float" in the nanodisc, leading to challenges in particle alignment and image processing. By contrast, selecting an MSP that forms nanodiscs of insufficient diameter might prevent protein incorporation altogether. MD simulations and DSC have shown that lipids in direct contact with the MSP (~15 Å) are perturbed due to hydrophobic mismatch, and have different properties compared to bulk lipids [62, 80–82]. Thus, a MSP that allows for

Table 2
Commonly used membrane scaffold proteins

MSP	Diameter	Type of MSP	Reference
MSP1D1ΔH5	8 nm	Conventional	[76]
NW9	8.5 nm	Circularized	[77]
MSP1D1	9.6 nm	Conventional	[58]
NW11	11 nm	Circularized	[77]
MSP1E3D1	12.1 nm	Conventional	[78]
NW30	15 nm	Circularized	[77]
MSP2 N2	16.5 nm	Conventional	[79]
MSP2N3	17 nm	Conventional	[79]
NW50	50 nm	Circularized	[77]

This is not an exhaustive list

the presence of additional layers of lipid molecules (15–20 Å) away from the scaffold protein might be required to mimic a planar lipid bilayer and preserve a native and full activity state of the incorporated target protein [62, 80–83]. Several MSP constructs of different sizes (Table 2) are readily available on Addgene and can be easily expressed in *Escherichia coli* and purified in large quantities from a relatively small amount of bacterial culture [60].

3. The final diameter of a nanodisc depends not only on the MSP but also on the amount of reconstituted lipids [19, 59] (Fig. 4). One strategy to counter this problem is to use circularized covalently linked MSPs (cMSP) [77], which assemble into nanodiscs with a defined homogeneous size. Circularized covalently linked MSPs (cMSPs) were developed by Wagner and colleagues and protocols for nanodisc assembly with this technology can be consulted at [77, 84, 85]. Before nanodisc assembly, the purified MSP needs to be circularized and requires a fresh preparation of sortase, adding several steps to the MSP preparation. While it remains unclear whether the incorporation efficiency into nanodiscs formed by cMSPs is comparable to conventional MSPs, a recent study demonstrated a successful application of cMSP for high-resolution cryo-EM [28].
4. The assembly of protein-nanodisc complexes is, to our knowledge, not limited by any buffer component used during protein purification, except for glycerol at concentrations above 4% [60]. Thus, conditions in which the protein is homogeneous and most stable should be used for the assembly. Alternatively,

nanodiscs can be assembled directly after membrane solubilization, performing purification of the target protein after its incorporation into nanodiscs [26]. While this minimizes the time in which the protein is exposed to detergent, it requires significantly higher amounts of MSPs and lipids, might lead to co-purification of other proteins, and prevents an accurate estimation of the target protein-to-lipid-to-MSP ratios [26].

5. Different lipid compositions require different lipid-to-MSP ratios, as lipids vary in their surface area [60, 81]. For each MSP and lipid mixture the optimal lipid-to-MSP ratio should be first determined in the absence of target protein, particularly when working with lipid extracts from natural sources.
6. Further, the lipid-to-MSP ratio has an effect on the nanodisc diameter and its homogeneity, in particular when using the large MSP2N2, and needs to be optimized [19, 79]. A large excess of lipids in the reconstitution reaction will result in the formation of nanodiscs with a heterogeneous size distribution and in the formation of liposomes by residual non-incorporated lipids (Figs. 3 and 4) [19, 59]. Conversely, the efficiency of reconstitution will also decrease if the lipid-to-MSP ratio is too low, leading to lipid-poor particles [59]. Another important parameter to consider during assembly is the ratio of target protein to assembled nanodiscs. To optimize assembly efficacy and to prevent multiple incorporation events of the target protein it is recommended to work with an excess of fully assembled nanodiscs [86], where empty nanodiscs can later be removed by affinity purification or size-exclusion chromatography.
7. The ternary mixture of target protein, lipids, and MSPs used during nanodisc assembly should be incubated at a temperature slightly above that of the phase transition of the selected lipids [59]. Note that once incorporated into nanodiscs the lipids show a broader phase transition [82].
8. A molar ratio of 2:10 of $TMEM16_{monomer}$:2N2 (one full dimer per five assembled nanodiscs) was selected to ensure that in most cases only one TMEM16 dimer is incorporated per nanodisc.
9. Separation of protein-nanodisc complexes from empty nanodiscs is easily accomplished by the use of affinity chromatography. The purification tag on the target protein can be used to isolate the protein-nanodisc complexes, while empty nanodiscs are removed during the wash steps. Alternatively, if the protein-nanodisc complex is significantly larger than the empty nanodiscs, both species can be directly separated by size-exclusion chromatography. Either way, due to the heterogeneity in nanodisc size, a final size-exclusion chromatography step is required to obtain a homogeneous sample for cryo-EM.

10. All buffers used during protein-nanodisc complex purification should be detergent-free to prevent solubilization of the nanodiscs.
11. The main peak is often broad, reflecting the heterogeneity of nanodisc sizes or multiple incorporations of a target protein per nanodisc (Fig. 3).
12. The estimation of the target protein concentration in nanodiscs is not straightforward, as the target protein and the MSPs, and to some extent also the lipids, contribute to the total absorbance at 280 nm. For a relative assessment of the protein concentration between batches one can compare the raw absorption value at 280 nm. Alternatively, one can calculate the molar concentration of the nanodisc sample by estimating the molar excitation coefficient (ε) of the entire complex ($\varepsilon_{\text{nanodisc-complex}} = \varepsilon_{\text{target protein}} + 2 * \varepsilon_{\text{MSP}}$). The molar concentration can then be estimated using the absorbance value at 280 nm and the Beer-Lambert equation.
13. The preferred orientation of particles in cryo-EM images leads to an uneven distribution of angular projections, which results in a map affected by anisotropic resolution [87, 88] and which attenuates the global Fourier shell correlation (FSC) [89]. It has become a good conduct in cryo-EM to calculate the distinct directional resolution values in X, Y, and Z directions (3DFSC) and to plot them against the global FSC resolution, which can be easily done online ([88]; https://3dfsc.salk.edu/). In case of anisotropic 3D reconstructions, it is also advised to perform a quantitative evaluation of the sampling compensation factor (SCF) criterion in order to evaluate the effect of nonuniform angular sampling on the global resolution [89].
14. Particle diffusion and adsorption to the air-water interface require little or no activation energy and occur in a few milliseconds [90, 91]. Once at the air-water interface, proteins partially lose their hydration shell, dry out, and unfold, retaining them in a specific orientation [92]. New sample preparation tools have been developed that allow to study this process in more detail [92]. However, these studies have so far been confined to soluble proteins. Although hydrophobic regions of a protein may be more prone to adhere to the air-water interface, it remains to be shown if membrane proteins and use of membrane-mimicking tools are indeed more affected.
15. The use of fluorinated surfactants, such as the non-solubilizing fluorinated octyl-maltoside or fluorinated Fos-choline 8, has been shown to improve the vitrification process and particle distribution on cryo-EM grids (Table 1) [12, 93–95]. Most likely, the surfactants form a hydrophilic, electron-transparent monolayer that reduces the access of the protein to the

hydrophobic side of the air-water interface [90]. Note that the presence of fluorinated detergents might affect the optimal sample concentration.

16. Grids of different metal coating material, mesh, and hole size can have an influence on the blotting process and the final curvature and thickness of the ice. Apart from their advantage to significantly reduce beam-induced motion [96, 97], holey gold-supporting films can be further chemically modified to optimize particle distribution and avoid particle adhesion to the supporting film [98].
17. If particles are bound to a structure-friendly support film, as long as the ice layer remains thick enough, there is no risk of adsorption to the air-water interface. Different types of chemically modified support films include continuous carbon film [99, 100], an additional layer of graphene oxide [101], hydrophilized graphene [102], functionalized graphene monolayer [103, 104], or even affinity-based monolayer support film [105–109].
18. The sample may be supplemented with other additives in order to improve particle orientation distribution and/or saturate the air-water interface and thereby shield the protein from denaturation. For example antibodies [110] or megabodies [31, 111, 112] attached to the target protein have shown to improve sample quality.
19. New sample freezing devices have been developed, e.g., Spotiton [113–116], Vitrojet [117], and cryoWriter [118], with the aim to substantially optimize cryo-EM sample preparation. In particular the Spotiton approach (currently being commercialized by TTP Labtech as Chameleon) allows to considerably reduce the spot-to-plunge time, giving particles not enough time to adhere to air-water interface and adopt preferential orientation in the first place.
20. It has been demonstrated that performing a few rounds of sample application and blotting before freezing could significantly increase particle density in a simple and cost-effective way [119]. This might however increase the risk of particles adhering to the air-water interface.
21. Ice thickness has a direct impact on data quality and ultimately on the resolution [120]. Therefore, data collection efficiency can be greatly improved if the ice thickness is measured as a criterion for hole selection before data acquisition (manuscript in preparation).
22. While images collected on thicker ice will be of lower quality, as evident from the drop in the estimated resolution of the CTF fit [120–122], thicker ice might allow to accommodate the particles in different, otherwise missing, orientations.

23. Collect more images to obtain sufficient number of particles in low-abundant views. During 3D reconstruction, the uneven distribution should be compensated by up-weighting under-represented views and lowering the particle number in over-represented views [88, 123]. This approach is not applicable if the view is entirely missing.
24. Additional images are collected at a defined nominal tilt angle. The defocus gradient across the images must be taken into account during image processing and might limit optimal high-resolution data collection [88, 124–126].
25. Alignment of the target protein reconstituted into nanodiscs is typically more difficult than the equivalent detergent samples because phospholipid headgroups scatter electrons stronger than the target protein, which is composed of lighter atoms. They contribute stronger to the overall signal, might obscure the target protein, and thereby hamper particle alignment. Further, nanodiscs often display a high degree of heterogeneity in size and morphology. Here, the target proteins might "float" in the nanodisc, leading to asymmetric particles where the position of the protein relative to the nanodisc boundaries differs. In case the target protein is not embedded in the center of the nanodisc, any potential intrinsic symmetry would be disrupted.
26. It was possible to achieve a high-resolution reconstruction on a synthetic dataset with a protein fully embedded in a nanodisc [127].
27. Despite all efforts to optimize the assembly parameters and additional purification steps, the datasets of nhTMEM16 in nanodisc complexes were heterogeneous [19]. This not only included different sizes of nhTMEM16-2N2 complexes but also the presence of empty nanodiscs observed during initial 2D and 3D classification steps. Although nhTMEM16 is a homodimer, it was beneficial to apply a C1 symmetry during initial 3D classification and only impose C2 symmetry at a final stage. To tackle the effect of heterogenous nanodisc sizes, increasingly smaller spherical masks were applied (220 Å during 2D classification, 180 Å during 3D classification, and by the end a tight mask around the protein was used). Ultimately, the nanodisc densities were subtracted and thereby entirely excluded during particle alignment. This approach not only improved the resolution, but also allowed a finer separation of distinct conformations found in one of the datasets (nhTMEM16 in 2N2 with Ca^{2+}).
28. For example Fab fragments or megabodies that bind to soluble regions of the target protein can facilitate its identification and guide particle alignment [11, 31, 111, 112].

29. During focused refinement, densities outside a selected region are temporarily masked out from the reference (e.g., the nanodisc) and their signal does not contribute to particle alignment [128, 129].
30. During image processing selected densities (e.g., corresponding to the nanodisc) are subtracted from the particles and will no longer contribute to particle alignment [8, 18–20, 130].

Acknowledgments

We thank Hendrik Siekkema and Dawid Deneka for valuable discussion and Jan Rheinberger and Chancievan Thangaratnarajah for critical reading of the manuscript. V.K was funded by the SNF early postdocmobility fellowship 187679. C.P. was funded by the NWO Veni grant 722.017.001 and the NWO Start-Up grant 740.018.016.

References

1. Kühlbrandt W (2014) The resolution revolution. Science 343(6178):1443. https://doi.org/10.1126/science.1251652
2. Zivanov J, Nakane T, Forsberg BO, Kimanius D, Hagen WJH, Lindahl E, Scheres SHW (2018) New tools for automated high-resolution cryo-EM structure determination in RELION-3. Elife 7:e42166. https://doi.org/10.7554/eLife.42166
3. Fan X, Wang J, Zhang X, Yang Z, Zhang JC, Zhao L, Peng HL, Lei J, Wang HW (2019) Single particle cryo-EM reconstruction of 52 kDa streptavidin at 3.2 Angstrom resolution. Nat Commun 10(1):2386. https://doi.org/10.1038/s41467-019-10368-w
4. Roh SH, Stam NJ, Hryc CF, Couoh-Cardel S, Pintilie G, Chiu W, Wilkens S (2018) The 3.5-Å cryoEM structure of nanodisc-reconstituted yeast vacuolar ATPase V_o proton channel. Mol Cell 69(6):993–1004. https://doi.org/10.1016/j.molcel.2018.02.006
5. Matthies D, Bae C, Toombes GES, Fox T, Bartesaghi A, Subramaniam S, Swartz KJ (2018) Single-particle cryo-EM structure of a voltage-activated potassium channel in lipid nanodiscs. Elife 7:e37558. https://doi.org/10.7554/eLife.37558
6. Autzen HE, Myasnikov AG, Campbell MG, Asarnow D, Julius D, Cheng Y (2018) Structure of the human TRPM4 ion channel in a lipid nanodisc. Science 359(6372):228–232. https://doi.org/10.1126/science.aar4510
7. Jojoa Cruz S, Saotome K, Murthy SE, Tsui CC, Sansom MSP, Patapoutian A, Ward AB (2018) Cryo-EM structure of the mechanically activated ion channel OSCA1.2. Elife 7:e41845. https://doi.org/10.7554/eLife.41845
8. Mi W, Li Y, Yoon SH, Ernst RK, Walz T, Liao M (2017) Structural basis of MsbA-mediated lipopolysaccharide transport. Nature 549:233–237. https://doi.org/10.1038/nature23649. https://www.nature.com/articles/nature23649#supplementary-information
9. Srivastava AP, Luo M, Zhou W, Symersky J, Bai D, Chambers MG, Faraldo-Gómez JD, Liao M, Mueller DM (2018) High-resolution cryo-EM analysis of the yeast ATP synthase in a lipid membrane. Science 360(6389):eaas9699
10. Taylor NMI, Manolaridis I, Jackson SM, Kowal J, Stahlberg H, Locher KP (2017) Structure of the human multidrug transporter ABCG2. Nature 546:504–509. https://doi.org/10.1038/nature22345
11. Jackson SM, Manolaridis I, Kowal J, Zechner M, Taylor NMI, Bause M, Bauer S, Bartholomaeus R, Bernhardt G, Koenig B, Buschauer A, Stahlberg H, Altmann K-H, Locher KP (2018) Structural basis of small-molecule inhibition of human multidrug transporter ABCG2. Nat Struct Mol Biol 25

(4):333–340. https://doi.org/10.1038/s41594-018-0049-1

12. Gatsogiannis C, Merino F, Prumbaum D, Roderer D, Leidreiter F, Meusch D, Raunser S (2016) Membrane insertion of a Tc toxin in near-atomic detail. Nat Struct Mol Biol 23:884–890. https://doi.org/10.1038/nsmb.3281. https://www.nature.com/articles/nsmb.3281#supplementary-information
13. Zhang S, Li N, Zeng W, Gao N, Yang M (2017) Cryo-EM structures of the mammalian endo-lysosomal TRPML1 channel elucidate the combined regulation mechanism. Protein Cell 8(11):834–847. https://doi.org/10.1007/s13238-017-0476-5
14. Chen Q, She J, Zeng W, Guo J, Xu H, Bai X-c, Jiang Y (2017) Structure of mammalian endo-lysosomal TRPML1 channel in nanodiscs. Nature 550:415. https://doi.org/10.1038/nature24035. https://www.nature.com/articles/nature24035#supplementary-information
15. Jin P, Bulkley D, Guo Y, Zhang W, Guo Z, Huynh W, Wu S, Meltzer S, Cheng T, Jan LY, Jan Y-N, Cheng Y (2017) Electron cryo-microscopy structure of the mechanotransduction channel NOMPC. Nature 547:118–122. https://doi.org/10.1038/nature22981. https://www.nature.com/articles/nature22981#supplementary-information
16. Gao Y, Cao E, Julius D, Cheng Y (2016) TRPV1 structures in nanodiscs reveal mechanisms of ligand and lipid action. Nature 534:347–351. https://doi.org/10.1038/nature17964
17. Fan C, Fan M, Orlando BJ, Fastman NM, Zhang J, Xu Y, Chambers MG, Xu X, Perry K, Liao M, Feng L (2018) X-ray and cryo-EM structures of the mitochondrial calcium uniporter. Nature 559(7715):575–579. https://doi.org/10.1038/s41586-018-0330-9
18. Dang S, Feng S, Tien J, Peters CJ, Bulkley D, Lolicato M, Zhao J, Zuberbühler K, Ye W, Qi L, Chen T, Craik CS, Jan YN, Minor DL Jr, Cheng Y, Jan LY (2017) Cryo-EM structures of the TMEM16A calcium-activated chloride channel. Nature 552:426–429. https://doi.org/10.1038/nature25024. https://www.nature.com/articles/nature25024#supplementary-information
19. Kalienkova V, Clerico Mosina V, Bryner L, Oostergetel GT, Dutzler R, Paulino C (2019) Stepwise activation mechanism of the scramblase nhTMEM16 revealed by cryo-EM. Elife 8:e44364. https://doi.org/10.7554/eLife.44364
20. Falzone ME, Rheinberger J, Lee B-C, Peyear T, Sasset L, Raczkowski AM, Eng ET, Di Lorenzo A, Andersen OS, Nimigean CM, Accardi A (2019) Structural basis of Ca^{2+}-dependent activation and lipid transport by a TMEM16 scramblase. Elife 8:e43229. https://doi.org/10.7554/eLife.43229
21. Alvadia C, Lim NK, Clerico Mosina V, Oostergetel GT, Dutzler R, Paulino C (2019) Cryo-EM structures and functional characterization of the murine lipid scramblase TMEM16F. Elife 8:e44365. https://doi.org/10.7554/eLife.44365
22. Kern DM, Oh S, Hite RK, Brohawn SG (2019) Cryo-EM structures of the DCPIB-inhibited volume-regulated anion channel LRRC8A in lipid nanodiscs. Elife 8:e42636. https://doi.org/10.7554/eLife.42636
23. Tang Q, Guo W, Zheng L, Wu J-X, Liu M, Zhou X, Zhang X, Chen L (2018) Structure of the receptor-activated human TRPC6 and TRPC3 ion channels. Cell Res 28 (7):746–755. https://doi.org/10.1038/s41422-018-0038-2
24. Hughes TET, Pumroy RA, Yazici AT, Kasimova MA, Fluck EC, Huynh KW, Samanta A, Molugu SK, Zhou ZH, Carnevale V, Rohacs T, Moiseenkova-Bell VY (2018) Structural insights on TRPV5 gating by endogenous modulators. Nat Commun 9(1):4198. https://doi.org/10.1038/s41467-018-06753-6
25. Shen PS, Yang X, DeCaen PG, Liu X, Bulkley D, Clapham DE, Cao E (2016) The structure of the polycystic kidney disease channel PKD2 in lipid nanodiscs. Cell 167(3):763–773. https://doi.org/10.1016/j.cell.2016.09.048
26. Willegems K, Efremov RG (2018) Influence of lipid mimetics on gating of ryanodine receptor. Structure 26(10):1303–1313. https://doi.org/10.1016/j.str.2018.06.010
27. Wild R, Kowal J, Eyring J, Ngwa EM, Aebi M, Locher KP (2018) Structure of the yeast oligosaccharyltransferase complex gives insight into eukaryotic N-glycosylation. Science 359 (6375):545–550. https://doi.org/10.1126/science.aar5140
28. McGoldrick LL, Singh AK, Saotome K, Yelshanskaya MV, Twomey EC, Grassucci RA, Sobolevsky AI (2017) Opening of the human epithelial calcium channel TRPV6. Nature 553:233–237. https://doi.org/10.1038/nature25182. https://www.nature.com/articles/nature25182#supplementary-information
29. Quentin D, Ahmad S, Shanthamoorthy P, Mougous JD, Whitney JC, Raunser S (2018)

Mechanism of loading and translocation of type VI secretion system effector Tse6. Nat Microbiol 3(10):1142–1152. https://doi.org/10.1038/s41564-018-0238-z

30. Rheinberger J, Gao X, Schmidpeter PAM, Nimigean CM (2018) Ligand discrimination and gating in cyclic nucleotide-gated ion channels from apo and partial agonist-bound cryo-EM structures. Elife 7:e39775. https://doi.org/10.7554/eLife.39775
31. Laverty D, Desai R, Uchański T, Masiulis S, Stec WJ, Malinauskas T, Zivanov J, Pardon E, Steyaert J, Miller KW, Aricescu AR (2019) Cryo-EM structure of the human α1β3γ2 GABAA receptor in a lipid bilayer. Nature 565:516–520. https://doi.org/10.1038/s41586-018-0833-4
32. Saotome K, Teng B, Tsui CC, Lee W-H, Tu Y-H, Kaplan JP, Sansom MSP, Liman ER, Ward AB (2019) Structures of the otopetrin proton channels Otop1 and Otop3. Nat Struct Mol Biol 26(6):518–525. https://doi.org/10.1038/s41594-019-0235-9
33. Walter JD, Sawicka M, Dutzler R (2019) Cryo-EM structures and functional characterization of murine Slc26a9 reveal mechanism of uncoupled chloride transport. Elife 8:e46986. https://doi.org/10.7554/eLife.46986
34. Davies KM, Anselmi C, Wittig I, Faraldo-Gómez JD, Kühlbrandt W (2012) Structure of the yeast F1Fo-ATP synthase dimer and its role in shaping the mitochondrial cristae. Proc Natl Acad Sci U S A 109(34):13602–13607. https://doi.org/10.1073/pnas.1204593109
35. Kosinski J, Mosalaganti S, von Appen A, Teimer R, DiGuilio AL, Wan W, Bui KH, Hagen WJH, Briggs JAG, Glavy JS, Hurt E, Beck M (2016) Molecular architecture of the inner ring scaffold of the human nuclear pore complex. Science 352(6283):363–365. https://doi.org/10.1126/science.aaf0643
36. von Appen A, Kosinski J, Sparks L, Ori A, DiGuilio AL, Vollmer B, Mackmull M-T, Banterle N, Parca L, Kastritis P, Buczak K, Mosalaganti S, Hagen W, Andres-Pons A, Lemke EA, Bork P, Antonin W, Glavy JS, Bui KH, Beck M (2015) In situ structural analysis of the human nuclear pore complex. Nature 526:140–143. https://doi.org/10.1038/nature15381. https://www.nature.com/articles/nature15381#supplementary-information
37. Kovtun O, Leneva N, Bykov YS, Ariotti N, Teasdale RD, Schaffer M, Engel BD, Owen DJ, Briggs JAG, Collins BM (2018) Structure of the membrane-assembled retromer coat determined by cryo-electron tomography. Nature 561(7724):561–564. https://doi.org/10.1038/s41586-018-0526-z
38. Mühleip AW, Dewar CE, Schnaufer A, Kuhlbrandt W, Davies KM (2017) In situ structure of trypanosomal ATP synthase dimer reveals a unique arrangement of catalytic subunits. Proc Natl Acad Sci U S A 114(5):992–997. https://doi.org/10.1073/pnas.1612386114
39. Mühleip AW, Joos F, Wigge C, Frangakis AS, Kühlbrandt W, Davies KM (2016) Helical arrays of U-shaped ATP synthase dimers form tubular cristae in ciliate mitochondria. Proc Natl Acad Sci U S A 113(30):8442–8447. https://doi.org/10.1073/pnas.1525430113
40. Tonggu L, Wang L (2018) Cryo-EM sample preparation method for extremely low concentration liposomes. bioRxiv:494997. https://doi.org/10.1101/494997
41. Kudryashev M, Castaño-Díez D, Deluz C, Hassaine G, Grasso L, Graf-Meyer A, Vogel H, Stahlberg H (2016) The structure of the mouse serotonin 5-HT3 receptor in lipid vesicles. Structure 24(1):165–170. https://doi.org/10.1016/j.str.2015.11.004
42. Pang SS, Bayly-Jones C, Radjainia M, Spicer BA, Law RHP, Hodel AW, Ekkel SM, Conroy PJ, Ramm G, Venugopal H, Bird PI, Hoogenboom BW, Voskoboinik I, Gambin Y, Sierecki E, Dunstone MA, Whisstock JC (2019) The structure of Macrophage Expressed Gene-1, a phagolysosome immune effector that is activated upon acidification. bioRxiv:580712. https://doi.org/10.1101/580712
43. Frauenfeld J, Löving R, Armache J-P, Sonnen AFP, Guettou F, Moberg P, Zhu L, Jegerschöld C, Flayhan A, Briggs JAG, Garoff H, Löw C, Cheng Y, Nordlund P (2016) A saposin-lipoprotein nanoparticle system for membrane proteins. Nat Methods 13:345–351. https://doi.org/10.1038/nmeth.3801. https://www.nature.com/articles/nmeth.3801#supplementary-information
44. Nagamura R, Fukuda M, Kawamoto A, Matoba K, Dohmae N, Ishitani R, Takagi J, Nureki O (2019) Structural basis for oligomerization of the prokaryotic peptide transporter PepTSo2. Acta Crystallogr F Struct Biol Commun 75(Pt 5):348–358. https://doi.org/10.1107/s2053230x19003546
45. Carlson ML, Young JW, Zhao Z, Fabre L, Jun D, Li J, Li J, Dhupar HS, Wason I, Mills AT, Beatty JT, Klassen JS, Rouiller I, Duong F (2018) The Peptidisc, a simple method for stabilizing membrane proteins in detergent-

free solution. Elife 7:e34085. https://doi.org/10.7554/eLife.34085

46. Knowles TJ, Finka R, Smith C, Lin Y-P, Dafforn T, Overduin M (2009) Membrane proteins solubilized intact in lipid containing nanoparticles bounded by styrene maleic acid copolymer. J Am Chem Soc 131 (22):7484–7485. https://doi.org/10.1021/ja810046q
47. Bayburt TH, Carlson JW, Sligar SG (1998) Reconstitution and imaging of a membrane protein in a nanometer-size phospholipid bilayer. J Struct Biol 123(1):37–44. https://doi.org/10.1006/jsbi.1998.4007
48. Flayhan A, Mertens HDT, Ural-Blimke Y, Martinez Molledo M, Svergun DI, Löw C (2018) Saposin lipid nanoparticles: a highly versatile and modular tool for membrane protein research. Structure 26(2):345–355. https://doi.org/10.1016/j.str.2018.01.007
49. Nguyen NX, Armache J-P, Lee C, Yang Y, Zeng W, Mootha VK, Cheng Y, Bai X-c, Jiang Y (2018) Cryo-EM structure of a fungal mitochondrial calcium uniporter. Nature 559 (7715):570–574. https://doi.org/10.1038/s41586-018-0333-6
50. Teo ACK, Lee SC, Pollock NL, Stroud Z, Hall S, Thakker A, Pitt AR, Dafforn TR, Spickett CM, Roper DI (2019) Analysis of SMALP co-extracted phospholipids shows distinct membrane environments for three classes of bacterial membrane protein. Sci Rep 9(1):1813. https://doi.org/10.1038/s41598-018-37962-0
51. Parmar M, Rawson S, Scarff CA, Goldman A, Dafforn TR, Muench SP, Postis VLG (2018) Using a SMALP platform to determine a sub-nm single particle cryo-EM membrane protein structure. Biochim Biophys Acta 1860 (2):378–383. https://doi.org/10.1016/j.bbamem.2017.10.005
52. Sun C, Benlekbir S, Venkatakrishnan P, Wang Y, Hong S, Hosler J, Tajkhorshid E, Rubinstein JL, Gennis RB (2018) Structure of the alternative complex III in a supercomplex with cytochrome oxidase. Nature 557 (7703):123–126. https://doi.org/10.1038/s41586-018-0061-y
53. Qiu W, Fu Z, Xu GG, Grassucci RA, Zhang Y, Frank J, Hendrickson WA, Guo Y (2018) Structure and activity of lipid bilayer within a membrane-protein transporter. Proc Natl Acad Sci U S A 115(51):12985–12990. https://doi.org/10.1073/pnas.1812526115
54. Swainsbury DJK, Scheidelaar S, Foster N, van Grondelle R, Killian JA, Jones MR (2017) The effectiveness of styrene-maleic acid (SMA) copolymers for solubilisation of integral membrane proteins from SMA-accessible and SMA-resistant membranes. Biochim Biophys Acta 1859(10):2133–2143. https://doi.org/10.1016/j.bbamem.2017.07.011
55. Dominguez Pardo JJ, Dorr JM, Iyer A, Cox RC, Scheidelaar S, Koorengevel MC, Subramaniam V, Killian JA (2017) Solubilization of lipids and lipid phases by the styrene-maleic acid copolymer. Eur Biophys J 46(1):91–101. https://doi.org/10.1007/s00249-016-1181-7
56. Oluwole AO, Danielczak B, Meister A, Babalola JO, Vargas C, Keller S (2017) Solubilization of membrane proteins into functional lipid-bilayer nanodiscs using a diisobutylene/maleic acid copolymer. Angew Chem Int Ed Engl. 56(7):1919–1924. https://doi.org/10.1002/anie.201610778
57. Bayburt TH, Grinkova YV, Sligar SG (2002) Self-assembly of discoidal phospholipid bilayer nanoparticles with membrane scaffold proteins. Nano Lett 2(8):853–856. https://doi.org/10.1021/nl025623k
58. Denisov IG, Grinkova YV, Lazarides AA, Sligar SG (2004) Directed self-assembly of monodisperse phospholipid bilayer Nanodiscs with controlled size. J Am Chem Soc 126 (11):3477–3487. https://doi.org/10.1021/ja0393574
59. Bayburt TH, Sligar SG (2010) Membrane protein assembly into Nanodiscs. FEBS Lett 584(9):1721–1727. https://doi.org/10.1016/j.febslet.2009.10.024
60. Ritchie TK, Grinkova YV, Bayburt TH, Denisov IG, Zolnerciks JK, Atkins WM, Sligar SG (2009) Reconstitution of membrane proteins in phospholipid bilayer nanodiscs. Methods Enzymol 464:211–231. https://doi.org/10.1016/s0076-6879(09)64011-8
61. Bayburt TH, Sligar SG (2003) Self-assembly of single integral membrane proteins into soluble nanoscale phospholipid bilayers. Protein Sci 12(11):2476–2481
62. Schuler MA, Denisov IG, Sligar SG (2013) Nanodiscs as a new tool to examine lipid-protein interactions. Methods Mol Biol 974:415–433. https://doi.org/10.1007/978-1-62703-275-9_18
63. Pedemonte N, Galietta LJ (2014) Structure and function of TMEM16 proteins (anoctamins). Physiol Rev 94(2):419–459. https://doi.org/10.1152/physrev.00039.2011
64. Brunner JD, Lim NK, Schenck S, Duerst A, Dutzler R (2014) X-ray structure of a calcium-activated TMEM16 lipid scramblase. Nature 516(7530):207–212. https://doi.

org/10.1038/nature13984. http://www.nature.com/nature/journal/v516/n7530/abs/nature13984.html#supplementary-information

65. Paulino C, Kalienkova V, Lam AKM, Neldner Y, Dutzler R (2017) Activation mechanism of the calcium-activated chloride channel TMEM16A revealed by cryo-EM. Nature 552(7685):421–425. https://doi.org/10.1038/nature24652
66. Paulino C, Neldner Y, Lam AK, Kalienkova V, Brunner JD, Schenck S, Dutzler R (2017) Structural basis for anion conduction in the calcium-activated chloride channel TMEM16A. Elife 6:e26232. https://doi.org/10.7554/eLife.26232
67. Mastronarde DN (2005) Automated electron microscope tomography using robust prediction of specimen movements. J Struct Biol 152(1):36–51. https://doi.org/10.1016/j.jsb.2005.07.007
68. Suloway C, Pulokas J, Fellmann D, Cheng A, Guerra F, Quispe J, Stagg S, Potter CS, Carragher B (2005) Automated molecular microscopy: the new Leginon system. J Struct Biol 151(1):41–60. https://doi.org/10.1016/j.jsb.2005.03.010
69. Biyani N, Righetto RD, McLeod R, Caujolle-Bert D, Castano-Diez D, Goldie KN, Stahlberg H (2017) Focus: The interface between data collection and data processing in cryo-EM. J Struct Biol 198(2):124–133. https://doi.org/10.1016/j.jsb.2017.03.007
70. Scheres SHW (2012) RELION: implementation of a Bayesian approach to cryo-EM structure determination. J Struct Biol 180(3):519–530. https://doi.org/10.1016/j.jsb.2012.09.006
71. Grant T, Rohou A, Grigorieff N (2018) cisTEM, user-friendly software for single-particle image processing. Elife 7:e35383. https://doi.org/10.7554/eLife.35383
72. Punjani A, Rubinstein JL, Fleet DJ, Brubaker MA (2017) cryoSPARC: algorithms for rapid unsupervised cryo-EM structure determination. Nat Methods 14:290–296. https://doi.org/10.1038/nmeth.4169. https://www.nature.com/articles/nmeth.4169#supplementary-information
73. Tang G, Peng L, Baldwin PR, Mann DS, Jiang W, Rees I, Ludtke SJ (2007) EMAN2: an extensible image processing suite for electron microscopy. J Struct Biol 157(1):38–46. https://doi.org/10.1016/j.jsb.2006.05.009
74. Moriya T, Saur M, Stabrin M, Merino F, Voicu H, Huang Z, Penczek PA, Raunser S, Gatsogiannis C (2017) High-resolution single particle analysis from electron cryomicroscopy images using SPHIRE. J Vis Exp 123:55448. https://doi.org/10.3791/55448
75. Hahn A, Vonck J, Mills DJ, Meier T, Kühlbrandt W (2018) Structure, mechanism, and regulation of the chloroplast ATP synthase. Science 360(6389):eaat4318. https://doi.org/10.1126/science.aat4318
76. Hagn F, Etzkorn M, Raschle T, Wagner G (2013) Optimized phospholipid bilayer nanodiscs facilitate high-resolution structure determination of membrane proteins. J Am Chem Soc 135(5):1919–1925. https://doi.org/10.1021/ja310901f
77. Nasr ML, Baptista D, Strauss M, Sun ZJ, Grigoriu S, Huser S, Pluckthun A, Hagn F, Walz T, Hogle JM, Wagner G (2017) Covalently circularized nanodiscs for studying membrane proteins and viral entry. Nat Methods 14(1):49–52. https://doi.org/10.1038/nmeth.4079
78. Denisov IG, Baas BJ, Grinkova YV, Sligar SG (2007) Cooperativity in cytochrome P450 3A4: linkages in substrate binding, spin state, uncoupling, and product formation. J Biol Chem 282(10):7066–7076. https://doi.org/10.1074/jbc.M609589200
79. Grinkova YV, Denisov IG, Sligar SG (2010) Engineering extended membrane scaffold proteins for self-assembly of soluble nanoscale lipid bilayers. Protein Eng Des Sel 23(11):843–848. https://doi.org/10.1093/protein/gzq060
80. Shih AY, Denisov IG, Phillips JC, Sligar SG, Schulten K (2005) Molecular dynamics simulations of discoidal bilayers assembled from truncated human lipoproteins. Biophys J 88(1):548–556. https://doi.org/10.1529/biophysj.104.046896
81. Efremov RG, Gatsogiannis C, Raunser S (2017) Lipid nanodiscs as a tool for high-resolution structure determination of membrane proteins by single-particle cryo-EM. Methods Enzymol 594:1–30. https://doi.org/10.1016/bs.mie.2017.05.007
82. Denisov IG, McLean MA, Shaw AW, Grinkova YV, Sligar SG (2005) Thermotropic phase transition in soluble nanoscale lipid bilayers. J Phys Chem B 109(32):15580–15588. https://doi.org/10.1021/jp051385g
83. Kawai T, Caaveiro JMM, Abe R, Katagiri T, Tsumoto K (2011) Catalytic activity of MsbA reconstituted in nanodisc particles is modulated by remote interactions with the bilayer. FEBS Lett 585(22):3533–3537. https://doi.org/10.1016/j.febslet.2011.10.015

84. Nasr ML, Wagner G (2018) Covalently circularized nanodiscs; challenges and applications. Curr Opin Struct Biol 51:129–134. https://doi.org/10.1016/j.sbi.2018.03.014
85. Johansen NT, Tidemand FG, Nguyen TTTN, Rand KD, Pedersen MC, Arleth L (2019) Circularized and solubility-enhanced MSPs facilitate simple and high-yield production of stable nanodiscs for studies of membrane proteins in solution. Febs Journal 286 (9):1734–1751. https://doi.org/10.1111/febs.14766
86. Hagn F, Nasr ML, Wagner G (2018) Assembly of phospholipid nanodiscs of controlled size for structural studies of membrane proteins by NMR. Nat Protoc 13(1):79–98. https://doi.org/10.1038/nprot.2017.094
87. Naydenova K, Russo CJ (2017) Measuring the effects of particle orientation to improve the efficiency of electron cryomicroscopy. Nat Commun 8(1):629. https://doi.org/10.1038/s41467-017-00782-3
88. Tan YZ, Baldwin PR, Davis JH, Williamson JR, Potter CS, Carragher B, Lyumkis D (2017) Addressing preferred specimen orientation in single-particle cryo-EM through tilting. Nat Methods 14(8):793–796. https://doi.org/10.1038/nmeth.4347
89. Baldwin PR, Lyumkis D (2019) Non-uniformity of projection distributions attenuates resolution in cryo-EM. bioRxiv:635938. https://doi.org/10.1101/635938
90. Glaeser RM, Han B-G (2017) Opinion: hazards faced by macromolecules when confined to thin aqueous films. Biophys Rep 3 (1):1–7. https://doi.org/10.1007/s41048-016-0026-3
91. Taylor KA, Glaeser RM (2008) Retrospective on the early development of cryoelectron microscopy of macromolecules and a prospective on opportunities for the future. J Struct Biol 163(3):214–223. https://doi.org/10.1016/j.jsb.2008.06.004
92. Noble AJ, Wei H, Dandey VP, Zhang Z, Tan YZ, Potter CS, Carragher B (2018) Reducing effects of particle adsorption to the air–water interface in cryo-EM. Nat Methods 15 (10):793–795. https://doi.org/10.1038/s41592-018-0139-3
93. Efremov RG, Leitner A, Aebersold R, Raunser S (2014) Architecture and conformational switch mechanism of the ryanodine receptor. Nature 517:39–43. https://doi.org/10.1038/nature13916. https://www.nature.com/articles/nature13916#supplementary-information
94. Johnson ZL, Chen J (2017) Structural basis of substrate recognition by the multidrug resistance protein MRP1. Cell 168 (6):1075–1085. https://doi.org/10.1016/j.cell.2017.01.041
95. Zhang Z, Chen J (2016) Atomic structure of the cystic fibrosis transmembrane conductance regulator. Cell 167(6):1586–1597. https://doi.org/10.1016/j.cell.2016.11.014
96. Russo CJ, Passmore LA (2014) Ultrastable gold substrates for electron cryomicroscopy. Science 346(6215):1377–1380. https://doi.org/10.1126/science.1259530
97. Russo CJ, Passmore LA (2016) Ultrastable gold substrates: properties of a support for high-resolution electron cryomicroscopy of biological specimens. J Struct Biol 193 (1):33–44. https://doi.org/10.1016/j.jsb.2015.11.006
98. Meyerson JR, Rao P, Kumar J, Chittori S, Banerjee S, Pierson J, Mayer ML, Subramaniam S (2014) Self-assembled monolayers improve protein distribution on holey carbon cryo-EM supports. Sci Rep 4:7084. https://doi.org/10.1038/srep07084
99. Nguyen THD, Galej WP, Bai X-c, Savva CG, Newman AJ, Scheres SHW, Nagai K (2015) The architecture of the spliceosomal U4/U6. U5 tri-snRNP. Nature 523:47–52. https://doi.org/10.1038/nature14548. https://www.nature.com/articles/nature14548#supplementary-information
100. Llaguno MC, Xu H, Shi L, Huang N, Zhang H, Liu Q, Jiang Q-X (2014) Chemically functionalized carbon films for single molecule imaging. J Struct Biol 185(3):405–417. https://doi.org/10.1016/j.jsb.2014.01.006
101. Palovcak E, Wang F, Zheng SQ, Yu Z, Li S, Betegon M, Bulkley D, Agard DA, Cheng Y (2018) A simple and robust procedure for preparing graphene-oxide cryo-EM grids. J Struct Biol 204(1):80–84. https://doi.org/10.1016/j.jsb.2018.07.007
102. D'Imprima E, Floris D, Joppe M, Sánchez R, Grininger M, Kühlbrandt W (2019) Protein denaturation at the air-water interface and how to prevent it. Elife 8:e42747. https://doi.org/10.7554/eLife.42747
103. Liu N, Zhang J, Chen Y, Liu C, Zhang X, Xu K, Wen J, Luo Z, Chen S, Gao P, Jia K, Liu Z, Peng H, Wang H-W (2019) Bioactive functionalized monolayer graphene for high-resolution cryo-electron microscopy. J Am Chem Soc 141(9):4016–4025. https://doi.org/10.1021/jacs.8b13038

104. Naydenova K, Peet MJ, Russo CJ (2019) Multifunctional graphene supports for electron cryomicroscopy. Proc Natl Acad Sci U S A:11718–11724. https://doi.org/10.1073/pnas.1904766116
105. Yu G, Li K, Huang P, Jiang X, Jiang W (2016) Antibody-based affinity cryoelectron microscopy at 2.6-Å resolution. Structure 24 (11):1984–1990. https://doi.org/10.1016/j.str.2016.09.008
106. Yu G, Li K, Jiang W (2016) Antibody-based affinity cryo-EM grid. Methods 100:16–24. https://doi.org/10.1016/j.ymeth.2016.01.010
107. Glaeser RM (2018) Proteins, interfaces and cryo-EM grids. Curr Opin Colloid Interface Sci 34:1–8. https://doi.org/10.1016/j.cocis.2017.12.009
108. Han BG, Watson Z, Cate JHD, Glaeser RM (2017) Monolayer-crystal streptavidin support films provide an internal standard of cryo-EM image quality. J Struct Biol 200 (3):307–313. https://doi.org/10.1016/j.jsb.2017.02.009
109. Wang F, Liu Y, Yu Z, Li S, Cheng Y, Agard DA (2019) General and robust covalently linked graphene oxide affinity grids for high-resolution cryo-EM. bioRxiv:657411. https://doi.org/10.1101/657411
110. Basu K, Green EM, Cheng Y, Craik CS (2019) Why recombinant antibodies—benefits and applications. Curr Opin Biotechnol 60:153–158. https://doi.org/10.1016/j.copbio.2019.01.012
111. Masiulis S, Desai R, Uchański T, Serna Martin I, Laverty D, Karia D, Malinauskas T, Zivanov J, Pardon E, Kotecha A, Steyaert J, Miller KW, Aricescu AR (2019) GABAA receptor signalling mechanisms revealed by structural pharmacology. Nature 565(7740):454–459. https://doi.org/10.1038/s41586-018-0832-5
112. Uchański T, Masiulis S, Fischer B, Kalichuk V, Wohlkönig A, Zögg T, et al. (2019) Megabodies expand the nanobody toolkit for protein structure determination by single-particle cryo-EM. bioRxiv 343, 812230. https://doi.org/10.1101/812230
113. Dandey VP, Wei H, Zhang Z, Tan YZ, Acharya P, Eng ET, Rice WJ, Kahn PA, Potter CS, Carragher B (2018) Spotiton: new features and applications. J Struct Biol 202 (2):161–169. https://doi.org/10.1016/j.jsb.2018.01.002
114. Jain T, Sheehan P, Crum J, Carragher B, Potter CS (2012) Spotiton: a prototype for an integrated inkjet dispense and vitrification system for cryo-TEM. J Struct Biol 179 (1):68–75. https://doi.org/10.1016/j.jsb.2012.04.020
115. Wei H, Dandey VP, Zhang Z, Raczkowski A, Rice WJ, Carragher B, Potter CS (2018) Optimizing "self-wicking" nanowire grids. J Struct Biol 202(2):170–174. https://doi.org/10.1016/j.jsb.2018.01.001
116. Razinkov I, Dandey V, Wei H, Zhang Z, Melnekoff D, Rice WJ, Wigge C, Potter CS, Carragher B (2016) A new method for vitrifying samples for cryoEM. J Struct Biol 195 (2):190–198. https://doi.org/10.1016/j.jsb.2016.06.001
117. Ravelli RBG, Nijpels FJT, Henderikx RJM, Weissenberger G, Thewessem S, Gijsbers A, Beulen BWAMM, López-Iglesias C, Peters PJ (2019) Automated cryo-EM sample preparation by pin-printing and jet vitrification. bioRxiv:651208. https://doi.org/10.1101/651208
118. Arnold SA, Albiez S, Bieri A, Syntychaki A, Adaixo R, McLeod RA, Goldie KN, Stahlberg H, Braun T (2017) Blotting-free and lossless cryo-electron microscopy grid preparation from nanoliter-sized protein samples and single-cell extracts. J Struct Biol 197 (3):220–226. https://doi.org/10.1016/j.jsb.2016.11.002
119. Snijder J, Borst AJ, Dosey A, Walls AC, Burrell A, Reddy VS, Kollman JM, Veesler D (2017) Vitrification after multiple rounds of sample application and blotting improves particle density on cryo-electron microscopy grids. J Struct Biol 198(1):38–42. https://doi.org/10.1016/j.jsb.2017.02.008
120. Kim LY, Rice WJ, Eng ET, Kopylov M, Cheng A, Raczkowski AM, Jordan KD, Bobe D, Potter CS, Carragher B (2018) Benchmarking cryo-EM single particle analysis workflow. Front Mol Biosci 5:50. https://doi.org/10.3389/fmolb.2018.00050
121. Downing KH, Glaeser RM (2018) Estimating the effect of finite depth of field in single-particle cryo-EM. Ultmi 184(Pt A):94–99. https://doi.org/10.1016/j.ultramic.2017.08.007
122. Rice WJ, Cheng A, Noble AJ, Eng ET, Kim LY, Carragher B, Potter CS (2018) Routine determination of ice thickness for cryo-EM grids. J Struct Biol 204(1):38–44. https://doi.org/10.1016/j.jsb.2018.06.007
123. Penczek PA (2010) Chapter 1: Fundamentals of three-dimensional reconstruction from projections. In: Jensen GJ (ed) Methods in enzymology, vol 482. Academic Press, New York, pp 1–33. https://doi.org/10.1016/S0076-6879(10)82001-4

124. Radermacher M (1988) Three-dimensional reconstruction of single particles from random and nonrandom tilt series. J Electron Microsc Tech 9(4):359–394. https://doi.org/10.1002/jemt.1060090405
125. Radermacher M, Wagenknecht T, Verschoor A, Frank J (1987) Three-dimensional reconstruction from a single-exposure, random conical tilt series applied to the 50S ribosomal subunit of Escherichia coli. J Microsc 146 (2):113–136. https://doi.org/10.1111/j.1365-2818.1987.tb01333.x
126. Leschziner AE, Nogales E (2006) The orthogonal tilt reconstruction method: an approach to generating single-class volumes with no missing cone for ab initio reconstruction of asymmetric particles. J Struct Biol 153 (3):284–299. https://doi.org/10.1016/j.jsb.2005.10.012
127. Asarnow D, Palovcak E, Gao Y, Julius D, Cheng Y (2017) Ion channel in lipid nanodisc by single particle cryo-EM – pushing the technology limit. Microsc Microanal 23 (S1):822–823. https://doi.org/10.1017/S1431927617004779
128. von Loeffelholz O, Natchiar SK, Djabeur N, Myasnikov AG, Kratzat H, Ménétret J-F, Hazemann I, Klaholz BP (2017) Focused classification and refinement in high-resolution cryo-EM structural analysis of ribosome complexes. Curr Opin Struct Biol 46:140–148. https://doi.org/10.1016/j.sbi.2017.07.007
129. Scheres SHW (2016) Processing of structurally heterogeneous cryo-EM data in RELION. Methods Enzymol 579:125–157. https://doi.org/10.1016/bs.mie.2016.04.012
130. Bai XC, Rajendra E, Yang G, Shi Y, Scheres SHW (2015) Sampling the conformational space of the catalytic subunit of human γ-secretase. Elife 4:e11182. https://doi.org/10.7554/eLife.11182

Chapter 18

Fast Small-Scale Membrane Protein Purification and Grid Preparation for Single-Particle Electron Microscopy

Natalie Bärland and Camilo Perez

Abstract

The ongoing development of single-particle cryo-electron microscopy (cryo-EM) is leading to fast data acquisition, data processing, and protein structure elucidation. Quick and reliable methods to go from protein purification and optimization to grid preparation will significantly improve the reach and power of cryo-EM. Such methods would particularly constitute a tremendous advantage in structural biology of membrane proteins, whose published structures stay still far behind the number of soluble protein structures. Here we describe a fast, low-cost, and user-friendly method for the purification and cryo-EM analysis of a recombinant membrane protein. This method minimizes the amount of starting material and manipulation steps needed to go from purification to grid preparation, and could potentially be expanded to other membrane protein purification systems for its direct application in structure determination by single-particle cryo-EM.

Key words Membrane proteins, Affinity-chromatography, Small-scale purification, Single-particle electron microscopy, Negative staining-EM, Cryo-EM

1 Introduction

The study of the structure and function of membrane proteins, which make up to nearly a third of the genome in eubacteria, archaea, and eukaryotes [1], is paved with multiple challenges. Membrane proteins have a broad variety of functions as transporters, channels, receptors, or enzymes, and are targeted by more than 50% of the marketed drugs [2, 3]. Recent developments in the field of single-particle cryo-EM have boosted the number of elucidated membrane protein structures. Higher sensitivity of direct detectors [4, 5], phase plates for contrast enhancement [6], implementation of graphic processor units for accelerated calculations [7], refined algorithms, and simplified software [8–10] speed up processes involved in data acquisition and processing. The bottleneck in high-throughput structural biology remains to be sample

Camilo Perez and Timm Maier (eds.), *Expression, Purification, and Structural Biology of Membrane Proteins*, Methods in Molecular Biology, vol. 2127, https://doi.org/10.1007/978-1-0716-0373-4_18,

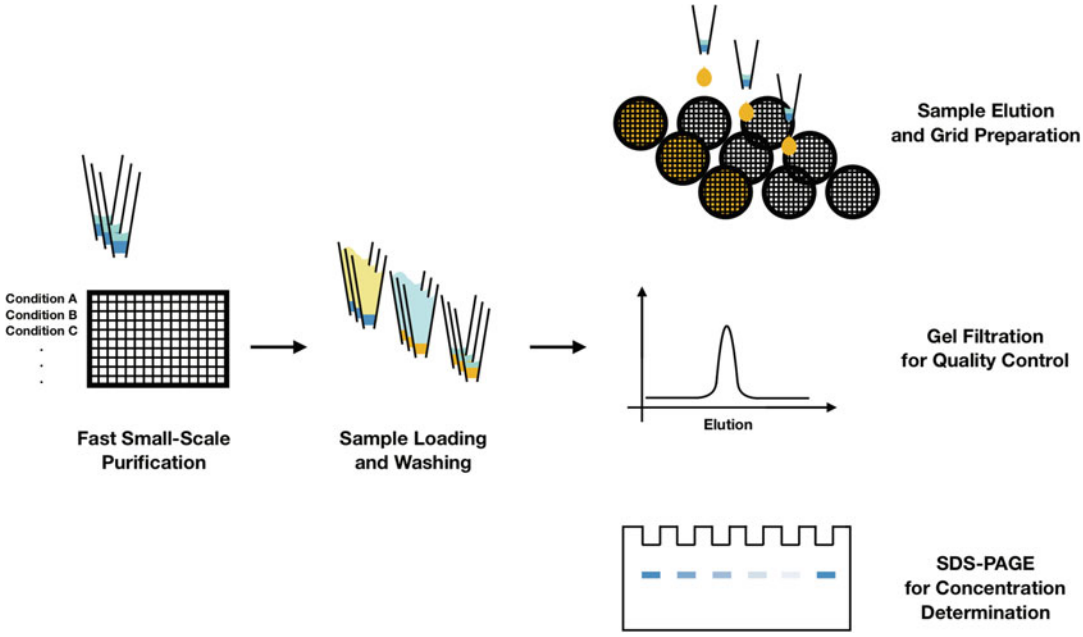

Fig. 1 Principle of the fast small-scale purification for single-particle EM (FASSP-EM) methodology. Low amounts of solubilized membrane protein[s] are distributed in a 96-well plate. Affinity chromatography using PureSpeed™ IMAC tips allows for quick protein loading and washing. The protein(s) of interest can be directly eluted on a glow-discharged grid for analysis by single-particle EM, analyzed via gel filtration and/or SDS-PAGE

preparation including refined methods in protein purification and grid preparation [11–14].

To meet the need of fast sample production of recombinant membrane proteins with minimal material usage and reduced cost, we present a fast small-scale method that uses PureSpeed™ IMAC tips and 96-well plates for purification, parallel buffer condition screening, and grid preparation for application to single-particle EM (Fig. 1). The advantage of parallelized purification is that it allows screening multiple stabilizing agents (e.g., detergents, protein binders, additives) and fast assessment of conditions targeted to trap particular conformations, and it facilitates working with multiple protein targets at the same time. In the current protocol, as *proof of principle* we perform the purification and EM analysis of a membrane protein linked to a poly-histidine tag. However, the method could be extended to purification of proteins with other affinity tags. The membrane protein studied here corresponds to the ATP-binding cassette (ABC) flippase PglK, a 130 kDa protein from *Campylobacter jejuni* [15].

2 Materials

2.1 Membrane Preparation and Purification

1. Centrifuge Sorvall LYNX 6000 (Thermo Fisher).
2. Microfluidizer LM10 (Microfluidics).
3. Rotor 70 Ti (Beckmann Coulter).
4. Rotor Fiberlite F9-6 × 1000 LEX Fixed Angle Rotor (Thermo Fisher).
5. Ultracentrifuge Optima XE-90 (Beckmann Coulter).
6. PureSpeed™ IMAC Tips 1 ml with 80 μl resin bed volume (Mettler Toledo).
7. Pyrex Dounce tissue grinder 40 ml (SciLabware).
8. Cell solubilisation buffer (CS), 50 mM Tris–HCl pH 8.0, 500 mM NaCl, 7 mM β-mercaptoethanol, 0.5 mM PMSF.
9. Membrane resuspension buffer (MR), 50 mM Tris–HCl pH 8.0, 500 mM NaCl, 7 mM β-mercaptoethanol.
10. Equilibration buffer (EQ), 50 mM Tris–HCl pH 8.0, 500 mM NaCl, 20 mM imidazole pH 8.0, 10% glycerol, 0.016% DDM, 7 mM β-mercaptoethanol.
11. Solubilisation buffer (SB), 50 mM Tris–HCl pH 8.0, 500 mM NaCl, 20 mM imidazol pH 8.0, 15% glycerol, 1% DDM, 1% $C_{12}E_8$, 7 mM β-mercaptoethanol.
12. Washing buffer (WB-1), 50 mM Tris–HCl pH 8.0, 500 mM NaCl, 50 mM imidazole pH 8.0, 10% glycerol, 0.016% DDM, 7 mM β-mercaptoethanol.
13. Washing buffer (WB-2), 50 mM Tris–HCl pH 8.0, 500 mM NaCl, 50 mM imidazole pH 8.0, 2% glycerol, 0.016% LMNG, 7 mM β-mercaptoethanol.
14. Elution buffer (EL), 50 mM Tris–HCl pH 8.0, 500 mM NaCl, 50 mM imidazole pH 8.0, 0.016% LMNG, 7 mM β-mercaptoethanol.

2.2 Electron Microscopy

1. FEI Talos TEM 200 kV transmission electron microscope (TEM) (FEI).
2. Lacey carbon grid mesh 400 copper grids (Electron Microscopy Sciences).
3. Leica EM GP plunge freezer (Leica Microsystems).
4. Tecnai G2 Spirit 120 kV TEM (FEI).
5. TG100/400 copper palladium rectangular mesh TEM carbon-coated grids.
6. Whatman™ Grade 556 dry pads (GE Healthcare).
7. Whatman™ Grade 1 circles (GE Healthcare).
8. 2% Uranyl acetate, kept away from light.

2.3 Software for Data Analysis

1. CTF4 [16].
2. ImageJ [17].
3. Relion 3.0 [8].
4. Origin (OriginLab Corp).

3 Methods

Protocols for expression need to be optimized separately. Samples and buffers should be pre-cooled at 4 °C. It is recommended to carry out the purification at 4 °C. Data acquisition for single-particle EM and data processing will not be discussed here.

3.1 Membrane Preparation and Purification of Recombinant Membrane Protein

1. Resuspend cell pellet in CS buffer using 8 ml buffer per 1 g cell dry weight. Let the solution stir at 4 °C until it is fully homogenized.
2. Disrupt cells using a Microfluidizer at 10,000 bar. Let the homogenized solution pass two times to break all cells.
3. Spin the disrupted cells at 4400 × *g* for 30 min at 4 °C in a pre-cooled rotor.
4. Spin the supernatant at 142,400 × *g* for 30 min at 4 °C.
5. Resuspend the pellet containing the membranes in MR buffer using 1 ml buffer for 1 g initial cell dry weight.
6. Aliquot membranes by 2.5 ml and flash freeze with liquid nitrogen. Store at −80 °C until further use.
7. Solubilize membranes in 6 ml SB buffer by stirring at 4 °C for 2 h.
8. Spin the solubilized sample at 29,600 × *g* and recover the supernatant.
9. Equilibrate a 1 ml PureSpeed™ IMAC tip with 80 µl resin volume with 2 × 1 ml equilibration buffer (*see* **Note 1**).
10. Load 2 × 1 ml supernatant on the equilibrated tip.
11. Wash two times with 1 ml WB-1.
12. Wash two times with 1 ml WB-2 (*see* **Note 2**).
13. Elute with 130 µl elution buffer by pipetting up and down four times. This facilitates to recover higher protein amounts (*see* **Note 3**) (Fig. 2a).
14. **Steps 9–13** can be carried out in parallel for other protein samples using a multichannel pipette or done individually with a regular pipette.

3.2 Determination of Protein Concentration

Due to the high absorbance of imidazole at 280 nm, using standard spectroscopy methods for the determination of protein

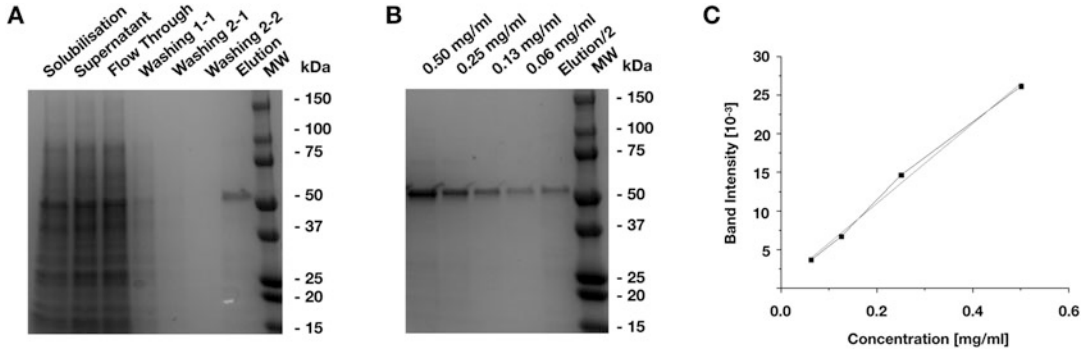

Fig. 2 SDS-PAGE analysis and protein concentration determination of FASSP-EM-purified PglK. (**a**) Gels were loaded with 7.5 μl of eluted PglK premixed with 2.5 μl of 4× loading dye. The standard molecular weight (MW) is indicated. The lane containing the eluted sample exhibits a strong band between 50 and 75 kDa, representing the expected molecular weight of the PglK monomer (65 kDa). (**b**) SDS-PAGE of PglK at known concentrations was used to generate a calibration curve. Elution corresponds to a twofold dilution of the eluted sample. (**c**) Plot of concentration against band intensity determined with ImageJ. The red line indicates a linear fit. The concentration estimated for the eluted protein is 0.4 mg/ml

concentration in the eluate is not recommended. To estimate protein concentration, we use SDS-PAGE and analysis with ImageJ to generate a calibration curve.

1. Prepare 10 μl protein dilutions of protein at known concentration [0.5 and 0.01 mg/ml] to use as standards for SDS-PAGE analysis. Load dilutions on the same gel as the eluted samples from the purification (Fig. 2b).
2. Take a picture of the gel for analysis in ImageJ and first adjust brightness and contrast in the drop-down menu Image > Adjust > Brightness/Contrast.
3. Select the first protein band on the gel with the rectangular tool and in the drop-down menu select Analyze > Gels > Select First Lane.
4. Move new rectangle to the next protein band and select Analyze > Gels > Select Next Lane. Repeat for all protein bands.
5. Select Analyze > Gels > Plot Lanes to calculate the profile of the density on the image and draw a baseline with the line tool to have a closed area.
6. Calculate the areas enclosed with the magic wand tool by clicking inside the profiles.
7. Plot the band intensities against the concentration of the protein in your program of choice and perform a linear fit (Fig. 2c).
8. Estimate protein concentration in the eluate using the calibration curve equation derived from the previous step.

3.3 Negative Staining EM

1. Prepare a series of dilutions of the eluted protein between 1:10 and 1:50 to be used for preparation of negative staining grids.
2. Load 5 μl of protein sample on a glow-discharged carbon-coated mesh 400 palladium grid and incubate for 1 min.
3. Wash three times with 20 μl ddH2O and blot with filter paper (*see* **Note 4**).
4. Wash one time with 5 μl 2% uranyl acetate and blot with filter paper.
5. Stain with 5 μl 2% uranyl acetate, incubate for 10–15 s, and blot with filter paper.
9. Examine grids and collect images in a transmission electron microscope (Fig. 3a, b). In this case we used a Tecnai G2 Spirit 120 kV TEM.

3.4 Plunge Freezing of Purified Sample for Cryo-EM Analysis

1. Start up the Leica plunge freezer according to the manual and cool down the instrument with liquid nitrogen and the plunge freezing bath with liquid ethane. Place a new Whatman blotting paper grade 1 and adjust the settings to 80% humidity in the chamber.
2. Place a freshly glow-discharged Lacey carbon grid on the Leica tweezers.
3. Apply 5 μl of the non-diluted protein purified with PureSpeed™ IMAC tips on a Lacey grid (*see* **Note 5**).
4. Adjust the tweezers on the Leica plunge freezer, transfer it into the chamber, blot for 3 s, and plunge freeze the grid.
5. Store the grid in a grid box in liquid nitrogen before usage or mount directly on a cryo-holder for screening and data collection at a TEM (Fig. 3c). In this case we used a FEI Talos TEM 200 kV TEM.

4 Notes

1. For the purification with the PureSpeed™ IMAC tips a 96 deep well plate can be used to distribute the protein sample and the different buffers in 1 ml aliquots using a multichannel pipet.
2. The second washing step is only necessary in the case of buffer or detergent exchange and can be excluded for other protein purifications. In the case of PglK the detergent DDM was exchanged for LMNG.
3. The elution volume can be further decreased to achieve a higher concentration in the sample.
4. The eluted sample should have less than 0.1% glycerol; otherwise it will produce artifacts after staining with uranyl acetate or

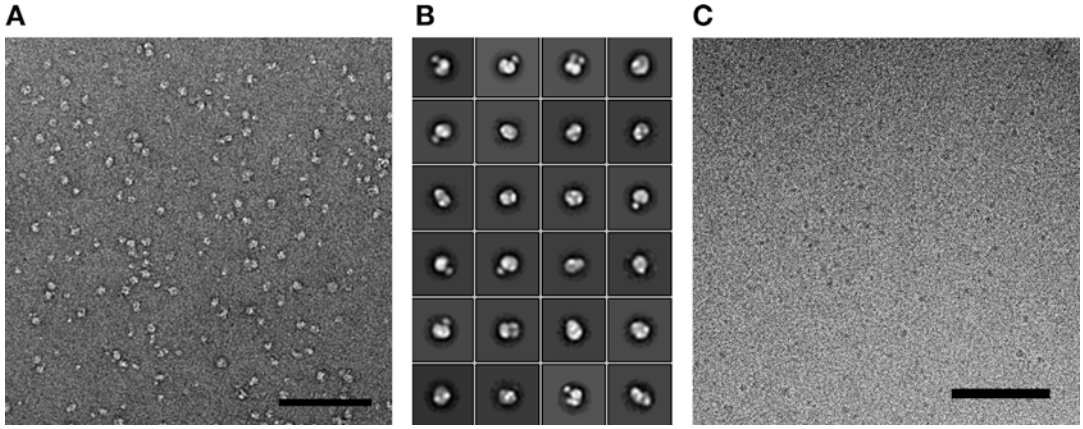

Fig. 3 EM analysis of purified protein. (**a**) Negative staining image of PglK purified with PureSpeed™ IMAC tips and diluted 1:35 times for staining with 2% uranyl acetate. Image was taken at a magnification of 105,000 and a pixel size of 5.6 Å. Black bar in the inset indicates 100 nm. (**b**) Selection of representative classes of a two-dimensional (2D) classification. Particles were picked automatically and 2D classified using Relion 3.0. No CTF correction was performed. (**c**) Cryo-EM micrograph of PglK in ice on a Lacey grid. The scale bar indicates a size of 100 nm. The image was recorded with a FEI Ceta 16 M Pixel CMOS camera at a magnification of 120,000× and a pixel size of 1.26 Å

freezing in liquid ethane. A high glycerol concentration will otherwise increase the signal-to-noise ratio in the recorded images. If the sample contains a high amount of glycerol, washing steps of up to ten times before staining with uranyl acetate can help.

5. It might be useful to prepare a small series of dilutions between 1:3 and 1:5 if the concentration is too high. If the protein concentration is on the other hand too low one can use an equilibrated concentrator for small volumes to concentrate the eluted sample to half or quarter of the volume.

Acknowledgments

We thank the staff at the BioEM Lab and Nano Imaging Lab of the University of Basel. This work was supported by the Swiss National Science Foundation (SNSF) (PP00P3_170607).

References

1. Wallin E, Von Heijne G (1998) Genome-wide analysis of integral membrane proteins from eubacterial, archaean, and eukaryotic organisms. Protein Sci 7:1029–1038
2. Arinaminpathy Y, Khurana E, Engelman DM, Gerstein MB (2009) Computational analysis of membrane proteins: the largest class of drug targets. Drug Discov Today 14:1130–1135
3. Oprea TI, Bologa CG, Brunak S et al (2018) Unexplored therapeutic opportunities in the human genome. Nat Rev Drug Discov 17:317

4. Faruqi AR, McMullan G (2018) Direct imaging detectors for electron microscopy. Nucl Instrum Methods Phys Res A 878:180–190
5. Song B, Lenhart J, Flegler VJ et al (2019) Capabilities of the Falcon III detector for single-particle structure determination. Ultramicroscopy 203:145–154
6. Li K, Sun C, Klose T et al (2019) Sub-3 Åapoferritin structure determined with full range of phase shifts using a single position of volta phase plate. J Struct Biol 206:225–232
7. Kimanius D, Forsberg BO, Scheres S, Lindahl E (2016) Accelerated cryo-EM structure determination with parallelisation using GPUs in RELION-2. Elife 5. https://doi.org/10.7554/eLife.18722
8. Zivanov J, Nakane T, Forsberg BO et al (2018) New tools for automated high-resolution cryo-EM structure determination in RELION-3. Elife 7:e42166
9. Punjani A, Rubinstein JL, Fleet DJ, Brubaker MA (2017) cryoSPARC: algorithms for rapid unsupervised cryo-EM structure determination. Nat Methods 14:290
10. Grant T, Rohou A, Grigorieff N (2018) cisTEM, user-friendly software for single-particle image processing. Elife 7:e35383
11. Schmidli C, Albiez S, Rima L et al (2019) Microfluidic protein isolation and sample preparation for high resolution cryo-EM. Proc Natl Acad Sci U S A 116 (30):15007–15012. bioRxiv 556068
12. Arnold SA, Albiez S, Opara N et al (2016) Total sample conditioning and preparation of nanoliter volumes for electron microscopy. ACS Nano 10:4981–4988
13. Stark H, Chari A (2016) Sample preparation of biological macromolecular assemblies for the determination of high-resolution structures by cryo-electron microscopy. Microscopy 65:23–34
14. Thompson RF, Walker M, Siebert CA et al (2016) An introduction to sample preparation and imaging by cryo-electron microscopy for structural biology. Methods 100:3–15
15. Perez C, Gerber S, Boilevin J et al (2015) Structure and mechanism of an active lipid-linked oligosaccharide flippase. Nature 524:433–438. https://doi.org/10.1038/nature14953
16. Rohou A, Grigorieff N (2015) CTFFIND4: fast and accurate defocus estimation from electron micrographs. J Struct Biol 192:216–221. https://doi.org/10.1016/j.jsb.2015.08.008
17. Abràmoff MD, Magalhães PJ, Ram SJ (2004) Image processing with ImageJ. Biophoton Int 11:36–42

Chapter 19

Stabilization and Crystallization of a Membrane Protein Involved in Lipid Transport

Bing Zhang and Camilo Perez

Abstract

Lipoteichoic acids (LTA) are ubiquitous cell wall components of Gram-positive bacteria. In *Staphylococcus aureus* LTA are composed of a polymer with 1,3-linked glycerol phosphate repeating units anchored to the plasma membrane. The anchor molecule is a lipid-linked disaccharide (anchor-LLD) synthesized at the cytoplasmic leaflet of the membrane. The anchor lipid becomes accessible at the outer leaflet of the membrane after the flippase LtaA catalyzes translocation. Recently we have elucidated the structure of LtaA using vapor diffusion X-ray crystallography and in situ annealing. We were able to obtain LtaA crystals after optimization of purification protocols that led to stabilization of LtaA isolated in detergent micelles. Here we report a protocol that describes the purification, stabilization, crystallization, and data collection strategies carried out to determine the structure of LtaA. We highlight key points that can be used to determine crystal structures of other membrane proteins.

Key words Membrane protein, Lipid flippases, X-ray crystallography, In situ annealing, TEV protease, Protein purification, Detergent micelles

1 Introduction

Gram-positive bacteria such as *S. aureus* are coated with an essential cell envelope composed of a thick peptidoglycan multilayer, in which teichoic acids (TAs) are embedded. TAs are long anionic polymers composed of repeating glycerol phosphate or ribitol phosphate units [1]. TAs are divided into two subtypes: lipoteichoic acids (LTA), which are anchored to the cell membrane, and wall teichoic acids (WTA), which are bound to the peptidoglycan layer [2]. LTA and WTA are both essential to resist antibacterial agents, localize the cell wall elongation and division machinery, contribute to immune evasion, and prevent recognition and opsonization by antibodies, and have been shown to be important for adhesion, colonization, and biofilm formation [3–12].

S. aureus LTA are composed of a polymer of 1,3-glycerol-phosphate repeat units attached to C-6 of the nonreducing glucosyl

Camilo Perez and Timm Maier (eds.), *Expression, Purification, and Structural Biology of Membrane Proteins*, Methods in Molecular Biology, vol. 2127, https://doi.org/10.1007/978-1-0716-0373-4_19,

of the disaccharide moiety of a gentiobiosyl-diacylglycerol anchor lipid (anchor-LLD). The anchor-LLD is found embedded in the extracellular leaflet of the plasma membrane [1, 2, 13–16], but its synthesis is carried out at the cytoplasmic leaflet by the action of the processive glycosyltransferase YpfP [17]. The anchor-LLD is translocated to the outer leaflet of the membrane by the flippase LtaA. Thus, LtaA regulates LTA synthesis by adjusting the extracellular concentration of anchor-LLD available for the polymerization reaction to happen [18].

LtaA is a 44 kDa monomeric membrane protein without prominent soluble domains. Thus, elucidation of a high-resolution structure of LtaA using cryo-electron microscopy (cryo-EM) methods is rather challenging at the current level of development of the technique. X-ray crystallography has shown to be successful in the determination of structures of membrane proteins with similar characteristics to LtaA in the past. However, obtaining well-diffracting crystals depends on several parameters including purity of the protein sample, stability of the protein in detergent micelles, presence of flexible regions that could preclude formation of well-ordered lattice structures, conformational diversity, surface properties that will dictate the formation of crystal contacts, stability of the protein at high concentrations, suitable cryo-protection strategies, etc. In this chapter we describe the experimental approaches that we used for the purification, stabilization, and crystallization of LtaA. We also describe the in situ annealing methodology used to increase the resolution of X-ray diffraction of LtaA crystals from 7 to 3.3 Å. We highlight important steps that could be applied to crystallographic studies of other membrane proteins.

2 Materials

2.1 Protein Expression

1. *E. coli* BL21-Gold (DE3) competent cells (Stratagene).
2. pET-19b expression vector (Novagen) carrying LtaA sequence: The vector contains an N-terminal His10 affinity tag followed by a Tobacco etch virus (TEV) protease site.
3. 1 M Ampicillin stock, dissolved in filtered ultrapure water: Store at −20 °C.
4. Terrific broth medium with 1% glucose (TB glucose) containing 100 μg/ml ampicillin.
5. Luria broth (LB) medium containing 100 μg/ml ampicillin.
6. LB agar plate containing 100 μg/ml ampicillin.
7. 1 M Isopropyl β-D-1-thiogalactopyranoside (IPTG) in filtered ultrapure water.
8. Miniprep DNA purification kit.

2.2 Protein Purification

1. Membrane preparation buffer (MP buffer), 50 mM Tris–HCl pH 8.0, 500 mM NaCl, 0.5 mM phenylmethylsulfonyl fluoride (PMSF), 5 mM β-mercaptoethanol (β-Me).
2. Membrane resuspension buffer (MR buffer), 50 mM Tris–HCl pH 8.0, 500 mM NaCl, 5 mM β-Me.
3. Nickel-nitrilotriacetic acid agarose matrix (Ni-NTA) for immobilized metal affinity chromatography (IMAC).
4. Superdex 200 Increase 10/300 GL column for size-exclusion chromatography (SEC) (GE Healthcare).
5. PD-10 desalting column (GE Healthcare).
6. Tobacco etch virus (TEV) protease: Self-preparation [19].
7. Solubilization buffer (Sol. buffer), 50 mM Tris–HCl pH 8.0, 200 mM NaCl, 15% glycerol, 1% lauryl maltose neopentyl glycol (LMNG, Anatrace), 1% *n*-dodecyl-β-D-maltoside (DDM, Anatrace), 5 mM β-Me. Detergents and β-Me are added freshly from stock solutions before usage.
8. Equilibration buffer (Eq. buffer), 50 mM Tris–HCl pH 8.0, 200 mM NaCl, 10% glycerol, 20 mM imidazole, 0.02% LMNG, 0.02% DDM, 5 mM β-Me.
9. Wash buffer-1, 50 mM Tris–HCl pH 8.0, 200 mM NaCl, 10% glycerol, 50 mM imidazole, 0.02% LMNG, 0.02% DDM, 5 mM β-Me.
10. Wash buffer-2, 50 mM Tris–HCl pH 8.0, 200 mM NaCl, 10% glycerol, 50 mM imidazole, 0.02% LMNG, 5 mM β-Me.
11. Elution buffer (Elu. buffer), 50 mM Tris–HCl pH 8.0, 200 mM NaCl, 10% glycerol, 200 mM imidazole, 0.02% LMNG, 5 mM β-Me.
12. Size-exclusion chromatography buffer (SEC buffer), 10 mM Tris–HCl pH 8.0, 150 mM NaCl, 0.02% LMNG.
13. Desalting buffer, 10 mM Tris–HCl pH 8.0, 150 mM NaCl, 0.1% Cymal-7 (Anatrace).
14. 30 kDa MWCO Vivaspin™ 20 concentrator (GE Healthcare).
15. Nanodrop (Thermo Fisher).

2.3 Protein Crystallization

1. MRC 96-well and MRC Maxi 48-well plates.
2. Stock solutions for crystallization: 1 M Magnesium acetate, 1 M glycine pH 9.5, 50% (v/v) polyethylene glycol 300 (PEG 300).
3. Cryo-buffers: (**1**) 15 mM Magnesium acetate, 150 mM NaCl, 10 mM Tris–HCl pH 8.0, 15 mM glycine pH 9.5, 0.1% Cymal-7, 26% PEG 300; (**2**) and (**3**) same composition as cryo-buffer (1) but containing 31% and 36% PEG 300, respectively.
4. Liquid nitrogen.
5. Cryoloops.

2.4 In Situ Annealing

1. X-ray beamline: X06SA-PXI at the SLS, Paul Scherrer Institut (PSI), provides fast and stable energy (wavelength) selection in the range from 5.7 to 17.5 keV (0.7–2.2 Å). Beamline X06SA-PXI is optimized for micro-focusing applications and features a beam down to $2 \times 1\ \mu m^2$. Beam size can be varied to match the dimensions of the crystal, thereby maximizing the diffraction signal.
2. Single-photon counting hybrid pixel area EIGER 16M (Dectris) detector [20]: The EIGER 16M at X06SA-PXI is a fast detector that allows collection of datasets at high speed. It has pixel-array detectors with low noise, fast frame rate, and negligible dead time.
3. Data collection software: The software suite developed at the SLS allows for fast scanning of crystals, automated data collection, and data processing [21–24].
4. Thin film to block nitrogen-gas stream.

3 Methods

3.1 Protein Expression

This protocol for LtaA expression comprises transformation of *E. coli* BL21-Gold (DE3) competent cells with recombinant vector carrying LtaA gene, cell culturing, and LtaA expression induction (*see* **Note 1**).

1. Thaw 50 μl of *E. coli* BL21-Gold (DE3) competent cell on ice, add 1 μl of pET19b-LtaA plasmid (approximately 30 ng), mix, and incubate on ice for 30 min.
2. Apply heat shock at 42 °C for 45 s followed by incubation on ice for 2 min.
3. Add 450 μl of pre-warmed LB medium and incubate for 1 h at 37 °C with mild shaking.
4. Centrifuge at $2000 \times g$ for 4 min, discard 400 μl of supernatant, resuspend the pellet gently, and spread on LB agar plate containing 100 μg/ml ampicillin. Leave incubating at 37 °C for about 16 h.
5. Inoculate a single colony in 100 ml of TB glucose medium containing 100 μg/ml ampicillin. Grow cells at 37 °C shaking at 200 rpm for about 16 h.
6. Inoculate the main culture (10 L of fresh TB glucose media containing 100 μg/ml ampicillin) to have initial $OD_{600} = 0.05$. Grow cells at 37 °C shaking at 130 rpm for about 3–4 h.
7. Add 0.2 mM IPTG and induce LtaA expression for 1 h.

8. Harvest cells by centrifugation at 10,000 × *g* at 4 °C for 15 min.
9. Weight pellet and store them at −80 °C.

3.2 Protein Purification

This protocol includes preparation of membrane vesicles, solubilization of membranes, and purification of LtaA by affinity chromatography and size-exclusion chromatography. All steps are carried out at 4 °C unless stated otherwise (*see* **Notes 2–5**).

3.2.1 Membrane Vesicle Preparation

1. Thaw cell pellets and resuspend on ice-cold MP buffer. Keep a proportion of 8 ml MP buffer for 1 g of dry cells.
2. Stir until a homogeneous suspension is obtained.
3. Disrupt the cells in a M-110L microfluidizer (Microfluidics) at 10,000 p.s.i.
4. Remove unbroken cells by centrifugation at 4400 × *g* for 30 min. Harvest membranes by ultracentrifugation at 140,000 × *g* for 30 min. Tubes used for centrifugation should be ice-chilled.
5. Resuspend pellet of membrane vesicles in MR buffer using Dounce homogenizer. Maintain a ratio of 1 ml MP buffer for every 1 g dry cells. Store homogenized membranes at −80 °C.

3.2.2 Purification and Stabilization

1. Solubilize membranes in ice-cold Sol. buffer for 2 h (*see* **Note 2**).
2. Centrifuge at 30,000 × *g* for 30 min using ice-chilled tubes.
3. Load supernatant onto pre-equilibrated Ni-NTA superflow affinity column.
4. Wash away nonspecific bound proteins by passing through buffer 1 and buffer 2 sequentially (*see* **Note 3**).
5. Elute LtaA from the column using elution buffer.
6. Equilibrate a PD-10 column or a HiPrep™ 26/10 desalting column with SEC buffer and exchange the buffer of the eluted protein.
7. Measure the concentration of eluted protein by nanodrop and add TEV protease at 1:5 (w:w) ratio to remove His10 affinity tag. Incubate for 16 h.
8. Remove TEV protease by passing through equilibrated Ni-NTA affinity column and collect the flow through (*see* **Note 4**) (*see* Fig. 1).
9. Concentrate eluted LtaA using a pre-chilled 30 kDa MWCO Vivaspin™ 20 concentrator.
10. Run LtaA sample on a pre-equilibrated Superdex 200 Increase 10/300 GL SEC column with a flow rate of 0.5 ml/min (*see* Fig. 1).

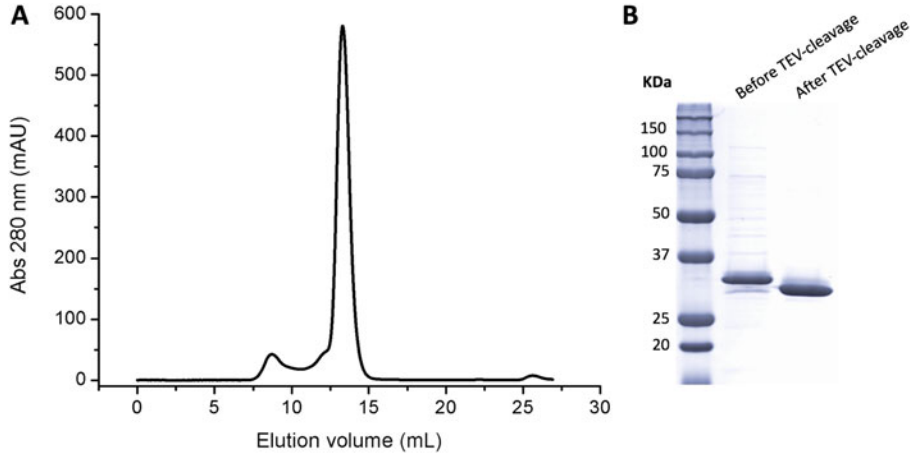

Fig. 1 LtaA purification. (**a**) Size-exclusion chromatography profile of purified LtaA. Superdex 200 Increase 10/300 GL. Void volume = 8.0 ml. (**b**) SDS-PAGE of purified LtaA before and after His-tag cleavage by TEV protease

11. Collect the main peak and change the buffer using a PD-10 column equilibrated in desalting buffer (*see* **Note 5**).
12. Collect eluate from PD-10 desalting column and measure concentration using a nanodrop.

3.3 Vapor Diffusion Crystallization

All steps are carried out at 4 °C unless stated otherwise (*see* **Notes 6** and 7).

1. Use the online "Make tray" tool of Hampton research (https://hamptonresearch.com/make_tray.aspx) to prepare a 8 × 6 crystallization screen, where the concentrations of components are varied: 30–50 mM magnesium acetate, 95–130 mM glycine pH 9.5, and 29–32% PEG 300.
2. Concentrate the protein using a 30 kDa MWCO Vivaspin™ 20 concentrator until the concentration reaches 6.0 mg/ml (*see* **Note 6**).
3. Centrifuge the concentrated protein at 20,000 × *g* for 5–15 min to remove heavy particles. Transfer protein to a new tube and keep it on ice.
4. Fill up the MRC Maxi 48-well plates with premade crystallization conditions (**step 1**).
5. Set up sitting-drop crystallization of LtaA by mixing drops of protein and reservoir solutions at 2:1 (1 μl:0.5 μl) ratios.
6. Seal the crystallization trays tightly with tape and carefully place them at 16 °C for crystals to grow.
7. Prepare cryo-protection buffers containing increasing concentrations of PEG 300 (up to 30% PEG 300).

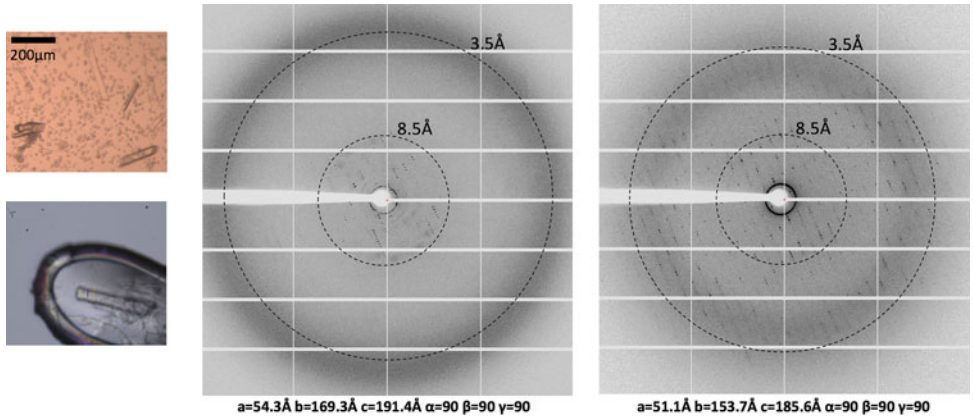

Fig. 2 Representative LtaA crystals and X-ray diffraction images before in situ annealing (*left*) and after in situ annealing (*right*). The difference in unit cell dimensions before and after in situ annealing demonstrates shrinking of the unit cell

8. Harvest LtaA crystals when they are fully grown in 1 week (*see* Fig. 2).
9. Perform sequential exchange of drop buffer and cryo-protection buffers under a light microscope. Let the solution to equilibrate for about 1 min every time the PEG 300 concentration is raised.
10. Harvest crystals using cryoloops and flash freeze them by immersion in liquid nitrogen.

3.4 In Situ Annealing and X-Ray Diffraction

1. Mount the crystal on goniometer at the beamline.
2. Perform in situ annealing by blocking the nitrogen-gas stream with a thin film for about 30 s while the crystal is still mounted on the goniometer [25]. It is important to not retract the cryojet and to observe that the flash-cooled drop turns slightly opaque (*see* **Note 7**) (*see* Fig. 2).
3. Expose the crystal to X-rays and collect datasets rotating the goniometer head 360° (*see* Fig. 2).

4 Notes

1. Optimizing expression conditions is an essential part of a crystallography project. Often large amounts of purified protein are necessary for screening crystallization conditions. We suggest carrying out screening of homologs, types of media, cell culture temperatures, and concentration of induction agents. A useful strategy for quick screening of homologs is to generate GFP fusion constructs and use in-gel fluorescence and fluorescence size-exclusion chromatography (FSEC).

2. As soon as a reliable expression protocol has been established, we recommend to use a GFP fusion construct to screen multiple detergents and buffer conditions in combination with in-gel fluorescence and FSEC to establish optimal solubilization parameters. Detergents that form small micelles promote formation of better crystal contacts; however in most cases they do not extract membrane proteins in high yields. Therefore, we recommend to screen for detergents that form large micelles and exchange them at a later point during purification for detergents that form small micelles.
3. A two-step washing strategy was applied to perform gently detergent exchange. Buffer 1 contains the same detergents as the solubilization buffer, whereas buffer 2 contains a different detergent (or mixture). Detergent exchange by using more than two buffers or by using concentration gradients can also be tested.
4. We recommend to test whether removing the affinity tag can have an impact on the stability and crystallization of the protein. In the case of LtaA, we noticed that removal of the tag was important to avoid aggregation during concentration (*see* Fig. 3).
5. We recommend to perform detergent exchange during SEC or after by using a PD-10 desalting column. In this particular case, exchanging to a detergent that forms small micelles was essential to obtain better protein crystals.
6. We recommend to test multiple protein concentrations and protein:mother-liquor ratios during early steps of crystallization screening experiments.
7. Flash-cooling and/or manipulation of protein crystals during flash-cooling can potentially cause lattice disorder. This is enhanced in crystals with high solvent content or with few intermolecular crystal contacts, as it is usually the case for membrane protein crystals. Lattice disorder results in increased mosaicity and reduced X-ray diffraction resolution. One potential way to resolve this issue is to use annealing techniques that involve warming the flash-cooled crystal and flash-cooling it again before data collection. In the case of LtaA crystals, the highest X-ray diffraction resolution achieved before annealing was 6–7 Å. We optimized a method for in situ annealing that included testing multiple annealing times, different thicknesses of films used to block the nitrogen-gas stream, and varying the distance of the cryo-stream to the crystal. The X-ray diffraction resolution achieved after crystal annealing was around 3.3–3.8 Å (*see* Fig. 2).

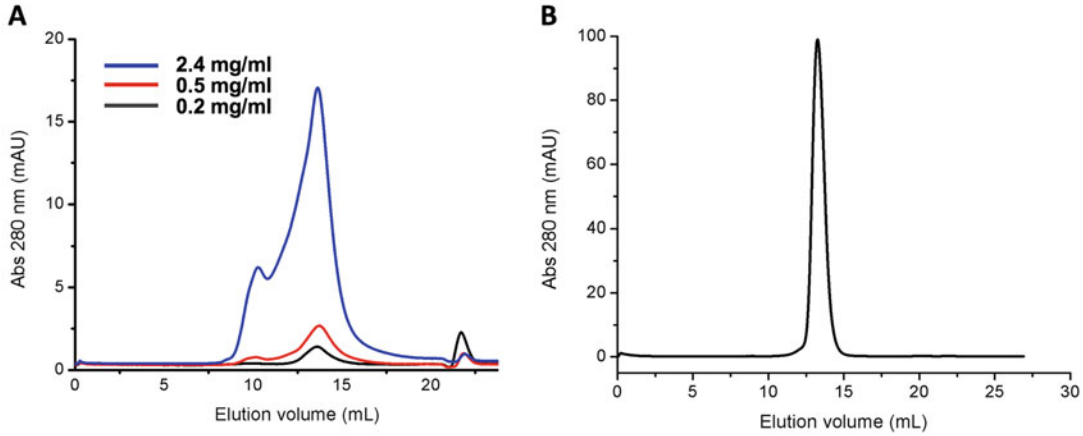

Fig. 3 Impact of His-tag removal on LtaA stability during concentration. (**a**) Size-exclusion chromatography profile of purified His_{10}-LtaA at different concentrations. (**b**) Size-exclusion chromatography profile of purified His-tag-less LtaA at 6 mg/ml. Superdex 200 Increase 10/300 GL. Void volume = 8.0 ml

Acknowledgments

We thank the staff at the PX beamline of the Swiss Light Source, Switzerland. This work was supported by the Swiss National Science Foundation (SNSF) (PP00P3_170607).

References

1. Neuhaus FC, Baddiley J (2003) A continuum of anionic charge: structures and functions of D-alanyl-teichoic acids in gram-positive bacteria. Microbiol Mol Biol Rev 67(4):686–723
2. Xia G, Kohler T, Peschel A (2010) The wall teichoic acid and lipoteichoic acid polymers of Staphylococcus aureus. Int J Med Microbiol 300(2–3):148–154. https://doi.org/10.1016/j.ijmm.2009.10.001
3. Saar-Dover R, Bitler A, Nezer R, Shmuel-Galia L, Firon A, Shimoni E, Trieu-Cuot P, Shai Y (2012) D-alanylation of lipoteichoic acids confers resistance to cationic peptides in group B streptococcus by increasing the cell wall density. PLoS Pathog 8(9):e1002891. https://doi.org/10.1371/journal.ppat.1002891
4. Fritz G, Mascher T (2014) A balancing act times two: sensing and regulating cell envelope homeostasis in Bacillus subtilis. Mol Microbiol 94(6):1201–1207. https://doi.org/10.1111/mmi.12848
5. Reichmann NT, Picarra Cassona C, Monteiro JM, Bottomley AL, Corrigan RM, Foster SJ, Pinho MG, Grundling A (2014) Differential localization of LTA synthesis proteins and their interaction with the cell division machinery in Staphylococcus aureus. Mol Microbiol 92(2):273–286. https://doi.org/10.1111/mmi.12551
6. Sewell EW, Brown ED (2014) Taking aim at wall teichoic acid synthesis: new biology and new leads for antibiotics. J Antibiot 67(1):43–51. https://doi.org/10.1038/ja.2013.100
7. Lee JH, Kim NH, Winstel V, Kurokawa K, Larsen J, An JH, Khan A, Seong MY, Lee MJ, Andersen PS, Peschel A, Lee BL (2015) Surface glycopolymers are crucial for in vitro anti-wall teichoic acid IgG-mediated complement activation and opsonophagocytosis of Staphylococcus aureus. Infect Immun 83(11):4247–4255. https://doi.org/10.1128/IAI.00767-15
8. Gautam S, Kim T, Lester E, Deep D, Spiegel DA (2016) Wall teichoic acids prevent antibody binding to epitopes within the cell wall of Staphylococcus aureus. ACS Chem Biol 11(1):25–30
9. Abachin E, Poyart C, Pellegrini E, Milohanic E, Fiedler F, Berche P, Trieu-Cuot P (2002) Formation of D-alanyl-lipoteichoic

acid is required for adhesion and virulence of Listeria monocytogenes. Mol Microbiol 43 (1):1–14

10. Bucher T, Oppenheimer-Shaanan Y, Savidor A, Bloom-Ackermann Z, Kolodkin-Gal I (2015) Disturbance of the bacterial cell wall specifically interferes with biofilm formation. Environ Microbiol Rep 7:990. https://doi.org/10.1111/1758-2229.12346
11. Peschel A, Otto M, Jack RW, Kalbacher H, Jung G, Gotz F (1999) Inactivation of the dlt operon in Staphylococcus aureus confers sensitivity to defensins, protegrins, and other antimicrobial peptides. J Biol Chem 274 (13):8405–8410. https://doi.org/10.1074/jbc.274.13.8405
12. Campbell J, Singh AK, Santa Maria JP Jr, Kim Y, Brown S, Swoboda JG, Mylonakis E, Wilkinson BJ, Walker S (2011) Synthetic lethal compound combinations reveal a fundamental connection between wall teichoic acid and peptidoglycan biosyntheses in Staphylococcus aureus. ACS Chem Biol 6(1):106–116. https://doi.org/10.1021/cb100269f
13. Percy MG, Grundling A (2014) Lipoteichoic acid synthesis and function in gram-positive bacteria. Annu Rev Microbiol 68:81–100. https://doi.org/10.1146/annurev-micro-091213-112949
14. Fischer W (1993) Molecular analysis of lipid macroamphiphiles by hydrophobic interaction chromatography, exemplified with lipoteichoic acids. Anal Biochem 208(1):49–56. https://doi.org/10.1006/abio.1993.1007
15. Fischer W, Koch HU, Rosel P, Fiedler F, Schmuck L (1980) Structural requirements of lipoteichoic acid carrier for recognition by the poly(ribitol phosphate) polymerase from Staphylococcus aureus H. A study of various lipoteichoic acids, derivatives, and related compounds. J Biol Chem 255(10):4550–4556
16. Brown S, Santa Maria JP Jr, Walker S (2013) Wall teichoic acids of gram-positive bacteria. Annu Rev Microbiol 67:313–336. https://doi.org/10.1146/annurev-micro-092412-155620
17. Kiriukhin MY, Debabov DV, Shinabarger DL, Neuhaus FC (2001) Biosynthesis of the glycolipid anchor in lipoteichoic acid of Staphylococcus aureus RN4220: role of YpfP, the diglucosyldiacylglycerol synthase. J Bacteriol 183(11):3506–3514. https://doi.org/10.1128/JB.183.11.3506-3514.2001
18. Lu D, Wormann ME, Zhang X, Schneewind O, Grundling A, Freemont PS (2009) Structure-based mechanism of lipoteichoic acid synthesis by Staphylococcus aureus LtaS. Proc Natl Acad Sci U S A 106(5):1584–1589. https://doi.org/10.1073/pnas.0809020106
19. Tropea JE, Cherry S, Waugh DS (2009) Expression and purification of soluble His(6)-tagged TEV protease. Methods Mol Biol 498:297–307. https://doi.org/10.1007/978-1-59745-196-3_19
20. Casanas A, Warshamanage R, Finke AD, Panepucci E, Olieric V, Noll A, Tampe R, Brandstetter S, Forster A, Mueller M, Schulze-Briese C, Bunk O, Wang M (2016) EIGER detector: application in macromolecular crystallography. Acta Crystallogr D Struct Biol 72(Pt 9):1036–1048. https://doi.org/10.1107/S2059798316012304
21. Wojdyla JA, Panepucci E, Martiel I, Ebner S, Huang CY, Caffrey M, Bunk O, Wang M (2016) Fast two-dimensional grid and transmission X-ray microscopy scanning methods for visualizing and characterizing protein crystals. J Appl Crystallogr 49(Pt 3):944–952. https://doi.org/10.1107/S1600576716006233
22. Huang CY, Olieric V, Howe N, Warshamanage R, Weinert T, Panepucci E, Vogeley L, Basu S, Diederichs K, Caffrey M, Wang M (2018) In situ serial crystallography for rapid de novo membrane protein structure determination. Commun Biol 1:124. https://doi.org/10.1038/s42003-018-0123-6
23. Wojdyla JA, Kaminski JW, Panepucci E, Ebner S, Wang X, Gabadinho J, Wang M (2018) DA+ data acquisition and analysis software at the Swiss Light Source macromolecular crystallography beamlines. J Synchrotron Radiat 25(Pt 1):293–303. https://doi.org/10.1107/S1600577517014503
24. Basu S, Kaminski JW, Panepucci E, Huang C-Y, Warshamanage R, Wang M, Wojdyla JA (2019) Automated data collection and real-time data analysis suite for serial synchrotron crystallography. J Synchrotron Radiat 26 (1):244–252. https://doi.org/10.1107/S1600577518016570
25. Heras B, Martin JL (2005) Post-crystallization treatments for improving diffraction quality of protein crystals. Acta Crystallogr D Biol Crystallogr 61(Pt 9):1173–1180. https://doi.org/10.1107/S0907444905019451

Chapter 20

In Meso In Situ Serial X-Ray Crystallography (IMISX): A Protocol for Membrane Protein Structure Determination at the Swiss Light Source

Chia-Ying Huang, Vincent Olieric, Martin Caffrey, and Meitian Wang

Abstract

The lipid cubic phases (LCP) have enabled the determination of many important high-resolution structures of membrane proteins such as G-protein-coupled receptors, photosensitive proteins, enzymes, channels, and transporters. However, harvesting the crystals from the glass or plastic plates in which crystals grow is challenging. The in meso in situ serial X-ray crystallography (IMISX) method uses thin plastic windowed plates that minimize LCP crystal manipulation. The method, which is compatible with high-throughput in situ measurements, allows systematic diffraction screening and rapid data collection from hundreds of microcrystals in in meso crystallization wells without direct crystal harvesting. In this chapter, we describe an IMISX protocol for in situ serial X-ray data collection of LCP-grown crystals at both cryogenic and room temperatures which includes the crystallization setup, sample delivery, automated serial diffraction data collection, and experimental phasing. We also detail how the IMISX method was applied successfully for the structure determination of two novel targets—the undecaprenyl-pyrophosphate phosphatase BacA and the chemokine G-protein-coupled receptor CCR2A.

Key words In situ, IMISX, Lipid cubic phase, Mesophase, Membrane proteins, Microcrystals, Serial crystallography, Synchrotron, X-ray, X-ray free-electron lasers

1 Introduction

Membrane proteins (MPs) play an important role in signal and energy transduction, metabolism, transport, as well as contributing to the structural integrity of cells. They account for approximately one-third of cellular proteins and represent close to 50% of drug targets in humans [1]. The atomic resolution structure of a MP serves as the basis for understanding a protein's mode of action and is valuable for structure-based drug design [2]. However, MPs are challenging to express, to purify, and to crystallize, in part, reflecting the complex membrane environment from which they derive. Traditionally, detergent micelles have been used to extract and

Camilo Perez and Timm Maier (eds.), *Expression, Purification, and Structural Biology of Membrane Proteins*, Methods in Molecular Biology, vol. 2127, https://doi.org/10.1007/978-1-0716-0373-4_20,

solubilize MPs by mimicking, to some degree, the lipid bilayer of the native membrane. Alas, micelles are imperfect mimics. The lipid bilayer of the lipid cubic phase (LCP) or in meso crystallization provides a closer analog to the native membrane and has been used successfully to support MP crystallization [3, 4]. The LCP enables MPs to stack in sheetlike assemblies giving rise to crystals with type I packing, which tend to be small and well ordered and can give rise to high-resolution diffraction [5]. The LCP method has had a major impact on the field of MP structural and functional biology, and has contributed to many high-impact structures including G-protein-coupled receptors, rhodopsins, transporters, ion channels, enzymes, and an assortment of complexes [6, 7]. It has also strongly contributed to the recent success of injector-based serial X-ray crystallography at both free-electron lasers (XFELs) [8–12] and synchrotrons [13–17].

The traditional glass plate designed for the LCP method provides stability during crystallization and the plate can be stored for long periods without water loss [18]. However, the process of harvesting crystals from the mesophase in the glass plate is technically demanding [19] and can lead to damage and/or crystal loss. We developed an improved method called in meso in situ serial X-ray crystallography (IMISX) which avoids direct crystal harvesting [20]. It employs a double-sandwich plate and its utility has been demonstrated with the structure determination of several MPs, including a GPCR [21]. The IMISX method has been further refined for data collection under cryogenic conditions (IMISXcryo) [21] and for heavy atom soaking directly in IMISX wells [22]. Independently, Broecker et al. have developed a similar method with lower X-ray scattering and absorption by using thinner plastic windows and for ease of use with 3D printed holders [23, 24].

A microfocus beam with a high flux density facilitates the detection of tiny crystals which are difficult to do otherwise with large synchrotron beams at conventional macromolecular X-ray crystallography (MX) experimental stations [25, 26]. Some of the more notable LCP case studies involving the use of a microfocus beam are those in the field of GPCRs [27–30]. The Nobel Prize in Chemistry awarded to Lefkowitz and Kobilka in 2012 recognized the important contributions made by the LCP method. While the method has been successful, it is still a challenge to obtain high-quality data from single LCP crystals of <20 μm in size. Accordingly, partial datasets from many crystals must be assembled to generate a complete dataset, hence the term serial X-ray crystallography [31]. The serial method was actually standard in 1980s for the measurement of virus crystals at room temperature, but its modern variants utilize hundreds to thousands of crystals in high-throughput manners by taking advantage of the advances in sample delivery methods [8, 13, 17, 32–35], detector technology

[36, 37], together with automation in data collection and processing [38–40].

Here, we review the LCP in situ serial crystallography method as implemented at the Swiss Light Source (SLS) and describe step-by-step procedures for the crystallographic structure determination of MPs, from IMISX plate assembly, well harvesting, heavy atom (HA), and ligand soaking to in situ serial data collection and experimental phasing (*see* **Note 1**).

2 Materials

2.1 IMISX Plate

In situ serial crystallography enables X-ray data collection directly on crystals where and as they grow. It significantly reduces the effort and time devoted to sample preparation and structure determination. It started with crystals in thin glass-walled capillaries (10 μm thickness) which were used for in situ data collection with counter-diffusion crystallization [41, 42]. The crystals in optically clear glass are easy to observe and the watertight property of the glass provides a hermetic seal and a reproducible environment for crystal growth. However, the viscous nature of the LCP makes it difficult to perform in meso crystallization and screening in such thin microcapillaries. Although the traditional LCP sandwich glass plate enables high-throughput screening of crystallization conditions, the glass sandwich plate cannot be used directly for X-ray diffraction screening due to poor X-ray transparency and strong scattering. Therefore, other materials have been explored to lower X-ray background scattering and increase transmission [43]. Thin plastic polymers have been tested including polydimethylsiloxane (PDMS, 14–45 μm), polyvinyl chloride (PVC, 50 μm), polyethylene terephthalate (PET, 50 μm), and cyclic olefin copolymer (COC, 50–100 μm), and applications have been reported in microfluidic devices for on-chip characterization [44–46] and for data collection on MPs [47, 48]. Of these materials, COC proved to be relatively watertight and to have good X-ray transparency and scattering properties which make it a useful material for in situ experiments. Importantly, easy-to-handle 50–100 μm thick COC film became commercially available. To date, COC has been used with 96-well SBS in situ plates including CrystalQuick™ X [49], CrystalDirect™ [50], and In Situ-1 Plates™ (MiTeGen) for in situ diffraction experiment at room temperature. The IMISX plate, which uses 25 μm thick COC film, was successfully used for structure determination of weakly diffracting LCP crystals [20–22, 51]. Subsequently, 13 μm thick cyclic olefin polymer (COP) with similar properties as COC [52] has been used for the structure determination of a GPCR [53]. Thinner materials like 3.5 μm biaxially oriented polyethylene terephthalate (Mylar) [23],

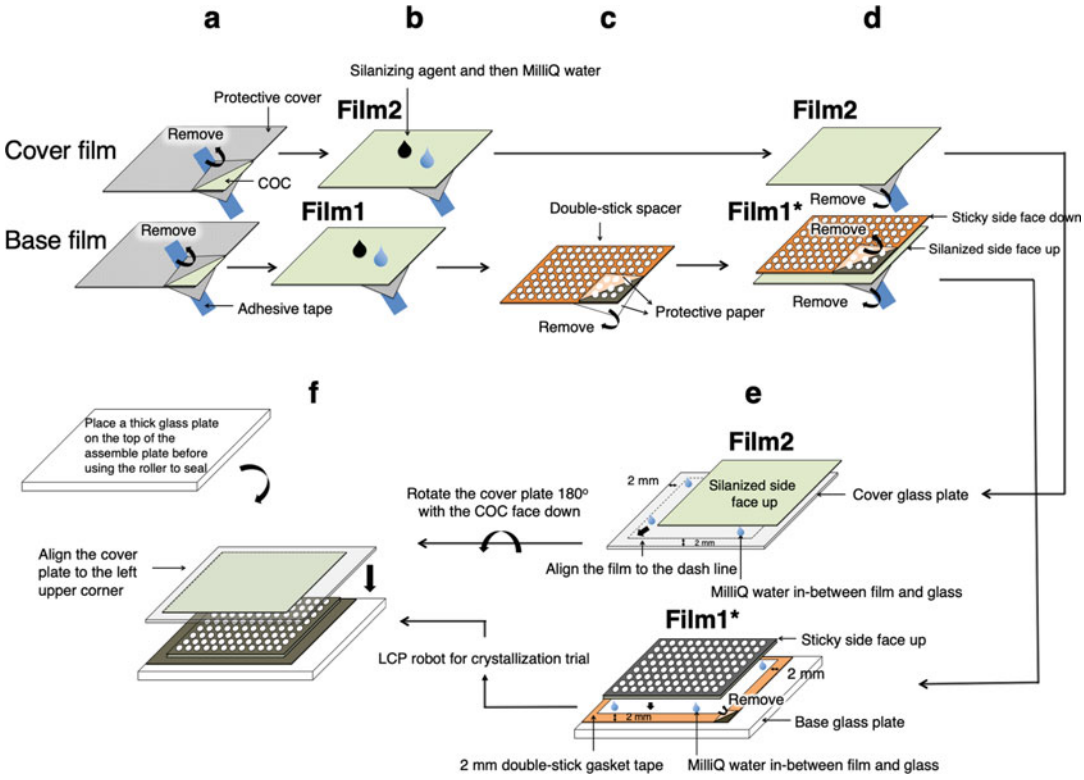

Fig. 1 Steps involved in assembling an IMISX plate. (**a**) Prepare two COC films. With the aid of a piece of adhesive tape, remove one of the protective covers from both COC films. (**b**) Treat the exposed surface with silanizing agent, rinse with water, and blot dry with a tissue. (**c**) Remove the protective white paper from one side of the perforated spacer tape. (**d**) Apply the spacer tape, sticky side down, to the silanized surface of the COC film from step (**b**) and remove the second protective covers from both COC films. Also remove the second protective paper from the upper surface of the double-stick tape from COC base plate. (**e**) Remove the protective paper from the upper surface of the double-stick gasket from the glass base plate. Place few drops of ultrapure water on the upper surface of the glass base plate and glass cover plate. Place the COC base plate and cover plate prepared in step (**d**) and place it bottom side down firmly onto the glass plate to be held in place by capillarity. (**f**) Use the LCP robot to dispense mesophase and precipitant on base glass plate with COC base plate, and seal using the cover glass plate with the COC film facing the sample. Place a standard glass plate on top of the cover glass plate and brayer to provide tight seals all around

250–500 nm graphene [54–56], and 1–20 μm silicon nitride [57–60] have been investigated as well for X-ray crystallography.

The thin film window material is normally combined with 96-well perforated double-stick tape for high-throughput LCP crystallization using a robot [61]. The detailed protocols for IMISX plate assembly (Fig. 1), sample harvesting (Fig. 2), as well as serial data collection implemented at the SLS are described below. All parts and materials can be purchased individually from commercial sources and assembled in-house (*see* **Note 2**).

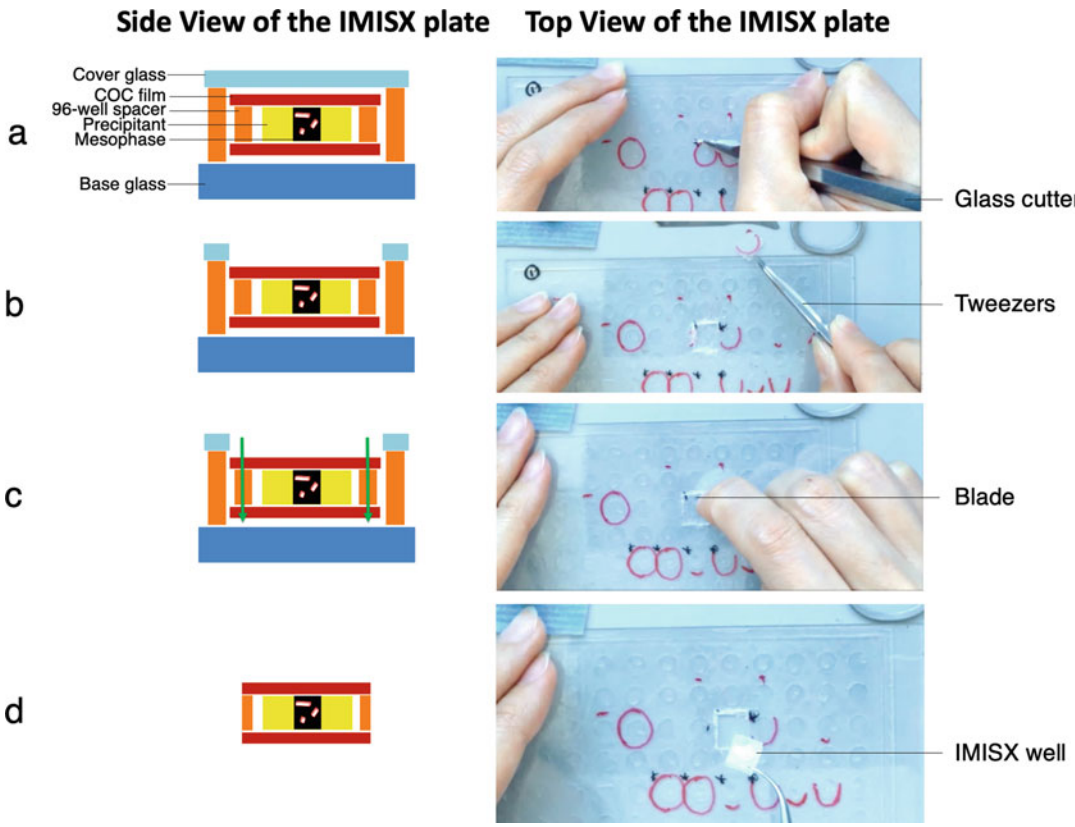

Fig. 2 Steps for removing a well from an IMISX plate. (**a**) Use a glasscutter to cut and to free a square of cover glass on the selected well. (**b**) Remove the freed cover glass. (**c**) Follow the edge of the square from the previous step to cut the inner plastic IMISX well using a blade or a scalpel. The arrows on the side view of the well indicate the cutting position. (**d**) Remove the freed plastic well using a tweezers (reproduced under a Creative Commons Attribution (CC-BY) License (https:/creativecommons.org/licenses/by/2.0) from [20, 21]. Copyright: © 2015, 2016 Huang et al.)

2.1.1 Thin Plastic Films

Two 112 mm × 77 mm pieces of 25 μm thick COC or of 13 μm thick COP are required. The COC film is available from MiTeGen (Ithaca, NY), Molecular Dimensions (Suffolk, UK), Zeonex (ZenorFilm, Düsseldorf, Germany), and SWISSCI (Neuheim, Switzerland). The COP film can be provided through Zeonex (ZenorFilm, Düsseldorf, Germany).

2.1.2 Perforated Double-Stick Spacer Tape

Double-stick spacer tape measuring 112 mm × 77 mm and 50, 64, or 140 μm thick with 5, 6, or 7 mm diameter perforations spaced 9 mm apart center-to-center and double-stick gasket 2 mm wide and 140 μm thick with outer dimensions of 118 mm × 83 mm and inner dimensions of 114 mm × 79 mm are required. The materials can be sourced from SAUNDERS (Chicago, IL, USA).

2.1.3 Glass Plates

124 mm × 84 mm No. 1.5 glass 0.15 mm thick thin glass plate and 127.8 mm × 85.5 mm standard 1 mm thick glass plate are required. These can be purchased from MARIENFELD (Lauda-Königshofen, Germany).

2.1.4 Other Materials and Tools Needed for the IMISX Plate Assembly

Ultrapure water, silanizing agent (RainX), tissue paper, adhesive tape, 10 or 20 μL pipette, and micro tip.

2.2 Sample Preparation Prior to the Data Collection

2.2.1 Sample Holder

To support in situ serial and high-throughput screening and data collection, many MX beamlines are equipped with a sample holder for SBS in situ 96-well plate [52, 62, 63] where protein crystals can be screened directly in situ and diffraction data can be recorded at room temperature. However, radiation damage of the sample at room temperature is a limiting factor and increases sample consumption [64–66]. The problem is often exacerbated when working with small LCP crystals. Later, thick polycarbonate plastic with 75 holes on a standard goniometer base that allowed LCP crystallization and data collection directly at room and cryogenic temperatures was developed [34]. Other supports for holding a single in situ well were made and modified for cryogenic measurements at a synchrotron. They include the DiffraX™ sample holder [52], 3D printed holders [23, 24], and Y-shaped IMISX sticker supports [21, 22].

The IMISX technology was designed around the MX facilities at the SLS. The original prototype used a square support made of 25 μm thick COC which imposed a very slight curvature (Fig. 3a) on the in situ sample once glued in place [21]. Although this curvature increased the rigidity of the sample in the cryostream, it turned out to be inconvenient for large-area grid scans because crystals distributed throughout the bolus were at different focus levels and on different rotation axes. Later, a Y-shaped sticker support (Fig. 3b) was designed to create a flat IMISX well and to facilitate large-area grid scans [22]. The Y-shaped support is made conveniently and in a medium-throughput fashion using a bespoke puncher which works directly with 25 μm COC on 141 μm double-stick tape (Fig. 4). Recently, the mounting of the sample on the support was simplified using a new 3D printed support which can hold most LCP sample preparation types [24]. We adapted the latter 3D design (unpublished results) to enable HA/ligand-soaking capability directly in the IMISX well for IMISX-experimental phasing (IMISX-EP) (Fig. 3c, d). The details method is described in Subheading 3.2.

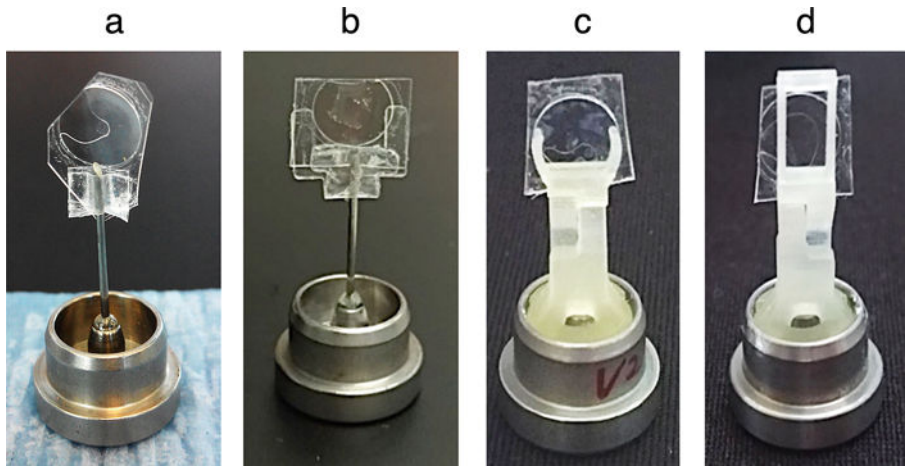

Fig. 3 Evolution of the IMISX support (**a**) Square support (adapted under a Creative Commons Attribution (CC-BY) License (https:/creativecommons.org/licenses/by/2.0) from [21]. Copyright: © 2016 Huang et al.) (**b**) Y-shaped support. (**c**) Round-shaped support. (**d**) Rectangular shaped support

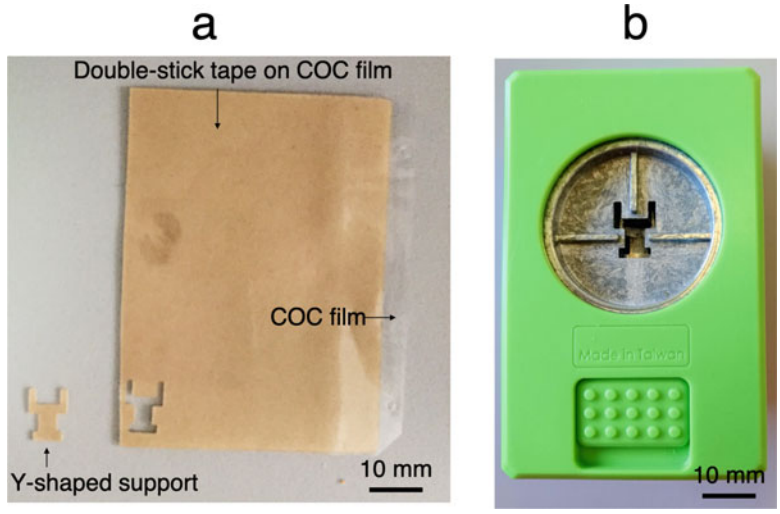

Fig. 4 The materials needed to make a sticker support. (**a**) Double-stick tape with the COC film and Y-shaped support. (**b**) Y-shaped puncher

2.2.2 Heavy Atoms

Currently, 40% of the unique MP structures on record in the PDB have been solved by the in meso crystallization method and most of them have had to be solved by experimental phasing with either selenomethionine (SeMet) labeling or HA soaking [22, 67]. The IMISX method is compatible with soaking in a manner that does not involve crystal handling [22]. Using dedicated sample holders, it is possible to add the HA soak solution to the LCP bolus and to remove it post-incubation, through the cut end of the IMISX well.

The optimal HA, concentration and soak time can be screened using a gel shift assay [68] or analyzed with the HATODAS II server [69] by uploading the protein sequence. The HA can be sourced from Hampton Research (CA, USA).

2.2.3 LCP Crystallization

Monoolein (9.9 MAG), 7.8 MAG, and cholesterol [70]. Gryphon LCP (Art Robbins) and mosquito® LCP (TTP Labtech), heat block, 50 or 100 µL Hamilton glass syringes, and coupler.

2.2.4 Other Materials and Tools Needed for Sample Preparation and Harvesting

Glass-cutting tool, tweezers, scissors, scalpel or blade, brayer or handheld roller, 3D printed rectangular or round support, 25 µm thick COC film, 141 µm double-stick tape, Y-shaped puncher, magnetic goniometer base, glove, magnetic wand, cotton bud, adhesive tape, microscope, 10 or 20 µL pipette, micro tip, incubator, timer, liquid nitrogen (LN_2), container for LN_2, sample-storing puck, and Dewar.

2.3 MX Beamlines

2.3.1 X-Ray Beam Characteristics

The IMISX method was developed at the two undulator beamlines X06SA-PXI and X10SA-PXII at the SLS, Paul Scherrer Institut (PSI). Both beamlines provide fast and stable energy (wavelength) selection in the range from 5.5 to 17.5 keV for X06SA-PXI and from 6 to 20 keV for X10SA-PXII. Beamline X06SA-PXI is optimized for micro-focusing applications and features a beam down to 2×1 µm^2. Beam size can be varied to match the dimensions of the crystal, thereby maximizing the diffraction signal. The X10SA-PXII beamline utilizes three apertures to resize the beam to a limiting dimension of 18×10 µm^2. A recent micro-focusing upgrade with kinoform diffractive lenses delivers a 5×2 µm^2 beam [71]. Both PX beamlines are equipped with a high-precision D3 diffractometer, which is essential for fast and continuous grid scanning [72].

2.3.2 Detector

For serial crystallography, a fast detector is required to expeditiously scan a large area, to locate microcrystals, and to collect hundreds of partial datasets at high speed. Both the EIGER 16M [37] at X06SA-PXI and the EIGER2 16M (Dectris Ltd.) at X10SA-PXII are state-of-the-art single-photon-counting, pixel-array detectors with low noise, fast frame rate, and negligible dead time, which make them ideal for serial synchrotron crystallography.

2.3.3 Software

The software suite developed at the SLS for IMISX applications includes (1) a fast scan program in DA+ GUI [73], (2) an automated serial data collection CY+ GUI [22], (3) an automated data processing (*adp*) program [74], and (4) an automated data merging (*adm*) pipeline [40]. The suite includes real-time data quality monitoring and feedback to inform concurrent data collection.

3 Methods

The optimized IMISX crystallization and serial data collection protocols described here are available at the SLS. All of the procedures are carried out at 20 °C unless indicated otherwise. Instructional, open-access videos describing implementation and effective use of the IMISX method are available online [21].

3.1 Performing an IMISX Crystallization Trial

3.1.1 Assembling the IMISX Plate

1. COC films come from the manufacturer sandwiched between two protective covers. Remove one protective cover from each of the two COC films with the help of a small piece of adhesive tape (Fig. 1a). Place the two films on a clean working surface with the exposed COC side face up. Apply 5–10 μL silanizing agent to the exposed surfaces and spread it evenly on the films with a tissue to create a hydrophobic surface (Fig. 1b). One film (Film1) will serve as the base film for the wells in which crystals grow. The other (Film2) functions as the cover for the well.
2. Rinse the silanizing agent off the treated films using 5–10 μL ultrapure water (Fig. 1b).
3. Remove the protective white paper from a 96-well double-stick spacer (6 mm diameter perforations) (Fig. 1c) and apply it—with its sticky surface down—to Film1 from the previous step (Fig. 1d). Use the roller or brayer to expel air from between the tape and Film1 and to ensure a tight bond between the two. This composite piece will be referred to hereafter as Film1∗ (*see* **Note 3**).
4. Remove the protective white paper from the double-stick tape gasket and apply it, sticky surface down, to a 1 mm thick base glass plate. The two should be arranged so that their upper left hand corners are aligned. Use the roller to make sure that the tape and glass stick firmly together (Fig. 1e).
5. At the middle and at the four corners of the 1 mm base glass plate from **step 4** and to a No. 1.5 cover glass plate apply 5–10 μL ultrapure water (Fig. 1e).
6. Use small pieces of adhesive tape to remove the protective cover from Film1∗ (with double-stick tape attached) and the protective brown paper from the 96-well double-stick spacer (Fig. 1d). Place Film1∗ with its COC film facing down on the 1 mm base glass plate carefully positioned and centered within the double-stick gasket (Fig. 1e).
7. Use adhesive tape to remove the second protective cover from Film2 (Fig. 1d). With Film2 oriented with its silanized surface up, place it on the No. 1.5 thin cover glass plate with at least 2 mm from the sides, as shown in Fig. 1e. Ultrapure water on the plate will help secure Film2 uniformly flat on the cover glass

plate. A paper tissue can be used to squeeze/absorb excess water from between the cover glass plate and Film2 and to ensure that the two are held firmly together by capillary forces.

3.1.2 High-Throughput Crystallization Trial Setup Using the LCP Robot

The Gryphon LCP and mosquito® LCP are popular robots for setting LCP crystallization trials. Both robots are equipped with a mesophase dispensing arm for dispensing the viscous protein-laden LCP. A protocol for using these robots that includes instructional online videos has been published [75]. Here, we describe a modification to this protocol specifically for setting up IMISX plates in a high-throughput fashion.

1. Melt the hosting lipid (usually monoolein 9.9 MAG with or without an additive lipid such as cholesterol) on a heat block at 42 °C and warm up a 100 μL Hamilton syringe on the same heat block. Prepare the protein solution at a concentration typically at or above 10 mg/mL.
2. Fill a 100 μL Hamilton syringe with 20 μL protein solution and fill the warm 100 μL syringe with 30 μL molten lipid. Connect the two syringes together with the narrow-bore coupler. Be careful not to over- or under-tighten the coupled syringe mixing device. Mix the contents of the two syringes immediately after connecting them. Our preference is to move the protein solution into the lipid as the first step in the mixing process. Continue to mix the contents until it becomes viscous and optical clear. The volume ratio of lipid to the protein solution is 3 to 2 based on the 9.9 MAG phase diagram and 1 to 1 for the short-chain lipid, 7.8 MAG [4].
3. Turn on the humidifier that provides a humid atmosphere over the deck of the robot for at least 10 min before use and make sure that the humidity level has reached 80% before dispensing mesophase onto plates.
4. When using the mosquito® LCP for the crystallization trial, first follow the LCP syringe wizard that is part of the mosquito® LCP protocol to assemble the Hamilton syringe complete with LCP from **step 2** and needle on the robot's LCP dispensing arm. The wizard will automatically calibrate the X and Y horizontal coordinates of the needle tip. The needle height can be adjusted manually to ~0.1 mm above the bottom of the well in the receiving plate to avoid damaging or making a tool mark on the IMISX film if the parameters of the standard glass plate type are used in the protocol of plate type. Alternatively, a new plate type can be set up and added using the Options| Plates menu of mosquito® LCP software without changing the needle height. Measure the plate height with a plastic film on the standard glass base plate by using vernier caliper. If the Gryphon LCP is being used, first prepare a Gryphon LCP syringe with a calibrated needle. The calibration

of the Gryphon syringe can be done by using Configuration| Configure Global Settings, Syringe menu in the Gryphon LCP software. The LCP sample then can be transferred from a Hamilton syringe to the Gryphon LCP syringe. Follow the instruction of the Exchange Solo Syringe of the Gryphon LCP protocol to assemble the Gryphon syringe on the LCP dispensing arm. Needle height can be adjusted manually to ~0.1 mm above the bottom of the well through the Dispense menu of the Gryphon software if the parameters of the standard glass plate type are used in the protocol of plate type. Alternatively, the new plate type will need to be set up for the IMISX plate through the Configuration| Open Labware Editor| Create New Labware menu of Gryphon LCP software without changing the needle height. Use the vernier caliper to measure the plate height with a plastic film on the glass base plate.

5. Activate the robot to dispense typically a 50 nL LCP bolus plus 800 nL precipitant solution sequentially into each well. When all 96 wells have been filled, cover the plate with No. 1.5 thin cover glass plate with Film2 attached (COC face down toward the sample) that was prepared in Subheading 3.1.1, **step 7** (Fig. 1f). Place a 1 mm thick glass plate on the top of the assembled IMISX plate and use a roller or brayer to effect a uniform and a hermetic seal. Note that the LCP bolus can deform by brayering action without a 1 mm thick glass plate on the top of assembled IMISX plate.
6. The IMISX plate described here has the same footprint as a SBS plate and can be directly stored in an incubator/imager (Rock Imager® RI1000, Formulatrix, Waltham, MA, USA) without a base plate frame support. The Rock Imager®, equipped with a top-of-plate barcode scanner, can be used for the IMISX plate incubation, storage, and crystallization progress monitoring. Add new plate type identifier as IMISX plate to the Plate Type list in the Rock Maker® software using the Plate Type Editor. Print a barcode with the IMISX plate type, apply it to the assembled plate from **step 5**, and incubate them in the Rock Imager® typically at 4 °C and/or 20 °C for quantitative tracking of crystallization progress.

3.2 Preparing the IMISX Well for Data Collection

3.2.1 Harvesting Using Sticker Support

1. Screen plates for crystals and mark the wells which contain crystals.
2. Use a glasscutter to cut and to free a square of cover glass on the selected well (Fig. 2a), remove the freed cover glass, and clean away glass shards using a brush or with a piece of adhesive tape (Fig. 2b).

3. Follow the edge of the square from **step 2** to cut the inner plastic IMISX well using a blade or a scalpel (Fig. 2c) and carefully remove the freed plastic well with its crystal-laden bolus using a tweezers (Fig. 2d).
4. Prepare a piece of 25 μm COC film and a 141 μm double-stick tape. Remove both protective covers from the COC film and remove the protective white paper from one side of the double-stick tape. Place the sticky side of double-stick tape down on the COC film and then use the roller or brayer to expel air from between the tape and film and to ensure a tight bond between the two (Fig. 4a).
5. Use the Y-shape puncher (Fig. 4b) on the film prepared in the previous step to generate a Y-shaped mount and then make a hole on the middle of the neck of the Y-shape support (Fig. 5a).
6. Remove the protective cover from one face of the Y-support (Fig. 5b). Pass the pin through the centering hole in the Y-support sticky face up (Fig. 5c).
7. Position the well on the exposed sticky surface of the Y-support (Fig. 5d).
8. Fold the Y-support back on itself and the two parts pressed together to secure the well firmly to the pin (Fig. 5e–g). Adjust the pin position to be just below the LCP bolus (Fig. 5h). Trim the edges of the IMISX well to fit it to the storage puck (Fig. 6a). The IMISX well securely attached to the pin on a base is now ready for precipitant removal, and HA or ligand soaking (Fig. 6b, c).
9. For snap cooling in liquid nitrogen, waft away by hand the stagnant warmer layer of gas above the liquid nitrogen that fills to the brim a small Dewar and rapidly snap-cool the mounted IMISX sample by plunging it edge down into the liquid nitrogen for long-term storage.

3.2.2 Mounting the Harvested IMISX Well on a 3D Printed Support

1. Prepare the IMISX sample as described in Subheading 3.2.1, **steps 1–3**.
2. Insert a 3D printed support into a standard goniometer base and mount the IMISX well on the support (Fig. 3c, d). Position the well so that the LCP bolus is approximately at the center of the support window (*see* **Note 4**). The round-shaped support is well suited for boluses in the sponge phase (Fig. 3c). The rectangular shaped support should be used for boluses that are in the cubic phase (Fig. 3d) (*see* **Note 5**).
3. Trim the edges of the IMISX well to fit the rectangular or round-shaped support (Fig. 6a). Use a cotton bud or tissue paper to remove precipitant solution from the cut well (Fig. 6b). Follow Subheading 3.2.3 for HA or ligand soaking, or Subheading 3.2.1, **step 9**, for sample storage.

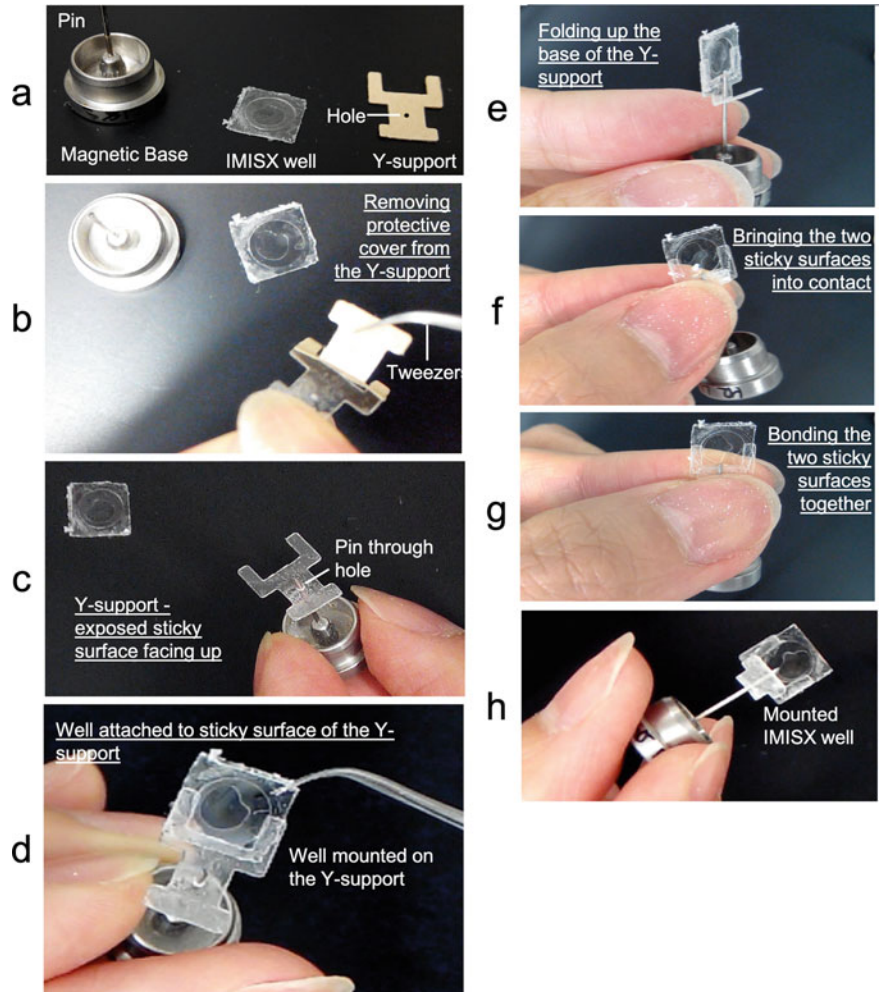

Fig. 5 Steps involved in securing an IMISX well to a Y-shaped support and subsequently to a mounting pin. (**a**) Parts: mounting pin in base, IMISX well, Y-shaped support with a centering hole and made from double-stick tape. (**b**) Protective cover is removed from one face of the Y-shaped support. (**c**) The pin is passed through the centering hole in the Y-shaped support sticky face up. (**d**) The well is positioned on the exposed sticky surface of the Y-shaped support. The precipitant that surrounds the crystal-laden mesophase is seen clearly in the IMISX well. (**e–g**) The Y-shaped support is folded back on itself and the two parts pressed together to secure the well firmly to the pin. (**h**) The IMISX well securely attached to the pin on a base ready for precipitant removal, heavy atom or ligand soaking, and/or snap cooling in liquid nitrogen (reproduced under a Creative Commons Attribution 4.0 International License (https:/creativecommons.org/licenses/by/4.0) from [22]. Copyright: © 2018 Huang et al.)

3.2.3 IMISX Soaking with HA or Ligand

The HA- or ligand-containing solution is applied directly to the IMISX wells without touching the crystals and in a closed environment (minimal air exposure). The method [22] is described below.

1. Prepare an IMISX sample as described in Subheading 3.2.1 or 3.2.2.
2. Snip off one corner of the well with a scissor (Fig. 6a) and wick away the precipitant solution from around the mesophase bolus using a cotton bud or tissue paper (Fig. 6b).

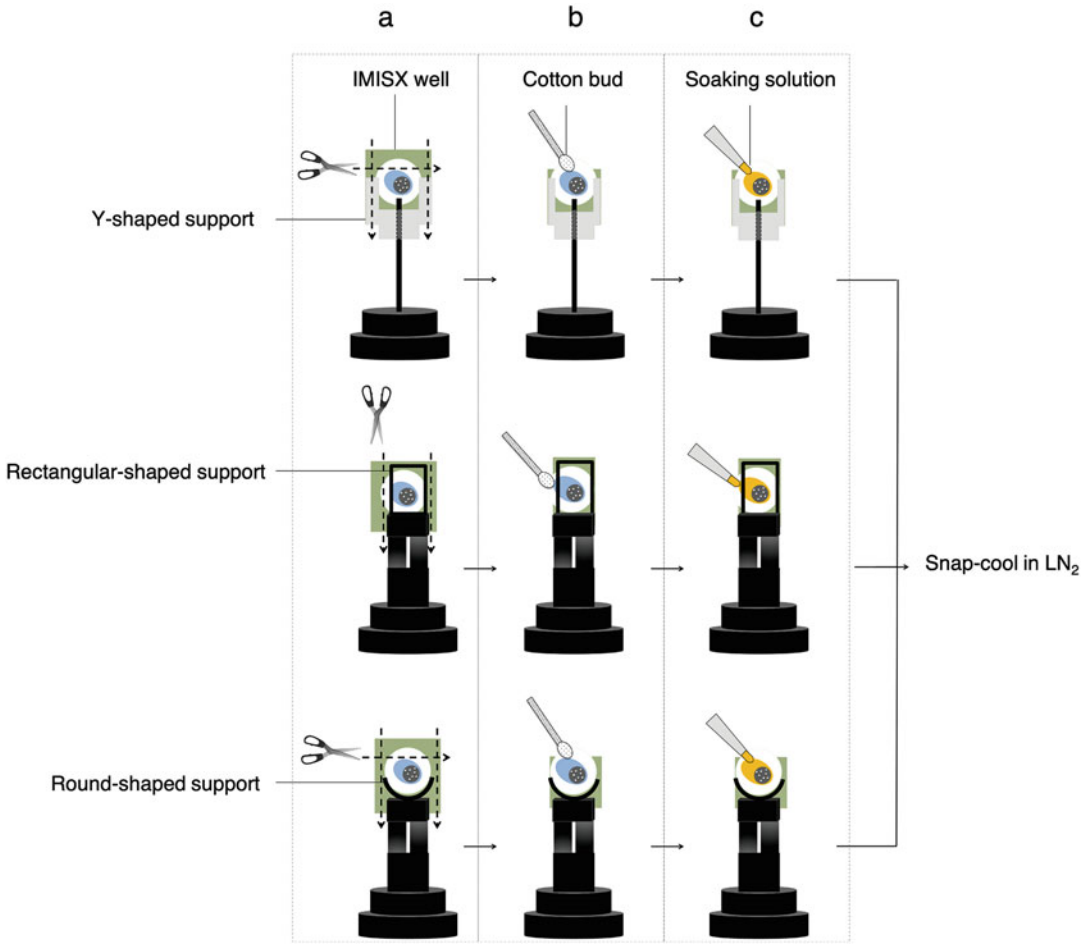

Fig. 6 Trimming an IMISX well and soaking with HA or ligand. (**a**) Snip off the top and both sides of the IMISX well. (**b**) Wick away precipitant solution from around the mesophase bolus using a cotton bud or tissue paper. (**c**) Pipet heavy atom reagent or ligand solution into the well via the open corner

3. Pipet the heavy atom reagent or ligand solution, dissolved in the same precipitant solution, into the well via the open corner and manipulate so as to make contact with and to fully bathe the crystal-laden mesophase bolus (Fig. 6c).
4. Store the samples in a box with wet tissues at 20 °C and then check the crystals at different time intervals under the microscope. The recommended time course is from 1 min, and every 10 min up to 1 h. If soaking is allowed to proceed for too long and/or at too high a concentration, it can lead to the crystal dissolving or fracturing. This should be avoided.
5. Snap-cool the IMISX well immediately in liquid nitrogen to terminate the derivatization process.

3.3 Serial Data Collection

3.3.1 Beamline Setup and Serial Data Collection

In what follows, we describe how serial data collection is performed at PXI-X06SA and PXII-X10SA at the SLS.

1. The SLS uses the data acquisition software DA+ GUI [74] and the automated serial data collection protocol CY+ GUI [40] for serial crystallography data collection. At the start of a measurement, adjust the beam size to the crystal dimensions to optimize the signal-to-noise ratio (10×10 μm^2 or 20×20 μm^2 typically). Place all sample pucks into the Dewar of the sample changer.
2. Set the data acquisition software (DA+) to sample changer mode and mount the strengthened COC sandwich on the magnetic head of the goniometer (Fig. 7).
3. Orient the IMISX well normal to the beam with the well/bolus positioned in the crosshairs of the high-resolution on-axis sample-viewing microscope which corresponds to the position of the beam (*see* **Note 6**). (For reference, we define the X, Y, and Z positioning of the crystal as follows. X corresponds to the crystal position along the rotation axis of the goniometer which is aligned to intersect orthogonally with the X-ray beam axis. Z corresponds to the position along the beam axis and Y to the position along the axis perpendicular to both X and Z.) This

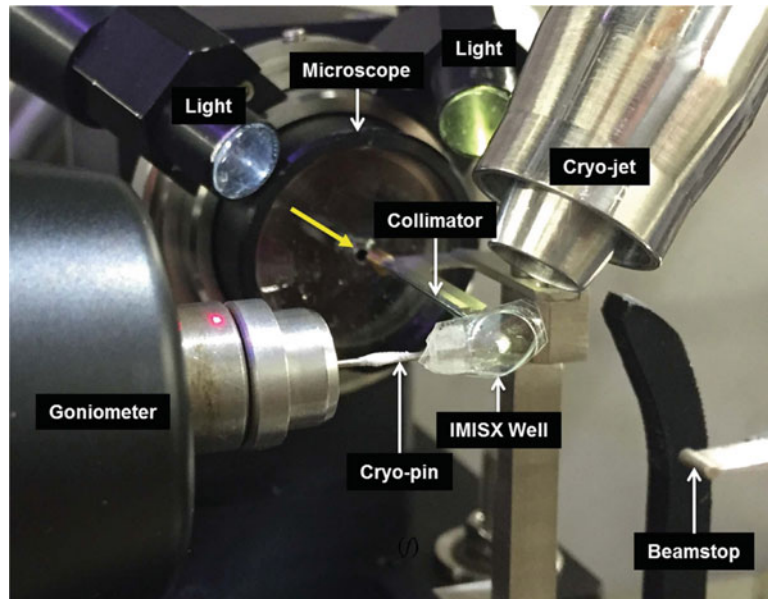

Fig. 7 Experimental setup of an IMISX well on a goniometer with the crystal-laden mesophase bolus positioned in the X-ray beam and in the cryostream at 100 K for SX data collection on beamline PXI-X06SA at the SLS (reproduced under a Creative Commons Attribution (CC-BY) License (https://creativecommons.org/licenses/by/2.0) from [21]. Copyright: © 2016 Huang et al.)

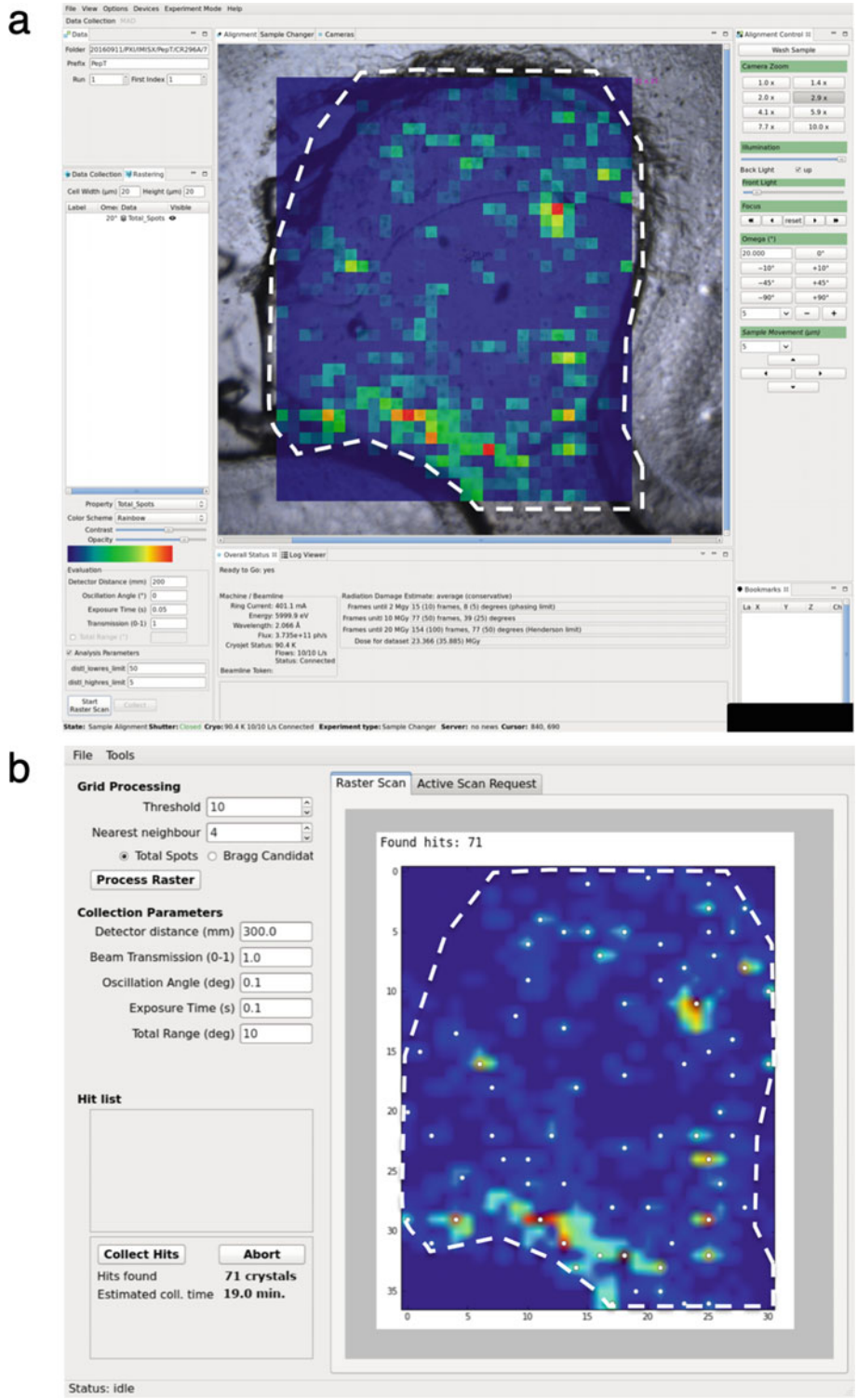

Fig. 8 Screenshots of the fast grid scan GUI (DA+) and automated serial data collection GUI (CY+). (**a**) DA+ GUI: A grid scan covers the complete LCP bolus (outlined with a dashed line) with the diffraction hits represented as a heatmap. The grid scan parameters are configured in the lower left panel of the GUI. (**b**) CY+ GUI: The selected crystal hits, identified by DA+ in (**a**), are labeled automatically with white dots and overlaid on the DA

step should be performed as quickly as possible to shroud the sample in a uniform stream of cryogenic nitrogen gas and to limit the possible ice formation. The same setup with the cryo-jet switched off can be used for in situ serial data collection at room temperature.

4. With the on-axis sample microscope, zoom in until a 1–2 mm diameter bolus can be seen, and refocus on the bolus itself (this is done by moving the sample along the beam or *Z*-axis). Make a 1–2 mm grid with the single-grid cell size 10×10 μm^2 or 20×20 μm^2 to fit to the size of crystals and to cover the entire bolus (Fig. 8a). For the initial screen, a raster scan at a typical speed of 50 Hz (20-ms exposure time per cell with a flux of 2×10^{12} photons/s) should provide enough diffracting spots for a successful spot-finding operation in the 5 to 50 Å resolution range using DISTL (Diffraction Image Screening Tool and Library) [76]. If the mesophase is of the more fluid sponge type, the crystal containing bolus may be spread over a bigger area ($>2 \times 2$ mm^2).
5. The resulting finely sampled grid map should accurately locate all diffracting crystals in the bolus (Fig. 8a) and provide a ranking of diffraction spots in heat map form (Fig. 8b).
6. Launch the automated data collection protocol CY+ after completing the grid scan for serial data collection on crystals above a defined diffraction quality threshold over a specified rotation range (typically 10–20°) and a defined beam attenuation (*see* **Note 7**). Note that such a data collection scheme does not align individual crystals to the goniometer rotation axis. In practice, this is not an issue because the rotation range is small (10–20°).
7. In case of problems with preferred orientation [20], repeat data collection with the IMISX chip through a range of angular sweeps (typically ±30°, ±45°, or ±60° with respect to the X-ray beam). Monitor processing and merging results for completeness (Fig. 9).

3.3.2 Strategy for Phasing the Structure and Structure Determination

1. Follow Subheading 3.3.1, **steps 1–4**, for centering the LCP bolus. Raster scan the LCP bolus to establish crystal coordinates in the bolus. If HAs are present, scan the absorption edge of the HA employed (note that the fluorescence signal may not

Fig. 8 (continued) + grid scan heatmap. The outline of the LCP bolus is shown so that panels (**a**) and (**b**) can be compared. The crystal hit selection criteria and parameters for serial data collection are configured in the left panel of the GUI (reproduced under a Creative Commons Attribution 4.0 International License (https://creativecommons.org/licenses/by/4.0) from [22]. Copyright: © 2018 Huang et al.)

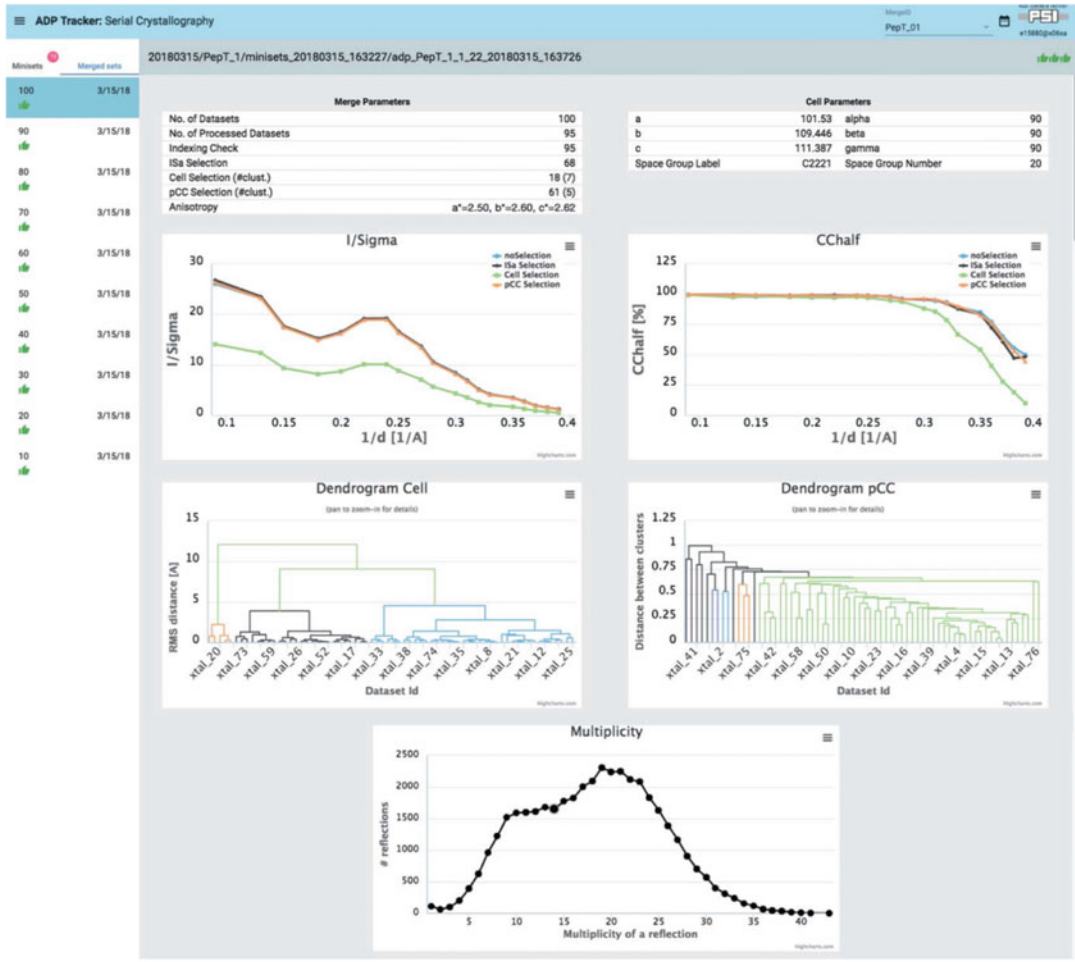

Fig. 9 The *adm* merging results and statistics of 100 $PepT_{St}$ LCP crystals in the *adp* tracker with "SX-View" mode (reproduced under a Creative Commons Attribution 4.0 International License (https:/creativecommons.org/licenses/by/2.0) from [40]. Copyright: © 2019 Basu et al.)

come from the crystal but from the surrounding mesophase). Adjust the energy to the peak of the absorption edge to maximize *f″* [77].

2. Check the quality of diffraction from the raster scan. Follow Subheading 3.3.1, **steps 5–7**, for data collection (*see* **Note 8**).
3. Where relevant, monitor the anomalous signal using *adp* [74] and *adm* [40] and continue to record diffraction until there is sufficient multiplicity in the anomalous data.
4. Determine the substructure using SHELXC/D [78].
5. Once the substructure is known, launch phasing programs such as SHELXE [78], CRANK2 [79], autoSHARP [80], or PHENIX AutoSol [81], which combine density modification and automatic model building.

3.4 Successful Cases and Applications

The IMISX method was introduced in 2015 and has been continually optimized for serial data collection and phasing of novel structures. In what follows, we present results obtained with two non-reference target MPs to demonstrate its usefulness with novel targets. The first successful use of the IMISX method was to solve the structure of undecaprenyl-pyrophosphate phosphatase (BacA) (PDB code 5OON) from *Bacillus subtilis* [51], a MP with a unique interdigitated inverted topology involved in the peptidoglycan synthesis (Fig. 10a). Crystals of 20 μm in maximum dimension were initially obtained using the LCP crystallization method in standard glass sandwich plates. A few of these diffracted to 2.8-Å resolution after conventional loop harvesting but they did not yield a complete dataset. The crystallization of BacA was readily reproduced using the IMISX plate with the same screen as for the glass sandwich plate. Experimental phasing was performed by $HgCl_2$ co-crystallization using the IMISX-EP method [22]. Without directly crystal handling and harvesting, two wells containing a total of 66 crystals with average dimension of $2 \times 15 \times 20$ μm^3 were collected (Fig. 10b). Of the 66 datasets collected, 36 came from well 1 recorded over a 30° wedge per crystal and 30 were from well 2 recorded over a 15° wedge per crystal. After merging 54 partial datasets, a complete dataset at 2.6-Å resolution provided enough Hg anomalous signal for phasing the structure by Hg-SAD. Later, the native BacA crystals were derivatized by directly soaking the $HgCl_2$ in IMISX well to demonstrate the in situ soaking protocol (Subheading 3.2.3). The merging of 360 partial datasets yielded an interpretable experimental SAD map using IMISX soaking with Hg. Parenthetically, the structure was also solved by the SIRAS method by merging 94 partial datasets from native crystals and 271 partial datasets from Hg-derivatized crystals.

The second case is from GPCR family—the prime target of LCP crystallization method and structure-based drug screening in industry. In a collaboration with Boehringer Ingelheim Pharma GmbH and leadXpro AG, we recently reported a CC Chemokine Receptor 2A (CCR2A) structure in complex with MK-0812 (PDB code 6GPX) at 2.7-Å resolution using the IMISX method (Fig. 10c) [53]. In this study, the IMISX method was used with a thin COP film of 13 μm. Partial datasets of 10–15° were collected from crystals of $80 \times 20 \times 10$ μm^3 in size on average (Fig. 10d). Finally, 77 small wedges of data were merged to yield a complete dataset and the structure was solved by molecular replacement (MR). The new CCR2A ligand (MK-0812) was clearly identified with well-defined hydrogen bonds to protein residues. The structure provided key information on the residue $E291^{7.39}$ for the antagonist binding and provides new insights for the drug design on the highly selective CCR2 antagonists.

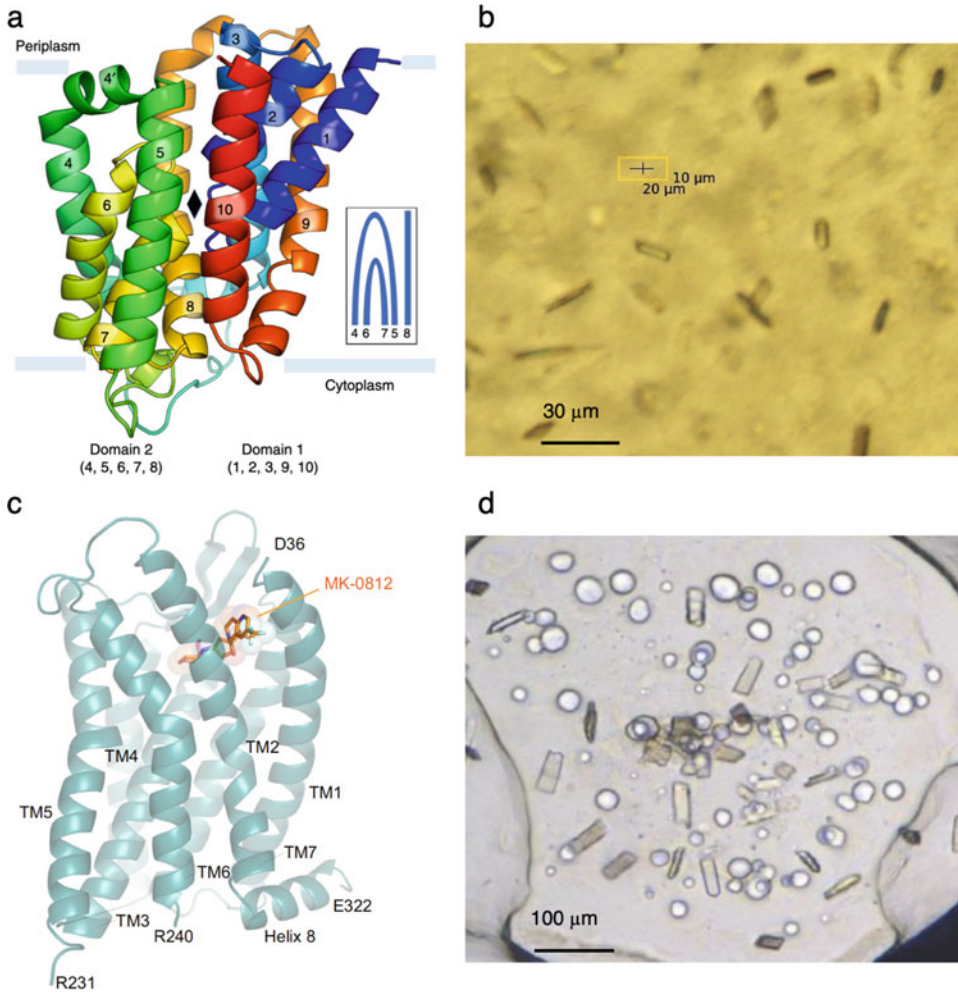

Fig. 10 Overall structures of the MPs solved by IMISX method and screenshots of the crystals in a well from an IMISX plate. (**a**) Overall structure of BacA (reproduced under a Creative Commons Attribution 4.0 International License (https:/creativecommons.org/licenses/by/4.0) from [51].) (**b**) Crystals of BacA. The size of the beam on the sample and scale bar are shown. (**c**) Overall structure of CCR2A. (**d**) Crystals of CCR2A. (Panels (**c**) and (**d**) are reproduced and adapted from [53] Copyright (2019), with permission from Elsevier)

In summary, IMISX has emerged as a valuable alternative for the structure determination of microcrystals grown in meso. As shown here, the method reduces crystal handling and makes the screening of the LCP crystals highly effective. It is generally applicable. In addition, the IMISX well is a suitable medium for serial femtosecond crystallography (SFX) applications at XFELs, providing an alternative to the well-established LCP injector-based methods. As a fixed-target method with small footprint, the IMISX setup can be used directly at both cryogenic and room temperatures as demonstrated in recent experiments at the Swiss X-ray free-electron lasers (SwissFEL) (unpublished results).

4 Notes

1. Some of the text included in this report is taken verbatim from [20–22].
2. IMISX kit that includes COC film, base glass plate with double-stick gasket, cover plate, and silanizing reagent is available from MiTeGen.
3. Large quantities of base and cover films (Film1∗ and Film2) can be prepared up to **step 3** in Subheading 3.1.1 (Fig. 1d) prior to the crystallization trial. The hydrophobic surface so created is stable for several months in storage under ambient conditions. For convenience, Film1∗ and Film2 can be placed on the base glass and cover glass plates (Fig. 1e), respectively, as outlined in Subheading 3.1.1 without removing the protective paper from double-stick gasket and base film. The base glass plate with Film1∗ and cover glass with Film2 are stable in storage for several months. Be careful to keep the plate and film in a dust-free environment.
4. It takes approximately 2 min per well to complete **steps 1** and **2** in Subheading 3.2.2. Mounted wells can be stored for a short time (~1.5 h) on moist tissue without dehydrating. In this way, IMISX wells can be conveniently prepared together in groups of 10–15.
5. Some precipitant solutions can cause the LCP to convert to the more fluid sponge phase. Sponge phase samples can move and spread in the well during harvesting. Therefore, the round-head or Y-shaped sticker support (Fig. 3b, c), which has a bigger area in which to perform the grid scan, is recommended for this kind of sample.
6. The mesophase bolus should be at or close to the center of the support. If the sticker support has been used, first look for the pin extending from the goniometer base. The bolus should be at the other end of the pin. The mesophase bolus appears brown in color when viewed with the in-line microscope and crystals should be visible if the precipitant solution has been removed properly.
7. Set up the parameters for serial data collection. First, set up the threshold and neighborhood number of the grid output to adjust the number of crystals to be shot. If known, one can provide the cell parameters, space group, and resolution range for data collection. For a new structure, the space group can be set to 0 for automatic space group identification. The program will provide an estimate of the time required to complete the data collection operation.

8. Unlike for native data collection, the dose per crystal should ideally not exceed ~5 MGy for phasing experiments [22, 77]. It can be estimated with knowledge of the incident flux, exposure time, wedge, crystal chemical composition, and size.

Acknowledgments

The assistance and support of beamline scientists at the Swiss Light Source beamlines X06SA-PXI and X10SA-PXII are acknowledged. C.-Y.H. was partially supported by the European Union's Horizon 2020 research and innovation program under the Marie Skłodowska Curie grant agreement No. 701647. The work was funded in part by Science Foundation Ireland (16/IA/4435).

References

1. Santos R, Ursu O, Gaulton A, Bento AP, Donadi RS, Bologa CG, Karlsson A, Al-Lazikani B, Hersey A, Oprea TI, Overington JP (2017) A comprehensive map of molecular drug targets. Nat Rev Drug Discov 16 (1):19–34. https://doi.org/10.1038/nrd.2016.230
2. Hendrickson WA (2016) Atomic-level analysis of membrane-protein structure. Nat Struct Mol Biol 23(6):464–467. https://doi.org/10.1038/nsmb.3215
3. Landau EM, Rosenbusch JP (1996) Lipidic cubic phases: a novel concept for the crystallization of membrane proteins. Proc Natl Acad Sci U S A 93(25):14532–14535
4. Caffrey M, Cherezov V (2009) Crystallizing membrane proteins using lipidic mesophases. Nat Protoc 4(5):706–731. https://doi.org/10.1038/nprot.2009.31
5. Caffrey M (2009) Crystallizing membrane proteins for structure determination: use of lipidic mesophases. Annu Rev Biophys 38:29–51. https://doi.org/10.1146/annurev.biophys.050708.133655
6. Caffrey M (2015) A comprehensive review of the lipid cubic phase or in meso method for crystallizing membrane and soluble proteins and complexes. Acta Crystallogr F Struct Biol Commun 71(Pt 1):3–18. https://doi.org/10.1107/S2053230X14026843
7. Cherezov V (2011) Lipidic cubic phase technologies for membrane protein structural studies. Curr Opin Struct Biol 21(4):559–566. https://doi.org/10.1016/j.sbi.2011.06.007
8. Weierstall U, James D, Wang C, White TA, Wang D, Liu W, Spence JC, Bruce Doak R, Nelson G, Fromme P, Fromme R, Grotjohann I, Kupitz C, Zatsepin NA, Liu H, Basu S, Wacker D, Han GW, Katritch V, Boutet S, Messerschmidt M, Williams GJ, Koglin JE, Marvin Seibert M, Klinker M, Gati C, Shoeman RL, Barty A, Chapman HN, Kirian RA, Beyerlein KR, Stevens RC, Li D, Shah ST, Howe N, Caffrey M, Cherezov V (2014) Lipidic cubic phase injector facilitates membrane protein serial femtosecond crystallography. Nat Commun 5:3309. https://doi.org/10.1038/ncomms4309
9. Liu W, Wacker D, Gati C, Han GW, James D, Wang D, Nelson G, Weierstall U, Katritch V, Barty A, Zatsepin NA, Li D, Messerschmidt M, Boutet S, Williams GJ, Koglin JE, Seibert MM, Wang C, Shah ST, Basu S, Fromme R, Kupitz C, Rendek KN, Grotjohann I, Fromme P, Kirian RA, Beyerlein KR, White TA, Chapman HN, Caffrey M, Spence JC, Stevens RC, Cherezov V (2013) Serial femtosecond crystallography of G protein-coupled receptors. Science 342(6165):1521–1524. https://doi.org/10.1126/science.1244142
10. Fromme R, Ishchenko A, Metz M, Chowdhury SR, Basu S, Boutet S, Fromme P, White TA, Barty A, Spence JC, Weierstall U, Liu W, Cherezov V (2015) Serial femtosecond crystallography of soluble proteins in lipidic cubic phase. IUCrJ 2(Pt 5):545–551. https://doi.org/10.1107/S2052252515013160
11. Johansson LC, Stauch B, McCorvy JD, Han GW, Patel N, Huang X-P, Batyuk A, Gati C, Slocum ST, Li C, Grandner JM, Hao S, Olsen RHJ, Tribo AR, Zaare S, Zhu L, Zatsepin NA, Weierstall U, Yous S, Stevens RC, Liu W, Roth BL, Katritch V, Cherezov V (2019) XFEL structures of the human MT2 melatonin

receptor reveal the basis of subtype selectivity. Nature 569:289. https://doi.org/10.1038/s41586-019-1144-0

12. Stauch B, Johansson LC, McCorvy JD, Patel N, Han GW, Huang X-P, Gati C, Batyuk A, Slocum ST, Ishchenko A, Brehm W, White TA, Michaelian N, Madsen C, Zhu L, Grant TD, Grandner JM, Shiriaeva A, Olsen RHJ, Tribo AR, Yous S, Stevens RC, Weierstall U, Katritch V, Roth BL, Liu W, Cherezov V (2019) Structural basis of ligand recognition at the human MT1 melatonin receptor. Nature 569:284. https://doi.org/10.1038/s41586-019-1141-3
13. Nogly P, James D, Wang DJ, White TA, Zatsepin N, Shilova A, Nelson G, Liu HG, Johansson L, Heymann M, Jaeger K, Metz M, Wickstrand C, Wu WT, Bath P, Berntsen P, Oberthuer D, Panneels V, Cherezov V, Chapman H, Schertler G, Neutze R, Spence J, Moraes I, Burghammer M, Standfuss J, Weierstall U (2015) Lipidic cubic phase serial millisecond crystallography using synchrotron radiation. IUCrJ 2:168–176. https://doi.org/10.1107/S2052252514026487
14. Botha S, Nass K, Barends TRM, Kabsch W, Latz B, Dworkowski F, Foucar L, Panepucci E, Wang MT, Shoeman RL, Schlichting I, Doak RB (2015) Room-temperature serial crystallography at synchrotron X-ray sources using slowly flowing free-standing high-viscosity microstreams. Acta Crystallogr D Biol Crystallogr 71:387–397. https://doi.org/10.1107/S1399004714026327
15. Weinert T, Olieric N, Cheng R, Brunle S, James D, Ozerov D, Gashi D, Vera L, Marsh M, Jaeger K, Dworkowski F, Panepucci E, Basu S, Skopintsev P, Dore AS, Geng T, Cooke RM, Liang M, Prota AE, Panneels V, Nogly P, Ermler U, Schertler G, Hennig M, Steinmetz MO, Wang M, Standfuss J (2017) Serial millisecond crystallography for routine room-temperature structure determination at synchrotrons. Nat Commun 8(1):542. https://doi.org/10.1038/s41467-017-00630-4
16. Martin-Garcia JM, Zhu L, Mendez D, Lee M-Y, Chun E, Li C, Hu H, Subramanian G, Kissick D, Ogata C, Henning R, Ishchenko A, Dobson Z, Zhang S, Weierstall U, Spence JCH, Fromme P, Zatsepin NA, Fischetti RF, Cherezov V, Liu W (2019) High-viscosity injector-based pink-beam serial crystallography of microcrystals at a synchrotron radiation source. IUCrJ 6(3):412–425. https://doi.org/10.1107/S205225251900263X
17. Martin-Garcia JM, Conrad CE, Nelson G, Stander N, Zatsepin NA, Zook J, Zhu L, Geiger J, Chun E, Kissick D, Hilgart MC, Ogata C, Ishchenko A, Nagaratnam N, Roy-Chowdhury S, Coe J, Subramanian G, Schaffer A, James D, Ketwala G, Venugopalan N, Xu S, Corcoran S, Ferguson D, Weierstall U, Spence JCH, Cherezov V, Fromme P, Fischetti RF, Liu W (2017) Serial millisecond crystallography of membrane and soluble protein microcrystals using synchrotron radiation. IUCrJ 4(Pt 4):439–454. https://doi.org/10.1107/S205225251700570X
18. Cherezov V, Caffrey M (2003) Nano-volume plates with excellent optical properties for fast, inexpensive crystallization screening of membrane proteins. J Appl Crystallogr 36(Part 6):1372–1377. https://doi.org/10.1107/S002188980301906X
19. Li D, Boland C, Aragao D, Walsh K, Caffrey M (2012) Harvesting and cryo-cooling crystals of membrane proteins grown in lipidic mesophases for structure determination by macromolecular crystallography. J Vis Exp 67:e4001. https://doi.org/10.3791/4001
20. Huang CY, Olieric V, Ma P, Panepucci E, Diederichs K, Wang M, Caffrey M (2015) In meso in situ serial X-ray crystallography of soluble and membrane proteins. Acta Crystallogr D Biol Crystallogr 71(Pt 6):1238–1256. https://doi.org/10.1107/S1399004715005210
21. Huang CY, Olieric V, Ma P, Howe N, Vogeley L, Liu X, Warshamanage R, Weinert T, Panepucci E, Kobilka B, Diederichs K, Wang M, Caffrey M (2016) In meso in situ serial X-ray crystallography of soluble and membrane proteins at cryogenic temperatures. Acta Crystallogr D Biol Crystallogr 72(Pt 1):93–112. https://doi.org/10.1107/S2059798315021683
22. Huang CY, Olieric V, Howe N, Warshamanage R, Weinert T, Panepucci E, Vogeley L, Basu S, Diederichs K, Caffrey M, Wang M (2018) In situ serial crystallography for rapid de novo membrane protein structure determination. Commun Biol 1:124. https://doi.org/10.1038/s42003-018-0123-6
23. Broecker J, Klingel V, Ou WL, Balo AR, Kissick DJ, Ogata CM, Kuo A, Ernst OP (2016) A versatile system for high-throughput in situ X-ray screening and data collection of soluble and membrane-protein crystals. Cryst Growth Des 16(11):6318–6326. https://doi.org/10.1021/acs.cgd.6b00950
24. Broecker J, Morizumi T, Ou WL, Klingel V, Kuo A, Kissick DJ, Ishchenko A, Lee MY, Xu S,

Makarov O, Cherezov V, Ogata CM, Ernst OP (2018) High-throughput in situ X-ray screening of and data collection from protein crystals at room temperature and under cryogenic conditions. Nat Protoc 13(2):260–292. https://doi.org/10.1038/nprot.2017.135

25. Cusack S, Belrhali H, Bram A, Burghammer M, Perrakis A, Riekel C (1998) Small is beautiful: protein micro-crystallography. Nat Struct Biol 5(Suppl):634–637. https://doi.org/10.1038/1325
26. Smith JL, Fischetti RF, Yamamoto M (2012) Micro-crystallography comes of age. Curr Opin Struct Biol 22(5):602–612. https://doi.org/10.1016/j.sbi.2012.09.001
27. Rosenbaum DM, Cherezov V, Hanson MA, Rasmussen SG, Thian FS, Kobilka TS, Choi HJ, Yao XJ, Weis WI, Stevens RC, Kobilka BK (2007) GPCR engineering yields high-resolution structural insights into beta2-adrenergic receptor function. Science 318 (5854):1266–1273. https://doi.org/10.1126/science.1150609
28. Rasmussen SG, Choi HJ, Rosenbaum DM, Kobilka TS, Thian FS, Edwards PC, Burghammer M, Ratnala VR, Sanishvili R, Fischetti RF, Schertler GF, Weis WI, Kobilka BK (2007) Crystal structure of the human beta2 adrenergic G-protein-coupled receptor. Nature 450(7168):383–387. https://doi.org/10.1038/nature06325
29. Cherezov V, Rosenbaum DM, Hanson MA, Rasmussen SG, Thian FS, Kobilka TS, Choi HJ, Kuhn P, Weis WI, Kobilka BK, Stevens RC (2007) High-resolution crystal structure of an engineered human beta2-adrenergic G protein-coupled receptor. Science 318 (5854):1258–1265. https://doi.org/10.1126/science.1150577
30. Rasmussen SG, DeVree BT, Zou Y, Kruse AC, Chung KY, Kobilka TS, Thian FS, Chae PS, Pardon E, Calinski D, Mathiesen JM, Shah ST, Lyons JA, Caffrey M, Gellman SH, Steyaert J, Skiniotis G, Weis WI, Sunahara RK, Kobilka BK (2011) Crystal structure of the beta2 adrenergic receptor-Gs protein complex. Nature 477(7366):549–555. https://doi.org/10.1038/nature10361
31. Diederichs K, Wang M (2017) Serial synchrotron X-ray crystallography (SSX). Methods Mol Biol 1607:239–272. https://doi.org/10.1007/978-1-4939-7000-1_10
32. Gañán-Calvo AM (1998) Generation of steady liquid microthreads and micron-sized monodisperse sprays in gas streams. Phys Rev Lett 80(2):285–288. https://doi.org/10.1103/PhysRevLett.80.285
33. DePonte DP, Weierstall U, Schmidt K, Warner J, Starodub D, Spence JCH, Doak RB (2008) Gas dynamic virtual nozzle for generation of microscopic droplet streams. J Phys D Appl Phys 41(19):195505. https://doi.org/10.1088/0022-3727/41/19/195505
34. Baxter EL, Aguila L, Alonso-Mori R, Barnes CO, Bonagura CA, Brehmer W, Brunger AT, Calero G, Caradoc-Davies TT, Chatterjee R, Degrado WF, Fraser JS, Ibrahim M, Kern J, Kobilka BK, Kruse AC, Larsson KM, Lemke HT, Lyubimov AY, Manglik A, McPhillips SE, Norgren E, Pang SS, Soltis SM, Song J, Thomaston J, Tsai Y, Weis WI, Woldeyes RA, Yachandra V, Yano J, Zouni A, Cohen AE (2016) High-density grids for efficient data collection from multiple crystals. Acta Crystallogr D Biol Crystallogr 72(Pt 1):2–11. https://doi.org/10.1107/S2059798315020847
35. Gati C, Bourenkov G, Klinge M, Rehders D, Stellato F, Oberthur D, Yefanov O, Sommer BP, Mogk S, Duszenko M, Betzel C, Schneider TR, Chapman HN, Redecke L (2014) Serial crystallography on in vivo grown microcrystals using synchrotron radiation. IUCrJ 1 (Pt 2):87–94. https://doi.org/10.1107/S2052252513033939
36. Mueller M, Wang M, Schulze-Briese C (2012) Optimal fine phi-slicing for single-photon-counting pixel detectors. Acta Crystallogr D Biol Crystallogr 68(Pt 1):42–56. https://doi.org/10.1107/S0907444911049833
37. Casanas A, Warshamanage R, Finke AD, Panepucci E, Olieric V, Noll A, Tampe R, Brandstetter S, Forster A, Mueller M, Schulze-Briese C, Bunk O, Wang M (2016) EIGER detector: application in macromolecular crystallography. Acta Crystallogr D Biol Crystallogr 72(Pt 9):1036–1048. https://doi.org/10.1107/S2059798316012304
38. Zander U, Bourenkov G, Popov AN, de Sanctis D, Svensson O, McCarthy AA, Round E, Gordeliy V, Mueller-Dieckmann C, Leonard GA (2015) MeshAndCollect: an automated multi-crystal data-collection workflow for synchrotron macromolecular crystallography beamlines. Acta Crystallogr D Biol Crystallogr 71(Pt 11):2328–2343. https://doi.org/10.1107/S1399004715017927
39. Yamashita K, Hirata K, Yamamoto M (2018) KAMO: towards automated data processing for microcrystals. Acta Crystallogr D Biol Crystallogr 74(Pt 5):441–449. https://doi.org/10.1107/S2059798318004576
40. Basu S, Kaminski JW, Panepucci E, Huang C-Y, Warshamanage R, Wang M, Wojdyla JA (2019) Automated data collection and real-time data analysis suite for serial synchrotron

crystallography. J Synchrotron Radiat 26 (1):244–252. https://doi.org/10.1107/S1600577518016570

41. Gavira JA, Toh D, Lopez-Jaramillo J, Garcia-Ruiz JM, Ng JD (2002) Ab initio crystallographic structure determination of insulin from protein to electron density without crystal handling. Acta Crystallogr D Biol Crystallogr 58:1147–1154. https://doi.org/10.1107/S0907444902006959
42. Yadav MK, Gerdts CJ, Sanishvili R, Smith WW, Roach LS, Ismagilov RF, Kuhn P, Stevens RC (2005) In situ data collection and structure refinement from microcapillary protein crystallization. J Appl Crystallogr 38:900–905. https://doi.org/10.1107/S002188980502649x
43. Martiel I, Olieric V, Caffrey M, Wang M (2018) Practical approaches for in situ X-ray crystallography: from high-throughput screening to serial data collection. In: Protein crystallography: challenges and practical solutions. The Royal Society of Chemistry, London. https://doi.org/10.1039/9781788010504-00001
44. Khvostichenko DS, Kondrashkina E, Perry SL, Pawate AS, Brister K, Kenis PJ (2013) An X-ray transparent microfluidic platform for screening of the phase behavior of lipidic mesophases. Analyst 138(18):5384–5395. https://doi.org/10.1039/c3an01174g
45. Soliman AS, Warkentin M, Apker B, Thorne RE (2011) Development of high-performance X-ray transparent crystallization plates for in situ protein crystal screening and analysis. Acta Crystallogr D Biol Crystallogr 67 (Pt 7):646–656. https://doi.org/10.1107/S090744491101883X
46. Sui S, Perry SL (2017) Microfluidics: from crystallization to serial time-resolved crystallography. Struct Dynam 4(3):032202. https://doi.org/10.1063/1.4979640
47. Li L, Fu Q, Kors CA, Stewart L, Nollert P, Laible PD, Ismagilov RF (2010) A plug-based microfluidic system for dispensing lipidic cubic phase (LCP) material validated by crystallizing membrane proteins in lipidic mesophases. Microfluid Nanofluid 8(6):789–798. https://doi.org/10.1007/s10404-009-0512-8
48. Perry SL, Roberts GW, Tice JD, Gennis RB, Kenis PJ (2009) Microfluidic generation of lipidic mesophases for membrane protein crystallization. Cryst Growth Des 9 (6):2566–2569. https://doi.org/10.1021/cg900289d
49. le Maire A, Gelin M, Pochet S, Hoh F, Pirocchi M, Guichou JF, Ferrer JL, Labesse G (2011) In-plate protein crystallization, in situ ligand soaking and X-ray diffraction. Acta Crystallogr D Biol Crystallogr 67 (Pt 9):747–755. https://doi.org/10.1107/S0907444911023249
50. Zander U, Hoffmann G, Cornaciu I, Marquette JP, Papp G, Landret C, Seroul G, Sinoir J, Rower M, Felisaz F, Rodriguez-Puente S, Mariaule V, Murphy P, Mathieu M, Cipriani F, Marquez JA (2016) Automated harvesting and processing of protein crystals through laser photoablation. Acta Crystallogr D Biol Crystallogr 72(Pt 4):454–466. https://doi.org/10.1107/S2059798316000954
51. Ghachi EM, Howe N, Huang CY, Olieric V, Warshamanage R, Touze T, Weichert D, Stansfeld PJ, Wang M, Kerff F, Caffrey M (2018) Crystal structure of undecaprenyl-pyrophosphate phosphatase and its role in peptidoglycan biosynthesis. Nat Commun 9 (1):1078. https://doi.org/10.1038/s41467-018-03477-5
52. Axford D, Aller P, Sanchez-Weatherby J, Sandy J (2016) Applications of thin-film sandwich crystallization platforms. Acta Crystallogr F Struct Biol Commun 72(Pt 4):313–319. https://doi.org/10.1107/S2053230X16004386
53. Apel AK, Cheng RKY, Tautermann CS, Brauchle M, Huang CY, Pautsch A, Hennig M, Nar H, Schnapp G (2018) Crystal structure of CC chemokine receptor 2A in complex with an orthosteric antagonist provides insights for the design of selective antagonists. Structure 27(3):427–438.e425. https://doi.org/10.1016/j.str.2018.10.027
54. Sui D, Huang Y, Huang L, Liang J, Ma Y, Chen Y (2011) Flexible and transparent electrothermal film heaters based on graphene materials. Small 7(22):3186–3192. https://doi.org/10.1002/smll.201101305
55. Sui S, Wang Y, Kolewe KW, Srajer V, Henning R, Schiffman JD, Dimitrakopoulos C, Perry SL (2016) Graphene-based microfluidics for serial crystallography. Lab Chip 16(16):3082–3096. https://doi.org/10.1039/c6lc00451b
56. Sui S, Wang YX, Dimitrakopoulos C, Perry SL (2018) A graphene-based microfluidic platform for electrocrystallization and in situ X-ray diffraction. Crystals 8(2):76. https://doi.org/10.3390/cryst8020076
57. Murray TD, Lyubimov AY, Ogata CM, Vo H, Uervirojnangkoorn M, Brunger AT, Berger JM (2015) A high-transparency, micro-patternable chip for X-ray diffraction analysis of microcrystals under native growth conditions. Acta Crystallogr D Biol Crystallogr 71:1987–1997.

https://doi.org/10.1107/S1399004715015011

58. Owen RL, Axford D, Sherrell DA, Kuo AL, Ernst OP, Schulz EC, Miller RJD, Mueller-Werkmeister HM (2017) Low-dose fixed-target serial synchrotron crystallography. Acta Crystallogr D Biol Crystallogr 73:373–378. https://doi.org/10.1107/S2059798317002996
59. Roedig P, Vartiainen I, Duman R, Panneerselvam S, Stube N, Lorbeer O, Warmer M, Sutton G, Stuart DI, Weckert E, David C, Wagner A, Meents A (2015) A micro-patterned silicon chip as sample holder for macromolecular crystallography experiments with minimal background scattering. Sci Rep 5:10451. https://doi.org/10.1038/srep10451
60. Cherezov V, Caffrey M (2007) Membrane protein crystallization in lipidic mesophases. A mechanism study using X-ray microdiffraction. Faraday Discuss 136:195–212. https://doi.org/10.1039/b618173b
61. Peddi A, Muthusubramaniam L, Zheng YR, Cherezov V, Misquitta Y, Caffrey M (2007) High-throughput automated system for crystallizing membrane proteins in lipidic mesophases. IEEE Trans Autom Sci Eng 4 (2):129–140. https://doi.org/10.1109/Tase.2006.880541
62. Axford D, Owen RL, Aishima J, Foadi J, Morgan AW, Robinson JI, Nettleship JE, Owens RJ, Moraes I, Fry EE, Grimes JM, Harlos K, Kotecha A, Ren J, Sutton G, Walter TS, Stuart DI, Evans G (2012) In situ macromolecular crystallography using microbeams. Acta Crystallogr D Biol Crystallogr 68(Pt 5):592–600. https://doi.org/10.1107/S0907444912006749
63. Bingel-Erlenmeyer R, Olieric V, Grimshaw JPA, Gabadinho J, Wang X, Ebner S, Isenegger A, Schneider R, Schneider J, Glettig W, Pradervand C, Panepucci EH, Tomizaki T, Wang M, Schulze-Briese C (2011) SLS crystallization platform at beamline X06DA—a fully automated pipeline enabling in situ X-ray diffraction screening. Cryst Growth Des 11:916–923. https://doi.org/10.1021/cg101375j
64. Garman E (1999) Cool data: quantity AND quality. Acta Crystallogr D Biol Crystallogr 55 (Pt 10):1641–1653
65. Garman E (2003) 'Cool' crystals: macromolecular cryocrystallography and radiation damage. Curr Opin Struct Biol 13(5):545–551
66. Garman EF, Schneider TR (1997) Macromolecular cryocrystallography. J Appl Crystallogr 30:211–237. https://doi.org/10.1107/S0021889897002677
67. Li DF, Pye VE, Caffrey M (2015) Experimental phasing for structure determination using membrane-protein crystals grown by the lipid cubic phase method. Acta Crystallogr D Biol Crystallogr 71:104–122. https://doi.org/10.1107/S1399004714010360
68. Boggon TJ, Shapiro L (2000) Screening for phasing atoms in protein crystallography. Structure 8(7):R143–R149
69. Sugahara M, Asada Y, Shimada H, Taka H, Kunishima N (2009) HATODAS II – heavy-atom database system with potentiality scoring. J Appl Crystallogr 42:540–544. https://doi.org/10.1107/S0021889809012370
70. Li D, Lee J, Caffrey M (2011) Crystallizing membrane proteins in lipidic mesophases. A host lipid screen. Cryst Growth Des 11 (2):530–537. https://doi.org/10.1021/cg101378s
71. Lebugle M, Dworkowski F, Pauluhn A, Guzenko VA, Romano L, Meier N, Marschall F, Sanchez DF, Grolimund D, Wang M, David C (2018) High-intensity X-ray microbeam for macromolecular crystallography using silicon kinoform diffractive lenses. Appl Opt 57(30):9032–9039. https://doi.org/10.1364/AO.57.009032
72. Fuchs MR, Pradervand C, Thominet V, Schneider R, Panepucci E, Grunder M, Gabadinho J, Dworkowski FS, Tomizaki T, Schneider J, Mayer A, Curtin A, Olieric V, Frommherz U, Kotrle G, Welte J, Wang X, Maag S, Schulze-Briese C, Wang M (2014) D3, the new diffractometer for the macromolecular crystallography beamlines of the Swiss Light Source. J Synchrotron Radiat 21 (Pt 2):340–351. https://doi.org/10.1107/S160057751400006X
73. Wojdyla JA, Panepucci E, Martiel I, Ebner S, Huang CY, Caffrey M, Bunk O, Wang M (2016) Fast two-dimensional grid and transmission X-ray microscopy scanning methods for visualizing and characterizing protein crystals. J Appl Crystallogr 49(Pt 3):944–952. https://doi.org/10.1107/S1600576716006233
74. Wojdyla JA, Kaminski JW, Panepucci E, Ebner S, Wang X, Gabadinho J, Wang M (2018) DA+ data acquisition and analysis software at the Swiss Light Source macromolecular crystallography beamlines. J Synchrotron Radiat 25(Pt 1):293–303. https://doi.org/10.1107/S1600577517014503
75. Li D, Boland C, Walsh K, Caffrey M (2012) Use of a robot for high-throughput crystallization of membrane proteins in lipidic

mesophases. J Vis Exp 67:4000. https://doi.org/10.3791/4000

76. Zhang Z, Sauter NK, van den Bedem H, Snell G, Deacon AM (2006) Automated diffraction image analysis and spot searching for high-throughput crystal screening. J Appl Crystallogr 39(1):112–119. https://doi.org/10.1107/S0021889805040677
77. Finke AD, Panepucci E, Vonrhein C, Wang M, Bricogne G, Olieric V (2016) Advanced crystallographic data collection protocols for experimental phasing. Methods Mol Biol 1320:175–191. https://doi.org/10.1007/978-1-4939-2763-0_11
78. Sheldrick GM (2010) Experimental phasing with SHELXC/D/E: combining chain tracing with density modification. Acta Crystallogr D Biol Crystallogr 66(Pt 4):479–485. https://doi.org/10.1107/S0907444909038360
79. Skubak P, Pannu NS (2013) Automatic protein structure solution from weak X-ray data. Nat Commun 4:2777. https://doi.org/10.1038/ncomms3777
80. Vonrhein C, Blanc E, Roversi P, Bricogne G (2007) Automated structure solution with autoSHARP. Methods Mol Biol 364:215–230. https://doi.org/10.1385/1-59745-266-1:215
81. Terwilliger TC, Adams PD, Read RJ, McCoy AJ, Moriarty NW, Grosse-Kunstleve RW, Afonine PV, Zwart PH, Hung LW (2009) Decision-making in structure solution using Bayesian estimates of map quality: the PHENIX AutoSol wizard. Acta Crystallogr D Biol Crystallogr 65(Pt 6):582–601. https://doi.org/10.1107/S0907444909012098

Chapter 21

Membrane Protein Preparation for Serial Crystallography Using High-Viscosity Injectors: Rhodopsin as an Example

Tobias Weinert and Valérie Panneels

Abstract

Membrane proteins are highly interesting targets due to their pivotal role in cell function and disease. They are inserted in cell membranes, are often intrinsically flexible, and can adopt several conformational states to carry out their function. Although most overall folds of membrane proteins are known, many questions remain about specific functionally relevant intramolecular rearrangements that require experimental structure determination. Here, using the example of rhodopsin, we describe how to prepare and analyze membrane protein crystals for serial crystallography at room temperature, a new technique allowing to merge diffraction data from thousands of injector-delivered crystals that are too tiny for classical single-crystal analysis even in cryogenic conditions. The application of serial crystallography for studying protein dynamics is mentioned.

Key words Membrane protein, GPCR, X-ray, Serial, Dynamics, Conformation, Crystallography, Lipidic cubic phase, LCP, Injector, Rhodopsin

1 Introduction

Serial crystallography (for definition see [1]) is a method to determine protein structures by merging diffraction patterns from many crystals. In serial femtosecond crystallography (SFX) at X-ray free-electron lasers (XFELs) [2, 3] diffraction patterns of thousands of crystals delivered by a jet into the extremely brilliant X-ray source of an XFEL are collected as single snapshots from crystals in random orientations. The XFEL delivers very short femtosecond X-ray pulses, resulting in a diffraction pattern before damaging the protein in the crystals [4]. A number of unknown membrane protein structures, relevant for drug discovery [5], have been determined by SFX [6] which is especially suitable for probing micron-sized crystals using a micrometer XFEL beam [7]. The lipidic cubic phase (LCP) as an ideal environment to surround the membrane proteins [8] has not only many advantages as a crystal growth medium.

Camilo Perez and Timm Maier (eds.), *Expression, Purification, and Structural Biology of Membrane Proteins*, Methods in Molecular Biology, vol. 2127, https://doi.org/10.1007/978-1-0716-0373-4_21,

Membrane proteins like G-protein-coupled receptors are notoriously difficult to crystallize but usually yield a shower of micron-sized crystals in LCP. This viscous medium is also ideal to deliver in a constant flow the crystals to the X-ray beam [9]. Using high-viscosity injectors in combination with LCP as a delivery medium dramatically reduced sample consumption for time-resolved serial crystallography [10]. Several flavors of serial crystallography have been developed since SFX was established. Serial millisecond crystallography (SMX) with high-viscosity injectors has been successfully used to determine room-temperature structures at synchrotrons [11]. Presenting crystals at room temperature or cryogenic temperature on solid supports for the collection of short rotation series at synchrotrons (SSX (serial synchrotron crystallography)) [12, 13] or thousands of still images at synchrotrons and XFELs [14] have also established their place in the repertoire of crystallography. While SFX is ideal for micron-sized crystals and ultrafast time-resolved studies, SMX consumes ten times less crystals and is a readily accessible technique [11, 15] and finally SSX consumes even less sample but is most suitable to determine structures at cryogenic temperatures.

Here we illustrate the workflow for preparing a membrane protein to determine its structure using serial crystallography with a high-viscosity injector at XFELs or synchrotrons. As an example, the crystallization, crystal diffraction, and SFX of the mammalian G-protein-coupled receptor (GPCR) responsible for vision, rhodopsin, are described.

2 Materials

2.1 Membrane Protein Crystallization

The amounts of membrane protein necessary for crystallization are not always easy to obtain and other chapters of this book will help the reader to optimize the protein expression and purification steps. Here, we present the preparation of rhodopsin as an example for crystallization and structure determination by serial crystallography. Depending on the aim of the serial crystallography experiment, the necessary amounts of protein range from a few micrograms to milligrams (*see* **Note 1**). Crystallization trials do not strictly require robotics, but high-throughput methods of crystallization screening will dramatically increase the efficiency and lower the required amounts of sample.

2.1.1 Initial LCP Crystallization of Rhodopsin

1. Preparation room with dimmed light (red filtered light; long-pass filter CWL 600 nm) using red screens and red lamps (Fig. 1).
2. Pure rhodopsin prepared according to Edwards [16].
3. UV-Vis spectrophotometer.

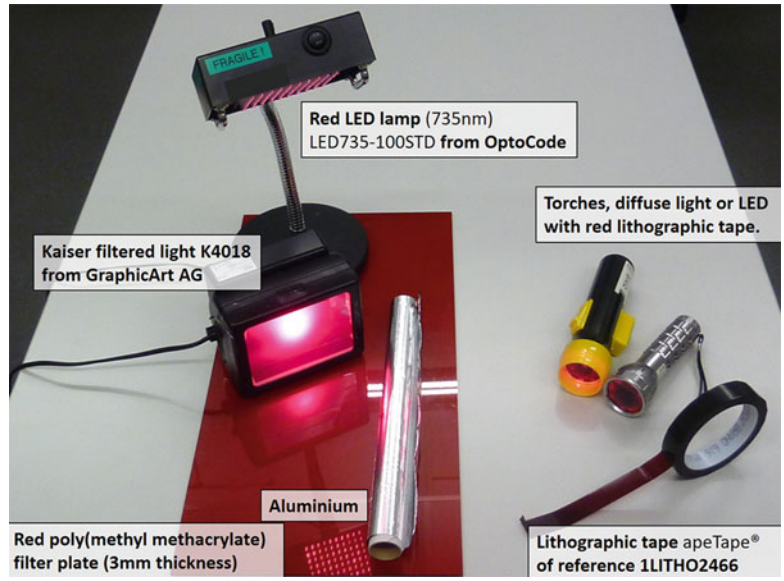

Fig. 1 Basic material for working in dark conditions with photoactivatable rhodopsin

4. Centrifugal concentrator (e.g., Amicon Ultra-0.5 mL from Millipore) with a molecular weight cutoff of 30 kDa.
5. Centrifuge for conical tubes and concentrators.
6. Monoolein M-219-1G from Nu-Chek Prep, Inc.
7. Two 100 µL Hamilton® syringes of type GASTIGHT® 1700RN.
8. Syringes two-way coupler 3072–01050 from TTP Labtech.
9. Thermoblock for 1.5 mL reaction tubes.
10. Various homemade or commercial crystallization screening kits for 96-well plates.
11. Laminex LCP crystallization plates (Molecular Dimensions).
12. Fully automated LCP dispenser (here, the mosquito®LCP from TTP Labtech) in a room which can be darkened.
13. Stereomicroscope with minimum 10 × 20 magnification equipped with a red filter.
14. Incubator for protein crystallization.
15. SONICC® imager for protein crystal detection (Formulatrix®).
16. Meshes and mounts for cryo-crystallography (e.g., MiTeGen). All the materials needed for harvesting crystals in LCP are described in [17].

2.1.2 Optimization of Crystal Quality and Quantity

1. Laminex plates (Molecular Dimensions).
2. Custom-prepared precipitant solution for screening around initial hit conditions.
3. Rhodopsin in LCP.
4. Meshes and mounts for cryo-crystallography.
5. 100 and 500 μL Hamilton® syringes of type GASTIGHT® 1700RN.
6. Incubator for protein crystallization.

2.2 Membrane Protein Diffraction

Membrane proteins and especially GPCRs tend to yield only small crystals of a few microns' size. In addition, due to the use of *in meso* LCP crystallization, they often grow crystals in two dimensions, literally piling up two-dimensional crystals, resulting in crystal plates. For this reason, we recommend to screen for first hits by imaging and not by random solid support diffraction where initial hits may be overlooked due to weakly diffracting crystals. In a second step, a powerful microfocused X-ray beam is used for diffraction tests. The focus of the X-ray beam has to be carefully chosen according to the size of the crystals in order to increase the signal-to-noise ratio, strongly affected by the scattering of the lipid phase embedding the crystal.

2.2.1 Final Quality Control Before the SFX/SMX Experiment: Diffraction at a Synchrotron

1. Rhodopsin crystals grown in Hamilton® syringes.
2. Manual LCP dispenser [optional].
3. IMISX plates kit™ from MiTeGen [12].
4. Few hours of beam time at a synchrotron with microfocus (*see* **Note 2**).

2.3 Serial Crystallography Using High-Viscosity Injectors

1. Rhodopsin crystal sample prepared with suitable injection medium in syringes.
2. High-viscosity injector system [9] and loading tools [18].
3. Visualization system for off-line jetting tests [18].
4. Beamline with microfocus beam and high-frame-rate detector or XFEL beamline.
5. Online hit-finding software.
6. High-performance computing cluster.
7. Data analysis software (CrystFEL [18, 19]).

3 Methods

3.1 Membrane Protein Crystallization

For serial crystallography, large quantities of crystals are needed. Crystallization trials will be successful if strong nucleation is observed, leading to showers of micron-sized crystals. In order to

reach the metastable supersaturation region of the phase diagram [20], the membrane protein concentration should be adjusted to the highest concentration not inducing heavy precipitation. In case of already established protocols for the production of high-quality single crystals, simply increasing the concentrations of protein and/or precipitant may be sufficient. Below, we describe the strategy used for obtaining rhodopsin crystals for SFX and time-resolved SFX experiments.

3.1.1 Initial LCP Crystallization of Rhodopsin

1. *Rhodopsin preparation*: Centrifuge fresh or flash-frozen rhodopsin for 20 min at 20,000 × *g*, at 18 °C. Measure the concentration of the supernatant using a spectrophotometer. Rhodopsin contains the covalently bound chromophore 11-cis retinal and displays an additional maximum of absorption at 500 nm. The final concentration of rhodopsin is calculated from the optical density at 500 nm ($\varepsilon = 40{,}600\ \mathrm{mol}^{-1}\ \mathrm{cm}^{-1}$) [21] and its purity is assessed by the ideal stoichiometry of 1 between the opsin and retinal chromophore, calculated by the ratio of the opsin OD at 280 nm over the retinal OD at 500 nm (*see* **Note 3**). Increase the rhodopsin concentration to 25 mg/mL using a centrifugal concentrator with regenerated cellulose membrane of 30 kDa molecular weight cutoff. Centrifuge the final solution for 20 min at 20,000 × *g*, at 18 °C, and verify the final concentration.
2. *Rhodopsin preparation in LCP*: In order to insert the rhodopsin into lipids, mix the protein solution with monoolein in a ratio of 2:3 to form a lipidic cubic phase (LCP) [22]: In a darkroom at 21 °C ± 2, fill the first 100 μL Hamilton syringe preheated at 42 °C with 30 μL of monoolein also preheated at 42 °C (liquid state). Then fill the other syringe with 20 μL of rhodopsin. Connect the two syringes with the coupling tool and mix 50–150 times until the sample loses its turbidity. A very transparent viscous phase is an evidence for the formation of a lipidic cubic phase (*see* **Note 4**).
3. *Crystallization trials with rhodopsin in LCP*: For the crystallization trials, perform a first high-throughput screening using several commercial crystallization screens to cover the diversity of precipitant and concentrations, buffer types, and pH values as well as successful additives. The following screens, a non-exhaustive list for membrane protein hit finding, were tested here: MemStart™ + MemSys™ HT-96, MemMeso™ HT-96, MemGold™ HT-96 (Molecular Dimensions), Classic Suite screens (Qiagen), and JBScreen Membrane HTS (Jena Bioscience). Using a fully automated LCP-dispensing robot in red dimmed light, mount the Hamilton syringe with rhodopsin-LCP on the motorized arm of the robot and dispense with needle contact 80 nL sample per well in the first

column of the plate under minimum 60% humidity (*see* **Note 5**). The robot then directly adds 700 nL of precipitant screen to the first column in order to avoid LCP dehydration. The same procedure is carried out for the 11 remaining columns. The Laminex plate is quickly sealed using a glass coverslip and incubated in a double layer of aluminum foil in the dark at 18 °C for 3 weeks. During this time, the crystallization drops are inspected under red dim light with a stereomicroscope.

4. *First crystal hit detection*: After 3 weeks, image the plates and screen for the presence of crystals. For serial crystallography, preferred hits present a shower of well-diffracting tiny crystals, rather than a single larger one. Depending on the available devices, bright light, cross-polarization, and/or UV imaging are used. Here, the SONICC/UV-TPEF imaging methods (*see* **Note 6**) were used.
   (a) Minimal modifications of the imager are necessary to work with bleaching proteins with the ROCK IMAGER SONICC: Ask the manufacturer to disconnect LED lamps inside the device (can be done remotely). Set the SONICC device on dark mode: set "Manual" mode in order to avoid automatic bright-light imaging of other plates in the queue. In the Plate Type Editor of Laminex plates, set the "Visible" mode on 3.21 ms exposure (minimum). Darken the room where the SONICC imager is located, and darken the window of the device. Switch off the monitor. Remove the protective aluminum foils in the red dimmed light and place the plates in the port. Close the transparent door covered with aluminum or red acrylic glass screen. Switch the monitor on and send the plates to the plate hotel.
   (b) Image first the plate using the SONICC mode (*see* **Note 7**). For finding a first hit, the sensitivity is set at "high SHG power" (450 mW laser power). Then, image the plate using UV-TPEF. This imaging is set at medium power because here there is a compromise to do between the signal and the noise which is usually very high with the LCP crystallization technique. A picture of the first crystal hit is shown in Fig. 2.
5. Test the best hits obtained above for diffraction. Open the Laminex plates under a stereomicroscope with light filtered with red screen, harvest with meshes, and flash freeze like described [17]. From now on, frozen crystals can be manipulated in the light. If the crystals are smaller than 20 μm, a microfocus beam of 5 μm × 5 μm will help increasing the signal-to-noise ratio (*see* **Note 8**). Complete diffraction raster scanning [13] as implemented at various synchrotron

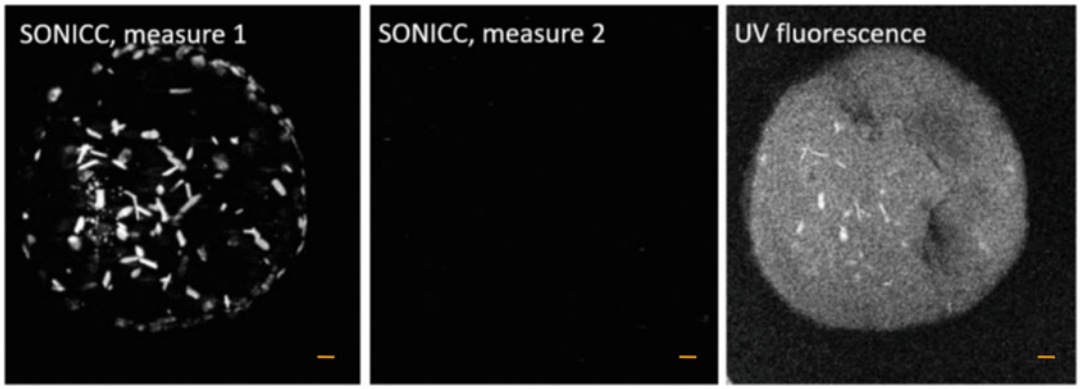

Fig. 2 Initial rhodopsin crystal hits visualized by SHG imaging. Left panel, measure 1: a picture of the rhodopsin-LCP bolus of 80 nL imaged at high SHG power. Middle panel, measure 2: second imaging of the very same drop. The SONICC emitted signal has a wavelength of 532 nm which bleaches the rhodopsin crystals. A second image of this same bolus taken again at high SHG power shows therefore an absence of signal, despite the presence of the crystals identified by UV-TPEF (right panel, measure 3). Orange scale bars show 50 μm

beamlines of the LCP covering the mesh is usually more successful than visual inspection.

3.1.2 Optimization of Crystal Quality and Quantity

The aim here is to scale up the quantity of crystal suspension from 80 nL to 20 μL, which is the minimal volume for serial crystallography with an injector. This step involves the switch from robotic to manual crystallization with syringes. Upscaling LCP crystallization is typically successful if volume and surface ratio are conserved in relation to the precipitant solution.

1. *Crystal optimization*: Reproduce the best conditions in Laminex plates. In the same time, optimize the crystallization protocol by analyzing the kinetics of growth using a normal stereomicroscope and test some similar conditions modified with increments of the precipitant concentration or the pH.
2. Test the quality of the crystals by X-ray diffraction as in **step 5** of Subheading 3.1.1.
3. *Scaling up*: Select the best crystallization condition (best diffraction combined with highest nucleation), load 180 μL of precipitant at room temperature in a 500 μL Hamilton syringe, and inject 20 μL of rhodopsin-LCP prepared in **step 2** of Subheading 3.1.1. Let it crystallize for a few days in the syringe at 18 °C. Further scaling-up to 100 μL LCP and more can be done by using plastic syringes for bio-viscous applications (1 ML syringes Luer-Lok Tip of reference 8049628, Becton Dickinson) and the fitting stainless steel luer connector (CAD6521 from Cadence Science). Handling crystals grown in a syringe is much easier than harvesting crystals from 96-well

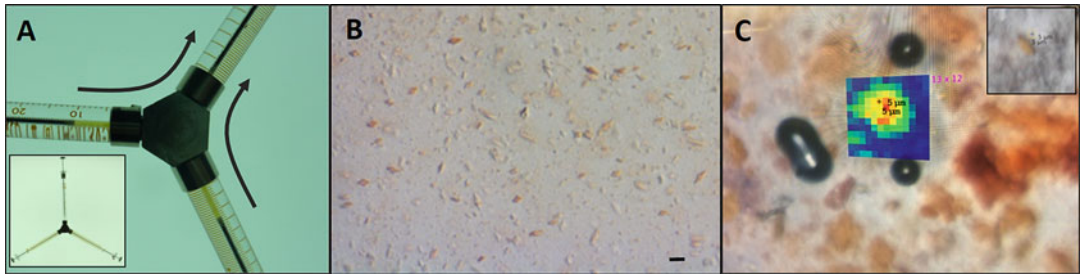

Fig. 3 Rhodopsin crystal preparation for diffraction tests at the synchrotron. (**a**) The crystals grown in LCP in the 500 μL Hamilton syringes are harvested in 100 μL syringes. The picture represents the mixing of LCP-embedded crystals using a three-way coupler [25]. (**b**) Rhodopsin crystals at a density which gives about 15% hit rate in a typical SFX experiment at the SACLA XFEL (the thickness of the LCP sample here is 100 μm). The scale bar is 20 μm. (**c**) Frozen rhodopsin crystals in sandwich between COC foils undergoing X-ray diffraction tests at the SLS synchrotron. The typical rastering grid shows the regions diffracting (in red) surrounded by lower diffracting regions (scale from orange to dark blue). The inset shows a single crystal and the black cross represents the position of the 5 × 5 μm^2 beam. Rhodopsin has a red color in the dark; the orange-to-yellow color is due to rhodopsin bleaching during the imaging

plates. Adapt a needle on the 500 μL syringe and extrude the sample. The precipitant will automatically flow first out of the syringe. Transfer the remaining rhodopsin crystals in LCP, in a 100 μL syringe—or smaller if necessary—as described in [23, 24]. In order to obtain a homogenous density of crystals, we recommend to mix the resulting crystal slurry, but **not** using a two-way coupler that often damages the crystals. Mix the crystal slurry using a three-way connector with three syringes [25] (*see* **Note 9**). The co-injection of two columns of LCP (Fig. 3) together improves the mixing efficiency and decreases the turbulence and shearing forces on the sample.

3.2 Membrane Protein Diffraction

Before starting a serial crystallography experiment at room temperature with an injector, which requires highly specialized setups at a synchrotron or at an XFEL, a quality control of each batch of the produced sample is necessary. Ranking the samples by best crystal density and diffraction will help serial crystallography experiments succeed (*see* **Note 10**).

3.2.1 Final Quality Control Before the SFX Experiment: Diffraction at a Synchrotron

1. Extrude the precipitant solution from the syringe. Mount the syringe containing the rhodopsin crystals on a manual dispenser tool (*see* **Note 11**). Dispense [26] the sample on a silanized foil of COC (synthetic cyclic olefin copolymer) as described in Huang et al. [12], and in Chap. 20 of this book, and close rapidly in sandwich with another sheet of this foil. Flash freeze the sample in liquid nitrogen, or analyze

diffraction at room temperature. For the latter option, the experimental hutch must be set in red dimmed light!

2. At the synchrotron microfocus beamline, mount the sample on the magnetic goniometer adapter from IMISX kit or using a 3D printed gonioclip (Huang et al., 3D-printed holders for in meso in situ fixed-target serial crystallography, submitted) raster scan and rate crystal diffraction (*see* **Note 12**).

3.3 Serial Crystallography Using High-Viscosity Injectors

In order to complete the workflow of a membrane protein serial crystallography experiment, we briefly list the necessary steps and provide experimental hints based on our work with rhodopsin. The experimental procedures and software used for serial crystallography experiments are readily comprehensible for experienced crystallographers. However, practical training on the specific injector system, data collection setup, and software on-site at the chosen site for data collection are usually required.

3.3.1 Preparation of Samples in Suitable High-Viscosity Medium/LCP

1. Adjust samples to form a jettable phase. For rhodopsin crystals, this requires diluting the sample by addition of LCP prepared using monoolein and crystallization buffer.
2. Make a simple extrusion test by squeezing LCP out of a 400 μm diameter two-way LCP coupler to ensure that the phase has the right consistence: a transparent solid phase.

3.3.2 Loading of the Sample in Reservoirs

1. Connect a loading tool to the Hamilton syringe containing the crystal-laden LCP.
2. Prepare a reservoir for loading.
3. Inject the sample slowly into the reservoir.
4. Prepare the injector head with a nozzle (*see* **Note 13**) and mount it on top of the loaded reservoir.

3.3.3 Extrusion Tests at an Off-Line System [25]

1. Mount the loaded injector on the off-line system and start slow extrusion.
2. Focus and zoom the camera to observe crystal extrusion.
3. Adjust HPLC pump to achieve the desired extrusion speed (*see* **Note 14**).
4. Record several short videos during the course of emptying one reservoir (*see* **Note 15**).
5. Analyze the videos by tracking the movements of several crystals in the recorded video and plot their movement speed (μm/s versus total volume extruded from the reservoir). The sample can be considered as ready for further time-resolved experiments when the graphical plot results in a flat line, showing homogeneous extrusion speeds.

3.3.4 Data Collection at Synchrotron Microfocus Beamlines with High-Frame-Rate Detectors

1. Install the injector at the beamline so that the extruded crystal-laden LCP intersects with the X-rays and the injector can be moved along x, y, and z. Mount the injector directly onto the goniometer. The sample head that typically holds and centers classical pins is removed before mounting the holder for the high-viscosity injector. This ensures maximum compatibility with other devices already installed at the beamline.
2. Connect the gas regulator to the beamline hardware so that it can be remotely controlled (*see* **Note 16**).
3. Connect the HPLC system to the injector and the beamline hardware to control the extrusion speed remotely.
4. Center and focus the nozzle to be able to see jet extrusion.
5. Start extrusion of the sample and adjust sheath gas flow and jet speed to form a stable jet.
6. Center the X-ray interaction region 20–50 μm below the nozzle tip at the center of the LCP jet.
7. Select the ideal beam size for data collection (*see* **Note 17**).
8. Select the ideal data collection frame rate based on jet speed, flux density, and crystal size (*see* **Note 18**) and start data collection.

3.3.5 Data Collection at XFEL Beamlines

Data collection at XFEL beamlines resembles a synchrotron experiment. Typically, jet speeds are faster (*see* **Note 14**), and the appropriate XFEL repetition rate instead of a detector frame rate is chosen. At the SPring-8 Angstrom Compact free electron LAser (SACLA, Japan), the Linac Coherent Light Source (LCLS, USA), and the Swiss free electron laser (SwissFEL, Switzerland), pre-configured high-viscosity injector systems with detailed documentation are available.

3.3.6 Online Hit Finding

Online hit finding is very important in order to ensure the success of the experiment as it gives a fast feedback on the sample quality. A variety of online systems have been described [27, 28], but they all require the adjustment of a basic set of criteria:

1. Optimize the hit finding criteria of the online hit finder by adjusting the number of pixels in a spot, the minimal signal-to-noise ratio of a spot, and the minimal number of spots per hit.
2. Analyze the success by visually inspecting the identified hits. It is also possible to create a virtual powder diffraction pattern by summing all frames identified as non-hits. If no diffraction rings show up in the low-resolution range, the hit finding criteria are useful. Hit finding criteria should be chosen so that 60–80% of the identified patterns are indexable.

3.3.7 Data Processing Using the CrystFEL Suite [18, 19]

Once the hits of a completed data collection run are identified, data processing can be started. Data are usually processed on high-performance computing systems since CrystFEL can be fully parallelized. The steps described here are a brief outline, and follow the available tutorials by Tom White and Takanori Nakane; for further details see http://www.desy.de/~twhite/crystfel/tutorial.html and https://github.com/biochem-fan/cheetah/wiki. A detailed step-by-step guide for CrystFEL processing has been published recently [30].

1. Prepare a geometry file with the best possible starting geometry and a beam center that is as close as possible to the reality (*see* **Note 19**).
2. Prepare lists of hits (*see* **Note 20**).
3. Optimize processing with the "indexamajig" program following available tutorials. Important aspects are unit cell parameters and space group, peak identification criteria (peak size in pixels, signal-to-noise, threshold), as well as beam center and detector distance.
4. Process all data with indexamajig.
5. Concatenate streams of compatible data collection runs into one stream file.
6. Use the "Ambigator" program to correct indexing ambiguity if needed (see www.desy.de/~twhite/crystfel/twin-calculator.pdf for a table).
7. Generate merged datasets using the "partialator" program (*see* **Note 21**).
8. Generate an mtz file by using the create-mtz script.

4 Notes

1. The useful amounts of material vary from about 12 μL of crystal-laden LCP per 8 h for SMX to around 120 μL of crystal-laden LCP per 8 h or 1.2 mg for SFX. This protocol can also be used for time-resolved (TR) serial crystallography experiments. For studying dynamics of photosensitive proteins, the SFX settings require in addition a pump laser which will activate the protein for a precise time delay before X-ray probe. TR-SFX requires more sample than SFX (around 1 mL of crystal slurry per 8 h corresponding to about 10 mg membrane protein), due to increased injector flow. The higher rate of crystal extrusion for TR-SFX is necessary to clear all activated materials between two photoactivation bursts of the pump laser.

2. Measuring crystals at the synchrotron requires either a collaboration or an independent online application from a proposal call.
3. Rhodopsin is theoretically pure at an optical density ratio OD 280 nm/OD 500 nm of 1.6.
4. The rhodopsin in LCP is quite stable and the crystallization trial can be made after 30 min or even 24 h. The crystals can be grown in a liquid mixture rather than in LCP and incorporated later to a viscous solid like grease, agarose, paraffin, or LCP itself [23]. The incorporation can be done with a spatula or using syringes.
5. The dispensing of one 96-well plate will require ((80 nL × 96 wells) × 0.4 (% protein in the LCP)) about 5 μL. We recommend to set the plates up in duplicate for imaging and diffraction trials, because the light of the imager might affect the crystal quality, especially with photosensitive proteins.
6. The SONICC-integrated ROCK IMAGER (Formulatrix) used here is a fully automated system analyzing plates using the two-photon excitation fluorescence (TPEF) principle. The UV-TPEF mode gives a signal from proteins or any other compound absorbing the UV light (Ex. 532 nm/Em. 340–400 nm ("Ex." is the maximal excitation wavelength from the laser source; "Em." is the range of maximal emission wavelengths emitted by the samples)), without distinction between precipitated and crystallized states. When the laser (Ex. 1064 nm/Em. 532 nm) is in the SONICC (second-order nonlinear imaging of chiral crystals) [29] second harmonic generation (SHG) mode [30], any material presenting ordered chiral molecules will emit a signal, with an intensity depending mostly on the chiral properties and the size of the object. UV-TPEF and SONICC are complementary to each other for the protein crystal detection. The two-photon excitation fluorescence method in general gives a very high signal-to-noise ratio, allowing for better hit finding than with classical UV absorption or imaging with cross-polarized light.
7. For photosensitive proteins, when the light of the imager irreversibly photoactivates the protein or induces large conformational changes that reduce the order of the crystals, like for rhodopsin, the SONICC measurement can be performed only once. We therefore recommend to set the plates in duplicate. It is not the case of the UV-TEPF measurement which is not dependent on the crystal order. For this reason, the SONICC measurement is performed first.
8. At this stage of the project, it is difficult to collect good diffraction data from <20 μm plate crystals due to several reasons: Laminex plates are optimal for imaging a first hit but not for in

situ diffraction of tiny crystals; the signal-to-noise ratio is too high; and harvesting crystals in the 80 nL LCP bolus in the dark is not straightforward.

9. The use of a three-way coupler improves the sample quality at diverse steps of the crystal sample preparation: adding a substance to modify the fluidity or stiffness of the phase or homogenizing the sample before serial crystallography.
10. Micron-sized crystals that do not diffract at all at synchrotrons (when probed at room temperature) do not diffract at FELs either (unless you have reasons to believe that it could be a signal-to-noise issue, especially when unit cells are large).
11. For LCP dispensing using the manual LCP dispenser (Hamilton Company), the use of a 10 μL syringe is appropriate, not only for saving material, but also for dispensing small quantities (the size of the aliquot is directly proportional to the syringe inner diameter).
12. Analyzing X-ray diffraction from LCP-embedded crystals in sandwich rather than on a mesh not only improves the signal-to-noise ratio, but helps as well to visualize tiny crystals through the viscous phase. The crystals can be individually sized and inspected for the shape and density, and correlation of those properties with X-ray diffraction is possible.
13. Nozzle sizes and their use cases: The smaller the nozzle diameter that is used, the lower the sample consumption. That said, it is typically not feasible to use nozzles below 50 μm diameter, because even crystals as small as 10 μm may accumulate at the "entrance" of the nozzle. Small nozzles also lead to less background diffraction, which in the case of LCP as a carrier medium improves data especially in the region from 5.5 to 3.5 Å resolution which is affected by the typical LCP diffraction ring. However, using larger nozzles may be beneficial if samples dry out upon extrusion (this is sometimes the case for high-salt samples) or for increasing hit rates (since also a larger volume is sampled when using the same beam size). Furthermore extrusion through large nozzles increases jet stability when the extruded phase is too soft (for example high-PEG samples).
14. Extrusion speeds: In order to test the jetting behavior under conditions suitable for measurements at synchrotrons one can use an off-line setup with a simple zoom camera since the extrusion rates are typically slow (about 250 μm per second at SLS). For optimizing a sample for extrusion at the FEL a high-speed camera is required, since crystal movement cannot be reliably traced at the fast extrusion rates necessary at an FEL, especially when doing time-resolved experiments that require complete removal of the illuminated portion of LCP (extrusion

rate of about 2 mm per second for a dark experiment at LCLS and up to 21 mm/s for a time-resolved experiment at LCLS) [31].

If crystals are colored as for rhodopsin stable extrusion is relatively easily observed by recording short movies and then tracking crystal movement over time. For colorless crystals cross-polarized light can be used to readily identify crystals. Note that for data collection at synchrotrons not only a stable extrusion speed is important, but also the extruded crystals do not tumble too much upon extrusion. Usually this is achieved by having a very stiff LCP phase. Crystal tumbling can be compensated for by faster frame rates. Faster frame rates should be accompanied by higher jet speeds and higher dose rates (if possible).

A stable extrusion at uniform speed is important in order to achieve maximal hit rates for simple structure determination experiments, and in order to know the dose applied to the crystals in SMX experiments. Stable extrusion is absolutely crucial for time-resolved experiments, where one relies on the extrusion rate to ensure using unilluminated material for consecutive shots. Note that the phase does not necessarily need to be as stiff for an XFEL experiment as for a synchrotron experiment. Crystal tumbling is negligible when the exposure times are only several femtoseconds.

15. Fast forwarding at synchrotron speed: Extruding a full reservoir at the speeds typically used at synchrotrons takes many hours. In order to still test extrusion over the course of an entire reservoir one can fast-forward by running the jet at quadrupled speed for a while, then readjust the speed back to a normal extrusion rate, wait for 10 min for the speed and pressure to stabilize, and then record another video.
16. Usefulness of sheath gas and pressure control: Being able to control the sheath gas pressure is important to keep the extruded jet stable and on axis. This is especially important at XFELs, where the pulses are strong enough to disrupt the jet. Furthermore, bursts of high-pressured sheath gas can be used to clear the nozzle tip from accumulating sample.
17. Beam size: At XFEL sources radiation damage is typically negligible, especially when dealing with proteins that do not contain metal centers and when using pulses shorter than 20 fs [4]. Due to the "self-termination" effect [2] also longer pulses of 50 fs do not lead to the site-specific radiation damage effects often observed in synchrotron structures. However, the impact of the beam typically leads to a complete destruction of the sample. Due to these facts, the beam size should be chosen based on signal-to-noise considerations for each individual type of crystal. If the beam has about half the size of the crystal

averaged over all dimensions, then in each possible orientation crystals are mostly hit by the full beam, whereas if the average crystal and beam size match exactly, the beam hits on average half a crystal and the other half is background causing carrier medium.

At synchrotron sources radiation damage effectively limits the achievable resolution at room temperature, since the maximal dose that can be deposited on a crystal without causing too much radiation damage is about 200 kGy. Hence, the beam size should take the maximum possible dose rate and the crystal size into account. Furthermore, the number of recorded diffraction patterns affects signal-to-noise of the assembled dataset and this number is higher if a larger portion of the extruded LCP is sampled by the beam. This means an informed decision has to be taken that allows to deliver the maximum possible dose onto as many as possible crystals in as short time as possible (then the jet speed and detector speed have to be adjusted). At Swiss Light Source beamline X06SA we found that a good compromise between signal-to-noise, dose rate, and hit rate is the crystal scanning approach [15].

18. Detector frame rate, extrusion speed, and flux density: The extrusion rate and the flux density of the beam together with the size of the crystals determine the dose rate in a typical experiment. The detector frame rate should be chosen in such a way that for each frame a new portion of the crystal is exposed to the beam. Ideally, during each detector frame the crystals are extruded by one beamwidth. Very high frame rates and low extrusion rates lead to multiple exposures of the same region and distort statistics dramatically if the consecutive patterns are used to create a combined dataset (since virtually all statistics used for serial crystallography depend on random half datasets and these become very similar when "the same" measurement is repeated over and over). But this mode of data collection may be useful in time-resolved experiments using high-frame-rate detectors (since one then analyzes the consecutive frames separately and they do differ in the temporal dimension; the resulting datasets will have been recorded on the same crystal which may help to make consecutive difference maps more comparable) [32].
19. Beam center and detector distance: Knowing the beam center and detector distance accurately is much more important in a serial crystallography experiment than in a synchrotron experiment in which long rotation series usually allow to determine these parameters quite well. This is especially true if the space group and unit cell parameters have not been previously determined by classical crystallography.

20. Preparing a list of hits: The hit list used in CrystFEL contains usually the path to a data file in hdf5 format followed by //XXX where XXX is the image number of that file. This number is later listed as Event: //XXX in the stream file resulting from processing.
21. Custom splitting: For time-resolved experiments the "custom splitting" option in indexamajig ensures that all datasets that are written out are indexed in the same way and the quality of smaller datasets usually improves if they are scaled together with other data.

Acknowledgments

We thank Thomas Gruhl for helping in developing the present protocol for rhodopsin serial crystallography and providing some pictures. We thank Edwards Stuttfeld for the continuous support and advices to work with the SONICC imager, and Timm Maier for the access to the SONICC imager. We acknowledge the Paul Scherrer Institut, Villigen, Switzerland, for provision of synchrotron radiation beam time at beamline PXI of the SLS and the continuous support from Andrea Prota and Takashi Tomizaki. This work was supported by the NCCR Molecular Systems Engineering 2015–2017 and Swiss National Science Foundation grant 173335 (to Gebhard Schertler). We acknowledge Filip Pamula and Maximilian Wranik for critical reading of the manuscript.

References

1. Standfuss J, Spence J (2017) Serial crystallography at synchrotrons and X-ray lasers. IUCrJ 4 (Pt 2):100–101. https://doi.org/10.1107/S2052252517001877
2. Barty A, Caleman C, Aquila A, Timneanu N, Lomb L, White TA, Andreasson J, Arnlund D, Bajt S, Barends TR, Barthelmess M, Bogan MJ, Bostedt C, Bozek JD, Coffee R, Coppola N, Davidsson J, Deponte DP, Doak RB, Ekeberg T, Elser V, Epp SW, Erk B, Fleckenstein H, Foucar L, Fromme P, Graafsma H, Gumprecht L, Hajdu J, Hampton CY, Hartmann R, Hartmann A, Hauser G, Hirsemann H, Holl P, Hunter MS, Johansson L, Kassemeyer S, Kimmel N, Kirian RA, Liang M, Maia FR, Malmerberg E, Marchesini S, Martin AV, Nass K, Neutze R, Reich C, Rolles D, Rudek B, Rudenko A, Scott H, Schlichting I, Schulz J, Seibert MM, Shoeman RL, Sierra RG, Soltau H, Spence JC, Stellato F, Stern S, Struder L, Ullrich J, Wang X, Weidenspointner G, Weierstall U, Wunderer CB, Chapman HN (2012) Self-terminating diffraction gates femtosecond X-ray nanocrystallography measurements. Nat Photonics 6:35–40. https://doi.org/10.1038/nphoton.2011.297
3. White TA, Barty A, Stellato F, Holton JM, Kirian RA, Zatsepin NA, Chapman HN (2013) Crystallographic data processing for free-electron laser sources. Acta Crystallogr D Biol Crystallogr 69(Pt 7):1231–1240. https://doi.org/10.1107/S0907444913013620
4. Neutze R, Wouts R, van der Spoel D, Weckert E, Hajdu J (2000) Potential for biomolecular imaging with femtosecond X-ray pulses. Nature 406(6797):752–757. https://doi.org/10.1038/35021099
5. Cheng RKY, Abela R, Hennig M (2017) X-ray free electron laser: opportunities for drug discovery. Essays Biochem 61(5):529–542. https://doi.org/10.1042/EBC20170031
6. Stauch B, Cherezov V (2018) Serial femtosecond crystallography of G protein-coupled

receptors. Annu Rev Biophys 47:377–397. https://doi.org/10.1146/annurev-biophys-070317-033239

7. Johansson LC, Stauch B, Ishchenko A, Cherezov V (2017) A bright future for serial femtosecond crystallography with XFELs. Trends Biochem Sci 42(9):749–762. https://doi.org/10.1016/j.tibs.2017.06.007
8. Landau EM, Rosenbusch JP (1996) Lipidic cubic phases: a novel concept for the crystallization of membrane proteins. Proc Natl Acad Sci U S A 93(25):14532–14535
9. Weierstall U, James D, Wang C, White TA, Wang D, Liu W, Spence JC, Bruce Doak R, Nelson G, Fromme P, Fromme R, Grotjohann I, Kupitz C, Zatsepin NA, Liu H, Basu S, Wacker D, Han GW, Katritch V, Boutet S, Messerschmidt M, Williams GJ, Koglin JE, Marvin Seibert M, Klinker M, Gati C, Shoeman RL, Barty A, Chapman HN, Kirian RA, Beyerlein KR, Stevens RC, Li D, Shah ST, Howe N, Caffrey M, Cherezov V (2014) Lipidic cubic phase injector facilitates membrane protein serial femtosecond crystallography. Nat Commun 5:3309. https://doi.org/10.1038/ncomms4309
10. Nogly P, Panneels V, Nelson G, Gati C, Kimura T, Milne C, Milathianaki D, Kubo M, Wu W, Conrad C, Coe J, Bean R, Zhao Y, Bath P, Dods R, Harimoorthy R, Beyerlein KR, Rheinberger J, James D, DePonte D, Li C, Sala L, Williams GJ, Hunter MS, Koglin JE, Berntsen P, Nango E, Iwata S, Chapman HN, Fromme P, Frank M, Abela R, Boutet S, Barty A, White TA, Weierstall U, Spence J, Neutze R, Schertler G, Standfuss J (2016) Lipidic cubic phase injector is a viable crystal delivery system for time-resolved serial crystallography. Nat Commun 7:12314. https://doi.org/10.1038/ncomms12314
11. Nogly P, James D, Wang D, White TA, Zatsepin N, S A, Nelson G, Liu H, Johansson L, Heymann M, J K, M M, Wickstrand C, Wu W, B P, B P, Oberthuer D, Panneels V, Cherezov V, Chapman H, Schertler G, Neutze R, Spence J, Moraes I, Burghammer M, Standfuss J, Weierstall U (2015) Lipidic cubic phase serial millisecond crystallography using synchrotron radiation. IUCrJ 2:168–176
12. Huang CY, Olieric V, Ma P, Panepucci E, Diederichs K, Wang M, Caffrey M (2015) In meso in situ serial X-ray crystallography of soluble and membrane proteins. Acta Crystallogr D Biol Crystallogr 71(Pt 6):1238–1256. https://doi.org/10.1107/S1399004715005210
13. Huang CY, Olieric V, Howe N, Warshamanage R, Weinert T, Panepucci E, Vogeley L, Basu S, Diederichs K, Caffrey M, Wang M (2018) In situ serial crystallography for rapid de novo membrane protein structure determination. Commun Biol 1:124. https://doi.org/10.1038/s42003-018-0123-6
14. Martiel I, Muller-Werkmeister HM, Cohen AE (2019) Strategies for sample delivery for femtosecond crystallography. Acta Crystallogr D Struct Biol 75(Pt 2):160–177. https://doi.org/10.1107/S2059798318017953
15. Weinert T, Olieric N, Cheng R, Brunle S, James D, Ozerov D, Gashi D, Vera L, Marsh M, Jaeger K, Dworkowski F, Panepucci E, Basu S, Skopintsev P, Dore AS, Geng T, Cooke RM, Liang M, Prota AE, Panneels V, Nogly P, Ermler U, Schertler G, Hennig M, Steinmetz MO, Wang M, Standfuss J (2017) Serial millisecond crystallography for routine room-temperature structure determination at synchrotrons. Nat Commun 8(1):542. https://doi.org/10.1038/s41467-017-00630-4
16. Edwards PC, Li J, Burghammer M, McDowell JH, Villa C, Hargrave PA, Schertler GF (2004) Crystals of native and modified bovine rhodopsins and their heavy atom derivatives. J Mol Biol 343(5):1439–1450. https://doi.org/10.1016/j.jmb.2004.08.089.S0022-2836(04)01089-7[pii].
17. Li D, Boland C, Aragao D, Walsh K, Caffrey M (2012) Harvesting and cryo-cooling crystals of membrane proteins grown in lipidic mesophases for structure determination by macromolecular crystallography. J Vis Exp 67:e4001. https://doi.org/10.3791/4001
18. White TA, Kirian RA, Martin AV, Aquila A, Nass K, Barty A, Chapman HN (2012) CrystFEL: a software suite for snapshot serial crystallography. J Appl Cryst 45:335–334
19. White TA, Mariani V, Brehm W, Yefanov O, Barty A, Beyerlein KR, Chervinskii F, Galli L, Gati C, Nakane T, Tolstikova A, Yamashita K, Yoon CH, Diederichs K, Chapman HN (2016) Recent developments in CrystFEL. J Appl Cryst 49(Pt 2):680–689. https://doi.org/10.1107/S1600576716004751
20. McPherson A, Gavira JA (2014) Introduction to protein crystallization. Acta Crystallogr F Struct Biol Commun 70:2–20. https://doi.org/10.1107/S2053230X13033141
21. Lin SW, Sakmar TP (1996) Specific tryptophan UV-absorbance changes are probes of the transition of rhodopsin to its active state. Biochemistry 35(34):11149–11159. https://doi.org/10.1021/bi960858u

22. Caffrey M, Cherezov V (2009) Crystallizing membrane proteins using lipidic mesophases. Nat Protoc 4(5):706–731. https://doi.org/10.1038/nprot.2009.31.nprot.2009.31[pii].
23. Ishchenko A, Cherezov V, Liu W (2016) Preparation and delivery of protein microcrystals in lipidic cubic phase for serial femtosecond crystallography. J Vis Exp 115. https://doi.org/10.3791/54463
24. Jaeger K, Dworkowski F, Nogly P, Milne C, Wang M, Standfuss J (2016) Serial millisecond crystallography of membrane proteins. Adv Exp Med Biol 922:137–149. https://doi.org/10.1007/978-3-319-35072-1_10
25. James D, Weinert T, Skopintsev P, Furrer A, Gashi D, Tanaka T, Nango E, Nogly P, Standfuss J (2019) Improving high viscosity extrusion of microcrystals for time-resolved serial femtosecond crystallography at X-ray lasers. J Vis Exp 144(e59087). https://doi.org/10.3791/59087
26. Caffrey M, Porter C (2010) Crystallizing membrane proteins for structure determination using lipidic mesophases. J Vis Exp 45. https://doi.org/10.3791/1712
27. Mariani V, Morgan A, Yoon CH, Lane TJ, White TA, O'Grady C, Kuhn M, Aplin S, Koglin J, Barty A, Chapman HN (2016) OnDA: online data analysis and feedback for serial X-ray imaging. J Appl Cryst 49 (Pt 3):1073–1080. https://doi.org/10.1107/S1600576716007469
28. Nakane T, Joti Y, Tono K, Yabashi M, Nango E, Iwata S, Ishitani R, Nureki O (2016) Data processing pipeline for serial femtosecond crystallography at SACLA. J Appl Cryst 49(Pt 3):1035–1041. https://doi.org/10.1107/S1600576716005720
29. Haupert LM, Simpson GJ (2011) Screening of protein crystallization trials by second order nonlinear optical imaging of chiral crystals (SONICC). Methods 55(4):379–386. https://doi.org/10.1016/j.ymeth.2011.11.003
30. Kissick DJ, Wanapun D, Simpson GJ (2011) Second-order nonlinear optical imaging of chiral crystals. Annu Rev Anal Chem 4:419–437. https://doi.org/10.1146/annurev.anchem.111808.073722
31. Nogly P, Weinert T, James D, Carbajo S, Ozerov D, Furrer A, Gashi D, Borin V, Skopintsev P, Jaeger K, Nass K, Bath P, Bosman R, Koglin J, Seaberg M, Lane T, Kekilli D, Brunle S, Tanaka T, Wu W, Milne C, White T, Barty A, Weierstall U, Panneels V, Nango E, Iwata S, Hunter M, Schapiro I, Schertler G, Neutze R, Standfuss J (2018) Retinal isomerization in bacteriorhodopsin captured by a femtosecond X-ray laser. Science 361(6398):eaat0094. https://doi.org/10.1126/science.aat0094
32. Weinert T, Skopintsev P, James D, Dworkowski F, Panepucci E, Kekilli D, Furrer A, Brunle S, Mous S, Ozerov D, Nogly P, Wang M, Standfuss J (2019) Proton uptake mechanism in bacteriorhodopsin captured by serial synchrotron crystallography. Science 365 (6448):61–65. https://doi.org/10.1126/science.aaw8634

Chapter 22

Hydrogen/Deuterium Exchange Mass Spectrometry for the Structural Analysis of Detergent-Solubilized Membrane Proteins

Darragh P. O'Brien, Véronique Hourdel, Alexandre Chenal, and Sébastien Brier

Abstract

Integral membrane proteins are involved in numerous biological functions and represent important drug targets. Despite their abundance in the human proteome, the number of integral membrane protein structures is largely underrepresented in the Protein Data Bank. The challenges associated with the biophysical characterization of such biological systems are well known. Most structural approaches, including X-ray crystallography, SAXS, or mass spectrometry (MS), require the complete solubilization of membrane proteins in aqueous solutions. Detergents are frequently used for this task, but may interfere with the analysis, as is the case with MS. The use of "MS-friendly" detergents, such as non-ionic alkyl glycoside detergents, has greatly facilitated the analysis of detergent-solubilized membrane proteins. Here, we describe a protocol, which we have successfully implemented in our laboratory to study the structure and dynamics of detergent-solubilized integral membrane proteins by Hydrogen/Deuterium eXchange and Mass Spectrometry (HDX-MS). The procedure does not require detergent removal prior to MS analysis, instead taking advantage of the ultra-high pressure chromatographic system to separate deuterated peptides from "MS-friendly" detergents.

Key words Integral membrane proteins, "MS-friendly" detergents, Ligand binding, Deuterium exchange, Mass spectrometry

1 Introduction

Hydrogen/Deuterium eXchange measured by Mass Spectrometry (HDX-MS) is a well-established and robust method to study the structure and dynamics of proteins [1–5]. The rate of exchange between backbone amide hydrogens and deuterium is directly influenced by the structure and dynamics of proteins. Disordered regions that lack stable hydrogen bonding networks exchange very rapidly, whereas folded elements, such as α-helices and β-sheets, exchange at much slower rates due to hydrogen bonding [6]. Over

Camilo Perez and Timm Maier (eds.), *Expression, Purification, and Structural Biology of Membrane Proteins*, Methods in Molecular Biology, vol. 2127, https://doi.org/10.1007/978-1-0716-0373-4_22,

the last 35 years, HDX-MS has been extensively used (mainly in the academic sector) to study the structure, folding, and dynamics of soluble proteins and to characterize their interactions with partners (e.g., DNA, peptides, membranes, lipids, and small molecules [7–11]). The structural information gathered by HDX-MS has proved to be extremely valuable and complementary to X-ray crystallography [12–14], SAXS [15–17], NMR spectroscopy [18], or other classical structural tools [19], underlining the utility of this technology in structural biology studies.

HDX-MS has long been perceived as a powerful but complex and time-consuming structural technique. The analysis of deuterated samples by MS necessitates quenching of the labeling reaction prior to monitoring the deuterium uptake by simultaneously adjusting the pH and the temperature to 2.5 and 0 °C, respectively. This step is critical to minimize as much deuterium loss as possible (i.e., back-exchange) during the chromatographic and MS steps. Under these so-called quench conditions, the exchange rate constant of backbone amide hydrogens is greatly reduced (i.e., by approximately five orders of magnitude compared to exchange at pH 7.0 and 25 °C) which provides "enough" time to perform LC-MS acquisition. However, such quench conditions must be maintained throughout the analysis, including during the digestion and chromatographic steps. This technical challenge has greatly hindered the expansion of HDX-MS, limiting its use to MS-specialized laboratories only. Over the past decade however, significant improvements in the HDX-MS workflow have resulted in the technology becoming more streamlined and robust, enhancing its accessibility in both academic and pharmaceutical environments. In particular, the development of dedicated robots for automated sample handling, the commercialization of refrigerated ultra-high performance liquid chromatography systems [20], and the automation of the rather labor-intensive data processing step have greatly simplified HDX-MS strategies [21–24].

Consequently, the use of modern HDX-MS workflows enables the structural analysis of more complex biological systems, such as entire viral particles [25] and membrane proteins [26–31]. One challenge still associated with this latter, however, remains their production and purification from their native environment, while maintaining a fully functional state. For this task, detergents have been traditionally used to extract and purify membrane proteins from biological membranes. Unfortunately, MS does not tolerate most detergents, due to their high ionization propensity, leading to ion signal suppression of peptides and proteins. Specific procedures for detergent removal have been developed, such as affinity-based spin columns [32] or filter-aided sample preparation [33]. Although these cleanup strategies work well, they are not compatible with the time constraints and/or the quench conditions imposed by the HDX-MS technology.

In this chapter, we report a HDX-MS protocol for the structural analysis of integral membrane proteins solubilized in "MS-friendly" detergent micelles. This protocol was initially developed in our laboratory to decipher the solvent accessibility and dynamics of the human glutamate transporter (EAAT1) solubilized in dodecanoyl sucrose micelles [12, 34]. Importantly, the procedure described below does not require any sample cleanup prior to MS analysis, and makes use of the refrigerated ultra-high performance liquid chromatography system to separate deuterated peptides from "MS-friendly" detergents, thus avoiding ion signal suppression.

2 Materials

2.1 Sample Preparation

Note that % refers to volume:volume (v:v) unless specified.

1. Deuterium oxide (D_2O), 99.9 atom % D.
2. Deuterium chloride solution (DCl), 35 wt. % in D_2O, 99 atom %D.
3. Sodium deuteroxide solution (NaOD), 40 wt. % in D_2O, 99 atom %D.
4. Immobilized agarose pepsin beads (50% slurry).
5. Acetonitrile (UPLC-MS grade).
6. Formic acid (UPLC-MS grade).
7. Highly pure detergents.
8. Ultrapure or UPLC-grade water.

The following buffers were used to study the uptake behavior of the human EAAT1 protein solubilized in dodecanoyl sucrose (DDS, CMC in H_2O ~ 0.016% (w:v)) in the presence and absence of the selective non-substrate EAAT1 inhibitor UCPH-101 [12]. The labeling and dilution buffers should both be identical to the initial protein buffer.

9. Dilution buffer: 50 mM HEPES-KOH, 200 mM NaCl, 1 mM L-aspartate, 5% glycerol, 0.0632% (w:v) DDS (~3 × CMC), 0.01264% (w:v) cholesteryl hemisuccinate (CHS), 0.5 mM TCEP, 2.2% DMSO, pH 7.4 (in H_2O).
10. Labeling buffer: 50 mM HEPES-KOH, 200 mM NaCl, 1 mM L-aspartate, 5% glycerol, 0.0632% (w:v) DDS, 0.01264% (w:v) CHS, 0.5 mM TCEP supplemented with either DMSO or 101.2 μM UCPH-101 prepared in 100% DMSO, pD 7.4 in D_2O (Final DMSO concentration = 2.2%) (*see* **Note 1**).
11. Quench buffer: ice-cold solution of 0.75% formic acid supplemented with 5% glycerol.

2.2 LC-MS Materials and Solutions

1. Empty 2 mm I.D. × 2-cm-long guard column with 2 μm frits.
2. ACQUITY UPLC BEH C18 VanGuard Pre-Column, 130 Å, 1.7 μm, 2.1 mm × 5 mm, or equivalent.
3. ACQUITY UPLC BEH C18 Analytical column, 130 Å, 1.7 μm, 1.0 mm × 100 mm, or equivalent.
4. Pepsin wash solution: 1% formic acid, 5% acetonitrile, 1.5 M guanidinium chloride, pH 1.7.
5. Lockmass solution: [Glu1]-fibrinopeptide B human prepared at 100 nM in 50% acetonitrile, 0.1% formic acid.

2.3 Computational Analysis

1. ProteinLynX Global Server 3.0 (PLGS; Waters Corporation).
2. DynamX 3.0 (Waters Corporation).
3. MEMHDX (http://memhdx.c3bi.pasteur.fr) [21].

3 Methods

1. The structural analysis of membrane proteins solubilized in "MS-friendly" detergents does not require changes to the classical HDX-MS workflow (Fig. 1). Before initiating the labeling, the protein is equilibrated at the desired temperature (depending on the stability of the biological system), in the presence or absence of a ligand (small molecules, proteins, peptides, etc.). The labeling starts by diluting the equilibrated sample with a large excess of deuterated buffer. The excess of deuterium favors the unidirectional exchange of labile backbone amide hydrogens (from H to D). The protein sample is incubated at the desired temperature; after defined periods of time, aliquots are removed and quenched by reducing the pH to 2.5, and the temperature to 0 °C. Quenched samples can be snap-frozen and stored at −80 °C or immediately digested by an acidic protease under quench conditions. The generated peptides are further separated on a C18 reverse phase column maintained at 0 °C and directly eluted onto the mass spectrometer.
2. The term "MS-friendly" detergents mainly refers to non-ionic alkyl glycoside detergents [R-O-$(CH_2)_n$-CH_3 with R = Glucose; or R-S-$(CH_2)_n$-CH_3 with R = glucose, maltose: e.g., *n*-Dodecyl-β-D-maltopyranoside (DDM), or sucrose monodecanoate] or zwitterionic detergents such as *n*-Tetradecyl-*N,N*-dimethyl-3-ammonio-1-propanesulfonate (Zwittergent 3–14). However, "MS-friendly" is not equivalent to "MS-compatible" (*see* **Note 2**). Hence, the co-elution of "MS-friendly" detergents with proteins or peptides during electrospray ionization-MS

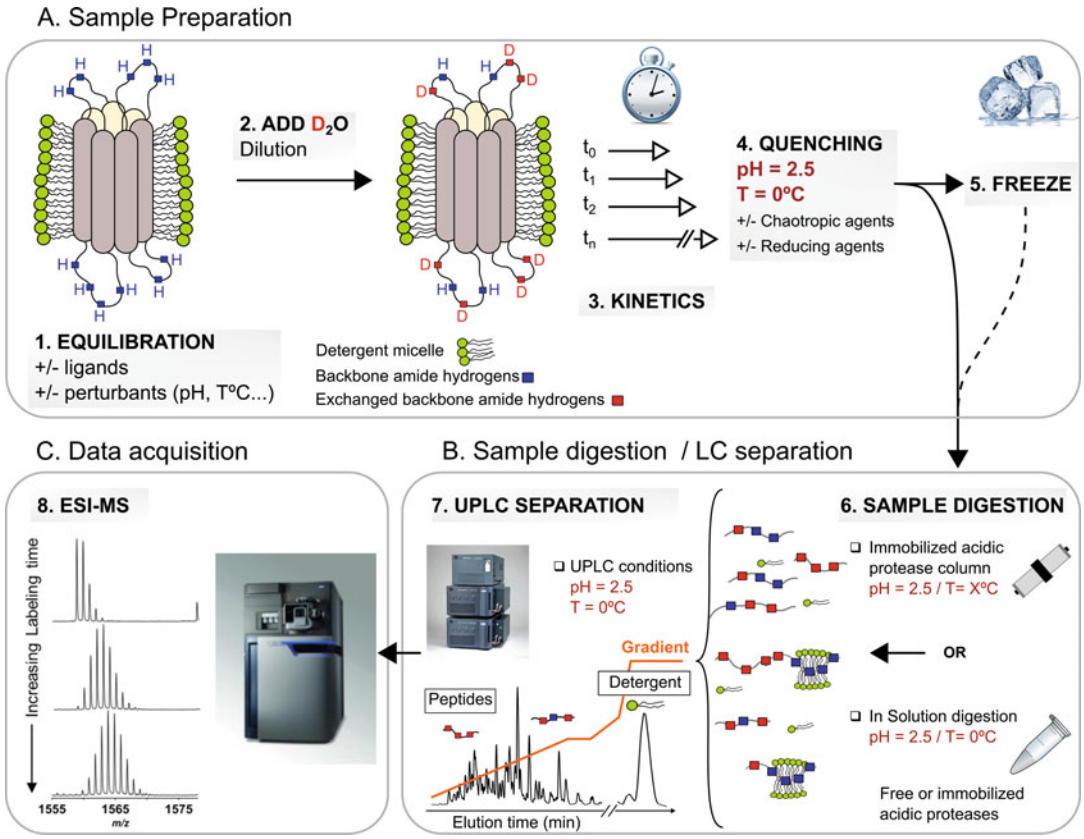

Fig. 1 Workflow of a typical HDX experiment. (**a**) The detergent-solubilized membrane protein is equilibrated in specific conditions (+/− ligands, presence of perturbants, etc.) at the desired temperature and for a specified amount of time. The labeling starts by adding a large excess of deuterated buffer. At defined periods, the reaction is quenched by decreasing both the pH and the temperature, to 2.5 and 0 °C. The quenching conditions "freeze" the protein in a specific labeling state by decreasing the exchange rate constant by five orders of magnitude. (**b**, **c**) Quenched samples can be immediately snap-frozen and conserved at −80 °C or digested either on line with an immobilized pepsin column or in solution. Peptides are further separated at 0 °C by reverse phase chromatography using an optimized gradient of acetonitrile and directly analyzed by MS.

analysis ultimately results in an almost complete loss of protein or peptide signal. One simple solution to overcome this is to use the chromatographic system to separate the deuterated peptides obtained after digestion from the detergent, based on their inherent differences in hydrophobicity. The HDX-MS protocol described in this chapter is based on this strategy, and was applied to investigate the changes of solvent accessibility occurring on a thermostabilized form of EEAT1, in the presence and absence of UCPH-101.

3.1 From Sample Preparation to Data Acquisition

3.1.1 Preparation of the "Home-Made" Pepsin Column

1. Assemble the analytical guard column following the vendor's instructions. Unscrew one side of the column, remove the frit, and attach the packing funnel. Connect a 1/16 inch syringe PEEK connector at the other extremity and attach an empty 10 mL syringe.
2. Mix the 50% pepsin slurry and load ~150 μL (i.e., ~ 75 μL of settled agarose beads) onto the packing funnel. Use the syringe to create a small and constant aspiration to pour the slurry. The 2 mm I.D. × 2 cm C-130B guard column can accommodate up to ~ 63 μL of pepsin beads (*see* **Note 3**).
3. Once the guard column is completely filled, remove the syringe and the packing funnel and place the frit onto the open end. Screw the column cap.
4. Connect the pepsin column to the UPLC system and flush with 10–20 column volume of 0.15% formic acid buffer, pH 2.5, at 40 μL/min and room temperature. At the end of the cleaning procedure, increase the flow rate to 100 μL/min for several minutes to finish packing the column.
5. Control the activity of the pepsin column by injecting a reference protein sample (*see* **Note 4**).
6. Close both ends of the column with a plug to avoid drying and place at 4 °C until use. When stored and used properly, the pepsin column lasts the entire life of a project (and more).

3.1.2 Optimizing the Digestion and LC Conditions

The first step of any HDX-MS project is to define and optimize the digestion and LC conditions. The generation of a good peptide map (i.e., high sequence coverage, redundancy, and signal quality) is essential and represents the most important criterion to evaluate the feasibility of a project [35]. The digestion can take place either online (using columns of immobilized acidic proteases) or offline (i.e., in solution) using solubilized or immobilized acidic proteases (*see* **Note 5**). The following steps describe the conditions employed to generate a peptide map of the DDS-solubilized EAAT1 protein with an immobilized pepsin column (Fig. 2).

1. Prepare the HDX-MS system: connect the pepsin column, the pre-column, and the analytical column to the UPLC system. Set the temperature of the HDX chamber to 0 °C and equilibrate the column and the pre-column for at least 2 h with 95% buffer A (0.15% formic acid, pH 2.5) and 5% buffer B (100% acetonitrile, 0.15% formic acid).
2. Equilibrate the pepsin column with the digestion buffer (0.15% formic acid, pH 2.5). The temperature of the pepsin column can be adjusted to improve the efficacy of the digestion. Low temperatures favor deuterium recovery but reduce the activity of the enzyme. We generally start to equilibrate the pepsin column at 20 °C.

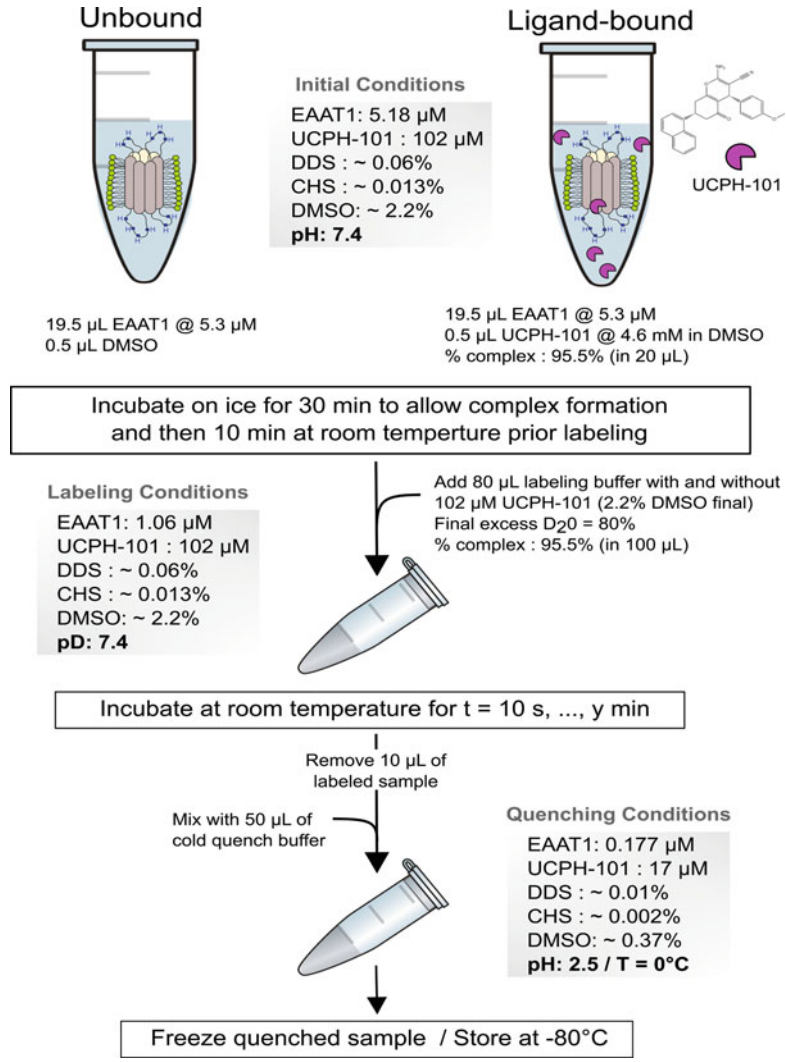

Fig. 2 Preparation of the deuterated EAAT1 samples in the presence and absence of UCPH-101. The DDS-solubilized EAAT1 membrane protein is incubated for 30 min on ice in the presence and absence of an excess of UCPH-101 and 2.2% final DMSO. Following an additional 10 min equilibration time at room temperature, the labeling is initiated by a fivefold dilution with the deuterated buffer. The concentration of the protein and the ligand was carefully selected and adjusted so that ~95.5% of the EAAT1 protein remains bound to the ligand before and after labeling (assuming a K_d value of ~ 4.5 µM) (*see* **Note 9**). At defined time points, the reaction is quenched by mixing 10 µL of labeled samples (10.6 pmols of EAAT1) with 50 µL of an ice-cold quenching solution. Quenched samples are immediately snap-frozen in liquid nitrogen and stored at −80 °C

3. Set the mass spectrometer to MS/MS mode (i.e., either in data-dependent or data-independent acquisition mode; we do recommend using the data-independent acquisition mode (MS^E) with the Synapt G2-Si HDMS instrument). Adjust the source conditions (voltages and temperatures) to minimize the back-exchange. Calibrate the instrument.
4. Prepare the membrane protein following the protocol described in Fig. 2 using H_2O in place of D_2O solutions (*see* **Note 6**).
5. Obtain a preliminary peptide digestion map of the membrane protein. Inject 50 μL of quenched sample (8.8 pmols) prepared in H_2O and perform the digestion for 2 min at 20 °C and 100 μL/min. The quantity of material required per injection mostly depends on the sensitivity of the mass spectrometer used (we do not inject more than 10 pmols on the Synapt G2-Si HDMS in resolution mode).
6. Elute peptides onto the mass spectrometer using a short gradient of buffer B at 0 °C (e.g., 5–35% in 8 min is a good starting point). Perform a quick analysis to generate a preliminary peptide map (see Subheading 3.2.1). Determine the optimal digestion conditions by changing the flow rate and temperature of the pepsin column, and/or the quenching conditions (*see* **Note 7**). Carefully adjust the gradient to optimize the separation of peptides from the detergent. Note the % of acetonitrile required to elute the detergent from the analytical column before adjusting the gradient.
7. Repeat **steps 5** and **6** with each new gradient.
8. Once the optimized experimental conditions are determined, generate the final peptide map in triplicate. The LC gradient, quench conditions, and digestion parameters should remain constant for the rest of the experiment with D_2O buffer.

3.1.3 Sample Preparation

1. Prepare the labeled samples following the procedure described in Fig. 2 (*see* **Note 8**).
2. Place the labeling buffer at room temperature for 1 h and the quench buffer on ice.
3. Equilibrate your system for "x" min at T°C. This step increases the probability of a uniform protein population, in terms of conformation, dynamics, etc., and favors the binding of the ligand (*see* **Note 9**). The temperature and time of equilibration depends on the intrinsic stability of the membrane protein (for instance, the DDS-solubilized EEAT1 membrane protein starts to lose its quaternary structure after 2 h incubation at room temperature).
4. Initiate the labeling by adding an excess of D_2O buffer. We generally use a fivefold dilution to reach a final D_2O ratio of

80%, but other dilution factors may be used (*see* **Note 9**). Incubate the samples at the desired temperature. It is common procedure to perform the reaction at room temperature although other labeling temperatures may be used (e.g., 4, 15, 25 °C using a thermoblock).

5. At defined periods of time, remove an aliquot of labeled sample and quench the reaction by mixing with an ice-cold quench buffer to decrease both the pH to 2.5 and the temperature to 0 °C. Snap-froze samples in liquid nitrogen and store at −80 °C until MS analysis (for less than a week).
6. Prepare one digestion control per condition following the procedure described in Subheading 3.1.2. This control will serve as a reference to calculate the level of deuterium incorporation per peptide and condition (Subheading 3.2.1, **step 3**).
7. Repeat **steps 3–5** to generate independent technical replicates. Triplicates are required to perform statistical analysis.

3.1.4 MS-Data Acquisition

1. Prepare the mass spectrometer and HDX system as described in Subheading 3.1.2 (**steps 1–3**). Set the mass spectrometer in MS acquisition mode and perform a new calibration. If using a Synapt G2-Si mass spectrometer, carefully adjust the StepWave and Source settings to reduce gas-phase deuterium loss and bimodal artifacts [36].
2. Before starting any injection, place a glass syringe (Hamilton 100 μL 710 SNR, 22 s Gauge, Point style 3) on ice for a minimum of 10 min.
3. Thaw one sample and immediately inject 50 μL into the cooled HDX system using the chilled glass syringe. Proceed to the digestion, peptide separation and MS acquisition using the conditions defined in Subheading 3.1.2, **step 8**.
4. At the end of each run, clean the pepsin column with two consecutive injections of pepsin wash solution maintained at room temperature (*see* **Note 10**).
5. Perform a blank between each run to confirm the absence of carryover (*see* **Note 11**).

3.2 From Data Extraction to Statistical Validation and Data Interpretation

3.2.1 HDX-MS Data Extraction Using Waters Software

1. Obtain the peptide map with PLGS using the default E-MS^{E} processing parameters (low energy threshold: 250 counts; elevated energy threshold: 100 counts; intensity threshold: 750 counts). Adjust the low and elevated energy thresholds based on the MS signal intensity (the default values represent a good starting point). Control the assignment of each fragmentation spectrum. Automatically generate the output file in *.csv* by clicking the Ion Accounting Output option in the IdentityE tab of the Automation Setup to "On."

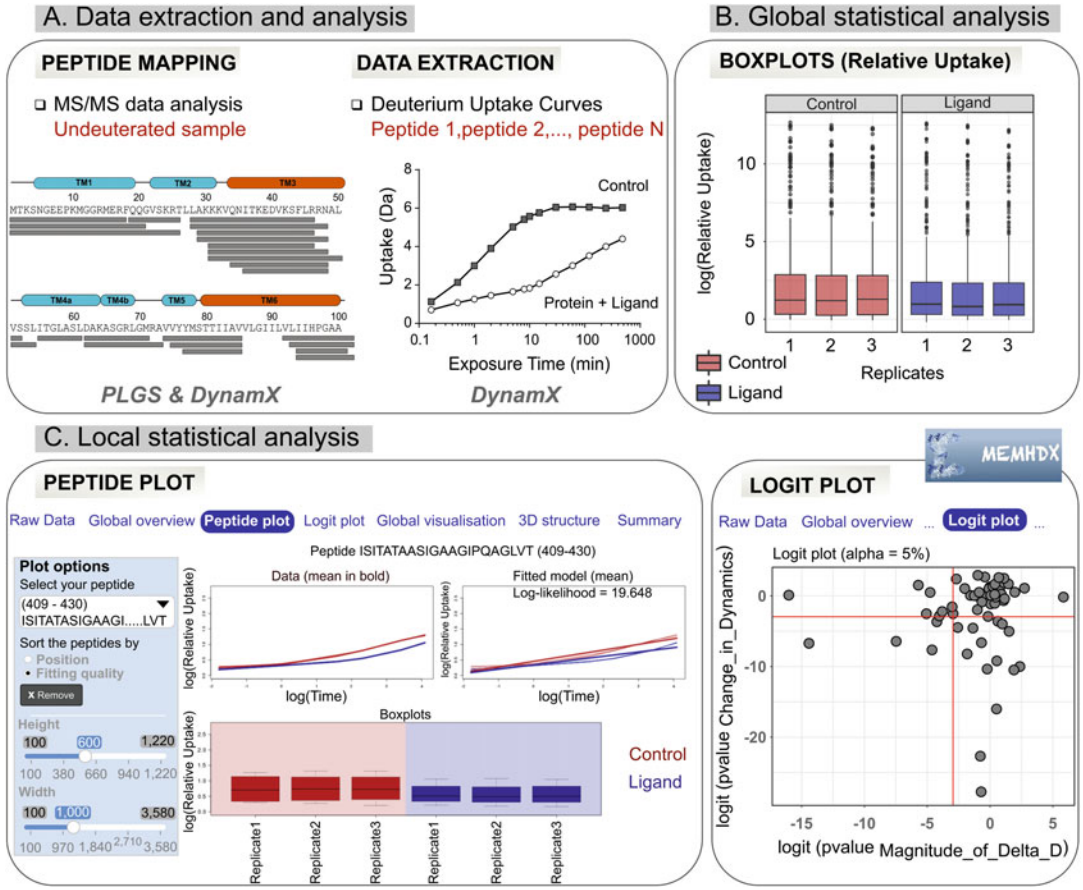

Fig. 3 Data extraction and statistical validation. (**a**) The initial peptide map is generated with PLGS and further refined in DynamX. The relative deuterium uptake values measured for each peptide and condition and at each time point are automatically extracted by DynamX and plotted as a function of incubation time. (**b**) Global statistical analysis is performed by MEMHDX on the entire HDX dataset. The boxplot representation summarizes variability across replicates and conditions. (**c**) The local statistical analysis is only initiated after validation of the whole HDX-MS dataset. The peptide plot panel of MEMHDX displays the results generated per peptide and shows the fitting quality of the mixed-effects model. Once each peptide has been inspected, the LogitPlot is used to summarize and identify all statistically significant peptides

2. Load the *.csv* file in DynamX 3.0 and refine the peptide map using the filtering options. Load all deuterated MS data and adjust the ion detection threshold (default value sets at 130) based on the spectral quality (Fig. 3a).
3. DynamX 3.0 automatically extracts the relative deuterium uptake values for each peptide and condition and generates the deuterium uptake plots. For each peptide, control the spectral quality and the peak picking.
4. Select one unique charge state per peptide to perform the statistical analysis with MEMHDX. Export the results in *.csv* using the CLUSTER export option in DynamX (MEMHDX does not run with STATE data) (*see* **Note 12**).

3.2.2 Statistical Validation with MEMHDX

1. Open the *.csv* file (CLUSTER data) in Excel. Your file **MUST** contain the following variables (all other variables can be removed from the *.csv* file, if needed):
   (a) **Start:** Peptide start position on the protein.
   (b) **End:** Peptide end position on the protein.
   (c) **Sequence:** Peptide sequence.
   (d) **State:** Name of the conditions.
   (e) **Exposure:** Value of the exposure time (min).
   (f) **Replicate:** Replicate number ($n >= 3$).
   (g) ***z*:** Peptide charge state.
   (h) **Center:** Centroid *m/z* value.
   (i) **MaxUptake:** Maximum number of exchangeable amide hydrogens per peptide.
2. Create the column "Replicate" and complete with the corresponding number (i.e., 1, 2,. . ., *n*). A minimum of three independent replicates is required (*see* **Note 13**). Check the *.csv* file before proceeding to the next step (i.e., number of replicates and conditions, etc.). Please note that at least one exposure time is required for each peptide, charge state, and condition.
3. Go to the MEMHDX website (http://memhdx.c3bi.pasteur.fr).
4. Go to the *Start Analysis* panel at the top of the application and upload the *.csv* file. MEMHDX automatically controls the global architecture of the *.csv* and the presence of each variable.
5. Adjust the MEMHDX options (*p*-value, $\%D_2O$, and biological threshold; the default values can be used as a starting point and adjusted later) and run the analysis.
6. In the HDX-MS results section, go to the *Global Overview* panel and explore your HDX-MS results using the different panels (*Box plot, PCA and Clustering)*. Pay particular attention to the quality control of the whole HDX-MS dataset (Fig. 3b). The box plot representation summarizes the variability across replicates and considers the deuterium values measured for all peptides, and at each time point. It is a good indication of the reproducibility between replicates. The principal component analysis (*PCA*) summarizes the effects of the variance on the entire datasets independent of either the conditions or labeling time.
7. Go to the *Peptide plot* panel and analyze the fitting quality of the model for each peptide. Peptides can be sorted by fitting quality (log-likelihood), or by position (from N- to

C-terminal), and further excluded from the statistical analysis using the "remove" button (Fig. 3c).

8. Go to the *Logit plot* panel to identify statistically significant peptides (Fig. 3c). The *p*-value, biological threshold, and % D_2O can be adjusted during the analysis.

3.2.3 Visualization and Interpretation

1. Use the "*Global visualization*" tool in MEMHDX to display the final HDX results. MEMHDX automatically plots the relative fractional uptake values (normalized values independent of the peptide length) as a function of peptide position and for each condition (e.g., free versus bound state). This representation gives both spatial and temporal information on the HDX behavior of the protein (Fig. 4a).
2. Identify peptides with statistically significant differences of deuterium uptake between states using the fractional uptake difference plot (Fig. 4b). Statistically significant peptides are highlighted in light blue.
3. Interpret the HDX results in light of the crystal structure of the protein (Fig. 4C) (*see* **Note 14**).

The HDX-MS protocol described in this chapter should be applicable to any membrane protein solubilized in "MS-friendly" detergents, upon careful selection of the quench conditions and optimization of the chromatographic separation. DDS does not affect the chromatographic system, as most of the detergent is eluted from the C18 analytical column at the end of the gradient. However, assays performed with DDM are less satisfactory in our hands, due to the incomplete elution of the detergent leading to a slow but constant increase of the column pressure with time and injections. Change of the pre-column and/or overnight back flushes of the analytical column at room temperature with mixtures of methanol/acetonitrile are therefore required from time to time to avoid overpressure of the chromatographic system and loss of deuterated samples.

Although detergent micelles facilitate the characterization of integral membrane proteins, they constitute poor mimics of the native membrane. HDX-MS protocols are now quickly evolving to investigate the conformation and dynamics of membrane proteins reconstituted in more "native-like" environments, such as those using liposomes or nanodiscs [37–42]. One elegant example of this is a recent HDX-compatible protocol that has been developed and applied to the analysis of prokaryotic integral membrane proteins in native conditions [43].

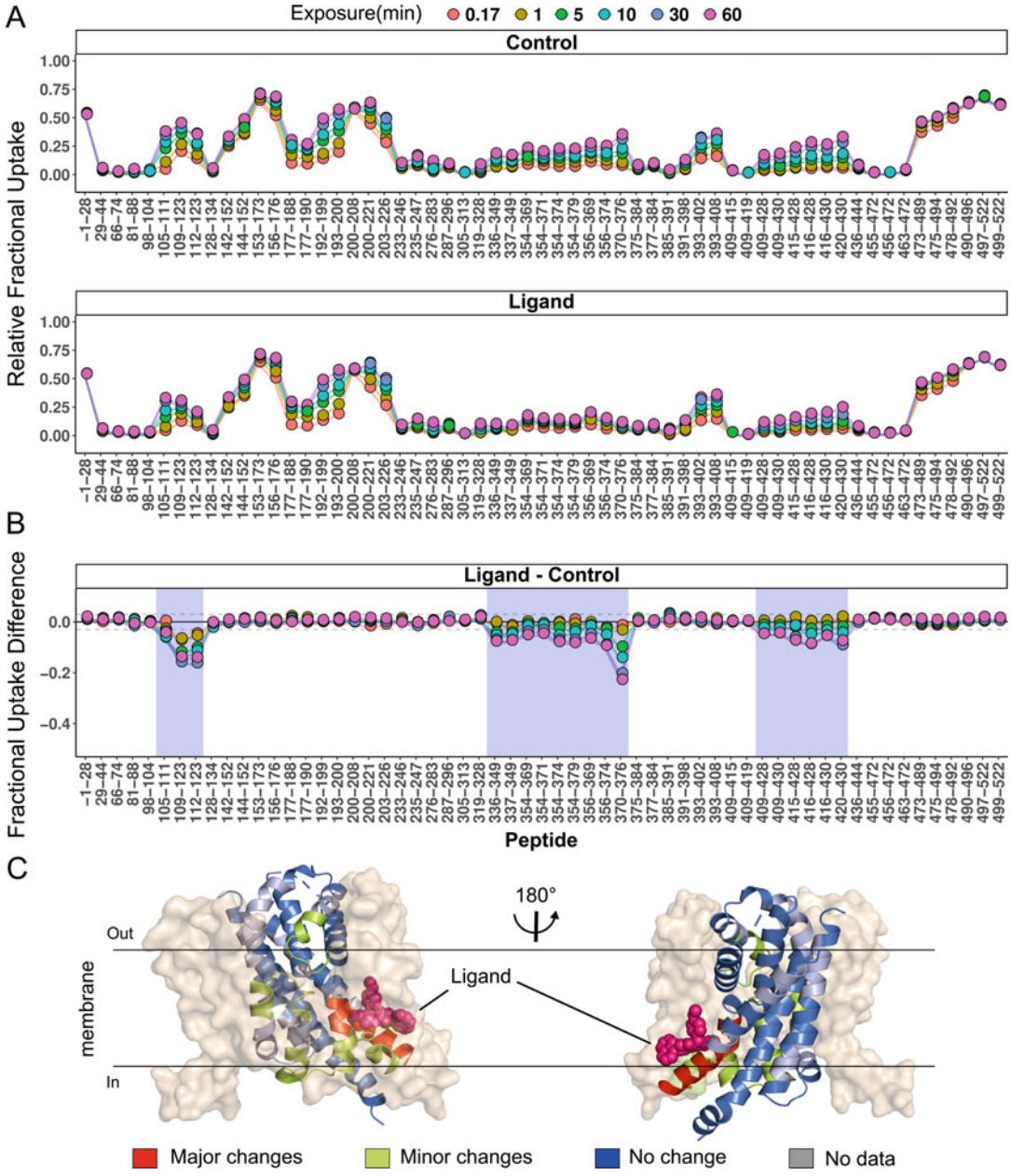

Fig. 4 Visualization of the HDX results with MEMHDX. (**a**) Relative fractional uptake plots obtained with the detergent-solubilized EAAT1 membrane protein alone (Control plot) or in the presence of an ~20-fold molar excess of ligand (UCPH-101). Each dot corresponds to an average of three independent technical replicates. (**b**) Fractional uptake difference plot showing the difference in deuterium uptake calculated between the ligand-bound and free EAAT1 protein. Negative values indicate a ligand-induced reduction of solvent accessibility. Statistically significant peptides are highlighted in light blue (Wald test; $p < 0.05$). (**c**) Visualization of the HDX-MS results on the crystal structure of EAAT1 (pdb # 5LM4) [12]

4 Notes

1. The labeling buffer is directly prepared in the 25 g D_2O bottle. 25 g of D_2O corresponds to a final volume of 22.6 mL at 25 °C (density = 1.107 g/cm^3). Once all components have been weighed and dissolved in the D_2O bottle, the pH is adjusted to the desired value using either concentrated DCl (~12 M) or NaOD (~14 M). Working solutions of DCl and NaOD are prepared by dilution in D_20. Keep in mind that the $pH_{reading}$ of a deuterated solution is 0.4 units lower than pD when using a classical hydrogen electrode (i.e., a $pH_{reading}$ of 7.0 corresponds to a pD value of 7.4).
2. "MS-compatible" detergents only refer to acid-labile surfactants such as RapiGest SF (Waters Corporation) or surfactant capable to degrade with time such as ProteaseMAX (Promega). These surfactants are commonly used in the preparation of classical proteomics samples.
3. The concentration of the cross-linked pepsin on agarose beads is unknown. The manufacturer recommends using 125 μL of settled resin to digest 10 mg of IgG. The guard column can accommodate 63 μL of the 50% slurry (i.e., 31.5 μL of settled resin) and thus handle up to 2.5 mg of protein per run (the quantity of injected material per assay should be in the μg range).
4. It is good practice to control the activity of your pepsin column before beginning to inject your protein samples. In our lab, we assess the activity of the column by injecting a known reference sample (Bet v 1; UniprotKB access number # P15494) prepared in 0.15% formic acid at 0.2 μM (10 pmols per injection (i.e., 0.17 μg), triplicate analysis). The elution profiles, spectral quality, and MS/MS data of each acquisition are compared to previous acquisitions performed in the exact same conditions to evaluate the activity and performance of the new pepsin column.
5. Digestions can take place online with immobilized acidic proteases packed into a column or offline (i.e., in solution) using solubilized acidic proteases or acidic protease immobilized on a solid support. Offline digestions are normally performed on ice to reduce back-exchange, thus increasing the time of digestion. In addition, the protein:acidic protease ratio must be optimized: a 1:1 (w:w) ratio is generally sufficient with pig pepsin, whereas higher ratios are required with type XIII and type XVIII proteases from *Aspergillus saitoi* and *Rhizopus species* [44]. Although solubilized acidic proteases work well in solution, we do recommend immobilized acidic proteases for both online and offline digestions to reduce the time of digestion

and to introduce more flexibility in the final composition of the quench buffer (*see* **Note 7**).

6. Before preparing and injecting your detergent-solubilized membrane protein prepared in H_2O, we highly recommend evaluating the effects of the detergent and other molecules (i.e., small ligands) on the activity of the pepsin column using a known protein sample prepared in the exact same conditions. In our lab, we use the Bet v 1 protein to evaluate the effects of distinct components of the digestion step. For instance, we noticed that 0.02% (w:v) DDM in the quench buffer reduces the activity of the pepsin column (presence of undigested material at the end of the gradient).
7. Optimization of the quench conditions is essential to generate the best sequence coverage possible and depends on the protein and the labeling conditions (i.e., buffer composition, etc.). The group of Patrick R. Griffith [31] elegantly showed how to select and optimize quench conditions to study the dynamics of the β2-adrenergic G-protein-coupled receptor. If the detergent-solubilized membrane protein contains disulfide bridges, then reducing agents such as TCEP can be added to the quench buffer. Electrochemical reduction using a μ-PrepCell thin-layer electrochemical reactor cell (Antec, Zoeterwoude, NL) may also be considered [45, 46]. In addition, some proteins might not digest very well using standard quench conditions. In this scenario, chaotropic agents such as guanidinium chloride or urea may be used to favor the denaturation of proteins. In our hands, 4 M urea works very well when performing online digestion. Bear in mind that solubilized acidic proteases are less resistant to chaotropic or reducing agents than immobilized enzymes.
8. Sample handling can be automated using a dedicated PAL-HDX autosampler [47].
9. The concentration of the detergent-solubilized membrane protein and the ligand must be carefully selected to avoid disruption of complexes during labeling. A good starting point is to fix the concentration of the detergent-solubilized membrane protein based on the MS signal quality and intensity of peptides obtained after digestion. The K_d value is then used to adjust the concentration of ligands so that >90% of the complex remains formed before and after dilution with the labeling buffer. Please note that this calculation must take into account the stoichiometry of the binding reaction. For the binding of UCPH-101 with EAAT1 ($K_d \sim 4.5$ μM; binding stoichiometry = 1), a 1:20 molar ratio was used to complex 95.5% of EAAT1 before labeling (Fig. 2). The concentration (in μM) and % of complex were calculated using equations in Fig. 5.

A

$$[\text{Complexe}] = \frac{(Kd + [\text{Protein}] + [\text{ligand}]) - \sqrt{(Kd + [\text{Protein}] + [\text{Ligand}])^2 - 4([\text{Protein}].[\text{Ligand}])}}{2}$$

B

$$\text{Complexe (\%)} = \frac{[\text{Complexe}]}{[\text{Protein}]}$$

Fig. 5 Equations used to calculate the concentration (**a**) and percentage (**b**) of complex during labeling

In addition, UCPH-101 was added to the labeling buffer to match the initial concentration of ligand during equilibration and prevent dissociation of the complex. If the K_d is not available, a 1:10 molar ratio (protein:ligand) represents a good starting point (depending on the tolerance of the pepsin column and the effect of the ligand of the MS signal).

10. This washing step should be performed to avoid carryover from previous samples. In most cases, the carryover is due to incomplete elution from the pepsin column leading to a false EX1 signature. One way to minimize the carryover is to add small quantities of detergent in the quench buffer [35], or to perform several extra washes of the acidic protease column with chaotropic agents such as guanidinium chloride (the concentration of guanidinium chloride should not exceed 2 M) [48].
11. To identify peptides prone to carryover in the LC system (i.e., "sticky peptides"), blank injections should be performed with the same elution gradient than that of the deuterated samples. We highly recommend introducing rapid sawtooth gradient cycles at the end of the analytical gradient to wash and regenerate the column. We generally perform two sawtooth cycles (Table 1) before equilibrating the column to preinjection conditions; the rapid changes of pressure of the system during these cycles also favor the elution of the remaining traces of detergent.
12. We use the bioinformatics solution provided by Waters (PLGS, MassLynX and DynamX) to identify peptides, extract deuterium uptake values, and analyze our results. Other bioinformatics solutions exist for this purpose [49].
13. The cluster *.csv* file of DynamX does not contain the "replicate" column required to run MEMHDX. Adding the replicate value in front of each time point and condition is a time-consuming task that we avoid by adding the replicate number at the end of each acquisition file name. We then use the convert function in Excel to automatically generate the "replicate" column.
14. HDX results can be analyzed in the absence of any crystal or NMR structure, but the strength and confidence of the interpretation is greatly reduced. For instance, the binding of a

Table 1
Example of HDX-MS gradient profile with two sawtooth cycles

Time (min)	Flow rate (μL/min)	Buffer A (%)	Buffer B (%)	
Initial	40	95	5	
8.00	40	70	30	Gradient
10.00	40	60	40	
10.50	40	5	95	Washing and regeneration
11.00	40	5	95	
11.10	40	95	5	
12.10	40	95	5	
12.20	40	5	95	
13.20	40	5	95	
13.30	40	95	5	
14.30	40	95	5	
14.40	40	5.0	95	
15.40	40	5.0	95	
15.5	40	95	5	
18.0	40	95	5	

ligand is expected to reduce the solvent accessibility of backbone amide hydrogens located at or near the binding site only. However, allosteric changes might occur upon binding thus leading to additional changes of accessibility in regions distal from the interaction site. Alternatively, the interaction sites might be formed by discontinuous segments of the protein, as observed with conformational epitopes [8, 14, 50].

Acknowledgments

The HDX-MS system was financed by the Equipex CACSICE (ANR-11-EQPX-0008). SB would like to thank Alexandre Chenal, Nadia Izadi-Prunyere, Mariette Matondo, Florence Cordier, Thierry Lang, Daniel Ladant, Iñaki Guijarro and Michael Nilges for their kindness and constant support over the last year.

References

1. Jaswal SS (2013) Biological insights from hydrogen exchange mass spectrometry. Biochim Biophys Acta 1834(6):1188–1201. https://doi.org/10.1016/j.bbapap.2012.10.011
2. Konermann L, Pan J, Liu YH (2011) Hydrogen exchange mass spectrometry for studying protein structure and dynamics. Chem Soc Rev 40(3):1224–1234. https://doi.org/10.1039/c0cs00113a
3. Oganesyan I, Lento C, Wilson DJ (2018) Contemporary hydrogen deuterium exchange mass spectrometry. Methods 144:27–42. https://doi.org/10.1016/j.ymeth.2018.04.023
4. Tsutsui Y, Wintrode PL (2007) Hydrogen/deuterium exchange-mass spectrometry: a powerful tool for probing protein structure, dynamics and interactions. Curr Med Chem 14(22):2344–2358

5. Wales TE, Engen JR (2006) Hydrogen exchange mass spectrometry for the analysis of protein dynamics. Mass Spectrom Rev 25 (1):158–170. https://doi.org/10.1002/mas.20064
6. Brier S, Engen JR (2008) Hydrogen exchange mass spectrometry: principles and capabilities. In: Chance M (ed) Mass spectrometry analysis for protein-protein interactions and dynamics. Wiley, New York, pp 11–43
7. Brier S, Fagnocchi L, Donnarumma D, Scarselli M, Rappuoli R, Nissum M, Delany I, Norais N (2012) Structural insight into the mechanism of DNA-binding attenuation of the Neisserial adhesin repressor NadR by the small natural ligand 4-hydroxyphenylacetic acid. Biochemistry 51(34):6738–6752. https://doi.org/10.1021/bi300656w
8. Faleri A, Santini L, Brier S, Pansegrau W, Lo Surdo P, Scarselli M, Buricchi F, Volpini G, Genovese A, van der Veen S, Lea S, Tang CM, Savino S, Pizza M, Finco O, Norais N, Masignani V (2014) Two cross-reactive monoclonal antibodies recognize overlapping epitopes on Neisseria meningitidis factor H binding protein but have different functional properties. FASEB J 28(4):1644–1653. https://doi.org/10.1096/fj.13-239012
9. Georgescauld F, Popova K, Gupta AJ, Bracher A, Engen JR, Hayer-Hartl M, Hartl FU (2014) GroEL/ES chaperonin modulates the mechanism and accelerates the rate of TIM-barrel domain folding. Cell 157 (4):922–934. https://doi.org/10.1016/j.cell.2014.03.038
10. Pirrone GF, Emert-Sedlak LA, Wales TE, Smithgall TE, Kent MS, Engen JR (2015) Membrane-associated conformation of HIV-1 Nef investigated with hydrogen exchange mass spectrometry at a Langmuir monolayer. Anal Chem 87(14):7030–7035. https://doi.org/10.1021/acs.analchem.5b01725
11. Trelle MB, Dupont DM, Madsen JB, Andreasen PA, Jorgensen TJ (2014) Dissecting the effect of RNA aptamer binding on the dynamics of plasminogen activator inhibitor 1 using hydrogen/deuterium exchange mass spectrometry. ACS Chem Biol 9(1):174–182. https://doi.org/10.1021/cb400619v
12. Canul-Tec JC, Assal R, Cirri E, Legrand P, Brier S, Chamot-Rooke J, Reyes N (2017) Structure and allosteric inhibition of excitatory amino acid transporter 1. Nature 544 (7651):446–451. https://doi.org/10.1038/nature22064
13. Chung KY, Rasmussen SG, Liu T, Li S, DeVree BT, Chae PS, Calinski D, Kobilka BK, Woods VL Jr, Sunahara RK (2011) Conformational changes in the G protein Gs induced by the beta2 adrenergic receptor. Nature 477 (7366):611–615. https://doi.org/10.1038/nature10488
14. Malito E, Faleri A, Lo Surdo P, Veggi D, Maruggi G, Grassi E, Cartocci E, Bertoldi I, Genovese A, Santini L, Romagnoli G, Borgogni E, Brier S, Lo Passo C, Domina M, Castellino F, Felici F, van der Veen S, Johnson S, Lea SM, Tang CM, Pizza M, Savino S, Norais N, Rappuoli R, Bottomley MJ, Masignani V (2013) Defining a protective epitope on factor H binding protein, a key meningococcal virulence factor and vaccine antigen. Proc Natl Acad Sci U S A 110 (9):3304–3309. https://doi.org/10.1073/pnas.1222845110
15. O'Brien DP, Brier S, Ladant D, Durand D, Chenal A, Vachette P (2018) SEC-SAXS and HDX-MS: a powerful combination. The case of the calcium-binding domain of a bacterial toxin. Biotechnol Appl Biochem 65(1):62–68. https://doi.org/10.1002/bab.1577
16. O'Brien DP, Durand D, Voegele A, Hourdel V, Davi M, Chamot-Rooke J, Vachette P, Brier S, Ladant D, Chenal A (2017) Calmodulin fishing with a structurally disordered bait triggers CyaA catalysis. PLoS Biol 15(12):e2004486. https://doi.org/10.1371/journal.pbio.2004486
17. O'Brien DP, Hernandez B, Durand D, Hourdel V, Sotomayor-Perez AC, Vachette P, Ghomi M, Chamot-Rooke J, Ladant D, Brier S, Chenal A (2015) Structural models of intrinsically disordered and calcium-bound folded states of a protein adapted for secretion. Sci Rep 5:14223. https://doi.org/10.1038/srep14223
18. Cavaliere P, Brier S, Filipenko P, Sizun C, Raynal B, Bonnete F, Levi-Acobas F, Bellalou J, England P, Chamot-Rooke J, Mayer C, Norel F (2018) The stress sigma factor of RNA polymerase RpoS/sigma(S) is a solvent-exposed open molecule in solution. Biochem J 475(1):341–354. https://doi.org/10.1042/BCJ20170768
19. Hamdi K, Salladini E, O'Brien DP, Brier S, Chenal A, Yacoubi I, Longhi S (2017) Structural disorder and induced folding within two cereal, ABA stress and ripening (ASR) proteins. Sci Rep 7(1):15544. https://doi.org/10.1038/s41598-017-15299-4
20. Wales TE, Fadgen KE, Gerhardt GC, Engen JR (2008) High-speed and high-resolution UPLC separation at zero degrees Celsius. Anal Chem 80(17):6815–6820. https://doi.org/10.1021/ac8008862

21. Hourdel V, Volant S, O'Brien DP, Chenal A, Chamot-Rooke J, Dillies MA, Brier S (2016) MEMHDX: an interactive tool to expedite the statistical validation and visualization of large HDX-MS datasets. Bioinformatics 32 (22):3413–3419. https://doi.org/10.1093/bioinformatics/btw420
22. Miller DE, Prasannan CB, Villar MT, Fenton AW, Artigues A (2012) HDXFinder: automated analysis and data reporting of deuterium/hydrogen exchange mass spectrometry. J Am Soc Mass Spectrom 23(2):425–429. https://doi.org/10.1007/s13361-011-0234-5
23. Pascal BD, Chalmers MJ, Busby SA, Mader CC, Southern MR, Tsinoremas NF, Griffin PR (2007) The Deuterator: software for the determination of backbone amide deuterium levels from H/D exchange MS data. BMC Bioinformatics 8:156. https://doi.org/10.1186/1471-2105-8-156
24. Pascal BD, Willis S, Lauer JL, Landgraf RR, West GM, Marciano D, Novick S, Goswami D, Chalmers MJ, Griffin PR (2012) HDX workbench: software for the analysis of H/D exchange MS data. J Am Soc Mass Spectrom 23(9):1512–1521. https://doi.org/10.1007/s13361-012-0419-6
25. Lim XX, Chandramohan A, Lim XY, Bag N, Sharma KK, Wirawan M, Wohland T, Lok SM, Anand GS (2017) Conformational changes in intact dengue virus reveal serotype-specific expansion. Nat Commun 8:14339. https://doi.org/10.1038/ncomms14339
26. Giladi M, Almagor L, van Dijk L, Hiller R, Man P, Forest E, Khananshvili D (2016) Asymmetric preorganization of inverted pair residues in the sodium-calcium exchanger. Sci Rep 6:20753. https://doi.org/10.1038/srep20753
27. Giladi M, van Dijk L, Refaeli B, Almagor L, Hiller R, Man P, Forest E, Khananshvili D (2017) Dynamic distinctions in the Na(+)/Ca(2+) exchanger adopting the inward- and outward-facing conformational states. J Biol Chem 292(29):12311–12323. https://doi.org/10.1074/jbc.M117.787168
28. Mehmood S, Domene C, Forest E, Jault JM (2012) Dynamics of a bacterial multidrug ABC transporter in the inward- and outward-facing conformations. Proc Natl Acad Sci U S A 109 (27):10832–10836. https://doi.org/10.1073/pnas.1204067109
29. West GM, Chien EY, Katritch V, Gatchalian J, Chalmers MJ, Stevens RC, Griffin PR (2011) Ligand-dependent perturbation of the conformational ensemble for the GPCR beta2 adrenergic receptor revealed by HDX. Structure 19 (10):1424–1432. https://doi.org/10.1016/j.str.2011.08.001
30. Yang L, Yang D, de Graaf C, Moeller A, West GM, Dharmarajan V, Wang C, Siu FY, Song G, Reedtz-Runge S, Pascal BD, Wu B, Potter CS, Zhou H, Griffin PR, Carragher B, Yang H, Wang MW, Stevens RC, Jiang H (2015) Conformational states of the full-length glucagon receptor. Nat Commun 6:7859. https://doi.org/10.1038/ncomms8859
31. Zhang X, Chien EY, Chalmers MJ, Pascal BD, Gatchalian J, Stevens RC, Griffin PR (2010) Dynamics of the beta2-adrenergic G-protein coupled receptor revealed by hydrogen-deuterium exchange. Anal Chem 82 (3):1100–1108. https://doi.org/10.1021/ac902484p
32. Antharavally BS, Mallia KA, Rosenblatt MM, Salunkhe AM, Rogers JC, Haney P, Haghdoost N (2011) Efficient removal of detergents from proteins and peptides in a spin column format. Anal Biochem 416(1):39–44. https://doi.org/10.1016/j.ab.2011.05.013
33. Wisniewski JR, Zougman A, Nagaraj N, Mann M (2009) Universal sample preparation method for proteome analysis. Nat Methods 6 (5):359–362. https://doi.org/10.1038/nmeth.1322
34. Cirri E, Brier S, Assal R, Canul-Tec JC, Chamot-Rooke J, Reyes N (2018) Consensus designs and thermal stability determinants of a human glutamate transporter. eLife 7. doi: https://doi.org/10.7554/eLife.40110
35. Hamuro Y, Coales SJ (2018) Optimization of feasibility stage for hydrogen/deuterium exchange mass spectrometry. J Am Soc Mass Spectrom 29(3):623–629. https://doi.org/10.1007/s13361-017-1860-3
36. Guttman M, Wales TE, Whittington D, Engen JR, Brown JM, Lee KK (2016) Tuning a high transmission ion guide to prevent gas-phase proton exchange during H/D exchange MS analysis. J Am Soc Mass Spectrom 27 (4):662–668. https://doi.org/10.1007/s13361-015-1330-8
37. Adhikary S, Deredge DJ, Nagarajan A, Forrest LR, Wintrode PL, Singh SK (2017) Conformational dynamics of a neurotransmitter:sodium symporter in a lipid bilayer. Proc Natl Acad Sci U S A 114(10):E1786–E1795. https://doi.org/10.1073/pnas.1613293114
38. Hebling CM, Morgan CR, Stafford DW, Jorgenson JW, Rand KD, Engen JR (2010) Conformational analysis of membrane proteins in phospholipid bilayer nanodiscs by hydrogen exchange mass spectrometry. Anal Chem 82 (13):5415–5419. https://doi.org/10.1021/ac100962c

39. Morgan CR, Hebling CM, Rand KD, Stafford DW, Jorgenson JW, Engen JR (2011) Conformational transitions in the membrane scaffold protein of phospholipid bilayer nanodiscs. Mol Cell Proteomics 10(9):M111.010876. https://doi.org/10.1074/mcp.M111.010876
40. Parker CH, Morgan CR, Rand KD, Engen JR, Jorgenson JW, Stafford DW (2014) A conformational investigation of propeptide binding to the integral membrane protein gamma-glutamyl carboxylase using nanodisc hydrogen exchange mass spectrometry. Biochemistry 53 (9):1511–1520. https://doi.org/10.1021/bi401536m
41. Redhair M, Clouser AF, Atkins WM (2019) Hydrogen-deuterium exchange mass spectrometry of membrane proteins in lipid Nanodiscs. Chem Phys Lipids 220:14. https://doi.org/10.1016/j.chemphyslip.2019.02.007
42. Vahidi S, Bi Y, Dunn SD, Konermann L (2016) Load-dependent destabilization of the gamma-rotor shaft in FOF1 ATP synthase revealed by hydrogen/deuterium-exchange mass spectrometry. Proc Natl Acad Sci U S A 113 (9):2412–2417. https://doi.org/10.1073/pnas.1520464113
43. Donnarumma D, Maestri C, Giammarinaro PI, Capriotti L, Bartolini E, Veggi D, Petracca R, Scarselli M, Norais N (2018) Native State Organization of Outer Membrane Porins Unraveled by HDx-MS. J Proteome Res 17 (5):1794–1800. https://doi.org/10.1021/acs.jproteome.7b00830
44. Cravello L, Lascoux D, Forest E (2003) Use of different proteases working in acidic conditions to improve sequence coverage and resolution in hydrogen/deuterium exchange of large proteins. Rapid Commun Mass Spectrom 17 (21):2387–2393. https://doi.org/10.1002/rcm.1207
45. Mysling S, Salbo R, Ploug M, Jorgensen TJ (2014) Electrochemical reduction of disulfide-containing proteins for hydrogen/deuterium exchange monitored by mass spectrometry. Anal Chem 86(1):340–345. https://doi.org/10.1021/ac403269a
46. Trabjerg E, Jakobsen RU, Mysling S, Christensen S, Jorgensen TJ, Rand KD (2015) Conformational analysis of large and highly disulfide-stabilized proteins by integrating online electrochemical reduction into an optimized H/D exchange mass spectrometry workflow. Anal Chem 87(17):8880–8888. https://doi.org/10.1021/acs.analchem.5b01996
47. Forest E, Man P (2016) Conformational dynamics and interactions of membrane proteins by hydrogen/deuterium mass spectrometry. Methods Mol Biol 1432:269–279. https://doi.org/10.1007/978-1-4939-3637-3_17
48. Majumdar R, Manikwar P, Hickey JM, Arora J, Middaugh CR, Volkin DB, Weis DD (2012) Minimizing carry-over in an online pepsin digestion system used for the H/D exchange mass spectrometric analysis of an IgG1 monoclonal antibody. J Am Soc Mass Spectrom 23 (12):2140–2148. https://doi.org/10.1007/s13361-012-0485-9
49. Claesen J, Burzykowski T (2017) Computational methods and challenges in hydrogen/deuterium exchange mass spectrometry. Mass Spectrom Rev 36(5):649–667. https://doi.org/10.1002/mas.21519
50. Brier S, Le Mignon M, Jain K, Lebrun C, Peurois F, Kellenberger C, Bordas-Le Floch V, Mascarell L, Nony E, Moingeon P (2018) Characterization of epitope specificities of reference antibodies used for the quantification of the birch pollen allergen bet v 1. Allergy 73(5):1032–1040. https://doi.org/10.1111/all.13364

Chapter 23

Mechanical Unfolding and Refolding of Single Membrane Proteins by Atomic Force Microscopy

Noah Ritzmann and Johannes Thoma

Abstract

Atomic force microscopy (AFM)-based single-molecule force spectroscopy allows direct physical manipulation of single membrane proteins under near-physiological conditions. It can be applied to study mechanical properties and molecular interactions as well as unfolding and folding pathways of membrane proteins. Here, we describe the basic procedure to study membrane proteins by single-molecule force spectroscopy and discuss general requirements of the experimental setup as well as common pitfalls typically encountered when working with membrane proteins in AFM.

Key words Single-molecule force spectroscopy, Atomic force microscopy, Membrane protein folding, Mechanical unfolding, Supported lipid bilayer

1 Introduction

Following the first appearance in 1986 [1], over the last decades atomic force microscopy (AFM) has evolved into an exceptional tool to study biological membranes and membrane proteins [2]. The latter is mainly owed to the ability to operate AFM in liquid environments, thereby allowing membranes to be studied under near-physiological conditions. In order to be studied by AFM, biological membranes are immobilized on a flat surface to form supported bilayers of 5–10 nm in height. Contouring the membrane surface with an atomically sharp tip at the free end of a microcantilever allows imaging of membrane topographies at sub-nanometer resolution. AFM has generated valuable insight into the molecular details of membrane proteins and their assemblies in biological membranes [3–6].

However, AFM also makes the direct physical manipulation of single membrane proteins possible. Single-molecule force spectroscopy (SMFS) allows probing the force-response of individual macromolecules under mechanical stress and can be used to study

Camilo Perez and Timm Maier (eds.), *Expression, Purification, and Structural Biology of Membrane Proteins*, Methods in Molecular Biology, vol. 2127, https://doi.org/10.1007/978-1-0716-0373-4_23,

the unfolding and folding behavior of membrane proteins [7, 8]. In order to mechanically unfold a membrane protein, the cantilever is first pushed onto the membrane surface applying a non-destructive force to facilitate the unspecific attachment of one terminus of the membrane protein to the tip of the cantilever by physisorption. Subsequent retraction induces the stepwise unfolding of the protein starting from the terminus which is tethered to the cantilever [9]. During retraction the deflection of the cantilever (correlated to the force required to unfold the protein) is recorded together with the retraction distance. Corrected for the cantilever deflection, this distance yields the effective length of the stretched molecule tethered between the tip of the cantilever and the sample surface. Plotting the unfolding force against this tip-sample-separation results in so-called force distance (FD) curves. FD curves recorded during unfolding of membrane proteins typically feature saw-tooth-shaped series of unfolding force peaks. These characteristic unfolding fingerprint patterns, which are determined by the interaction-network stabilizing the structural segments of a protein, are unique for each membrane protein. The unfolding fingerprint patterns can therefore be used to identify proteins [10], structural alterations within proteins, different conformational states [11, 12], or to distinguish folded and misfolded states of membrane proteins [13, 14].

SMFS can yield information not only on the unfolding pathways of membrane proteins but also on their folding behavior [15, 16]. To this end, a mechanically unfolded membrane protein is brought into close proximity of the membrane surface in a relaxed state. While still bound to the cantilever, the unfolded protein can reinsert into the lipid bilayer to adopt a folded state, which is then probed by unfolding the protein again [17]. The FD curves resulting from the two successive unfolding processes allow direct comparison of the conformations the protein adopted before and after refolding. This way SMFS helped to reveal to what extent membrane proteins can fold in a self-guided process [14, 18] and how external factors such as molecular chaperones influence the folding pathways of membrane proteins [19, 20].

2 Materials

1. Membrane protein sample: Ideal samples for force spectroscopy are proteoliposomes containing the membrane protein of interest embedded in a lipid bilayer at high purity and density. These can either be native membranes, which are naturally rich in a certain protein, or bilayers reconstituted from purified components. If possible, one of the protein's termini should be elongated to ensure efficient attachment to the cantilever during SMFS (*see* **Notes 1** and **2**).

2. Buffer: SMFS experiments are typically performed under physiological buffer conditions. However, the buffer should also facilitate firm adsorption of proteoliposomes to mica supports, which might require optimization. A good starting point is the storage buffer the proteoliposomes are supplied in since this buffer should ensure sample stability. Other buffers frequently used in SMFS include sodium or potassium-based PBS (20 mM (Na/K)P_i, pH 7.5, 100–150 mM (Na/K)Cl) and Tris buffers (20 mM Tris–HCl, pH 8, 100–300 mM NaCl) (*see* **Note 6**). All buffers should be freshly prepared from analytical grade reagents and ultrapure deionized water (using stock solutions is not recommended) in freshly cleaned glass bottles (*see* **Note 4**).
3. AFM: SMFS of membrane proteins can be performed using most commercial AFMs equipped with a 3-axis piezo positioning system. It should support an *xy* range of $>15 \times 15$ μm and a *z* range of >1 μm. Moreover, the capability of designing and recording multi-segment force-distance curves is required. To ensure optimal stability during the measurements, the AFM should be placed on an active damping table and acoustically shielded (*see* **Notes 3** and **4)**.
4. Cantilevers: Soft silicon nitride cantilevers with spring constants in the range 0.01–0.1 N/m and a tip radius <10 nm are the cantilevers of choice and offer a good balance between the ability to image the sample topography prior to and good force resolution during SMFS.
5. Mica supports: Muscovite mica is widely used to immobilize biological membranes for AFM studies due to its atomically flat and negatively charged surface. To prepare supports a mica disk with a diameter of 5 mm and a thickness of ~0.5 mm is glued either to a microscopy glass slide or to a Teflon foil covered metal disk (depending on the sample holder of the AFM) using two-component epoxy glue (*see* **Note 5**). It is important that the entire surface of the mica disk is covered in an even thin layer of glue and no air is entrapped in the glue.
6. Fluid cell: It is important that the AFM is equipped with a fluid cell, which can either be a closed design or an open design holding a liquid volume of ≥ 1 mL. Using a fluid cell ensures maximal stability of the setup during the measurement, minimizes thermal drift and allows measurements to be maintained for longer durations, especially when using a closed design.
7. Cleaning agents: 1% solution of household detergent in a spray bottle, laboratory-grade ethanol and ultrapure deionized water in wash bottles.
8. Compressed air or nitrogen to dry equipment.
9. Scotch tape or other adhesive tape for cleaving mica supports.

3 Methods

All preparations and experiments can be performed at room temperature.

3.1 Sample Adsorption and Imaging

1. Wash supports thoroughly with detergent solution, rinse several times iteratively with ethanol and water, dry using compressed air or nitrogen.
2. Cleave the top layer of the mica. To this end push a stripe of adhesive tape onto the mica surface and detach the top layer by pulling the tape off. Inspect the detached mica layer on the tape to ensure it was removed across the entire area of the support. Inspect the freshly cleaved support surface for visible edges. If necessary, repeat until an even and smooth surface is obtained.
3. Add 50 μL of proteoliposome suspension at a concentration of 10 μg/mL to the freshly cleaved mica and allow to adsorb for ~15 min (*see* **Note 6** for optimal conditions). Cover the support with a glass dish while adsorbing to prevent contamination with dust particles.
4. To wash out unbound material, remove 45 μL of sample solution then add 45 μL of fresh buffer and repeat seven times. Avoid direct contact with the mica surface when pipetting.
5. Transfer the sample to the AFM, fill the fluid cell with fresh buffer and engage the cantilever. Allow to equilibrate for at least 15 min or until the system is stabilized and thermal drift of the cantilever is no longer observed.
6. Approach the cantilever to the sample surface. Choose approach parameters conservatively using only minimal target force and approach velocity to prevent damaging the tip upon surface contact.
7. Record a topography of the sample at low to medium magnification and low resolution in contact mode (scan area $\geq 10 \times 10$ μm, 256×256 pixels). The topography can be recorded at rather high imaging velocity (up to five lines per second). Try to apply as low imaging force as possible in order not to damage the sample. The topography should give an initial impression of the sample quality. Adsorbed proteoliposomes should be visible as separated individual single-layered membrane patches of 5–10 nm in height. Areas of empty mica between membrane patches should be smooth and free of particulates (*see* **Notes 5–9**).
8. Select an area with a clean mica surface devoid of proteoliposomes and record a few force distance curves. Approach and subsequently retract the AFM cantilever without pausing using a constant velocity of 500 nm/s (*see* **Note 10**).

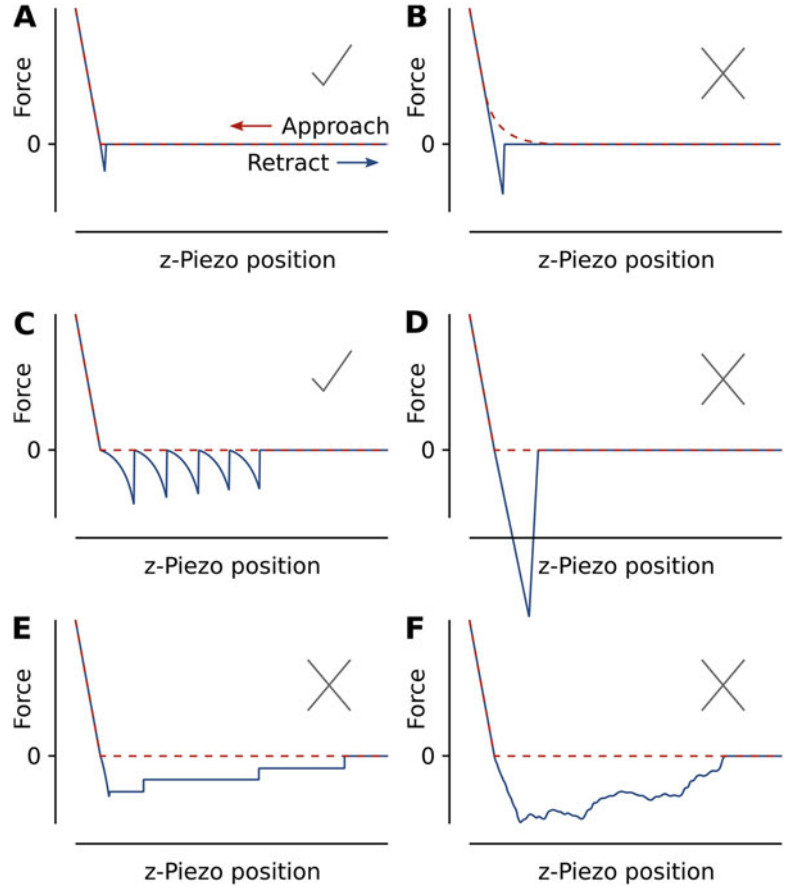

Fig. 1 Typical shapes of FD curves. (**a**) Ideal FD curves as measured on empty mica showing a sharp bend at the transition between non-contact and contact regime. No hysteresis is observed between the FD curves recorded during the approach (red) and following retract segment (blue). Upon retraction, only a weak surface adhesion event is registered. (**b**) A smooth bend at the transition between non-contact and contact regime in the approach curve is indicative of debris contaminating the cantilever. (**c**) Typical sawtooth-shaped series of force peaks as it occurs upon the stepwise unfolding of a membrane protein. (**d**) Pronounced force peaks with linear force increase resulting from strong surface adhesion can be caused by unfavorable tip geometries. (**e**) Elongated force plateaus caused by membrane tethers, which often occur when using blunt cantilevers with a large tip radius. (**f**) Highly irregular and irreproducible force patterns resembling a mountain range indicate sample degradation

9. Assess the quality of the FD curves (Fig. 1, *see* **Note 13**). FD curves should not deviate from zero force level in the non-contact regime and increase linearly with piezo-movement in the contact regime. If no hysteresis and no strong adhesion are observed, use one of the recorded FD curves to determine

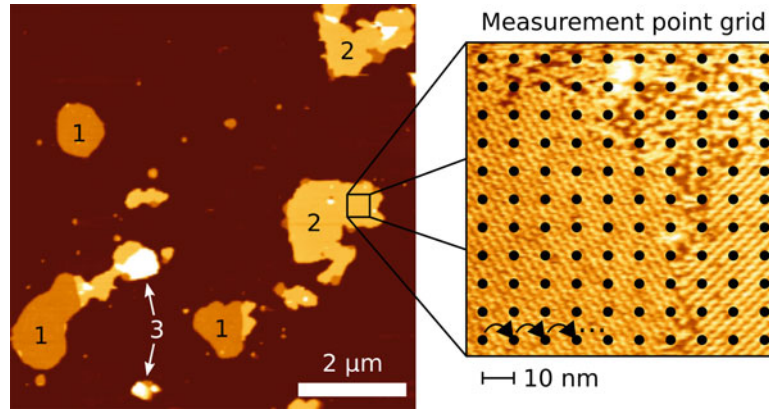

Fig. 2 Exemplary AFM topography. Proteoliposomes of FhuA reconstituted in *E. coli* polar lipids adsorbed to mica in buffer (20 mM Tris–HCl, pH 8, 150 mM NaCl). The topography shows membrane patches containing sparsely distributed membrane proteins (*1*) and membrane proteins at high density (*2*). Features protruding far from the surface indicate intact proteoliposomes, which did not break open upon adsorption (*3*). Areas containing densely packed membrane proteins provide ideal conditions for mechanical unfolding or refolding experiments and should be chosen to set the grid of consecutive measurement points

the cantilever's deflection sensitivity in the linear regime of the contact region of the FD curve.

10. Retract the cantilever from the surface for at least 1 µm and calibrate the cantilever's spring constant using the thermal noise method [21].
11. Re-approach the cantilever to the sample surface, select areas of interest and record topographies at increased magnification. It is not necessary to obtain very high resolution; however, the image quality should be sufficient to discern protein-rich regions within membrane patches from regions containing mainly empty lipid (Fig. 2).

3.2 Mechanical Unfolding of Membrane Proteins

1. Select a protein-rich region within a membrane patch with an area of min. 100 × 100 nm and set up a grid of consecutive measurement points with ~10 nm spacing (Fig. 2).
2. For each measurement point, repeat an approach-pause-retract cycle to record FD curves with the following settings: Approach and retract the AFM cantilever with a constant velocity of 500 nm/s (*see* **Note 11**). Use a target force of 1 nN for the approach and pause at constant force for 0.5 s (*see* **Note 12**). Set the retraction distance ≥2 times the contour length of the studied protein (*see* **Note 13**).
3. Assess the quality of initial FD curves (Fig. 1, *see* **Note 14**). If no irregular force patterns are observed in these FD curves, pass through the point grid repeating the approach-pause-

retract cycle for every measurement point and save all the recorded FD curves. The point grid can be sampled several times.

4. Interrupt the measurement every 1–2 h to record a new topography. Ensure that the membrane patch is still intact and that the measurement area is set on the correct sample position. Reposition the point grid if sample drift occurred.
5. Keep recording FD curves until the repetitively occurring characteristic unfolding fingerprint pattern of the studied membrane protein can be clearly recognized (*see* **Note 15**).

3.3 Refolding of Membrane Proteins

In contrast to the previously described unfolding of membrane proteins, setting up refolding experiments requires pre-existing knowledge of the characteristic unfolding fingerprint pattern of a protein, which can be established in unfolding experiments. Only then the fraction of the protein that is to be refolded can be selected based on the unfolding pattern. Moreover, since the throughput of refolding experiments is substantially lower, prior knowledge of the unfolding fingerprint pattern simplifies analysis of the resulting data. Otherwise the setup follows the same principles as mechanical unfolding experiments.

1. Select a protein-rich region within a membrane patch with an area of min. 100 × 100 nm and apply a grid of measurement points with ~10 nm spacing.
2. For each measurement point set up an approach-pause-retract-approach-pause-retract cycle to record FD curves with the following settings: Approach and retract the AFM cantilever with a constant velocity of 500 nm/s. Use a target force of 1 nN for the first approach and pause at constant force for 0.5 s. The retraction distance of the first retract depends on the unfolding fingerprint pattern of the studied membrane protein. Set the retraction distance depending on the length of the protein segments that are to be unfolded and subsequently refolded (*see* **Note 16**). Thereby take into account that the piezo travels a certain distance while the cantilever is in contact with the sample and deflected (Fig. 3).

   The distance of the second approach segment depends on the length of the first retract segment relative to the sample surface and should be chosen to end 5–10 nm above the contact point with the sample surface (*see* **Note 17**). Set the second pause at constant height for 1 s and the second retraction distance to ≥2 times the contour length of the studied membrane protein (Fig. 3).
3. Interrupt the measurement every 1–2 h to record a new topography. Ensure that the membrane patch is still intact and that the measurement area is still set on the correct sample position. Reposition the point grid if sample drift occurred.

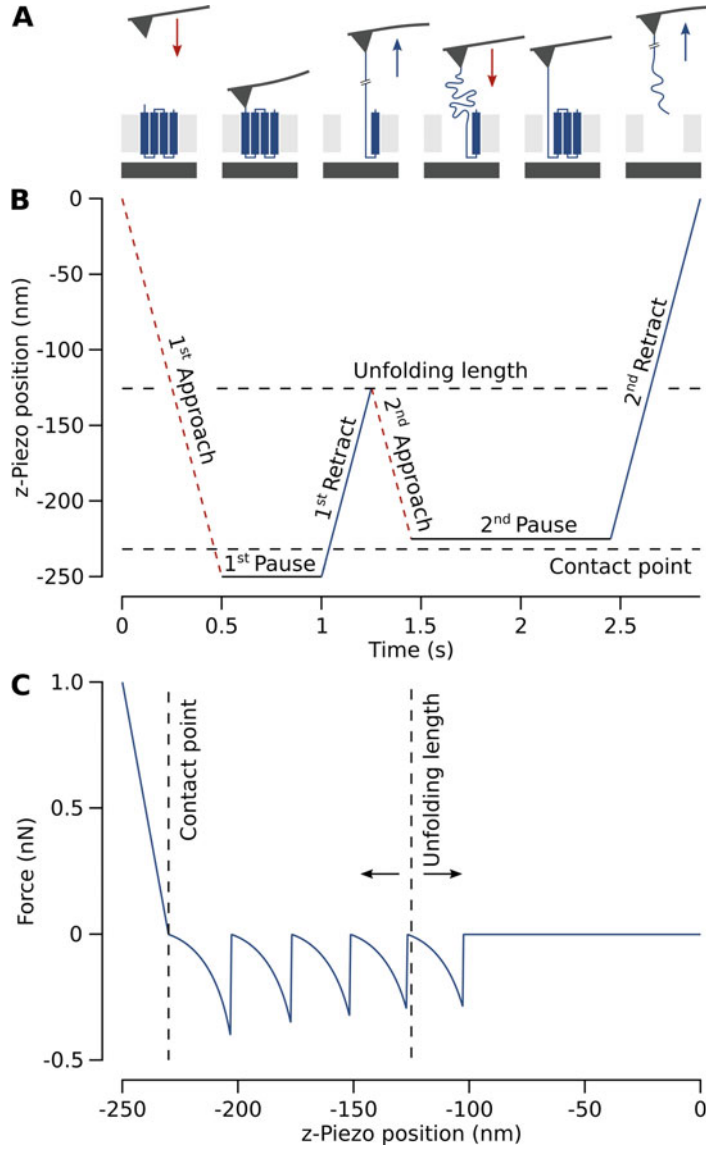

Fig. 3 Refolding setup. (**a**) Experimental sequence for protein refolding experiments. First, the cantilever is approached to and then pushed onto the membrane surface to facilitate the attachment of the membrane protein. Subsequent retraction of the cantilever induces unfolding of a predefined fraction of the protein. The unfolded protein is then held in close proximity of the membrane surface, upon which the unfolded polypeptide can reinsert into the membrane. The resulting fold is probed by unfolding the protein again. (**b**) Exemplary time sequence showing movement of the z-piezo during the experiment. The cantilever is approached with a velocity of 500 nm/s. A target force of 1 nN is maintained during the first pause segment for 0.5 s. Note that during the first pause segment, the cantilever is in contact with the sample surface. The cantilever is then retracted for 125 nm and re-approached for 100 nm, taking into account 20 nm the cantilever travels while in contact with the surface (see

3.4 Data Processing

1. Correct FD curves for cantilever deflection by subtracting the cantilever deflection from the z-piezo position to obtain the actual tip-sample separation (*see* **Note 18**). Correct for force offset by setting the non-contact regime of the FD curve to zero force. To this end use 20% of the data points in the non-contact regime of the FD curve most distant from the contact regime. Correct for distance offset by setting the contact regime of the FD curve to zero distance (*see* **Note 19**). For representation FD curves are typically oriented to display unfolding force peaks as positive forces. Flip FD curves if necessary.
2. Full unfolding events are typically registered only in a small fraction (<1/1000) of all recorded FD curves, while in the majority of the approach-retract cycles no protein adhered to the cantilever tip, which results in FD curves showing no significant force peaks. FD curves corresponding to protein unfolding events can be selected by applying an automated coarse filtering step to the data of the retract segment. To this end define a force threshold (>100 pN), which substantially exceeds the noise level of the FD curves and a distance threshold corresponding to >75% of the contour length of the membrane protein being unfolded (Fig. 4, *see* **Note 20**). For refolding experiments, set the distance threshold to >75% of the length of the first retract segment.
3. Inspect all resulting FD curves in order to select for FD curves showing the typical saw-tooth-shaped unfolding pattern corresponding to the stepwise unfolding of a membrane protein (Fig. 1) and sort out FD curves showing irregular force patterns.
4. The following detailed analysis of the resulting filtered dataset strongly depends on the type of experiment. Recently, several computational tools were developed to largely automate routine operations in the analysis and processing of force spectroscopy data, such as the alignment of FD curves, the automated fitting of force peaks, or the identification of unfolding pathways [22–24]. However, in particular the analysis of data obtained in refolding experiments remains a specialized task which needs to be adapted to the membrane protein under investigation.

Fig. 3 (continued) c) this places the cantilever 5 nm above the surface contact point. The cantilever is then held at this distance for 1 s and subsequently retracted for 225 nm. (**c**) Typical sawtooth-shaped series of force peaks as it occurs upon the stepwise unfolding of a membrane protein. Based on the unfolding pattern of the protein, the distance of the first retract segment can be chosen to unfold a predefined length of the protein (or the entire protein)

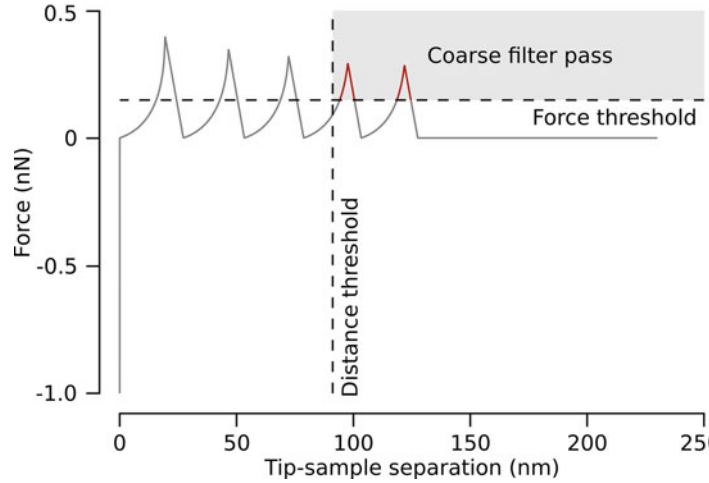

Fig. 4 Transformation and coarse filtering. FD curves are corrected for cantilever deflection shifted to zero force and zero distance. In order to select FD curves corresponding to the full unfolding of a membrane protein, a force threshold and a distance threshold corresponding to >75% of the contour length of the membrane protein being unfolded are defined (grey area). FD curves featuring force peaks within this region (red) pass the coarse filtering step and are taken into account for further analysis

4 Notes

1. Elongation of a terminus can also help to determine from which terminus the protein was unfolded in SMFS experiments since it strongly increases the probability of unfolding from the elongated terminus. Alternatively, this can be achieved through sequence alterations in the protein, e.g., through proteolytic cleavage or presence/absence of a disulfide bridge connecting two segments of the protein. Each of these alterations should result in a shift of either the entire or a part of the unfolding fingerprint pattern of the protein, which will allow determination of the unfolding direction.
2. Purple membrane from *H. salinarium* containing Bacteriorhodopsin at high density represents an ideal reference sample for newcomers, since it is commercially available (e.g., from Cube Biotech, Monheim am Rhein, Germany), easy to handle, and well-studied by SMFS, allowing direct comparison of the obtained results [9, 25].
3. The described method follows the procedure as carried out on a commercially available NanoWizard AFM (JPK Instruments, Berlin, Germany). However, it should be readily adaptable to most AFMs independent of model and manufacturer, under

the premise that a basic knowledge of the working principles of AFM is existing and instrument-specific routine procedures such as cantilever mounting, laser alignment, and cantilever calibration can be performed.

4. All parts of the AFM, all tools used to handle cantilevers, fluid cells, etc., as well as all glassware used to prepare buffers must be meticulously clean. This is best achieved by lathering all surfaces extensively using detergent solution, followed by rinsing them several times alternately with ethanol and deionized water and drying them in a stream of nitrogen or compressed air.
5. Ready-to-use mica discs are commercially available in various diameters (e.g., from Electron Microscopy Sciences, Hatfield, USA); however, they can also be prepared from mica sheets using a punch and die set.
6. A proteoliposome concentration of ~10 μg/mL should result in dense but separated membrane patches upon adsorption to mica for many membrane protein samples. Decrease the concentration and adsorption duration if the density is too high and overlapping membrane patches are observed. Increase the concentration and adsorption duration if only few membrane patches are observed. Adding divalent ions can also help to improve adsorption (add $MgCl_2$ or $CaCl_2$ at concentrations of up to 20 mM to the adsorption buffer).
7. Typically, the majority of proteoliposomes will break open to form supported bilayers when adsorbed to the mica surface. However, in some cases a large fraction remains intact. These unbroken proteoliposomes are then visible as bulky blobs, which protrude highly from the surface. If this is the case, one can make use of the AFMs ability to physically interact with the sample and repeatedly image the proteoliposomes in contact mode, iteratively increasing the imaging force until open bilayers become visible (*careful, might contaminate tip*). If this procedure remains ineffective, another approach can be breaking the proteoliposomes by sonication prior to adsorption using a bath sonicator. To this end several samples should be prepared with varying sonication time and power, in order to find a condition where the proteoliposomes are destabilized enough to form open bilayers on the mica surface but not fragmented. Increased osmotic pressure by using buffers with a reduced salt content during adsorption can aid the formation of open bilayers as well.
8. If large numbers of small particles are observed, clean all equipment thoroughly and ensure all buffers are free from contaminants. However, also the sample itself may contain particulate contaminations such as protein/lipid aggregates, other

precipitates, or dust particles. If contaminants are soluble, collect the proteoliposomes by centrifugation (rcf $> 20000 \times g$ for >30 min), remove the supernatant, and resuspend the membrane pellet in fresh buffer. If contaminants are insoluble, collect the precipitate by centrifugation (rcf $< 5000 \times g$ for <10 min), then recover the supernatant containing the proteoliposomes.

9. Proteoliposome preparations sometimes contain large populations of vesicles, which are too small to perform appropriate SMFS experiments. In such case it can help to repeatedly collect the proteoliposomes by centrifugation, remove the supernatant and resuspend the membrane pellet in fresh buffer. Thereby lower centrifugal forces and shorter centrifugation times help to select for larger proteoliposomes.
10. Prior to calibration, the instrument-specific set point (typically in V) corresponding to a force of 1 nN is not known but can be estimated from previous experience with cantilevers of the same type.
11. A velocity of 500 nm/s represents a good starting value, but of course the velocity can be varied. Choose the sampling rate for approach and retract segments to a value resulting in 8–10 data points per nm (e.g., 4096 Hz at 500 nm/s). Adjust the sampling rate accordingly to obtain an equal number of data points per distance if the velocity is changed.
12. The duration of the pause segment can be increased if a contact time of 0.5 s results in a very low probability of attaching a polypeptide to the cantilever (unfolding events registered in $\ll 1/1000$ of FD curves).
13. Calculate the contour length of the protein, which is the length at maximum extension, based on the protein sequence using a length of 0.36 nm per amino acid.
14. Replace the cantilever and/or prepare a fresh sample if multiple FD curves show irregular force patterns. Recording FD curves with a non-ideal setup rarely results in interpretable data and unnecessarily complicates downstream data processing.
15. Beware that a single protein species can yet result in more than one characteristic unfolding pattern, for example, if not all proteins are unfolded from the same terminus or if proteins are probed in different conformational states.
16. The protein can either be unfolded partially with the final segments remaining embedded in the lipid bilayer or fully. For partial unfolding, choose a retraction distance not exceeding the position of the last unfolding force peak. For full unfolding choose a retraction distance clearly exceeding the length of the fully stretched protein.

17. Decrease the approach distance used for the second approach if contact with the sample surface is observed (visible as a force increase close to the sample surface).
18. After correction, the contact regime of the FD curve should resemble a vertical line. If not, check whether the deflection sensitivity was determined correctly.
19. Data processing software included with commercially available AFMs should support these operations, otherwise they can be adapted from the procedure described by Bosshart et al. [26].
20. Check whether the AFM control software allows online-filtering of FD curves already during data acquisition. This way only FD curves passing the coarse-filtering step will be saved, which can substantially reduce the post-processing time.

Acknowledgment

We thank Nico Strohmeyer for proofreading the manuscript. Johannes Thoma was supported by a long-term European Molecular Biology Organization (EMBO) fellowship (ALTF 413-2018).

References

1. Binnig G, Quate C, Gerber C (1986) Atomic force microscope. Phys Rev Lett 56:930–934
2. Bippes CA, Muller DJ (2011) High-resolution atomic force microscopy and spectroscopy of native membrane proteins. Reports Prog Phys 74:086601
3. Butt HJ, Downing KH, Hansma PK (1990) Imaging the membrane protein bacteriorhodopsin with the atomic force microscope. Biophys J 58:1473–1480
4. Fotiadis D, Liang Y, Filipek S et al (2003) Atomic-force microscopy: rhodopsin dimers in native disc membranes. Nature 421:127–128
5. Hoogenboom BW, Suda K, Engel A, Fotiadis D (2007) The supramolecular assemblies of voltage-dependent anion channels in the native membrane. J Mol Biol 370:246–255
6. Shibata M, Yamashita H, Uchihashi T et al (2010) High-speed atomic force microscopy shows dynamic molecular processes in Photoactivated bacteriorhodopsin. Nat Nanotechnol 5:208–212
7. Kedrov A, Janovjak H, Sapra KT, Müller DJ (2007) Deciphering molecular interactions of native membrane proteins by single-molecule force spectroscopy. Annu Rev Biophys Biomol Struct 36:233–260
8. Engel A, Gaub HE (2008) Structure and mechanics of membrane proteins. Annu Rev Biochem 77:127–148
9. Oesterhelt F, Oesterhelt D, Pfeiffer M et al (2000) Unfolding pathways of individual bacteriorhodopsins. Science 288:143–146
10. Thoma J, Manioglu S, Kalbermatter D et al (2018) Protein-enriched outer membrane vesicles as a native platform for outer membrane protein studies. Commun Biol 1:23
11. Kedrov A, Ziegler C, Muller DJ (2006) Differentiating ligand and inhibitor interactions of a single antiporter. J Mol Biol 362:925–932
12. Bippes CA, Ge L, Meury M et al (2013) Peptide transporter DtpA has two alternate conformations, one of which is promoted by inhibitor binding. Proc Natl Acad Sci U S A 110:E3978–E3986
13. Serdiuk T, Sugihara J, Mari SA et al (2015) Observing a lipid-dependent alteration in single lactose permeases. Structure 23:754–761
14. Thoma J, Bosshart P, Pfreundschuh M, Müller DJ (2012) Out but not in: the large transmembrane β-barrel protein FhuA unfolds but cannot refold via β-hairpins. Structure 20:2185–2190
15. Kessler M, Gottschalk KE, Janovjak H et al (2006) Bacteriorhodopsin folds into the

membrane against an external force. J Mol Biol 357:644–654

16. Yu H, Siewny MGW, Edwards DT et al (2017) Hidden dynamics in the unfolding of individual bacteriorhodopsin proteins. Science 355:945–950
17. Kedrov A, Ziegler C, Janovjak H et al (2004) Controlled unfolding and refolding of a single sodium-proton antiporter using atomic force microscopy. J Mol Biol 340:1143–1152
18. Bosshart PD, Iordanov I, Garzon-Coral C et al (2012) The transmembrane protein KpOmpA anchoring the outer membrane of Klebsiella Pneumoniae unfolds and refolds in response to tensile load. Structure 20:121–127
19. Thoma J, Burmann BM, Hiller S, Müller DJ (2015) Impact of Holdase chaperones Skp and SurA on the folding of β-barrel outer-membrane proteins. Nat Struct Mol Biol 22:795–802
20. Serdiuk T, Steudle A, Mari SA et al (2019) Insertion and folding pathways of single membrane proteins guided by translocases and Insertases. Sci Adv 5:eaau6824
21. Butt H-J, Jaschke M (1995) Calculation of thermal noise in atomic force microscopy. Nanotechnology 6:1–7
22. Bosshart PD, Frederix PLTM, Engel A (2012) Reference-free alignment and sorting of single-molecule force spectroscopy data. Biophys J 102:2202–2211
23. Thoma J (2017) Unfolding and folding pathways of Escherichia Coli outer membrane proteins. PhD thesis (ETH Zürich). https://doi.org/10.3929/ethz-b-000214458
24. Galvanetto N, Perissinotto A, Pedroni A, Torre V (2018) Fodis: software for protein unfolding analysis. Biophys J 114:1264–1266
25. Müller D, Heymann J, Oesterhelt F et al (2000) Atomic force microscopy of native purple membrane. Biochim Biophys Acta 1460:27–38
26. Bosshart PD, Casagrande F, Frederix PLTM et al (2008) High-throughput single-molecule force spectroscopy for membrane proteins. Nanotechnology 19:384014

Chapter 24

Sample Preparation and Technical Setup for NMR Spectroscopy with Integral Membrane Proteins

Hundeep Kaur, Anne Grahl, Jean-Baptiste Hartmann, and Sebastian Hiller

Abstract

NMR spectroscopy is a method of choice to characterize structure, function, and dynamics of integral membrane proteins at atomic resolution. Here, we describe protocols for sample preparation and characterization by NMR spectroscopy of two integral membrane proteins with different architecture, the α-helical membrane protein MsbA and the β-barrel membrane protein BamA. The protocols describe recombinant expression in *E. coli*, protein refolding, purification, and reconstitution in suitable membrane mimetics, as well as key setup steps for basic NMR experiments. These include experiments on protein samples in the solid state under magic angle spinning (MAS) conditions and experiments on protein samples in aqueous solution. Since MsbA and BamA are typical examples of their respective architectural classes, the protocols presented here can also serve as a reference for other integral membrane proteins.

Key words Nuclear magnetic resonance, Solid-state NMR, Magic angle spinning NMR, MsbA, BamA, Protein reconstitution, Membrane proteins, Dynamics

1 Introduction

1.1 Structural Studies of Integral Membrane Proteins

Membrane proteins mediate essential biological processes, including signal transduction, cellular homeostasis, and metabolite transport, and they account for up to one-third of cellular proteomes [1], making them key targets for academic and pharmaceutical research [2]. To elucidate mechanisms underlying membrane protein function, it is essential to resolve interactions as well as dynamics of the protein backbone and individual side chains at the atomic level. This can be achieved by NMR spectroscopy, a technique that can provide structural and functional insights complementary to other structural biology techniques such as X-ray crystallography [3, 4], cryo-electron microscopy [5], and electron paramagnetic resonance [6–8]. In the past three decades, multidimensional NMR methods have been developed to facilitate structure determination of membrane proteins in aqueous solution [9, 10] and in the solid

Camilo Perez and Timm Maier (eds.), *Expression, Purification, and Structural Biology of Membrane Proteins*, Methods in Molecular Biology, vol. 2127, https://doi.org/10.1007/978-1-0716-0373-4_24,

state [11–13]. In addition, NMR spectroscopy efficiently provides spectral fingerprints of backbone and side chain moieties, which can be used to monitor changes in structure and dynamics upon ligand interaction and complex formation.

There are two main architectural classes of membrane proteins: α-helical and β-barrel membrane proteins [14, 15]. α-helical membrane proteins are the predominant architectural class in the prokaryotic, mitochondrial, and chloroplast inner membranes and in the eukaryotic plasma and endoplasmic reticulum (ER) membranes. For NMR studies, bacterial α-helical membrane proteins can often be overexpressed in a functional form into the inner membrane of *E. coli* and from there they can be extracted and transferred into a suitable membrane mimetic environment [16]. In contrast, β-barrel membrane proteins have their origin in the bacterial, mitochondrial, and chloroplast outer membranes. Most members of this class of proteins can be produced in high yields in *E. coli* inclusion bodies, from where they can frequently be refolded into their native conformation [17–19].

Due to the amphiphilic topology of biological membranes, integral membrane proteins comprise large hydrophobic as well as large hydrophilic patches on their surfaces. For biochemical and biophysical studies of membrane proteins, specific amphiphilic solubilization conditions, so-called membrane mimetics, are required to retain the native protein structure in the absence of the native membrane. These membrane mimetics can be composed of detergent and lipid molecules to form micelles, bicelles, or proteoliposomes [20–25]. Alternatively, amphiphilic polymers and lipids can form larger membrane-mimicking molecular assemblies, such as styrene maleic acid lipid particles (SMALPs) and lipid bilayer nanodiscs [26, 27].

In this chapter, we present a collection of protocols for sample preparation of two selected *E. coli* membrane proteins for NMR studies and a toolbox for basic solid-state and solution NMR experiments for their characterization. The two proteins are the α-helical membrane protein MsbA, an ABC-transporter from *E. coli* that is involved in the translocation of lipid A from cytosol to periplasm [28–30], and the outer membrane β-barrel protein BamA that is involved as the key catalytic unit in outer membrane protein biogenesis, i.e., folding and insertion into the outer membrane [31–34].

1.2 NMR Spectroscopy

1.2.1 Basic Experiments in Solid-State NMR

In solid-state NMR spectroscopy, spectral resolution and sensitivity are strongly determined by the orientation dependence of nuclear spin interactions, such as dipolar coupling or chemical shift anisotropy. In unoriented samples, these anisotropic interactions manifest as extremely broad resonance lines, making atomic resolution studies of proteins impossible. The obstacle can be overcome by subjecting the samples to a fast rotation around an axis that is tilted

relative to the static B_0-field of the spectrometer by the "magic" angle of 54.73°. Such "Magic Angle Spinning" (MAS) effectively reduces all anisotropic interactions because these show an angle dependency of $(3\cos^2\theta - 1)$, which is zero at the magic angle [35, 36]. MAS combined with high-power proton decoupling results in sharp resonance lines even for very big biomolecules. Traditionally, the rotors used for integral membrane proteins have a diameter of 4 or 3.2 mm, which can be spun at frequencies between 10 and 25 kHz, facilitating ^{13}C- and ^{15}N-detected experiments [35, 37–39]. Very recent developments have resulted in rotors with a diameter as small as 0.5 mm. These allow the use of spinning frequencies above 60 up to 110 kHz, which in turn allow ^{1}H-detected experiments, drastically increasing experimental sensitivity and resolution [40–45]. While methods exist to statically orient membrane proteins relative to the magnetic field [46–48], MAS is the method of choice for solid-state analysis for membrane proteins [49–52].

Two types of membrane mimetics are well suited for the reconstitution of membrane proteins for MAS-NMR: proteoliposomes and lipid bilayer nanodiscs [53–57]. The reconstitution of membrane proteins from detergent micelles into liposomes is typically achieved by a dilution approach with or without pre-destabilization of the lipid vesicles by suitable detergents [58–60].

A spectroscopic key technique to increase experimental sensitivity in MAS-NMR is cross-polarization (CP), which enhances the signal by a magnetization transfer from an abundant and sensitive nuclei such as ^{1}H to a dilute insensitive spin such as ^{13}C or ^{15}N (X-spins) by dipolar interactions [61–63]. Polarization transfer occurs when the ^{1}H and X spin lock fields fulfill the Hartmann–Hahn matching condition:

$$\omega_1^{\mathrm{H}} = \omega_1^{\mathrm{X}} \pm n\omega_{\mathrm{rot}}$$

where ω_1^{H} and ω_1^{X} are the ^{1}H and X nutation frequencies, ω_{rot} is the rotor spinning frequency and n is an integer. A CP transfer typically starts from the proton polarization, leading to an overall signal enhancement equivalent to the ratio of the gyromagnetic ratios $\gamma^{\mathrm{H}}/\gamma^{\mathrm{X}}$. The CP magnetization transfer is based on dipolar coupling and is efficient only for the rigid parts of the protein which do not experience local motion relative to the spinning rotor. Therefore, when detected on ^{13}C- or ^{15}N-channel, the experiment effectively acts as a motion filter to suppress signal from mobile segments of the sample. The experiment thus can provide an efficient first glance into the rigid segments of a protein [37].

The most common 2D MAS-NMR experiment to assess the quality of a protein sample is the proton-driven spin diffusion (PDSD), a homonuclear through-space correlation experiment

[64]. This experiment can provide qualitative conclusions about the sample based on cross peak size, line width, and sometimes can provide an approximate distance between the nuclei based on the mixing time. There are two kinds of heteronuclear correlation experiments, through-bond and through-space, which are generally employed. For sequential assignment of the protein backbone, through-bond heteronuclear correlation experiments (NCACX/NCOCX) are typically used [13, 65, 66]. In order to establish this correlation, the experiments employ two CP steps, first between ^{1}H and ^{15}N and then between ^{13}C and ^{15}N during the mixing step. This is followed by a DARR step to obtain information about the side chains [67, 68]. On the other hand, Transferred Echo Double Resonance (TEDOR) NMR is a method to measure heteronuclear dipolar couplings. In principle, this experiment is based on spin echoes, which interfere with the MAS averaging process and therefore recouple the averaged dipole couplings [69–71]. The intensity of signal depends on the strength of dipolar coupling, which in turn depends on the inverse third power of the internuclear distance r, i.e., as $1/r^3$. Therefore, the TEDOR experiment can be typically used to determine distances between nuclei under MAS conditions to structurally characterize the biomolecules [72].

1.2.2 Basic Experiments in Solution NMR

Solution NMR spectroscopy is a powerful technique that can be employed to investigate structure, function, and dynamics of membrane proteins in solubilized form. When molecules in solution undergo rotational molecular tumbling on the nanosecond timescale due to Brownian motion, it results in an NMR spectrum with sharp resonance lines. Inherent molecular tumbling slows down with increasing molecular size leading to rapid decay of signal and thus decreased resolution and sensitivity. It is therefore crucial to solution NMR that membrane mimetics with particle sizes as small as possible are chosen. Membrane proteins can typically be studied by solution NMR in detergent micelles, bicelles, or lipid bilayer nanodiscs [73].

Solution NMR spectroscopy of membrane proteins requires samples with a protein concentration in the range 10–1000 μM. Various experimental methods to maximize the molecular size limit in solution have been developed. On the spectroscopic side, these are the transverse relaxation optimized spectroscopy (TROSY) techniques, which minimize signal losses during the pulse sequence [74]. In addition, deuteration of proteins reduces dipolar couplings between spins and thus line broadening [75, 76]. Furthermore, segmental or selective labeling can reduce the signal overlap, which is especially relevant for α-helical regions [77–79]. Altogether, these techniques enable structural studies up to sizes of 50 kDa and functional studies up to several 100 kDa, in favorable cases up to 1 MDa [80–86]. For an initial characterization of samples and

for probing the conformational states at atomic level, spectra of backbone or side chain moieties are typically recorded and are often referred to as "fingerprint" spectra. Subsequent experiments include triple-resonance sequences that correlate spins through bonds for backbone assignment, and NOESY spectroscopy that correlates spins through space for structural information [87–91]. A large arsenal of different experiment is available to characterize protein dynamics of backbone or side chain moieties on different time scales from nanoseconds to seconds [87, 88, 90, 92–102].

A fingerprint spectrum of backbone amide moieties is obtained by correlating chemical shifts of amide nitrogen and amide proton in a two-dimensional experiment. For membrane proteins in detergent micelles, this is achieved in the most sensitive way with the 2D [^{15}N,^{1}H]-TROSY experiment, which has optimal relaxation properties due to its selection of specific magnetization transfer pathways [103–105]. Thereby, proper handling of the water resonance is essential to minimize magnetization losses due to spin diffusion [106, 107]. At the same time, NMR signals of detergent resonances can cause acquisition problems including spectral T_1-noise. These detergent signals can be handled by three different means. (1) A longitudinal z-filter gradient after the first INEPT step. (2) Selective presaturation of detergent resonances. (3) Use of deuterated detergents. In cases of high-molecular-weight assemblies, 2D [^{15}N,^{1}H]-CRIPT or 2D [^{15}N,^{1}H]-CRINEPT experiments may be useful alternatives to the 2D [^{15}N,^{1}H]-TROSY [82, 108, 109]. Alternatively, and in particular with upcoming ultra-high-field NMR spectrometers, ^{15}N-detected experiments may be a method of choice to record backbone amide fingerprints [110].

Fingerprint spectra of side chain methyl groups require suitable isotope labeling schemes. Classical side chain labeling protocols for isoleucines, valines, and leucines have recently been extended to alanines, methionines, and threonines [85, 111–113]. For production of suitable samples, the cells are grown in minimal medium with a combination of labeling molecules chosen for the desired labeling scheme [114–118]. The NMR pulse sequence employed to record the most sensitive fingerprint spectra of side chain methyl groups in proteins is a 2D [^{13}C,^{1}H]-HMQC with water handling, also referred to as a 2D [^{13}C,^{1}H]-TROSY [116]. Handling of detergent signals is as described for backbone amide spectra. The use of deuterated detergents is at the same time optimal for NOESY-type spectra to avoid spin diffusion. As a final measure, the recording in 100%-D_2O buffer further optimizes overall spectral sensitivity and quality by minimizing spin diffusion.

2 Materials

2.1 Medium and Stocks for Expression of Membrane Proteins

1. LB agar plates and LB medium (25 g/L).
2. Stocks: 1 M antibiotic solution, 1 M IPTG solution.
3. Minimal medium (amount/L), 10.5 g K_2HPO_4, 4.5 g KH_2PO_4, 0.5 g NaCl, 2 mM $MgSO_4$, 1 g ^{15}N-NH_4Cl, 2 g ^{13}C-Glucose, 0.01 mM $FeCl_3$, 1 mL vitamin solution∗∗.
4. Vitamin solution (amount/500 mL)∗∗, 100 mg $CaCl_2{\cdot}2H_2O$, 100 mg $ZnSO_4{\cdot}7H_2O$, 100 mg $MnSO_4{\cdot}H_2O$, 2.5 g Thiamine, 2.5 g Niacin, 50 mg Biotin.

2.2 Buffers for Purification and Reconstitution of MsbA

Prepare all buffers with ultrapure water and filter with 0.22 μm filter for storage. Add detergent from stock just before use.

1. Stocks: DDM 10% w/v, 1 M DTT.

2.2.1 Expression and Purification

2. Lysis Buffer (pH 7.5), 10 mM Tris–HCl, 250 mM Sucrose, 150 mM NaCl, 2.5 mM $MgSO_4$.
3. Resuspension Buffer (pH 7.3), 50 mM HEPES, 300 mM NaCl, 5 mM $MgCl_2$, 10 mM Imidazole, 10% w/v Glycerol. 1.25% w/v DDM added in powder.
4. Wash Buffer (pH 7.3), 50 mM HEPES, 300 mM NaCl, 5 mM $MgCl_2$, 50 mM Imidazole, 10% w/v Glycerol, 0.015% w/v DDM.
5. Elution Buffer (pH 7.3), 50 mM HEPES, 300 mM NaCl, 5 mM $MgCl_2$, 400 mM Imidazole, 10% w/v Glycerol, 0.015% w/v DDM.
6. SEC buffer (pH 7.3), 50 mM HEPES, 150 mM NaCl, 5 mM $MgCl_2$, 0.015% w/v DDM.
7. Lipid/ssNMR Buffer (pH 7.3), 50 mM HEPES, 50 mM NaCl, 0.015% w/v DDM.

2.2.2 Reconstitution

1. Dry lipid powder stocks stored at −20 °C.
2. Chloroform: Methanol mixture in the ratio of 2:1 v/v.
3. Water bath.
4. Lipid Extruder with membranes of different pore sizes (Avanti lipids).
5. 10% w/v DDM stock.
6. Biobeads (SM2, 20–50 mesh; Bio-Rad).

2.2.3 MAS Rotor Packing

1. Beckman Coulter ultracentrifuge with SW Ti60 Rotor.
2. MAS rotor 4 mm or 3.2 mm Zirconia with vespel caps.

2.3 Buffers for Purification and Refolding of BamA

1. Buffer 1 (pH 8.0), 50 mM Tris–HCl, 300 mM NaCl.
2. Buffer 2 (pH 8.0), 50 mM Tris–HCl, 300 mM NaCl, 6 M Guanidine-HCl.
3. Buffer 3 (pH 8.0), 50 mM Tris–HCl, 300 mM NaCl, 6 M Guanidine-HCl, 200 mM Imidazole.
4. Buffer 4 (pH 8.0), 50 mM Tris–HCl, 300 mM NaCl, 500 mM Arginine, 0.5% w/v LDAO, 10 mM DTT.
5. Buffer 5 (pH 8.0), 50 mM Tris–HCl.
6. Ion Exchange Buffer A (pH 8.0), 50 mM Tris–HCl, 0.1% w/v LDAO.
7. Ion Exchange Buffer B (pH 8.0), 50 mM Tris–HCl, 500 mM NaCl, 0.1% w/v LDAO.
8. NMR Buffer (pH 7.5), 20 mM NaPi, 150 mM NaCl, 0.1% w/v LDAO, 5% v/v D_2O.

3 Methods

3.1 Overexpression of Membrane Proteins in Bacteria

Following crucial parameters should be considered for optimizing the expression of a membrane protein in *E. coli* cells for NMR spectroscopy:

1. Type of *E. coli* expression strain (*see* **Note 1**).
2. Composition of the minimal medium including isotope labeling (*see* **Note 2**) [119].
3. Concentration of the inducing agent, temperature, and duration of overexpression [16].

3.2 Expression of the α-Helical Membrane Protein MsbA [120]

1. Transform a pET19b plasmid encoding MsbA with an N-terminal 10XHis-tag and a linker peptide (-SSGHIDDDDKH-) in C43(DE3) cells.
2. Inoculate 1 L LB medium with a 10 mL overnight preculture and incubate at 37 ° C, 220 rpm until OD_{600} reaches 0.6 (*see* **Note 2**).
3. Harvest cells by centrifugation at 5,000 × *g* for 10 min at 4 °C. In order to remove the traces of LB medium, wash the cell pellet by resuspending in 15 mL minimal medium and pelleting by centrifugation.
4. Resuspend the final cell mass from 1 L LB medium in 500 mL isotope-labeled minimal medium and incubate at 37 ° C, 220 rpm.
5. After 1 h, induce protein overexpression by adding 1 mM IPTG at 20 °C for 17 h.
6. Harvest cells by centrifugation at 5,000 × *g* for 10 min at 4 °C.

7. Weigh cell pellet and resuspend in the lysis buffer along with protease inhibitor and 1 mM DTT.
8. Lyse cells using a constant cell systems cell disruptor by passaging at 1.5 kbar for 2–3 times. Centrifuge the suspension at 8′000 g for 15 min to remove cell debris.
9. Ultracentrifuge supernatant at 140,000 × *g*, 4 °C, for 1 h.
10. Discard supernatant. Solubilize membrane pellet using the resuspension buffer + 1.25% w/v DDM for 17 h.
11. Ultracentrifuge the solution at 140,000 × *g*, 4 °C, for 1 h to separate the lipids from solubilized protein.
12. Load the supernatant on Ni-NTA beads preequilibrated with wash buffer.
13. After 2 h incubation, wash the beads with five column volumes of wash buffer to remove nonspecifically bound proteins.
14. Elute MsbA using 2–3 column volumes of elution buffer.
15. Run the purified protein on an S200 size-exclusion column to obtain a pure homogenous protein in 0.015% w/v DDM. Characterize the purified protein using MALDI mass spectrometry (Fig. 1a, b).

3.3 Reconstitution of MsbA into a Lipid Bilayer

1. Weigh calculated amounts of lipids (DMPC:DMPA in the ratio of 9:1) for a final lipid:protein ratio of 75:1 mol/mol in a clean dried round-bottomed flask and solubilize in a 2:1 chloroform: methanol mixture.
2. Dry lipid-containing solution under a continuous nitrogen flow and overnight in vacuum rotary evaporator. This step ensures the complete absence of the organic solvent.
3. Resuspend the lipids in the lipid buffer/ssNMR (at a concentration of 4 mg/mL) at 27 °C, i.e., above the transition temperature of the lipids forming multilamellar liposome (LMVs), which is 25 °C.
4. For initial optimization extrude the resuspended solution through membranes with pore sizes of 0.4 μm, 0.2 μm, and 0.1 μm to test for homogeneity of reconstituted sample (*see* **Note 3**).
5. Reconstitute 5 mg MsbA in 0.015% w/v DDM into DMPC: DMPA (9:1) liposomes by increasing DDM concentration for each sample until the liposome solution becomes clear and then adding protein solution to the softened lipids in a dropwise manner (Fig. 1c).
6. Wash biobeads thoroughly with water and store in NMR buffer for long-term use. For each preparation, remove the detergent by incubation with ~80 mg/mL of wet biobeads in a two- to three-step process over a total time period of 16–18 h.

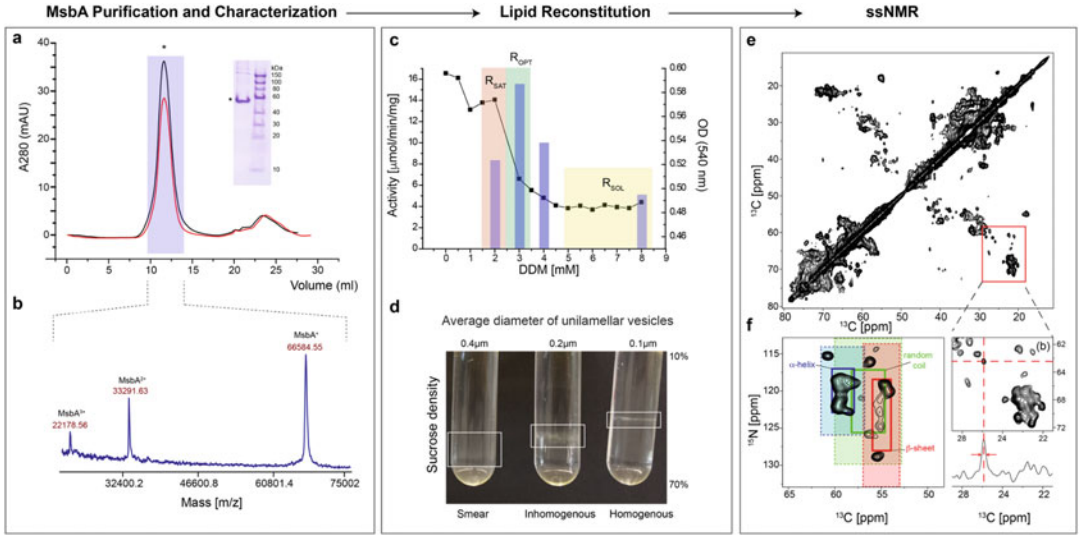

Fig. 1 Sample preparation and MAS-NMR of the α-helical membrane protein MsbA. (**a**) Size-exclusion chromatogram of purified MsbA in 0.015% w/v DDM along with SDS-PAGE of the same sample. (**b**) MALDI mass spectrum of the sample after size-exclusion chromatography. (**c**) Determination of the optimal DDM concentration (R_{OPT}) for destabilization of 9:1 DMPC:DMPA liposomes for homogenous MsbA proteoliposome preparation. The black solid squares connected by solid line show changes in optical density 540 nm. Liposomes are fully saturated still maintaining their vesicular state at R_{SAT} and fully solubilized in DDM at R_{SOL}. At each point of detergent concentration, ATPase activity of the protein in proteoliposomes was measured. Based on that an optimal DDM concentration called R_{OPT} corresponding to maximum ATPase activity was determined. This assay is based on [60]. (**d**) Sucrose density gradients (10–70% w/v) on MsbA reconstituted in lipids extruded through different pore size. Based on the distribution of proteoliposome particles in the gradient, the sample has reduced homogeneity as the size of extruded lipid vesicles increase from 0.1 µm to 0.4 µm. (**e**) Aliphatic region of a [^{13}C,^{13}C]-PDSD spectrum acquired using 20 ms mixing time on reconstituted [^{13}C,^{15}N-DEQGHKTS]-MsbA. The inset shows a representative isolated peak with a linewidth of 106 Hz at half height. (**f**) [^{15}N,^{13}C]-NCA spectrum of [^{13}C,^{15}N-K]-MsbA. Spectral areas with peaks from different secondary structure elements of the protein are highlighted. All spectra were acquired at 11.4 kHz sample spinning at –3 °C on a 600 MHz Avance spectrometer equipped with a 4 mm E-free MAS probe

7. Analyze the resulting proteoliposomes for homogeneity by a sucrose gradient (10–70% w/v).
   (a) This gradient is prepared by layering 1 mL of 10, 30, 50, and 70% w/v sucrose in lipid buffer.
   (b) Add sample (400 µl) on the top of gradient and centrifuge at 14,000 × *g* in a swing bucket rotor for 16 h at 4 °C.

   Under the given conditions, MsbA is most homogenously incorporated by 0.1 µm lipid vesicles (Fig. 1d).
8. Assay protein functionality by measuring the ATPase activity:
   (a) Incubate MsbA and ATP (5 mM) in buffer with 10 mM $MgCl_2$ at 37 °C for 20 min. Keep control samples for each reaction on ice.

(b) Quench the reaction by adding 12% w/v SDS solution.

(c) Measure the release of inorganic phosphate (Pi) using the molybdenum blue method [120, 121].

Based on these optimizations, the finalized protocol used for preparing the reconstituted NMR sample is as follows:

1. Soften the extruded lipids with 3 mM DDM for 20 mins with continuous stirring at 25–27 °C.
2. Add the protein (<1 mg/mL) dropwise to the stirring lipids and incubate at room temperature for 30 mins.
3. Remove detergent by adding biobeads (80 mg/mL) three times, first time at 4 °C for overnight, i.e., 16 h and then twice at room temperature for 2 h each.
4. Remove biobeads using a cell sorting filter and centrifuging at 1,000 × *g* for 10 mins.

3.4 Packing the Sample into MAS-NMR Rotor

1. Concentration of proteoliposomes without the ultracentrifugal packing tool:
   (a) Pellet the buffer-suspended liposomes via high-speed centrifugation (up to 100,000 × *g*).
   (b) Discard the supernatant. The proteoliposome pellet has a gel-like consistency.
   (c) Resuspend the proteoliposome pellet in small amounts of buffer to get the final desired concentration in lesser volumes.
2. Concentration of proteoliposomes by the use of swinging bucket ultracentrifugal packing tool [53].
   (a) Place an empty MAS rotor without cap into the open packing tool.
   (b) Pipet the aqueous sample suspension into the device.
   (c) The device may be inserted into an empty centrifuge tube, in order to catch inadvertent sample leakage.

A detailed review of how these tools are used has been provided by Mandal et al. [122].

3.5 An Optimized Protocol for the Expression of the β-Barrel Membrane Protein BamA

1. Transform a pET15b-based plasmid encoding BamA construct (residues 426–810 of wt-BamA plus an initial methionine residue and without any expression tags) into BL21 Lemo cells. Alternatively, the construct $BamA^{+9}$ can be used (above construct plus 9 additional residues MENVALDFS at the C-terminus).
2. Inoculate 1 L minimal medium with 10 mL overnight preculture and incubate at 37 ° C, 220 rpm, until OD_{600} reached 0.8.

3. Induce protein overexpression by adding 1 mM IPTG at 37 °C for 5 h.
4. Harvest cells by centrifugation at 5,000 × *g* for 10 min at 4 °C.
5. Resuspend cell pellet in Buffer 1, freshly supplemented with lysozyme (0.5–1 mg/mL), DNase I, and protease inhibitors.
6. Lyse cells by sonication on ice and centrifuge for 30 min at 16,000 × *g*.
7. Solubilize the inclusion bodies in Buffer 2.
8. After 1 h of centrifugation at 16,000 × *g*, mix supernatant with 5 mL of Ni-beads (Genscript) for 1 h at room temperature.
9. Elute protein using Buffer 3.
10. Dialyze eluate against ultrapure H_2O overnight with a snakeskin membrane of 3.5 kDa molecular weight cutoff (MWCO) and resuspend the precipitate in Buffer 2.
11. Dilute BamA to 5 mg/mL and add DTT to a final concentration of 10 mM prior to refolding.

3.6 Refolding and Purification of BamA

1. Refold at 4 °C by dropwise addition of 20 mL of the BamA/6 M Gdm-HCl solution into 80 mL of Buffer 4 while stirring the refolding solution to a final protein concentration of 1 mg/mL.
2. Stir solution for another 24 h and dialyze against Buffer 5 with a snakeskin membrane of 3.5 kDa cutoff.
3. Apply BamA to a HiTrap Q HP ion exchange column (GE) preequilibrated with Ion Exchange Buffer A. Elute the protein with a step gradient of Ion Exchange Buffer B (0% B, 40% B, 65% B, 100% B). Well-refolded protein elutes between 40 and 65% B (Fig. 2a).
4. Pool the eluted fractions and concentrate using a concentrator with 30 kDa MWCO to protein concentrations of 500 μM. Exchange buffer to NMR Buffer (Fig. 2b).
5. Freeze samples and store at −80 ° C.
6. Prior to measurements, thaw samples and fill into Shigemi NMR tubes.

3.7 Toolbox of MAS-NMR Experiments for Membrane Proteins

3.7.1 Cross Polarization

1. Adjust temperature of the NMR probe to a desired value.
2. Check that the cap of the rotor is properly closed and that the magic angle is correctly adjusted.
3. Insert sample into the NMR magnet and start spinning the rotor at desired frequency. Make sure that the spinning and the temperature are stable (*see* **Note 4**).
4. Match resonance conditions of the resonance circuits on all channels.

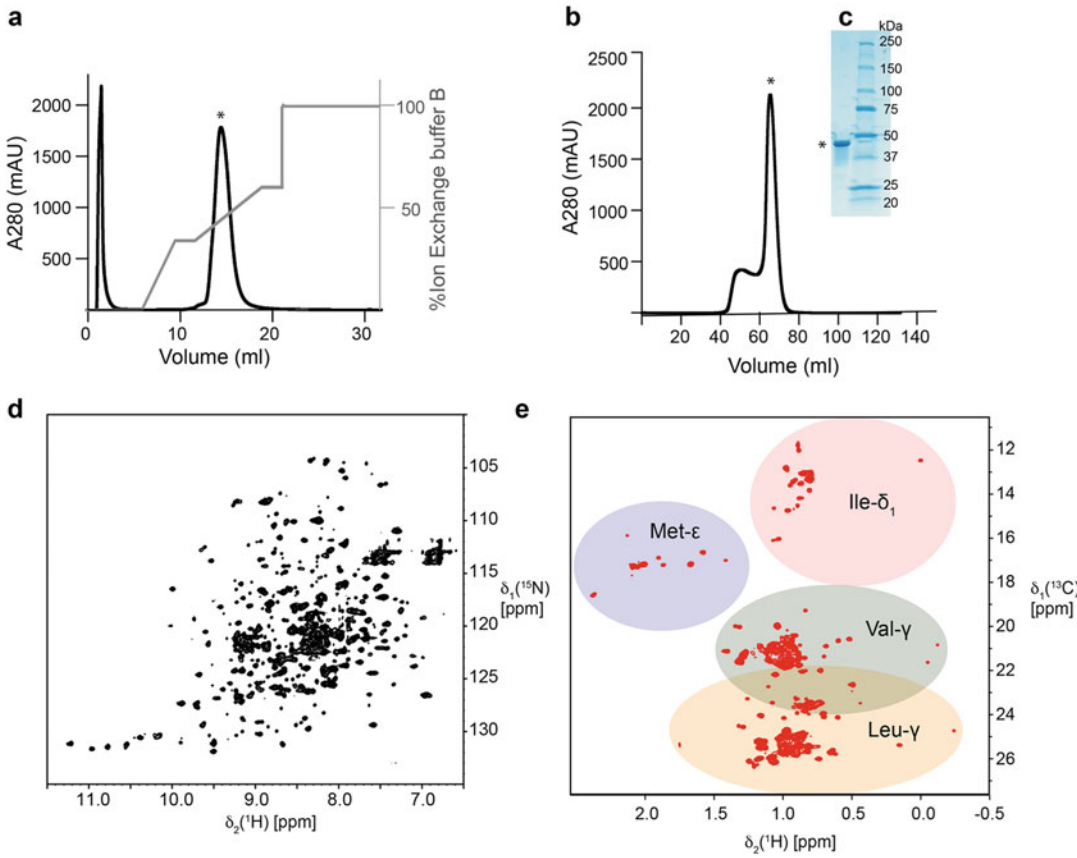

Fig. 2 Sample preparation and solution NMR spectroscopy of the β-barrel membrane protein BamA. (**a**) Ion exchange elution profile of refolded BamA in 0.1% w/v LDAO from a HiTrap Q 5 mL HP column. The asterisks in a–c indicate the position of BamA. (**b**) Size-exclusion chromatogram of BamA. (**c**) SDS-PAGE of purified BamA in 0.1% w/v LDAO micelles. (**d**) 2D [^{15}N,^{1}H]-TROSY spectrum of BamA in LDAO detergent recorded on a 700 MHz Bruker spectrometer equipped with a cryogenic probe at 37 °C. (**e**) 2D [^{13}C,^{1}H]-HMQC spectrum of [*U*-^{2}H, ^{1}H$_3$^{13}C-MILV]-labeled BamA^{+9} in LDAO detergent micelles. The typical spectral regions of different side chain types are marked in color

5. Homogenize the magnetic field across the sample volume by adjusting the shim coil currents.
6. In order to record the first 1D MAS-NMR spectrum, conditions for polarization transfer from ^{1}H and X spin lock fields fulfilling the Hartmann–Hahn matching conditions are optimized [123]. This is done by first setting the offset of X-channel corresponding to the frequency of signal of interest.
7. Determine the radio frequency (rf) power of the proton 90° pulse.
8. Determine the rf power of the X-channel 90° pulse.
9. Use these values as a starting condition for obtaining the CP condition on X-channel.

10. Thereafter, optimize the following parameters to maximize polarization transfer:
    (a) Power level for CP power on X-channel.
    (b) Power level for CP power on ^{1}H-channel.
    (c) Pulse length of CP for the specific rotation frequency.
11. Sharper line shapes can be obtained by using SPINAL64 decoupling sequence on the ^{1}H-channel while acquisition of the signal [124].

3.7.2 Homonuclear Through Space Correlation Spectroscopy: Proton-Driven Spin Diffusion (PDSD)

1. Set up CP transfer as described above. Spin diffusion is driven by protons; therefore, no decoupling is carried out during this step in the PDSD experiment.
2. Select mixing time.
    (a) Shorter mixing times (10–20 ms) lead to intraresidue magnetization transfer, i.e., up to two covalent bonds.
    (b) Longer mixing times (500 ms –1 s) lead to inter-residue magnetization transfer.

An example spectrum of [^{13}C,^{15}N-DEQGHKTS]-labeled MsbA is shown in Fig. 1e.

3.7.3 Heteronuclear Correlation for Sequential Assignment (NCACX/ NCOCX)

1. Set up the ^{1}H, ^{15}N CP as described above.
2. Adjust to the NCA/NCO match by setting the ^{15}N-offset on the resonance of amide backbone and ^{13}C-offset corresponding to CA or CO resonance, respectively, considering the matching condition:

$$\omega_{\mathrm{RF}}^{\mathrm{N}} = \frac{5}{2}\omega_r \quad \omega_{\mathrm{RF}}^{\mathrm{CA}} = \frac{3}{2}\omega_r \quad \omega_{\mathrm{RF}}^{\mathrm{CO}} = \frac{7}{2}\omega_r$$

ω_r = spinning frequency

3. Apply rotational recoupling in the form of DARR [67, 68], to achieve magnetization transfer from CA or CO to the side chains. Recover the ^{13}C–^{1}H dipolar interaction by CW irradiation on ^{1}H with rf field intensity satisfying the rotary-resonance condition $\omega_{1\mathrm{H}} = \omega_{\mathrm{MAS}}$ [125].

An example NCA spectrum of selectively [^{13}C,^{15}N-K]-labeled MsbA is shown in Fig. 1f.

3.7.4 Heteronuclear Dipolar Coupling: TEDOR (Transferred Echo Double Resonance) NMR

1. Adjust the parameters for optimal ^{1}H and ^{13}C CP transfer.
2. Adjust the value for ^{13}C and ^{15}N hard pulses and mixing time, considering that the experiment requires rotor-synchronized 180° pulses (l0; for details of parameters and pulse sequence, please refer [72]).

3.8 Toolbox of Basic Solution NMR Experiments for Membrane Proteins

3.8.1 2D [^{15}N,^{1}H]-TROSY

1. Adjust temperature of the NMR probe to a desired value.
2. Insert sample into the NMR magnet.
3. Activate field-frequency lock. Adjust field lock parameters.
4. Match resonance conditions of the resonance circuits on all channels.
5. Homogenize the magnetic field across the sample volume by adjusting the shim coil currents.
6. Determine the proton 90° pulse on the water resonance.
7. Determine the length and duration of soft pulses for water flip-back.
8. Insert all values into the 2D [^{15}N,^{1}H]-TROSY and adjust final Watergate interactively [126].
9. Adjust spectral resolution and number of transients.
10. Record experiment.

A 2D [^{15}N,^{1}H]-TROSY spectrum of 300 μM BamA in LDAO is shown in Fig. 2d.

3.8.2 Side Chain Methyl Groups' Fingerprint Spectra

1. Prepare a sample with suitable isotope labeling of the side chains of interest (*see* **Note 5**).
2. Repeat **steps 1**–**7** from above.
3. Insert values into the 2D [^{13}C,^{1}H]-HMQC pulse sequence and adjust water suppression interactively [127].
4. Adjust number of transients and spectral resolution.
5. Record experiment.

A 2D [^{13}C,^{1}H]-HMQC spectrum of 300 μM of [U-^{2}H, $^{1}H_3{}^{13}$C-MILV]-labeled BamA in LDAO is shown in Fig. 2e.

4 Notes

1. *E. coli* is the organism of choice for expression of most membrane proteins for NMR studies, due to a variety of available options for uniform and selective labeling. A major caveat with heterologous expression of recombinant membrane protein constructs can be aggregation of the protein in cytoplasm. Generally, it has been established that the T7 RNA polymerase-based expression system is a successful and efficient system leading to high yields of proteins based on IPTG induction. *E. coli* strains that have been successfully used from membrane protein production are BL21(DE3)-derived strains such as C41(DE3) and C43(DE3) [128]. Very recently two more strains have been isolated, namely C44(DE3) and C45(DE3), which have been shown to improve the yield and quality of

several bacterial membrane proteins [129]. In addition the overexpression for a membrane proteins can be improved based on screening of expression temperature, inducer concentrations, and duration of overexpression [16].

2. NMR measurements require proteins labeled with NMR-active nuclei, several of which are of low natural abundance such as 0.4% for nitrogen-15, or 1.109% for carbon-13. Therefore, proteins have to be produced in minimal medium supplemented with ^{15}N-ammonium chloride as the nitrogen source and ^{13}C-glucose or ^{13}C-glycerol as the carbon source. A substantial increase in protein yields can be obtained by inducing protein expression at unusually high cell densities in minimal medium. Such densities are obtained by growing the cells in unlabeled medium until an OD_{600} of 0.6, and then transferring the cells into half the volume of a freshly prepared minimal medium with appropriate isotope labeling [130]. Recently, it has also been shown that increasing the buffering capacity of the minimal medium can increase protein yields by up to twofold [119]. Since α-helical segments of proteins generally feature low signal dispersion in the amide proton compared to β-sheets, amide-based experiments of α-helical membrane proteins suffer particularly from spectral crowding. One way to decrease the number of resonances is by using a specifically labeled ^{13}C source such as (1,3-^{13}C)-glycerol or (2-^{13}C)-glycerol [131, 132] or 10% Glucose [133] in the minimal medium. To reduce spectral crowding further, residue-specific labeling schemes can be employed by adding specific amino acids to minimal medium [134, 135].
3. Three crucial protein-dependent parameters should be optimized to obtain a stable sample preparation for MAS-NMR:
   (a) Lipid composition for stability
   Different lipids and lipid mixtures with varying head group and acyl chain length can be tested for the stability of the protein.
   (b) Vesicle size for homogenous protein insertion
   Multilamellar liposomes are often an undesirable form of proteoliposomes and therefore it is necessary to create unilamellar vesicles of defined size for reconstitution of membrane proteins. There are SUVs (small unilamellar vesicles) and LUVs (large unilamellar vesicles) that can be generated by the following methods:
   SUVs can typically be formed by sonication in a water-bath set above the phase transition temperature of lipids. This generates a clear solution containing vesicles of 30–50 nm diameter.

LUVs can be formed by repeatedly extruding the lipid mixture through a polycarbonate membrane with a specific pore size.

(c) Lipid-to-protein ratio

Achieving low lipid-to-protein ratios of proteoliposomes is key to maximize the amount of protein in the filled rotor. The optimal lipid-to-protein ratio is the minimal value at which the protein is stable and functional. Maximal filling of the rotor maximizes experimental sensitivity and thus minimizes the acquisition time of the experiments.

4. For proteoliposomal sample, initial sample spinning can be unstable until the sample is uniformly distributed in the rotor. Therefore, it is suggested to start spinning at lower frequency like 5000 Hz until the spinning is stable and then increase it to desired value. If the spinning does not stabilize within a minute, it is essential to stop the spinning and take the rotor out. At this point following things can cause an instability:

   (a) Cap of the rotor is either damaged or not properly closed.

   (b) The rotor is not marked properly at the bottom.

   Notably for MsbA, experiments under MAS conditions have been performed at low probe temperatures, and the sample is not frozen because rotor spinning and pulses generate heat, thus the actual temperature of the measured sample is between 10 and 15 °C. The low temperature minimizes residual protein dynamics and preserves the sample stability. For temperature-sensitive samples and kinetic experiments, the temperature calibration should be done before every measurement.

5. For selective $^{13}CH_3$-labeling of methyl groups on a deuterated background, two schemes can be distinguished, which differ in the labeling of the other carbon nuclei of the side chain. These other nuclei can be uniformly ^{12}C-labeled ("NOESY-type labeling") or uniformly ^{13}C-labeled ("COSY-type labeling"). COSY-type labeling allows for correlation experiments of the methyl groups to the backbone nuclei [136–138], however, at the cost of a one-bond $J_{C\text{-}C}$ coupling between the methyl group of interest and to the adjacent carbon (Cγ in isoleucine, Cβ in valine, Cγ in leucine). This $J_{C\text{-}C}$ coupling is difficult or impossible to refocus during chemical shift evolution periods in ^{13}C-filtered NOESY experiments, leading to magnetization loss and multiplet line broadening. NOESY-type labeling removes these couplings, leading to optimized spectral quality in NOESY experiments. The different labeling schemes are achieved by expressing the protein in medium of either ^{12}C- or ^{13}C-glucose and with suitably labeled precursor compounds for amino acid biosynthesis [114, 117, 139–141].

Acknowledgment

This work was supported by the Swiss National Science Foundation and the NFP 72 (grants 31003A_166426 and 407240_167125 to S.H.).

References

1. Wallin E, von Heijne G (1998) Genome-wide analysis of integral membrane proteins from eubacterial, archaean, and eukaryotic organisms. Protein Sci 7(4):1029–1038. https://doi.org/10.1002/pro.5560070420
2. Lundstrom K (2007) Structural genomics and drug discovery. J Cell Mol Med 11 (2):224–238. https://doi.org/10.1111/j.1582-4934.2007.00028.x
3. Muchmore SW, Sattler M, Liang H, Meadows RP, Harlan JE, Yoon HS, Nettesheim D, Chang BS, Thompson CB, Wong SL, Ng SL, Fesik SW (1996) X-ray and NMR structure of human Bcl-xL, an inhibitor of programmed cell death. Nature 381 (6580):335–341. https://doi.org/10.1038/381335a0
4. Hartmann JB, Zahn M, Burmann IM, Bibow S, Hiller S (2018) Sequence-specific solution NMR assignments of the beta-barrel Insertase BamA to monitor its conformational Ensemble at the Atomic Level. J Am Chem Soc 140(36):11252–11260. https://doi.org/10.1021/jacs.8b03220
5. Sborgi L, Ravotti F, Dandey VP, Dick MS, Mazur A, Reckel S, Chami M, Scherer S, Huber M, Bockmann A, Egelman EH, Stahlberg H, Broz P, Meier BH, Hiller S (2015) Structure and assembly of the mouse ASC inflammasome by combined NMR spectroscopy and cryo-electron microscopy. Proc Natl Acad Sci U S A 112(43):13237–13242. https://doi.org/10.1073/pnas.1507579112
6. Kaur H, Abreu B, Akhmetzyanov D, Lakatos-Karoly A, Soares CM, Prisner T, Glaubitz C (2018) Unexplored nucleotide binding modes for the ABC exporter MsbA. J Am Chem Soc 140(43):14112–14125. https://doi.org/10.1021/jacs.8b06739
7. Wiegand T, Lacabanne D, Keller K, Cadalbert R, Lecoq L, Yulikov M, Terradot L, Jeschke G, Meier BH, Bockmann A (2017) Solid-state NMR and EPR spectroscopy of Mn(2+)-substituted ATP-fueled protein engines. Angew Chem Int Ed Engl 56 (12):3369–3373. https://doi.org/10.1002/anie.201610551
8. Hellmich UA, Lyubenova S, Kaltenborn E, Doshi R, van Veen HW, Prisner TF, Glaubitz C (2012) Probing the ATP hydrolysis cycle of the ABC multidrug transporter LmrA by pulsed EPR spectroscopy. J Am Chem Soc 134(13):5857–5862. https://doi.org/10.1021/ja211007t
9. Liang B, Tamm LK (2007) Structure of outer membrane protein G by solution NMR spectroscopy. Proc Natl Acad Sci U S A 104 (41):16140–16145. https://doi.org/10.1073/pnas.0705466104
10. Hiller S, Garces RG, Malia TJ, Orekhov VY, Colombini M, Wagner G (2008) Solution structure of the integral human membrane protein VDAC-1 in detergent micelles. Science 321(5893):1206–1210. https://doi.org/10.1126/science.1161302
11. Lee M, Wang T, Makhlynets OV, Wu Y, Polizzi NF, Wu H, Gosavi PM, Stohr J, Korendovych IV, DeGrado WF, Hong M (2017) Zinc-binding structure of a catalytic amyloid from solid-state NMR. Proc Natl Acad Sci U S A 114(24):6191–6196. https://doi.org/10.1073/pnas.1706179114
12. Milikisiyants S, Wang S, Munro RA, Donohue M, Ward ME, Bolton D, Brown LS, Smirnova TI, Ladizhansky V, Smirnov AI (2017) Oligomeric structure of Anabaena sensory rhodopsin in a lipid bilayer environment by combining solid-state NMR and long-range DEER constraints. J Mol Biol 429(12):1903–1920. https://doi.org/10.1016/j.jmb.2017.05.005
13. Pauli J, Baldus M, van Rossum B, de Groot H, Oschkinat H (2001) Backbone and side-chain 13C and 15N signal assignments of the alpha-spectrin SH3 domain by magic angle spinning solid-state NMR at 17.6 tesla. Chembiochem 2(4):272–281
14. Karyolaimos A, Ampah-Korsah H, Zhang Z, de Gier JW (2018) Shaping Escherichia coli for recombinant membrane protein production. FEMS Microbiol Lett 365(15). https://doi.org/10.1093/femsle/fny152

15. von Heijne G (1999) Recent advances in the understanding of membrane protein assembly and structure. Q Rev Biophys 32(4):285–307
16. Drew D, Lerch M, Kunji E, Slotboom DJ, de Gier JW (2006) Optimization of membrane protein overexpression and purification using GFP fusions. Nat Methods 3(4):303–313. https://doi.org/10.1038/nmeth0406-303
17. Bannwarth M, Schulz GE (2003) The expression of outer membrane proteins for crystallization. Biochim Biophys Acta 1610(1):37–45
18. Tamm LK, Hong H, Liang B (2004) Folding and assembly of beta-barrel membrane proteins. Biochim Biophys Acta 1666 (1–2):250–263. https://doi.org/10.1016/j.bbamem.2004.06.011
19. Hiller S, Abramson J, Mannella C, Wagner G, Zeth K (2010) The 3D structures of VDAC represent a native conformation. Trends Biochem Sci 35(9):514–521. https://doi.org/10.1016/j.tibs.2010.03.005
20. Raschle T, Hiller S, Etzkorn M, Wagner G (2010) Nonmicellar systems for solution NMR spectroscopy of membrane proteins. Curr Opin Struct Biol 20(4):471–479. https://doi.org/10.1016/j.sbi.2010.05.006
21. Sanders CR 2nd, Landis GC (1995) Reconstitution of membrane proteins into lipid-rich bilayered mixed micelles for NMR studies. Biochemistry 34(12):4030–4040. https://doi.org/10.1021/bi00012a022
22. Prosser RS, Evanics F, Kitevski JL, Al-Abdul-Wahid MS (2006) Current applications of bicelles in NMR studies of membrane-associated amphiphiles and proteins. Biochemistry 45(28):8453–8465. https://doi.org/10.1021/bi060615u
23. Brown LS, Ladizhansky V (2015) Membrane proteins in their native habitat as seen by solid-state NMR spectroscopy. Protein Sci 24(9):1333–1346. https://doi.org/10.1002/pro.2700
24. Warschawski DE, Arnold AA, Beaugrand M, Gravel A, Chartrand E, Marcotte I (2011) Choosing membrane mimetics for NMR structural studies of transmembrane proteins. Biochim Biophys Acta 1808(8):1957–1974. https://doi.org/10.1016/j.bbamem.2011.03.016
25. Krueger-Koplin RD, Sorgen PL, Krueger-Koplin ST, Rivera-Torres IO, Cahill SM, Hicks DB, Grinius L, Krulwich TA, Girvin ME (2004) An evaluation of detergents for NMR structural studies of membrane proteins. J Biomol NMR 28(1):43–57. https://doi.org/10.1023/B:JNMR.0000012875.80898.8f
26. Mio K, Sato C (2018) Lipid environment of membrane proteins in cryo-EM based structural analysis. Biophys Rev 10(2):307–316. https://doi.org/10.1007/s12551-017-0371-6
27. Mineev KS, Nadezhdin KD, Goncharuk SA, Arseniev AS (2016) Characterization of small isotropic Bicelles with various compositions. Langmuir 32(26):6624–6637. https://doi.org/10.1021/acs.langmuir.6b00867
28. Doerrler WT, Raetz CR (2002) ATPase activity of the MsbA lipid flippase of Escherichia coli. J Biol Chem 277(39):36697–36705. https://doi.org/10.1074/jbc.M205857200
29. Mi W, Li Y, Yoon SH, Ernst RK, Walz T, Liao M (2017) Structural basis of MsbA-mediated lipopolysaccharide transport. Nature 549 (7671):233–237. https://doi.org/10.1038/nature23649
30. Siarheyeva A, Sharom FJ (2009) The ABC transporter MsbA interacts with lipid a and amphipathic drugs at different sites. Biochem J 419(2):317–328. https://doi.org/10.1042/BJ20081364
31. Knowles TJ, Scott-Tucker A, Overduin M, Henderson IR (2009) Membrane protein architects: the role of the BAM complex in outer membrane protein assembly. Nat Rev Microbiol 7(3):206–214. https://doi.org/10.1038/nrmicro2069
32. Han L, Zheng J, Wang Y, Yang X, Liu Y, Sun C, Cao B, Zhou H, Ni D, Lou J, Zhao Y, Huang Y (2016) Structure of the BAM complex and its implications for biogenesis of outer-membrane proteins. Nat Struct Mol Biol 23(3):192–196. https://doi.org/10.1038/nsmb.3181
33. Malinverni JC, Werner J, Kim S, Sklar JG, Kahne D, Misra R, Silhavy TJ (2006) YfiO stabilizes the YaeT complex and is essential for outer membrane protein assembly in Escherichia coli. Mol Microbiol 61 (1):151–164. https://doi.org/10.1111/j.1365-2958.2006.05211.x
34. Wu T, Malinverni J, Ruiz N, Kim S, Silhavy TJ, Kahne D (2005) Identification of a multicomponent complex required for outer membrane biogenesis in Escherichia coli. Cell 121 (2):235–245. https://doi.org/10.1016/j.cell.2005.02.015
35. Wasylishen R, Fyfe C (1982) High-resolution NMR of solids. In: Annual reports on NMR spectroscopy, vol 12. Elsevier, Amsterdam, pp 1–290
36. Dudley R, Fyfe C, Stephenson P, Deslandes Y, Hamer G, Marchessault RJJACS (1983) High-resolution carbon-13 CP/MAS NMR

spectra of solid cellulose oligomers and the structure of cellulose II. J Am Chem Soc 105(8):2469–2472

37. Duer MJ (2008) Solid state NMR spectroscopy: principles and applications. Wiley
38. Apperley DC, Harris RK, Hodgkinson P (2012) Solid-state NMR: basic principles and practice. Momentum Press
39. Schaefer J, Stejskal EO (1976) Carbon-13 nuclear magnetic resonance of polymers spinning at the magic angle. J Am Chem Soc 98(4):1031–1032
40. Agarwal V, Penzel S, Szekely K, Cadalbert R, Testori E, Oss A, Past J, Samoson A, Ernst M, Bockmann A, Meier BH (2014) De novo 3D structure determination from sub-milligram protein samples by solid-state 100 kHz MAS NMR spectroscopy. Angew Chem Int Ed Engl 53(45):12253–12256. https://doi.org/10.1002/anie.201405730
41. Chevelkov V, Rehbein K, Diehl A, Reif B (2006) Ultrahigh resolution in proton solid-state NMR spectroscopy at high levels of deuteration. Angew Chem Int Ed Engl 45 (23):3878–3881. https://doi.org/10.1002/anie.200600328
42. Ishii Y, Tycko R (2000) Sensitivity enhancement in solid state (15)N NMR by indirect detection with high-speed magic angle spinning. J Magn Reson 142(1):199–204. https://doi.org/10.1006/jmre.1999.1976
43. Ishii Y, Yesinowski JP, Tycko R (2001) Sensitivity enhancement in solid-state (13)C NMR of synthetic polymers and biopolymers by (1) H NMR detection with high-speed magic angle spinning. J Am Chem Soc 123 (12):2921–2922. https://doi.org/10.1021/ja015505j
44. Linser R, Dasari M, Hiller M, Higman V, Fink U, Lopez del Amo JM, Markovic S, Handel L, Kessler B, Schmieder P, Oesterhelt D, Oschkinat H, Reif B (2011) Proton-detected solid-state NMR spectroscopy of fibrillar and membrane proteins. Angew Chem Int Ed Engl 50 (19):4508–4512. https://doi.org/10.1002/anie.201008244
45. Reif B, Griffin RG (2003) 1H detected 1H,15N correlation spectroscopy in rotating solids. J Magn Reson 160(1):78–83
46. Gopinath T, Mote KR, Veglia G (2013) Sensitivity and resolution enhancement of oriented solid-state NMR: application to membrane proteins. Prog Nucl Mag Res Sp 75:50–68. https://doi.org/10.1016/j.pnmrs.2013.07.004
47. Hansen SK, Bertelsen K, Paaske B, Nielsen NC, Vosegaard T (2015) Solid-state NMR methods for oriented membrane proteins. Prog Nucl Magn Reson Spectrosc 88-89:48–85. https://doi.org/10.1016/j.pnmrs.2015.05.001
48. Park SH, Das BB, Casagrande F, Tian Y, Nothnagel HJ, Chu M, Kiefer H, Maier K, De Angelis AA, Marassi FM, Opella SJ (2012) Structure of the chemokine receptor CXCR1 in phospholipid bilayers. Nature 491 (7426):779–783. https://doi.org/10.1038/nature11580
49. Eddy MT, Ong TC, Clark L, Teijido O, van der Wel PC, Garces R, Wagner G, Rostovtseva TK, Griffin RG (2012) Lipid dynamics and protein-lipid interactions in 2D crystals formed with the beta-barrel integral membrane protein VDAC1. J Am Chem Soc 134 (14):6375–6387. https://doi.org/10.1021/ja300347v
50. Li Y, Berthold DA, Frericks HL, Gennis RB, Rienstra CM (2007) Partial (13)C and (15)N chemical-shift assignments of the disulfide-bond-forming enzyme DsbB by 3D magic-angle spinning NMR spectroscopy. Chembiochem 8(4):434–442. https://doi.org/10.1002/cbic.200600484
51. Shi L, Ahmed MA, Zhang W, Whited G, Brown LS, Ladizhansky V (2009) Three-dimensional solid-state NMR study of a seven-helical integral membrane proton pump--structural insights. J Mol Biol 386 (4):1078–1093. https://doi.org/10.1016/j.jmb.2009.01.011
52. Retel JS, Nieuwkoop AJ, Hiller M, Higman VA, Barbet-Massin E, Stanek J, Andreas LB, Franks WT, van Rossum BJ, Vinothkumar KR, Handel L, de Palma GG, Bardiaux B, Pintacuda G, Emsley L, Kuhlbrandt W, Oschkinat H (2017) Structure of outer membrane protein G in lipid bilayers. Nat Commun 8:2073. https://doi.org/10.1038/s41467-017-02228-2
53. Lacabanne D, Kunert B, Gardiennet C, Meier BH, Bo Ckmann A (2017) Sample preparation for membrane protein structural studies by solid-state NMR. Methods Mol Biol 1635:345–358. https://doi.org/10.1007/978-1-4939-7151-0_19
54. Ward ME, Shi L, Lake E, Krishnamurthy S, Hutchins H, Brown LS, Ladizhansky V (2011) Proton-detected solid-state NMR reveals intramembrane polar networks in a seven-helical transmembrane protein proteorhodopsin. J Am Chem Soc 133 (43):17434–17443. https://doi.org/10.1021/ja207137h

55. Kijac AZ, Li Y, Sligar SG, Rienstra CM (2007) Magic-angle spinning solid-state NMR spectroscopy of nanodisc-embedded human CYP3A4. Biochemistry 46 (48):13696–13703. https://doi.org/10.1021/bi701411g
56. Ladizhansky V (2017) Applications of solid-state NMR to membrane proteins. Biochim Biophys Acta Proteins Proteom 1865(11 Pt B):1577–1586. https://doi.org/10.1016/j.bbapap.2017.07.004
57. Cross TA, Opella SJ (1994) Solid-state NMR structural studies of peptides and proteins in membranes. Curr Opin Struct Biol 4 (4):574–581. https://doi.org/10.1016/S0959-440x(94)90220-8
58. Rigaud JL, Levy D (2003) Reconstitution of membrane proteins into liposomes. Methods Enzymol 372:65–86. https://doi.org/10.1016/S0076-6879(03)72004-7
59. Rigaud JL, Pitard B, Levy D (1995) Reconstitution of membrane proteins into liposomes: application to energy-transducing membrane proteins. Biochim Biophys Acta 1231(3):223–246
60. Geertsma ER, Nik Mahmood NA, Schuurman-Wolters GK, Poolman B (2008) Membrane reconstitution of ABC transporters and assays of translocator function. Nat Protoc 3(2):256–266. https://doi.org/10.1038/nprot.2007.519
61. Morris GA, Freeman R (2011) Selective excitation in Fourier transform nuclear magnetic resonance. 1978. J Magn Reson 213 (2):214–243. https://doi.org/10.1016/j.jmr.2011.08.031
62. Kolodziejski W, Klinowski J (2002) Kinetics of cross-polarization in solid-state NMR: a guide for chemists. Chem Rev 102 (3):613–628
63. Pines A, Gibby MG, Waugh JS (1973) Proton-enhanced NMR of dilute spins in solids. J Chem Phys 59(2):569–590. https://doi.org/10.1063/1.1680061
64. Bloembergen N (1949) On the interaction of nuclear spins in a crystalline lattice. Physica 15 (3–4):386–426. https://doi.org/10.1016/0031-8914(49)90114-7
65. Petkova AT, Baldus M, Belenky M, Hong M, Griffin RG, Herzfeld J (2003) Backbone and side chain assignment strategies for multiply labeled membrane peptides and proteins in the solid state. J Magn Reson 160(1):1–12
66. Baldus M, Petkova AT, Herzfeld J, Griffin RG (1998) Cross polarization in the tilted frame: assignment and spectral simplification in heteronuclear spin systems. Mol Phys 95 (6):1197–1207. https://doi.org/10.1080/002689798166215
67. Takegoshi K, Nakamura S, Terao T (2001) C-13-H-1 dipolar-assisted rotational resonance in magic-angle spinning NMR. Chem Phys Lett 344(5–6):631–637. https://doi.org/10.1016/S0009-2614(01)00791-6
68. Takegoshi K, Nakamura S, Terao T (2003) C-13-H-1 dipolar-driven C-13-C-13 recoupling without C-13 rf irradiation in nuclear magnetic resonance of rotating solids. J Chem Phys 118(5):2325–2341. https://doi.org/10.1063/1.1534105
69. Hing AW, Vega S, Schaefer J (1992) Transferred-echo double-resonance NMR. J Magnetic Reson 96(1):205–209. https://doi.org/10.1016/0022-2364(92)90305-Q
70. Mcdowell LM, Klug CA, Studelska DR, Tasaki K, Beusen DD, Mckay RA, Schaefer J (1995) Applications of REDOR NMR-spectroscopy. J Cell Biochem:18–18
71. Michal CA, Jelinski LW (1997) REDOR 3D: Heteronuclear distance measurements in uniformly labeled and natural abundance solids. J Am Chem Soc 119(38):9059–9060. https://doi.org/10.1021/ja9711730
72. Jaroniec CP, Filip C, Griffin RG (2002) 3D TEDOR NMR experiments for the simultaneous measurement of multiple carbon-nitrogen distances in uniformly (13)C,(15)N-labeled solids. J Am Chem Soc 124 (36):10728–10742. https://doi.org/10.1021/ja026385y
73. Liang B, Tamm LK (2016) NMR as a tool to investigate the structure, dynamics and function of membrane proteins. Nat Struct Mol Biol 23(6):468–474. https://doi.org/10.1038/nsmb.3226
74. Pervushin K, Riek R, Wider G, Wuthrich K (1997) Attenuated T2 relaxation by mutual cancellation of dipole-dipole coupling and chemical shift anisotropy indicates an avenue to NMR structures of very large biological macromolecules in solution. Proc Natl Acad Sci U S A 94(23):12366–12371. https://doi.org/10.1073/pnas.94.23.12366
75. Wang AC, Grzesiek S, Tschudin R, Lodi PJ, Bax A (1995) Sequential backbone assignment of isotopically enriched proteins in D2O by deuterium-decoupled HA(CA)N and HA(CACO)N. J Biomol NMR 5 (4):376–382
76. Sattler M, Fesik SW (1996) Use of deuterium labeling in NMR: overcoming a sizeable problem. Structure 4(11):1245–1249
77. Yagi H, Tsujimoto T, Yamazaki T, Yoshida M, Akutsu H (2004) Conformational change of

H+-ATPase beta monomer revealed on segmental isotope labeling NMR spectroscopy. J Am Chem Soc 126(50):16632–16638. https://doi.org/10.1021/ja045279o

78. Sim DW, Lu Z, Won HS, Lee SN, Seo MD, Lee BJ, Kim JH (2017) Application of solution NMR to structural studies on alpha-helical integral membrane proteins. Molecules 22(8). https://doi.org/10.3390/molecules22081347
79. Fiaux J, Bertelsen EB, Horwich AL, Wuthrich K (2004) Uniform and residue-specific 15N-labeling of proteins on a highly deuterated background. J Biomol NMR 29 (3):289–297. https://doi.org/10.1023/B:JNMR.0000032523.00554.38
80. Arora A, Tamm LK (2001) Biophysical approaches to membrane protein structure determination. Curr Opin Struct Biol 11 (5):540–547
81. Fernandez C, Wuthrich K (2003) NMR solution structure determination of membrane proteins reconstituted in detergent micelles. FEBS Lett 555(1):144–150. https://doi.org/10.1016/s0014-5793(03)01155-4
82. Riek R, Wider G, Pervushin K, Wuthrich K (1999) Polarization transfer by cross-correlated relaxation in solution NMR with very large molecules. Proc Natl Acad Sci U S A 96(9):4918–4923
83. Matzapetakis M, Turano P, Theil EC, Bertini I (2007) 13C- 13C NOESY spectra of a 480 kDa protein: solution NMR of ferritin. J Biomol NMR 38(3):237–242. https://doi.org/10.1007/s10858-007-9163-9
84. Wider G, Wuthrich K (1999) NMR spectroscopy of large molecules and multimolecular assemblies in solution. Curr Opin Struct Biol 9(5):594–601
85. Kerfah R, Plevin MJ, Sounier R, Gans P, Boisbouvier J (2015) Methyl-specific isotopic labeling: a molecular tool box for solution NMR studies of large proteins. Curr Opin Struct Biol 32:113–122. https://doi.org/10.1016/j.sbi.2015.03.009
86. Huang R, Perez F, Kay LE (2017) Probing the cooperativity of Thermoplasma acidophilum proteasome core particle gating by NMR spectroscopy. Proc Natl Acad Sci U S A 114 (46):E9846–E9854. https://doi.org/10.1073/pnas.1712297114
87. Grzesiek S, Bax A (1992) Correlating backbone amide and side-chain resonances in larger proteins by multiple relayed triple resonance NMR. J Am Chem Soc 114 (16):6291–6293. https://doi.org/10.1021/ja00042a003
88. Grzesiek S, Bax A (1993) Amino-acid type determination in the sequential assignment procedure of uniformly C-13/N-15-enriched proteins. J Biomol NMR 3(2):185–204
89. Kushlan DM, LeMaster DM (1993) Resolution and sensitivity enhancement of heteronuclear correlation for methylene resonances via 2H enrichment and decoupling. J Biomol NMR 3(6):701–708
90. Yamazaki T, Lee W, Arrowsmith CH, Muhandiram DR, Kay LE (1994) A suite of triple-resonance NMR experiments for the backbone assignment of N-15, C-13, H-2 labeled proteins with high-sensitivity. J Am Chem Soc 116(26):11655–11666. https://doi.org/10.1021/ja00105a005
91. Zhu G, Kong XM, Sze KH (1999) Gradient and sensitivity enhancement of 2D TROSY with water flip-back, 3D NOESY-TROSY and TOCSY-TROSY experiments. J Biomol NMR 13(1):77–81. https://doi.org/10.1023/A:1008398227519
92. Ikura M, Kay LE, Bax A (1990) A novel approach for sequential assignment of 1H, 13C, and 15N spectra of proteins: heteronuclear triple-resonance three-dimensional NMR spectroscopy. Application to calmodulin. Biochemistry 29(19):4659–4667. https://doi.org/10.1021/bi00471a022
93. Lundstrom P, Vallurupalli P, Hansen DF, Kay LE (2009) Isotope labeling methods for studies of excited protein states by relaxation dispersion NMR spectroscopy. Nat Protoc 4 (11):1641–1648. https://doi.org/10.1038/nprot.2009.118
94. Neudecker P, Lundstrom P, Kay LE (2009) Relaxation dispersion NMR spectroscopy as a tool for detailed studies of protein folding. Biophys J 96(6):2045–2054. https://doi.org/10.1016/j.bpj.2008.12.3907
95. Mittermaier A, Kay LE (2006) New tools provide new insights in NMR studies of protein dynamics. Science 312(5771):224–228. https://doi.org/10.1126/science.1124964
96. Sattler M, Schleucher J, Griesinger C (1999) Heteronuclear multidimensional NMR experiments for the structure determination of proteins in solution employing pulsed field gradients. Prog Nucl Mag Res Sp 34 (2):93–158. https://doi.org/10.1016/S0079-6565(98)00025-9
97. Farrow NA, Zhang O, Forman-Kay JD, Kay LE (1994) A heteronuclear correlation experiment for simultaneous determination of 15N longitudinal decay and chemical exchange rates of systems in slow equilibrium. J Biomol NMR 4(5):727–734

98. Li Y, Palmer AG 3rd (2009) TROSY-selected ZZ-exchange experiment for characterizing slow chemical exchange in large proteins. J Biomol NMR 45(4):357–360. https://doi.org/10.1007/s10858-009-9385-0
99. Vallurupalli P, Bouvignies G, Kay LE (2012) Studying "invisible" excited protein states in slow exchange with a major state conformation. J Am Chem Soc 134(19):8148–8161. https://doi.org/10.1021/ja3001419
100. Vallurupalli P, Sekhar A, Yuwen T, Kay LE (2017) Probing conformational dynamics in biomolecules via chemical exchange saturation transfer: a primer. J Biomol NMR 67 (4):243–271. https://doi.org/10.1007/s10858-017-0099-4
101. Loria JP, Rance M, Palmer AG 3rd (1999) Transverse-relaxation-optimized (TROSY) gradient-enhanced triple-resonance NMR spectroscopy. J Magn Reson 141 (1):180–184. https://doi.org/10.1006/jmre.1999.1891
102. Bibow S, Hiller S (2019) A guide to quantifying membrane protein dynamics in lipids and other native-like environments by solution-state NMR spectroscopy. FEBS J 286 (9):1610–1623. https://doi.org/10.1111/febs.14639
103. Pervushin K (2000) Impact of transverse relaxation optimized spectroscopy (TROSY) on NMR as a technique in structural biology. Q Rev Biophys 33(2):161–197
104. Pervushin KV, Wider G, Wuthrich K (1998) Single transition-to-single transition polarization transfer (ST2-PT) in [15N,1H]-TROSY. J Biomol NMR 12(2):345–348. https://doi.org/10.1023/A:1008268930690
105. Salzmann M, Pervushin K, Wider G, Senn H, Wuthrich K (1998) TROSY in triple-resonance experiments: new perspectives for sequential NMR assignment of large proteins. Proc Natl Acad Sci U S A 95 (23):13585–13590
106. Hiller S, Wider G, Etezady-Esfarjani T, Horst R, Wuthrich K (2005) Managing the solvent water polarization to obtain improved NMR spectra of large molecular structures. J Biomol NMR 32(1):61–70. https://doi.org/10.1007/s10858-005-3070-8
107. Bruschweiler R, Ernst RR (1992) Molecular-dynamics monitored by Cross-correlated Cross relaxation of spins quantized along orthogonal axes. J Chem Phys 96 (3):1758–1766
108. Dalvit C (1992) 1H to 15N polarization transfer via 1H chemical-shift anisotropy—1H-15N dipole-dipole cross correlation. J Magn Reson 97(3):645–650
109. Brüschweiler R, RRJTJocp E (1992) Molecular dynamics monitored by cross-correlated cross relaxation of spins quantized along orthogonal axes. 96(3):1758–1766
110. Chhabra S, Fischer P, Takeuchi K, Dubey A, Ziarek JJ, Boeszoermenyi A, Mathieu D, Bermel W, Davey NE, Wagner G, Arthanari H (2018) (15)N detection harnesses the slow relaxation property of nitrogen: delivering enhanced resolution for intrinsically disordered proteins. Proc Natl Acad Sci U S A 115(8):E1710–E1719. https://doi.org/10.1073/pnas.1717560115
111. Rossi P, Monneau YR, Xia Y, Ishida Y, Kalodimos CG (2019) Toolkit for NMR studies of methyl-labeled proteins. Methods Enzymol 614:107–142. https://doi.org/10.1016/bs.mie.2018.08.036
112. Kay LE, Gardner KH (1997) Solution NMR spectroscopy beyond 25 kDa. Curr Opin Struct Biol 7(5):722–731
113. Gardner KH, Rosen MK, Kay LE (1997) Global folds of highly deuterated, methyl-protonated proteins by multidimensional NMR. Biochemistry 36(6):1389–1401. https://doi.org/10.1021/bi9624806
114. Velyvis A, Ruschak AM, Kay LE (2012) An economical method for production of (2)H, (13)CH3-threonine for solution NMR studies of large protein complexes: application to the 670 kDa proteasome. PLoS One 7(9): e43725. https://doi.org/10.1371/journal.pone.0043725
115. Tugarinov V, Kay LE (2005) Quantitative 13C and 2H NMR relaxation studies of the 723-residue enzyme malate synthase G reveal a dynamic binding interface. Biochemistry 44 (49):15970–15977. https://doi.org/10.1021/bi0519809
116. Tugarinov V, Kay LE (2004) An isotope labeling strategy for methyl TROSY spectroscopy. J Biomol NMR 28(2):165–172. https://doi.org/10.1023/B:JNMR.0000013824.93994.1f
117. Ruschak AM, Velyvis A, Kay LE (2010) A simple strategy for (1)(3)C, (1)H labeling at the Ile-gamma2 methyl position in highly deuterated proteins. J Biomol NMR 48 (3):129–135. https://doi.org/10.1007/s10858-010-9449-1
118. Ollerenshaw JE, Tugarinov V, Skrynnikov NR, Kay LE (2005) Comparison of 13CH3, 13CH2D, and 13CHD2 methyl labeling strategies in proteins. J Biomol NMR 33

(1):25–41. https://doi.org/10.1007/s10858-005-2614-2

119. Azatian SB, Kaur N, Latham MP (2019) Increasing the buffering capacity of minimal media leads to higher protein yield. J Biomol NMR 73:11. https://doi.org/10.1007/s10858-018-00222-4
120. Kaur H, Lakatos A, Spadaccini R, Vogel R, Hoffmann C, Becker-Baldus J, Ouari O, Tordo P, McHaourab H, Glaubitz C (2015) The ABC exporter MsbA probed by solid state NMR - challenges and opportunities. Biol Chem 396(9–10):1135–1149. https://doi.org/10.1515/hsz-2015-0119
121. González-Romo P, Sánchez-Nieto S, MJAb G-R (1992) A modified colorimetric method for the determination of orthophosphate in the presence of high ATP concentrations. Anal Biochem 200(2):235–238
122. Mandal A, Boatz JC, Wheeler TB, van der Wel PC (2017) On the use of ultracentrifugal devices for routine sample preparation in biomolecular magic-angle-spinning NMR. J Biomol NMR 67(3):165–178. https://doi.org/10.1007/s10858-017-0089-6
123. Hartmann SR, Hahn EL (1962) Nuclear double resonance in rotating frame. Phys Rev 128(5):2042. https://doi.org/10.1103/PhysRev.128.2042
124. Bräuniger T, Wormald P, Hodgkinson P (2002) Improved proton decoupling in NMR spectroscopy of crystalline solids using the S PINAL-64 sequence. In: Current developments in solid state NMR spectroscopy. Springer, Wien, pp 69–74
125. Takegoshi K, Nakamura S, Terao T (2001) 13C–1H dipolar-assisted rotational resonance in magic-angle spinning NMR. Chem Phys Lett 344(5):631–637
126. Liu ML, Mao XA, Ye CH, Huang H, Nicholson JK, Lindon JC (1998) Improved WATERGATE pulse sequences for solvent suppression in NMR spectroscopy. J Magn Reson 132(1):125–129. https://doi.org/10.1006/jmre.1998.1405
127. Tugarinov V, Hwang PM, Ollerenshaw JE, Kay LE (2003) Cross-correlated relaxation enhanced 1H[bond]13C NMR spectroscopy of methyl groups in very high molecular weight proteins and protein complexes. J Am Chem Soc 125(34):10420–10428. https://doi.org/10.1021/ja030153x
128. Miroux B, Walker JE (1996) Overproduction of proteins in Escherichia coli: mutant hosts that allow synthesis of some membrane proteins and globular proteins at high levels. J Mol Biol 260(3):289–298. https://doi.org/10.1006/jmbi.1996.0399
129. Angius F, Ilioaia O, Amrani A, Suisse A, Rosset L, Legrand A, Abou-Hamdan A, Uzan M, Zito F, Miroux B (2018) A novel regulation mechanism of the T7 RNA polymerase based expression system improves overproduction and folding of membrane proteins. Sci Rep 8(1):8572. https://doi.org/10.1038/s41598-018-26668-y
130. Marley J, Lu M, Bracken C (2001) A method for efficient isotopic labeling of recombinant proteins. J Biomol NMR 20(1):71–75
131. Castellani F, van Rossum B, Diehl A, Schubert M, Rehbein K, Oschkinat H (2002) Structure of a protein determined by solid-state magic-angle-spinning NMR spectroscopy. Nature 420(6911):98–102. https://doi.org/10.1038/nature01070
132. Higman VA, Flinders J, Hiller M, Jehle S, Markovic S, Fiedler S, van Rossum BJ, Oschkinat H (2009) Assigning large proteins in the solid state: a MAS NMR resonance assignment strategy using selectively and extensively 13C-labelled proteins. J Biomol NMR 44(4):245–260. https://doi.org/10.1007/s10858-009-9338-7
133. Schubert M, Manolikas T, Rogowski M, Meier BH (2006) Solid-state NMR spectroscopy of 10% 13C labeled ubiquitin: spectral simplification and stereospecific assignment of isopropyl groups. J Biomol NMR 35(3):167–173. https://doi.org/10.1007/s10858-006-9025-x
134. Lacabanne D, Meier BH, Bockmann A (2018) Selective labeling and unlabeling strategies in protein solid-state NMR spectroscopy. J Biomol NMR 71(3):141–150. https://doi.org/10.1007/s10858-017-0156-z
135. Hong M, Jakes K (1999) Selective and extensive 13C labeling of a membrane protein for solid-state NMR investigations. J Biomol NMR 14(1):71–74
136. Meissner A, Sorensen OW (2001) Sequential HNCACB and CBCANH protein NMR pulse sequences. J Magn Reson 151(2):328–331. https://doi.org/10.1006/jmre.2001.2374
137. Tugarinov V, Kay LE (2003) Side chain assignments of Ile delta 1 methyl groups in high molecular weight proteins: an application to a 46 ns tumbling molecule. J Am Chem Soc 125(19):5701–5706. https://doi.org/10.1021/ja021452+
138. Tugarinov V, Kay LE (2003) Ile, Leu, and Val methyl assignments of the 723-residue malate

synthase G using a new labeling strategy and novel NMR methods. J Am Chem Soc 125 (45):13868–13878. https://doi.org/10.1021/ja030345s

139. Tugarinov V, Choy WY, Orekhov VY, Kay LE (2005) Solution NMR-derived global fold of a monomeric 82-kDa enzyme. Proc Natl Acad Sci U S A 102(3):622–627. https://doi.org/10.1073/pnas.0407792102
140. Gelis I, Bonvin AM, Keramisanou D, Koukaki M, Gouridis G, Karamanou S, Economou A, Kalodimos CG (2007) Structural basis for signal-sequence recognition by the translocase motor SecA as determined by NMR. Cell 131(4):756–769. https://doi.org/10.1016/j.cell.2007.09.039
141. Ayala I, Sounier R, Use N, Gans P, Boisbouvier J (2009) An efficient protocol for the complete incorporation of methyl-protonated alanine in perdeuterated protein. J Biomol NMR 43(2):111–119. https://doi.org/10.1007/s10858-008-9294-7

Chapter 25

Exploring Lipid and Membrane Protein Dynamics Using Lipid-Bilayer Nanodiscs and Solution-State NMR Spectroscopy

Stefan Bibow

Abstract

The relationship of membrane protein function and the surrounding lipid bilayer goes far beyond simple hydrophobic interactions. At least from the 1980s, it is speculated that a certain fluid lipid state may be important not only for the lateral diffusion of membrane proteins (MPs) but also for modulating the catalytic activity of MPs (Lenaz. Bioscience Rep 7 (11):823-837, 1987). Indeed, acyl chain length, hydrophobic mismatch, and lipid headgroups are determinants for enzymatic and transport activities of MPs (Dumas et al. Biochemistry 39(16):4846-4854, 2000; Johannsson et al. Biochim Biophys Acta 641 (2):416-421, 1981; Montecucco et al. FEBS Lett 144(1):145-148, 1982; Martens et al. Nat Struct Mol Biol 23(8):744-751, 2016). Moreover, it is speculated that changes in membrane lipid dynamics are important in the field of thermosensation (Vriens J, Nilius B, Voets T, Nat Rev Neurosci 15:573-589, 2014). Atomic insights into lipid-mediated modulation of membrane protein dynamics would therefore provide new insights with the potential to fundamentally extend our understanding on dynamic lipid–protein interdependencies.

This chapter describes the expression and purification of nanodiscs assembled from membrane scaffold protein (MSP) as well as the expression and purification of the outer membrane protein X (OmpX). Subsequently, the incorporation of OmpX into MSP-derived nanodiscs is explained in detail. The chapter concludes with the setup of nuclear magnetic resonance (NMR) relaxation experiments and the extraction of relaxation rates for OmpX and the surrounding lipids.

Key words NMR, OmpX, Relaxation, cpmg, lipid dynamics, R1, R2, membrane protein dynamics, Thermosensation

1 Introduction

The lipid diversity in membranes of prokaryotic and eukaryotic organisms is immense, reflected by the fact that 5% of the genome encodes for lipids [7]. Remarkably, the lipid compositions are vastly different between the three kingdoms of life, between cellular organelles within the same cell and even between the two leaflets of the same membrane [7–9]. In addition to physically separating

Camilo Perez and Timm Maier (eds.), *Expression, Purification, and Structural Biology of Membrane Proteins*, Methods in Molecular Biology, vol. 2127, https://doi.org/10.1007/978-1-0716-0373-4_25,

two environments, biomembranes provide anchor points for the cytoskeleton and harbor membrane-spanning proteins that enable the directed transfer of molecules and signals. It is well documented that the lipid composition of the bilayer has the capability to modulate enzymatic and transport activities of membrane proteins through their phase state, fluidity, head groups, and thickness [1–5, 10]. An increasing body of evidence furthermore suggests an influence of membrane composition to the function of membrane proteins by an interplay of lipid dynamics and membrane protein dynamics [11, 12], providing a regulatory or even environment-sensing mechanism as suggested in infrared sensing of bats and snakes [6, 13, 14]. In the past, MPs were investigated using detergent molecules as mimics for a lipid bilayer. Although detergents have favorable capabilities regarding extraction, refolding, and crystallization of MPs, they frequently reduce or abolish MP function and stability or interfere with functional assays and ligand binding [15–17]. Alternatives to detergent micelles include the development of detergent–lipid bicelle preparations which ideally harbor the MP within the lipid-bilayer core that is segregated from the circumference of detergents. Unfortunately, lipids and detergents mix under conditions usually used for solution NMR studies (that is having a bicelle with a q-value below 1) [18]. Hence it is difficult to assess how "lipidic" the MP surrounding actually is given the fact that usually no "lipid-only" NMR spectrum for that particular MP exists. A detergent-free lipid bilayer would therefore provide a more natural environment to asses ligand binding, as well as the structure and dynamics of MPs [19–23]. Indeed, recent efforts culminated in the development of non-detergent alternatives such as styrene maleic acid [24, 25], amphipols, and fluorinated surfactants [26, 27] as well as lipid-bilayer nanodiscs composed of the membrane scaffolding protein (MSP) [28–31] (Fig. 1).

Combining nuclear magnetic resonance (NMR) spectroscopy and MPs incorporated into nanodiscs opens a new avenue to study MP structure [30, 32], MP dynamics [33, 34], as well as lipid dynamics [35–37] with atomic resolution in a lipid-bilayer environment. Nanodiscs are composed of MSP, which is an elongated or shortened version of apolipoprotein A-I, a naturally occurring protein in high-density lipoprotein (HDL) particles [29]. Two MSP proteins wrap around a lipid-bilayer patch in an antiparallel fashion, corresponding to one MSP per lipid leaflet [38]. NMR is a uniquely powerful method to probe molecular dynamics in solution over a wide range of timescales with atomic resolution. NMR relaxation experiments can extract dynamics parameters from picoseconds to seconds from basically every atom of a molecule. However, by far the most frequently studied dynamics are ^{15}N dynamics of the ^{1}H–^{15}N protein backbone bond [39, 40]. Motions faster than the molecular tumbling, τ_c, can be probed by nuclear spin relaxation experiments [41, 42] such as the longitudinal relaxation rate R_1

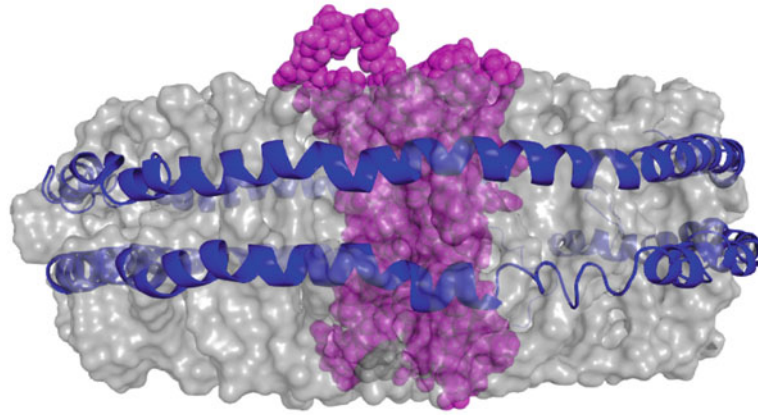

Fig. 1 Schematic representation of the OmpX-containing nanodisc. The membrane scaffolding protein (MSP, colored blue) encircles a lipid-bilayer patch. Here, the structure of MSPΔH5 is shown (pdb entry 2N5E). OmpX (shown in magenta, pdb entry 2MNH) is surrounded by DMPC lipids (shown in gray). Ca. 40 lipids per leaflet are present in the OmpX-MSPΔH5 assembly

that probes picosecond and nanosecond motions up to the tumbling time. A second relaxation parameter is the transverse relaxation rate R_2 that is the sum of transverse relaxation (often denoted R_2^0) and exchange contributions (often denoted R_{ex}). R_{ex} is due to stochastic fluctuations of the chemical environment near the residue of interest, either due to conformational plasticity or due to solvent exchange phenomena. R_{ex} reduces the NMR signal intensities of affected residues that is exploited in CPMG (Carr-Purcell-Meiboom-Gill) and the R_{1rho} experiments. To recover lost signal intensities, the CPMG (Carr-Purcell-Meiboom-Gill) and R_{1rho} experiment apply pulse trains that increase the signal intensities of affected residues [43–45]. Correlations between signal recovery and radiofrequency field strengths then reveal exchange rates and equilibria between interconverting species [46]. Please note that a detailed explanation of nuclear spin relaxation and the physical background of relaxation experiments is beyond the scope of this chapter. The interested reader is referred to reviews [47–53]. We recently used NMR dynamics experiments to study the outer membrane protein X (OmpX) and lipid dynamics in nanodiscs over a wide range of temperatures and lipid compositions using essentially the same sample. The data revealed a direct modulatory capability of the membrane to regulate protein function through lipid dynamics ranging from picoseconds to milliseconds [54].

Here, the production and purification of OmpX and MSP are described. Then a method is presented which reconstitutes OmpX into a saturated, unsaturated, and cholesterol-containing lipid-bilayer nanodisc. Subsequently, the setup of the timescale-specific NMR relaxation experiments for the protein and lipids will be

described [55, 56]. Lastly, NMR relaxation rates will be extracted using the software NMRFAM-SPARKY [57] and the Bruker Software TopSpin.

2 Materials

Prepare all solutions using ultrapure water. Filter the prepared buffers using a 0.22 μm membrane. Store the prepared solutions at 4 °C.

2.1 Protein Expression, Purification, and Nanodiscs Reconstitution

1. LB agar plates with kanamycin (50 μg/ml).
2. MSPΔH5 plasmid (pET-28a) and OmpX plasmid (pET-28b) with kanamycin resistance (*see* **Note 1**).
3. Granulated LB powder (Miller) in nanopure water with kanamycin for expression of MSPΔH5.
4. Freshly prepared M9 minimal medium for OmpX expression (amount per 1 L): 990 ml of 99.8% D_2O (Sigma), 6.8 g Na_2HPO_4 (anhydrous), 3 g KH_2PO_4, 0.5 g NaCl, 1 g $^{15}NH_4Cl$ (Sigma), 240 mg $MgSO_4$, 10 ml Vitamin Mix (100x) prepared in D_2O, 2.5 g ^{12}C,^{2}H-Glucose (Sigma), Kanamycin.
5. *E. coli* BL21 (DE3∗) cells.
6. SM-2 BioBeads (e.g., Bio-Rad).
7. Ni-NTA resin.
8. OmpX buffer 1, 20 mM Tris, 5 mM EDTA, pH 8.0.
9. OmpX buffer 2, 20 mM Tris, 2% (vol/vol) Triton-X100, 5 mM EDTA, pH 8.0.
10. OmpX buffer 3, 20 mM Tris, 6 M GuHCl, 5 mM EDTA, pH 8.0.
11. OmpX buffer 4, 50 mM Tris, 100 mM NaCl, 0.5% dodecylphosphocholine (FC-12), 500 mM L-arginine, pH 8.5.
12. NMR buffer, 20 mM Tris, 100 mM NaCl, pH 7.4.
13. MSP buffer 1, 20 mM Tris, 500 mM NaCl, pH 8.0.
14. MSP buffer 2, 20 mM Tris, 500 mM NaCl, pH 8.0, 1% (vol/vol) Triton-X100.
15. MSP buffer 3, 20 mM Tris, 500 mM NaCl, pH 8.0, 50 mM Sodium cholate.
16. MSP buffer 4, 20 mM Tris, 500 mM NaCl, pH 8.0, 50 mM imidazole.
17. MSP buffer 5, 20 mM Tris, 500 mM NaCl, pH 8.0, 500 mM imidazole.

18. 9-cis-unsaturated 1,2-dimyristoyl-sn-glycero-3-phosphocholine (DMPC14:1) (Avanti)
19. 9-cis-saturated 1,2-dimyristoyl-sn-glycero-3-phosphocholine (DMCP14:0) (Avanti)
20. Cholesterol (Avanti).

2.2 1 L Vitamin Mix (100×)

1. 100 mg D-Biotin, 100 mg choline chloride,
2. 100 mg Folic acid,
3. 200 mg Myo-Inositol,
4. 100 mg Nicotinamide,
5. 100 mg D-pantothenic acid hemicalcium,
6. 100 mg Pyridoxal HCl,
7. 10 mg Riboflavin,
8. 100 mg Thiamine HCl,
9. 8.5 g NaCl.
10. Set the pH between 6.8–7.2 and sterile filter the solution.
11. Aliquot the solution into 10 ml. Store at −20 °C.
12. Add 10 ml Vitamin mix (100×) per 1 L minimal medium.

2.3 NMR Relaxation Data

1. Computer with Bruker Software TopSpin (Version 3) and NMRFAM-SPARKY. Both programs are freely available for academic use.
2. Excel, for organizing the tables of relaxation data.

   If required, an additional program for data analysis can be used. For example, IGOR pro (WaveMetrix) is a powerful data analysis tool with many possibilities to present data in a clear and appealing way, but still rather simple to use. Exported as vector graphics, the data can be arranged for high-quality publication figures, for example, in Adobe Illustrator.

3 Methods

3.1 Expression and Purification of MSPΔH5

1. Express MSPΔH5 in the *E. coli* strain BL21(DE3∗) in LB medium at 37 °C until an $OD_{600} = 0.8$ (*see* **Note 1**).
2. Initiate protein overexpression by the addition of 0.5 mM isopropyl β-D-1-thiogalactopyranoside (IPTG; Invitrogen, Carlsbad).
3. Reduce temperature after 1 h to 28 °C for 4 h.
4. Harvest cells by centrifugation (4000 g for 15 min at 4 °C).
5. Resuspend the cell pellet in ca. 30 ml of MSP buffer 1 and store at −80 °C until further use.

6. Thaw frozen MSPΔH5 at room temperature and fill to 50 ml with MSP buffer 1.
7. Stirr the solution and add 5 mg of DNAse deoxyribonuclease I and 1% (Vol/vol) Triton-X100 at room temperature (Triton-X100 tends to clog at low temperature) and stirr for additional 30 min.
8. Sonicate the solution for 20 min (2 seconds pulses, 20% power on a Branson digital sonifier model 250) in a glass beaker placed on ice.
9. Separate the supernatant containing MSPΔH5 from the insoluble cell fraction by centrifugation (20,000 × *g* for 30 min at 4 °C). Filter the supernatant using a 50 ml syringe with a 0.20 μm disposable, non-pyrogenic sterile filter attached to it.
10. Equilibrate 3 ml of fresh Ni-NTA (bed volume) with MSP buffer 2 in a gravity flow column.
11. Add 50 ml of the filtered supernatant to the Ni-NTA and adjust the flow rate to around 1 drop every 2 seconds, corresponding to around 1 ml/min.
12. Apply 100 ml of MSP buffer 2 with the same flow rate.
13. Apply 100 ml of MSP buffer 3 with 1–2 drops every second (2–4 ml/min).
14. Apply 100 ml of MSP buffer 1 (2–4 ml/min) to wash away excess of sodium cholate (*see* **Note 2**).
15. Eliminate unspecific binding of proteins by washing with 100 ml of MSP buffer 4.
16. Elute MSP with around 12 ml of MSP buffer 5.
17. Exchange the MSP buffer 5 directly after the elution with NMR buffer using PD10 desalting columns. PD10 columns have the advantage that they can be reused several times.
18. Cleave the his-tag at room temperature incubating for 10 h using TEV in a ratio of 1:100.
19. Concentrate cleaved MSPΔH5 protein using an Amicon Ultra-4 10 kDa molecular weight cutoff (MWCO) concentrator to around 300 μM and freeze in a − 80 °C freezer containing TEV and the His-tag (*see* **Note 3**).

3.2 Expression and Purification of OmpX from Inclusion Bodies

1. The used OmpX plasmid encodes for 148 residues (*see* **Note 1**).
2. In the morning, inoculate a new agar plate with transfected *E. coli* cells and leave for 8 h at 37 °C.
3. Prepare 1 L of 99.8% deuterated M9 minimal medium with $^{15}NH_4Cl$ for the ^{15}N isotope labeling and deuterated ^{12}C.

4. In the late evening of the same day, use 50 ml from M9 minimal medium for an overnight preculture with *E. coli* cells from the ca. 8 h inoculation plate.
5. In the next morning add the preculture to the remaining 950 ml of M9 medium to reach a starting OD of 0.1 and grow to an OD_{600} of 0.6–0.8.
6. Induce overexpression of OmpX by adding 1 mM isopropyl β-D-1-thiogalactopyranoside (IPTG) and grow cells overnight at 37 °C.
7. After 15 h of overexpression, harvest the cells by centrifuging at 5000 g, 4 °C for 10 min.
8. Resuspend the cells in 100 mL OmpX buffer 1.
9. After gently stirring for 30 min at room temperature, break the cells by passing through a microfluidizer at a pressure of 42 psi twice. Alternatively, the cells can also be broken by sonication (as described for MSP). Cell lysis should be complete because OmpX is purified from inclusion bodies and intact cells sediment together with the inclusion bodies upon centrifugation, thus contaminating the preparation (*see* **Note 4**).
10. Centrifuge the solution for 1 h at 5000 × *g* and 4 °C.
11. Resuspend the pellet in OmpX buffer 2 and shake for 20 min at 37 °C. A washing step with low concentrations of chaotropic agents (e.g., 0.5–1 M guanidine-HCl or urea) or detergents (e.g., 1–2% Triton X-100) removes contaminants that have absorbed onto the hydrophobic inclusion bodies during processing. This washing step will also dissolve membranes and membrane proteins, resulting in purer inclusion bodies. A short sonication (3 × 10 s) during this washing step can help to resuspend all the inclusion bodies and break unbroken cells as well as shear DNA.
12. Centrifuge the solution again for 1 h at 5000 × *g* and 4 °C.
13. Wash the pellet with OmpX buffer 1.
14. Subsequently, dissolve the pellet with OmpX buffer 3 for 2 h at 37 °C.
15. Centrifuge the solution for 30 min at 15,000 × *g* and 4 °C. Aliquot the supernatant in 5 ml Eppendorf tubes and store in a −80 °C freezer.
16. Refold OmpX at room temperature by adding 5 mL of the OmpX solution to 50 mL of OmpX buffer 4 in a dropwise manner using a flow rate of 0.5 ml/min.
17. Gently stir the solution for 2 h at room temperature.
18. Dialyze OmpX three times against 4 L of NMR buffer using a 6–8 kDa dialysis membrane.

19. Concentrate OmpX using an Amicon Ultra-4 10 kDa molecular weight cutoff (MWCO) concentrator to a concentration of ~600 μM and store at −80 °C until further usage. OmpX is stable for at least 1 year in FC-12 at −80 °C.

3.3 Assembly of MSP and OmpX

1. Mix 100 mM DMPC14:1 in a molar ratio of 4:1 with cholesterol and dissolve in chloroform in a glass vial. Remove the solvent under speed vacuum centrifugation at 3000 g and 37 °C until a transparent homogenous pellet is observed. Resuspend the pellet in a 200 mM sodium cholate solution until the solution is transparent.
2. For the DMPC14:0 and DMPC14:1 solution, dissolve the cholate in water first. Then add 100 mM DMPC14:0 and perform cycles of freezing, thawing, and vortexing until DMPC14:0 is completely dissolved and the solution is clear.
3. For the reconstitution of OmpX into MSPΔH5 nanodiscs, use a molar ratio of 1:2:80:160 of OmpX:MSPΔH5:lipids:sodium cholate.
4. Add the lipids first into a glass vial, followed by the membrane protein and finally add MSPdH5 to the solution. Shake the assembly solution at 185 rpm for 2 h at 27 °C. Make sure you **assemble above the lipid phase transition temperature**, which means within the liquid phase of the lipids (*see* **Note 5**).
5. Add then 1 g Biobeads SM-2 (Bio-Rad) per mL assembly solution to the mixture and shake at 185 rpm for 3 h at 27 °C (*see* **Note 6**).
6. Separate Biobeads from the solution by slow speed centrifugation using a hand centrifuge.
7. Concentrate the solution to 400 μl using Amicon Ultra-4 10 kDa concentrators.
8. Using a 500 μl loop, inject the 400 μl into an FPLC (e.g., Äkta) using a Superdex 200 10/300 GL to perform a size-exclusion chromatography (SEC). On this column, the empty as well as OmpX-containing nanodiscs elute at around 12.5–13 ml. If you use larger nanodiscs, they elute earlier, e.g., MSP1D1 would elute at around 11–12 ml. During the SEC, the cleaved His-tag (1–2 kDa) and TEV protease (ca. 27 kDa) can be separated from the nanodiscs assembly (108 kDa), resulting in a very pure assembly for NMR and other spectroscopic methods (Fig. 2) (*see* **Note 7**).
9. Run an SDS gel from the appropriate fractions to assure and compare the incorporation of the membrane protein. A subsequent His-trap step can be conducted to separate the membrane protein containing nanodiscs from the empty nanodiscs if the membrane protein has a His-tag and if the His-tag is

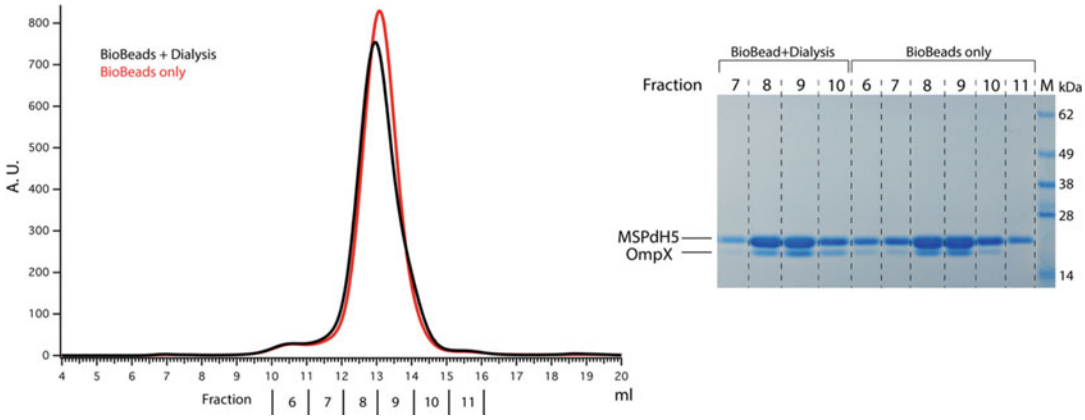

Fig. 2 SEC profile and SDS page of OmpX incorporated in MSPΔH5 nanodiscs. Left panel: A size-exclusion chromatogram (SEC) using a S200 column is shown. Empty and OmpX-containing nanodiscs will come at similar positions since the MSP protein determines the size of the assembly. Right panel: Fractions from the SEC are used for an SDS gel to confirm the presence of OmpX within the nanodiscs. A BioBeads detergent removal simultaneously with a dialysis against 4 L of NMR buffer does not perform better than a detergent removal procedure using only BioBeads. After the SEC, the nanodiscs fractions are very pure

accessible, which very much depends on the membrane protein.

10. For dynamics studies the assembly should be concentrated and used right away or within a couple of days. Although the assembly can be stored for several months at −80 °C until further usage, the quality of the spectra deteriorates over time. This may not challenge assignment procedures, but can provide inaccurate results for dynamics studies.

3.4 General Considerations in Setting Up Relaxation Experiments

Every assembly needs to be checked to exhibit the same high-quality spectra. High-quality is defined here as a (2D) spectrum with minimal peak overlap and peaks that exhibit similar sharp peak shapes and heights across assemblies. For dynamics measurements, especially for slow dynamics measurements of microsecond–millisecond (μs–ms) dynamics, the visual inspection of the spectral quality provides a direct measure on the comparability of assemblies using the same lipids. Commonly, a 2D ^{1}H,^{15}N-TROSY-HSQC spectrum (e.g., using the standard Bruker pulse sequence trosyetf3gpsi2) provides a good assessment into the spectral quality. The original TROSY sequences for ^{15}N-R_1, ^{15}N-R_2, and ^{15}N-R_{1rho} from Lakomek et al. were used [55, 56] (*see* **Note 8** for Bruker sequences). These experiments are recorded as a pseudo-3D experiment, meaning that several 2D experiments were recorded in an interleaved fashion. The pseudo-3D experiment needed to be split after a successful completion into 2D experiments. Splitting of experiments was done using the build-in au-program "split" (for a list of all Bruker au-programs type "edau"). We restricted our

relaxation measurements to four relaxation delays because of the following: (i) four delays are enough to provide very good relaxation rates; (ii) a pseudo-3D experiment with four interleaved 2D experiments already takes 3–4 days due to a long recycle delay of up to 10 s. As a rule of thumb, the longest relaxation delay should reduce the signal intensity to around 1/e (36%) compared to the experiment without any relaxation delay. However, this is sometimes difficult to assess since signals from the structured region will relax faster (stronger signal reduction) than signals from flexible loop regions, which is why signals from unstructured regions at around 8.5–8.0 ppm in the proton spectrum will dominate the spectrum. Hence, the spectroscopist should focus on signal intensities from structured regions that are found between 10 and 8.5 ppm in the proton 1D spectrum. Those signals should be no less than 36% for the longest relaxation delay when compared to the experiment without any relaxation delay. Note that there is no way to extract reliable relaxation values from peaks that disappear in the noise. All experiments contain a so-called temperature compensation element, assuring the same amount of heat from the radio frequency pulses as well as the same amount of time for all relaxation experiments.

3.4.1 Setting Up Protein ^{15}N-R_1 and ^{15}N-R_2 Relaxation Experiments

1. The ^{15}N-R_1 experiment uses a vc ("variable counter") list containing the number of loops the pulse sequence has to execute during the relaxation delay. It takes a certain amount of time to execute one loop, meaning that the number of loops directly corresponds to the relaxation delay.
2. It is important for the R_1 experiment to allow for a sufficiently long recycle delay (d1 in Bruker pulse sequences). A typical ^{15}N-R_1 rate for OmpX in nanodiscs is around 0.3 s^{-1}, corresponding to a longitudinal relaxation time T_1 of 3.33 s.
3. Using therefore a recycle delay of 7–9 s (2–3 times the T_1) between experiments is an adequate compromise to allow the nuclear spins to relax back to equilibrium and to record the experiment in a timely manner.
4. The R_2 experiment uses a "vd" (variable delay) list. This list is called up and incremented for each experiment and contains the relaxation delay according to the values set in the list.
5. The lists can be found at /opt/topspinX.X.X/exp./stan/nmr/lists/ (whereas the "X" indicate the version number of the TopSpin software).
6. Setting up R_1 and R_2 experiments is relatively straight forward.
7. It is important to look in the pulse sequence to check how often the lists are called to set the relaxation delay as intended.

3.4.2 Setting Up Protein ^{15}N-R_{1rho} Relaxation Experiments

1. The R_{1rho} experiment is slightly more difficult to set up. It uses a "vp" (variable pulse) list, meaning that the spin-lock pulse length itself is modulated according to the values set in the vp list.
2. The lists can also be found at /opt/topspinX.X.X/exp./stan/nmr/lists/ (whereas the "X" indicate the version number of the TopSpin software). There, folders for vc, vd, and vp are found which usually contain files that can serve as templates.
3. In the ^{15}N-R_{1rho} experiment, the ^{15}N spin-lock frequency determines which motions are probed. A spin-lock frequency of 2000 Hz refocuses motions slower than $1/(2*\pi*2000) = 80$ μs. Hence, ^{15}N dynamics around 80 μs are probed.
4. It is advisable to take extra care in setting up an R_{1rho} experiment since the build-in security measures in TopSpin may not prevent damage to the probehead from an incorrect power level for the spin-lock (see below).
5. The spin-lock period is preceded and followed by adiabatic half-passage (AHP) pulses. Each pulse is 3 ms in duration and corresponds to the first and second half of a tangent hyperbolic tangent (tanh/tan) adiabatic inversion pulse, respectively [58]. The half-passage pulses are amplitude and phase-modulated [58] and defined with 3000 μs duration, 100 kHz total sweep width, $\zeta = 10$, and $\tan(\kappa) = 20$ [55]. ζ and tan(κ) are numerically optimized constants [59].
6. To set up a spin-lock field of 2000 Hz, the power level needs to be calculated using:

$$20 * \log * \left(\frac{p_{\text{new}}}{p_{\text{reference}}}\right) = \textit{c}\text{hange in dB}$$

7. with $p_{\text{reference}}$ as the reference pulse power having a predetermined power level, and p_{new} as a 2000 Hz 90° pulse (p_{new}):

$$p_{\text{new}} = \frac{1}{4 * 2000} = 125\ \mu\text{s}$$

8. Keep in mind that it is not a 125 μs pulse that is applied but a 2000 Hz pulse of variable length (taken from the vp list). The shaped pulses are available upon request.
9. It is possible to check how well the adiabatic pulse can align the nuclear spin magnetization with a certain offset from the applied spin-lock field.
10. For that type "stdisp" to enter the shape tool analysis display in TopSpin.

11. Select the full-passage amplitude and phase-modulated adiabatic RF pulse from the shapes folder (the pulse should be saved under /opt/topspinX.X.X/exp/stan/nmr/lists/wave/user).
12. Select the pulse, go to simulate, and use 6000 μs pulse length.
13. Then click the start NMR-SIM button. Depending on your TopSpin version, in the newly opened window either click the dropdown menu "Waveform analysis" (e.g., for TopSpin 3.2) or click the button with "A."
14. Type for P0 = 6000 μs, SP0 = 2000 (spin-lock field frequency), and SPOFF0 = offset frequency. The offset frequency is the difference in the frequency where the spin-lock field is applied and where the spin of interest resonates. In a case where the spin lock is applied at 119 ppm (^{15}N) and the ^{15}N spin resonates at 129 ppm, the offset is 10 ppm.
15. On a 600 MHz spectrometer, 10 ppm offset for a ^{15}N nuclei corresponds to 600 Hz offset in frequency units which needs to be entered in SPOFF0. In the "theta" window, two lines are present.
16. If the spin at 129 ppm can be aligned by the 2000 Hz spin-lock field applied at 119 ppm, the two lines overlap. The further away the spin is from the spin-lock field, the worse the alignment will be.
17. For ^{15}N-R_{1rho} the minimal relaxation value is 1 ms (instead of 0 ms).

3.4.3 Setting Up the TRACT Experiment

1. The TRACT experiment [60] reveals the rotational correlation time of the molecule. If OmpX is ^{15}N labeled, the rotational correlation time of OmpX in nanodiscs can be determined. If MSP is ^{15}N-labeled and OmpX is not isotope-labeled, the rotational correlation time of the nanodiscs itself can be determined.
2. The TRACT experiment uses 1D experiments to determine the bulk relaxation rates of the slowly relaxing α-state and fast relaxing β-state of ^{15}N.
3. Single exponential fits of the bulk relaxation rates R_α and R_β of the corresponding spin states were derived from an integral [61].
4. It is important to choose a region from the 1D spectrum that does not contain residues from flexible loops, which are located around 8 ppm. Loop residues relax slowly (see above), and will therefore dominate the 1D proton spectrum at longer relaxation times, hence the TRACT experiment will provide the "tumbling" of flexible loops.

5. β-strand residues are found at around 9 ppm. A safe region to integrate in the resulting proton spectrum is therefore from 9.5 to 8.5 ppm.
6. A typical τ_c-value for OmpX in nanodiscs at 316 K is ca. 34 ns. TRACT provides the lower limit of τ_c because the fastest tumbling areas will relax the slowest.
7. Notably, the TROSY-R_2 experiment from Lakomek et al. measures the slowly relaxing α-spin state of ^{15}N. It is very easy to change this 2D sequence to measure the fast relaxing β-spin state of ^{15}N (see Fig. S14 in the supporting information of ref. [56]). This provides 2D measurements of transverse ^{15}N chemical shift anisotropy (CSA)-dipolar cross-correlated relaxation rates η_{xy} for every residue, which can be converted into residue-specific τ_c-values (see supplementary material in ref. [61]).
8. For exact values of relaxation rates used for OmpX in nanodiscs and other membrane-mimicking environments, see ref. [34, 54].
9. For an in-depth description of the TROSY-relaxation experiments, see ref. [55, 56]. Please also keep in mind that the usage of Bruker versions of these sequences might be different, especially regarding the usage of lists (*see* **Note 8**). The original sequences from Lakomek et al are freely available (https://spin.niddk.nih.gov/bax/).

3.4.4 Setting Up Lipid Relaxation Experiments

1. It is very fortunate that lipid dynamics can be investigated along with membrane protein dynamics within the same NMR sample. Lipids are ca. 80 times more abundant in the nanodiscs than OmpX and very flexible, allowing the exploitation of carbon dynamics using ^{13}C natural abundance measurements on NMR cryoprobes (Fig. 3B).
2. ^{13}C R_1 inversion recovery (called t1irpg in the Bruker library) experiments with proton decoupling during the full sequence were used to determine the lipid R_1 rates.
3. Eight relaxation delays (vd list with 0.01, 0.05, 0.5, 1, 2, 4, 8, and 10 s) and a recovery delay of 15 s were used.
4. The standard Bruker 1D CPMG experiment (called cpmg in the Bruker library) was modified to include proton decoupling during the full sequence and to record ^{13}C coherence. The proton carrier was set to 2 ppm, the carbon carrier was set to 50 ppm.
5. The recycling delay was 5 s.
6. The cpmg experiment uses a vc list containing the number of loops. The cpmg block is d20—180° pulse—d20. A d20 delay

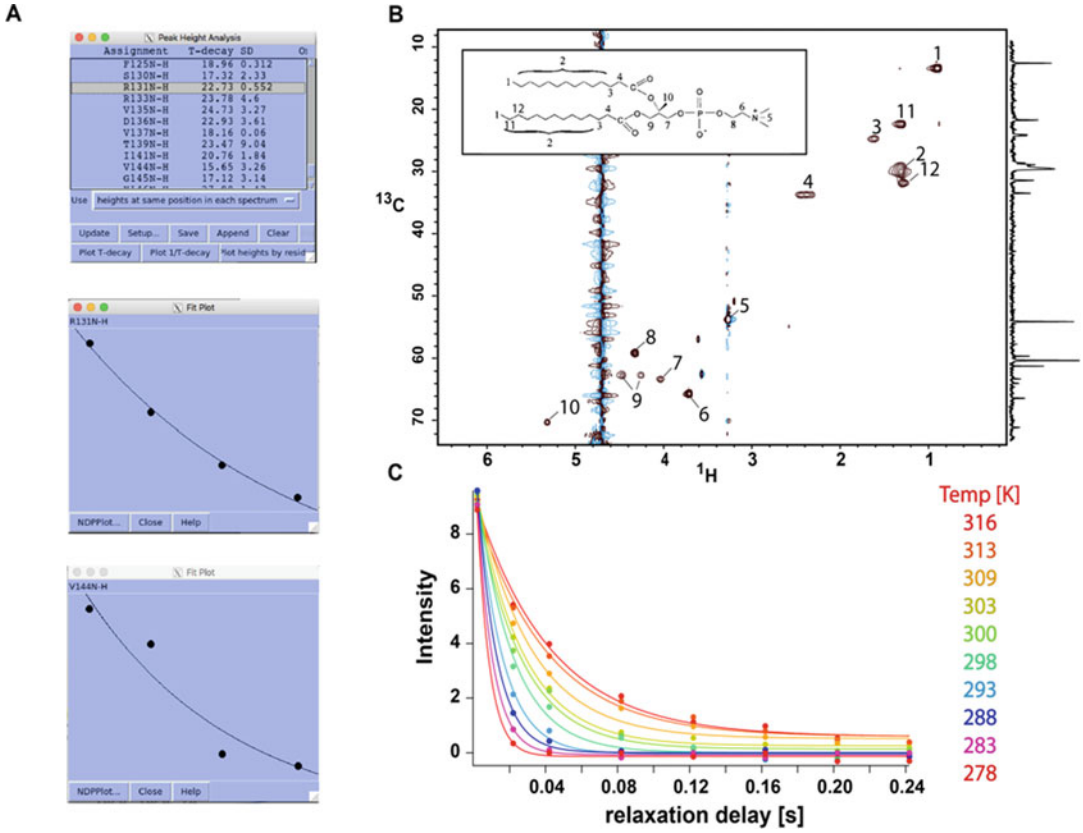

Fig. 3 Relaxation data analysis. (A) NMRFAM-SPARKY windows of the relaxation data analysis (appears upon typing "rh"). After the rate analysis from the program, the quality of the fits can be assessed by clicking on the respective assignment (good fit is found in the middle panel). It is advisable to check every amino acids with bad fits thoroughly (lower panel) which may be due to peak overlap. (B) 2D ^{1}H,^{13}C-HSQC using the ^{13}C natural abundance of lipids. The inset shows a DMPC molecule with the respective assignment indicated on the molecule and within the spectrum. A 1D ^{13}C spectrum is shown on the right side which were used for relaxation data measurements. (C) CPMG intensity ratios were extracted using the t1t2 module of TopSpin and then fitted in IGOR pro using a monoexponential curve fit

of 1 ms means that one loop takes 2 ms (plus a couple of μs for the 180° pulse). Since the experiment executes the cpmg block already once until it reaches the loop statement in the pulse program, zero loops in the vc list correspond to a relaxation time of 2 ms, 1 loop corresponds to a relaxation time of 4 ms, and 120 loops correspond to a relaxation delay of 242 ms.

7. The t1irpg and cpmg experiment are recorded as pseudo-2D experiments with the number of relaxation delays as the F1 ("indirect") dimension.

3.5 Analysis of Relaxation Experiments

3.5.1 Analysis of Protein Relaxation Experiments

1. Once high-quality relaxation spectra could be recorded, the analysis is rather straightforward.
2. The described procedure is the same for the R_1, R_2, and R_{1rho} experiments.
3. Interleaved pseudo-3D experiments can be split with the command "split" in TopSpin.
4. The 2rr files within each experiment (found in a subfolder of each experiment folder) can be changed to a ucsf file format, necessary for older Sparky version using the command (*see* **Note 9**): "bruk2ucsf 2rr NewFilename.ucsf."
5. Or it can be read directly with the newer NMRFAM-SPARKY version [57] (available free of charge here: http://pine.nmrfam.wisc.edu/download_packages.html).
6. If the new filename contains the relaxation delay time, it will avoid confusion at a later stage.
7. Although Sparky is a fast and easy-to-learn NMR spectra visualization tool (youtube contains some introductory videos), spectra processing such as phasing or baseline corrections needs to be done in either TopSpin or NMRPipe [62].
8. Also keep in mind the "hidden" processing parameter nc_proc in TopSpin (intensity scaling factor), which is only visible in the status parameter view in the Processing Parameters tab in TopSpin.
9. Keep the same nc_proc value for each set of 2D relaxation experiments by processing the 2D spectrum with "xfb nc_proc X," with X as a one-digit negative value.
10. Once all spectra are processed correctly, convert them in NMRFAM-SPARKY format and save them separately into a folder of your choice and as a project.
11. Transfer the assignment to each spectrum: "pa" (pick all assignments) -->"oc" (ornament copy) --> "op" (ornament paste).
12. Make sure you comply with the SPARKY annotation scheme.
13. Assignments can also be read from the BMRB (see the YouTube videos of NMRFAM-SPARKY).
14. With "yt" you can synchronize the views between the different 2D spectra, meaning that the same area of a spectrum is shown for every 2D experiment.
15. It is important to compute the noise floor of every spectrum for a correct signal-to-noise value.
16. For that type "st" and enter the value 10,000 in the box next to "noise as median of."

17. Then click recompute several times and look at the estimated noise value.
18. The value should be approximately the same for all 2D spectra of one relaxation dataset.
19. Once this is done, type "rh" and click on setup.
20. In the time/condition parameter, type the relaxation delay time (in this step confusion can be avoided if the filenames contain the relaxation delay values).
21. Select the spectra from the same relaxation series and use 10 random trials for error estimation. Click apply and close.
22. Then select all peaks from one spectrum of the relaxation series (it does not matter which spectrum) by using "pa" and run the relaxation rate calculation by typing "rh." This can take a couple of minutes.
23. When the "Peak Height Analysis" window is open, you should see a number that is increasing rapidly.
24. Afterwards the assignment should be listed in this window with a relaxation rate and a standard deviation (SD, Fig. 3A upper panel).
25. By clicking on the entries, the quality of the fit can be assessed visually (Fig. 3a). Among very good fits with a low SD (Fig. 3a middle panel), worse fits will be present (Fig. 3a lower panel), and it is important to check each peak again for peak overlap and shifts.
26. Overlapped peaks should be removed from data analysis.
27. Be aware that SPARKY calculates relaxation time T, whereas relaxation rates R are commonly reported in publications:

$$T = \frac{1}{R}$$

28. The SD is reported for time Tas well and needs to be converted to the rate R. Relaxation times from SPARKY can be saved as a .txt file and imported from within Excel to obtain an excel file with separate columns.

3.5.2 Analysis of Lipid Relaxation Experiments

1D lipid relaxation rates are extracted from peak intensity reductions upon increasing relaxation delays. The process is illustrated using TopSpin 3.5 pl7 (patchlevel 7) and the t1irpg experiment. Start TopSpin and load the pseudo-2D experiment.

1. Process the pseudo-2D using "xf2," phase the first ser file to absorption.
2. Type ".md" to scan through the rows (using scan rows) to visualize the intensity signal reduction. Exit this modus.
3. Type "t1t2," a new tab line appears.

4. Click the tab FID, select spectrum, and slice number 1.
5. Zoom into the area of interest in the spectrum and click Peaks/Range tab and use manual integration.
6. New buttons on top of the spectral window appear, click the button with "d," which lets you define the region for the integral. Remember the region since the integral boundaries should be the same for all 1D experiments from this pseudo-2D dataset.
7. Then save region as ... (Button with the floppy disc and the "A").
8. Export regions to relaxation module, the buttons should disappear.
9. Click on Tab Relaxation and a new window will appear, possibly with an error message due to wrong assumptions of the program regarding the relaxation parameter settings.
10. Select the vdlist in the relaxation parameter settings. The same window appears after clicking the Fitting tab.
11. Fitting type should be Area and upon clicking the Calculation tab, the T_1 will be calculated (a simple monoexponential fit is conducted).
12. Click on report and export the data as a .txt file.
13. Import the text file into excel (open the .txt file from within excel to obtain correct columns) to use the intensity values either for excel or another data visualization program, such as IGOR pro. Convert T_1 into R_1,
14. Alternatively, you can read out the signal intensity ratios and calculate T_1 yourself.

The same steps are valid for extracting R_2 from the cpmg experiment. However, TopSpin cannot read out the correct delay times from the vclist (see the report and the values for tau), which means that the calculated relaxation time is wrong. Hence, TopSpin is only used to extract the intensity data from the pseudo-2D which are then read into Excel (open the .txt file from within excel to obtain correct columns). The intensity ratio data together with the correct relaxation times (written down manually by the user) are used for a monoexponential fit in excel or another program such as IGOR pro (Fig. 3C).

3.5.3 Analysis of TRACT Data

The TRACT experiment is analyzed in a similar fashion. It is recorded in an interleaved fashion, meaning that the data for the relaxation rates of the slow relaxing α-spin and fast relaxing β-spin state of ^{15}N need to be separated using "split" (that also means that a TRACT experiment with 32 increments needs 64 increments in total). Process the data with xf2 and phase the first ser file. Extract

the data using the t1t2 procedure. The tumbling time is calculated using the formulas from Lee et al. [60]. A Mathematica script can be send by me upon request.

4 Notes

1. Addgene offers various plasmids for MSP, e.g., also the plasmid for MSPΔH5. The MSPΔH5 plasmid used in the studies encodes for a truncated apoA-I protein missing residues 1–54 (the G-domain and half of helix 1) and 121–142 (Helix 5) and contains an N-terminal TEV (Tobacco Etch Virus) protease cleavable hexahistidine tag. OmpX is expressed without the signaling sequence (residues 1–23). The protein therefore accumulates in inclusion bodies. Expression of OmpX with the signaling sequence leads to OmpX accumulation in the outer membrane, however, with much lower yields. The protein without the signaling sequence has 148 residues and is assigned with residue numbers 1–148 in NMR studies, ignoring the first 23 residues of the pre-protein.
2. It is tempting to shortcut the MSP purification steps with faster flow rates or different volumes. In my experience, the final quality and stability of the nanodisc assembly depend on the exact execution of these steps. If the purification is executed with the same relative amounts and flow rates of MSP buffers as described, very stable nanodiscs will form resulting in high-quality spectra of the embedded membrane protein and even for the nanodisc itself [61].
3. It is possible to separate MSP from the His-tag and TEV by another Ni-NTA gravity flow column. Be aware, however, that MSP has a tendency to bind Ni-NTA even without the His-tag. It is therefore necessary to either add 20 mM imidazole to the NMR buffer or use a TALON resin (e.g., GE lifescience) to keep MSP in the flow trough. However, the His-tag as well as TEV can also be separated from the assembled MSP nanodiscs later on using the size-exclusion chromatography and an S200 column. It is advisable to check the completeness of cleavage on an SDS gel. The gel needs to run rather long with diluted samples in order to observe the differences in the height of bands for cleaved and uncleaved MSP. The yield of MSP after purification and cleavage is around 40 mg of protein per L. If MSPΔH5 does not aggregate upon concentration, the purification was successful and a high-quality sample can be assembled (be aware that MSP will show smears upon pipetting in the concentrator, which disappear and a clear solution should result).

4. A complete cell lysis can be checked for example by using a light microscope.
5. From personal experience, the assembly process works best when the pH is at or above 7. Previous assembly protocols use a pH of 7.4. The concentration of the membrane protein may also determine if 1 or 2 membrane proteins incorporate per nanodiscs. Lower membrane protein concentrations during the assembly reduce the probability of incorporating two membrane proteins into one nanodisc. However, this is only a problem for larger nanodiscs and not for MSPΔH5 but needs to be kept in mind. When NMR spectra need to be recorded at low temperature, it is recommended to use lipids with a low melting temperature to assure a fluid and highly dynamic lipid environment for the membrane protein [54].
6. I also tested the removal of cholate by a BioBead extraction with a simultaneous dialysis (10 kDa MWCO Spectrum labs Float-A-Lyzer), which gives similar results to a BioBeads-only procedure (see Fig. 2). If the protein aggregates during the detergent removal step, it is recommended to use a stepwise and possibly softer removal of detergent. For this, start with 100 mg of BioBeads per 1 ml for 1 h, add another 200 mg of BioBeads for 1 h and keep adding BioBeads to around 800 mg per 1 ml of solution. 3–4 h of BioBeads are enough to remove any remaining detergent. A temperature-sensitive membrane protein might also be incorporated at a lower temperature. For this procedure, a lipid with a low melting temperature is recommended to assemble within the lipids liquid phase.
7. The incorporation of a membrane protein does not change the size of the assembly which is solely determined by the surrounding scaffolding protein. The variable lipid–MSP ratio is therefore a determinant specific to every membrane protein. The occupied space by the membrane protein is accounted for by the removal of lipids upon assembly. Empty MSPΔH5 nanodiscs contain around 50 lipids per lipid leaflet, which means that the optimal molar ratio of assembling empty MSPΔH5 nanodiscs is 2:100:200 (MSPΔH5:DMPC:cholate), corresponding to ca. 50 lipids per leaflet. Remember that for the reconstitution of 8-beta-stranded OmpX into MSPΔH5 nanodiscs, a molar ratio of 1:2:80:160 (OmpX:MSPdH5: lipids:sodium cholate) was used, corresponding to ca. 40 lipids per leaflet. In another assembly using the 16-beta-stranded BamA, a molar ratio of 1:6:132:264 (OmpX:MSPdH5:DMPC:sodium cholate) was used, corresponding to ca. 22 lipids per leaflet [63]. See ref. [64] for more details on how to estimate the amount of lipids, e.g., per transmembrane helix.

8. In the new Bruker software distribution of TopSpin (4.0.6), the pulse programs for [^{1}H],^{15}N-hetNOE, R1, and T1rho are included with the pulse sequence names trnoeetf3gpsi3d.3, trt1etf3gpsitc3d.3, and trtretf3gpsitc3d.3, respectively, as pseudo-3D experiments.
9. To execute this command, open a terminal window and navigate to the experiment folder. There the command must be typed. However, the command can only be executed in this folder when the .chsrc file contains the line:alias bruk2ucsf /path/path/path/path/Sparky/Resources/bin/bruk2ucsf

   The bruk2ucsf and pipe2ucsf files are part of the package of older sparky versions (https://www.cgl.ucsf.edu/home/sparky/).

References

1. Lenaz G (1987) Lipid fluidity and membrane-protein dynamics. Bioscience Rep 7 (11):823–837 https://doi.org/10.1007/Bf01119473
2. Dumas F, Tocanne JF, Leblanc G, Lebrun MC (2000) Consequences of hydrophobic mismatch between lipids and melibiose permease on melibiose transport. Biochemistry 39 (16):4846–4854
3. Johannsson A, Smith GA, Metcalfe JC (1981) The effect of bilayer thickness on the activity of (Na+ + K+)-ATPase. Biochim Biophys Acta 641(2):416–421
4. Montecucco C, Smith GA, Dabbeni-sala F, Johannsson A, Galante YM, Bisson R (1982) Bilayer thickness and enzymatic activity in the mitochondrial cytochrome c oxidase and ATPase complex. FEBS Lett 144(1):145–148
5. Martens C, Stein RA, Masureel M, Roth A, Mishra S, Dawaliby R, Konijnenberg A, Sobott F, Govaerts C, McHaourab HS (2016) Lipids modulate the conformational dynamics of a secondary multidrug transporter. Nat Struct Mol Biol 23(8):744–751. https://doi.org/10.1038/nsmb.3262
6. Vriens J, Nilius B, Voets T (2014) Peripheral thermosensation in mammals. Nat Rev Neurosci 15(9):573–589. https://doi.org/10.1038/nrn3784
7. van Meer G, Voelker DR, Feigenson GW (2008) Membrane lipids: where they are and how they behave. Nat Rev Mol Cell Biol 9 (2):112–124. https://doi.org/10.1038/nrm2330
8. Alberts B (2002) Molecular biology of the cell, 4th edn. Garland Science, New York
9. Stryer L (1995) Biochemistry, 4th edn. W.H. Freeman, New York
10. Martin M, de Mendoza D (2013) Regulation of Bacillus subtilis DesK thermosensor by lipids. Biochem J 451(2):269–275. https://doi.org/10.1042/BJ20121825
11. Gao Y, Cao E, Julius D, Cheng Y (2016) TRPV1 structures in nanodiscs reveal mechanisms of ligand and lipid action. Nature 534 (7607):347–351. https://doi.org/10.1038/nature17964
12. Baenziger JE, Darsaut TE, Morris ML (1999) Internal dynamics of the nicotinic acetylcholine receptor in reconstituted membranes. Biochemistry 38(16):4905–4911. https://doi.org/10.1021/bi9901811
13. Gracheva EO, Cordero-Morales JF, Gonzalez-Carcacia JA, Ingolia NT, Manno C, Aranguren CI, Weissman JS, Julius D (2011) Ganglion-specific splicing of TRPV1 underlies infrared sensation in vampire bats. Nature 476 (7358):88–91. https://doi.org/10.1038/nature10245
14. Gracheva EO, Ingolia NT, Kelly YM, Cordero-Morales JF, Hollopeter G, Chesler AT, Sanchez EE, Perez JC, Weissman JS, Julius D (2010) Molecular basis of infrared detection by snakes. Nature 464(7291):1006–1011. https://doi.org/10.1038/nature08943
15. Sanders CR, Landis GC (1995) Reconstitution of Membrane-Proteins into Lipid-Rich Bilayered Mixed Micelles for Nmr-Studies. Biochemistry 34 (12):4030–4040. doi:Doi https://doi.org/10.1021/Bi00012a022
16. Poget SF, Cahill SM, Girvin ME (2007) Isotropic bicelles stabilize the functional form of a

small multidrug-resistance pump for NMR structural studies. J Am Chem Soc 129 (9):2432–+. doi:https://doi.org/10.1021/ja0679836

17. Hwang PM, Bishop RE, Kay LE (2004) The integral membrane enzyme PagP alternates between two dynamically distinct states. Proc Natl Acad Sci USA 101(26):9618–9623. https://doi.org/10.1073/pnas.0402324101
18. Caldwell TA, Baoukina S, Brock AT, Oliver RC, Root KT, Krueger JK, Glover KJ, Tieleman DP, Columbus L (2018) Low- q Bicelles are mixed micelles. J Phys Chem Lett 9 (15):4469–4473. https://doi.org/10.1021/acs.jpclett.8b02079
19. Chung KY, Kim TH, Manglik A, Alvares R, Kobilka BK, Prosser RS (2012) Role of detergents in conformational exchange of a G protein-coupled receptor. J Biol Chem 287 (43):36305–36311. https://doi.org/10.1074/jbc.M112.406371
20. Zoonens M, Comer J, Masscheleyn S, Pebay-Peyroula E, Chipot C, Miroux B, Dehez F (2013) Dangerous liaisons between detergents and membrane proteins. The case of mitochondrial uncoupling protein 2. J Am Chem Soc 135(40):15174–15182. https://doi.org/10.1021/ja407424v
21. Ding Y, Fujimoto LM, Yao Y, Plano GV, Marassi FM (2015) Influence of the lipid membrane environment on structure and activity of the outer membrane protein ail from Yersinia pestis. BBA-Biomembranes 1848 (2):712–720. https://doi.org/10.1016/j.bbamem.2014.11.021
22. Dehez F, Schanda P, King MS, Kunji ERS, Chipot C (2017) Mitochondrial ADP/ATP carrier in Dodecylphosphocholine binds Cardiolipins with non-native affinity. Biophys J 113 (11):2311–2315. https://doi.org/10.1016/j.bpj.2017.09.019
23. Kurauskas V, Hessel A, Ma P, Lunetti P, Weinhaupl K, Imbert L, Brutscher B, King MS, Sounier R, Dolce V, Kunji ERS, Capobianco L, Chipot C, Dehez F, Bersch B, Schanda P (2018) How detergent impacts membrane proteins: atomic-level views of mitochondrial carriers in Dodecylphosphocholine. J Phys Chem Lett 9(5):933–938. https://doi.org/10.1021/acs.jpclett.8b00269
24. Lee SC, Knowles TJ, Postis VL, Jamshad M, Parslow RA, Lin YP, Goldman A, Sridhar P, Overduin M, Muench SP, Dafforn TR (2016) A method for detergent-free isolation of membrane proteins in their local lipid environment. Nat Protoc 11(7):1149–1162. https://doi.org/10.1038/nprot.2016.070
25. Scheidelaar S, Koorengevel MC, Pardo JD, Meeldijk JD, Breukink E, Killian JA (2015) Molecular model for the solubilization of membranes into nanodisks by styrene maleic acid copolymers. Biophys J 108(2):279–290. https://doi.org/10.1016/j.bpj.2014.11.3464
26. Chae PS, Rasmussen SG, Rana RR, Gotfryd K, Kruse AC, Manglik A, Cho KH, Nurva S, Gether U, Guan L, Loland CJ, Byrne B, Kobilka BK, Gellman SH (2012) A new class of amphiphiles bearing rigid hydrophobic groups for solubilization and stabilization of membrane proteins. Chemistry 18 (31):9485–9490. https://doi.org/10.1002/chem.201200069
27. Breyton C, Pucci B, Popot JL (2010) Amphipols and fluorinated surfactants: two alternatives to detergents for studying membrane proteins in vitro. Methods Mol Biol 601:219–245. https://doi.org/10.1007/978-1-60761-344-2_14
28. Bayburt TH, Carlson JW, Sligar SG (1998) Reconstitution and imaging of a membrane protein in a nanometer-size phospholipid bilayer. J Struct Biol 123(1):37–44. https://doi.org/10.1006/jsbi.1998.4007
29. Bayburt TH, Grinkova YV, Sligar SG (2002) Self-assembly of discoidal phospholipid bilayer nanoparticles with membrane scaffold proteins. Nano Lett 2(8):853–856
30. Hagn F, Etzkorn M, Raschle T, Wagner G (2013) Optimized phospholipid bilayer Nanodiscs facilitate high-resolution structure determination of membrane proteins. J Am Chem Soc 135(5):1919–1925. https://doi.org/10.1021/ja310901f
31. Nasr ML, Baptista D, Strauss M, Sun ZJ, Grigoriu S, Huser S, Pluckthun A, Hagn F, Walz T, Hogle JM, Wagner G (2017) Covalently circularized nanodiscs for studying membrane proteins and viral entry. Nat Methods 14 (1):49–52. https://doi.org/10.1038/nmeth.4079
32. Bibow S, Carneiro MG, Sabo TM, Schwiegk C, Becker S, Riek R, Lee D (2014) Measuring membrane protein bond orientations in nanodiscs via residual dipolar couplings. Protein Sci 23(7):851–856. https://doi.org/10.1002/pro.2482
33. Kofuku Y, Ueda T, Okude J, Shiraishi Y, Kondo K, Mizumura T, Suzuki S, Shimada I (2014) Functional dynamics of deuterated beta (2)-adrenergic receptor in lipid bilayers revealed by NMR spectroscopy. Angew Chem Int Ed 53(49):13376–13379. https://doi.org/10.1002/anie.201406603

34. Frey L, Lakomek NA, Riek R, Bibow S (2017) Micelles, Bicelles, and Nanodiscs: comparing the impact of membrane mimetics on membrane protein backbone dynamics. Angew Chem Int Ed 56(1):380–383. https://doi.org/10.1002/anie.201608246
35. Mors K, Roos C, Scholz F, Wachtveitl J, Dotsch V, Bernhard F, Glaubitz C (2012) Modified lipid and protein dynamics in nanodiscs. Bba-Proteins Proteom 1828 (4):1222–1229. https://doi.org/10.1016/j.bbamem.2012.12.011
36. Martinez D, Decossas M, Kowal J, Frey L, Stahlberg H, Dufourc EJ, Riek R, Habenstein B, Bibow S, Loquet A (2017) Lipid internal dynamics probed in Nanodiscs. ChemPhysChem 18:2651. https://doi.org/10.1002/cphc.201700450
37. Brainard JR, Knapp RD, Morrisett JD, Pownall HJ (1984) 13C NMR studies of the thermal properties of a model high density lipoprotein. Apolipoprotein A-I-dimyristoylphosphatidylcholine complex. J Biol Chem 259 (16):10340–10347
38. Bibow S, Polyhach Y, Eichmann C, Chi CN, Kowal J, Albiez S, McLeod RA, Stahlberg H, Jeschke G, Guntert P, Riek R (2017) Solution structure of discoidal high-density lipoprotein particles with a shortened apolipoprotein A-I. Nat Struct Mol Biol 24(2):187–193. https://doi.org/10.1038/nsmb.3345
39. Kay LE, Torchia DA, Bax A (1989) Backbone dynamics of proteins as studied by 15N inverse detected heteronuclear NMR spectroscopy: application to staphylococcal nuclease. Biochemistry 28:8972–8979
40. Wagner G (1995) The importance of being floppy. Nat Struct Mol Biol 2(4):255–257
41. Igumenova TI, Frederick KK, Wand AJ (2006) Characterization of the fast dynamics of protein amino acid side chains using NMR relaxation in solution. Chem Rev 106(5):1672–1699. https://doi.org/10.1021/cr040422h
42. Jarymowycz VA, Stone MJ (2006) Fast time scale dynamics of protein backbones: NMR relaxation methods, applications, and functional consequences. Chem Rev 106 (5):1624–1671. https://doi.org/10.1021/cr040421p
43. Bibow S, Hiller S (2018) A guide to quantifying membrane protein dynamics in lipids and other native-like environments by solution-state NMR spectroscopy. FEBS J
44. Kleckner IR, Foster MP (2011) An introduction to NMR-based approaches for measuring protein dynamics. Bba-Proteins Proteom 1814 (8):942–968. https://doi.org/10.1016/j.bbapap.2010.10.012
45. Morin S (2011) A practical guide to protein dynamics from N-15 spin relaxation in solution. Prog Nucl Mag Res Sp 59(3):245–262. https://doi.org/10.1016/j.pnmrs.2010.12.003
46. Palmer AG 3rd (2014) Chemical exchange in biomacromolecules: past, present, and future. J Magn Reson 241:3–17. https://doi.org/10.1016/j.jmr.2014.01.008
47. Kempf JG, Loria JP (2004) Measurement of intermediate exchange phenomena. Methods Mol Biol 278:185–231. https://doi.org/10.1385/1-59259-809-9:185
48. Jarymowycz VA, Stone MJ (2006) Fast time scale dynamics of protein backbones: NMR relaxation methods, applications, and functional consequences. Chem Rev 106 (5):1624–1671. https://doi.org/10.1021/cr040421p
49. Kleckner IR, Foster MP (2011) An introduction to NMR-based approaches for measuring protein dynamics. Biochimica et biophysica acta 1814 (8):942–968. doi:Doi https://doi.org/10.1016/J.Bbapap.2010.10.012
50. Morin S (2011) A practical guide to protein dynamics from 15N spin relaxation in solution. Prog Nucl Magn Reson Spectrosc 59 (3):245–262. https://doi.org/10.1016/j.pnmrs.2010.12.003
51. Bibow S, Hiller S (2018) A guide to quantifying membrane protein dynamics in lipids and other native-like environments by solution-state NMR spectroscopy. FEBS J 286 (9):1610–1623. https://doi.org/10.1111/febs.14639
52. Ishima R, Bagby S (2018) Protein dynamics revealed by CPMG dispersion. In: Webb GA (ed) Modern magnetic resonance. Springer International Publishing, Cham, pp 435–452. https://doi.org/10.1007/978-3-319-28388-3_44
53. Stetz MA, Caro JA, Kotaru S, Yao X, Marques BS, Valentine KG, Wand AJ (2019) Characterization of internal protein dynamics and conformational entropy by NMR relaxation. Methods Enzymol 615:237–284. https://doi.org/10.1016/bs.mie.2018.09.010
54. Frey L, Hiller S, Riek R, Bibow S (2018) Lipid- and cholesterol-mediated time-scale-specific modulation of the outer membrane protein X dynamics in lipid bilayers. J Am Chem Soc 140 (45):15402–15411
55. Lakomek NA, Ying J, Bax A (2012) Measurement of (1)(5)N relaxation rates in

perdeuterated proteins by TROSY-based methods. J Biomol NMR 53(3):209–221. https://doi.org/10.1007/s10858-012-9626-5

56. Lakomek NA, Kaufman JD, Stahl SJ, Louis JM, Grishaev A, Wingfield PT, Bax A (2013) Internal dynamics of the homotrimeric HIV-1 viral coat protein gp41 on multiple time scales. Angew Chem Int Ed Engl 52 (14):3911–3915. https://doi.org/10.1002/anie.201207266
57. Lee W, Tonelli M, Markley JL (2014) NMRFAM-SPARKY: enhanced software for biomolecular NMR spectroscopy. Bioinformatics 31(8):1325–1327
58. Mulder FA, de Graaf RA, Kaptein R, Boelens R (1998) An off-resonance rotating frame relaxation experiment for the investigation of macromolecular dynamics using adiabatic rotations. J Magn Reson 31:351–357
59. Garwood M, Ke Y (1991) Symmetric pulses to induce arbitrary flip angles with compensation for RF inhomogeneity and resonance offsets. J Magn Reson (1969) 94(3):511–525
60. Lee D, Hilty C, Wider G, Wuthrich K (2006) Effective rotational correlation times of proteins from NMR relaxation interference. J Magn Reson 178(1):72–76
61. Bibow S, Polyhach Y, Eichmann C, Chi CN, Kowal J, Albiez S, McLeod RA, Stahlberg H, Jeschke G, Guntert P, Riek R (2017) Solution structure of discoidal high-density lipoprotein particles with a shortened apolipoprotein A-I. Nat Struct Mol Biol 24 (2):187–193. https://doi.org/10.1038/nsmb.3345
62. Delaglio F, Grzesiek S, Vuister GW, Zhu G, Pfeifer J, Bax A (1995) NMRPipe: a multidimensional spectral processing system based on UNIX pipes. J Biomol NMR 6(3): 277–293
63. Hartmann JB, Zahn M, Burmann IM, Bibow S, Hiller S (2018) Sequence-specific solution NMR assignments of the beta-barrel Insertase BamA to monitor its conformational Ensemble at the Atomic Level. J Am Chem Soc 140(36):11252–11260. https://doi.org/10.1021/jacs.8b03220
64. Ritchie TK, Grinkova YV, Bayburt TH, Denisov IG, Zolnerciks JK, Atkins WM, Sligar SG (2009) Chapter 11 - reconstitution of membrane proteins in phospholipid bilayer nanodiscs. Methods Enzymol 464:211–231. https://doi.org/10.1016/S0076-6879(09)64011-8

INDEX

A

Affinity chromatography 130, 136, 139–149, 253, 255, 262, 276, 287
Amphipol 106, 192–194, 196, 197, 200, 231, 398
Arabidopsis thaliana ..... v, 82, 87, 89
Atomic force microscopy (AFM) 359–371
ATPase assay 98–101
Avi tag 153, 154, 156–162

B

Baculovirus 63–79
Bicelles 99, 192–194, 196–198, 200, 374, 375
Biotin 110, 113, 133, 135, 152–154, 156, 157, 159–164, 378

C

Cell lysis 18, 22, 24, 40, 78, 148, 403, 415
Chloroplast 82, 83, 86, 90–91, 374
Cryo-electron microscopy (Cryo-EM) 245, 284

D

Detergent 15, 18, 22–24, 34, 38, 39, 42, 43, 49, 50, 56, 57, 59, 69, 77, 93–101, 106, 109, 110, 114, 122, 123, 129–131, 133–136, 141, 143, 147, 148, 159, 162, 173, 182, 186, 192, 193, 196–200, 210, 220, 221, 227–242, 251–259, 262, 265, 280, 284, 290, 293, 340, 341, 343, 346, 350, 353, 354, 361, 362, 369, 374, 375, 377, 378, 380–382, 384, 398, 405, 415
Detergent exchange 280, 290
Deuterium exchange 339–355
Dynamics 246, 331, 339–341, 346, 350, 353, 373–375, 377, 388, 397–416

E

Electroporation 20, 32, 35, 36, 40, 41, 53
Envelope 82, 84, 90, 91, 283
Escherichia coli 13–26, 41, 43, 44, 47, 48, 50–54, 105, 130, 133, 140–145, 149, 152–157, 161, 167, 169–171, 180, 247, 249, 260, 261, 284, 286, 364, 374, 379, 386, 400–403

F

Fermentation 48, 49, 56, 57
FlashBac Gold 70, 73
Fluorescence-detection size-exclusion chromatography (FSEC) 18, 24, 107, 108, 111, 113–116, 123, 133, 135, 162, 289, 290
Fluorescent ligand binding assay 109, 120–122
Fluorimetry 75
FX cloning 154–158, 160, 161, 180

G

Glow discharging 228, 231, 232
G-protein-coupled receptors (GPCRs) 63, 65, 69, 72, 105, 106, 108, 139, 168, 209, 294, 324
Grid preparation 229–233, 235, 257, 275–281

H

Homolog screening 14
Hydrogen/Deuterium eXchange and Mass Spectometry (HDX-MS) ..... vi, 339–344, 347–351, 355

I

Immobilized metal affinity chromatography (IMAC) 15, 16, 24, 72, 78, 95, 97, 100, 132, 134, 140–142, 176, 182, 276–278, 280, 281, 285
In-gel fluorescence 110, 113, 123, 124, 289, 290
Injector 322, 324, 326, 328–331
In Meso In Situ Serial X-ray Crystallography (IMISX) 293–314, 324, 329
Insect cells Sf9 ..... 65, 67, 77, 79
In situ annealing 284, 286, 289, 290
Inverted vesicles 34, 38
Ion channel 63, 139, 168, 193, 195, 209, 210, 294
Ion flux assay 210, 212, 213

L

Lactococcus lactis 29–44, 47
Ligand binding 109, 111–112, 119–121, 187, 398

Camilo Perez and Timm Maier (eds.), *Expression, Purification, and Structural Biology of Membrane Proteins*, Methods in Molecular Biology, vol. 2127, https://doi.org/10.1007/978-1-0716-0373-4,

Lipid cubic phase (LCP) ..... vi, 294–296, 298–300, 302–304, 309–313, 321–335
Lipid dynamics 398, 399, 409
Lipid flippases 207
Lipid transport 208, 218, 283–290
Lipids 23, 49, 59, 81, 94, 99, 106, 115, 186, 193–200, 207–211, 214, 216–218, 221, 222, 229, 246, 247, 249, 251–256, 259, 261–263, 325, 340, 364, 374, 378, 380–382, 387, 397–399, 403, 405, 409, 410, 415
Liposome reconstitution 211

M

Magic angle spinning (MAS) NMR ..... vi, 375, 376, 381–384, 387
Mass spectrometry 31, 43, 57, 69, 154, 160, 162, 163, 339–355, 380
Mechanical unfolding 359–371
Membrane protein 13–26, 106, 108, 120, 129–133, 135, 136, 140, 141, 143, 144, 147, 198–200, 227–242, 246, 252, 275–281, 283–290, 293–314, 321–329, 331, 343, 345, 346, 350, 351, 353, 360, 363, 365–369, 373, 374, 379–381, 383, 384, 386, 397–416
Membrane protein complexes 1–11, 169, 230
Membrane protein folding 360
Membrane scaffold 99, 196, 251, 253, 261, 398, 399
Mesophase 294, 296, 302, 305–307, 309, 310, 313
Microcrystals 300, 312
Microsome 84, 88, 89
Mitochondria 1, 55–57, 82, 84, 86–88
Mitochondrial membrane protein 1–11
Multi-subunit expression 1–11

N

Nanobody 151, 167, 169, 171–174, 176, 178–182
Nanobody enlargement 168
Nanobody expression 175, 176, 181
Nanodisc 194–196, 199, 200, 251–253, 255, 256, 258–263, 265, 266, 399, 414, 415
Negative staining 228, 231–234, 240, 256, 280, 281
Neutravidin 152
NICE expression system 31, 41
Nisin A 30, 33, 37, 40
Non-selective channel 207–222
Nuclear Magnetic Resonance (NMR) ..... vi, 191, 194, 198, 200, 245, 340, 354, 373–388, 397–416

O

On-column proteolytic cleavage 140
Organelle ..... v, 81–83, 85, 89, 397

P

Panning 151, 152
Phage display 167
Phospholipids 43, 200, 207–227, 246, 251, 265
Protein expression 13, 15–17, 20–22, 24, 30, 38, 50, 57, 63–79, 123, 134, 156, 159, 174, 284, 286, 287, 322, 387, 400–401
Protein extraction 93
Protein purification 15, 22, 23, 31, 34, 38–40, 49, 50, 56–59, 115, 129–131, 135, 196, 197, 208, 261, 275–281, 285, 287–288

R

Recombinant protein 13, 16–19, 67, 107, 129, 147
Reconstitution 20, 106, 107, 191–201, 208, 209, 211, 213–219, 222, 231, 246, 252, 254–256, 262, 375, 378, 380–382, 387, 400–401, 403, 415

S

Saccharomyces cerevisiae 1–11, 47–59
Scramblases 207–211, 218, 219, 252, 256
Scrambling 207–222
SDS-PAGE 5, 9, 17, 19, 20, 38, 39, 42, 49, 55–59, 69, 72, 77–79, 96, 110, 113, 116, 131, 135, 136, 142, 146, 147, 149, 154, 156, 160, 163, 164, 173, 175, 176, 178, 179, 182, 195, 198–200, 214, 215, 222, 276, 279, 288, 381, 384
Serial crystallography 295, 300, 307, 321–336
Serial femtosecond crystallography (SFX) 312, 321, 322, 324, 325, 328, 331
Single-molecule force spectroscopy (SMFS) 359–361, 368, 370
Single particle electron microscopy 275–281
Size exclusion chromatography (SEC) 19, 24, 26, 69, 77, 132, 134, 135, 158–160, 162, 176, 177, 179, 285, 287, 290, 378, 404, 405
Small-scale purification 108, 110, 113, 137
Solid-state NMR ..... vi, 200, 374
Spodoptera frugiperda 65
Strep-II tag 129, 130
Streptactin 130
Streptavidin 152, 154, 156, 160, 163, 164
Sucrose gradient 84, 88–91, 381

Supported lipid bilayer 360, 370
Sybody 151, 188, 189
Synchrotron 294, 298, 300, 324, 326, 328–330, 332, 334–336

T

Thermal shift assay 106, 114
Transfection 70, 73, 156, 158, 159
Transformation 2–4, 7, 10, 14–16, 20, 31–33, 35, 36, 40, 41, 50–54, 141, 144, 170, 173, 174, 180, 286, 368
Transporter 63, 93–101, 139, 161, 168, 169, 186, 252, 294, 341

V

VHH 167
Vitrification 228, 236, 263

X

X-ray 49, 284, 286, 289, 290, 294, 295, 300, 307, 309, 312, 321, 322, 324, 326, 328, 330, 331, 333
X-ray crystallography 65, 191, 227, 245, 246, 284, 294, 296, 340, 373
X-ray free electron lasers (XFELs) ..... vi, 294, 312, 321, 322, 324, 328, 330, 334